BIOMASS-BASED SUPERCAPACITORS

DESIGN, FABRICATION AND SUSTAINABILITY

EDITED BY

MD. ABDUL AZIZ • SYED SHAHEEN SHAH

WILEY

Biomass-Based Supercapacitors

Biomass-Based Supercapacitors

Design, Fabrication and Sustainability

Edited by

Md. Abdul Aziz
Interdisciplinary Research Center for Hydrogen and Energy Storage, King Fahd University of Petroleum and Minerals, Dhahran, Saudi Arabia

Syed Shaheen Shah
Department of Material Chemistry
Graduate School of Engineering, Kyoto University
Nishikyo-ku, Kyoto, Japan

WILEY

Cover images: © edge69/Getty Images, © browndogstudios/iStockphoto, © petovarga/Adobe Stock, © chombosan/Shutterstock, © ksyproduktor/Shutterstock, Pixabay, © Elnur/Shutterstock
Cover design by Wiley

Set in 9.5/12.5pt STIXTwoText by Integra Software Services Pvt. Ltd, Pondicherry, India

Contents

About the Editors

Dr. Md. Abdul Aziz is a Research Scientist-II (Associate Professor) at the Interdisciplinary Research Center for Hydrogen and Energy Storage (IRC-HES), King Fahd University of Petroleum & Minerals (KFUPM), Saudi Arabia. He also served as research scientist-III (Assistant Professor) at the Center of Research Excellence in Nanotechnology (CENT), KFUPM. He worked as a postdoctoral fellow of the Japan Society for the Promotion of Science (JSPS) in the Department of Material Chemistry, Kyoto University, from 2009–2011. He is a serving editorial board member of ChemistrySelect-Wiley; Current Nanomaterials – Bentham Science and served/serving as guest editor of The Chemical Record-Wiley; Chemistry-an Asian Journal-Wiley; Chemistry – a European Journal-Wiley. Dr. Aziz has authored 187 papers in well-reputed peer-reviewed journals in addition to numerous numbers of conference proceedings/presentations/book chapters, and holds 30 US patents. His research interests are the preparation and characterization of nanomaterial and carbonaceous materials for different electrochemical applications such as energy storage and generation, sensor, CO_2 conversion, water splitting, sensors etc. Dr. Aziz received his B.Sc. in Chemistry in 1999 and M.Sc. in organic chemistry in 2001 from University of Dhaka, Bangladesh. In 2009, he earned his PhD in chemistry from BioMEMS and Nanoelectrochemistry Laboratory, Department of Chemistry, Pusan National University, Republic of Korea.

Dr. Syed Shaheen Shah is a JSPS Post-Doctoral Fellow in the Department of Material Chemistry, Graduate School of Engineering, Kyoto University, Japan. Dr. Shah received his Bachelor's degree in 2015 and Master's degree in 2017 from the Department of Physics, University of Peshawar, Pakistan. He earned his PhD degree in 2022 from the Physics Department, King Fahd University of Petroleum & Minerals, Saudi Arabia. His research interests focus on the development and mechanistic investigation of advanced nanomaterials for energy harvesting and storage applications, such as supercapacitors, electrochemical water splitting, and electrochemical sensors.

Preface

Due to recent technological developments energy demands are rising with time, and our planet currently faces enormous energy-related challenges, including fossil fuel consumption and CO_2 emission. Renewable energy resources provide a considerable alternative to meet global energy demands. However, due to its time-dependent operations, a powerful energy storage system is required that can store vast amounts of energy in a short time. In this regard, supercapacitors based on biomass materials have recently received tremendous attention. A supercapacitor is an energy storage device with high energy and power densities and can be completely charged in seconds. Supercapacitors can be developed to store renewable energy on a larger scale by carefully selecting electrode materials and electrolytes and using cost-effective and simple preparation methods. Supercapacitors are now a reality in the market and are used in various wearable and automobile systems. When intermittent renewable sources are added to the energy mix, supercapacitors can also help stabilize the output energy and power. Supercapacitors are currently commercially accessible; however, they still need to be improved, mainly to increase their energy density. In addition to enhancing electrode materials, electrolytes present, and system integration, a thorough comprehension of their properties and precise operating principles is required. All of these issues over the decade greatly influenced both academia and business.

One fundamental technical and financial development is turning biomass into energy, transport, and storage. R&D and industrial applications for collecting all types of biomass resources have made significant progress in recent years. All the non-fossilized biological materials on Earth are referred to as biomass, including animal and plant wastes, agricultural residues, industrial residues, food wastes, municipal wastes, forest residues, and agricultural residues. Biomass has been utilized as a renewable resource for both energy and non-energy purposes, including the production of fuels and power as well as uses in agriculture and industry. As a result, biomass meets roughly 10% of the global energy demand and 35% of that in developing nations. Biomass and its derivatives have increased as science and technology have advanced, not only for use in producing energy and fuel but also in applications such as energy storage, sensors, and catalysis. Producing electrodes, electrolytes, binder materials, separators, and packaging materials from biomass has sparked a prospective interest in developing electrochemical supercapacitors.

Our book, *Biomass-Based Supercapacitors*, provides extensive knowledge about the developments of supercapacitors, with a complete package of using biomass-based materials and

their various industrial applications. No other thorough book has dealt extensively with the subject of biomass-based supercapacitors. A comprehensive study is necessary due to the new concepts that have emerged over the last few years, including a better explanation of how biomass can efficiently be utilized in developing high-performance supercapacitors. This book has been specifically designed to satisfy the academic and scientific needs of students, aspiring researchers, and material scientists working in the area of biomass-based materials and their numerous applications in the field of electrochemical energy storage devices. The book was written in collaboration with experts in the field of supercapacitors from around the world, and state-of-the-art studies are covered in detail. This book is structured into several sections that discuss different aspects of biomass in the field of supercapacitors. We are confident that this book will satisfy all of needs and expectations. There are 26 chapters in the book: the first three chapters being devoted to an introduction to biomass, the environmental aspects for utilization in supercapacitors, and circular economy. The next three chapters explain the basic concepts, fundamental electrochemical principles, electrochemical characterization methods, and fundamental supercapacitor attributes to enable reading the book without any prior knowledge. Afterward, fifteeen chapters are devoted to very important component of supercapacitors i.e., biomass-derived carbonaceous electrode materials, including non-activated carbon, carbon from pretreated biomass, carbonate salts-activated carbon, KOH/NaOH-activated carbon, chloride salt-activated carbon, CO_2-activated carbon, steam-activated carbon, hard carbon, carbon nanofibers, graphene, nitrogen-doped carbon, sulfur-doped carbon, composites of biomass-derived carbon and metal oxides, composites of biomass-derived materials and conducting polymers, and composites of biomass-derived materials and conductive materials excluding conducting polymers. Next, three further chapters explains the production of supercapacitor's electrolytes, separators, binding agents, and packaging materials from biomass, and the last two chapters provide a comprehensive insight into the industrial applications, future directions, and challenges in biomass-based supercapacitors. Each chapter strives to provide the most comprehensive information possible using everyday language.

We are pleased that we were able to bring together the top experts in biomass-based supercapacitors research and technology in one book. They all graciously consented to offer their time to write chapters, for which we are grateful. We would also like to thank the Wiley team for their patience and for providing us with this amazing opportunity to provide an excellent platform for researchers and students working in electrochemical energy storage. Finally, we would like to dedicate this book to our teachers and parents, who would be incredibly proud of our small contributions to assist in resolving global issues facing humanity.

Dr. Md. Abdul Aziz
Dr. Syed Shaheen Shah

List of Contributors

A. J. Saleh Ahammad
Department of Chemistry
Jagannath University
Dhaka, Bangladesh

Md. Rajibul Akanda
Department of Chemistry
Jagannath University
Dhaka, Bangladesh

Ashika Akhtar
Department of Botany
University of Dhaka
Dhaka, Bangladesh

Md. Akhtaruzzaman
Solar Energy Research Institute (SERI)
Universiti Kebangsaan
Malaysia

Runa Akter
Institute of Forestry and Environmental
Sciences
University of Chittagong
Chittagong, Bangladesh

Md. Almujaddade Alfasane
Department of Botany
Curzon Hall Campus
University of Dhaka
Dhaka, Bangladesh

Syeda Ramsha Ali
Universidad Autónoma de Nuevo León
UANL, Facultad de Ciencias Químicas
Av. Universidad, Cd. Universitaria
San Nicolás de los Garza
Nuevo León, México

Awais Ali
Department of Chemical Engineering
Technology
Government College University
Faisalabad, Pakistan

Ahmar Ali
Physics Department
King Fahd University of Petroleum &
Minerals
Dhahran, Saudi Arabia

Muhammad Ali
Interdisciplinary Research Center for
Hydrogen and Energy Storage (IRC-HES)
King Fahd University of Petroleum &
Minerals
Dhahran, Saudi Arabia

Shahid Ali
Interdisciplinary Research Center for
Hydrogen and Energy Storage (IRC-HES)
King Fahd University of Petroleum &
Minerals
Dhahran, Saudi Arabia

Abdul-Rahman Al-Betar
Chemistry Department
King Fahd University of Petroleum
and Minerals
Dhahran, Saudi Arabia

Interdisciplinary Research Center
for Hydrogen and Energy Storage
(IRC-HES)
King Fahd University of Petroleum &
Minerals
KFUPM, Dhahran, Saudi Arabia

Atif Saeed Alzahrani
Interdisciplinary Research Center for
Hydrogen and Energy Storage (IRC-HES)
King Fahd University of Petroleum &
Minerals
Dhahran, Saudi Arabia

Materials Science and Engineering
Department
King Fahd University of Petroleum &
Minerals
Dhahran Saudi Arabia

Muhammad Ammar
Department of Chemical Engineering
Technology
Government College University
Faisalabad, Pakistan

Ahtisham Anjum
Physics Department
King Fahd University of Petroleum & Minerals
Dhahran, Saudi Arabia

Abdul Awal
Department of Chemistry
Jagannath University
Dhaka, Bangladesh

Md. Abdul Aziz
Interdisciplinary Research Center for
Hydrogen and Energy Storage
King Fahd University of Petroleum
and Minerals
Dhahran, Saudi Arabia

K. A. CARE Energy Research and
Innovation Center
King Fahd University of Petroleum &
Minerals
Dhahran, Saudi Arabia

T. Elango Balaji
Department of Chemistry
Utkal University
Bhubaneswar
Odisha, India

Hasi Rani Barai
Department of Mechanical Engineering
School of Mechanical and IT Engineering
Yeungnam University
Republic of Korea

Jaber Bin Abdul Bari
Department of Oceanography
Noakhali Science and Technology University
Noakhali, Bangladesh

Biswa Nath Bhadra
International Center for Materials
Nanoarchitectonics (WPI-MANA)
National Institute for Materials Science (NIMS)
Tsukuba, Ibaraki, Japan

Md. Raquibul Hassan Bhuiyan
Department of Architecture
Bangladesh University of Engineering
and Technology
Dhaka

Saidur R. Chowdhury
Department of Civil Engineering
College of Engineering
Prince Mohammad Bin Fahd University
(PMU)
Al khobar
Saudi Arabia

SC Environmental Solutions
Toronto ON, Canada

Himadri Tanaya Das
Centre for Advance Materials and
Applications
Utkal University
Bhubaneswar, Odisha, India

Nigamananda Das
Department of Chemistry
Utkal University
Bhubaneswar, Odisha, India

Thuhin Kumar Dey
Department of Leather Engineering
Khulna University of Engineering &
Technology
Khulna, Bangladesh

Guodong Du
Department of Chemistry
University of North Dakota
Grand Forks, North Dakota
United States

Swapnamoy Dutta
Bredesen Center for Interdisciplinary
Research and Graduate Education
University of Tennessee
Knoxville, TN, USA

Muhammad Ali Ehsan
Interdisciplinary Research
Center for Hydrogen and Energy Storage
(IRC-HES)
King Fahd University of Petroleum &
Minerals
Dhahran, Saudi Arabia

Mian Muhammad Faisal
Universidad Autónoma de Nuevo León
UANL, Facultad de Ciencias Químicas
Av. Universidad, Cd. Universitaria
San Nicolás de los Garza
Nuevo León, México

Salman Farsi
Department of Materials Science &
Engineering
Khulna University of Engineering &
Technology
Khulna, Bangladesh

K.C. Sanal
Universidad Autónoma de Nuevo León
UANL, Facultad de Ciencias Químicas
Av. Universidad, Cd. Universitaria
San Nicolás de los Garza
Nuevo León, México

Eman Gul
Institute of Chemical Sciences
University of Peshawar
Peshawar, Pakistan

Md. Akib Hasan
Department of Chemistry
University of Dhaka
Bangladesh

Abbas Saeed Hakeem
Interdisciplinary Research
Center for Hydrogen and Energy Storage
(IRC-HES)
King Fahd University of Petroleum and
Mineral
Dhahran, Saudi Arabia

Md. Mehedi Hasan
Department of Chemistry
Jagannath University
Dhaka, Bangladesh

Khizar Hayat
Department of Physics Abdul Wali
Khan University
Mardan, Khyber Pakhtunkhwa
Pakistan

Muhammad Humayun
Wuhan National Laboratory for
Optoelectronics
Huazhong University of Science and
Technology
Wuhan, China

Abdulmajeed H. Hendi
Physics Department
King Fahd University of Petroleum and
Minerals
Dhahran, Saudi Arabia

Md. Mominul Islam
Department of Chemistry
Faculty of Sciences
Dhaka University
Bangladesh

Santa Islam
Department of Chemistry
Jagannath University
Dhaka, Bangladesh

Naseem Iqbal
U.S. Pakistan Center for Advanced Studies
in Energy (USPCAS−E)
National University of Sciences and
Technology (NUST)
Islamabad, Pakistan

Muhammad Zahir Iqbal
Nanotechnology Research Laboratory
Faculty of Engineering Sciences
GIK Institute of Engineering Sciences
and Technology
Topi, Khyber Pakhtunkhwa, Pakistan

Mamun Jamal
Department of Chemistry
Khulna University of Engineering &
Technology (KUET)
Khulna, Bangladesh

Mohammad Rezaul Karim
Center of Excellence for Research in
Engineering Materials (CEREM)

Deanship of Scientific Research (DSR)
College of Engineering
King Saud University
Riyadh, Saudi Arabia

K.A. CARE Energy Research and
Innovation Center
King Saud University
Riyadh, Saudi Arabia

Nazmul Abedin Khan
Department of Mathematical
and Physical Sciences
East West University
Dhaka, Bangladesh

Ibrahim Khan
School of Chemical Engineering &
Materials Science
Chung-Ang University
Seoul, Republic of Korea

Syed Niaz Ali Shah
Center for Integrative Petroleum Research
King Fahad University of Petroleum and
Minerals
Dhahran, Saudi Arabia

Sikandar Khan
Department of Mechanical Engineering
King Fahd University of Petroleum
and Minerals
Dhahran, Saudi Arabia

Abuzar Khan
Interdisciplinary Research Center for
Hydrogen and Energy Storage
(IRC-HES) King Fahd University of
Petroleum and Minerals
Dhahran, Saudi Arabia

Nasrin Siraj Lopa
Center for Environmental & Energy
Research
Ghent University Global Campus
Incheon, Republic of Korea

Wael Mahfoz
Chemistry Department
King Fahd University of Petroleum &
Minerals
Dhahran, Saudi Arabia

Narayan Chandra Deb Nath
Department of Chemistry
University of North Dakota
Grand Forks, North Dakota, United States

S.M. Abu Nayem
Department of Chemistry
Jagannath University
Dhaka, Bangladesh

Munetaka Oyama
Department of Material Chemistry
Graduate School of Engineering
Kyoto University
Kyotodaigaku Katsura
Nishikyo-ku, Kyoto, Japan

Md. Mahbubur Rahman
Department of Energy and Materials
Konkuk University
Chungju, Republic of Korea

Mushfiqur Rahman
Department of Materials Science &
Engineering
Khulna University of Engineering &
Technology
Khulna, Bangladesh

Muhammad Muhitur Rahman
Department of Civil and Environmental
Engineering
College of Engineering
King Faisal University
Al-Ahsa, Saudi Arabia

Madhusudan Roy
Department of Physics
National Taiwan University
Taipei, Taiwan

Falak Niaz
Materials Research Laboratory
Department of Physics
University of Peshawar
Peshawar, Pakistan

Syed Masiur Rahman
Applied Research Center for Environment
& Marine Studies
King Fahd University of Petroleum &
Minerals
Dhahran, Eastern Province
Saudi Arabia

Mohammad Anikur Rahman
Department of Chemistry
University of Dhaka
Dhaka, Bangladesh

Haroon Ur Rahman
Department of Physics
Abdul Wali Khan University
Mardan, Khyber Pakhtunkhwa
Pakistan

Nafeesa Sarfraz
School of Chemical Engineering &
Materials Science
Chung-Ang University
Seoul, Republic of Korea

Syed Adil Shah
National Laboratory of Solid-States
Microstructures
Department of Physics
Nanjing University
Nanjing, China

Syed Shaheen Shah
Department of Material Chemistry
Graduate School of Engineering
Kyoto University, Nishikyo-ku
Kyoto, Japan

M. Nasiruzzaman Shaikh
Interdisciplinary Research Center for
Hydrogen and Energy Storage (IRC-HES)
King Fahd University of Petroleum &
Minerals Dhahran
Saudi Arabia

Farrukh Shehzad
Department of Chemical Engineering
King Fahd University of Petroleum &
Minerals
Dhahran, Saudi Arabia

Abubakar Dahiru Shuaibu
Material Science and Engineering
Department
King Fahd University of Petroleum
and Minerals
Dhahran, Saudi Arabia

Nasrin Sultana
Department of Chemistry
Jagannath University
Dhaka, Bangladesh

Sami Ullah
K. A. CARE Energy Research and
Innovation Center
King Fahd University of Petroleum &
Minerals
Dhahran, Saudi Arabia

Muhammad Usman
Interdisciplinary Research Center for
Hydrogen and Energy Storage
King Fahd University of Petroleum
and Minerals
Dhahran, Saudi Arabia

Md. Abdul Wahab
Australian Institute for Bioengineering and
Nanotechnology (AIBN)
The University of Queensland
St. Lucia, QLD, Australia

Laiq Zada
Department of Microbiology
Faculty of Biological Sciences
Quaid-i-Azam University
Islamabad, Pakistan

Md. Hasan Zahir
Interdisciplinary Research Center for
Renewable Energy and Power Systems
(IRC-REPS)
King Fahd University of Petroleum &
Minerals
Dhahran, Saudi Arabia

Serge Zhuiykov
Center for Environmental & Energy
Research
Ghent University Global Campus
Yeonsu-gu, Incheon, South Korea

Part 1

Biomass

1

Introduction to Biomass

Md. Almujaddade Alfasane[1,], Ashika Akhtar[1], Nasrin Siraj Lopa[2], and Md. Mahbubur Rahman[3,*]*

[1] *Department of Botany, University of Dhaka, Dhaka-1000, Bangladesh*
[2] *Center for Environmental & Energy Research, Ghent University Global Campus, 119–5 Songdomunhwa-ro, Yeonsu-gu, Incheon 21985, Republic of Korea*
[3] *Department of Applied Chemistry, Konkuk University, Chungju 27478, Republic of Korea*
* Corresponding authors

1.1 Introduction

Biomass refers to the organic materials that come from biological bodies [1]. Carbon, hydrogen, oxygen, and nitrogen are the major elements of biomass-based organic compounds that can be derived from plants, animals, and microorganisms in both terrestrial and aquatic ecosystems [1, 2]. Terrestrial biomass consists of various plants, animals, and microorganisms, whereas aquatic biomass mainly comprises micro-/macro-algae, phytoplankton, zooplankton, aquatic plants and animals, and other microorganisms [3–5]. Biomass encompasses different compounds such as cellulose, hemicelluloses, starches, sugars, lipids, proteins, lignin, hydrocarbons, and trace amounts of Si, Na, K, Mg, Al, Fe, Mn, Ca, P, and S contained in inorganic ash [6–8]. Among them, lignocellulosic materials, including cellulose, hemicellulose, and lignin, are the major compounds of the biomass (Figure 1.1) [6–8].

Humans have utilized biomass since time immemorial and its use has fostered the birth of civilization. Among all the sources of biomass, plant-derived biomasses are significantly used for energy and fuel production. Plants produce biomass by absorbing solar energy through photosynthesis and converting carbon dioxide (CO_2) and water into carbohydrates [1, 2]. This chemical energy produced by biomass can be converted to usable heat and electrical energy or can be processed into biofuel through pyrolysis [9]. Thus, biomass is currently regarded as the fourth energy source in the world after oil, coal, and natural gas. With the world's increasing energy demand, biomass utilization has been growing substantially to fulfill a significant proportion of this demand as one of the cheap, available, and renewable energy sources [10]. For example, in 2019, biomass satisfied approximately 10% of the energy requirement worldwide [11]. However, biomass has not been utilized equally by the world's countries for energy production. Developing countries depend more on
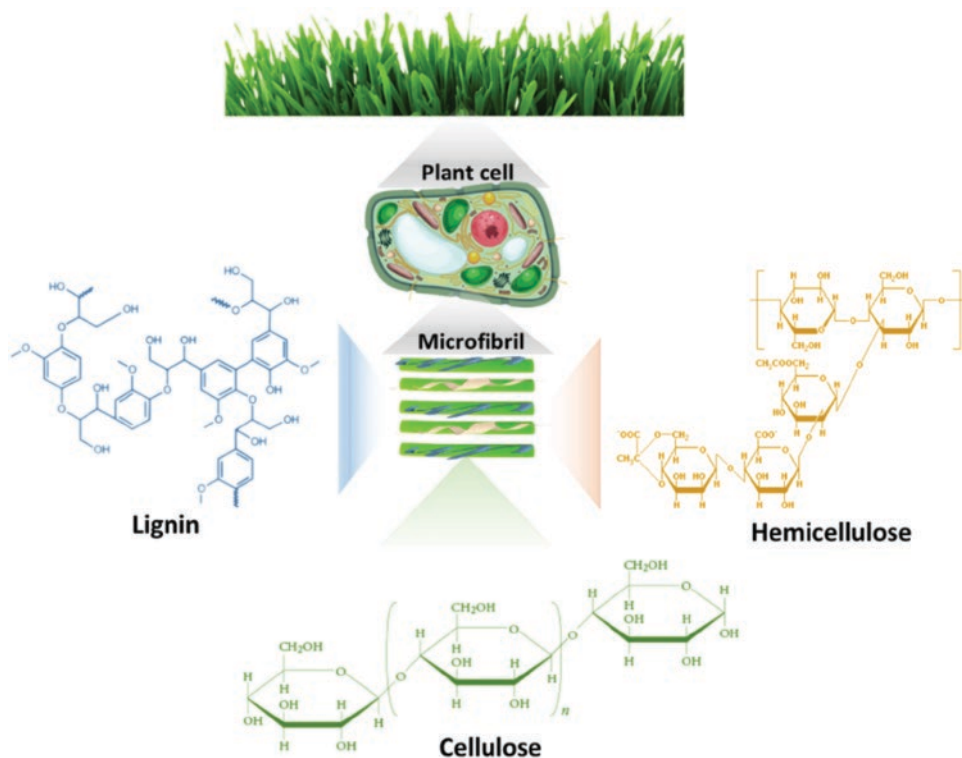
Figure 1.1 The main compounds and the chemical structures of lignocellulosic biomass.

biomass-based energy than industrialized countries due to their limited technology, infrastructure, and poor economies [12]. For instance, almost half of the energy supply in Africa comes mainly from biomass-based sources, whereas in Europe, only about 10% of the energy supply comes from renewables, the lowest among the continents [13]. Meanwhile, considering the total global production of biomass (~150 billion tons/year), a large amount of these biomasses is still underutilized for energy and fuel production [14]. Interestingly, most of them are generally considered waste materials, commonly to be decomposed or subjected to waste management methods.

Awareness and concern among the world population have increased regarding the use and valorization of biomass not only for energy and fuel production but also for synthesizing nanomaterials and dyes for various applications [15, 16]. The utilization of biological residue materials obtained from biomass represents ecologically friendly and considerably higher-value alternatives to conventional fossil fuels [17]. For example, peanut shells, which was previously considered waste and was given low value, has the potential to be applied to hydrogen, biodiesel, bioethanol, carbon nano-sheet, and dye production [18, 19]. Another example is phytoplankton, which was earlier considered a disturbance and a hazardous ecosystem component. It is now being commercially cultured for biofuels, bioactive pigments, lipids, and energy production [20]. Similarly, many examples of biomass that have never been considered valuable previously are now valorized as precious materials. Accordingly, researchers' interest in using biomass for energy production increased steeply, as is evident from the number of publications that appeared in the last decade (Figure 1.2).
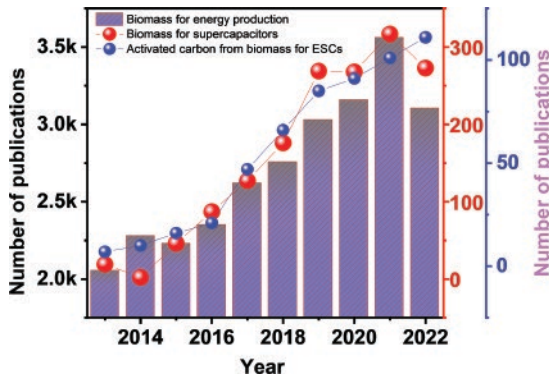
Figure 1.2 The number of publications having keywords of "biomass for energy production", "biomass for supercapacitors", and "activated carbon from biomass for supercapacitors" from 2013 to October 17, 2022. *Source: Scopus.*

In addition to energy and fuel production, biomass can be utilized to produce biochar (BC), a lightweight black carbon residue, through the carbonization processes (e.g., pyrolysis and hydrothermal carbonization) [21]. The biochar can be treated for producing activated carbon (AC) through various chemical, physical, and mechanical activation methods [22, 23]. Moreover, AC can be produced from biomass using a single step [23]. These ACs derived from biomass could solve environmental problems such as air and water pollution and the accumulation of industrial, food, and agricultural wastes. Furthermore, using ACs from lignocellulosic biomass instead of fossil fuels such as coal can reduce global warming effects. ACs derived from lignocellulosic biomass can potentially be utilized in various industrial sectors such as chemical processes, petroleum refining, wastewater and air pollution treatment, volatile organic compounds adsorption, catalysis, gas separation, deodorization, and purification [24]. This is due to the rich carbon content of ACs derived from BC with high surface area, microporous structure, and favorable pore size [24, 25]. Along with this improved physical property, facile controlling of the dimensions and structures, heteroatom doping, chemical functionalization, and enhanced degree of graphitization of ACs prepared from suitable biomass help to increase its electrical conductivity, which is beneficial for the development of high-performance electrochemical energy storage devices such as electrochemical supercapacitors (ESCs) and batteries [26–30].

In particular, the application of ACs derived from biomass has increased sharply for ESC applications, as is evident from the number of publications that appeared in the last decade (Figure 1.2). ESCs have received tremendous recognition as energy storages device in recent years due to their intermediate energy density between battery and capacitor [31]. The ultra-high-power density, extended life cycles, and prompt charge/discharge rate of ESC widen its application in various technologies, including consumer electronics, voltage stabilizers, micro-grids, low-power equipment, etc [32]. Principally, ESCs fabricated using carbons or ACs store the charge by reversible adsorption of ions in a non-Faradaic process and are commonly known as electric double-layer capacitors (EDLCs) [33, 34]. To develop high-performance ESCs based on ACs derived from biomass, the optimal pores corresponding to the size of the electrolyte ions, high degree of graphitization for improved electrical conductivity, heteroatom doping (e.g., N and P), and chemical functionalization

(e.g., carboxylic, carbonyl, and hydroxyl) are significantly important [35, 36]. Moreover, enduring cyclic stability and capacitance retention in ESCs can be obtained by tuning the structural stability of the AC framework [29, 37–40]. All other main parts of supercapacitors, including binder, electrolyte, and membrane (separator), can be produced via biochar and biomass derivatives [41–45]. Therefore, biomass could be considered a complete material source for the fabrication of efficient energy storage devices, supercapacitors, and for future research (Figure 1.2). Considering the importance of biomass for energy and fuel production and ESCs applications, this chapter briefly discusses the fundamentals of biomass by highlighting its classification, environmental and energy aspects, and pyrolysis process. Additionally, the application of biomass for ESCs is discussed briefly by highlighting the current challenges and future directions.

1.2 Categories of Biomass

A wide range of materials, including agricultural and forest residues, food wastes, animal wastes, wastes of the wood processing industry, wastes of the zoo-technical industry, biodegradable industrial/household solid wastes, and algal and other aquatic organisms with varying compositions of lignocellulosic compounds are termed as biomass [46–48]. Accordingly, biomass can be mainly classified as plant and organic wastes/residues (Figure 1.3).

1.2.1 Plant Biomass

Plants are the largest biomass energy source worldwide and can be categorized mainly as woody and non-woody biomass based on the plant's origin and chemical compositions [49]. Woody biomass is primarily derived from stems and branches of trees and shrubs or their residue products [50]. The proportions of lignocellulosic compounds are not the same
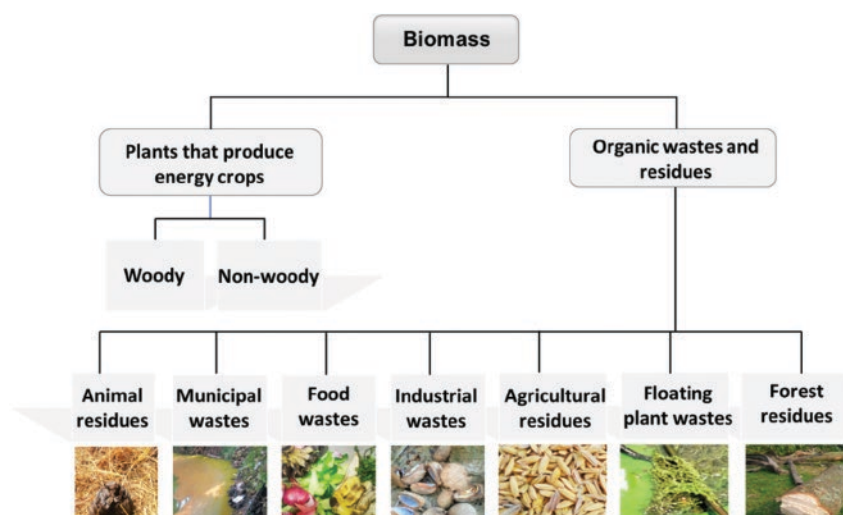
Figure 1.3 Types of biomasses based on the sources.

in all woody biomass. Accordingly, woody biomass can be reclassified as hardwoods and softwoods [51]. Hardwoods generally contain higher proportions of cellulose and hemicelluloses than softwoods, but the amount of lignin is higher in softwoods (Table 1.1) [52]. Generally, hardwoods contain approximately 35% hemicelluloses and 22% lignin by dry weight. In contrast, softwoods have a composition of approximately 43% cellulose, 28% hemicelluloses, and 29% lignin by dry weight [50, 52].

In contrast, non-woody biomass is described as those plants with weak stems, such as herbaceous plants, grasses, and agricultural crops. In non-woody biomass, the proportion of hemicellulose is generally higher, with a low proportion of lignin [52]. However, the chemical composition of non-woody plants is highly dependent on the soil properties and climate conditions. Furthermore, their chemical compositions are also varied based on the structure of cell walls, species, and maturity. Other than lignocellulosic compounds, non-woody biomass is richer in silicate and various nutrient contents than is woody biomass [53]. Also, the plant biomass's chemical composition depends on the plant's type and portions (e.g., root, leaves, trunk). For example, *Albizia procera* leaves contain a significant amount of protein and lignocellulosic components [54]. It is well known that protein is used to develop bioelectrolyte for supercapacitor fabrication.

1.2.2 Organic Wastes and Residues-based Biomass

Organic wastes and residues from different sources, such as forest products, agricultural, industrial, municipal and urban activities, and animals, produce a massive amount of biomass, more than 13×10^9 tons/year [55]. Based on the sources, this type of biomass can be generated in different stages of its processing, growing, production, and uses. For example, agricultural wastes are produced during crop harvesting, such as wheat straw, rice husk, rice straw, etc. Industrial waste, such as sawdust, is produced in the timber and furniture industry. All these different forms of organic waste biomass are also rich in lignocellulosic materials (Table 1.2) and are potential energy sources. Among all these sources, residues from agriculture account for 87% of the total supply of organic wastes and residues-based biomass, while municipal and industrial wastes occupy 5% [13]. However, almost 99% of this form of biomass remains unused due to the lack of proper knowledge and ability to commercialize it [56].

Table 1.1 Chemical composition of lignocellulosic hardwood and softwood biomass.

Biomass	Source	Cellulose (%)	Hemicellulose (%)	Lignin (%)
Hardwood	Eucalyptus	54.1	18.4	21.5
	Oak	40.4	35.9	15.5–16.3
	Poplar	50.8–53.3	26.2–28.7	21 – 26
Softwood	Douglas fir	44.0	11.0	27.0
	Spruce	45.5	22.9	27.9
	Pine	42.0–50.0	24.0–27.0	20.0

Table 1.2 Composition of different organic waste biomass.

Biomass	Hemicellulose (%)	Cellulose (%)	Lignin (%)	Ref.
Barley straw	24–29	31–34	14–15	[57]
Coconut coir	26	48	18	[58]
Nut shells	25–30	25–30	30–40	[59]
Leaves	80–85	15–20	0	[60]
Sugarcane bagasse	26.9	38.1	18.4	[61]
Wheat straw	24.8	36	14.5	[62]
Waste papers from chemical pulps	10–20	60–70	5–10	[63]
Sugarcane tops	24.2	33.3	36.1	[64]
Rice straw	24	32.1	18	[65]
Rice husk	24	31	14	[60]
Grasses (average)	25–50	25–40	10–30	[66]
Oat straw	27–38	31–37	16–19	[67]
Sweet sorghum bagasse	25	45	18	[68]
Banana waste	14.8	13.2	14	[69]

1.3 Utilization of Biomass

Biomass can be utilized as an energy and non-energy source to produce fuels and power, and for agricultural and industrial uses (Figure 1.4). For example, woody biomass is mainly used for household heating, cooking, and electricity generation, and for producing paper, particle boards, and furniture. Moreover, woody biomass is also used as animal food and as a raw material for chemical synthesis. While fast-growing vegetal species, which are not fit for agriculture, are generally cultivated for biofuel production [70]. Agricultural biomass residue is widely applied in generating electric and thermal energies [71]. Other than the production of energy and fuels, biomass is extensively used to produce animal feed and food, construction materials, compost, and composite materials. In particular, composites from natural fibers have gained considerable attention in the manufacturing industry, particularly for transportation, automotive, and electronics applications [72–84]. This is due to their light weight, resistance to corrosion, abundance, and biodegradability [85].

Furthermore, biomass polymer composites can provide a sustainable, eco-friendly, and cheap structural material with improved mechanical properties different from traditional polymer-reinforced glass and carbon composite materials [85]. For instance, carbon derived from feedstock waste or undervalued sources such as coir fibers, shell particles, coffee ground powder, and olive seed flour can be used to prepare carbon/poly(propylene) as an effective composite for automobile parts with light weight and low-cost [86–89]. Binoj et al. reported that an optimized amount of tamarind fruit fiber incorporated into polyester resins substantially improves the thermal stability and aquatic properties suitable for lightweight automotive and marine applications [90]. Biomass/polymer composites are also used to produce hybrid particle boards with improved mechanical properties. For example, a hybrid particle board was
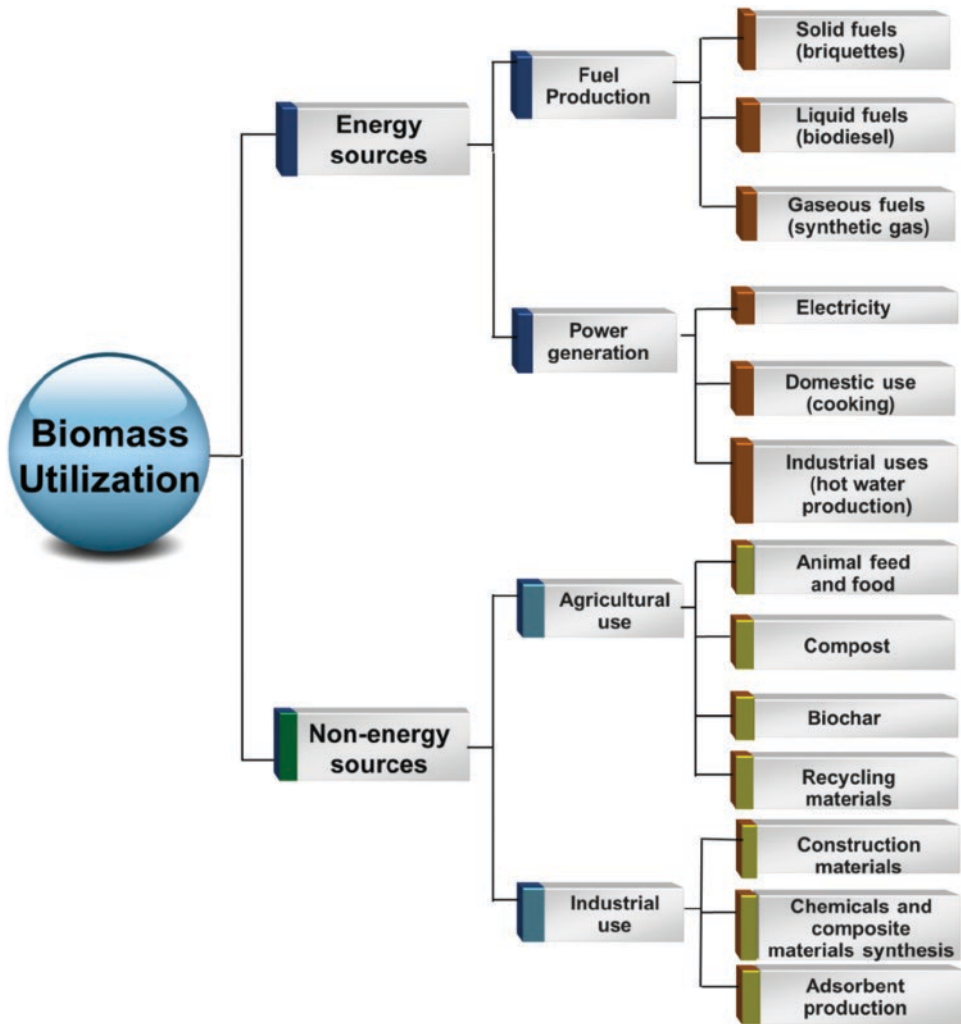
Figure 1.4 Utilization of biomass for practical applications.

prepared by reinforcing rice straws/coir fibers in phenol formaldehyde resin [91]. This particle board possibly improves the toughness, vibration damping, and flame retardancy compared to the board made with only phenol formaldehyde resin. Some other researchers embedded celery root fibers, poplar seed hair fibers, and hazelnut shell flour into the polylactic acid matrix to prepare biodegradable plastic films, bottles, and medical devices [92, 93].

1.4   Biomass as an Energy Source

The resources that meet the basic needs of energy demand for humans and civilizations can be divided into primary resources (renewable and non-renewable energy resources) and secondary resources obtained by converting primary energy resources [94]. Primary energy sources can be classified as non-renewable (e.g., coal, natural gas, oil) and renewable

energy sources (e.g., solar, hydrothermal, biomass, etc.) [95–97]. Biomass is a renewable energy source that can provide a sustainable energy supply at a low cost and mitigate global warming by reducing greenhouse gas emissions. Energy generation from biomass is growing faster due to the quick depletion of conventional fossil fuels. Plants, rice husks, waste plastics, sawdust, algae, and trees are the common biomass sources for producing different energy and products (Figure 1.4). Currently, biomass energy sources produce 50×10^{18} J, accounting for 10% of the world's energy demand and 35% of that of developing countries [98]. These sources include the production of electrical and thermal energy, fuels (gaseous, liquid, and solid), and valuable chemicals (e.g., ethanol and methanol) through thermal (e.g., pyrolysis, gasification, and combustion) and chemical treatments.

Considering the chemical compositions of biomass and fossil oils, biomass's main disadvantage in producing biofuels is its higher oxygen content with less carbon and hydrogen ratio (C/H) [99]. To replace fossil oils with biofuels, the C/H ratio in biomass must be improved by removing oxygen from the biomass in the form of H_2O, CO, and CO_2 [100]. This is challenging and costly since pyrolysis, gasification, combustion, and chemical processes for energy production and the enhancement of C/H ratio are still required for using other primary and secondary energy sources and chemical reagents. However, the high O/C atomic ratio in lignocellulosic biomass is advantageous for synthesizing valuable chemicals and residues.

1.5 Pyrolysis of Biomass

Pyrolysis is a process that decomposes the lignocellulosic polymer chains in biomass by thermal treatment in the absence of air or an inert atmosphere [101]. This led to the use of BC to generate solid fuels, bio-oil as liquid fuels, and non-condensable gases (Figure 1.5) [102, 103]. In the process of biomass pyrolysis, first the biomass feed materials are
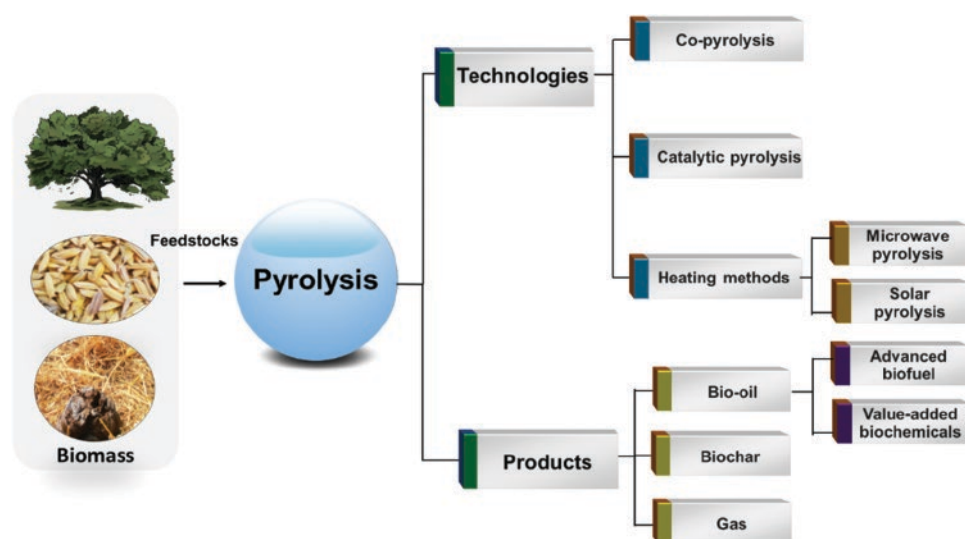
Figure 1.5 Schematic representation of the products and technologies of the pyrolysis of biomass.

decomposed by the removal of moisture contents [104]. This also induces the breaking of bonds in lignocellulosic polymers and the formation of CO, CO_2, and residues [105–107]. The remaining compounds or materials are further converted to secondary BC, crude bio-oil, and gases using cracking and polymerization processes. The pyrolysis products and their yields are highly dependent on the conditions and parameters of the pyrolysis technologies and biomass sources. These include the reactor's temperature, gas flow rate, heating rate, residence time, catalysts, and reactor configurations [105, 106].

Depending on the operating conditions, the pyrolysis process can be categorized as either slow, fast, or flash pyrolysis [108]. In the slow pyrolysis process, lower temperature (550–950 K), slow heating rate, and long residence time (several hours to days) are applied to prepare BC as the primary product [109]. While in the fast pyrolysis method, moderate temperature (850–1250K), high heating rates (on the order of 100 °C/sec), and short residence time are used to prepare bio-oil with a maximum yield of ~75% [109]. The prepared crude pyrolytic bio-oil can be further upgraded and purified to advanced biofuels or biochemicals through fast pyrolysis. In contrast, flash pyrolysis is based on heat treatment at a higher temperature (1050–1300 K) for less than two seconds producing a higher yield of bio-oil than gas and BC [109]. However, bio-oil produced by flash pyrolysis is acidic, unstable, and highly viscous, and contains solids and dissolved water [110, 111]. Hence, reducing the oxygen content in the final product (bio-oil) is essential by using advanced methods, such as hydrogenation and catalytic cracking. To improve the yield and properties of bio-oil, BC, and gas-derived from biomass, many pyrolysis techniques, including co-pyrolysis [112], catalytic pyrolysis [113], microwave pyrolysis [114], and solar pyrolysis [115] have already been developed (Figure 1.5).

1.6 Biomass-derived Carbon for Electrochemical Supercapacitors

The main component of an ESC consists of two electrodes separated by a thin and porous insulator soaked in an electrolyte. Various materials are used to fabricate ESC electrodes, including metal oxides, carbon-based compounds, and conducting polymers [116]. The energy storage mechanism in ESCs depends on the types and properties of electrode materials, broadly classified as EDLC and pseudocapacitor (Figure 1.6) [117]. In particular, both non-activated carbon (NAC) and AC derived from biomass sources are attractive materials for fabricating high-performance EDLC-type ESCs due to their low cost, easy processing, availability, and improved physicochemical properties [118–120]. NAC and AC materials can be prepared from a wide variety of biomass sources such as coffee beans, rice husk, coffee endocarp, bamboo species, apricot shell, sugarcane bagasse, rubberwood sawdust, jute stick, wood, anthracite, bitumen charcoal, peat shells, date seeds, coconut, etc [23, 29, 120, 121]. NAC, which is generally obtained from biomass by simple hydrothermal/pyrolysis method, generally exhibits inferior physical and chemical properties and energy storage capacity in ESCs compared to the ACs [119]. For example, Saini et al. compared the energy storage capacity of AC and NAC derived from sugar [119]. Results demonstrated that the sugar-derived AC exhibited a 35% improved energy storage capacity compared to the NAC. This research further revealed a significantly high capacity of ACs compared to the reduced
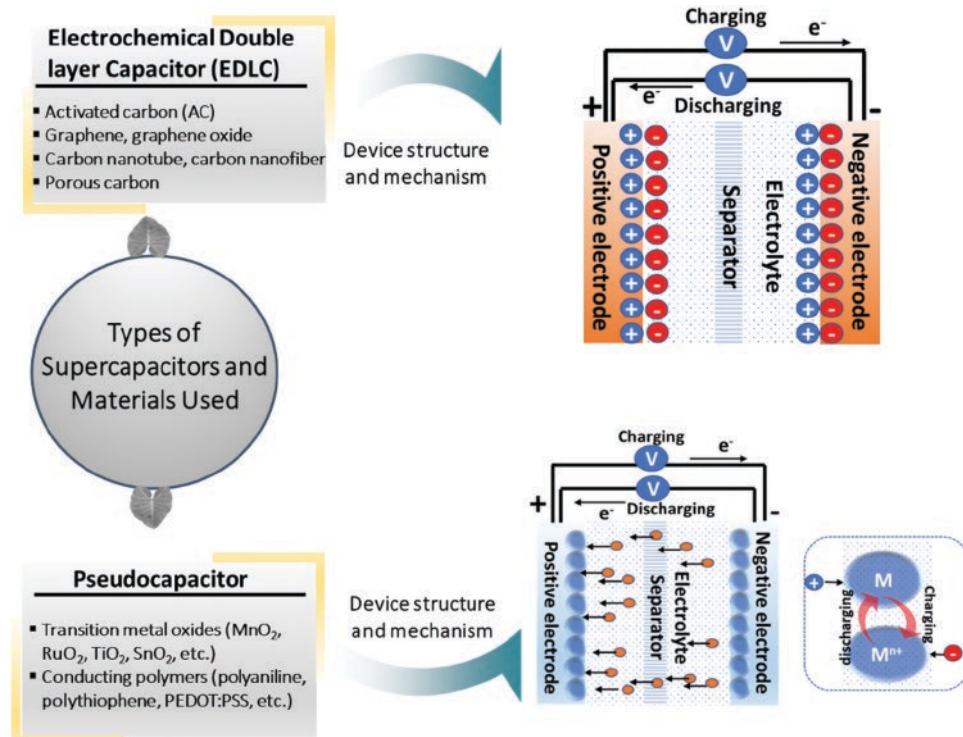
Figure 1.6 Types of electrochemical supercapacitor and their electrode materials along with the schematic of device structure and operation principle. In an EDLC, energy is stored electrostatically via reversible ions adsorption/desorption in a non-Faradaic process, while in pseudocapacitors, energy is stored based on the fast and reversible Faradaic redox reactions that occurred at or near the electrode surface and the electrochemical adsorption/desorption (i.e., intercalation/de-intercalation) of ions into the tunnels of electrode materials through the Faradaic charge transfer process.

graphene oxide. In another report, Kalyani and Anitha prepared AC and NAC from tea dust refuse. The as-prepared AC delivered 31.50% improved specific capacitance after the 25th cyclic voltammetric cycle compared to the NAC [122].

This is mainly due to the robust pore architecture, high porosity, high specific surface area, and ample pore functionalities of ACs for the intercalation/de-intercalation of electrolyte ions compared to NAC. Nevertheless, the properties and the ESCs performance of ACs derived from biomass are highly dependent on the carbonization conditions of biomass and the activators. ACs with a high percentage of carboxyl (–COOH), carbonyl (C = O), phenolic, lactonic, pyrrolic, and pyridinic functional groups, along with various heteroatoms (S, O, N) within the porous framework with the high carbon content can deliver high energy storage capacity in ESCs [24, 25]. These physical and chemical properties of ACs derived from a wide range of biomass can be tuned by varying the carbonization conditions and activation methods (e.g., physical, chemical, electrochemical, microwave (MW), ultrasound, and plasma methods) [123–126]. Specifically, the physical, chemical, and electrochemical characteristics of the chemically prepared ACs are highly dependent on the type of activation agents (e.g., NaOH, KOH, $ZnCl_2$, K_2CO_3, H_3PO_4, $FeCl_3$, CO_2,

steam, N_2, O_3, O_2) and methods [123–126]. For example, Alhebshi et al. prepared AC from palm fronds using a NaOH activator that exhibited a much higher surface area (1011 m^2/g) and specific capacitance (C_s = 125.9 F/g) in ESCs [125]. The ACs prepared from the same biomass using the physical activation method delivered the C_s of 125.9 F/g with a surface area of 603.5 m^2/g. In another report, ACs prepared using an H_3PO_4 activator from rubber-wood waste biomass showed the C_s of 129 F/g and high surface area (605–693 m^2/g) compared to the NaOH activator-based ACs (C_s = 69 F/g and surface area = 429 m^2/g) [127]. Similarly, numerous reports are available on the preparation of ACs derived from biomass using various activation methods and activators for ESCs as summarized in Table 1.3.

1.7 Environmental Aspects of Biomass

Biomass is a potential renewable energy source due to its balanced emission of environmentally harmful CO_2 gas compared to conventional nuclear and gasoline-based energy production [136]. This can be attributed to the fact that a certain amount of CO_2 from the atmosphere can be absorbed by a plant during its growing phase, while the same amount of CO_2 can be released into the atmosphere during the combustion of plant-derived biomass for energy production (Figure 1.7). Biomass can also be co-fired with other fossil fuels to decrease the content of additional CO_2 released into the atmosphere [137]. Moreover, modern biomass combustion systems offer lower CO_2 emission levels and better combustion efficiency than the best fossil fuel boilers [138]. Furthermore, biomass contains a lower percentage of nitrogen and sulfur, thus, releasing a lower amount of sulfur oxides (SO_x) and nitrogen oxides (NO_x) into the atmosphere, which are responsible for acid rain [139].

The utilization of biomass as a fuel instead of conventional fossil fuels allows the consumer to manage woodland and agriculture in an economical way, also improving biodiversity and soil fertility [140, 141]. Moreover, using biomass as renewable energy can avoid

Table 1.3 Comparison of ESCs performance of various biomass-derived ACs.

Biomass	Activators	Surface area of AC ($m^{[2]}$/g)	Specific capacitance (F/g)	Electrolyte	Ref.
Peanut shell	$ZnCl_2$	1549	340 at 1 A/g	1 M H_2SO_4	[128]
Watermelon rind	KOH	2277	333.4 at 1 A/g	6 M KOH	[129]
Tea leaves	KOH	2841	330 at 1 A/g	2 M KOH	[130]
Withered rose flower	KOH/ KNO_3	1980	350 at 1 A/g	6 M KOH	[131]
Plastic waste (Polyethylene terephthalate)	KOH	2326	169 at 0.2 A/g	6 M KOH	[132]
Soybean pods	NaOH	2612	352.6 at 0.5 A/g	1M Na_2SO_4	[133]
Onion husk	K_2CO_3	2571	188 at 1 A/g	1M $TEABF_4$/ AC	[134]
Coconut shell	Steam	1532	228 at 5 mV s^{-1}	6 M KOH	[135]
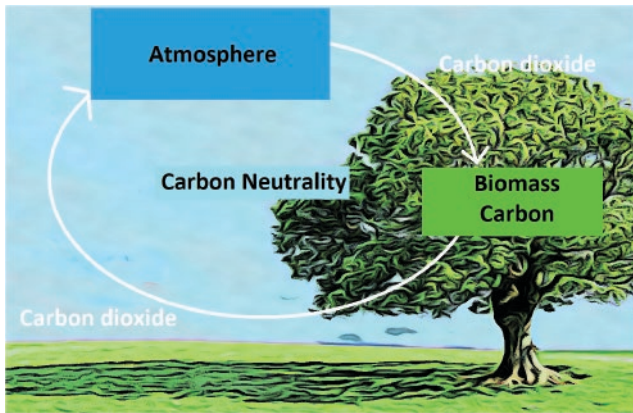
Figure 1.7 Biomass derived from plants is carbon-neutral. A plant absorbs and emits the same amount of CO_2 during its growing and combustion phase, respectively.

possible man-made catastrophes like the oil spill in the Gulf of Mexico in 2010 and the nuclear reactor destruction in Fukushima, Japan, in 2011. The oil spill in the Gulf of Mexico continued for about three months and discharged over 130 million gallons of crude oil, killing millions of aquatic animals [142]. On the other hand, the Fukushima nuclear disaster resulted in fatal radioactive emissions harmful to humans and aquatic and biotic life [143].

Biomass-derived energy is gaining attention for economic development owing to its flexibility and potential for integration encompassing all development strategies [136]. Biomass production and its conversion into energy can also create new business possibilities and support the rural and industrial economy and trading [144]. For different environmental legislations, biomass has high demand worldwide, creating huge opportunities to trade biomass. One of the major ongoing environmental legislations is the UN Climate Change Conferences to meet net zero emissions by 2050 [144, 145]. Net-zero emissions mean that the released greenhouse gasses (e.g., CO_2, SO_x, NO_x) should be offset by eliminating the same amount of these gases from the atmosphere by storing them in soil, plants, or other materials [146]. Thus, if a nation exceeds the limit of using a fixed amount of carbon per annum, they must absorb an equivalent amount of carbon through forest absorption or carbon capture. Therefore, every nation, especially developed countries, is attempting to reduce greenhouse gas emissions. Biomass utilization can help as it is considered the world's most essential and abundant renewable energy source [137, 138]. Accordingly, the use of biomass energy in Europe is increasing, and by 2050 it will increase from 70% to 150% for the production of energy and materials [147]. Thus, European countries are the prime markets for biomass trade. Additionally, there are huge opportunities to trade biomass in countries with limited biomass resources.

Global demand for biofuels is also expected to grow sharply, driven partly by biofuel mandates from various countries. Again, the current record high crude oil and gas price induced by the COVID-19 pandemic and the war between Russia and Ukraine is expected to push global energy industries for biofuel production [148]. Thus, financing in biomass-based biofuel production has become very attractive for investors. Biomass can be easily collected locally, and it has the potential to contribute significantly to any nation's energy

supply security. Governments of different countries offered renewable energy aid to fulfill their energy demand by decreasing carbon emissions. Many industrialized countries set a trajectory and implemented the extensive use of bioenergy to meet their energy needs. Thus, a large amount of biomass resources must be produced, mobilized, and possibly imported to fulfill the trajectory [136].

1.8 The Challenges

The global interest in biomass use has been increasing steeply due to its renewability, decentralized production, and potential role in climate change mitigation [149]. However, many challenges still need to be resolved for the proper utilization of biomass. One of the major challenges is finding the best biomass sources and finding novel ways to valorize industrial or agricultural wastes and residues. More scientific exploration, research, and development on biomass resources is required to improve their utilization. Also, sustainable systems must be developed for harvesting and processing biomass resources. It is high time to improve the efficiency and performance of conversion and distribution processes along with developing technologies for a multitude of products from biomass.

The rapid advancement of energy production from biomass, fossil fuels, and other renewable sources has triggered the development of low-cost and sustainable materials for energy storage applications. Recently, biomass-derived materials such as NAC and AC and their composites are gaining special attention for developing high-performance energy storage devices (e.g., ESCs and batteries), catalysts, and sensors [118, 150–152]. The foremost challenge is the high production cost of ACs from biomass. Thus, the least expensive method must be developed for large-scale activation of BC. Selecting precursors from an extensive range of biomass sources to ensure the improved physical and chemical properties of NAC and AC with high device performance is another prime challenge. The presence of inorganic materials and other existing impurities in biomass-derived ACs can significantly affect the performance of these technologies. So, all the impurities must be removed carefully, which is sometimes costly and time-consuming [153]. Thus, low-cost, fast, and efficient technologies must be developed for preparing ACs from biomass with high functionality, surface area, and controlled dimensions.

Contrary to the world's large commodity trade, the number of credit-worthy companies that supply biomass is insufficient to meet the demand. Biomass supply-chain companies capable of providing predictable and reliable long-term deliveries of a sufficient amount of biomass need to be established to support power generators worldwide. At this point we suggest investment in converting the existing coal-fired power plants into biomass treatment plants would be a good decision. Besides, many investors do not prefer to invest in the whole value chain; rather, they are interested in getting the final product to be delivered. Therefore it is very important to ensure the environment of regulation and market necessary for the increased development and use of bio-based products. Increasing awareness among the general populous can be the most important and efficient way to valorize biomass. In most cases, developing countries lag behind developed countries in utilizing biomass at a high level, although biomass production is higher in developing countries. So, developed countries should support developing countries for the proper valorization of biomass.

1.9   Conclusions

This chapter discusses the chemical and physical properties, the classification of biomass, and the utilization of biomass for producing energy, fuels, and products. A brief overview of the fundamentals of ESCs and biomass utilization is also presented by highlighting the environmental impact and the challenges of biomass utilization. Even though a significantly high amount of energy (50×10^{18} J) is being produced worldwide from biomass, a large amount of biomass is still being wasted by natural decomposition. More research, development, and industrial implementation should be promoted to valorize biomass. The advancement of science and technology has enabled the utilization of biomass-derived ACs for developing high-performance energy storage devices, sensors, and catalysts. Specifically, developing ESCs electrodes by utilizing biomass-derived ACs has received potential interest from scientists and industrialists. This is mainly due to the robust pore architecture, high porosity, high specific surface area, and abundant pore functionalities of ACs prepared from a wide variety of biomass sources through sequential thermal (pyrolysis) treatment and chemical/physical activation. However, the energy storage capacity of biomass-based ACs still needs to be improved by selecting a suitable biomass precursor with high carbon content. Furthermore, the development of a safe, eco-friendly, and low-cost technology is required for the large-scale production of ACs from biomass. Finally, the authors are confident that this chapter can guide the researchers in understanding the fundamentals of biomass, its energy and environmental aspects, and the utilization of biomass for ESCs.

Acknowledgments

References

1 R. Saidur, E.A. Abdelaziz, A. Demirbas, M.S. Hossain, S. Mekhilef, *Renew. Sust. Energ. Rev.* **2011**, *15*, 2262–2289.

2 L. R. Amjith, B. Bavanish, *Chemosphere* **2022**, *293*, 133579.

3 P. Biller, Hydrothermal Liquefaction of Aquatic Feedstocks in *Direct Thermochemical Liquefaction for Energy Applications*, (Ed.: L. Rosendahl), Woodhead Publishing, **2018**, Chapter 4, pp. 101–125, https://doi.org/10.1016/B978-0-08-101029-7.00003-5.

4 A. C. Ernesto, C.-H. Alejandra, Biomass from the Sea in *Biomass Now*, (Ed.: M. M. Darko), IntechOpen, Rijeka, **2013**, Chapter 21, https://doi.org/10.5772/54520.

5 Y. M. Bar-On, R. Phillips, R. Milo, *Proc. Natl. Acad. Sci.* **2018**, *115*, 6506–6511.

6 A. Kumar, D. Dutt, A. Gautam, *J. Genet. Eng. Biotechnol.* **2016**, *14*, 107–118.

7 S. Nanda, J. Mohammad, S. N. Reddy, J. A. Kozinski, A. K. Dalai, *Biomass Convers. Biorefin.* **2014**, *4*, 157–191.

8 X. Zhao, L. Zhang, D. Liu, *Biofuel. Bioprod. Biorefin.* **2012**, *6*, 465–482.

9 M. de Wit, A. Faaij, *Biomass Bioenerg.* **2010**, *34*, 188–202.

10 D. Gielen, F. Boshell, D. Saygin, M. D. Bazilian, N. Wagner, R. Gorini, *Energy Strategy Rev.* **2019**, *24*, 38–50.

11 IEA. World Total Energy Supply by Source. *Key World Energy Statistics 2021* **2021** [cited 22-10, **2022**]; Available from: https://www.iea.org/reports/key-world-energy-statistics-2021/supply.

12 D. Khatiwada, P. Purohit, E. K. Ackom, *Sustainability* **2019**, *11*, 7091.

13 W. B. Association. Global Bioenergy Statistics 2020. *World Bioenergy Association* **2020** [cited October 22, **2022**]; Available from: http://www.worldbioenergy.org/uploads/201210%20 WBA%20GBS%202020.pdf.

14 B.-H. Cheng, B.-C. Huang, R. Zhang, Y.-L. Chen, S.-F. Jiang, Y. Lu, X.-S. Zhang, H. Jiang, H.-Q. Yu, *Sci. Adv.* **2020**, vol.*6*, eaay0748.

15 E. Pfab, L. Filiciotto, R. Luque, *J. Chem. Educ.* **2019**, *96*, 3030–3037.

16 P. Ning, G. Yang, L. Hu, J. Sun, L. Shi, Y. Zhou, Z. Wang, J. Yang, *Biotechnol. Biofuels* **2021**, *14*, 102.

17 N. M. Clauser, G. González, C. M. Mendieta, J. Kruyeniski, M. C. Area, M. E. Vallejos, *Sustainability* **2021**, *13*, 794.

18 P.A. Duc, P. Dharanipriya,B.K.Velmurugan, M. Shanmugavadivu, *Biocatal. Agric. Biotechnol.* **2019**, *20*, 101206.

19 N. F. Zaaba, H. Ismail, M. Jaafar, *BioResources* **2014**, *9*, 15.

20 G. Ghedini, D. J. Marshall, M. Loreau, *Funct. Ecol.* **2022**, *36*, 446–457.

21 Y. X. Seow, Y. H. Tan, N. M. Mubarak, J. Kansedo, M. Khalid, M. L. Ibrahim, M. Ghasemi, *J. Environ. Chem. Eng.* **2022**, *10*, 107017.

22 A. K. Sakhiya, A. Anand, P. Kaushal, *Biochar* **2020**, *2*, 253–285.

23 A. Aziz, S. S. Shah, A. Kashem, *Chem. Rec.* **2020**, *20*, 1074–1098.

24 E. I. Ugwu, J. C. Agunwamba, *Environ. Monit. Assess.* **2020**, *192*, 240.

25 Y. X. Gan, *C.* **2021**, *7*, 39.

26 G. S. Dos Reis, S. H. Larsson, H. P. de Oliveira, M. Thyrel, E. Claudio Lima, *Nanomaterials* **2020**, *10*, 1398.

27 R. Mehdi, A. H. Khoja, S. R. Naqvi, N. Gao, N. A. S. Amin, *Catalysts* **2022**, *12*, 798.

28 S. S. Shah, H. T. Das, H. R. Barai, M. A. Aziz, *Polymers* **2022**, *14*, 270.

29 S. S.Shah, M. N. Shaikh, M. Y. Khan, M. A. Alfasane, M. M. Rahman, M. A. Aziz, *Chem. Rec.* **2021**, *21*, 1631–1665.

30 S. M. Abu Nayem, A. Ahmad, S. S. Shah, A. Saeed Alzahrani, A. J. Saleh Ahammad, M. A. Aziz, *Chem. Rec.* **2022**, e202200181, https://doi.org/10.1002/tcr.202200181.

31 S. A. Ansari, N. A. Khan, Z. Hasan, A. A. Shaikh, F. K. Ferdousi, H. R. Barai, N. S. Lopa, M. M. Rahman, *Sustain. Energy Fuels* **2020**, *4*, 2480–2490.

32 Y. M.Volfkovich, *Russ. J. Electrochem.* **2021**, *57*, 311–347.

33 H. R.Barai, M. M. Rahman, M.Adeel, S. W. Joo, *Mater. Res. Bull.* **2022**, *148*, 111678.

34 H. R.Barai, M. M. Rahman, S. W.Joo, *J. Power Sources* **2017**, *372*, 227–234.

35 Z.Kang, C. Wu, L. Dong, W.Liu, J. Mou, J. Zhang, Z. Chang, B. Jiang, G. Wang, F. Kang, C. Xu, *ACS Sustain. Chem. Eng.* **2019**, *7*, 3364–3371.

36 S. Yang, S. Wang, X. Liu, L. Li, *Carbon* **2019**, *147*, 540–549.

37 S.Rawat, R. K. Mishra, T. Bhaskar, *Chemosphere* **2022**, *286*, 131961.

38 H. Liu, T. Xu, K. Liu, M. Zhang, W. Liu, H. Li, H. Du, C. Si, *Ind. Crops Prod.* **2021**, *165*, 113425.

39 S.S. Shah, E.Cevik, M. A. Aziz, T. F. Qahtan, A. Bozkurt, Z. H. Yamani, *Synth. Met.* **2021**, *277*, 116765.

40 N. C. Deb Nath, S. S. Shah, M. A. A. Qasem, M. H. Zahir, M. A. Aziz, *ChemistrySelect* **2019**, *4*, 9079–9083.

41 H.Parsimehr, A. Ehsani, *Chem. Rec.* **2020**, *20*, 1163–1180.

42 M. A. Islam, H. L. Ong, A. R. Villagracia, K. A. A. Halim, A. B. Ganganboina, R.-A. Doong, *Ind. Crops Prod.* **2021**, *170*, 113694.

43 C. Gao, Y. Duan, Y. Liu, J. Gu, Z. Guo, P. Huo, *J. Power Sources* **2022**, *541*, 231658.

44 P.Ruschhaupt, A. Varzi, S. Passerini, *ChemSusChem* **2020**, *13*, 763–770.

45 X. Wang, X. Xu, P. Chatterjee, C. Lv, J. Popovich, Z. Song, L. Dai, M. Y. S. Kalani, S. E. Haydel, H. Jiang, *Adv. Mater. Technol.* **2016**, *1*, 1600059.

46 M. H. Duku, S. Gu, E. B. Hagan, *Renew. Sust. Energ. Rev.* **2011**, *15*, 404–415.

47 S. Jha, J. A.Okolie, S. Nanda, A. K. Dalai, *Chem. Eng. Technol.* **2022**, *45*, 791–799.

48 S. S. Shah, M. A. Aziz, *Bangladesh J. Plant Taxon.* **2020**, *27*, 467–478.

49 T. Tabata, Environmental Impacts of Utilizing Woody Biomass for Energy: A Case Study in Japan in *Waste Biorefinery*, (Eds: T. Bhaskar, A. Pandey, S. V. Mohan, D.-J.Lee, S. K.Khanal), Elsevier, **2018**, Chapter 26, pp.751–778, https://doi.org/10.1016/B978-0-444-63992-9.00026-4.

50 A. Demirbaş, *Energy Sources* **2005**, *27*, 761–767.

51 X. Xu, R. Pan, R. Chen, *Processes* **2021**, *9*, 1598.

52 F. H. Isikgor, C. R. Becer, *Polym. Chem.* **2015**, *6*, 4497–4559.

53 L. Zhong, W. Huimei, H. Lanfeng, Pulping and Papermaking of Non-Wood Fibers in *Pulp and Paper Processing*, (Ed.: K. S.Newaz), IntechOpen, Rijeka, **2018**, Chapter 1, https://doi.org/10.5772/intechopen.79017.

54 A. K. Mohamedkhair, M. A. Aziz, S. S. Shah, M. N. Shaikh, A. K. Jamil, M. A. A. Qasem, I. A. Buliyaminu, Z. H. Yamani, *Arab. J. Chem.* **2020**, *13*, 6161–6173.

55 S. Chavan, B. Yadav, A. Atmakuri, R. D. Tyagi, J. W. C. Wong, P. Drogui, *Bioresour. Technol.* **2022**, *344*, 126398.

56 R. A. Jansen, Biomass in *Second Generation Biofuels and Biomass: Essential Guide for Investors, Scientists and Decision Makers*, (Ed.:R. A. Jansen), **2012**, Chapter 8 pp., 113–125, https://doi.org/10.1002/9783527652976.ch8.

57 S. Naik, V.V. Goud, P. K. Rout, K. Jacobson, A. K. Dalai, *Renew. Energy* **2010**, *35*, 1624–1631.

58 K. Raveendran, A. Ganesh,K. C. Khilar, *Fuel* **1995**, *74*, 1812–1822.

59 S. Prasad, A. Singh, H. C. Joshi, *Resour. Conserv. Recycl.* **2007**, *50*, 1–39.

60 R. Howard, E. Abotsi, E. J. Van Rensburg, S. Howard, *Afr. J. Biotechnol.* **2003**, *2*, 602–619.

61 J. Lee, *J. Biotechnol.* **1997**, *56*, 1–24.

62 M. A. Kabel, M. J. E. C. van der Maarel, G. Klip, A. G. J. Voragen, H. A. Schols, *Biotechnol. Bioeng.* **2006**, *93*, 56–63.

63 M. C. Monte, E. Fuente, A. Blanco, C. Negro, *Waste Manage.* **2009**, *29*, 293–308.

64 V. Ferreira-Leitão, C. C. Perrone, J. Rodrigues, A. P. M. Franke, S. Macrelli, G. Zacchi, *Biotechnol. Biofuels* **2010**, *3*, 7.

65 H. Li, N.-J. Kim, M. Jiang, J. W. Kang, H. N. Chang, *Bioresour. Technol.* **2009**, *100*, 3245–3251.

66 S. Malherbe, T. E. Cloete, *Rev. Environ. Sci. Biotechnol.* **2002**, *1*, 105–114.

67 C. Sánchez, *Biotechnol. Adv.* **2009**, *27*, 185–194.

68 S. Nanda, P. Mohanty, K. K. Pant, S. Naik, J. A. Kozinski, A. K. Dalai, *BioEnergy Res.* **2013**, *6*, 663–677.

69 M. Ballesteros, J. M. Oliva, M. J. Negro, P. Manzanares, I. Ballesteros, *Process Biochem.* **2004**, *39*, 1843–1848.

70 J. J. Lafont, A. A. Espitia, J. R. Sodré, *Mater. Renew. Sustain. Energy* **2015**, *4*, 1.

71 D. Janiszewska, L. Ossowska, *Energies* **2022**, *15*, 6756.

72 S. S. Shah, M. A. Aziz, Z. H. Yamani, *Chem. Rec.* **2022**, *22*, e202200018.

73 S. O. Adio, S. A. Ganiyu, M. Usman, I. Abdulazeez, K. Alhooshani, *Chem. Eng. J.* **2020**, *382*, 122964.

74 M. Daud, M. S. Kamal, F. Shehzad, M. A. Al-Harthi, *Carbon* **2016**, *104*, 241–252.

75 M. D. Garba, M. Usman, S. Khan, F. Shehzad, A. Galadima, M. F. Ehsan, A. S. Ghanem, M. Humayun, *J. Environ. Chem. Eng.* **2021**, *9*, 104756.

76 S. Khan, Y. Khulief, A. Al-Shuhail, *Int. J. Glob. Warm.* **2018**, *14*, 462–487.

77 S. Khan, Y. A. Khulief, A. Al-Shuhail, *Mitig. Adapt. Strat. Gl. Chan.* **2019**, *24*, 23–52.

78 S. Khan, Y. A. Khulief, A. A. Al-Shuhail, *Environ. Earth Sci.* **2020**, *79*, 294.

79 M. Usman, *Membranes* **2022**, *12*, 507.

80 M. Usman, A. S. Ghanem, S. N. A. Shah, M. D. Garba, M. Y. Khan, S. Khan, M. Humayun, A. L. Khan, *Chem. Rec.* **2022**, *22*, e202200039.

81 M. Usman, A. Helal, M. M. Abdelnaby, A. M. Alloush, M. Zeama, Z. H. Yamani, *Chem. Rec.* **2021**, *21*, 1771–1791.

82 M. Usman, N. Iqbal, T. Noor, N. Zaman, A. Asghar, M. M. Abdelnaby, A. Galadima, A. Helal, *Chem. Rec.* **2022**, *22*, e202100230.

83 M. Usman, M. Y. Khan, T. Anjum, A. L. Khan, B. Hoque, A. Helal, A. S. Hakeem, B. A. Al-Maythalony, *Membranes* **2022**, *12*, 1055.

84 M. Usman, Z. Zeb, H. Ullah, M. H. Suliman, M. Humayun, L. Ullah, S. N. A. Shah, U. Ahmed, M. Saeed, *J. Environ. Chem. Eng.* **2022**, *10*, 107548.

85 M. A. Usman, I. Momohjimoh, A. S. Gimba, *J. Miner. Mater. Charac. Engin.* **2016**, *4*, 228.

86 H. Essabir, M. O. Bensalah, D. Rodrigue, R. Bouhfid, A. Qaiss, *Mech. Mater.* **2016**, *93*, 134–144.

87 D. García-García, A. Carbonell, M. D. Samper, D. García-Sanoguera, R. Balart, *Compos. B. Eng.* **2015**, *78*, 256–265.

88 I. Naghmouchi, P. Mutjé, S. Boufi, *Ind. Crops Prod.* **2015**, *72*, 183–191.

89 E. Watt, M. A. Abdelwahab, M. R. Snowdon, A. K. Mohanty, H. Khalil, M. Misra, *Sci. Rep.* **2020**, *10*, 10714.

90 J. S. Binoj, R. Edwin Raj, B. S. S. Daniel, *J. Clean. Prod.* **2017**, *142*, 1321–1331.

91 L. Zhang, Y. Hu, *Mater. Des.* **2014**, *55*, 19–26.

92 I. Spiridon, R. N. Darie-Nita, A. Bele, *J. Clean. Prod.* **2018**, *172*, 2567–2575.

93 J. F. Balart, V. Fombuena, O. Fenollar, T. Boronat, L. Sánchez-Nacher, *Compos. B. Eng.* **2016**, *86*, 168–177.

94 K. Alper, K. Tekin, S. Karagöz, A. J. Ragauskas, *Sustain. Energy Fuels* **2020**, *4*, 4390–4414.

95 A. Bauen, G. Berndes, M. Junginger, M. Londo, F. Vuille, R. Ball, T. Bole, C. Chudziak, A. Faaij, H. Mozaffarian, *IEA* **2009**, *20113044518*, 108.

96 M. Rauf, S. S. Shah, S. K. Shah, S. N. A. Shah, T. U. Haq, J. Shah, A. Ullah, T. Ahmad, Y. Khan, M. A. Aziz, K. Hayat, *J. Saudi Chem. Soc.* **2022**, *26*, 101514.

97 S. S. Shah, K. Hayat, S. Ali, K. Rasool, Y. Iqbal, *Mater. Sci. Semicond. Process.* **2019**, *90*, 65–71.

98 M. Sanjay, G. Arpitha, L. L. Naik, K. Gopalakrishna, B. Yogesha, *Nat. Resourc.* **2016**, *7*, 108–114.

99 J. A. Melero, J. Iglesias, A. Garcia, *Energy Environ. Sci.* **2012**, *5*, 7393–7420.

100 C. Wang, Z. Du, J. Pan, J. Li, Z. Yang, *J. Anal. Appl. Pyrolysis* **2007**, *78*, 438–444.

101 G. Wang, Y. Dai, H. Yang, Q. Xiong, K. Wang, J. Zhou, Y. Li, S. Wang, *Energy Fuel* **2020**, *34*, 15557–15578.

102 S. Wang, G. Dai, H. Yang, Z. Luo, *Prog. Energy Combust. Sci.* **2017**, *62*, 33–86.

103 V. Chintala, *Renew. Sust. Energ. Rev.* **2018**, *90*, 120–130.

104 E. Leng, Y. Zhang, Y. Peng, X. Gong, M. Mao, X. Li, Y. Yu, *Fuel* **2018**, *216*, 313–321.

105 T. Kan, V. Strezov, T. J. Evans, *Renew. Sust. Energ. Rev.* **2016**, *57*, 1126–1140.

106 A. V. Bridgwater, *Biomass Bioenerg* **2012**, *38*, 68–94.

107 I. U. Din, M. Usman, S. Khan, A. Helal, M. A. Alotaibi, A. I. Alharthi, G. Centi, *J. CO2 Util.* **2021**, *43*, 101361.

108 X. Hu, M. Gholizadeh, *J. Energy Chem.* **2019**, *39*, 109–143.

109 M. I. Jahirul, M. G. Rasul, A. A. Chowdhury, N. Ashwath, *Energies* **2012**, *5*, 4952–5001.

110 R. Aguado, M. Olazar, B. Gaisán, R. Prieto, J. Bilbao, *Ind. Eng. Chem. Res.* **2002**, *41*, 4559–4566.

111 T. Cornelissen, J. Yperman, G. Reggers, S. Schreurs, R. Carleer, *Fuel* **2008**, *87*, 1031–1041.

112 F. Abnisa, W. M. A. Wan Daud, *Energy Convers. Manage.* **2014**, *87*, 71–85.

113 B. Luna-Murillo, M. Pala, A. L. Paioni, M. Baldus, F. Ronsse, W. Prins, P. C. A. Bruijnincx, B. M. Weckhuysen, *ACS Sustain. Chem. Eng.* **2021**, *9*, 291–304.

114 J. Robinson, C. Dodds, A. Stavrinides, S. Kingman, J. Katrib, Z. Wu, J. Medrano, R. Overend, *Energy Fuel* **2015**, *29*, 1701–1709.

115 S. Morales, R. Miranda, D. Bustos, T. Cazares, H. Tran, *J. Anal. Appl. Pyrolysis* **2014**, *109*, 65–78.

116 S. Rajagopal, R. Pulapparambil Vallikkattil, M. Mohamed Ibrahim, D. G. Velev, *Condens. Matter* **2022**, *7*, 6.

117 L. M. Da Silva, R. Cesar, C. M. R. Moreira, J. H. M. Santos, L. G. De Souza, B. M. Pires, R. Vicentini, W. Nunes, H. Zanin, *Energy Storage Mater.* **2020**, *27*, 555–590.

118 S. Ghosh, R. Santhosh, S. Jeniffer, V. Raghavan, G. Jacob, K. Nanaji, P. Kollu, S. K. Jeong, A. N. Grace, *Sci. Rep.* **2019**, *9*, 16315.

119 S. Saini, P. Chand, A. Joshi, *J. Energy Storage* **2021**, *39*, 102646.

120 B. Zhang, Y. Jiang, R. Balasubramanian, *J. Mater. Chem. A* **2021**, *9*, 24759–24802.

121 V. S. Bhat, S. Supriya, G. Hegde, *J. Electrochem. Soc.* **2020**, *167*, 037526.

122 P. Kalyani, A. Anitha, *Port. Electrochimica Acta* **2013**, *31*, 165–174.

123 A. M. Abioye, F. N. Ani, *Renew. Sust. Energ. Rev.* **2015**, *52*, 1282–1293.

124 Z. Heidarinejad, M. H. Dehghani, M. Heidari, G. Javedan, I. Ali, M. Sillanpää, *Environ. Chem. Lett.* **2020**, *18*, 393–415.

125 N. A. Alhebshi, N. Salah, H. Hussain, Y. N. Salah, J. Yin, *Nanomaterials* **2022**, *12*, 122.

126 R. K. Gupta, M. Dubey, P. Kharel, Z. Gu, Q. H. Fan, *J. Power Sources* **2015**, *274*, 1300–1305.

127 U. Thubsuang, S. Laebang, N. Manmuanpom, S. Wongkasemjit, T. Chaisuwan, *J. Mater. Sci.* **2017**, *52*, 6837–6855.

128 Z. Xiao, W. Chen, K. Liu, P. Cui, D. Zhan, *Int. J. Electrochem. Sci.* **2018**, *13*, 5370–5381.

129 P. Bai, S. Wei, X. Lou, L. Xu, *RSC Adv.* **2019**, *9*, 31447–31459.

130 C. Peng, X.-B. Yan, R.-T. Wang, J.-W. Lang, Y.-J. Ou, Q.-J. Xue, *Electrochim. Acta* **2013**, *87*, 401–408.

131 A. Khan, R. Arumugam Senthil, J. Pan, Y. Sun, X. Liu, *Batter. Supercaps* **2020**, *3*, 731–737.

132 Y. Wen, K. Kierzek, J. Min, X. Chen, J. Gong, R. Niu, X. Wen, J. Azadmanjiri, E. Mijowska, T. Tang, *J. Appl. Polym. Sci.* **2020**, *137*, 48338.

133 X. Kong, Y. Zhang, P. Zhang, X. Song, H. Xu, *Appl. Surf. Sci.* **2020**, *516*, 146162.

134 D. Wang, S. Liu, G. Fang, G. Geng, J. Ma, *Electrochim. Acta* **2016**, *216*, 405–411.

135 J. Mi, X.-R. Wang, R.-J. Fan, W.-H. Qu, W.-C. Li, *Energy Fuel* **2012**, *26*, 5321–5329.

136 A. Welfle, R. Slade, The Supply of Biomass for Bioenergy Systems in *Biomass Energy with Carbon Capture and Storage (BECCS): Unlocking Negative Emissions, First*, (Eds: G. Clair, T. S. Patricia, M.V. Naomi, F. Temitope), **2018**, Chapter 2, pp.17–46, https://doi.org/10.1002/9781119237716.ch2.

137 N. Thibanyane, P. Agachi, G. Danha, *Procedia Manufacturing* **2019**, *35*, 477–487.

138 L. J. R. Nunes, J. C. O. Matias, J. P. S. Catalão, *Renew. Sust. Energ. Rev.* **2016**, *53*, 235–242.

139 W. Moroń, W. Rybak, *Atmos. Environ.* **2015**, *116*, 65–71.

140 G. N. Furey, D. Tilman, *Proc. Natl. Acad. Sci.* **2021**, *118*, e2111321118.

141 R. Dybzinski, J. E. Fargione, D. R. Zak, D. Fornara, D. Tilman, *Oecologia* **2008**, *158*, 85–93.

142 J. Meiners. Ten Years Later, BP Oil Spill Continues to Harm Wildlife—especially Dolphins. National Geographic **2020** [cited October 22, 2022]; Available from: https://www.nationalgeographic.com/animals/article/how-is-wildlife-doing-now--ten-years-after-the-deepwater-horizon.

143 M. Penn. We Don't Know When It Will End': 10 Years after Fukushima. **2021** [cited October 22, 2022]; Available from: https://www.aljazeera.com/news/2021/3/9/fallout-fukushima-10-years-after.

144 F. Birol. World Energy Outlook 2021. **2021** [cited October 22, 2022]; Available from: https://iea.blob.core.windows.net/assets/88dec0c7-3a11-4d3b-99dc-8323ebfb388b/WorldEnergyOutlook2021.pdf.

145 J. Thakur. COP26: What Is Net Zero Emissions Pledged By Many Countries Including India. **2021** [cited October 22, 2022]; Available from: https://www.indiatimes.com/explainers/news/cop26-what-is-net-zero-emissions-pledged-by-many-countries-553541.html.

146 Is It Possible to Achieve Net-zero Emissions? **2022** [cited October 22, 2022]; Available from: https://www.nationalacademies.org/based-on-science/is-it-possible-to-achieve-net-zero-emissions.

147 New Report Details Way Forward as Future Biomass Demand May Exceed Supply. **2021** [cited October 22, 2022]; Available from: https://www.climate-kic.org/in-detail/new-report-shows-future-biomass-demand-may-exceed-supply.

148 K. R. Bandyopadhyay, *Energies* **2022**, *15*, 2884.

149 T. Gumartini, *Biomass Energy in the Asia-Pacific Region*: *Current Status*, *Trends and Future Setting* **2009**, *Working Paper Series* Working Paper No. APFSOS II/WP/2009/26.

150 S. Sharma, M. Kaur, C. Sharma, A. Choudhary, S. Paul, *ACS Omega* **2021**, *6*, 19529–19545.

151 P. Pang, F. Yan, M. Chen, H. Li, Y. Zhang, H. Wang, Z. Wu, W. Yang, *RSC Adv.* **2016**, *6*, 90446–90454.

152 K. Ojha, B. Kumar, A. K. Ganguli, *J. Chem. Sci.* **2017**, *129*, 397–404.

153 T. T. Duignan, X. S. Zhao, *J. Phys. Chem. C.* **2019**, *123*, 4085–4093.

2

Environmental Aspects of Biomass Utilization in Supercapacitors

Runa Akter[1], Jaber Bin Abdul Bari[2], Saidur R. Chowdhury[3,4],
Muhammad Muhitur Rahman[5], and Syed Masiur Rahman[6,*]

[1] *Institute of Forestry and Environmental Sciences, University of Chittagong, Chittagong 4331, Bangladesh*
[2] *Department of Oceanography, Noakhali Science and Technology University, Noakhali 3814, Bangladesh*
[3] *Department of Civil Engineering, College of Engineering, Prince Mohammad Bin Fahd University, Al Khobar, Saudi Arabia*
[4] *SC Environmental Solutions, Greystone Walk Dr, Toronto ON, M1K 5J3, Canada*
[5] *Department of Civil and Environmental Engineering, College of Engineering, King Faisal University, Al-Ahsa 31982, Saudi Arabia*
[6] *Applied Research Center for Environment & Marine Studies, King Fahd University of Petroleum & Minerals (KFUPM), Dhahran 31260, Eastern Province, Saudi Arabia*
* *Corresponding author*

2.1 Introduction

Energy is essential in modern civilization, from everyday living to advanced research and technology. Unfortunately, it has become a bottleneck impeding our progress with rising energy consumption and negative environmental impacts. Renewable energy sources have gained attention as feasible, low-cost, and environmentally acceptable energy sources due to the possible climate change and fossil fuels depletion. Non-fossil energy sources must be used to establish a sustainable future; ideally, they should be reliable, economical, and limitless. The key to attaining global energy sustainability is energy conversion and storage. Numerous energy conversion and storage technologies are available, such as solar panels, flywheels, pressurized air, fuel cells, supercapacitors, and batteries, have been created to harness sustainable energy sources like solar, wind, thermal, hydro, or biomass energy. The most efficient electrochemical energy conversion and storage technologies for everyday use have been demonstrated to be supercapacitors (SC) and batteries [1].

SCs are clean energy storage devices that function like batteries and capacitors in power delivery and energy storage. SCs and batteries are considered the most reliable electrochemical energy transformation and storage technologies for practical applications. Batteries immediately transform chemical energy into electrical energy via redox reactions, while SCs reserve charges at the electrode or electrolyte interface through the electrical dual layer or reversible Faradaic processes [2, 3]. The energy performance of SCs may be adjusted and made application-specific depending on the charge storage method [4]. Fuel

cells and batteries are high-energy sources but lack power delivery. Conversely, conventional capacitors have outstanding power delivery capabilities, but energy density remains a constraint [5]. SCs are gaining popularity as a viable alternative to fuel cells and batteries due to their capacity to offer high power at high energy and long life. They are classified into electric double-layer capacitors (EDLCs) and pseudocapacitors (PCs) based on charge storage mechanisms [6, 7]. The electrochemical performance of supercapacitors is entirely dependent on the selection of its constructing components, such as electrodes, binders, separators, electrolytes, packaging material, etc. The following section provides a summary of the various supercapacitor components.

2.2 Supercapacitor Components

2.2.1 Electrodes

The potential elements of SCs mainly include carbon-based materials. Because of their physicochemical qualities, carbon-based elements have been widely used for SC electrodes [8]. Carbon-based materials include anything from basic ACs to sophisticated nanostructured carbons like graphene and carbon nanotubes (CNTs). Some of their characteristics are high specific surface area, strong chemical stability, superior electrical conductivity, and controlled porosity [9]. Various biomass resources have been used as precursor materials to prepare carbon electrodes for SCs to date, including multiple types of wood and plant tissues, agricultural residues, industrial effluent, and domestic waste. They have gained considerable interest due to their widespread availability and low cost.

2.2.2 Electrolytes

An essential component of electrochemical supercapacitors is the electrolyte that provides ionic conductivity and facilitates charge adjustment on each electrode of the cell. It also allows connectivity between various components of SCs. In SC electrolytes, the organic compounds derived from the extraction or conversion of biomass materials in the form of gel polymer electrolytes and solid-state electrolytes have been extensively studied. These organic electrolyte-based energy storage devices (ESs) now dominate the commercial market due to their large operation potential window, which is generally between 2.5 and 2.8 V. The energy and power densities may be significantly enhanced by their large operation potential window and the higher operating cell voltage [6, 10–17]. This remarkable electrochemical performance of biomass-based hierarchical porous carbon (PC) material in electric double-layer capacitors (EDLC) is a result of its high specific surface area (SSA) and unique hollow tubular hierarchical porous structure [18].

In carbon-based ESs, the capacitances derived from organic electrolytes are often less than those obtained from aqueous electrolytes because the specific capacitance of an ES depends on the specific surface area and the pore size/size distribution of the carbon components [19]. Therefore, the compatibility between electrolyte ions and pore structure may increase the specific capacitance. Due to their porous and interconnected architectures, carbon materials generated from biomass can facilitate convenient and efficient electron transport and offer enough electrolyte contact [20].

2.2.3 Separators

To reduce the conduction of electrons between the electrodes, separators between electrodes in supercapacitors have been used, which are made of rubber, plastic, aqua gel, resorcinol formaldehyde polymers, polyolefin films, etc. However, inclusion of binders would result in several adverse consequences, including higher electrical resistance, poor adhesion, unfavorable electrolyte diffusion, and inadequate capacitive performance [21, 22]. The commercially available Nafion membrane has qualities for it to function efficiently as a supercapacitor separator. Still, the high cost and scarcity of raw materials derived from fossil resources prevent its widespread usage [23, 24]. Developing biomass-based porous carbon membranes can remove the limitations of their powdered counterparts for use in SCs. Permeability and porosity are the most crucial characteristics of EES membranes. Biomass-derived carbon materials have considerable potential for application in these SCs due to their extremely high porosity, large specific surface area, and outstanding electrical conductivity. The membranes generated from biomass may be utilized directly as electrodes for SCs, eliminating the need for binders, additives, and current collectors, hence simplifying the electrode assembly procedures and decreasing the cost of SC manufacture [25, 26].

A micro-supercapacitor prepared using micro-electro-mechanical technology is referred to as MEMS supercapacitor, with vast application possibilities in implantable biomedical devices, micro-sensors, micro-robots, etc. The MEMS supercapacitor features a huge energy storage capacity, miniaturization, many charge/discharge cycles, and batch manufacturing. The optimization of the specific surface area of membrane materials is applied to the investigation of the maximal electrical double-layer capacitor per square centimeter or per gram [27]. In addition, the carbon membrane's structural integrity would allow for high cycle stability. These fundamental characteristics make biomass-derived carbon membranes a highly promising electrode material for SCs.

2.2.4 Binders

The purpose of the binder is to bind the active material in the electrode and enhance adhesion between the electrode and current collectors. The binders might create a compact arrangement for the electrodes, ensuring a favorable electrical connection between the active substances [28]. Activated carbon is now the most common material used in SCs due to its high specific surface area, low cost, and capacity for mass production. Similarly, graphene has generated much attention in the energy storage sector as a novel carbon material since supercapacitors and polymers are frequently mixed onto graphene for various enhanced or novel features [29]. Utilizing conducting polymers (CPs) in supercapacitors allows for quick charge and discharge and high specific capacitance; nevertheless, the primary problem of using CPs alone as the supercapacitor electrode is that they are unstable over lengthy cycle life [30]. Compound CPs with graphene, in this instance, extend the lifespan of a CP-based supercapacitor. Another ecofriendly compound, nanocellulose is a good choice for developing green renewable energy storage systems due to its low cost, abundant availability, and straightforward production procedures [31]. Nano cellulose has a unique mix of features, such as flexible surface chemistry, transparency, minimal thermal expansion, high elasticity, anisotropy, and the ability to bind to other conductive materials, allowing for widespread application in supercapacitors [32].

2.2.5   Packaging Materials

The use of ecofriendly packing materials guarantees optimal safety for supercapacitors. Aluminum or iron is used to coat the majority of energy storage devices. Replacing metal cans and coin cells with eco-friendly polymer materials like biomass-derived polymers in supercapacitors is extremely desirable. Even while aluminum or steel cans do not represent a threat to the environment, they nonetheless can generate ash [33].

Although significant advances have been achieved in the electrochemical performance of electrode materials, additional mechanical support is essential for the flexibility, strength, and stability of these devices. These supports are required to support substantial mechanical loads [34]. In practical applications, the substrates and packaging materials of these devices accounts for a significant amount of their total weight/volume and significantly reduces their overall energy density.

2.3   Biomass Use

SCs rely on porous carbons. Porous carbons are predicted to be in high demand in the future for various technologies because of their vital function and the expected constant increase in output. The production of porous carbons necessitates specific methods to be chosen based on two fundamental criteria: (i) an abundance of carbon precursors and (ii) the method must be flexible and ecologically sustainable, using resources that are easily accessible, cost-effective, and renewable (i.e., biomass or biomass-based products), and non-corrosive and non-toxic constituents [35]. Due to its widespread availability, sustainability, renewable nature, unique structure, and low cost, biomass has been studied and exploited by researchers all over the world for various applications such as carbon dioxide (CO_2) capture [36], hydrogen storage [37], dye-sensitized solar cells [38], water treatment [39], and energy storage [12, 13]. Agriculture waste, also known as lignocellulosic materials, is a renewable resource available in large quantities. Lignin, cellulose, and hemicellulose are the three types of cellulose. Lignin and cellulose are excellent resources for synthesizing activated carbon compounds [40].

Biomass-derived carbon materials are eco-friendly; thus, they ensure clean and green energy. Moreover, using these materials can be cost-effective. The ionic and electrical conductivity of biomass-derived carbon materials ranges from moderate to high for rapid and efficient diffusion of electrolyte ions. They are compatible with almost all ranges of electrolytes, like aqueous, organic, and ionic liquids. Because of their higher power density, longer cycle life, and faster charge-discharge rate, SCs have recently gained a lot of interest as a type of superior energy storage technology [41, 42].

Many studies have shown that biomass-based carbon materials with 1D or 2D structures are viable for developing flexible electrodes with good electrochemical performance at the scale of laboratory experiments. However, developing generic and practical procedures to weave them on a large scale remains challenging [43]. Several studies found that using a cost-effective self-template method to mass-produce 3D hierarchically porous carbon from corn husks is a sustainable biomass carbon source [44]. The corn husk-derived hierarchical porous carbons (CHHPCs) exhibited a three-dimensional architecture with meso- or micro-porous carbon walls and a hierarchically interconnected micro-, meso-, or macro-porous

pore structure, as well as a huge surface area (814,928 m^2 g^{-1}) and a high proportion of oxygen-containing groups (12.71%) [45]. SCs can be obtained from biomass by adopting a general process. Figure 2.1 explains how we can obtain SCs from simple biomass resources like cellulose, hemicellulose, and lignin fibers with an application of simple techniques.

Nonetheless, several recent studies relied on an extra chemical agent to produce the unique structure, resulting in low carbon yield and biomass structural disruption due to the generation of substantial amounts of by-products [17, 47, 48]. In order to create methods for the effective use of biomass resources, greater attention should be applied to the structural development, from an organic biomass precursor to an inorganic carbon material and to how additional agents can be utilized to change the characteristics of the carbon material.

2.4 Green Biomass Resources

SC electrodes are made from carbon compounds derived from biomass. Because these materials are plentiful and high in carbon content, they can be used to create enriched carbon compounds in high quantities. In order to create a fresh and long-lasting energy storage device, the synthesis process and the precursor used are crucial. Although fossil fuels are frequently used as precursors, they are limited and nonrenewable resources. As a result, carbon products made from these sources are unappealing. Therefore, attention has been given to biomass materials for generating energy storage devices [49]. Crops and their waste, woodland crops and waste, aquatic, residential, and industrial by-products are all examples of green biomass sources. Figure 2.2 outlines some biomasses that can be efficiently used as recycled waste. In the first step of the carbonization process, these raw
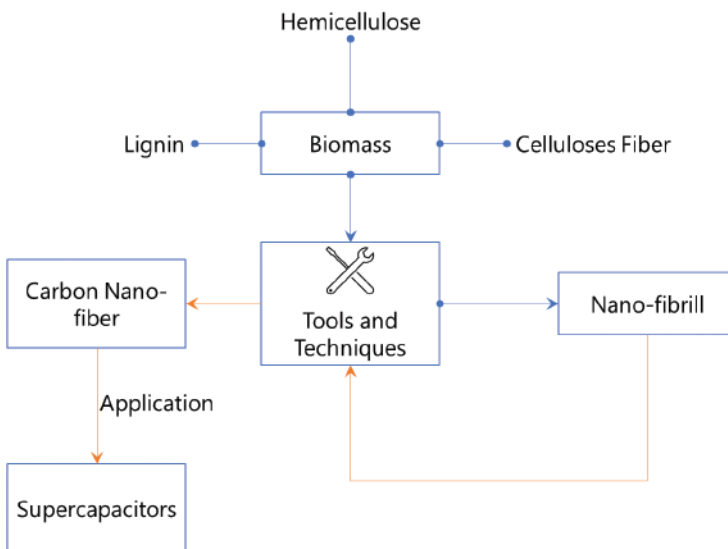
Figure 2.1 Graphical representation of obtaining supercapacitors from biomass. *Redrawn from refs* [28, 46].
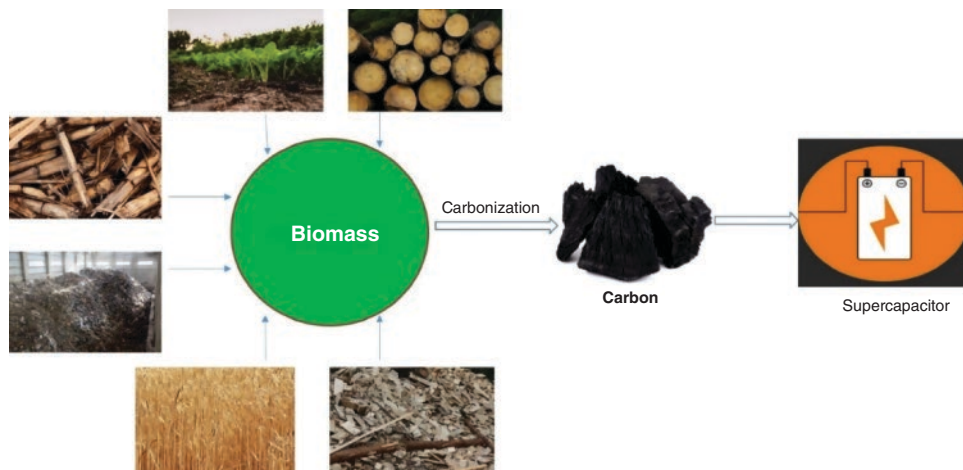
Figure 2.2 Natural biomass resources and their applications to fabricate supercapacitor cells for green energy storage. *Redrawn from refs* [1, 4].

biomass ingredients are combusted into chars with a rudimentary pore structure inside an inert environment at a high temperature. Under elevated temperatures and pressures, the carbon ratio enriches the precursor by degrading carbon-rich material.

Catalyst-free-carbon nanospheres were manufactured by some researchers utilizing simple one-step pyrolysis employing biowaste sago bark [50], seaweed [51], and leather waste [52] as precursors, with no chemical release because no activating agents were utilized. Usually, most biomass resources require different activating agents, which release various hazardous compounds into the environment and may cause serious environmental damage. The utilization of biomass to fabricate SC's other components like electrolytes, membranes, separators, binding materials, and packaging materials is also reported. These biomass applications will be discussed in later chapters in this book.

2.5 Green Synthetic Strategies for Biomass-derived Carbon

Currently, massive development has been achieved in the sector of catalysis, adsorption/separation, energy conversion, and storage using a mix of efficient synthesis methodologies and sustainable biomass. Various methods of obtaining energy from biomass have been attempted to date [35, 53]. These methods are typically divided into two categories: thermochemical processes (such as combustion, gasification, and pyrolysis) and biochemical processes (e.g., fermentation and anaerobic digestion). Figure 2.3 explains how activated carbon is achieved from different biomass resources by physical and chemical activation processes. Hydrothermal carbonization (HTC), hydrochar activation, and final carbonization and reduction are the three primary phases of the processes. Carbon atoms are rearranged during the carbonization process of physical activation to produce graphitic-like structures, which give the carbonized material its original porosity. Carbonized material, char, or biochar is the ultimate result of the carbonization process, which is high in aromatic rings.
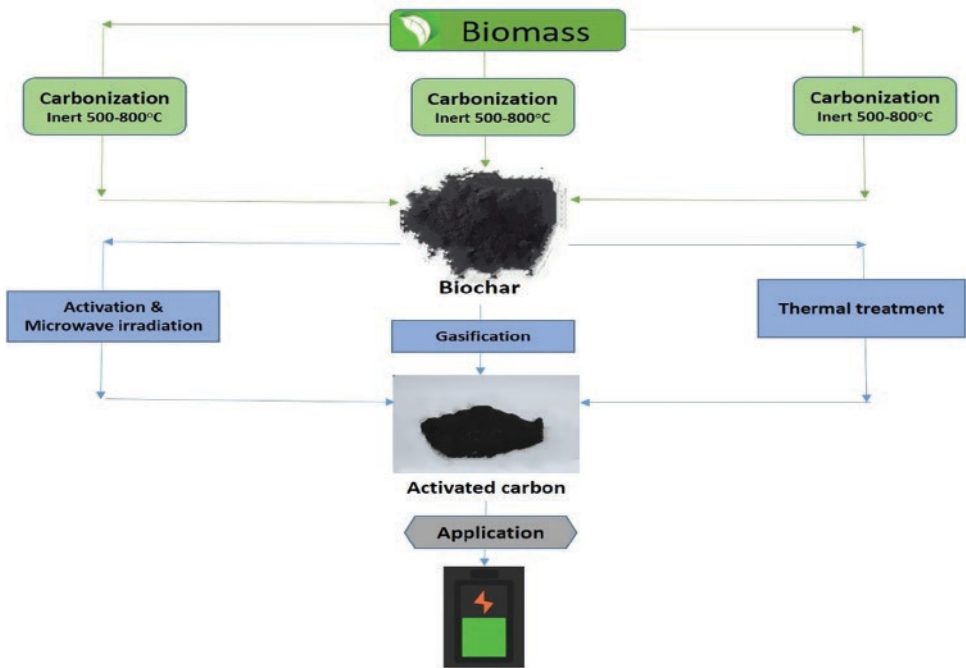
Figure 2.3 Synthetic routes towards activated carbon from biomass and its application as electrodes for supercapacitors. *Redrawn from refs* [22, 38].

Biochar is further activated using steam, carbon dioxide, air, or a combination of gases as an activating agent at temperatures between 350 and 1000°C, increasing carbon porosity. The chemical activation procedure may be done using raw biomass or carbonized biochar. This procedure is carried out at relatively low temperatures (about 300–800°C) depending on the precursor material. Activated carbon is rinsed multiple times with water to eliminate any trace residues of the activating agent in the last phase of chemical activation. A quick overview of various conversion methods is provided in the next sections.

2.6 Pyrolysis of Biomass

Pyrolysis is either a high-temperature hydrothermal treatment (700–900°C) in an inert environment or a high-temperature carbonization procedure. When calcined under inert gas, the three primary components of biomass, cellulose, hemicellulose, and lignin, may take various chemical paths. Moisture is the principal component that volatilizes in the initial stage (about 100°C). Hemicellulose degrades quickly when the temperature is raised (220– 315°C) [8]. The pyrolysis of cellulose occurs between 315°C and 400°C, but lignin pyrolysis occurs across a wide temperature range. The structural and textural properties, including porosity, shape, and physicochemical property, of direct pyrolysis-produced carbon (DPC), which may be created by the prudent choice of organic precursors and processing conditions, are particularly important for electrochemical performance.

2.7 Carbon Activation

To update the characteristics of biomass-derived carbons, activation, including chemical and physical activation, is required. A physical activation is a two-step approach that begins with the carbonization of precursor materials at a certain temperature (typically about 800°C) and ends with the activation of the conserved char at a higher temperature in the presence of appropriate catalysts such as air, CO_2, and steam. Chemical activation, however, combines the two stages, namely combining the biomass with the activator and then calcining at an appropriate temperature [54]. The activators significantly impact the qualities of the end products throughout the activation process. Potassium hydroxide (KOH) is the most promising of these activators because it has a lower activation temperature, resulting in higher outputs and well-defined pore size distribution with extremely high SSA (up to 3000 m^2/g). Microspores and tiny mesoporous may be inserted into the system of differently patterned carbons by activating them with KOH [55]. For carbon activation with KOH, three primary activation methods are available [56]:

- During the calcination process, potassium compounds such as KOH and some compounds (K_2CO_3 and K_2O) interact with carbon, forming the pore system;
- Carbon gasification leads to the subsequent development of porosity via by-products (H_2O and CO_2); and
- The metal potassium efficiently directly interacts with the carbon lattices of the carbon matrix, causing the carbon lattices to expand.

2.8 Hydrothermal Carbonization

Hydrothermal carbonization (HTC) is a potential approach for converting cellulose into coal-like compounds in particular. It is often used at low temperatures (130°C–250°C) and under self-generated pressures in water. It is found to be a viable method for producing a variety of carbonaceous materials [57]. Hydrolysis, dehydration, decarboxylation, polymerization, and aromatization are the five techniques usually used in the hydrothermal treatment of biomass. Various carbon sources produce different precursors, which influence the structures and morphologies of the final products. During the early phases of the hydrothermal treatment, hexoses (such as glucose, sucrose, and starch) and pentoses (xylose, ribose) are dehydrated, resulting in the formation of hydroxyethyl furfural (HMF) and furfural, and also different organic acids. These acids reduce pH and accelerate carbohydrate dehydration in situ. Under moderate processing conditions, the temperature may be used to regulate both the chemical composition and the shape of HTCs.

HTC has been found to be a minimal-cost approach for directly generating porous carbon-based materials from biomass [57, 58]. HTC-derived compounds, on the other hand, have fewer pores and a smaller specific surface area than ACs, which is unfavorable for applications involving nanometer-scale regulated porosity, such as catalysis, adsorption, or energy storage [4].

2.9   Ionothermal Carbonization

Ionic liquids (ILs), which are liquids with a temperature below 100°C, were first created as molten electrolytes for use in batteries. Because of their superior biomass solubility, low solvent volatility, and great thermal stability, ILs are now being used as a benign solvent in biomass-derived carbon synthesis [59]. The capacity to create hydrogen bonds with solutes may improve carbohydrate solubility, and the latent acidity function can accelerate carbohydrate dehydration. Ionothermal carbonization (ITC) can be handled much more effectively with an open vessel than HTC, where water creates huge autogenous forces at extreme temperatures. Furthermore, ITC-derived carbon compounds (ITCCs) have a somewhat greater specific surface area (SSA) and carbonization yield [60]. Although ILs may be recovered and reused without additional purification following the carbonization step, their cost prevents their widespread application in industry. ITC, on the other hand, is an excellent supplementary procedure for converting biomass into useful carbon compounds.

2.10   Molten Salt Carbonization

High temperatures treatment of carbon materials used in electrical devices is required for both HTCs and ITCs and results in an increased electro-conductivity and a very well-porous structure. Molten salt carbonization (MSC) does not require any further raised temperature treatment. Molten salt synthesis is an extension and successful complement to the ITC and HTC techniques in this regard. In this way, molten salt synthesis is an effective supplement to the ITC and HTC procedures. In a solid-state reaction mechanism, the reaction rates are often limited by the sluggish diffusion of reactants [61].

2.11   Environmental Benefits

In many places, wood-processing leftovers, urban wood wastes, and some food-processing residues are landfilled. The majority of agricultural leftovers used as fuel are burnt. Agricultural residual fuels are sometimes plowed into the soil. The majority of in-forest wastes are left in the forest, where their long-term accumulation increases the danger of forest fires and degrades ecosystems. Instead of being left in the forest, some in-forest items, notably logging wastes, are pile burnt, eliminating this material as a source of fuel loading but contributing to air pollution. However, using these materials to produce biomass that will later be used in SCs may have environmental and economic benefits. Biomass seems to have the prospects to be a cost-effective and long-term source of energy in the future if the government and industry collaborate to ensure that harvesting biomass compounds and producing bioenergy crops are both ecologically friendly, all while helping countries fulfil their greenhouse gas (GHG) reduction targets [11, 62]. Figure 2.4 shows a simple diagram of the different benefits obtained from biomass energy production. The consequences of disposing of biomass as waste will be severe. Biomass burning in the open
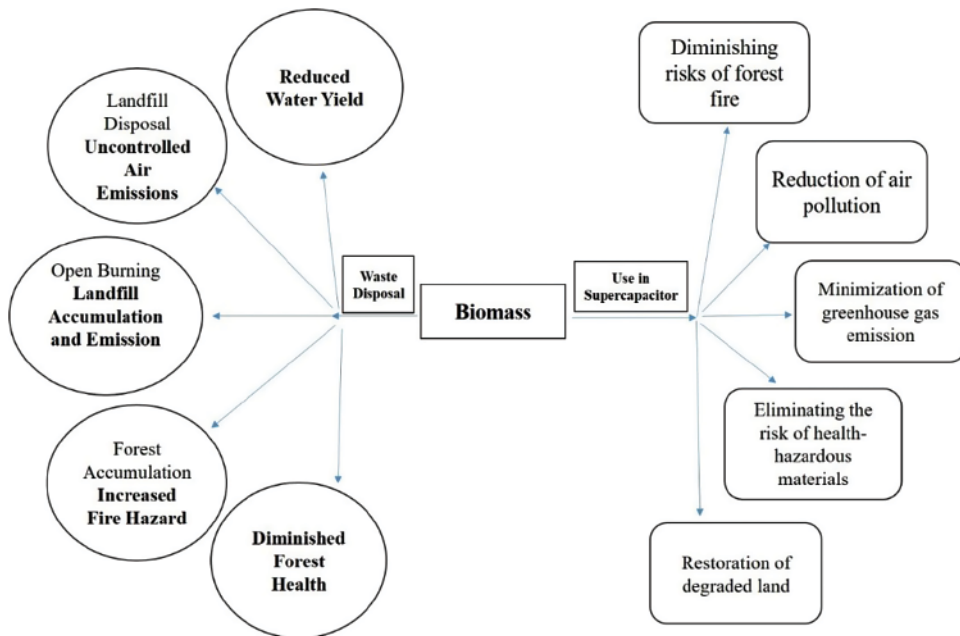
Figure 2.4 Benefits of biomass energy production. *Redrawn from refs* [3, 44].

emits toxic and harmful chemicals and fumes. Furthermore, when biomass accumulates in the forest, forest fire risk grows. These undesirable biomass elements represent a threat to the ecosystem as a whole. On the other hand, using these materials to make carbon materials for SCs may be extremely beneficial.

2.12 Eliminating Hazardous Materials

Municipal waste is a collection of a city's solid and semisolid waste. It mostly consists of home or residential garbage although commercial and industrial garbage may be included, except for toxic wastes, which are usually managed separately in compliance with environmental requirements [63, 64]. Food and kitchen trash, such as meat trimmings or vegetable peelings, yard or green garbage, and paper, are all considered biodegradable parts of municipal waste. The hazardous materials are sometimes left over in open areas, thus generating threats to human health and the ecosystem. Sometimes these hazardous wastes are landfilled, resulting in the production of methane. As a result, they can be employed as raw materials to reduce the detrimental effects. Another promising path towards a more environmentally friendly and sustainable energy source is to utilize harmful particles produced by automobiles and industry to produce more useful nano-sized carbon compounds. Soot particles (vegetable oil soot, diesel soot, wood soot, charcoal soot), leather waste, and waste tires are a few major challenges contributing to global warming and human health issues [4]. Therefore, using these compounds may help to decrease the threat they produce.

2.13   Diminishing Risks of Forest Fire

Existing old and damaged wood, fallen wooden debris of various kinds, and forest growth stock, whose density is generally increasing, are all sources of fuel accumulating in the woods. In terms of forest fire danger, the build up of old and damaged timber, both rising and falling, can be problematic since it contains less moisture content than young stock, making it easier to ignite, quicker to burn, and more likely to spread the fire. As the amount of fuel in forests increases, out-of-control fires become far more intense and devastating than the pre-industrial fires. In drier regions flames burn far hotter than fires in damper regions, consuming much larger areas and causing far more damage. Hence, using these materials may diminish the risks of a forest fire.

2.14   Enhancement of Ecosystems

Fuel loading can lead to declining forest and watershed health and ecosystem function. Many modern forests have a high canopy closure level, but healthy, generally undisturbed forest ecosystems have low canopy closure. This indicates that more accessible rainfall enters the evapotranspiration cycle than in the original ecosystem, and therefore less precipitation reaches the watersheds as runoff. Decreased runoff means less water reaches the grassland and lowland, where it is stored throughout the rainy season and gradually released during the dry. Thus, using forest fuels to generate biomass may improve the health of a given ecosystem [65].

2.15   Minimizing Air Pollution

People have been polluting the air since they learned how to use the fire. Still, anthropogenic air pollution, also known as man-made air pollution, has increased drastically since the dawn of civilization. Air pollution and landfill loading are two of traditional biomass waste disposal's most significant environmental consequences. The open burning of biomass leftovers causes significant air pollution, including smoke, particles, and hydrocarbon emissions. These activities release many volatile organic compounds and toxic metals into the atmosphere. It also emits large amounts of NO_x, CO, and hydrocarbons, all contributing to ozone formation in the atmosphere. In many locations, agricultural burning significantly hinders meeting air quality criteria [66]. Pollutants discharged into the atmosphere are not limited to the immediate vicinity of the emission source or the local environment but may travel considerable distances, causing regional and worldwide environmental issues [67]. In addition, landfill loading with biomass waste produces methane, a greenhouse gas. However, rather than burning these biomass resources, they might be used to produce activated carbon for SCs, which could help to alleviate air pollution.

2.16   Greenhouse Gas Emission Reduction

Biomass is a well-known clean energy source that may assist in reducing the use of fossil fuels, therefore minimizing the greenhouse effect [68]. The utilization of biomass resources that are often considered a third-world energy source, might contribute a critical role in

assisting the developed countries in reducing the detrimental effect of using fossil fuels to generate electricity, but only if major replanting is promptly undertaken. Biomass is a carbon-neutral renewable energy source that burns cleaner than fossil fuels. Therefore, biomass production may help to minimize global warming, and there are likely to be environmental advantages if intensive agriculture is substituted with less intensively managed energy crops, such as reduced fertilizer leaching and pesticide usage. Biofuels and chemicals made from biomass for various applications, including supercapacitors, are becoming increasingly popular worldwide to enhance energy resources and combat global warming [69, 70].

2.17   Solid Waste Management

Landfilling wood leftovers that can be collected and transformed into fuel for the power plant has the same positive environmental consequences as other organic wastes. Many cities generate a large amount of solid waste, ultimately ending up in landfill and may pose serious environmental risks in the form of waste materials, a situation that has become a prominent and pressing issue in civilized human societies [70, 71]. When organic waste is dumped in a landfill, it decomposes and produces methane, a powerful greenhouse gas. As a result, diverting these wastes for biomass generation lowers landfill volume and methane emissions. Hence, using rather than dumping solid waste eliminates a considerable amount of organic material from the landfill.

2.18   Restoration of Degraded Land

When considering the use of biomass to help offset global warming, the time lag between the initial release of CO_2 from fossil fuel burning and its eventual absorption as biomass, which may take many years, is a critical factor that is sometimes overlooked. A similar problem affects developing countries, which utilize biomass for energy production but do not have a plant replacement program. A number of crops have been proposed or are being explored for commercial energy farming. Woody crops, grasses/herbaceous plants (all perennial crops), starch and sugar crops, and oilseeds are all potential energy crops. Biomass production may help rehabilitate degraded areas if suitable crops are chosen. Compared to present agricultural practice, higher biodiversity may be produced depending on the crops utilized and how biomass is farmed [72].

2.19   Environmental Externalities

Use of agricultural and forest residues and the production of woody, herbaceous, and aquatic crops are among the biomass feedstock manufacturing methods. Agricultural residues, such as leaves and roots, stover, straw, and stalks, remain after harvesting and contribute to erosion control, nutrient and water retention, and soil organic matter maintenance. However, using these resources to produce energy may introduce severe environmental problems.

The major environmental issues related to biomass production are associated with land, water, and fertilizer. More specific environmental issues from biomass-based supercapacitors involve soil degradation, nutrient loss, water quality deterioration, and air pollution [73], which may create anxieties related to environmental protection [64]. Recently, numerous crops have been produced that are later used as raw materials for energy production. However, using woody crops and aquatic plants as raw materials has drawn attention due to long-term negative implications.

Short-rotation intensively farmed plants are utilized to produce woody crops that are used for energy conversion. Large areas of agricultural land will be required for the large-scale development of short-rotation plants, potentially causing a conflict with food and fiber production. Also, severe impacts such as soil disturbance, soil degradation, and compression may arise from the converting forest sites to short-rotation plantations. Furthermore, fertilizers are utilized in developing these crops, which are then carried into neighboring water bodies through surface runoff. Aquatic plants that are used for energy production directly or indirectly contribute to land-use changes, including displacement of wildlife habitat and rangeland grazing, groundwater impacts such as aquifer drawdown, land subsidence, and freshwater contamination from pond seepage and interaction among aquifers [74]. The degradation of these aquatic plants may prompt algae to grow rapidly, thus creating algal blooms and, subsequently, hypoxia and death of aquatic organisms in the water bodies [75].

Major problems arising from using biomass for SCs are from different conversion methods such as fermentation, direct combustion, gasification, and pyrolysis. Various volatile and non-volatile pollutants, such as high carbon monoxide (CO), unburned hydrocarbons, sulfur dioxide (SO_2), carbon dioxide (CO_2), ammonia (NH_3), hydrogen sulfide (H_2S), hydrogen cyanide (HCN), carbonyl sulfide (COS), and carbon disulfide (CS_2), are emitted as a result of these conversion methods. Solid wastes exist in the form of stillage, wastewater treatment sludge, combustion debris, and sulfur scrubber effluent, as well as liquid wastewaters from equipment wash waters and power plant blowdown streams containing biodegradable organic compounds [11, 67, 76].

2.20 Conclusions

Supercapacitors (SCs) are clean energy storage devices considered the most efficient electrochemical energy transformation and storage methods in real-world applications. SCs have gained traction as cost-effective and environmentally acceptable energy sources as concerns about climate change grow and the depletion of fossil fuels becomes more imminent. SCs have shown enormous promise in meeting the growing energy demands of fast-evolving portable electronics, electric car markets, and other industries, as biowaste has been making steady progress in supercapacitor technologies.

SC electrodes have been made using a variety of carbon-based substances, ranging from basic ACs to sophisticated nanostructured carbons. Biomass resources have been employed as precursors to manufacture carbon electrodes and other components for SCs, and their widespread availability and inexpensive costs have sparked an interest. Biomass resources and their exploitation have piqued the world's energy sector's attention, and their relevance will only grow as the focus shifts to renewable energy sources and energy conservation.

Using biomass in SCs will give a good chance to reduce greenhouse gas emissions and global warming.

The production of porous carbons derived from wood and plant tissues, agricultural residues, industrial effluents, and municipal waste materials has been used as precursor materials to prepare carbon electrodes for supercapacitors. Lignin, cellulose fiber, and hemicellulose obtained from biomass are excellent resources for synthesizing activated carbon compounds to develop flexible electrodes for SCs. Thermochemical processes and biochemical processes are methods for obtaining energy from biomass.

The production of activated carbons using these methods requires more investigation in terms of environmental and economic issues. It should be noted that different volatile and non-volatile toxic gases can be emitted during conversion processes. Biomass has the potential to offer a cost-effective and long-term source of energy. Using biomass in SCs manufacturing instead of biowaste disposal can help to reduce air pollution, forest fire danger, GHG emissions, hazardous material release, and land degradation. Organic waste decomposes in landfills and emits methane. As a result, diverting these wastes for biomass production reduces landfill volume and methane emissions.

Although biomass-based supercapacitors are environmentally friendly and cost effective, they do cause soil erosion, nutrient depletion, water quality degradation, and air pollution. Thus, waste SCs are classified as hazardous products and require a special treatment facility. Researchers have not paid enough attention to waste supercapacitor recycling yet. Nonetheless, the potential risks from certain traditional electrolytes, solvents, and polymer binders should be considered after the device's life cycle. SCs with binder-free electrodes are gaining considerable popularity to eliminate the redundancy of using additional materials and their potential hazards.

Acknowledgment

References

1 Z. Gao, Y. Zhang, N. Song, X. Li, *Mater. Res. Lett.* **2017**, *5*, 69–88.

2 S. S. Shah, M. A. Aziz, Z. H. Yamani, *Chem. Rec.* **2022**, *22*, e202200018.

3 S. S. Shah, S. M. Abu Nayem, N. Sultana, A. J. Saleh Ahammad, M. Abdul Aziz, *ChemSusChem* **2022**, *15*, e202101282.

4 R. B. Marichi, V. Sahu, R. K. Sharma, G. Singh, *Handb. Ecomater.* **2017**, 1–26.

5 T. Christen, M. W. Carlen, *J. Power Sources* **2000**, *91*, 210–216.

6 S. S. Shah, M. A. Alfasane, I. A. Bakare, M. A. Aziz, Z. H. Yamani, *J. Energy Storage* **2020**, *30*, 101562.

7 N. C. Deb Nath, S. S. Shah, M. A. A. Qasem, M. H. Zahir, M. A. Aziz, *ChemistrySelect* **2019**, *4*, 9079–9083.

8 H. Yang, R. Yan, H. Chen, D. H. Lee, C. Zheng. *Fuel* **2007**, *86*, 1781–1788.

9 S. S. Shah, H. T. Das, H. R. Barai, M. A. Aziz. *Polymers (Basel)* **2022**, *14*, 270.

10 C. Zhong, Y. Deng, W. Hu, J. Qiao, L. Zhang, J. Zhang. *Chem. Soc. Rev.* **2015**, *44*, 7484–7539.

11 S. S. Shah, M. A. Aziz, E. Cevik, M. Ali, S. T. Gunday, A. Bozkurt, Z. H. Yamani. *J. Energy Storage* **2022**, *56*, 105944.

12 S. S. Shah, M. N. Shaikh, M. Y. Khan, M. A. Alfasane, M. M. Rahman, M. A. Aziz. *Chem. Rec.* **2021**, *21*, 1631–1665.

13 A. K. Mohamedkhair, M. A. Aziz, S. S. Shah, M. N. Shaikh, A. K. Jamil, M. A. A. Qasem, I. A. Buliyaminu, Z. H. Yamani. *Arab. J. Chem.* **2020**, *13*, 6161–6173.

14 M. A. Aziz, S. S. Shah, S. M. A. Nayem, M. N. Shaikh, A. S. Hakeem, I. A. Bakare. *J. Energy Storage* **2022**, *50*, 104278.

15 A. Helal, S. Shaheen Shah, M. Usman, M. Y. Khan, M. A. Aziz, M. Mizanur Rahman, *Chem. Rec.* **2022**, *22*, e202200055.

16 M. Usman, M. Humayun, S. S. Shah, H. Ullah, A. A. Tahir, A. Khan, H. Ullah, *Energies.* **2021**, *14*, 2281.

17 I. Khan, N. Baig, S. Ali, M. Usman, S. A. Khan, K. Saeed, *Energy Storage Mater* **2021**, *35*, 443–469.

18 Z. Chen, X. Wang, Z. Ding, Q. Wei, Z. Wang, X. Yang, J. Qiu. *ChemSusChem* **2019**, *12*, 5099–5110.

19 J. Chmiola, G. Yushin, Y. Gogotsi, C. Portet, P. Simon, P. L. Taberna. *Science (80-.).* **2006**, *313*, 1760–1763.

20 J. Zhou, S. Zhang, Y. N. Zhou, W. Tang, J. Yang, C. Peng, Z. Guo. *Electrochem. Energy Rev.* **2021**, *4*, 219–248.

21 E. Taer, Sugianto, M. A. Sumantre, R. Taslim, Iwantono, D. Dahlan, M. Deraman. *Adv. Mater. Res.* **2014**, *896*, 66–69.

22 J. M. Yang, H. Z. Wang, C. C. Yang. *J. Memb. Sci.* **2008**, *322*, 74–80.

23 H. Yu, Q. Tang, J. Wu, Y. Lin, L. Fan, M. Huang, J. Lin, Y. Li, F. Yu. *J. Power Sources* **2012**, *206*, 463–468.

24 B. G. Choi, J. Hong, W. H. Hong, P. T. Hammond, H. Park. *ACS Nano* **2011**, *5*, 7205–7213.

25 T. Ye, Y. Sun, X. Zhao, B. Lin, H. Yong, X. Zhang, L. Guo. *J. Mater. Chem.* **2018**, *6*, 18994–19003.

26 J. Liu, S. Min, F. Wang, Z. Zhang. *J. Power Sources* **2020**, *466*, 228347.

27 E. Senokos, V. Reguero, L. Cabana, J. Palma, R. Marcilla, J. José Vilatela, E. Senokos, J. Palma, R. Marcilla, V. Reguero, L. Cabana, J. J. Vilatela. *Adv. Mater. Technol.* **2017**, *2*, 1600290.

28 S. Rajeevan, S. John, S. C. George. *J. Power Sources* **2021**, *504*, 230037.

29 Y. Gao. *Nanoscale Res. Lett.* **2017**, *12*, 387.

30 W. Li, J. Chen, J. Zhao, J. Zhang, J. Zhu. *Mater Lett.* **2005**, *59*, 800–803.

31 J. Jose, V. Thomas, V. Vinod, R. Abraham, S. Abraham. *J. Sci. Adv. Mater. Devices* **2019**, *4*, 333–340.

32 M. E. L. Hu, G. Zheng, J. Yao, N. Liu, B. Weil. *Energy Environ. Sci.* **2013**, *6*, 513–518.

33 B. Dyatkin, V. Presser, M. Heon, M. R. Lukatskaya, M. Beidaghi, Y. Gogotsi. *ChemSusChem* **2013**, *6*, 2269–2280.

34 C. Shen, Y. Xie, B. Zhu, M. Sanghadasa, Y. Tang, L. Lin. *Sci. Rep.* **2017**, *7*, 1–8.

35 L. Borchardt, M. Oschatz, S. Kaskel. *Chem. Eur. J.* **2016**, *22*, 7324–7351.

36 G. Singh, K. S. Lakhi, S. Sil, S. V. Bhosale, I. Y. Kim, K. Albahily, A. Vinu. *Carbon* **2019**, *148*, 164–186.

37 L. S. Blankenship, R. Mokaya. *Energy Environ. Sci.* **2017**, *10*, 2552–2562.

38 L. Wang, Y. Shi, Y. Wang, H. Zhang, H. Zhou, Y. Wei, S. Tao, T. Ma. *Chem. Commun.* **2014**, *50*, 1701–1703.

39 A. Bhatnagar, M. Sillanpää, A. Witek-Krowiak. *Chem. Eng. J.* **2015**, *270*, 244–271.

40 P. J. M. Carrott, M. M. L. R. Carrott. *Bioresour. Technol.* **2007**, *98*, 2301–2312.

41 D. Zhao, Q. Zhang, W. Chen, X. Yi, S. Liu, Q. Wang, Y. Liu, J. Li, X. Li, H. Yu. *ACS Appl. Mater. Interfaces* **2017**, *9*, 13213–13222.

42 C. K. Roy, S. S. Shah, A. H. Reaz, S. Sultana, A. Chowdhury, S. H. Firoz, M. H. Zahir, M. A. Ahmed Qasem, M. A. Aziz. *Chem. – An Asian J.* **2021**, *16*, 296–308.

43 Z. Bi, Q. Kong, Y. Cao, G. Sun, F. Su, X. Wei, X. Li, A. Ahmad, L. Xie, C.-M. Chen. *J. Mater. Chem. A* **2019**, *7*, 16028–16045.

44 C. Mensah-Darkwa, K. Zequine, P. K. Kahol, G. R. K. *Sustainability* **2019**, *11*, 414.

45 S. Song, F. Ma, G. Wu, D. Ma, W. Geng, J. Wan. *J. Mater. Chem. A* **2015**, *3*, 18154–18162.

46 P. Zhu, T. Cai. *Sensors Actuators B Chem.* **2015**, *213*, 202–208.

47 C. Wang, H. Wang, B. Dang, Z. Wang, X. Shen, C. Li, Q. Sun. *Renew. Energy* **2020**, *156*, 370–376.

48 M. Ashraf, S. S. Shah, I. Khan, M. A. Aziz, N. Ullah, M. Khan, S. F. Adil, Z. Liaqat, M. Usman, W. Tremel, M. N. Tahir. *Chem. - A Eur. J.* **2021**, *27*, 6973–6984.

49 M. Rauf, S. S. Shah, S. K. Shah, S. N. A. Shah, T. U. Haq, J. Shah, A. Ullah, T. Ahmad, Y. Khan, M. A. Aziz, K. Hayat. *J. Saudi Chem. Soc.* **2022**, *26*, 101514.

50 G. Hegde, S. A. Abdul Manaf, A. Kumar, G. A. M. Ali, K. F. Chong, Z. Ngaini, K. V. Sharma. *ACS Sustain. Chem. Eng.* **2015**, *3*, 2247–2253.

51 E. Raymundo-Piñero, M. Cadek, F. Béguin. *Adv. Funct. Mater.* **2009**, *19*, 1032–1039.

52 N. Konikkara, N. Punithavelan, L. J. Kennedy, J. J. Vijaya. *Clean Technol. Environ. Policy* **2017**, *19*, 1087–1098.

53 N. Balahmar, A. C. Mitchell, R. Mokaya. *Adv. Energy Mater.* **2015**, *5*, 1500867.

54 P. Williams, A. Reed. *Biomass Bioenergy* **2006**, *30*, 144–152.

55 M. Sevilla, C. Falco, -M.-M. Titirici, A. B. Fuertes. *RSC Adv* **2012**, *2*, 12792–12797.

56 J. Wang, S. Kaskel. *J. Mater. Chem.* **2012**, *22*, 23710–23725.

57 T. Wang, Y. Zhai, Y. Zhu, C. Li, G. Zeng. *Renew. Sustain. Energy Rev.* **2018**, *90*, 223–247.

58 M. Heidari, A. Dutta, B. Acharya, S. Mahmud. *J. Energy Inst.* **2019**, *92*, 1779–1799.

59 P. Zhang, Y. Gong, Y. Lv, Y. Guo, Y. Wang, C. Wang, H. Li. *Chem. Commun.* **2012**, *48*, 2334–2336.

60 P. Zhang, Y. Gong, Z. Wei, J. Wang, Z. Zhang, H. Li, S. Dai, Y. Wang. *ACS Appl. Mater. Interfaces* **2014**, *6*, 12515–12522.

61 X. Liu, N. Fechler, M. Antonietti. *Chem. Soc. Rev.* **2013**, *42*, 8237–8265.

62 A. Demirbas. *Energy Educ. Sci. Technol.* **2006**, *16*, 53.

63 G. Genon, D. Panepinto, F. Viggiano, *WIT Trans. Ecol. Environ.*, WIT Press, **2014**, pp. 995–1006.

64 M. Ashraf, I. Khan, M. Usman, A. Khan, S. S. Shah, A. Z. Khan, K. Saeed, M. Yaseen, M. F. Ehsan, M. N. Tahir, N. Ullah. *Chem. Res. Toxicol.* **2020**, *33*, 1292–1311.

65 I. Ahmed, M. A. Zia, H. Afzal, S. Ahmed, M. Ahmad, Z. Akram, F. Sher, H. M. N. Iqbal. *Sustainability.* **2021**, *13*, 4200.

66 A. M. Omer. *Sustain. Energy Rev.* **2008**, *12*, 1562–1587.

67 J. Vasco-Correa, S. Khanal, A. Manandhar, A. Shah. *Bioresour. Technol.* **2018**, *247*, 1015–1026.

68 G. Berndes, M. Hoogwijk, R. van den Broek. *Biomass Bioenergy* **2003**, *25*, 1–28.

69 M. Yaseen, M. A. K. Khattak, M. Humayun, M. Usman, S. S. Shah, S. Bibi, B. S. U. Hasnain, S. M. Ahmad, A. Khan, N. Shah, A. A. Tahir, H. Ullah. *Energies* **2021**, *14*, 7779.

70 I. Hadjipaschalis, A. Poullikkas, V. Efthimiou. *Renew. Sustain. Energy Rev.* **2009**, *13*, 1513–1522.

71 S. Khandaker, M. M. Bashar, A. Islam, M. T. Hossain, S. H. Teo, M. R. Awual. *Renew. Sustain. Energy Rev.* **2022**, *157*, 112051.

72 T. Abbasi, S. A. Abbasi. *Renew. Sustain. Energy Rev.* **2010**, *14*, 919–937.

73 A. Kumar, T. Bhattacharya, S. M. Mozammil Hasnain, A. Kumar Nayak, M. S. Hasnain. *Mater. Sci. Energy Technol.* **2020**, *3*, 905–920.

74 A. Arabameri, S. Saha, J. Roy, J. P. Tiefenbacher, A. Cerda, T. Biggs, B. Pradhan, P. T. Thi Ngo, A. L. Collins. *Sci. Total Environ.* **2020**, *726*, 138595.

75 B. Bhagowati, K. U. Ahamad. *Ecohydrol. Hydrobiol.* **2019**, *19*, 155–166.

76 D. Gielen, F. Boshell, D. Saygin, M. D. Bazilian, N. Wagner, R. Gorini. *Energy Strateg. Rev.* **2019**, *24*, 38–50.

3

Biomass Utilization in Supercapacitors for the Circular Economy

Runa Akter[1], Md. Raquibul Hassan Bhuiyan[2], Saidur R. Chowdhury[3,4], Muhammad Muhitur Rahman[5], and Syed Masiur Rahman[6,*]

[1] *Institute of Forestry and Environmental Sciences, University of Chittagong, Chittagong 4331, Bangladesh*

[2] *Department of Architecture, Bangladesh University of Engineering and Technology, Dhaka 1000*

[3] *Department of Civil Engineering, College of Engineering, Prince Mohammad Bin Fahd University (PMU), Al khobar, KSA*

[4] *SC Environmental Solutions, 1 Greystone Walk Dr, Toronto ON, M1K 5J3, Canada*

[5] *Department of Civil and Environmental Engineering, College of Engineering, King Faisal University, Al-Ahsa 31982, Saudi Arabia*

[6] *Applied Research Center for Environment & Marine Studies, King Fahd University of Petroleum & Minerals (KFUPM), Dhahran 31260, Eastern Province, Saudi Arabia*

* *Corresponding author*

3.1 Introduction

The old open-ended system, sometimes dubbed the linear economy, creates severe problems with economic, social, and environmental sustainability [1]. In a typical linear economy (Figure 3.1), natural resources (R) are used to generate (P) consumer and capital goods (C), which in turn generate (U) utility or well-being. By relying on the wasteful take-make-discard loop, the linear economy's fundamental mechanics are destructive to the environment, incapable of providing necessary services to our planet's rising population, and naturally results in strained profitability.

To counter this, circular economy (CE) is an economic system that focuses on resource conservation, repurposing, recycling, and reuse throughout the entire value chain from production to consumption. At the micro, meso, and macro levels, it aims to achieve sustainable development, resulting in enhanced environmental quality, economic prosperity, and social equality for existing generations and the generations to come. Innovative business models and attentive customers make this feasible [3]. Reducing dependence on virgin resources and recycling waste-derived resources is a sustainable flow paradigm that reduces negative environmental impacts [4]. Product-service systems, remanufacturing, corporate social responsibility, the sharing economy, and zero waste are all components of industrial ecology. For example, CE stresses (i) remanufacturing, refurbishing and repair, (ii) utilization of renewable energy throughout the value chain and the cradle-to-cradle life cycle, and (iii) reuse of product, component, and material [5]. A researcher provides a simplified model of a circular model [2], as shown in Figure 3.2. Adding (R) for recycling and
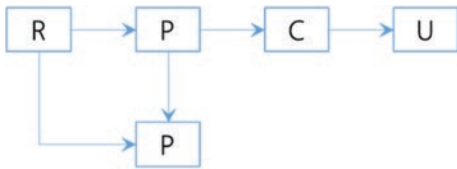
Figure 3.1 A schematic diagram of the conventional linear economy. *Redrawn from ref* [2].
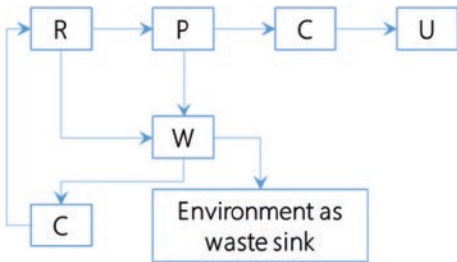

Figure 3.2 A simplified illustration of a circular economy model. *Redrawn from ref* [2].

(W) for waste completes the cycle and circularize the economy, as shown in this model. Due to missed opportunities and physical laws, it is impossible to recycle all waste.

Any industrial product, including supercapacitors, requires a sustainable supply of raw materials for SCs. A linear production path that depletes resources and throws away their value-added products will exacerbate climate change and other environmental issues. It's no secret that many resources, such as food and water, are becoming increasingly scarce as time goes on (Figure 3.3). A logarithmic scale represents the amount of each element in the Earth's crust and atmosphere, with the larger tiles representing more of the element. It's important to note that the man-made elements technetium and promethium (shown in white in the Figure 3.3) do occur naturally on Earth but in extremely small quantities. This image calls attention to the rapid depletion of elemental resources as well as the fact that many of these elements come from countries where mining rights are contested [6].

The automotive and stationary industries are driving an increase in the demand for electrochemical energy storage. In the future, obtaining essential raw materials and managing end-of-life systems will be challenging tasks. From the perspective of the CE, it is vital to identify reuse and recycling solutions that can make the demand for goods and services sustainable [8]. This chapter will mainly elaborate on the role of biomass-based SC in waste elimination, environmental pollution, biodiversity protection, renewable energy, renewable resources, reduced chemical substance use, greenhouse gas (GHG) emission reduction, healthy and resilient soils, and economic benefits.

3.2 Circular Economy Framework

The production of bioenergy and bioproducts from biomass, especially bio-waste streams, has sparked global interest in developing a circular economy [9]. Incorporating biomass into the circular economy can substantially increase the production of sustainable bioproducts,
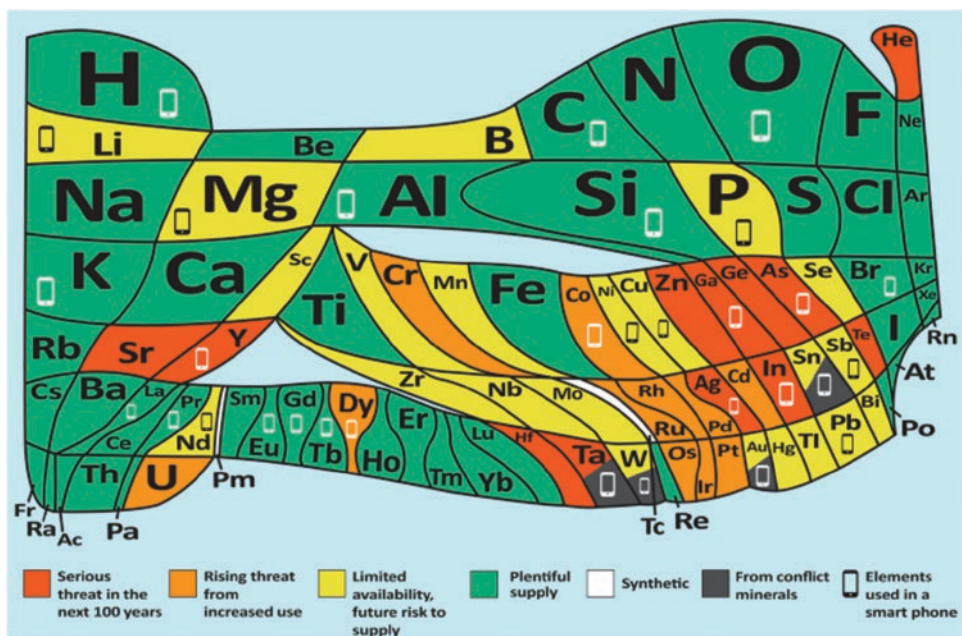
Figure 3.3 The periodic table in light of the rarity of the elements. *Reproduced with permission* [7]. *Reproduced under the term CC-BY-ND-4.0. Copyright 2021, European Chemical Society.*

including SCs. A conceptual circular economy framework consisting of significant material and energy flows for biomass-based SCs is presented in Figure 3.4. Different elements of a SC, including an electrode, electrolyte, separator, binding materials, current collector, and packaging materials, are produced from biomass. After their design lives, different elements of biomass containing carbon, cellulose, gelatin, protein, fibre, and other materials can be recovered and used for producing the same or other elements of SCs. The unused biomass after material recovery will be returned to the biological environment or could be used for energy generation and water treatment after appropriate modifications. The manufacturing process of the elements of SCs requires energy, water, and other resources, which the recovery and bioenergy development could support. Finally, the circular economy approach will ensure significant methane emissions from the biomass used in SCs. However, this conceptual framework is mainly adopted to explain circular economy features pertinent to SCs.

3.3 Elimination of Waste through Biomass Utilization in Supercapacitors

Large volumes of waste are generated by municipal, industrial and agricultural activities around the globe. Continuous improvement in the handling, management, or disposal of waste from the manufacturing industry or other activities has been identified as one of the most important tasks within the scientific community.
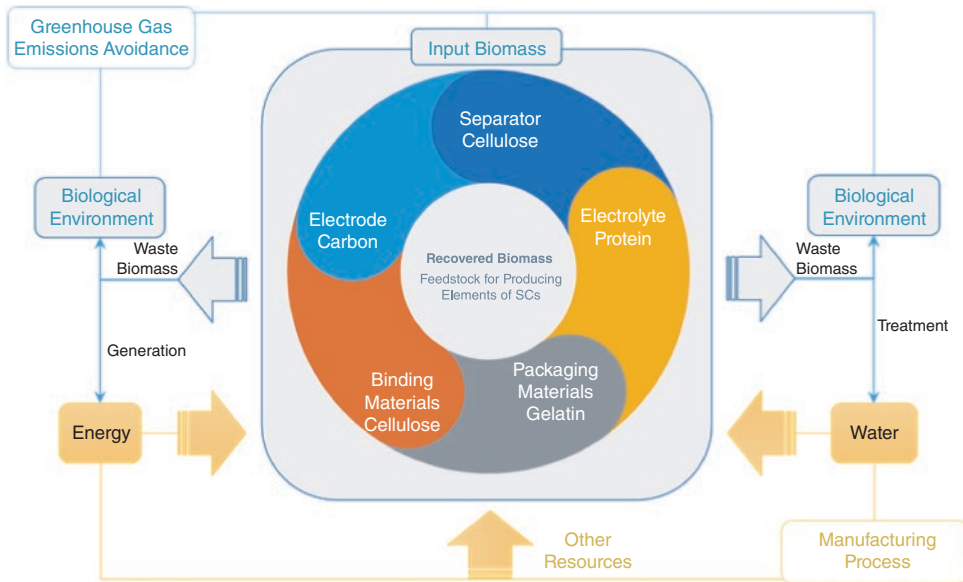
Figure 3.4   A conceptual circular economy framework consists of major material and energy flows for biomass-based SCs.

   The ability to minimize waste has the potential to generate environmental gains. In manufacturing, sustainability has come to mean creating products that can be recycled entirely, using environmentally friendly or green production methods, and reusing or recycling products at the end of their useful lives. Waste disposal is closely associated with sustainable development. Waste reduction is an important part of environmental protection and improvement, and of social and economic satisfaction maximization. This could be achieved through recycling, reuse processes, or the discovery of devices from biowaste products. Biomass or biowaste can be eliminated through the uses in SC creation (referred to as green production processes) [10]. SCs can use carbon derived from biowaste, including waste greenery, dead or dying leaves and flowers residues, waste cereals, vegetables and fruits, fruit peels, nuts, shells, plant seeds/roots, and hazardous sewage (desk, domestic and industrial effluent by-products, etc.), as well as animal and microorganisms wastes [10, 11]. Biowaste materials generated by households, industries, animals, and municipal waste can be used to develop activated carbon (AC) electrodes. Carbon-based biomass can be used as a form of energy storage because it is readily available and has unique porous structures that make it environmentally friendly, renewable, and free of harmful chemicals [12, 13]. To synthesize AC, biowaste can be used as a carbon-rich organic material. Researchers examined various biowaste materials, such as coconut shells, soybeans, bamboo, eggshells, dead neem leaves, cow dung, and banana peels, to produce high porosity AC for use in SCs [14, 15].

   Biowaste, such as from animals, minerals, plants, and vegetables, have been used to produce activated carbon for use as electrode material in electrochemical energy systems [10, 11]. In addition, the researchers studied various porous carbon derived from biowaste for electrochemical energy storage systems, as well as various performance parameters and

Table 3.1 Renewable biowastes-derived carbons for supercapacitors.

Biowastes derived carbons	Surface area $(m^2\ g^{-1})$	Specific capacitance $(F\ g^{-1})$	Energy density $(Wh\ kg^{-1})$	Remarks/ challenges for bio-waste supercapacitor	Ref.
Remains of trees, plants, wood, dead leaves, and flowers	475– 3550	21–406	12–80	...	[11, 30]
Food wastes, vegetables, fruit peels, and shells	350–3831	127–591	3–53	Compatibility (ecotoxicity and leaching control)	[31, 32]
Nuts shells, plant seeds/roots	644–3549	120–440	5–79	...	[33, 34]
Office, household, and industrial wastes	50–2616	122.8– 480	15–45	Chemical activation	[35, 36]
Human, animal, and microorganisms wastes	109– 2570	41– 410	7–67.5	Challenges for industrialization standard	[30, 37]
Miscellaneous wastes (e.g., cigarette butts, tobacco wastes, milk powder, paper pulp mill sludge etc.)	1095 –3300	95 ($0.12A\ g^{-1}$)– 442 ($0.5A\ g^{-1}$)	7 –31	Sufficient energy density, low yield	[11]

storage mechanisms of the different kinds of SCs investigated by the scientists (as shown in Table 3.1). Because of this, a country's economy gets a boost from using biowaste for SC applications, which not only helps to eliminate waste but also generates revenue [16, 17]. Biomass-derived activated carbons, which can be used as electrode material in SC applications, are becoming increasingly popular as a solution to waste disposal and waste elimination issues [18–29]. It transforms waste into a valuable product and offers an economical solution for supercapacitor technology. Table 3.1 shows different types of renewable biowastes-derived carbons for SCs.

3.4 Resource Recovery through Biomass Utilization in Supercapacitors

Biomass is a rich, dispatchable, durable, and environmentally friendly resource that is gaining traction in the field of electrochemical capacitors technology. It's an excellent raw material for making carbon materials. Global demand for renewable energy sources has piqued scientists' interest in recent decades. As a result of their high surface area, strong conductivity, and long-term stability, supercapacitor electrode materials like carbon and carbon-based materials are becoming increasingly popular in the field. Clean energy from renewable sources necessitates developing and improving new materials for energy storage (such as biomass in supercapacitors). The biowastes form and shape mix is equivalent to diverse carbon materials with varying architectures and performance levels. In addition to making the activation process more accessible, the porous structure of biowastes also makes it easier to create porous carbons with a greater specific surface area. As an added

benefit, the hard carbons generated from biowaste have a tube that adds strength, making them ideal for solid-state batteries (SSBs).

Biomass resources with a high degree of graphitization, manageable flaws, low oxygen, and high nitrogen content can be more efficient in terms of conductivity and yield when compared to other biomass resources [11, 30]. As a result of this, the availability of nitrogen and phosphorus and different substituents in fruit peels or fruit-based biomass provide more suitable circumstances for creating AC. Due to their porous structure, their high specific surface area (SSA) and heteroatom enrichment, seeds, flowers, and nuts-based wastes are more promising for manufacturing AC [10]. Using activated carbons derived from biowaste is a viable strategy for developing small pores (such as micropores and mesopores) and heteroatom dosing [31, 32]. Figure 3.5 demonstrates green resource recovery through biomass utilization in SCs. The outcome of biomass resources in a supercapacitor is closely associated with clean energy production, thus contributing to sustainable development.

3.4.1 Electrolyte

Supercapacitors, a novel energy storage device, have distinct advantages over traditional energy storage technologies, including safety and environmental friendliness, quick charging and discharging, low power consumption, and superior power density and sturdy construction [38–42]. One crucial component that affects electrochemically effective supercapacitors is the electrolyte. Polymer electrolyte compounds, in contrast to non-renewable electrolytes, include polyethylene oxide, polyvinyl chloride, poly methyl methacrylate, and polyvinylidene fluoride (PVDF). [43]. The capacitances produced from organic electrolytes in carbon-based ethylene sulfide (ES) are frequently lower than those
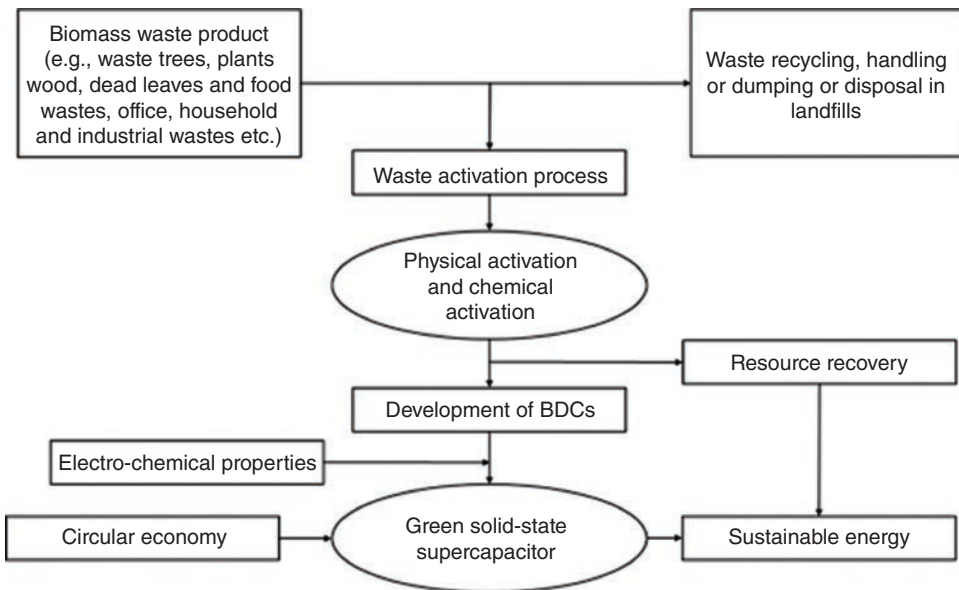

Figure 3.5 Green resource recovery through biomass utilization in SC. *Redrawn from the concept in ref* [30].

from aqueous electrolytes because the specific surface area and pore size/size distribution of the carbon components of an ES's affect its specific capacitance [44]. After membrane production, pure SPI (solid permeable interface) has weak mechanical strength and water resistance, so it typically needs to be changed physically or chemically. SPI/PAM/PTGE cross-linked composite films were created by Xu et al. by doping polyacrylamide (PAM) and 1,2,3-propanetriol-diglycidyl ether (PTGE) in the SPI. As a result, the film's mechanical performance and water resistance were greatly enhanced [45]. Gao et al. performed a straightforward ammonium persulphate start to graft-modify SPI with AA (SPI-g-PAA (polyacrylic acid)). After sufficient adsorption of 1 M lithium sulfate (Li_2SO_4) aqueous solution by the membrane material, the polymer electrolyte was subsequently created. Finally, they created supercapacitors that can function steadily within a voltage window of 0–2 V by mixing the polymer electrolytes and activated carbon electrodes. With a power density of 734.38 $W\,kg^{-1}$ and an optimized single electrode specific capacitance of up to 293.08 $F\,g^{-1}$ and 38.76 $Wh\,kg^{-1}$, this device has promising application potential [46].

3.4.2 Electrodes

Electrochemical double-layer capacitors (EDLCs) are a high-power energy storage technology with a long life. The use of EDLCs in the expanding renewable energy ecosystem is increasing as more efforts are made to address climate change, and they already have a range of unique applications. Their energy storage approach relies on fast ions from an electrolyte and reversible ion adsorption onto a high-surface-area porous material. Commercial electrodes composed of activated carbon and organic electrolytes with an operating voltage of about three volts are most commonly used [47]. These devices are made by coating enormous sheets of metal (Al) current collectors with quick, low-cost roll-to-roll techniques. Various biomass resources have been used as precursor materials to prepare carbon electrodes for SCs to date, including multiple types of wood and plant tissues, agricultural residues, industrial effluent, and domestic waste. They have gained considerable interest due to their widespread availability and low cost. According to a recent study, Guar gum (GG), potato starch (PS), and wheat starch were examined and compared to the commonly used aqueous binder carboxymethyl cellulose (CMC) in EDLCs. The 3:1 blend of PS and GG produced the best coating rheology, allowing for high solid contents and flexible high-mass-loading electrodes. PS75/GG25 could withstand bending tests at up to 7 $mg\,cm^{-2}$, which is twice as much as CMC. SEM microscopy revealed good active material, conductive additive dispersion, and minimized crack formation during drying [48].

3.4.3 Packaging Materials and Separators

To meet the increasing global energy demand, one of the most challenging problems is to store and transfer energy into many accessible forms. Currently, fossil fuels are being consumed at an alarming rate, causing significant environmental consequences. To meet the demands of energy-driven applications, building a sustainable and renewable electrical energy storage device is critical. The electrochemical performance of a SC is determined by four crucial components, namely electrode, electrolyte, current collector, and separator. The separator is one of these four components that plays two crucial roles; it is responsible

for preventing internal short-circuits between the anode and cathode, as well as allowing ions to move freely throughout the interconnected electrolyte-soaked porous structure [49, 50]. Biopolymer membranes made from biomass have received substantial interest due to their critical role in environmental protection and supercapacitor electrochemical performance. A recent study demonstrated that cellulose nanofibril (CNF) membranes of varying thicknesses can be made from agricultural rice straw waste using a simple and cost-effective solution casting method and then employed as supercapacitor separators. Among the constructed membranes, CNF membranes with a thickness of $30\,\mu m$ (CNF 30) had 51% porosity, 225% electrolyte absorption, and the highest mesopore (17.2%) with uniform pore size distribution. The supercapacitors (CNF 30-SC) with CNF 30 as the supercapacitor separator had the maximum specific capacitance, energy density, and power density of $150.7\,F\,g^{-1}$, $30.2\,Wh\,kg^{-1}$, and $240.0\,W\,kg^{-1}$, respectively [51]. In addition, CNF 30 membrane from rice straw can be a good alternative to commercial membranes for high-performance supercapacitor devices [51].

3.5 Reduction of Chemical Substances through Biomass Utilization in Supercapacitors

In SCs, electrochemical double-layer capacitors, activated carbon, carbon nanofibers, and graphene are utilized as electrode materials, and electrolytes (such as KOH, H_2SO_4 and biomass-derived electrolytes) are employed between the electrodes. Pseudocapacitors can also be made from polymer electrolytes and molecules with O and N functional groups, as well as metallic oxides, hydroxides, and sulfides. Carbon nanotubes, often known as graphene, exhibit outstanding mechanical and chemical properties [52, 53]. Energy storage substances continue to pose several challenges despite these chemicals' improved performance. Chemical vapour deposition is used to make graphene, which has environmental impacts and is unsustainable [52, 54]. Active carbon generated from graphite and petroleum coke is non-renewable and harmful to the environment. Furthermore, nanostructured carbons derived from graphite and petroleum coke are frequently developed under challenging conditions and at a high cost [11]. In contrast, biomass is a renewable carbon source that offers several advantages. Because of their availability, cheapness, renewability, and environmental friendliness, biomass has been exploited to produce critical nanoparticles of carbon materials that could lessen dependence on ACs made from graphene, petroleum coke-derived active carbon, and fossil fuels [55–59]. As a result, incorporating biomass into the electrode manufacturing process reduces the need for non-renewable carbon in SC production and operation. It is sustainable and low cost to use abundant biomass to create biomass-based materials with outstanding characteristics for SC. The capacity of biomass-based materials to conduct electrochemical processes is influenced by chemical content, pore structure, and experimental conditions. Carbon nanoparticles made from biomass have shown promise in energy storage due to their unique properties (high electrical conductivity, surface area, thermal and chemical stability, etc.) particularly in electric double-layer capacitors [52].

Carbon materials derived from biomass are undeniably more effective and resilient energy storage and conversion devices, resulting in fewer non-renewable chemicals being used in SC manufacturing. Direct carbonization of biomass, hydrothermal carbonization, and carbonization are all environmentally acceptable ways to make hetero atoms-functionalized

carbon with excellent electrochemical performance, high-rate capability, and cycle capacity. However, biowaste can disintegrate and release harmful substances into the natural environment, damaging land and water if not properly managed. Thus, it can be concluded that using biowaste in SC manufacturing can drastically lower the chance of this kind of pollution.

3.6 Environmental Pollution Control by Using Biomass in Supercapacitors

In recent years, as energy demand and fossil fuel usage have risen fast and environmental pollution has worsened, it has become critical to discover and develop alternative, ecologically friendly energy sources and high-efficiency renewable energy conversion and storage systems [53, 60, 61]. Porous carbon derived from natural biomass wastes is prominent as electrode material in SCs due to its good qualities of large surface area, cost-effectiveness, readily available precursor, ease of manufacture, and ecofriendly nature. Biomass-based SCs also address the challenges of safe waste ingredient recycling and fossil fuel use.

Carbon-based electrode materials derived from biomass/waste materials such as human hair, waste coffee grounds, ginkgo shells, sugarcane bagasse, wood, banana peel, fallen leaves, leather waste, tea leaves, stiff silkworm, and waste paper, in comparison to traditional electrode materials, are well-known and environmentally friendly high-performance renewable energy conversion and storage devices [62]. Agricultural biomass, also known as lignocellulosic biomass, is among the most abundant biodegradable materials. Lignin, cellulose, and hemicellulose materials are separated from lignocellulosic materials. Lignin and cellulose are essential ingredients in the production of activated carbon molecules [63]. Carbon compounds are often created through direct pyrolysis of biomass (also known as physical activation) or chemical activation to achieve a high value of Brunauer, Emmett and Teller (BET) surface area. Both activation methods have their own set of benefits [64–66]. It is possible to control environmental pollution using biomass-based supercapacitors, described in detail below.

3.6.1 Reduction of Air Pollution

Traditional biomass waste disposal has two significant environmental consequences: air pollution and landfill overcrowding. Open burning of biomass waste produces a lot of pollutants, including smoke, particulates, and hydrocarbon emissions. Furthermore, agricultural waste is burned in an open fire, producing significant amounts of visible smoke and particles. It also produces a lot of NOx, CO, and hydrocarbons, all contributing to ozone depletion in the atmosphere. Agricultural burning is a severe impediment to air quality standards in many areas [67]. It follows that using biomass waste to create supercapacitors will have a significant positive impact on the environment.

3.6.2 Reduction of Solid Waste

It is one of the significant aspirations for developing a more sustainable and environmentally friendly energy source using nano-sized carbon compounds derived from vehicle and company emissions. A few of the primary contributors to global warming and human

health issues are soot particles (vegetable oil, diesel, wood, and charcoal soot), leather waste, and waste tires [68]. Therefore, using these compounds may help to deplete the threat they produce. When organic waste is dumped in a landfill, it decomposes and produces methane, a powerful greenhouse gas. As a result, diverting these wastes for energy generation lowers landfill volume and methane emissions [69].

3.6.3 Enhancing Ecosystems

Dead and diseased trees, felled woody debris of various types, and forest growth stock with increasing density are all sources of fuel in the woods. In terms of forest fire danger, dead and diseased wood, both standing and felled, is more prone to ignite, burn hotter, and spread fire than healthy wood. Increasing forest fuel loads make wildfires fiercer and more destructive than pre-industrial flames. Using biomass in SCs may therefore reduce the risk of forest fires. Fuel loading degrades forest and watershed health and ecosystem function. Contrary to healthy, largely undisturbed forest ecosystems, most modern forests have significant canopy closure levels. In this habitat, less rainwater enters the water table as runoff. Reduced runoff means less water reaches the meadows and lowlands, water which is usually retained throughout the wet season and slowly released during the dry season. Using forest fuels to produce biomass may thereby improve ecosystem health.

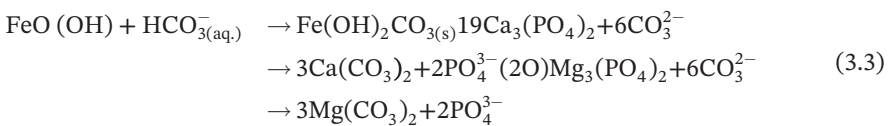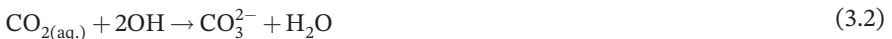## 3.7 Greenhouse Gas Emission Reduction

The depletion of natural resources and the degradation of the global environment have made the need for environmentally friendly and renewable energy sources imperative. As a result of human actions, such as the combustion of fossil fuels, CO_2 has been released into the atmosphere worldwide, a significant contributor to global warming [70]. CO_2 concentrations in the air are currently substantially beyond the highest allowed limit for climatic safety (350 parts per million) for a habitable planet and are expected to reach 700 parts per million over the twenty-first century [71]. As a result, global warming is predicted to lead to a rise in global temperature and potentially alter the entire ecosystem irreversibly [72, 73]. The breach of the climatic safety threshold emphasizes the critical nature of corrective efforts to rein in anthropogenic greenhouse gas (GHG) emissions. CO_2 capturing and storage has been considered the most viable strategy for resolving this global warming issue [74–78]. Along with environmental concerns, continued reliance on fossil fuels raises an urgent concern about the resource's possible depletion, which, combined with rising global energy demand, has sparked widespread interest in energy storage technologies such as SCs. Nowadays, biomass is intensively researched for its environmentally friendly and renewable features. At the moment, thermochemical converting biomass is among the most efficient methods, owing to the flexibility of natural resources and numerous derivatives such as synthesis gas, liquid fuel, and porous activated carbon. Porous carbon has several benefits, including a large specific surface area, high conductivity, and desirable physicochemical qualities [79, 80]. CO_2 biomaterials and catalysts in supercapacitors can benefit from microporous carbon, which has many catalytic surfaces for preserving gas molecules and small ions [81, 82].

3.7.1   Role of Biomass in Emission Mitigation

As biomass-based SCs sequester a significant amount of carbon, the use of SCs can be considered as a case of carbon emissions avoidance, at least for the short term. In addition, using biomass in SCs also contributes to avoiding methane formation resulting from anaerobic decomposition. Biomass has two distinct advantages when it comes to reducing GHG emissions. To begin, biomasses fix atmospheric CO_2 via photosynthesis and then undergo pyrolysis to preserve carbon as activated carbon. Secondly, these types of materials can be used as adsorbing materials to capture CO_2 in different industrial operations. Recent technological advancements in manufacturing activated carbon have heightened the importance of CO_2 mitigation research. Numerous types of biomass have been examined recently for use in the construction of activated carbons for CO_2 collection, including coconut shells, crab shells, rice husks, saw residue, and poplar anthers [83, 84]. These study findings are incredibly encouraging and demonstrate the potential for activated porous carbons to be used in real-world CO_2 capture applications. These materials are relatively affordable and quickly synthesized. Additionally, they have a high capacity for CO_2 capture at it both high and low pressures. By adding primary functional groups to such activated porous carbons, their attraction to acidic CO_2 molecules can be further enhanced.

3.7.2   Mechanism of CO_2 Capture by Supercapacitor Through Activated Carbon

To better understand the CO_2 capture process, it is necessary to describe the mechanisms so far discovered. According to research [85–87], the primary mechanism of adsorption is physisorption mediated by weak van der Waals forces. The investigators believe that the CO_2's quadrupole structure is a helpful characteristic for dispersing and stimulating the activated carbon onto its surface. Furthermore, they asserted that total surface area was the key factor regulating CO_2 physisorption on the activated carbon. According to some researchers [88], the size and form of the pores in activated carbon affect CO_2 absorption. According to their findings, small microspores were packed via physisorption and exhibited curved adsorption isotherms, but larger microspores exhibited rectilinear isotherms. In other research [89], the authors used three distinct types of carbons to conduct steady-state batch experiments for converting CO_2 heterogeneity through adsorption. Chemisorption, the group proposed, occurred as a consequence of inorganic metals such as calcium, iron, potassium, and magnesium with CO_2 ions, resulting in about 17 to 51% adsorption of CO_2. These gas particles first enter the aqueous phase, resulting in the formation of calcite and caustic anion species on the surface, which subsequently undertake chemical reactions to yield a range of products as below [84]:

$$CO_{2(gas)} \rightarrow CO_{2(aq.)} \tag{3.1}$$

$$CO_{2(aq.)} + 2OH \rightarrow CO_3^{2-} + H_2O \tag{3.2}$$

$$\begin{aligned} FeO\,(OH) + HCO_{3(aq.)}^- \quad &\rightarrow Fe(OH)_2CO_{3(s)}19Ca_3(PO_4)_2 + 6CO_3^{2-} \\ &\rightarrow 3Ca(CO_3)_2 + 2PO_4^{3-}(2O)Mg_3(PO_4)_2 + 6CO_3^{2-} \\ &\rightarrow 3Mg(CO_3)_2 + 2PO_4^{3-} \end{aligned} \tag{3.3}$$

$$Ca^{2+} + 2K^+ + 2CO_3^{2-} \rightarrow K_2\,Ca(CO_3)_2 \tag{3.4}$$

3.7.3 The Capability of Biomass to Reduce CO_2

CO_2 can be harvested from the atmosphere or the exhaust gas streams of industrial processes in various ways. It might subsequently be used differently to create future-generation clean energy fuels or as a carbon precursor for producing industrially significant compounds [90, 91]. Over the years, various types of adsorbents for CO_2 capture have been proposed. As illustrated in Figure 3.6, an ideal CO_2 adsorbent should possess good adsorption capacity, superior selectivity, microporosity, high restoration capability, and be inexpensive [83, 84]. Recent research on CO_2 capture has concentrated on approaches that involve different biomaterials, aqueous amine solutions, cryogenic separation, and membrane separation at shallow temperatures. Each procedure has several disadvantages, including toxic products, deterioration, and degradation of apparatus, dumping issues, and significant initial investment and operating expenditure. However, numerous researchers have recently used activated porous carbons generated from biomass, which are very promising and inexpensive for CO_2 capture [92–94]. Otherwise, pyrolysis can be used to convert undesirable biomass resources into extremely effective porous carbon absorbents that may be used on an industrial level for CO_2 extraction [95].

Regarding adsorbing CO_2 emissions, several types of carbons from diverse biomasses have been tested and compared as shown in Figure 3.7 [84]. Numerous biomass predecessors were investigated, and a substantial amount of work exists on developing several forms of activated carbons for efficient CO_2 capture by altering the experimental circumstances and type of activating agent. Porous carbon materials can help mitigate the reduction of carbon dioxide from the atmosphere in three distinct ways: i) by lowering CO_2 emissions from decomposing biomass, ii) by supplementing soils with activated carbon,
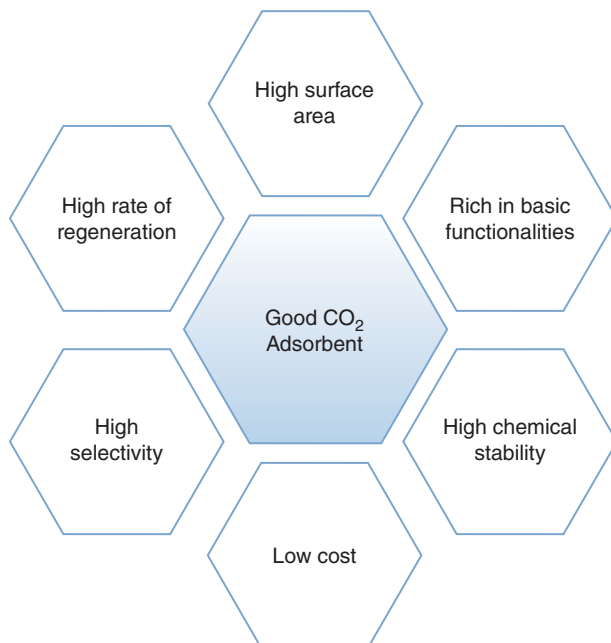

Figure 3.6 Core characteristics of an ideal adsorbent for CO_2 capture [83, 84].
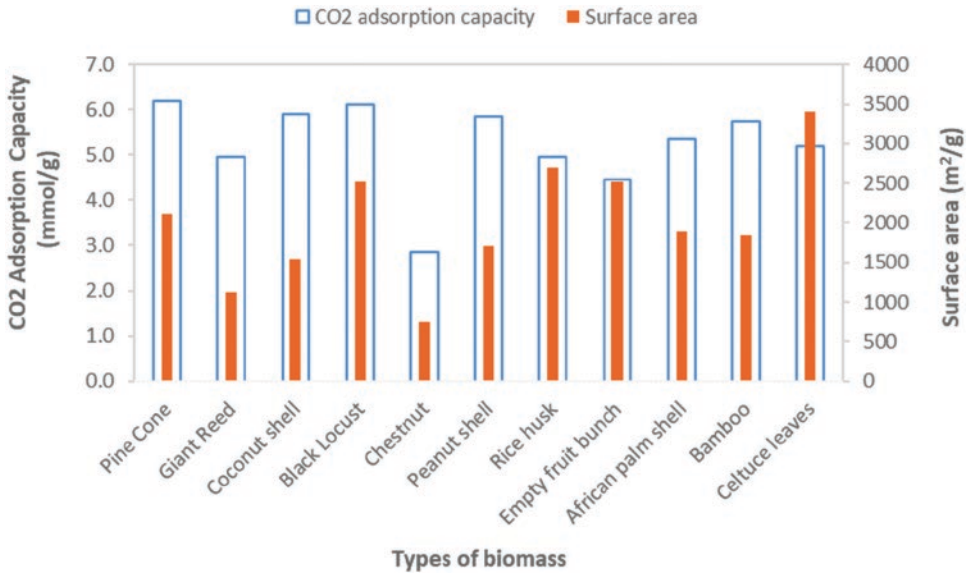
Figure 3.7 CO_2 adsorption capabilities of different biomass-based activated carbon [84].

and iii) by carbon dioxide capture in exhaust gas streams. Because virgin biochar is highly impervious, it is ineffective for CO_2 extraction. It must be triggered to enhance the area of its surface and pore volume before being used to this end.

3.8 Economics of Biomass Utilization in Supercapacitors

Difficulties beset biomass usage due to the poor profit margins of biomass products [33]. The economics of biomass consumption in supercapacitors are determined by the comparative feasibility of various carbon activation processes and resource management. Commercial active carbon is currently manufactured using costly and environmentally harmful fossil fuels. A cost-effective and environmentally friendly alternative might be biomass from homes, businesses, animals, and municipal waste [76]. It also provides extra benefits regarding sustainability and rural economic growth, particularly in underdeveloped nations [96, 97].

3.8.1 Economic Feasibility Factors

An organic source of clean and renewable energy is found in agricultural wastes, algae, the organic portion of sludge and other organic materials like cardboard and waste products, as well as municipal solid waste [98]. However, creating an effective and economically viable institution is the deciding criterion for feasibility. Some of the main issues impacting the commercial aspects of production include biomass supply, profit margin uncertainty, policy and regulations, and so on [99].

Careful consideration must be given to all of these factors, including economic growth, reducing environmental emissions, increasing co-product emissions, and the availability of

feedstock resources [100]. In different contexts, the cost and availability of the feedstock vary greatly [101]. The feedstock type, collection technique, storage facility, and other factors play a role [4, 102]. When all these factors are considered, the industry's economic viability is determined by the particular context and site-specific solutions. For different types of feedstocks, analyzing the cost and other financial performance indicators for different thermochemical conversion paths requires a comprehensive and innovative review [103].

3.8.2 Alternatives to Transportation

Another key consideration is the cost of transportation. When the processing plant is located far from the feedstock source, the cost of transporting biomass feedstock such as mill and forest leftovers is exceptionally high [104]. Because these feedstocks are preserved as waste products, the only expense is transportation. Densification of feedstock biomass by chipping, installing on-site pre-processing machines for better mobility and higher density [105], and other methods can be employed to minimize costs and establish a sustainable and economically viable approach to resource feedstock.

3.8.3 Utilization of By-products

The fly ash from the biomass boiler contains incompletley combusted carbons that can be used to make activated carbon for the SC after pyrolysis and combustion. The task now is to improve their pore architectures so they can be widely used [99]. Templating pathways, carbonization-activation routes, one-step carbonization routes, and other sophisticated processes for synthesizing activated carbon exist [39]. Non-templating routes, in comparison to templating routes, give a low-cost fabrication procedure. Fly ash is currently regarded as a by-product of biomass power plants, and it causes water contamination and air pollution. The unburned carbon can be used after proper pyrolysis, combustion, and other processes [99].

3.8.4 Comparison of Different Preparation Routes

There is a range of synthetic methodologies for carbon activation after the pre-carbonization process, including chemical, physical, and microwave-assisted activation methods. Physical techniques are preferred just at the industrial level. Although the chemical procedure produces superior quality, the cost of using hazardous chemicals and the risk of chemical handling remain. Although H_3PO_4 activation is less polluting, it is more expensive. A combination of H_3PO_4 and hydrothermal carbanization (HTC) may be a more cost-effective option without sacrificing quality or yield amount [74]. Although the microwave approach is efficient in terms of time and cost, it is most commonly utilized at the beginning of the industrial process [11].

Biocompatibility of biowaste, a limited yield of active carbon, modest energy density, maintaining industry standards, and other significant issues persist [11]. In order to identify biowaste products that may represent a problem, ecotoxicity tests are used. To be considered economically viable, at least one of its biological tests must be positive for biowaste material [11]. The poor yield of the production is the critical worry here, so scaling up from

the laboratory to the industrial level is vital. The evaluation of practical applications should be based on agronomic effectiveness and financial profitability. To determine the best production line, conducting cost-benefit analysis research is crucial [106].

3.9 Conclusions

The take-make-discard cycle is used in the linear economy, generating waste materials. The circular economy system shows benefits by utilizing resources more wisely through reuse, recycling, and resource recovery. To solve resource scarcity, cyclic material flow is necessary, particularly for industrial materials like SCs and this market is expanding. Thus, renewable energy sources like biomass are essential. The circular economy enhances sustainable bioproducts by creating various SC components, such as electrodes, electrolytes, separators, binding materials, current collectors, and packaging materials. Carbon, cellulose, gelatin, protein, fiber, and other biomasses can all be used to create the elements. After material recovery, the leftover biomass could be recycled or used for electricity and water purification. In contrast, burning openly releases pollutants and landfilling releases greenhouse gases. Therefore, a circular economy will cut emissions by avoiding methane generation from biomass degradation: methane has a much higher potential to cause global warming than carbon dioxide.

SCs can be manufactured using biowaste that can be recycled to create AC. There are numerous ways to prepare different biomass for producing AC, potentially reducing waste. An economical and environmentally favorable product is biomass-activated carbon. Biomass thermochemical conversion results in the production of a carbon dioxide absorber and a SC electrode. A cost-effective alternative biomass utilization system should be produced by comparing the costs of various carbon activation technologies, resource management, and economic viability. It is crucial to consider the cost of creating activated carbon, the type of biomass used, and other aspects. Relevant research should be carried out to develop a commercially feasible and environmentally responsible manufacturing process for utilizing biomass in SCs, considering a thorough lifecycle approach beginning with the product design to guarantee the circular economy principles.

The traditional linear economy is based on virgin input products, uses the take-make-discard loop, and generates a constant cycle of waste materials. In contrast, a circular economy improves the system through resource design, reuse, recycling, and recovery. It is based on a cradle-to-cradle material life cycle, which reduces the current system's massive waste. It is especially critical for industrial materials such as SCs, which require a cyclic material flow to alleviate the issue of finite resources. The market for electrical energy storage is expanding, as is the potential for material demand. As a result, renewable sources such as biomass are critical in satisfying demand sustainably. Biowaste can be recycled to make activated carbons used in SCs. Many methods can be used to prepare various types of biomass for producing AC, potentially alleviating the growing waste dilemma. The use of biomass is determined by the degree of graphitization, cell structure, and composition. In SCs, electrode materials such as AC, carbon nanotubes, and graphene are employed, while liquid electrolytes are used between the electrodes.

Biomass-activated carbon can be produced in a sustainable and low-cost manner. Carbon sequestration has shown to be one of the most viable approaches for reducing greenhouse

gases. The reliance on fossil fuels aggravates the situation. As a result, thermochemical conversion of biomass can produce porous carbon, which can be employed as a CO_2 absorber and SC electrode at the industrial level. A cost-effective alternative biomass use system should be created by comparing the costs of various carbon activation procedures, resource management, and numerous economic feasibility considerations. Feedstock type, collecting technique, storage facility, transportation, densification, installation of pre-processing on-site machinery, and special individual context mainly impact cost-effectiveness. Unburned by-products can also be used to generate alternating currents for SCs. Each of the physical, chemical, and microwave techniques of preparing AC has advantages. Therefore, depending on the desired output, such as quality or quantity, these approaches should be investigated using a cost-benefit analysis.

Future research needs to be focused on bendable portable devices, hybrid electric automobiles, and other advanced technologies to enhance SC's performance. The cost of activated carbon generation, the biomass used, and other parameters are crucial for progress toward large-scale industrial outputs. The SC properties of various biowaste products should be thoroughly researched. The long-term viability of the method is vital. Air pollutants should not be emitted directly into the environment during activation. All research efforts should be extended to the industrial and commercial levels to develop an economically feasible manufacturing strategy for biomass-based SCs.

References

1 J. Korhonen, A. Honkasalo, J. Seppälä, *Ecol. Econ.* **2018**, *143*, 37–46.

2 M. S. Andersen, *Sustain. Sci.* **2007**, *2*, 133–140.

3 J. Kirchherr, D. Reike, M. Hekkert, *Resour. Conserv. Recycl.* **2017**, *127*, 221–232.

4 S. S. Shah, M. N. Shaikh, M. Y. Khan, M. A. Alfasane, M. M. Rahman, M. A. Aziz, *Chem. Rec.* **2021**, *21*, 1631–1665.

5 V. Ranta, L. Aarikka-Stenroos, P. Ritala, S. J. Mäkinen, *Resour. Conserv. Recycl.* **2018**, *135*, 70–82.

6 T. Keijer, V. Bakker, J. C. Slootweg, *Nat. Chem.* **2019**, *11*, 190–195.

7 Element Scarcity – EuChemS Periodic Table. European Chemical Society **2019** [cited October 29, 2022]; Available from: https://www.euchems.eu/euchems-periodic-table.

8 C. Ferrara, R. Ruffo, E. Quartarone, P. Mustarelli, *Adv. Energy Sustainability Res.* **2021**, *2*, 2100047.

9 A. Jain, S. Sarsaiya, M. K. Awasthi, R. Singh, R. Rajput, U. C. Mishra, J. Chen, J. Shi, *Fuel* **2022**, *307*, 121859.

10 K. Mensah-Darkwa, C. Zequine, P. K. Kahol, R. K. Gupta, *Sustainability* **2019**, *11*, 414.

11 S. Sundriyal, V. Shrivastav, H. D. Pham, S. Mishra, A. Deep, D. P. Dubal, *Resour. Conserv. Recycl.* **2021**, *169*, 105548.

12 S. Sundriyal, V. Shrivastav, M. Sharma, S. Mishra, A. Deep, *ChemistrySelect* **2019**, *4*, 2585–2592.

13 M. Ashraf, I. Khan, M. Usman, A. Khan, S. S. Shah, A. Z. Khan, K. Saeed, M. Yaseen, M. F. Ehsan, M. N. Tahir, N. Ullah, *Chem. Res. Toxicol.* **2020**, *33*, 1292–1311.

14 H. Zhou, T. Fan, D. Zhang, *ChemSusChem* **2011**, *4*, 1344–1387.

15 A. Demirbaş, *Energy Convers. Manage.* **2001**, *42*, 1357–1378.

16 A. M. Abioye, F. N. Ani, *Renew. Sust. Energ. Rev.* **2015**, *52*, 1282–1293.

17 L. Zhang, Z. Liu, G. Cui, L. Chen, *Prog. Polym. Sci.* **2015**, *43*, 136–164.

18 S. I. Basha, S. S. Shah, S. Ahmad, M. Maslehuddin, M. M. Al-Zahrani, M. A. Aziz, *Chem. Rec.* **2022**, e202200134, https://doi.org/10.1002/tcr.202200134.

19 T. Islam, M. M. Hasan, S. S. Shah, M. R. Karim, F. S. Al-Mubaddel, M. H. Zahir, M. A. Dar, M. D. Hossain, M. A. Aziz, A. J. S. Ahammad, *J. Energy Storage* **2020**, *32*, 101908.

20 M. Ashraf, S. S. Shah, I. Khan, M. A. Aziz, N. Ullah, M. Khan, S. F. Adil, Z. Liaqat, M. Usman, W. Tremel, M. N. Tahir, *Chem. Eur. J.* **2021**, *27*, 6973–6984.

21 S. S. Shah, E. Cevik, M. A. Aziz, T. F. Qahtan, A. Bozkurt, Z. H. Yamani, *Synth. Met.* **2021**, *277*, 116765.

22 S. S. Shah, M. A. Alfasane, I. A. Bakare, M. A. Aziz, Z. H. Yamani, *J. Energy Storage* **2020**, *30*, 101562.

23 C. K. Roy, S. S. Shah, A. H. Reaz, S. Sultana, A.-N. Chowdhury, S. H. Firoz, M. H. Zahir, M. A. A. Qasem, M. A. Aziz, *Chem. Asian J.* **2021**, *16*, 296–308.

24 S. S. Shah, H. Yang, M. Ashraf, M. A. A. Qasem, A. S. Hakeem, M. A. Aziz, *Chem. Asian J.* **2022**, *17*, e202200567.

25 S. S. Shah, S. M. A. Nayem, N. Sultana, A. J. S. Ahammad, M. A. Aziz, *ChemSusChem* **2022**, *15*, e202101282.

26 M. M. Hasan, T. Islam, S. S. Shah, A. Awal, M. A. Aziz, A. J. S. Ahammad, *Chem. Rec.* **2022**, *22*, e202200041.

27 S. S. Shah, M. A. Aziz, Z. H. Yamani, *Chem. Rec.* **2022**, *22*, e202200018.

28 M. Yaseen, M. A. K. Khattak, M. Humayun, M. Usman, S. S. Shah, S. Bibi, B. S. U. Hasnain, S. M. Ahmad, A. Khan, N. Shah, A. A. Tahir, H. Ullah, *Energies* **2021**, *14*, 7779.

29 S. S. Shah, M. A. Aziz, E. Cevik, M. Ali, S. T. Gunday, A. Bozkurt, Z. H. Yamani, *J. Energy Storage* **2022**, *56*, 105944.

30 C. Zhang, X. Zhu, M. Cao, M. Li, N. Li, L. Lai, J. Zhu, D. Wei, *ChemSusChem* **2016**, *9*, 932–937.

31 K. Lee, L. Shabnam, S. N. Faisal, V. G. Gomes, *J. Energy Storage* **2020**, *27*, 101152.

32 H. Jin, S. Wu, T. Li, Y. Bai, X. Wang, H. Zhang, H. Xu, C. Kong, H. Wang, *Appl. Surf. Sci.* **2019**, *488*, 593–599.

33 X. Liu, S. Zhang, X. Wen, X. Chen, Y. Wen, X. Shi, E. Mijowska, *Sci. Rep.* **2020**, *10*, 3518.

34 R. Thangavel, A. G. Kannan, R. Ponraj, V. Thangavel, D.-W. Kim, Y.-S. Lee, *J. Mater. Chem. A* **2018**, *6*, 17751–17762.

35 G. Li, Q. Li, J. Ye, G. Fu, J. Han, Y. Zhu, *J. Solid State Electrochem.* **2017**, *21*, 3169–3177.

36 C. Wei, J. Yu, X. Yang, G. Zhang, *Nanoscale Res. Lett.* **2017**, *12*, 379.

37 W. Si, J. Zhou, S. Zhang, S. Li, W. Xing, S. Zhuo, *Electrochim. Acta* **2013**, *107*, 397–405.

38 X. Su, W. Jia, H. Ji, Y. Zhu, *J. Energy Storage* **2021**, *41*, 102830.

39 J. Yang, Z. Tan, X. Chen, Y. Liang, M. Zheng, H. Hu, H. Dong, X. Liu, Y. Liu, Y. Xiao, *J. Colloid Interface Sci.* **2021**, *599*, 381–389.

40 M. Rauf, S. S. Shah, S. K. Shah, S. N. A. Shah, T. U. Haq, J. Shah, A. Ullah, T. Ahmad, Y. Khan, M. A. Aziz, K. Hayat, *J. Saudi Chem. Soc.* **2022**, *26*, 101514.

41 R. Shakil, M. N. Shaikh, S. S. Shah, A. H. Reaz, C. K. Roy, A.-N. Chowdhury, M. A. Aziz, *Asian J. Org. Chem.* **2021**, *10*, 2220–2230.

42 M. M. Hasan, T. Islam, S. S. Shah, M. A. Aziz, A. Awal, M. D. Hossain, M. A. Ehsan, A. J. S. Ahammad, *Int. J. Hydrog. Energy* **2022**, *47*, 28740–28751.

43 S. B. Aziz, T. J. Woo, M. Kadir, H. M. Ahmed, *J. Sci-Adv. Mater. Dev.* **2018**, *3*, 1–17.

44 J. Chmiola, G. Yushin, Y. Gogotsi, C. Portet, P. Simon, P.-L. Taberna, *Science* **2006**, *313*, 1760–1763.

45 F. Xu, Y. Dong, W. Zhang, S. Zhang, L. Li, J. Li, *Ind. Crops Prod.* **2015**, *67*, 373–380.

46 C. Gao, Y. Duan, J. Liu, J. Gu, Z. Guo, P. Huo, *J. Power Sources* **2022**, *541*, 231658.

47 C. Schütter, S. Pohlmann, A. Balducci, *Adv. Energy Mater.* **2019**, *9*, 1900334.

48 P. Ruschhaupt, A. Varzi, S. Passerini, *ChemSusChem* **2020**, *13*, 763–770.

49 J. Zhang, Q. Kong, Z. Liu, S. Pang, L. Yue, J. Yao, X. Wang, G. Cui, *Solid State Ion* **2013**, *245*, 49–55.

50 N. Blomquist, T. Wells, B. Andres, J. Bäckström, S. Forsberg, H. Olin, *Sci. Rep.* **2017**, *7*, 39836.

51 M. A. Islam, H. L. Ong, A. R. Villagracia, K. A. A. Halim, A. B. Ganganboina, R.-A. Doong, *Ind. Crops Prod.* **2021**, *170*, 113694.

52 C. Wang, H. Wang, B. Dang, Z. Wang, X. Shen, C. Li, Q. Sun, *Renew. Energy* **2020**, *156*, 370–376.

53 E. Gul, G. Rahman, Y. Wu, T. H. Bokhari, A. U. Rahman, A. Zafar, Z. Rana, A. Shah, S. Hussain, K. Maaz, S. Karim, S. Javaid, H. Sun, M. Ahmad, G. Xiang, A. Nisar, *New J. Chem.* **2022**, *46*, 16280–16288.

54 M. Usman, *Membranes* **2022**, *12*, 507.

55 M. Daud, M. S. Kamal, F. Shehzad, M. A. Al-Harthi, *Carbon* **2016**, *104*, 241–252.

56 S. M. Abu Nayem, S. S. Shah, N. Sultana, M. A. Aziz, A. J. Saleh Ahammad, *Chem. Rec.* **2021**, *21*, 1039–1072.

57 S. M. Abu Nayem, S. S. Shah, N. Sultana, M. A. Aziz, A. J. Saleh Ahammad, *Chem. Rec.* **2021**, *21*, 1038-1038.

58 S. Islam, S. S. Shah, S. Naher, M. A. Ehsan, M. A. Aziz, A. J. S. Ahammad, *Chem. Asian J.* **2021**, *16*, 3516–3543.

59 S. M. A. Nayem, S. S. Shah, N. Sultana, M. A. Aziz, A. J. S. Ahammad, *Chem. Rec.* **2021**, *21*, 1073–1097.

60 J. Yan, Q. Wang, T. Wei, Z. Fan, *Adv. Energy Mater.* **2014**, *4*, 1300816.

61 D. Yu, K. Goh, H. Wang, L. Wei, W. Jiang, Q. Zhang, L. Dai, Y. Chen, *Nat. Nanotechnol.* **2014**, *9*, 555–562.

62 S. Koohi-Fayegh, M. A. Rosen, *J. Energy Storage* **2020**, *27*, 101047.

63 P. Carrott, M. R. Carrott, *Bioresour. Technol.* **2007**, *98*, 2301–2312.

64 A. J. S. Ahammad, P. R. Pal, S. S. Shah, T. Islam, M. Mahedi Hasan, M. A. A. Qasem, N. Odhikari, S. Sarker, D. M. Kim, M. A. Aziz, *J. Electroanal. Chem.* **2019**, *832*, 368–379.

65 A. K. Mohamedkhair, M. A. Aziz, S. S. Shah, M. N. Shaikh, A. K. Jamil, M. A. A. Qasem, I. A. Buliyaminu, Z. H. Yamani, *Arab. J. Chem.* **2020**, *13*, 6161–6173.

66 S. S. Shah, M. A. Aziz, A. K. Mohamedkhair, M. A. A. Qasem, A. S. Hakeem, M. K. Nazal, Z. H. Yamani, *J. Mater. Sci. - Mater. Electron.* **2019**, *30*, 16087–16098.

67 G. Genon, D. Panepinto, F. Viggiano, *WIT Trans. Ecol. Environ.* **2014**, *190*, 995–1006.

68 M. Z. Jacobson, *J. Geophys. Res. Atmos.* **2010**, *115*.

69 M. D. Garba, M. Usman, S. Khan, F. Shehzad, A. Galadima, M. F. Ehsan, A. S. Ghanem, M. Humayun, *J. Environ. Chem. Eng.* **2021**, *9*, 104756.

70 M. Höök, X. Tang, *Energy Policy* **2013**, *52*, 797–809.

71 D. Coskun, D. T. Britto, H. J. Kronzucker, *J. Plant Physiol.* **2016**, *203*, 95–109.

72 M. Usman, M. Humayun, S. S. Shah, H. Ullah, A. A. Tahir, A. Khan, H. Ullah, *Energies* **2021**, *14*, 2281.

73 M. A. Aziz, S. S. Shah, S. M. A. Nayem, M. N. Shaikh, A. S. Hakeem, I. A. Bakare, *J. Energy Storage* **2022**, *50*, 104278.

74 J. Chaparro-Garnica, D. Salinas-Torres, M. J. Mostazo-López, E. Morallon, D. Cazorla-Amorós, *J. Electroanal. Chem.* **2021**, *880*, 114899.

75 X. Li, J. Zhang, B. Liu, Z. Su, *J. Clean. Prod.* **2021**, *310*, 127428.

76 Z. Li, D. Guo, Y. Liu, H. Wang, L. Wang, *Chem. Eng. J.* **2020**, *397*, 125418.

77 B. K. Saikia, S. M. Benoy, M. Bora, J. Tamuly, M. Pandey, D. Bhattacharya, *Fuel* **2020**, *282*, 118796.

78 S. Saini, P. Chand, A. Joshi, *J. Energy Storage* **2021**, *39*, 102646.

79 H. Meng, S. Wang, L. Chen, Z. Wu, J. Zhao, *Fuel* **2015**, *158*, 602–611.

80 L. Rao, S. Liu, L. Wang, C. Ma, J. Wu, L. An, X. Hu, *Chem. Eng. J.* **2019**, *359*, 428–435.

81 F. Sher, S. Z. Iqbal, S. Albazzaz, U. Ali, D. A. Mortari, T. Rashid, *Fuel* **2020**, *282*, 118506.

82 X. Ma, Y. Yang, Q. Wu, B. Liu, D. Li, R. Chen, C. Wang, H. Li, Z. Zeng, L. Li, *Fuel* **2020**, *282*, 118727.

83 N. Abuelnoor, A. AlHajaj, M. Khaleel, L. F. Vega, M. R. Abu-Zahra, *Chemosphere* **2021**, *282*, 131111.

84 G. Singh, K. S. Lakhi, S. Sil, S. V. Bhosale, I. Kim, K. Albahily, A. Vinu, *Carbon* **2019**, *148*, 164–186.

85 A. E. Creamer, B. Gao, M. Zhang, *Chem. Eng. J.* **2014**, *249*, 174–179.

86 M. Usman, Z. Zeb, H. Ullah, M. H. Suliman, M. Humayun, L. Ullah, S. N. A. Shah, U. Ahmed, M. Saeed, *J. Environ. Chem. Eng.* **2022**, *10*, 107548.

87 M. Usman, A. S. Ghanem, S. N. A. Shah, M. D. Garba, M. Y. Khan, S. Khan, M. Humayun, A. L. Khan, *Chem. Rec.* **2022**, *22*, e202200039.

88 J. Martin-Martinez, R. Torregrosa-Macia, M. Mittelmeijer-Hazeleger, *Fuel* **1995**, *74*, 111–114.

89 X. Xu, Y. Kan, L. Zhao, X. Cao, *Environ. Pollut.* **2016**, *213*, 533–540.

90 Z. Chen, S. Deng, H. Wei, B. Wang, J. Huang, G. Yu, *Front. Environ. Sci. Eng.* **2013**, *7*, 326–340.

91 A. Samanta, A. Zhao, G. K. Shimizu, P. Sarkar, R. Gupta, *Ind. Eng. Chem. Res.* **2012**, *51*, 1438–1463.

92 J. Kou, L.-B. Sun, *J. Mater. Chem. A* **2016**, *4*, 17299–17307.

93 T. Wei, Q. Zhang, X. Wei, Y. Gao, H. Li, *Sci. Rep.* **2016**, *6*, 22646.

94 B. Zhu, K. Qiu, C. Shang, Z. Guo, *J. Mater. Chem. A* **2015**, *3*, 5212–5222.

95 Y. Li, G. Ruan, A. S. Jalilov, Y. R. Tarkunde, H. Fei, J. M. Tour, *Carbon* **2016**, *107*, 344–351.

96 M. Parvez, M. Elias, N. Rahim, N. Osman, *Sol. Energy* **2016**, *135*, 29–42.

97 P. Tanger, J. L. Field, C. E. Jahn, M. W. DeFoort, J. E. Leach, *Frontiers in Plant Science* **2013**, *4*, 218.

98 K. Zhang, A. Isella, J. M. Carpenter, G. A. Blake, *Astrophys. J.* **2014**, *791*, 42.

99 S. Song, F. Ma, G. Wu, D. Ma, W. Geng, J. Wan, *J. Mater. Chem. A* **2015**, *3*, 18154–18162.

100 J. Malinauskaite, H. Jouhara, D. Czajczyńska, P. Stanchev, E. Katsou, P. Rostkowski, R. J. Thorne, J. Colon, S. Ponsá, F. Al-Mansour, *Energy* **2017**, *141*, 2013–2044.

101 J. Speirs, C. McGlade, R. Slade, *Energy Policy* **2015**, *87*, 654–664.

102 A. Aziz, S. S. Shah, A. Kashem, *Chem. Rec.* **2020**, *20*, 1074–1098.

103 M. Brodin, M. Vallejos, M. T. Opedal, M. C. Area, G. Chinga-Carrasco, *J. Clean. Prod.* **2017**, *162*, 646–664.

104 E. Searcy, P. Flynn, E. Ghafoori, A. Kumar, *Appl. Biochem. Biotechnol.* **2007**, *137*, 639–652.

105 K. Homagain, C. Shahi, N. Luckai, M. Sharma, *For. Ecosyst.* **2016**, *3*, 21.

106 Y. Qiang, L. Guo, H. Li, X. Lan, *Chem. Eng. J.* **2021**, *406*, 126863.

Part 2

Fundamentals of Supercapacitors

4

Introduction to Supercapacitors

*Syed Shaheen Shah[1,2], Mohammad Rezaul Karim[3,4], Md. Abdul Wahab[5],
Muhammad Ali Ehsan[1], and Md. Abdul Aziz[1,6,*]*

[1] *Interdisciplinary Research Center for Hydrogen and Energy Storage (IRC-HES), King Fahd University of Petroleum & Minerals, KFUPM Box 5040, Dhahran 31261, Saudi Arabia*

[2] *Physics Department, King Fahd University of Petroleum & Minerals, KFUPM Box 5047, Dhahran 31261, Saudi Arabia*

[3] *Center of Excellence for Research in Engineering Materials (CEREM), Deanship of Scientific Research (DSR), College of Engineering, King Saud University, Riyadh 11421, Saudi Arabia*

[4] *K.A. CARE Energy Research and Innovation Center, King Saud University, Riyadh 11421, Saudi Arabia*

[5] *Australian Institute for Bioengineering and Nanotechnology (AIBN), The University of Queensland, St. Lucia, QLD 4072, Australia*

[6] *K. A. CARE Energy Research and Innovation Center, King Fahd University of Petroleum & Minerals, Dhahran, 31261, Saudi Arabia*

* *Corresponding author*

4.1 Introduction

Researchers have been working on developing sustainable energy technologies, such as solar and wind, in response to the rapid depletion of nonrenewable resources and increased concern over environmental concerns in recent years. Fossil fuel usage is reduced when energy is extracted from renewable sources. Gases released by the combustion of fossil fuels damages our air, and waste products such as fly ash discharged in the open atmosphere affect land and water [1]. Because of these serious problems there is a critical need for the long-term development of renewable energy sources. Solar and wind account for a large portion of the total renewable energy generated; additional energy sources include biomass, hydropower plants, and geothermal [2]. The intermittency of renewable energy sources is one of the most significant challenges. The wind does not blow continuously, and the sun does not shine at night. Effective energy storage devices are required to circumvent these constraints, which can store a considerable quantity of energy from renewable sources and release it when needed [3]. During the energy storage process, one type of energy is transformed into a form that can be stored and delivered across the country. Electrochemical energy storage devices (EESDs), such as batteries and supercapacitors, were developed in this line for societal progress.

EESD-based technologies, such as batteries and supercapacitors, allow efficient energy storage and supply [4–7]. Because of their high specific energy, batteries have been widely employed among these modern EESDs of various sizes. However, they have drawbacks like heat generation, poor specific power, a relatively low charging rate, a limited rechargeable

life, and safety hazards. Alternatively, supercapacitors have high specific power and may charge and discharge for many cycles. Nonetheless, most supercapacitors have a low specific energy [8]. Therefore, developing modern, durable, and compact supercapacitors with high specific energy and specific power will revolutionize the landscape of electric energy storage and supply for industrial and home uses. As a result, scientists are working on high-performance supercapacitors that are meant to have the benefits of both batteries and capacitors [9].

It is critical to understand the performance of various EESDs, which have been compared using the Ragone plot (Figure 4.1). It is a relationship between the energy density $(Wh\,kg^{-1})$ and the power density $(W\,kg^{-1})$ that can be achieved. The research's ultimate goal is to develop an EESD with high energy density and high power density. This implies the energy storage device can hold a lot of energy and distribute it rapidly. Batteries are high energy density devices that store a lot of energy but deliver it slowly. Traditional capacitors can discharge their charge on demand but cannot store much energy. Supercapacitors are used to create high energy and high power density devices. Electrochemical capacitors, also known as supercapacitors, can bridge the gap between traditional capacitors and batteries, as illustrated in the Ragone plot. Supercapacitors can bridge the gap by many orders of magnitude in terms of power density and energy density. Batteries, to the best of our knowledge, produce the highest specific energy $(>1000\,Wh\,kg^{-1})$ among the currently available EESDs, but have a short charge/discharge cyclic life $(<20000$ cycles). Although supercapacitors have the highest specific power $(>300\,kW\,kg^{-1})$ and charge/discharge cyclic life $(>100,000$ cycles), they have the lowest specific energy $(<200\,Wh\,kg^{-1})$ [10, 11]. Supercapacitors have recently been extensively researched in order to fulfill the EESDs' growing needs for quick charge/discharge, long cycle life, high specific power, and high specific energy [12, 13].

The large energy capacity of surface/bulk Faradaic electrode materials makes them excellent for building high-performance supercapacitors [14]. As a result, the fabrication of high-performance supercapacitors configurations constituted of Faradaic and non-Faradaic electrode materials [15–22]. A high power density (non-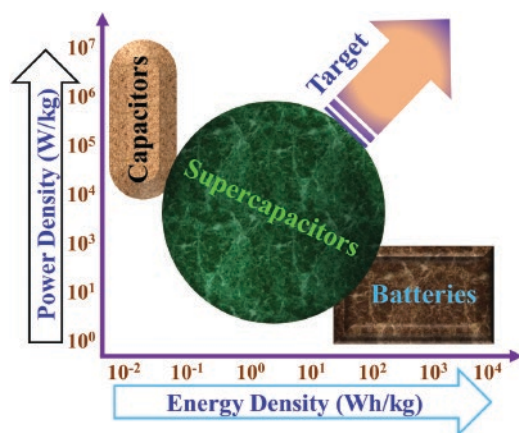Faradaic) and high specific energy (Faradaic) supercapacitor with two different (asymmetric) electrodes is an excellent technique for integrating high power density (non-Faradaic) and high specific energy (Faradaic) in a single device [14, 23]. However, because of the substantial difference in charging rates between non-Faradaic and Faradaic electrodes, these devices typically fail to achieve their planned specific energy level, particularly when redox electrodes are used [24–27]. Another step forward in this field is using an asymmetric supercapacitor construction with one carbon-based electrode and the other

Figure 4.1 Ragone plot for various EESDs.

a hybrid composite-based electrode. Real carbonaceous nanostructure and redox-active oxides/sulfides hybrid composites that use each component's synergistic performance and solve the obstacles associated with the lower rate of the Faradaic component in supercapacitors [14, 23].

Evans et al. [28] pioneered and patented a high-performance supercapacitor by describing an electrolytic-based capacitor with a pseudocapacitive electrode. The nature of the electrode materials, including shape, size, and composition, influences the performance of a supercapacitor. As a result, nanostructure materials are thought to be particularly effective for use in high-performance supercapacitors [29, 30]. This piqued the interest of researchers since such power sources are in great demand for wearable electronics, electric cars, and security alarm systems [31]. However, complete commercialization remains a challenge. Some supercapacitors are less efficient in terms of high specific energy, while others have stability issues.

Supercapacitors have attracted a lot of attention from the scientific community because of their high charge propagation dynamic, long cycle life, fast charge-discharge rate, high Coulombic efficiencies, and wide operating temperatures to bridge the gap between batteries and conventional capacitors. Table 4.1 shows a quick comparison of the capacitor, supercapacitor, and battery.

Because of their high power density, long cycle life, and safe operation, supercapacitors are viable EESDs for mobile power supply [32]. Light rail, military services, shape memory, wind turbine systems, aerospace, electric cars, and hybrid batteries are only a few of the applications [33, 34]. Supercapacitors, on the other hand, have lower specific energy, which restricts their industrial uses. As a result, scientists have been working to create new electrolytes and electrode materials for high-performance output in order to boost supercapacitors' energy

Table 4.1 Comparison of various EESDs (i.e., battery, supercapacitor, and capacitor).

Parameters	Battery	Supercapacitor	Capacitor
Charge storage mechanism	Chemical (redox reactions)	Both physical and chemical (electrostatic double-layer formation and Faradaic charge transfer)	Physical (electrostatic)
Capacitance (F)	Not possible	500–3000	< 2.5
Specific energy ($Wh\,kg^{-1}$)	10–100	1–10	< 0.1
Specific power ($W\,kg^{-1}$)	> 1000	500–10000	> 10000
Charging time (sec)	10^3–10^4	1–10	10^{-6}–10^{-3}
Discharging time (sec)	10^3–10^4	1–10	10^{-6}–10^{-3}
Coulombic efficiency	70–85%	85–98%	~100%
Cycle life (in thousands)	~1	> 500	infinite

density. The electrode material, current collector, electrolyte, and separator make up a conventional supercapacitor (Figure 4.2). Two electrodes (electrode materials) separated by an ion-permeable membrane (separator), current collectors (thin metallic films), and an electrolyte (medium containing positive and negative ions) are utilized in the fabrication of a supercapacitor. Supercapacitors are classified into two categories based on their design: symmetry and asymmetric supercapacitors. The same electrodes are used in symmetric supercapacitors (i.e., the same active materials for both positive and negative electrodes). On the other hand, asymmetric supercapacitors have two distinct electrodes (i.e., the active materials on both the positive and negative electrodes) [35]. Furthermore, supercapacitors are divided into three groups: (i) electrochemical double-layer capacitors (EDLCs), (ii) pseudocapacitors, and (iii) hybrid supercapacitors, based on charge-storage mechanisms such as charge accommodation at the electric double layer, Faradaic reaction, and a combination of EDLCs and pseudocapacitors [36, 37]. An EDLC stores electrochemical energy by adsorbing and desorbing electrolyte ions and forming a double layer at the electrode–electrolyte interface. Pseudocapacitors, on the other hand, utilize redox-active materials (such as transition metal oxides/hydroxides and conducting polymers) to store charges via redox processes. The kind of electrode materials and their specific surface area (SSA) are crucial [38–43]. Carbon-based materials are the most widely used electrodes, with more than 80% of commercially manufactured supercapacitors. Porous carbonaceous materials have been shown to have greater SSA than metal phosphides, oxides, and sulfides. Activated carbon is rated good in terms of performance among the carbonaceous materials described by researchers for supercapacitors. Activated carbon used as electrode materials for supercapacitors is generally made from biowaste and has high electrical conductivity, porosity, thermal and chemical stability, outstanding power density, high packing density, and good reversibility [36, 40, 41, 43–46].
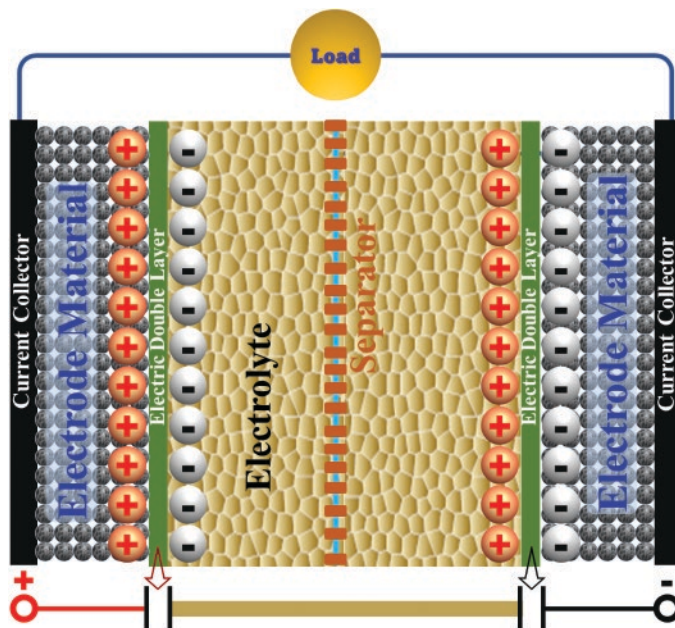

Figure 4.2 Schematic representation of a supercapacitor.

Supercapacitors comprising composites of carbonaceous and redox-active materials have been found to improve the overall electrochemical performance of hybrid supercapacitors. Hybrid supercapacitors using redox-active material electrodes comprised of transition metal sulfides, oxides, and hydroxides have been examined. However, certain flaws exist, such as sluggish electrolyte ion transport and poor electrode material electrical conductivity. Electrochemical energy storage capacities are limited as a result of these factors. Superior transition metals-based electrode materials with a fast charge/discharge rate, high specific power, and high specific energy are important for hybrid supercapacitors [47]. Using hybrid composites of carbonaceous and redox-active materials can improve conductivity, increase ions/electrons diffusion, and improve hybrid supercapacitors' electrochemical performance. The electrode development, fundamental concepts, and device design of hybrid supercapacitors based on carbonaceous and redox-active materials have all been thoroughly investigated. Much research has been done in the last several years to generate new composites of active electrode materials for hybrid supercapacitors [7, 15, 48–50].

4.2 Supercapacitor Background

The effectiveness of energy storage units is critical to developing modern electronics, including portable and wearable smart devices. It is anticipated that supercapacitors will take the lead in the energy storage devices field because of their high-power densities, large specific capacitance, improved cyclic ability, and secure usage [51]. The phenomenon of charge storage in capacitors at the electrode–electrolyte interface has been known for a very long time. In 1879, Hermann von Helmholtz was the first person to predict this phenomenon [52]. Later in 1957, H. I. Becker of General Electric Corp. created and patented the first double-layer capacitor that could be used in practical applications [53]. The first commercially available supercapacitor was produced by the SOHIO firm in 1969, utilizing carbon-based material and a non-aqueous electrolyte [54]. This process took around ten years to complete. It was not until several years after the introduction of carbon-based capacitors that a new class of supercapacitors consisting of Ru_2O as electrode materials were developed. The charge storage mechanism in these supercapacitors was a Faradaic redox reaction, yet the form of the capacitance-voltage (CV) curve was still similar to the rectangular geometry of the supercapacitors. Therefore, this category of supercapacitors was given the term pseudocapacitors because they store charges via a Faradaic redox process at the electrode–electrolyte interface. Additional research in this sector expanded the concept of pseudocapacitors to practically all of the metal oxides and conducting polymers using battery-like redox reactions [39, 55–57].

4.3 Characteristic Features of Supercapacitors

Supercapacitors are classified into three categories based on their charge-storing techniques: EDLCs, pseudocapacitors, and hybrid supercapacitors, as shown in Figure 4.3(a) [36, 49, 58]. A typical supercapacitor comprises four major parts described in Figure 4.3(b). Specifically, current collectors (metal contacts/conductive substrates), electrode materials (carbon and/or
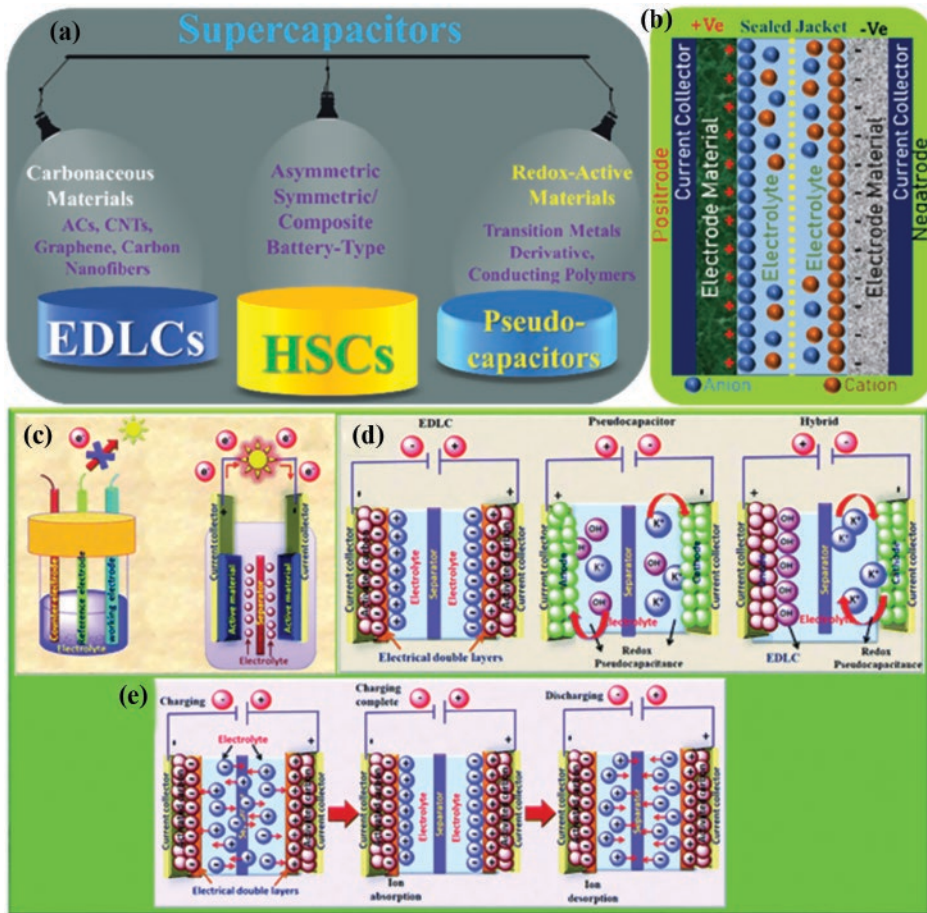
Figure 4.3 (a) Supercapacitors classifications, (b) a standard supercapacitor, (c) three/two electrodes electrochemical systems, (d) supercapacitor types, and (e) absorption or desorption of electrolyte ions at the electrode–electrolyte interface. *Reproduced with permission [50, 58].Copyright 2022, Wiley [50]. Reproduced under the terms of the CC BY-NC 3.0 license. Copyright 2019, Pal et al. [58].*

redox-active materials), separator (porous/ion-permeable membrane), and electrolyte (ionic liquids, aqueous, and non-aqueous electrolytes) [33, 59]. The electrolyte and electrode materials are active components of supercapacitors, whereas the remainder are passive components. In supercapacitor applications, the operating potential window is critical for both electrodes and electrolytes. When the operating potential window range is reached, electrolytes should not be oxidized or reduced. In the creation of high-performance supercapacitors, choosing appropriate electrode materials is crucial. During charging and discharging, the electrode materials collect and release electrolyte ions on their surfaces. The most important characteristics of electrode materials are high specific surface area, light weight, superior electrical conductivity, chemical and thermal durability, and cheap cost. The most appropriate electrode materials for fabricating high-performance supercapacitors are carbonaceous materials, transition metal oxides/hydroxides, and conductive polymers.

For the performance investigation of supercapacitors, there are two types of systems: three-electrode and two-electrode systems, as shown in Figure 4.3(c). A three-electrode electrochemical system uses a counter electrode made of corrosion resistant platinum or graphite wire/mesh. Saturated Ag/AgCl or Hg/HgCl are utilized as reference electrodes (having a well-known and stable electrode potential used to maintain the electrochemical cell potential). The working electrode is the third electrode, and it is here that researchers are testing the performance of electrode materials in supercapacitors. Supercapacitors are two-electrode devices with two metal plates called current collectors as electrodes. These plates are covered with active electrode materials and layered with a separator between them. The separator is saturated in electrolytes and physically separates the two electrodes while also allowing electrolyte ions to flow between them.

Symmetric supercapacitors are those in which both electrodes are made of the same material. The supercapacitor is referred to as an asymmetric supercapacitor when the two electrodes are made of different materials. During charging and discharging, the electrode materials play an important role in energy storage and delivery. Ions in the electrolyte travel towards opposing electrodes when voltage is supplied (Figure 4.3(d, e)). Charge recombination is prevented by forming a double layer at each electrode in the EDLCs. To store the charges, pseudocapacitors use redox processes. The pseudocapacitors can have higher capacitance than EDLCs, thanks to this redox method. Hybrid supercapacitors are better at storing energy than EDLCs and pseudocapacitors because of the simultaneous adsorption/desorption of electrolyte ions and redox processes [23, 60, 61].

Electrolytes are also important components of supercapacitors, and their chemical and physical characteristics affect their overall performance. They enable ionic conductivity and charge correction on each electrode in the device. The electrolyte in a supercapacitor influences not only the production of electric-double layers and reversible redox processes but also the overall performance of the supercapacitor. The ideal supercapacitor electrolyte must meet the following criteria: exhibit a wide operating potential window, have a broad operating temperature range, high ion concentration, low viscosity, high ionic conductivity, environmental friendliness, electrolyte-electrode materials interaction, good electrochemical stability, low-cost, and ion-solvent interaction [62–67]. All of these electrolyte parameters affect the electrochemical performance of supercapacitors (specific capacitance, specific energy, specific power, and cyclic life). Various types of electrolytes now employed in supercapacitors are aqueous, solid gel type, organic, and ionic liquids. Organic electrolytes with operating potential window values ranging from 2.5 to 2.8 V are commonly employed in commercial supercapacitors. Several alternative electrolytes for supercapacitors have been developed and reported in the literature [55, 59, 63, 68–70].

Below are the key criteria that define a supercapacitor's quality.

i)   The EDLC capacitance (C_d) is represented by equation (4.1) [71].

$$C_\mathrm{d} = \frac{\varepsilon_\mathrm{r}\varepsilon_\mathrm{o}A}{d} \tag{4.1}$$

where, ε_r is the electrolyte dielectric constant, ε_o is the permittivity of vacuum, A is the active materials surface area which is accessible to the ions of electrolyte, and d is the effective thickness of the electric double layer.

ii) The redox-active materials pseudocapacitance (C_p) can be measured using equation (4.2) [72].

$$C_p = \frac{n \times F}{M \times \Delta V} \tag{4.2}$$

where, n signify the average number of electrons engaged in redox reactions, M is the redox-active material molar mass, F shows the Faraday's constant, and ΔV is the operating potential window.

iii) The supercapacitor's energy density (E) can be achieved by applying equation (4.3) [73].

$$E = \frac{C \times V^2}{2} \tag{4.3}$$

where, V is the operating potential window and C is the nominal capacitance.

iv) The supercapacitor's power density (P) can be determined by employing equation (4.4) [73].

$$P = \frac{V^2}{4R} \tag{4.4}$$

where, R is the equivalent series resistance (ESR), and V is the operating potential window.

v) The cyclic voltammetry (CV) can be used to measure the specific capacitance (C_{CV}) from equation (4.5) [72].

$$C_{CV} = \frac{\int I \times dV}{m \times \nu \times \Delta V} \tag{4.5}$$

where, $\int I \times dV$ is the area under CV curve, ν is the scan rate, m is the active material mass, and ΔV is the operating potential window.

vi) Similarly, galvanostatic charge-discharge (GCD) can be used to measure the specific capacitance (C_{GCD}) using equation (4.6) [72].

$$C_{GCD} = \frac{I \times \Delta t}{m \times \Delta V} \tag{4.6}$$

where, I is the discharging current, Δt is the discharging time, m is active material mass, and ΔV is the discharging operating potential window.

vii) Coulombic efficiency (η) is the ratio of discharging and charging times, which may be derived using equation (4.7) [73].

$$\eta = \frac{t_d}{t_c} \times 100\% \tag{4.7}$$

4.4   Supercapacitor Components

A supercapacitor is made up of four different components, each of which plays a specific role. The four components include electrodes, electrolytes, separators, and current collectors. The interaction of electrolyte ions with the electrode allows for charge storage via a capacitive or Faradaic process. The electrolyte enables the charge and discharge process, which supplies the required ions. The separator performs the function of a barrier, therefore preventing the device from experiencing any short circuits. The current collector makes a conducting channel available for the electrons to go from the electrode to the external circuit. The following subsections provide a brief discussion of each component.

4.4.1   Electrodes

The performance of a supercapacitor is heavily influenced by the electrodes, which play a significant part in the charge storage process. When a potential is applied to the electrodes, it stores charges. The supercapacitor electrodes should have high conductivity, allowing for easy electron transfer to the external circuit. The following are the fundamental characteristics of the optimal electrode:

High electronic conductivity: determines the electrode material's rate capabilities and power density. High conductivity reduces resistance and makes electron passage from the electrode to the current collector easier.

High specific surface area: the electrode surface interacts with the electrolytic ions. A large specific surface area allows more electrode materials to be exposed to electrolyte ions. This increases the electrode material's specific capacitance and energy density.

Surface electroactive sites: attract electrolytic ions, promoting pseudocapacitance. Many electroactive species, such as the oxygen and nitrogen functional groups, experience pseudocapacitance, which increases the electrode material's conductivity.

Controlled porosity: has an impact on the electrode material's specific capacitance and rate capabilities. The pores must be larger than the electrolytic ions to get adsorbed at the electrode surface.

Easy solvation: the electrode pores are responsible for the easy solvation of electrolyte ions where solvation reduces the charge over screening effect.

Low-cost and environment-friendly: the entire price of the supercapacitor device is reduced due to the low cost of the electrode. A sustainable approach is provided by using an electrode made of environmentally appropriate materials.

High thermal chemical and electrochemical stability: electrolyte ions motions are engaged during repeated charge/discharge cycles, which can raise the device's temperature. The electrode should also be chemical and corrosion-resistant since this enhances the electrode's durability.

The electrode materials in supercapacitors may be divided into two categories based on the charge storage mechanisms: EDLC electrodes, which store charges electrostatically at the electrode/electrolyte interface, and pseudocapacitive electrodes which store charge by fast reversible Faradaic processes. Where the non-Faradaic process is engaging, and charges are

stored at the electrode surface, carbon-based materials display EDLC-like behavior. These materials are appropriate for the EDLC electrode because they have a large surface area and an adjustable pore size. Nanostructured materials with high conductivity, such as carbon nanotubes (CNTs), carbon nanofibers, activated carbon, and graphene, reduce supercapacitor resistance [36, 41, 43, 45, 46, 57, 65, 74]. Corrosion resistance and environmental friendliness are two characteristics of carbon allotropes. On the other hand, metal oxide and conducting polymers exhibit a pseudocapacitive charge storage mechanism. This is a Faradaic process in which the electrode undergoes reversible redox reactions. Metal oxides can gain and release electrons throughout the charge/discharge process because they can exist in changing oxidation states. During charging and discharging, a conducting polymer also exhibits Faradaic behavior through doping and de-doping. Because the entire material is engaged in the charge storage process, it has an extraordinarily high capacitance value, which raises the material's energy density. The materials utilized in supercapacitor electrodes have various restrictions, for example, carbon materials have high conductivity, huge specific surface area, and high cyclic stability, but they don't have a lot of capacitance. Supercapacitors have a high capacitance for metal oxides; however, they are unstable. In addition, metal oxides, with the exception of RuO_2, have low conductivity. Due to swelling and shrinking, the conducting polymer degrades after a few charge/discharge cycles. Composite materials combining EDLC and pseudocapacitive material have been developed to overcome these disadvantages. The EDLC electrode offers conductivity and stability, while the surface of the pseudocapacitive material conducts reversible redox reactions. This method has the potential to deliver high power and energy density, as well as improved rate capability and cycle stability.

4.4.2 Electrolytes

One of the most important components of the EESDs is the electrolyte. The physical and chemical qualities of the electrolyte are crucial in defining the supercapacitor's efficiency and performance. It has an impact on the supercapacitor's capacitance, energy density and power density, rate capability, cycle life, and safety. It is responsible for balancing the charges between two electrodes. Electrolyte selection is critical because it significantly impacts electrode–electrolyte interactions. Currently there is no ideal electrolyte that can fulfill all the requirements for supercapacitors. The following are the essential electrolytes capabilities needed for supercapacitors.

Salt effect: The conductivity of an electrolyte varies depending on the solvent. In the same solvent, conductivity changes with salt content. The quantity of free ions determines ionic conductivity; optimal conductivity can boost the electrolyte's ionic conductivity.

Electrolyte conductivity: A high-conductivity electrolyte is required for a high-performance supercapacitor. The conductivity of an electrolyte is determined by concentration of ions, mobility of ions, elementary charges, and valency of mobile ion charges.

Solvent effect: The solvent's composition significantly impacts the electrolyte's conductivity. The viscosity and dielectric constant are the two most important parameters that determine the conductivity of an electrolyte. Salt dissociation and viscosity have an impact on ionic mobility, which is determined by the dielectric's nature. As a result, a good supercapacitor solvent should have a low viscosity and a high dielectric constant.

Thermal stability: The thermal stability of electrolytes is critical for high-temperature supercapacitor operations. Electrolytes should also be stable throughout multiple charge/discharge cycles due to heat release. The composition of electrolytes, such as additives, salt, and solvent, significantly impacts thermal stability.

Electrochemical stability: Supercapacitor stability and safety are linked to electrochemical stability. The electrochemical stability is determined by the electrolyte's interaction with the electrode materials and the electrolyte's component elements.

Aqueous electrolytes, organic electrolytes, and ionic electrolytes are the three types of electrolytes used in electrochemical devices. Aqueous electrolytes, for example, have high conductivity and capacitance at a reasonable cost. Despite its short operating potential window, it has a low energy density. This is owing to the 1.23 V potential difference in water electrolysis. Although organic and ionic electrolytes may operate at higher operating potential windows, their ionic conductivity is lower. The organic electrolyte is poisonous and has problems with handling. Because of the larger ions, ionic electrolytes are more costly and can reach a lower electrode surface. When the supercapacitor is being charged or discharged, the electrolyte is a source of charges and ions moving between the electrodes. There is a wide variety of electrolytes, the most popular of which are ionic liquids, aqueous electrolytes, and organic electrolytes. Aqueous electrolytes are simply salt solutions that have salts dissolved in water. These solutions can either be acidic, such as H_2SO_4, or basic, such as NaOH, or neutral, for example, K_2SO_4 [58, 63]. These electrolytes have a low viscosity in addition to their great ionic conductivity. They are common due to their inexpensive cost, the simplicity with which they may be prepared, the fact that they are not combustible, and the convenience with which they can be acquired. On the other hand, they have a few drawbacks, the most prominent of which is the restricted thermodynamical stability of water at a potential window of 1.23 volts. These constraints prevent them from being used in practical applications. On the other hand, organic electrolytes offer a large operating potential window that is stable at 3 volts. Due to the fact that the equation that defines energy density has a square dependency of the potential window, this, in turn, enhances the energy density of the supercapacitors. The restricted ionic conductivity, the toxic character, and the flammability of the substance are the most significant drawbacks of organic electrolytes. Ionic liquids are a family of non-aqueous electrolytes that take the form of salts that are liquid at normal temperatures. This type of electrolyte can exist in aqueous or non-aqueous forms. These salts are ionic, which indicates that they contain ions in their composition. They have a large operating potential window and a high level of stability. Still, at the same time, they are plagued by high prices and limited abundance, which restricts the commercialization of their products. On the other hand, these ionic liquid electrolytes are now being used, albeit in very small quantities, as a component in various electrolytes that are less expensive.

It has recently been discovered that adding redox compounds to some ionic liquids improves their performance. The use of hydroquinone as a redox additive to an ionic liquid electrolyte increased the specific capacitance of a carbon-based supercapacitor from $42\,F\,g^{-1}$ to $72\,F\,g^{-1}$ [75]. A significant rise in the specific energy value was also reported, which increased from $18.40\,Wh\,kg^{-1}$ to $31.22\,Wh\,kg^{-1}$. Similar results were reported by Navalpotro et al. [76] where they added hydroquinone to N-butyl-N-methylpyrrolidinium bis(triflouromethane sulfonylimide) electrolyte. The capacitance and the specific energy

value increased significantly, going from $70\,F\,g^{-1}$ to $156\,F\,g^{-1}$ and from $10.3\,Wh\,kg^{-1}$ to $30.0\,Wh\,kg^{-1}$, respectively. Lee et al. [77] described the fabrication of nanoporous carbon-based supercapacitors with promising electrochemical properties. They used an aqueous redox electrolyte containing $VOSO_4$ and $SnSO_4$ and were able to achieve specific energy of up to $75.4\,Wh\,kg^{-1}$. Researchers that introduced redox additives to gel polymer electrolytes have also reported on supercapacitor performance [78–80]. Cevik et al. [81] described the production of flexible carbon-based supercapacitor using ammonium molybdate as a redox additive in the electrolyte poly(2-acrylamido-2-methyl-1-propanesulfonic acid). The operating potential window was increased from 1 V to 2 V since a redox mediator was added in this scenario, resulting in a high specific energy value of $73\,Wh\,kg^{-1}$. Gel polymer electrolytes, which are electrolytes based on polymers, are becoming increasingly popular. In addition to its non-corrosiveness, gel polymer electrolyte's capacity to seal is well-known. An electrolyte and polymer matrix are mixed in a separate container to create a gel polymer electrolyte. Polymer matrices can originate from both natural and man-made sources, such as rice starch, chitosan, and alginate (PVA, PVP, PVDF-HFP etc.). The non-toxic, cost-effective, and ecologically friendly properties of natural or biopolymer electrolytes make them popular choices among polymer electrolytes [82].

4.4.3 Separators

A separator is used to separate two electrodes from one another, and its primary function is to prevent the device from shorting out. It enables smooth ion transit in a supercapacitor without enduring any chemical modifications. As a result, selecting separators is a critical prerequisite for the supercapacitor's successful operation. Some of the important separator features arethat it should not conduct electricity, with electrolyte ion permeability it should have a low ionic resistance, it should be easy to wet with the electrolyte, and it should be able to sustain the supercapacitor mechanically. Glass, paper, and ceramics can be used as separator materials. Because of their low cost, porous nature, and flexibility, polymer-based separators are extensively utilized in supercapacitors [83, 84].

4.4.4 Current Collectors

The electrode active materials are coated with a collection of conductive substrates called current collectors. Conductivity, chemical, and electrochemical stability, thermal stability, flexibility, and cost-effectiveness of supercapacitors are all influenced by the choice of current collectors. The supercapacitor's total resistance is heavily influenced by the resistance at the current collector/electrode material interface. A smooth, binder-free contact between the electrode and the current collector will provide maximum charge transfer with the lowest electrochemical series resistance [85]. Electrochemical series resistance is a critical factor in determining the power output of a supercapacitor, therefore selecting an appropriate collector is critical. If certain electrolytes oxidize the metals of the current collector, the device will have a shorter life span. In neutral electrolytes, aluminum current collectors are recommended; stainless steel current collectors are favored in severe electrolytes. Metals and alloys, including copper, aluminum, stainless steel, nickel foam, graphitic carbon, FTO/ITO-coated glass conductive substrate-coated PET flexible sheet, have all been used

as current collectors in the supercapacitors. Current collectors are responsible for transporting electrons from the supercapacitor electrodes to the external circuit. It should have a high electrical conductivity to allow electrons to flow from the electrode to the external circuit without resistance. Because supercapacitor devices employ a variety of electrode and electrolyte materials, the current collector must be corrosion resistant. It should also have strong mechanical strength because it mechanically supports the entire supercapacitor device. Aluminum, graphite, iron, nickel foam, and steel alloys are commonly employed as current collectors. The active material is coated over the current collector to reduce contact resistance. Currently, nickel mesh, metal foams, and carbon cloth are employed to offer effective surface areas for electrode material. These lower contact resistance and allow for homogeneous active electrode materials dispersion. To enhance the current collector's properties, the thickness, size and form, and accessible surface area should be increased, which may give low internal resistance and high stability by preventing delamination between the current collector and the electrode.

4.5   Conclusions

One of the most promising EESDs is supercapacitors. They have the capability of bridging the gap between batteries and traditional capacitors. They have a higher energy density and a higher power density than ordinary capacitors and batteries, respectively. Short charge/discharge time, high-rate capability, and wide operating temperature range are all electrochemical features of supercapacitors. This is due to the charge storage method involving electrolytic ions being adsorbed at the electrode surface, forming an EDLC. Because no chemical processes are involved, this gives excellent cyclic stability. The supercapacitor demonstrates a different sort of charge storage called pseudocapacitance, which involves reversible redox processes. This increases the supercapacitor's capacitance and energy density. In a hybrid supercapacitor, various combinations of Faradaic and non-Faradaic electrode materials are employed to improve the supercapacitor's performance. An asymmetric capacitor, composite electrode, and battery-type capacitor make up the hybrid capacitor. This results in a synergistic approach to increasing efficiency. Supercapacitor devices come in a variety of materials and architectures, each of which is suited to a certain target application. Nonetheless, major research is being conducted in order to build a supercapacitor with a high energy density that can be used as a battery without compromising other features. This chapter discusses the introduction of supercapacitors and highlights the features of various aspects of supercapacitors, including the supercapacitor components and their various parameters.

Acknowledgments

References

1 M. Höök, X. Tang, *Energy Policy* **2013**, *52*, 797–809.

2 D. Millstein, R. Wiser, M. Bolinger, G. Barbose, *Nat. Energy* **2017**, *2*, 17134.

3 E. T. Sayed, T. Wilberforce, K. Elsaid, M. K. H. Rabaia, M. A. Abdelkareem, K.-J. Chae, A. G. Olabi, *Sci. Total Environ.* **2021**, *766*, 144505.

4 A. Rahman, O. Farrok, M. M. Haque, *Renew. Sust. Energ. Rev.* **2022**, *161*, 112279.

5 S. S. Shah, M. A. Aziz, A.-R. Al-Betar, W. Mahfoz, *Arab. J. Chem.* **2022**, *15*, 104058.

6 M. Rauf, S. S. Shah, S. K. Shah, S. N. A. Shah, T. U. Haq, J. Shah, A. Ullah, T. Ahmad, Y. Khan, M. A. Aziz, K. Hayat, *J. Saudi Chem. Soc.* **2022**, *26*, 101514.

7 S. Islam, M. M. Mia, S. S. Shah, S. Naher, M. N. Shaikh, M. A. Aziz, A. J. S. Ahammad, *Chem. Rec.* **2022**, *22*, e202200013.

8 S. Zhang, N. Pan, *Adv. Energy Mater.* **2015**, *5*, 1401401.

9 V. T. Chebrolu, B. Balakrishnan, A. R. Selvaraj, H.-J. Kim, *Sustain. Energy Fuels* **2020**, *4*, 4848–4858.

10 L. F. Chen, Z. H. Huang, H. W. Liang, Q. F. Guan, S. H. Yu, *Adv. Mater.* **2013**, *25*, 4746–4752.

11 A. Khan, R. A. Senthil, J. Pan, S. Osman, Y. Sun, X. Shu, *Electrochim. Acta* **2020**, *335*, 135588.

12 J. Zhu, W. Sun, D. Yang, Y. Zhang, H. H. Hoon, H. Zhang, Q. Yan, *Small* **2015**, *11*, 4123–4129.

13 P. Yu, Z. Zhang, L. Zheng, F. Teng, L. Hu, X. Fang, *Adv. Energy Mater.* **2016**, *6*, 1601111.

14 D. P. Chatterjee, A. K. Nandi, *J. Mater. Chem. A* **2021**, *9*, 15880–15918.

15 S. Li, C. Shi, Y. Pan, Y. Wang, *Diamond Relat. Mater.* **2021**, *115*, 108358.

16 J. Zhu, J. Jiang, Z. Sun, J. Luo, Z. Fan, X. Huang, H. Zhang, T. Yu, *Small* **2014**, *10*, 2937–2945.

17 L. Su, Q. Zhang, Y. Wang, J. Meng, Y. Xu, L. Liu, X. Yan, *J. Mater. Chem. A* **2020**, *8*, 8648–8660.

18 W. Zuo, R. Li, C. Zhou, Y. Li, J. Xia, J. Liu, *Adv. Sci.* **2017**, *4*, 1600539.

19 B. Mordina, R. Kumar, N. S. Neeraj, A. K. Srivastava, D. K. Setua, A. Sharma, *J. Energy Storage* **2020**, *31*, 101677.

20 Z. Wu, X. Yang, H. Gao, H. Shen, H. Wu, X. Xia, X. Wu, W. Lei, J. Yang, Q. Hao, *J. Alloys Compd.* **2022**, *891*, 162053.

21 A. M. Zardkhoshoui, S. S. Hosseiny Davarani, *Sustain. Energy Fuels* **2021**, *5*, 900–913.

22 S. S. Patil, D. P. Dubal, V. G. Deonikar, M. S. Tamboli, J. D. Ambekar, P. Gomez-Romero, S. S. Kolekar, B. B. Kale, D. R. Patil, *ACS Appl. Mater. Interfaces* **2016**, *8*, 31602–31610.

23 A. Muzaffar, M. B. Ahamed, K. Deshmukh, J. Thirumalai, *Renew. Sust. Energ. Rev.* **2019**, *101*, 123–145.

24 M. M. Hasan, T. Islam, A. Imran, B. Alqahtani, S. S. Shah, W. Mahfoz, M. R. Karim, H. F. Alharbi, M. A. Aziz, A. J. S. Ahammad, *Electrochim. Acta* **2021**, *374*, 137968.

25 S. S. Shah, K. Hayat, S. Ali, K. Rasool, Y. Iqbal, *Mater. Sci. Semicond. Process.* **2019**, *90*, 65–71.

26 M. M. Faisal, S. R. Ali, S. S. Shah, M. W. Iqbal, S. Pushpan, M. A. Aziz, N. P. Aguilar, M. M. Alcalá Rodríguez, S. L. Loredo, K. C. Sanal, *Ceram. Int.* **2022**, *48*, 28565–28577.

27 S. S. Shah, H. Yang, M. Ashraf, M. A. A. Qasem, A. S. Hakeem, M. A. Aziz, *Chem. Asian J.* **2022**, *17*, e202200567.

28 D. A. Evans, T. A. Murphy, *Packaged hybrid capacitor*, *US Patents*, **2004**, US 6,721,170 B1.

29 X. He, X. Mao, C. Zhang, W. Yang, Y. Zhou, Y. Yang, J. Xu, *J. Mater. Sci. - Mater. Electron.* **2020**, *31*, 2145–2152.

30 C. Guo, H. Wang, Y. Liu, Y. Zhang, S. Cui, Z. Guo, C. Ma, *Energy Fuel* **2021**, *35*, 4524–4532.

31 V. T. Chebrolu, B. Balakrishnan, D. Chinnadurai, H.-J. Kim, *Adv. Mater. Technol.* **2020**, *5*, 1900873.

32 Z. Li, S. Gadipelli, H. Li, C. A. Howard, D. J. L. Brett, P. R. Shearing, Z. Guo, I. P. Parkin, F. Li, *Nat. Energy* **2020**, *5*, 160–168.

33 N. Wu, X. Bai, D. Pan, B. Dong, R. Wei, N. Naik, R. R. Patil, Z. Guo, *Adv. Mater. Interfaces* **2021**, *8*, 2001710.

34 M. Zhang, L. He, T. Shi, R. Zha, *Chem. Mater.* **2018**, *30*, 7391–7412.

35 Y. Shao, M. F. El-Kady, J. Sun, Y. Li, Q. Zhang, M. Zhu, H. Wang, B. Dunn, R. B. Kaner, *Chem. Rev.* **2018**, *118*, 9233–9280.

36 S. S. Shah, E. Cevik, M. A. Aziz, T. F. Qahtan, A. Bozkurt, Z. H. Yamani, *Synth. Met.* **2021**, *277*, 116765.

37 Z. Bi, Q. Kong, Y. Cao, G. Sun, F. Su, X. Wei, X. Li, A. Ahmad, L. Xie, C.-M. Chen, *J. Mater. Chem. A* **2019**, *7*, 16028–16045.

38 M. Ashraf, I. Khan, M. Usman, A. Khan, S. S. Shah, A. Z. Khan, K. Saeed, M. Yaseen, M. F. Ehsan, M. N. Tahir, N. Ullah, *Chem. Res. Toxicol.* **2020**, *33*, 1292–1311.

39 M. Ashraf, S. S. Shah, I. Khan, M. A. Aziz, N. Ullah, M. Khan, S. F. Adil, Z. Liaqat, M. Usman, W. Tremel, M. N. Tahir, *Chem. Eur. J.* **2021**, *27*, 6973–6984.

40 A. Helal, S. S. Shah, M. Usman, M. Y. Khan, M. A. Aziz, M. Mizanur Rahman, *Chem. Rec.* **2022**, *22*, e202200055.

41 S. S. Shah, M. A. A. Qasem, R. Berni, C. Del Casino, G. Cai, S. Contal, I. Ahmad, K. S. Siddiqui, E. Gatti, S. Predieri, J.-F. Hausman, S. Cambier, G. Guerriero, M. A. Aziz, *Sci. Rep.* **2021**, *11*, 6945.

42 M. Usman, M. Humayun, S. S. Shah, H. Ullah, A. A. Tahir, A. Khan, H. Ullah, *Energies* **2021**, *14*, 2281.

43 M. Yaseen, M. A. K. Khattak, M. Humayun, M. Usman, S. S. Shah, S. Bibi, B. S. U. Hasnain, S. M. Ahmad, A. Khan, N. Shah, A. A. Tahir, H. Ullah, *Energies* **2021**, *14*, 7779.

44 T. Islam, M. M. Hasan, S. S. Shah, M. R. Karim, F. S. Al-Mubaddel, M. H. Zahir, M. A. Dar, M. D. Hossain, M. A. Aziz, A. J. S. Ahammad, *J. Energy Storage* **2020**, *32*, 101908.

45 S. S. Shah, H. T. Das, H. R. Barai, M. A. Aziz, *Polymers* **2022**, *14*, 270.

46 M. A. Aziz, S. S. Shah, S. M. A. Nayem, M. N. Shaikh, A. S. Hakeem, I. A. Bakare, *J. Energy Storage* **2022**, *50*, 104278.

47 H. Wang, Y. Zhu, Q. Zong, Q. Wang, H. Yang, Q. Zhang, *Electrochim. Acta* **2019**, *321*, 134746.

48 K. C. S. Lakshmi, X. Ji, T.-Y. Chen, B. Vedhanarayanan, T.-W. Lin, *J. Power Sources* **2021**, *511*, 230434.

49 S. K. Shinde, H. M. Yadav, G. S. Ghodake, A. D. Jagadale, M. B. Jalak, D.-Y. Kim, *Ceram. Int.* **2021**, *47*, 15639–15647.

50 S. S. Shah, M. A. Aziz, Z. H. Yamani, *Chem. Rec.* **2022**, *22*, e202200018.

51 Y. Wang, Y. Song, Y. Xia, *Chem. Soc. Rev.* **2016**, *45*, 5925–5950.

52 J. F. Mulligan, *Am. J. Phys.* **1989**, *57*, 68–74.

53 H. I. Becker, *Low voltage electrolytic capacitor*, **1957**, *2,800,616*, US2800616A.

54 D. L. Boos, *Electrolytic capacitor having carbon paste electrodes*, **1970**, *US3536963A*, 3,536,963.

55 S. S. Shah, S. M. A. Nayem, N. Sultana, A. J. S. Ahammad, M. A. Aziz, *ChemSusChem* **2022**, *15*, e202101282.

56 S. S. Shah, M. A. Alfasane, I. A. Bakare, M. A. Aziz, Z. H. Yamani, *J. Energy Storage* **2020**, *30*, 101562.

57 S. S. Shah, M. A. Aziz, W. Mahfoz, A.-R. Al-Betar, Conducting Polymers Based Nanocomposites for Supercapacitors in *Nanostructured Materials for Supercapacitors*, (Eds: S. Thomas, A. B. Gueye, R. K. Gupta), Springer, Cham, **2022**, Chapter 22, pp. 485–511, Vol. *1*.

58 B. Pal, S. Yang, S. Ramesh, V. Thangadurai, R. Jose, *Nanoscale Adv.* **2019**, *1*, 3807–3835.

59 X. Tian, Q. Zhu, B. Xu, *ChemSusChem* **2021**, *4*, 2501–2515.

60 J. A. Staser, J. W. Weidner, *J. Electrochem. Soc.* **2014**, *161*, E3267–E3275.

61 W. Gu, G. Yushin, *Wiley Interdiscip. Rev. Energy Environ.* **2014**, *3*, 424–473.

62 C. Xu, G. Yang, D. Wu, M. Yao, C. Xing, J. Zhang, H. Zhang, F. Li, Y. Feng, S. Qi, M. Zhuo, J. Ma, *Chem. Asian J.* **2021**, *16*, 549–562.

63 C. Zhong, Y. Deng, W. Hu, J. Qiao, L. Zhang, J. Zhang, *Chem. Soc. Rev.* **2015**, *44*, 7484–7539.

64 I. U. Din, M. Usman, S. Khan, A. Helal, M. A. Alotaibi, A. I. Alharthi, G. Centi, *J. CO2 Util.* **2021**, *43*, 101361.

65 M. D. Garba, M. Usman, S. Khan, F. Shehzad, A. Galadima, M. F. Ehsan, A. S. Ghanem, M. Humayun, *J. Environ. Chem. Eng.* **2021**, *9*, 104756.

66 S. Khan, Y. A. Khulief, A. Al-Shuhail, *Mitig. Adapt. Strat. Gl. Chan.* **2019**, *24*, 23–52.

67 M. Usman, A. S. Ghanem, S. Niaz Ali Shah, M. D. Garba, M. Yusuf Khan, S. Khan, M. Humayun, A. Laeeq Khan, *Chem. Rec.* **2022**, *22*, e202200039.

68 K. D. Verma, P. Sinha, M. K. Ghorai, K. K. Kar, *Diamond Relat. Mater.* **2022**, *123*, 108879.

69 C. K. Roy, S. S. Shah, A. H. Reaz, S. Sultana, A.-N. Chowdhury, S. H. Firoz, M. H. Zahir, M. A. A. Qasem, M. A. Aziz, *Chem. Asian J.* **2021**, *16*, 296–308.

70 N. C. Deb Nath, S. S. Shah, M. A. A. Qasem, M. H. Zahir, M. A. Aziz, *ChemistrySelect* **2019**, *4*, 9079–9083.

71 L. L. Zhang, X. Zhao, *Chem. Soc. Rev.* **2009**, *38*, 2520–2531.

72 R. S. Kate, S. A. Khalate, R. J. Deokate, *J. Alloys Compd.* **2018**, *734*, 89–111.

73 C. Zhong, Y. Deng, W. Hu, D. Sun, X. Han, J. Qiao, J. Zhang, Electrolytes for Electrochemical Supercapacitors in *Electrolytes for Electrochemical Supercapacitors*, 1st ed., (Ed.: C. Zhong), CRC Press, Boca Raton, FL, **2016**, Chapter 2, p. 362, Vol. *1*.

74 M. Daud, M. S. Kamal, F. Shehzad, M. A. Al-Harthi, *Carbon* **2016**, *104*, 241–252.

75 S. Sathyamoorthi, V. Suryanarayanan, D. Velayutham, *J. Power Sources* **2015**, *274*, 1135–1139.

76 P. Navalpotro, J. Palma, M. Anderson, R. Marcilla, *J. Power Sources* **2016**, *306*, 711–717.

77 J. Lee, B. Krüner, A. Tolosa, S. Sathyamoorthi, D. Kim, S. Choudhury, K.-H. Seo, V. Presser, *Energy Environ. Sci.* **2016**, *9*, 3392–3398.

78 J. Zhong, L.-Q. Fan, X. Wu, J.-H. Wu, G.-J. Liu, J.-M. Lin, M.-L. Huang, Y.-L. Wei, *Electrochim. Acta* **2015**, *166*, 150–156.

79 G. Ma, M. Dong, K. Sun, E. Feng, H. Peng, Z. Lei, *J. Mater. Chem. A* **2015**, *3*, 4035–4041.

80 E. Feng, G. Ma, K. Sun, Q. Yang, H. Peng, Z. Lei, *RSC Adv.* **2016**, *6*, 75896–75904.

81 E. Cevik, A. Bozkurt, M. Hassan, M. A. Gondal, T. F. Qahtan, *ChemElectroChem* **2019**, *6*, 2876–2882.

82 T. Xu, K. Liu, N. Sheng, M. Zhang, W. Liu, H. Liu, L. Dai, X. Zhang, C. Si, H. Du, K. Zhang, *Energy Storage Mater.* **2022**, *48*, 244–262.

83 Q. Meng, K. Cai, Y. Chen, L. Chen, *Nano Energy* **2017**, *36*, 268–285.

84 A. Clemente, S. Panero, E. Spila, B. Scrosati, *Solid State Ion.* **1996**, *85*, 273–277.

85 H. Trivedi, K. D. Verma, P. Sinha, K. K. Kar, Current Collector Material Selection for Supercapacitors in *Handbook of Nanocomposite Supercapacitor Materials III: Selection*, (Ed.: K. K. Kar), Springer, Cham, **2021**, pp. 271–311, https://doi.org/10.1007/978-3-030-68364-1_8.

5

Electrochemical Techniques for Supercapacitors

Syed Shaheen Shah[1],*, Md. Abdul Aziz[2,3],*, and Munetaka Oyama[4]

[1] *JSPS International Research Fellow, Department of Material Chemistry, Graduate School of Engineering, Kyoto University, Kyotodaigaku Katsura, Nishikyo-ku, Kyoto 615-8520, Japan*
[2] *Interdisciplinary Research Center for Hydrogen and Energy Storage (IRC-HES), King Fahd University of Petroleum & Minerals, KFUPM Box 5040, Dhahran 31261, Saudi Arabia*
[3] *K. A. CARE Energy Research and Innovation Center, King Fahd University of Petroleum & Minerals, Dhahran, 31261, Saudi Arabia*
[4] *Department of Material Chemistry, Graduate School of Engineering, Kyoto University, Kyotodaigaku Katsura, Nishikyo-ku, Kyoto 615-8520, Japan*
* *Corresponding authors*

5.1   Introduction

Researchers have been encouraged to investigate renewable energy supplies because of the finite fossil fuel resources and the long-term harmful impacts of greenhouse emissions. The intermittent nature of wind and solar renewable energy poses a significant barrier to harnessing the abundant renewable energy that these sources provide, necessitating the development of energy conversion and storage technologies [1, 2]. There are a variety of electrical energy storage devices (EESDs) that are useful in this situation and EESDs, such as batteries and supercapacitors, are used in our daily lives and are critical to industry. Batteries have been widely employed for their remarkable performance, although they have drawbacks such as poor power density, heat generation, safety issues, and limited cyclic life. Therefore, developing durable, compact, and secure EESDs with high energy and power performance would unquestionably revolutionize the landscape of electric energy generation, distribution, and utility for industrial and military applications [1–3].

Several advantages of using supercapacitors as an EESD are their high-power capacity, ease of operation, great reversibility, extremely long cyclic life, low thermochemical heat, and low cost of manufacture [4–9]. The industrial sector has succeeded using supercapacitors in power electronics, data storage, and backup systems. Supercapacitors, also known as ultra-capacitors, power capacitors, or gold capacitors, have a substantially larger stored specific energy than regular capacitors. The specific power of supercapacitors is considerably higher than that of typical batteries, despite having a lower specific energy density. As a result of this design, their specific energy and specific power may be raised by many orders of magnitude, allowing them to be utilized as an independent energy supply or a hybrid system (in combination with batteries). Since supercapacitors have unique properties of

high specific energy and specific power capabilities, they may be used in various applications [10–14].

The easiest way to evaluate supercapacitor performance is to look at three parameters: specific capacitance, operating potential window, and equivalent series resistance. These characteristics are heavily influenced by the electrode materials, supercapacitor design, and electrolytes. Cyclic voltammetry (CV), galvanostatic charge-discharge (GCD), and electrochemical impedance spectroscopy (EIS) are the commonly used techniques to evaluate the performance of supercapacitors. This chapter mainly focuses on understanding the various electrochemical techniques for supercapacitors, including CV, GCD, and EIS, and explains the essential measurement parameters.

5.2 Electrochemical Techniques for Supercapacitors

Electrochemistry is the study of the processes that take place on the electrodes of an energy storage device, such as Faradaic and non-Faradaic reactions. There are two ways to track the electrochemical reactions in electrode materials: ions or electrons. To generate a current, electrolyte ions in the electrolyte solution are engaged in the movement of electrons between electrodes. Electrons travel from negative to positive when charging and vice versa while discharging [15]. In a setup with three electrodes and two electrodes, an electrochemical workstation known as a potentiostat is utilized in order to perform the electrochemical studies. The three-electrode setup has working (the prepared electrode), reference (Ag/AgCl), and counter (platinum wire) electrodes. The working electrode was the one that was being investigated. Both the positive and negative electrodes used the same materials being explored in the two-electrode system [11, 16–20]. The three- and two-electrode configurations that are used for electrochemical experiments are depicted in Figure 5.1. There is a subtle difference in the ways in which three-electrode and two-electrode electrochemical systems are configured; specifically, in the two-electrode system, the counter electrode is adjusted in conjunction with the reference electrode, whereas in the three-electrode system, each of the three electrodes is adjusted in its own unique manner.

Two- and three-electrode assemblies are used to perform electrochemical characterizations on the produced supercapacitors. An electrochemical workstation (potentiostat) is used to perform CV, GCD, and EIS measurements. The CV of the supercapacitor device is carried out at various scan rates, and the GCD of the supercapacitor device is carried out at various current densities. In contrast, the EIS of a supercapacitor device is carried out at various applied frequencies and various applied potentials. Different electrochemical methods, including CV, GCD, and EIS, are utilized in order to assess the electrochemical properties of newly developed supercapacitors [8, 13, 20–22].

5.2.1 Cyclic Voltammetry

The cyclic voltammetry (CV) method is a potentiodynamic electrochemical evaluation technique that uses a predetermined voltage scan rate to sweep the working electrode's potential between two different voltage limits. In a standard CV experiment, the voltage at the working electrodes is made to rise at a certain scan rate until it reaches a potential value
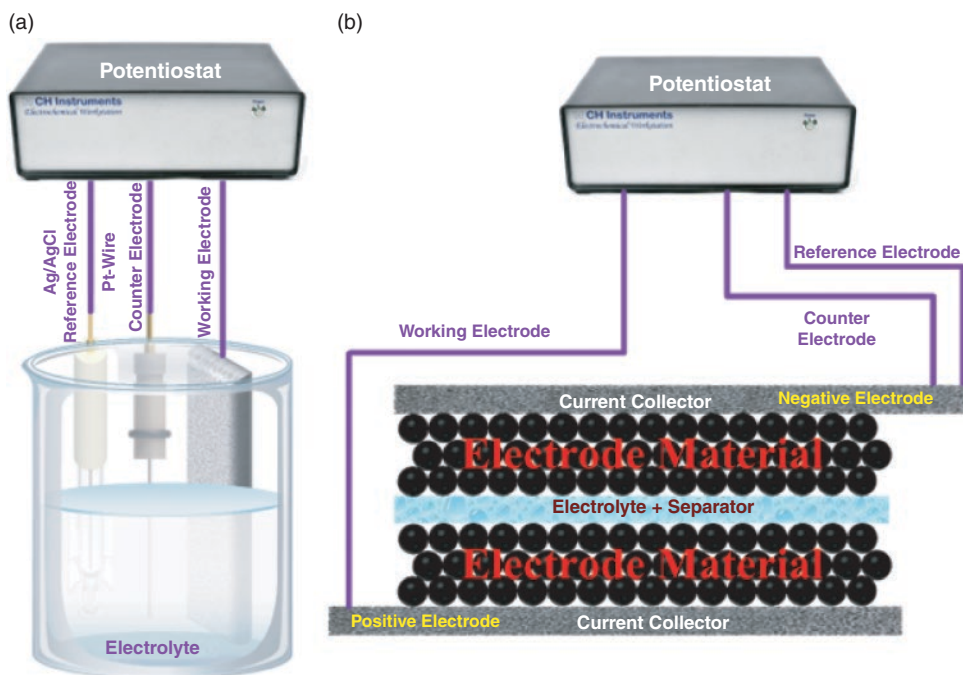
(a)

(b)

Potentiostat

CH Instruments

Ag/AgCl Reference Electrode

Pt-Wire Counter Electrode

Working Electrode

Electrolyte

Potentiostat

CH Instruments

Reference Electrode

Counter Electrode

Working Electrode

Current Collector

Negative Electrode

Electrode Material

Electrolyte + Separator

Electrode Material

Positive Electrode

Current Collector

Figure 5.1 Schematic representation for (a) three-electrode and (b) two-electrode electrochemical systems connected to a potentiostat.

that has been defined in advance. When the desired potential value has been reached, the procedure is then inverted to decrease the potential while maintaining the same scan rate. This continues until the desired lower potential value has been achieved [1, 2, 10, 18]. The voltage sweep approach creates a voltage differential between the working electrode and the counter electrode. This allows electrons to move freely between the working electrode and the counter electrode, which in turn causes current to flow in the external circuit. The resultant current and voltage are both measured and analyzed, yielding informative data on the charge transfer kinetics, redox behaviour of the electrode material, specific capacitance, reversibility, and the cyclic stability of the supercapacitors [23–25]. The voltage-current curves of an ideal supercapacitor often take the form of perfect rectangles and have a constant current. However, the rectangular shape of CV curves deviates in practical applications due to the existence of Faradaic reactions or the resistive nature of electrode materials. CV is considered the primary approach for characterizing supercapacitors, regardless of whether they have two or three electrodes configured in their setup [26]. The CV analysis is done by making linear adjustments to the potential difference between the supercapacitor's negative and positive electrodes. The pace at which this potential shift is referred to as the scan rate or the sweep rate, and it is measured in volts per second (V/sec). It is possible to differentiate between the different charge storage systems based on the form of the CV profile [27]. The electrochemical double-layer capacitors (EDLC) type of charge storage mechanism is indicated by the rectangular shape of the CV curve. On the other hand, a small deviation from the rectangular shape and the appearance of redox peaks in a

highly reversible manner are indicators of a pseudocapacitive charge storage mechanism. Various CV curves and GCD profiles of supercapacitors are shown in Figure 5.2.

Analyzing the supercapacitor electrochemical behaviour could be accomplished using CV measurements. A type of supercapacitor, EDLC or pseudocapacitor, could be determined by the shape of the CV curve, where the reaction mechanisms of the electrod material may be seen in the CV shapes. The CV is often used to display the redox potential of the electrode material and to gather qualitative data about the electrode material. The current response is captured as cyclic voltammograms at a constant scan rate within a predefined operating potential window by applying a voltage across the relevant electrode. The CV depicts the oxidation and reduction peaks of the Faradaic processes on the electrode material's surface. Further, the CV data can be used to calculate the key performance parameter such as specific capacitance (C_s) and arial capacitance (C_A) of the supercapacitor using equations (5.1) and (5.2), respectively [22, 29].

$$C_s(F/g) = \frac{\int I \times \Delta V}{m \times \Delta V \times \nu} \tag{5.1}$$

$$C_A(F/cm^2) = \frac{\int I \times \Delta V}{A \times \Delta V \times \nu} \tag{5.2}$$
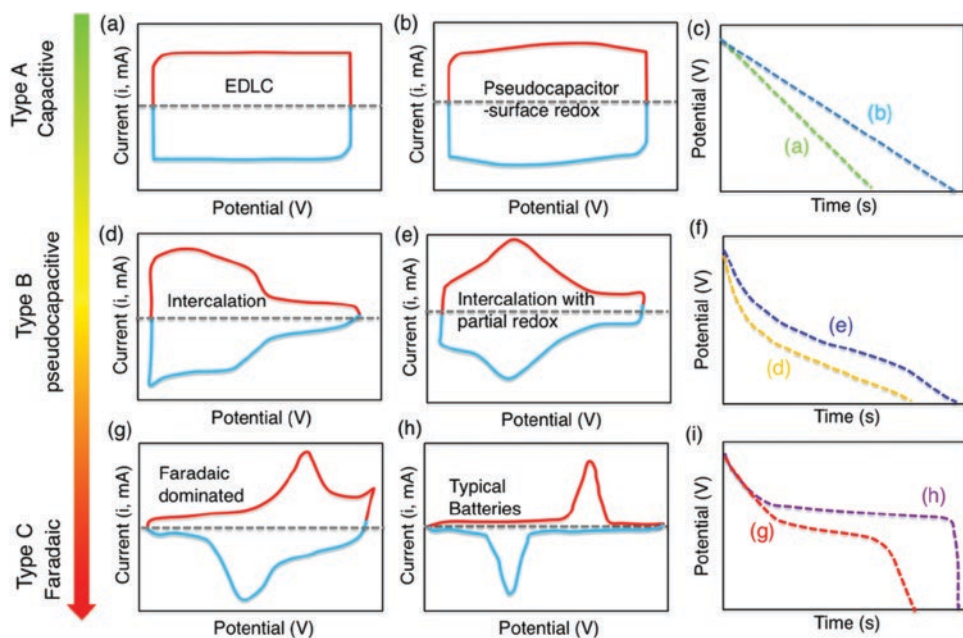
Figure 5.2 CV curves and GCD profiles of supercapacitors demonstrating charge storage mechanisms for EDLC, pseudocapacitors, and hybrid supercapacitors. *Reproduced with permission [28]. Copyright 2018, American Chemical Society.*

where, $\int I \times \Delta V$ represent the area under CV curve (in watt), m stands for the mass of active material of electrodes (in gram), A stands for the working area of electrodes (in cm^2), v is the scan rate (in volt/sec), and ΔV is the operating potential window (in volt).

The CV analysis can also be used to quantify the contribution from both mechanisms using power law. This method deals with the cyclic voltammograms obtained at the same scan rates at a constant operating potential window. The value of cathodic and anodic peak current is important and recorded in each case. The total current can be given as a sum of capacitive and diffusion-controlled currents. The charge storage mechanism can be studied using power law relation for CV peak current (i_p) and scan rate (v), using equation (5.3) [30, 31].

$$i = i_{\mathrm{cap}} + i_{\mathrm{diff}} = a v^{\mathrm{b}} \tag{5.3}$$

Here a and b are constants, i is the output current for a fixed potential, i_{cap} is the capacitive current, and i_{diff} is the diffusive current. Taking log on both sides to get equation (5.4) [30, 31].

$$\log i = \log \mathrm{a} + \mathrm{b}\, \log v \tag{5.4}$$

The slope of the graph obtains the value of b plotted between the log of cathodic or anodic peak current and the log of scan rate following equation (5.4). The charge storage follows diffusion-controlled kinetics if the value of b is 0.5 and surface-controlled kinetics if the value of b is 1.0. Whereas from b = 0.5 to 1.0 is the transitional zone between capacitive and battery-type materials, as shown in Figure 5.3.

5.2.2 Galvanostatic Charge-discharge

Using galvanostatic charge-discharge (GCD), a well-established electrochemical measurement technique may provide valuable information on the electrochemical characteristics of supercapacitors. The GCD method is used in an operating potential window to maintain a consistent current density when charging and discharging the supercapacitor. When the supercapacitor is charged or discharged at a certain current density, the charge transfer capacity between the electrodes stays constant. The potential and time are monitored and altered based on the applied current density. Learning a great deal about an electrode material's electrochemical properties is possible by studying its voltage and time dynamics with current density. GCD curves are the most practical and reliable way to calculate the specific capacitance of supercapacitors [2, 7, 22]. For an ideal supercapacitor, the GCD curve is linear and symmetric; however, it can deviate for a real supercapacitor.
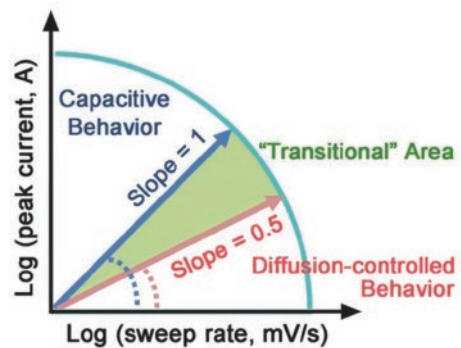
Figure 5.3 Power law dependency on the peak current and sweep rate for supercapacitors. *Reproduced with permission [30]. Reproduced under the term CC-BY-4.0. Copyright 2017, Liu et al., Wiley.*

Capacitance, IR drop, Coulombic efficiency, power density, and energy density may all be studied using GCD analysis. Charge and discharge the device while maintaining a constant current are the cornerstones of GCD analysis. As with CV, the GCD curve's appearance may be utilized to infer the charge storage method. Redox reactions may be viewed as little bumps in the GCD curves [32, 33]. In contrast, capacitive type EDLC mechanisms are represented by the highly reversible triangular form of the GCD curve, as shown in Figure 5.2.

Because of the total ohmic resistance of the electrodes, electrolyte, and contact resistances in the system, an immediate voltage decrease occurs when the supercapacitor changes from charging to discharging. This voltage drop is referred to as an IR drop. The overall useable voltage window (in volts) is decreased due to the IR drop [34]. It is important to remember the impacts of IR drop when attempting to interpret electrochemical data since IR drop significantly impacts these measurements [35, 36]. There are some factors that influence the amount of IR drop: the distribution of both current and potential within the electrolyte, i.e., changing the working electrode's size or shape, will change the shape of the equipotential lines; the location of the reference electrode in relation to the working electrode; the electrolyte solution and electrode material's ability to conduct electricity, i.e., the lower the conductivity of the electrolyte and electrode material, the higher the IR drop. A three-electrode electrochemical system could be used to find the actual IR drop of electrode materials, increasing the amount of totally dissociated electrolytes in the solution with an increase in the overall conductivity, keeping the tip of the reference electrode near to the working electrode surface, using low current densities, and using a small area of the working electrode [35, 36].

The electrochemical performance of the supercapacitors may be evaluated with the use of GCD measurements. The electrochemical measurements are carried out in the galvanostatic mode, which involves the potential change while the current remains the same. The specific capacitance (C_s in Farad/gram) and arial capacitance (C_A in Farad/cm^2) of the supercapacitors could be calculated from GCD measurements using equations (5.5) and (5.6), respectively [22, 29, 37].

$$C_s = \frac{I \times \Delta t}{m \times \Delta V} \tag{5.5}$$

$$C_A = \frac{I \times \Delta t}{A \times \Delta V} \tag{5.6}$$

where, I shows the constant current (in ampere), Δt corresponds to the discharging time (sec), m corresponds to the active material mass (in gram), A represents the electrodes working area (in cm^2), and ΔV denotes the discharge operating potential window (in Volts).

The supercapacitor device's energy density (E, Wh/cm^2 or Wh/kg) is an essential performance characteristic, and it may be evaluated in line with the equation (5.7) [11, 12, 16, 17, 22].

$$E = \frac{1}{2} \frac{C_s \times \Delta V^2}{3.6} \tag{5.7}$$

Research on supercapacitors has also shown that power density (P, W/cm^2 or W/kg) is an important factor. This can be calculated by applying the formula given in equation (5.8).

$$P = \frac{E \times 3600}{\Delta t} \tag{5.8}$$

In a similar manner, the Coulombic efficiency (η) of supercapacitors may be determined by using equation (5.9) [12].

$$\eta = \frac{t_d}{t_c} \times 100\% \tag{5.9}$$

Where is the Coulombic efficiency expressed as a percentage, t_d and t_c are the times in seconds required to discharge and charge the supercapacitor, respectively.

5.2.3 Electrochemical Impedance Spectroscopy

Electrochemical impedance spectroscopy (EIS) analysis is used to investigate various resistance properties of supercapacitors as a frequency function. Typically, a frequency in the range of mHz to MHz is overlaid on a steady state potential. The data from the EIS analysis may be used to create a graph (also known as a Bode plot) by plotting the phase angle on the y-axis and frequency on the x-axis. At low frequencies, phase angles close to 90° suggest optimum capacitive behaviour. The Nyquist plot, including real and imaginary components of the impedance, may also be drawn using the EIS data. As shown in Figure 5.4, the x-intercept in the high-frequency zone represents electrode resistance or bulk resistance. In contrast, the semi-circle linked with the mid-range frequency represents charge transfer resistance. The capacitive nature of the device can be seen in the low-frequency area, which has a rapidly rising curve. The EIS method could be used to determine the electrochemical nature of the electrode materials that had been applied in supercapacitors. Using EIS, researchers may learn more about the kinetics of electrochemical processes at the electrode's surface, as well as the charge transfer behaviour of materials [38–41]. An EIS study of electrode materials could be conducted at zero bias potential to determine their various resistance components. A semi-circle is seen during the high-frequency range, whereas a straight line emerges in the lower-frequency range. At low frequencies, the Warburg resistance is shown by a straight line, but at higher frequencies, the charge transfer resistance is represented by a semi-circle. Materials are more resistive when the semi-circle is greater; on the other hand, materials are more conductive when the semi-circle is smaller [1, 2, 11, 22].

In order to show EIS analysis, a Nyquist plot is employed, which depicts imaginary vs. real sections of the complicated impedance of an electrochemical cell. Using the EIS approach, one is able to examine the conductivity as well as the charge transport characteristics of the electrode–electrolyte interface [11, 44]. Nyquist plots have typically been interpreted through analogous resistor capacitor (RC) circuits and/or by applying physical intuition. On the other hand, the interpretations that follow are not unique in the literature and are usually inconsistent. Physical interpretations of EIS data for EDLCs and pseudocapacitors were published by Mei et al. [42, 43]. They used a physicochemical transport model

that accounted for electrode charge transport, electric double-layer generation at the electrode–electrolyte interface, and ion diffusion in symmetric/binary electrolytes to replicate Nyquist plots numerically. To record typical EDLC Nyquist plots, different electrolyte ions sizes, electrolyte domain thickness, diffusion coefficients, concentrations, and electrode thickness and conductivity were numerically reproduced. The electrolyte and electrode resistances and equilibrium differential capacitances were calculated using Nyquist plots without employing comparable RC circuits. As can be seen in Figure (5.4a), the Nyquist plots of individual EDLC electrodes and devices were simulated using a modified Poisson-Nernst-Planck model and closely matched the real results. This was accomplished through the use of computational modeling. Based on these discoveries it is possible to directly read equilibrium differential capacitance, diffuse layer resistance, bulk electrolyte resistance, and electrode resistance from Nyquist plots. In a similar manner, the physical interpretation of the EIS data, which can be seen in Figure (5.4b), explains the normal behaviour of pseudocapacitors.

The majority of supercapacitor devices deviate from the ideal capacitive behavior because they do not fulfill the set criterion that the imaginary and real components of the impedance should be out of phase by 90°. This criterion states that the imaginary and real components of the impedance should be in opposition to one another. The existence of various resistance characteristics inside the capacitive element is the primary cause of the behavior of the capacitive element deviating from the ideal behavior of a capacitive element. This frequency-dependent capacitive reactance is sometimes referred to as electrochemical series resistance since it will always produce a phase difference that is greater than 0°. The equivalent series resistance (ESR) accounts for a portion of the total internal resistance of a supercapacitor and is often stated in parallel with the capacitor. As was previously mentioned, the observed potential decrease in the discharge curve
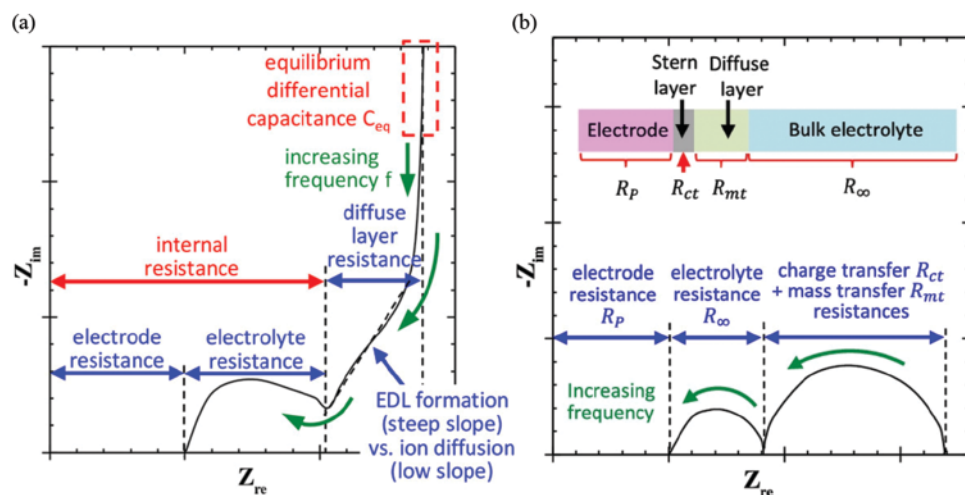
Figure 5.4 A typical interpretation of EIS with Nyquist Plot for supercapacitors with (a) EDLC electrodes and (b) pseudocapacitive electrodes. *Reproduced with permission [42, 43]. Copyright 2017 and 2018, American Chemical Society.*

of the GCD study can be attributed, in part, to the value of the ESR [45, 46]. Another important feature in EIS analysis is to perform the fitting of the Nyquist plot with the proposed circuit model. The validity of the proposed equivalent circuit can be projected from the fitted curve of the Nyquist plot, which should match reasonably well with the experimental curve of the Nyquist plot obtained at various frequency regions. The components of the equivalent circuit are chosen with higher accuracy (i.e., $\chi2 < 0.1$), with the first component as an electrode or bulk resistance (R_B) at high frequency followed by the charge transfer resistance (R_{CT}) at medium frequency. Another important parameter in the equivalent circuit is CPE, known as the constant phase element, which can be defined by the following impedance equation (5.10) [47].

$$Z_{CPE} = \frac{1}{Q_{CPE}\left(j2\pi f\right)^n} \tag{5.10}$$

Where, Q_{CPE} represents the CPE coefficient, and n is referred to as the exponent. The value of exponent (n) is –1 for a pure inductor, 0 for a pure resistor, and +1 for a pure capacitor [47, 48]. To explain the shape of the Nyquist plot in terms of electric components and their combination some of the equivalent circuit models are shown in Figure 5.5.

5.3 Conclusions

The use of supercapacitors in future energy storage systems appears promising. For the development of supercapacitors, several materials and production choices are available. The entire behaviour and electrochemical performance of energy storage devices are heavily influenced by the physicochemical parameters of the supercapacitor electrode materials. Because of their superior performance, supercapacitors are garnering an ever-increasing amount of attention. However, the electrochemical performance of supercapacitors, including capacitance, rate capabilities, cyclic stability, potential profile, and safety, is highly dependent on the supercapacitor's structural and morphological nature well as ion diffusion, electron transportation, and rebuilding the electrode–electrolyte interface during the GCD processes. It is essential to have an in-depth knowledge of the electrochemical processes involved in the development of supercapacitors in order to maximize their effectiveness in manufacturing, design, and prospective applications. There are three primary electrochemical techniques that are used to measure the critical performance parameters of a supercapacitor. These techniques are CV, GCD, and EIS. In all of these methods, the electrochemical workstation is utilized to measure important parameters such as voltage, current, time, equivalent series resistance, and capacitance in three- or two-electrode systems. The field of supercapacitors has seen a great deal of advancement in the last decade. Energy storage devices have made significant progress in recent years; nevertheless, further work is needed to ensure that the devices are scalable and consistent enough to meet commercial needs. New scientific breakthroughs and discoveries should address these problems in the near future.
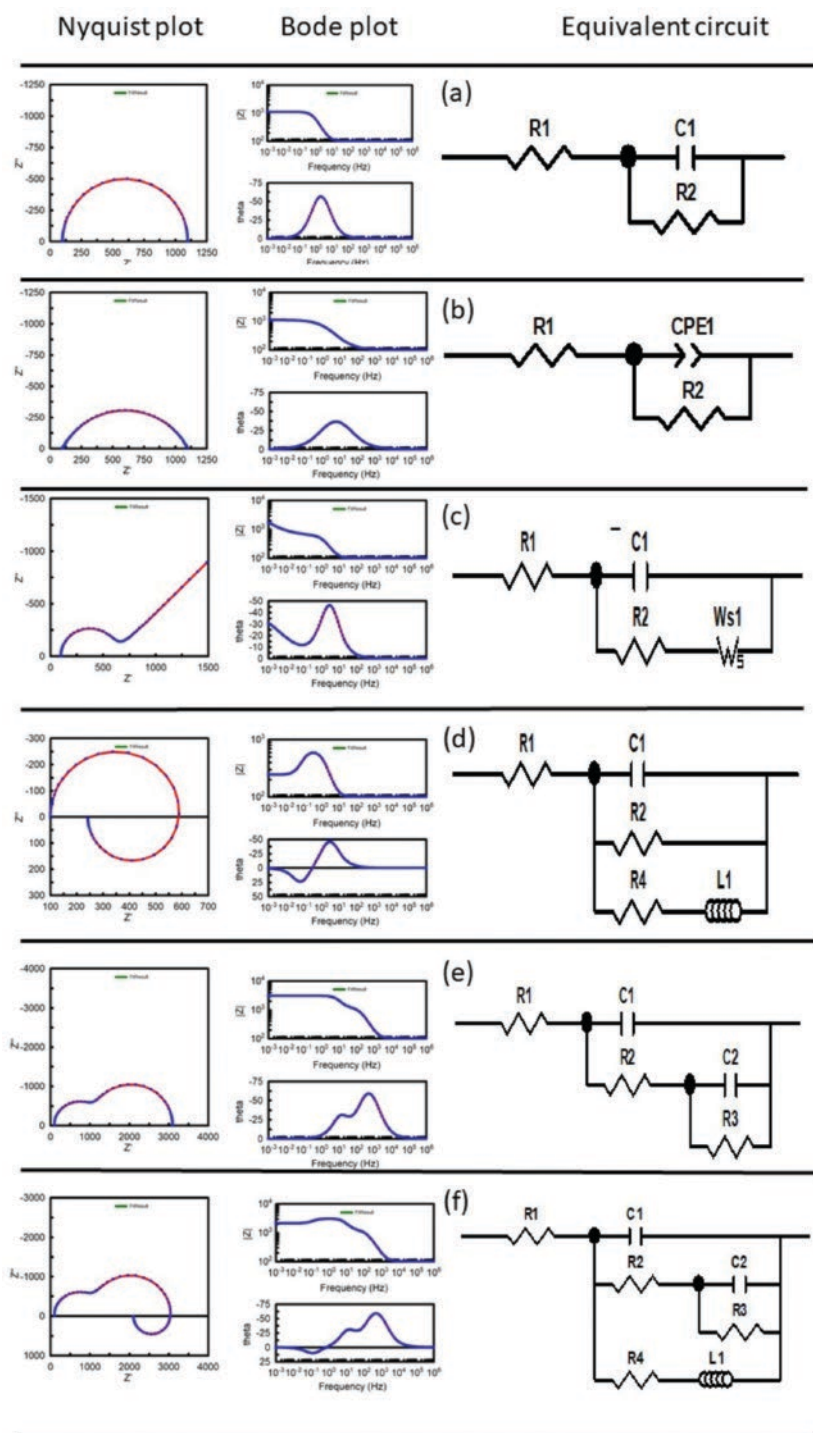
Figure 5.5 Equivalent circuit analysis from simple to advanced circuits obtained by fitting the Nyquist plot. *Reproduced with permission. Reproduced under the term CC-BY-4.0 license. Copyright 2020, Feliu et al.* [49], *MDPI.*

Acknowledgements

References

1 S. S. Shah, M. A. Aziz, Z. H. Yamani, *Chem. Rec.* **2022**, *22*, e202200018.

2 S. S. Shah, S. M. A. Nayem, N. Sultana, A. J. S. Ahammad, M. A. Aziz, *ChemSusChem* **2022**, *15*, e202101282.

3 M. R. Biradar, S. V. Bhosale, P. P. Morajakar, S. V. Bhosale, *Fuel* **2022**, *310*, 122487.

4 V. Venkataraman, M. Pérez-Fortes, L. Wang, Y. S. Hajimolana, C. Boigues-Muñoz, A. Agostini, S. J. McPhail, F. Maréchal, J. Van Herle, P. V. Aravind, *J. Energy Storage* **2019**, *24*, 100782.

5 B. K. Roy, I. Tahmid, T. U. Rashid, *J. Mater. Chem. A* **2021**, *9*, 17592–17642.

6 M. Ashraf, I. Khan, M. Usman, A. Khan, S. S. Shah, A. Z. Khan, K. Saeed, M. Yaseen, M. F. Ehsan, M. N. Tahir, N. Ullah, *Chem. Res. Toxicol.* **2020**, *33*, 1292–1311.

7 S. S. Shah, M. A. Aziz, E. Cevik, M. Ali, S. T. Gunday, A. Bozkurt, Z. H. Yamani, *J. Energy Storage* **2022**, *56*, 105944.

8 S. S. Shah, M. A. Aziz, W. Mahfoz, A.-R. Al-Betar, Conducting Polymers Based Nanocomposites for Supercapacitors in *Nanostructured Materials for Supercapacitors*, (Eds: S. Thomas, A. B. Gueye, R. K. Gupta), Springer, Cham, **2022**, Chapter 22, pp. 485–511, Vol. 1.

9 M. Usman, M. Humayun, S. S. Shah, H. Ullah, A. A. Tahir, A. Khan, H. Ullah, *Energies* **2021**, *14*, 2281.

10 M. Yaseen, M. A. K. Khattak, M. Humayun, M. Usman, S. S. Shah, S. Bibi, B. S. U. Hasnain, S. M. Ahmad, A. Khan, N. Shah, A. A. Tahir, H. Ullah, *Energies* **2021**, *14*, 7779.

11 S. S. Shah, E. Cevik, M. A. Aziz, T. F. Qahtan, A. Bozkurt, Z. H. Yamani, *Synth. Met.* **2021**, *277*, 116765.

12 M. A. Aziz, S. S. Shah, S. M. A. Nayem, M. N. Shaikh, A. S. Hakeem, I. A. Bakare, *J. Energy Storage* **2022**, *50*, 104278.

13 T. Islam, M. M. Hasan, S. S. Shah, M. R. Karim, F. S. Al-Mubaddel, M. H. Zahir, M. A. Dar, M. D. Hossain, M. A. Aziz, A. J. S. Ahammad, *J. Energy Storage* **2020**, *32*, 101908.

14 M. Rauf, S. S. Shah, S. K. Shah, S. N. A. Shah, T. U. Haq, J. Shah, A. Ullah, T. Ahmad, Y. Khan, M. A. Aziz, K. Hayat, *J. Saudi Chem. Soc.* **2022**, *26*, 101514.

15 Z. A. Feng, F. El Gabaly, X. Ye, Z.-X. Shen, W. C. Chueh, *Nat. Commun.* **2014**, *5*, 4374.

16 A. K. Mohamedkhair, M. A. Aziz, S. S. Shah, M. N. Shaikh, A. K. Jamil, M. A. A. Qasem, I. A. Buliyaminu, Z. H. Yamani, *Arab. J. Chem.* **2020**, *13*, 6161–6173.

17 R. Shakil, M. N. Shaikh, S. S. Shah, A. H. Reaz, C. K. Roy, A.-N. Chowdhury, M. A. Aziz, *Asian J. Org. Chem.* **2021**, *10*, 2220–2230.

18 M. M. Hasan, T. Islam, S. S. Shah, A. Awal, M. A. Aziz, A. J. S. Ahammad, *Chem. Rec.* **2022**, *22*, e202200041.

19 A. Helal, S. S. Shah, M. Usman, M. Y. Khan, M. A. Aziz, M. Mizanur Rahman, *Chem. Rec.* **2022**, *22*, e202200055.

20 M. Ashraf, S. S. Shah, I. Khan, M. A. Aziz, N. Ullah, M. Khan, S. F. Adil, Z. Liaqat, M. Usman, W. Tremel, M. N. Tahir, *Chem. Eur. J.* **2021**, *27*, 6973–6984.

21 S. S. Shah, M. A. Alfasane, I. A. Bakare, M. A. Aziz, Z. H. Yamani, *J. Energy Storage* **2020**, *30*, 101562.

22 S. S. Shah, H. T. Das, H. R. Barai, M. A. Aziz, *Polymers* **2022**, *14*, 270.

23 M. M. Hasan, T. Islam, A. Imran, B. Alqahtani, S. S. Shah, W. Mahfoz, M. R. Karim, H. F. Alharbi, M. A. Aziz, A. J. S. Ahammad, *Electrochim. Acta* **2021**, *374*, 137968.

24 M. M. Hasan, T. Islam, S. S. Shah, M. A. Aziz, A. Awal, M. D. Hossain, M. A. Ehsan, A. J. S. Ahammad, *Int. J. Hydrog. Energy* **2022**, *47*, 28740–28751.

25 S. S. Shah, M. A. Aziz, A.-R. Al-Betar, W. Mahfoz, *Arab. J. Chem.* **2022**, *15*, 104058.

26 P. Forouzandeh, P. Ganguly, R. Dahiya, S. C. Pillai, *J. Power Sources* **2022**, *519*, 230744.

27 F. Marken, A. Neudeck, A. M. Bond, Cyclic Voltammetry in *Electroanalytical Methods: Guide to Experiments and Applications*, (Eds: F. Scholz), Springer, Berlin, Heidelberg, **2002**, Chapter 4, pp. 51–97, https://doi.org/10.1007/978-3-662-04757-6_4.

28 Y. Gogotsi, R. M. Penner, *ACS Nano* **2018**, *12*, 2081–2083.

29 M. Grundy, Z. Ye, *J. Mater. Chem. A* **2014**, *2*, 20316–20330.

30 J. Liu, J. Wang, C. Xu, H. Jiang, C. Li, L. Zhang, J. Lin, Z. X. Shen, *Adv. Sci.* **2018**, *5*, 1700322.

31 M. M. Faisal, S. R. Ali, S. S. Shah, M. W. Iqbal, S. Pushpan, M. A. Aziz, N. P. Aguilar, M. M. Alcalá Rodríguez, S. L. Loredo, K. C. Sanal, *Ceram. Int.* **2022**, *48*, 28565–28577.

32 L. Zeng, T. Wu, T. Ye, T. Mo, R. Qiao, G. Feng, *Nat. Comput. Sci.* **2021**, *1*, 725–731.

33 S. Fleischmann, J. B. Mitchell, R. Wang, C. Zhan, D.-e. Jiang, V. Presser, V. Augustyn, *Chem. Rev.* **2020**, *120*, 6738–6782.

34 K. Yang, K. Cho, D. S. Yoon, S. Kim, *Sci. Rep.* **2017**, *7*, 40163.

35 R. D. Oliveira, C. S. Santos, J. R. Garcia, M. Vidotti, L. F. Marchesi, C. A. Pessoa, *J. Electroanal. Chem.* **2020**, *878*, 114662.

36 S. R. S. Prabaharan, R. Vimala, Z. Zainal, *J. Power Sources* **2006**, *161*, 730–736.

37 X. Zhang, C. Peng, R.-t. Wang, J.-w. Lang, *RSC Adv.* **2015**, *5*, 32159–32167.

38 A. Sacco, *Renew. Sust. Energ. Rev.* **2017**, *79*, 814–829.

39 P. L. Taberna, C. Portet, P. Simon, *Appl. Phys. A* **2006**, *82*, 639–646.

40 P. L. Taberna, P. Simon, J. F. Fauvarque, *J. Electrochem. Soc.* **2003**, *150*, A292.

41 T. Ramesh, R. Vedarajan, N. Rajalakshmi, L. R. G. Reddy, *J. Mater. Sci. - Mater. Electron.* **2020**, *31*, 1681–1690.

42 B.-A. Mei, O. Munteshari, J. Lau, B. Dunn, L. Pilon, *J. Phys. Chem. C* **2018**, *122*, 194–206.

43 B.-A. Mei, J. Lau, T. Lin, S. H. Tolbert, B. S. Dunn, L. Pilon, *J. Phys. Chem. C* **2018**, *122*, 24499–24511.

44 W. Mahfoz, M. A. Aziz, S. S. Shah, A.-R. Al-Betar, *Chem. Asian J.* **2020**, *15*, 4358–4367.

45 J.-B. Jorcin, M. E. Orazem, N. Pébère, B. Tribollet, *Electrochim. Acta* **2006**, *51*, 1473–1479.

46 N. A. Cañas, K. Hirose, B. Pascucci, N. Wagner, K. A. Friedrich, R. Hiesgen, *Electrochim. Acta* **2013**, *97*, 42–51.

47 P. Navalpotro, M. Anderson, R. Marcilla, J. Palma, *Electrochim. Acta* **2018**, *263*, 110–117.

48 F. O. Ochai-Ejeh, M. J. Madito, D. Y. Momodu, A. A. Khaleed, O. Olaniyan, N. Manyala, *Electrochim. Acta* **2017**, *252*, 41–54.

49 S. Feliu Jr, *Metals*, **2020**, *10*, 775.

6

Types of Supercapacitors

Syed Shaheen Shah[1,2,3], Md. Abdul Aziz[1,4,], Wael Mahfoz[5], and Md. Akhtaruzzaman[6]*

[1] Interdisciplinary Research Center for Hydrogen and Energy Storage (IRC-HES), King Fahd University of Petroleum & Minerals, KFUPM Box 5040, Dhahran Saudi Arabia
[2] Physics Department, King Fahd University of Petroleum & Minerals, KFUPM Box 5047, Dhahran Saudi Arabia
[3] JSPS International Research Fellow, Department of Material Chemistry, Graduate School of Engineering, Kyoto University, Kyotodaigaku Katsura, Nishikyo-ku, Kyoto Japan
[4] K. A. CARE Energy Research and Innovation Center, King Fahd University of Petroleum & Minerals, Dhahran, Saudi Arabia
[5] Chemistry Department, King Fahd University of Petroleum & Minerals, Dhahran Saudi Arabia
[6] Solar Energy Research Institute (SERI), Universiti Kebangsaan, Malaysia
* Corresponding author

6.1 Introduction

Researchers have been motivated to investigate various renewable energy sources due to the finite availability of fossil fuels and the long-term damaging impacts of greenhouse emissions. It is necessary to develop energy conversion and storage technologies in order to overcome the major obstacle posed by the intermittent nature of renewable energy that comes from solar and wind sources. This obstacle prevents the full exploitation of the abundant renewable energy that can be generated from these resources. Several electrical energy storage technologies have been used in this setting, allowing efficient power storage, rectification, transportation, and delivery [1–3]. Such energy storage technologies as batteries and fuel cellsare quite close to our daily lives. Others, including flywheels, compressed air, pumped hydro, superconducting magnets, and supercapacitors, are crucial from the industrial point of view. Batteries have been widely employed of various sizes because of their exceptional performances, yet, they have several drawbacks like low power density, safety concerns, heat generation, and limited cyclic life [4–6]. Therefore, developing a durable, small, and secure energy storage device with high electrochemical performance would surely revolutionize the design of electric energy generation, distribution, and utility for industry and the military [1, 2, 5–12].

Specific capacitance, energy density, and power density are the three fundamental concepts that are utilized in the process of characterizing the effectiveness of supercapacitors. The device's capacitance measures a device's capacity to hold an electric charge. The capacity of an object to store an electric charge proportional to its mass is referred to as the substance's specific capacitance. The cyclic voltammetry method and the galvanostatic charge-discharge
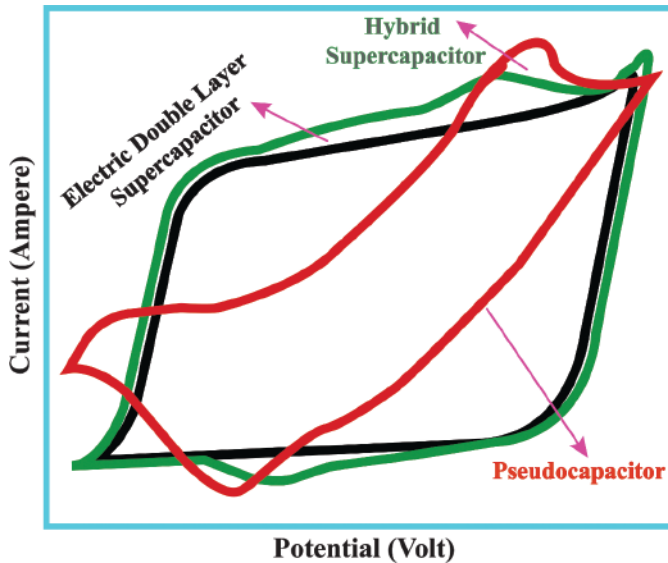
Figure 6.1   Supercapacitor classification based on cyclic voltammetry.

process are typically utilized in order to obtain information about the type of supercapacitors [5, 6, 10–14]. Different underlying phenomena can lead to different types of supercapacitors. The charge-storing mechanism of a supercapacitor can be broken down into the following categories. Electric double-layer supercapacitors (EDLCs) are supercapacitors that store energy by accumulating an electrostatic charge at the electrode/electrolyte interface (EEI), where ions are physically adsorbed and desorbed, storing energy [15–20]. Figure 6.1 shows that the cyclic voltammetry of Faradaic reactions does not participate in the energy storage process of EDLCs. Carbonaceous materials like activated carbon are commonly used in EDLCs. The EDLCs have a higher power density than pseudocapacitors.

They are extremely rapid in terms of charging and discharging, but their low energy density remains an issue. Pseudocapacitors are supercapacitors that store energy through reversible redox reactions (Faradaic reactions). The Faradaic reaction occurs at the electrode surfaces. The Faradaic reactions have oxidation and reduction peaks, which are depicted in Figure 6.1 as upper and lower peaks, respectively. Pseudocapacitors outperform EDLCs in terms of specific capacitance and energy density. These are often made up of oxides, sulfides, and conductive polymers. Hybrid supercapacitors are those that have properties of both EDLCs and pseudocapacitors [21–23]. Such supercapacitors use Faradaic and non-Faradaic reactions for charge storage. These retain both high energy density and powered density at the same time. Their cyclic voltammetry curve differs somewhat from the rectangular shape of EDLCs and has a little hump, as seen in Figure 6.1.

6.2   Types of Supercapacitors

There are various ways supercapacitors can be divided into different types, i.e., based on charge storage mechanisms, assembly of electrodes, and size and shapes.

6.2.1 Types of Supercapacitors Based on Charge Storage Mechanisms

Supercapacitors can be classified into three types on the basis of their working principle of charge storage, i.e., EDLC, pseudocapacitor, and hybrid supercapacitor.

6.2.1.1 Electric Double-layer Supercapacitors

Electric Double-layer Supercapacitors (EDLC) are a type of supercapacitor that stores energy through the accumulation of electrostatic charges at the electrode–electrolyte interface (EEI) (i.e., physical adsorption or desorption of electrolyte ions) [24–26]. Activated carbon, graphene, and carbon nanofibers are examples of carbonaceous nanomaterials typically used to construct the electrodes of EDLCs. These materials have a large specific surface area and a wide range of pore sizes [5, 12, 13, 27, 28]. Because carbon materials have a hierarchical porosity, the diffusion of electrolyte ions to the surfaces will be sped up, especially at higher scan rates and current densities. Consequently, it is essential to exercise control over both the pore size and the pore size distribution of the electrode materials, both of which substantially impact supercapacitors. In order to build carbon materials with regulated surface chemistry, interconnected pore structures, small pore size distributions (that are susceptible to electrolyte ion diffusion), and short pore lengths are required [5, 11, 19, 29–31]. The Helmholtz double-layer model provides an explanation for the energy storage process of an EDLC. According to this model, the two oppositely charged layers that arise at the EEI are split by small gaps (usually atomic level), as demonstrated in Figure 6.2. Within the Stern layer, the term "inner-Helmholtz plane" refers to the highly adsorbed ions that are produced by the electrode. A known as the outer-Helmholtz plane comprises particularly adsorbed ions as well as counter ions that are not specifically adsorbed at the EEI [32, 33]. Because of the mechanism through which they store electrostatic charge, EDLCs do not undergo a Faradaic redox reaction, and a rectangular pattern characterizes the behavior of their CV curves [34].

The application of voltage to EDLC electrodes causes a double layer to form, and the ions of electrolytes flow alongside the double layer's surface. Two charged surfaces determine the specific capacitance, while the movement of electrolyte ions provides a potential due to the compression of the two layers, which the zeta potential of the electrodes can ascribe [36]. When it comes to high power density, EDLCs offer a lot of desirable properties, such
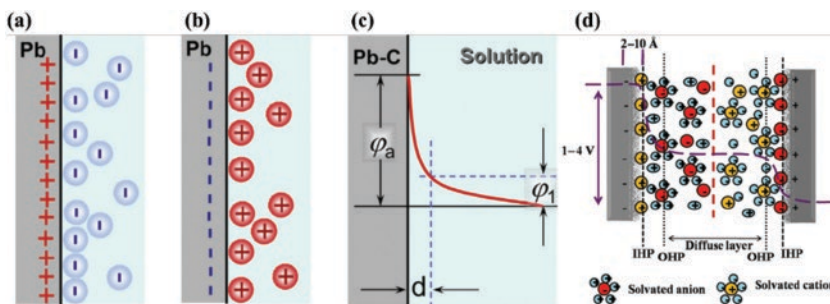
Figure 6.2 EDLCs potential and charge distributions at the EEI of (a) positive electrode, (b) negative electrode, and (c) Helmholtz double-layer. *Reproduced with permission [35]. Copyright 2013, Elsevier. (d) Stern model at the EEI, and diffused layer. Reproduced with permission [33]. Copyright 2018, Elsevier.*

as being able to charge in a matter of seconds and having long-term cyclic stability. EDLCs have been the subject of great interest ever since General Electric published the first patent on the technology in 1957 [37]. Because of its exceptionally high power density, which can have a capacity of up to ten times more than that of rechargeable batteries, EDLC has been successfully utilized in various industries, including computers, LED flash devices, memory backup power, and load-lifting equipment [38]. There is no involvement of Faradaic processes in the electrostatic charge storage that takes place in EDLCs; rather, it takes place predominately due to the electrolyte ions adsorption onto the electrode materials surfaces, as shown in Figure 6.2(a). Carbon materials with a high specific surface area are frequently reported to act in this way due to high electrical conductivity and a high number of surface adsorption sites [12, 14, 39]. Nevertheless, because of the limitation placed on the electrode surface area, the energy density of commercial EDLCs can only reach a maximum of $6\,\mathrm{Wh\,kg}^{-1}$, a value significantly lower than that of batteries [40]. From this point of view, one feasible strategy for the development of electrode materials with high energy and power density is to combine the benefits of EDLCs and rechargeable batteries.

6.2.1.2 Pseudocapacitors

Pseudocapacitors have electrodes made of redox-active nanomaterials, which are typically transition metals-based materials and conducting polymers. The electrical energy is stored in the rapidly reversible Faradaic redox processes that take place at the electrode surface [5, 41–43]. Pseudocapacitors have a relatively high energy density, but because of the quick redox reactions that occur during the charging and discharging processes, they also accumulate irreversible components. Consequently, this results in a decline in cyclic stability performance [34, 41]. The pseudocapacitor electrode materials go through fast reversible Faradaic redox processes, resulting in the Faradaic current being conducted via the supercapacitor device. Oxidation and reduction peaks are involved in the Faradaic process, as shown in Figure 6.3. The process of charging and discharging batteries is analogous to the behavior of this mechanism. Since 1971, researchers have investigated a wide selection of pseudocapacitive redox-active electrode materials, for example, transition metal oxides/hydroxides. The first evidence of the pseudocapacitance of RuO_2 in a supercapacitor was found and published by Trasatti et al. [44] When subjected to electrochemical cycling in aqueous electrolytes of elevated pH values, RuO_2 demonstrates the properties of pseudocapacitance. It is generally accepted that the pseudocapacitive behavior of RuO_2 may be traced back to a chain of reversible reactions, one of which is the transfer of electrons at the electrode surface (represented by equation (6.1)) [45].

$$Ru^{IV}O_2 + xH^+ + xe^- \leftrightarrow Ru^{IV}_{1-x}Ru^{III}_xO_2H_x \tag{6.1}$$
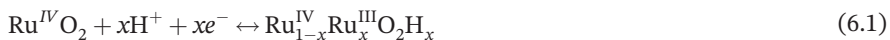
Furthermore, several known transition metal-based materials, such as MnO_2 and Fe_3O_4, also exhibit core Faradaic reactions. Because of their many valence states they outperform EDLCs in initiating fast and reversible redox reactions at the electrode surface. This allows them to store a substantially greater amount of energy at a much faster rate during charge and discharge. Equation (6.2) shows that surface and bulk redox processes in MnO_2 can store charges between the +4 and +3 manganese oxidation states [46]. Where, A describes an alkaline cation (i.e., Li^+, Na^+, and K^+).

$$MnO_2 + xA^+ + xe^- \leftrightarrow A_xMnO_2 \tag{6.2}$$

This type of supercapacitor has fast surface redox or intercalation processes and a double-layer capacitance to increase energy density while keeping EDLC-like fast timings for charging and discharging [47]. In 1991, the term pseudocapacitance was coined by Conway et al. [48]. EDLCs and batteries are two extremes of the energy storage spectrum. Pseudocapacitance energy storage, however, comes somewhere in the middle. There are three pseudocapacitance types: the surface Faradaic reaction, the intercalation, and the monolayer adhesion, as shown in Figure 6.3. A monolayer adsorption happens when two metals with different redox potentials come together to form an adsorbent monolayer on the surface of each other (this is called underpotential deposition). Underpotential lead (Pb) depositions on gold (Au) electrodes are well-known examples [49]. Due to the increased contact between Au and Pb in crystal-like Pb metal, it is easier for Pb to be deposited onto Au than it is for Pb to be deposited onto itself. Surface Faradaic redox pseudocapacitance on the electrode materials results from charge-transfer mechanisms that adsorb alkali ions onto or near the electrode surface. Pseudocapacitance is a phenomenon that can occur when the intercalation or deintercalation processes that are of interest are not kinetically constrained by the slow solid-state diffusion that occurs when alkali ions migrate slowly through the crystal structure of electrode materials. Bulk intercalation pseudocapacitance takes the place of surface redox pseudocapacitance, which is unique to the electrode surface or the area immediately adjacent to it [50].

6.2.1.3 Hybrid Supercapacitors

Another technique has been developed to integrate both the mechanisms of charge storage of pseudocapacitors and EDLCs to build an efficient device that could emulate the excellent energy density of pseudocapacitors/batteries and the high-power density of EDLCs. These high-performance devices are referred to as hybrid supercapacitors, and they are able to sustain high energy and power densities concurrently [51, 52]. Instead of using carbon, transition metal-based materials, and conducting polymers individually, scientists prepared hybrid composites of these active materials for hybrid supercapacitors. These hybrid composites are inexpensive, chemically stable, mechanically flexible, and demonstrate excellent electrical conductivity. To govern the hybrid supercapacitors energy storage principle, EDLCs and pseudocapacitors are connected (Figure 6.3(f)). Because pseudocapacitors lack the limiting property of EDLCs, and vice versa, the combination of these two components allows the restrictions of the combining components to be concealed, which results in an increase in capacitance. Hybrid supercapacitors can either be symmetric (shown in Figure 6.3(g)) or asymmetric (shown in Figure 6.3(h)), and this depends on the architecture of the assembly. The electrochemical behavior is better when hybrid supercapacitors are created from independent electrodes made of dissimilar materials than when the electrodes are used independently. Both cyclic stability and affordability, two key variables in determining whether pseudocapacitors would be successful, are preserved in hybrid systems. Because of its higher specific capacitance values and wider operating potential windows than symmetrical EDLCs, the hybrid type offers a higher energy density than those devices [5, 6, 19, 31, 53]. The CV curves of hybrid supercapacitors have
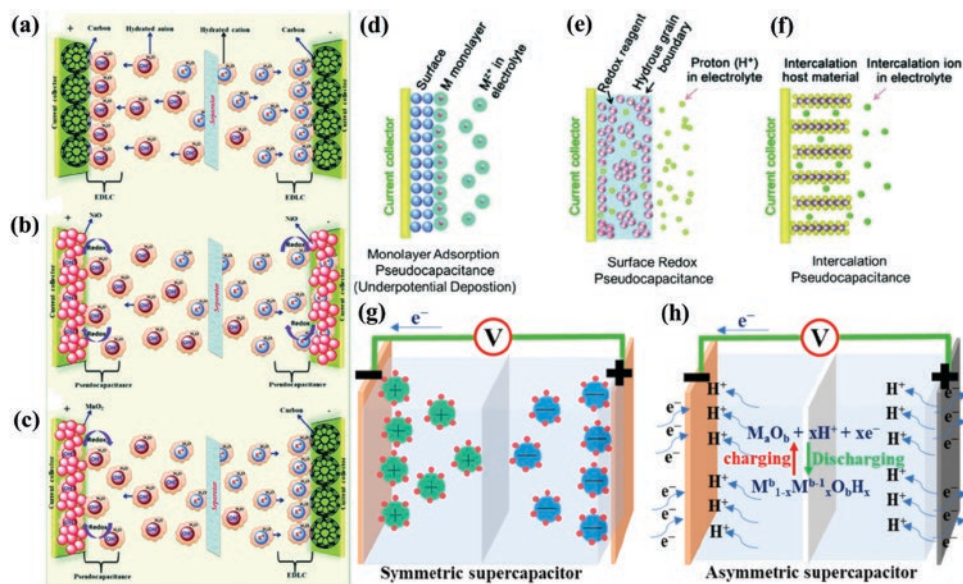
Figure 6.3 (a) EDLCs, (b) pseudocapacitors, and (c) hybrid supercapacitors charge storage mechanisms. *Reproduced with permission [56]. Reproduced under the terms of the CC BY-NC 3.0 license. Copyright 2019, Pal et al.* (d-f) Various pseudocapacitance methods. *Reproduced with permission [40]. Reproduced under the terms of the CC BY-NC 3.0 license. Copyright 2019, Huang et al.* (g, h) Symmetric/asymmetric hybrid supercapacitors. *Reproduced with permission [57]. Reproduced under the terms of the CC BY 4.0 license. Copyright 2022, Zhang et al.*

some oxidation/reduction peaks, which are shown as minor bumps in Figure 6.1. This is a departure from the rectangular shape of CV curves for EDLCs. Hybrid supercapacitors are regarded as a potential game changer for future energy storage systems development. They have developed as an alternative to electrochemical energy storage systems with the aim of achieving higher energy density demand. The performance of hybrid supercapacitors depends on the materials that make up their electrodes when it comes to practical applications. The hybrid supercapacitors have high specific capacitance, greater power density, and better energy density than the pseudocapacitors and EDLCs that are already on the market. This is due to the fact that the hybrid supercapacitors utilize two distinct charge-storing processes. In most cases, the asymmetric method of hybrid supercapacitors, which is the combination of pseudocapacitors and EDLCs, performs the function of an amplifier in the respective capacitance values. The asymmetric hybrid supercapacitors are made up of a positive electrode that contains redox-active materials and a negative electrode that is created by combining a carbon material with an electrolyte and a separator in between. During the process of charging and discharging, the counter electrolyte ions migrate towards the positive and negative electrodes. EDLC behavior is provided by the adsorption/desorption of positive electrolyte ions at the negative electrode surface, while pseudocapacitive behavior is caused by fast reversible Faradaic reactions at the positive electrode surface caused by negative electrolyte ions. This asymmetric methodology illustrates a bright start in the direction of the extremely needed pollution-free, durable, and beneficial energy storage appearances in terms of hybrid supercapacitors. Large pore volumes and

high specific surface area of electrode materials are the key criteria for energy-efficient hybrid supercapacitors. These factors enable the electrolyte ions accessibility and boost the device's capacitance. In a similar vein, the ability to tune the morphology of the electrode material for hybrid supercapacitors has been considered to be another crucial aspect. Careful morphological adjustment of the nanostructures changes the unique properties of nanomaterials. It exposes active sites and distinct crystal facets, both of which can frequently considerably impact the hybrid supercapacitors electrochemical performances [30, 54, 55].

6.2.2 Supercapacitor Types Based on Electrode Configuration

Depending on the type of electrodes, a supercapacitor can have two configurations, i.e., symmetric and asymmetric. A symmetric supercapacitor is made up of positive and negative electrodes of the same material, which is typically carbon. In contrast, as illustrated in Figure 6.4, an asymmetric supercapacitor can have a variety of electrode material combinations [58]. The positive and negative electrodes of a symmetric device have identical active materials and the same mass loading ($m_+ = m_-$). EDLC-based materials or materials with EDLC and Faradaic capacitance contributions are typically used to fabricate symmetric supercapacitors. Using only Faradaic materials results in symmetric supercapacitors, which are rarely used because redox reactions only occur at either positive or negative voltages [59]. Within the same electrolyte, asymmetric supercapacitors combine two distinct types of active electrode materials, one of which is EDLC and the other of which is pseudocapacitive. Asymmetric supercapacitors are another name for supercapacitors that have the same kind of active electrode material on each electrode but have different masses of materials ($m_+ \neq m_-$) on each electrode (Figure 6.4). Even in EDLC-based devices in which both positive and negative electrodes contain the same active material, optimizing the mass ratio between the positive and negative electrodes is important. Because the hydrated anions and cations in the electrolyte have different sizes, the surface area of the electrolyte

Figure 6.4 Schematic representation for the symmetric and asymmetric configuration of supercapacitors.

that is accessible to the anions or cations also has different sizes. The decrease directly improves the kinetics in the size of the hydrated ions. Therefore, loading the active electrode materials with the same mass amount could prevent the EDLC-based supercapacitor from achieving its maximum possible supercapacitive performance [58]. Therefore, to counterbalance the device's specific capacitance and energy, it is necessary to balance the mass loading of the negative and positive electrodes.

6.2.3 Supercapacitor Types Based on Device Configuration

In addition to the material itself, the performance of a supercapacitor cell can be significantly altered by several factors relating to the processing conditions of the electrodes and the cell assembly. These factors include electrode thickness and density, cell pressure, and the pre-conditioning process. The production of a supercapacitor only requires a few steps, including the preparation of a homogeneous mixture of components, the creation of an electrode layer on a current collector sheet, the assembly of the cells, and the packaging of the finished product. When evaluating an electrode material in a full cell configuration in a laboratory, it is common practice to pack a pair of tiny electrodes with a few cm^2 areas or mF capacity into a coin cell or one of its derivatives, such as a Swagelok cell. This allows for evaluating the electrode material in a full-cell configuration. Nevertheless, a demonstration of a large-capacity cell is necessary to evaluate the cell's performance from a practical standpoint and as a first step toward commercialization. A cylindrical or pouch-shaped container is required to package a high-capacity cell. Sadly, the research that has been published provides very little information, and the guidelines for producing a cell in such a large container are considered to be proprietary information in the commercial sphere. Recently, it was reported that efforts had been made to scale up the size of supercapacitors to coin cells and even to a more oversized format, most notably a pouch cell, highlighting challenges with electrode preparation. These efforts were reported to have successfully scaled up the size of supercapacitors to coin cells. According to the available research, pouch cell packaging appears to be the format of choice due to its user-friendliness, low cost of processing, compatibility with industrial settings, and minimal footprint design [60].

Porous/functionalized/activated carbon [61, 62], oxides [63], hydroxides [64], and conductive polymers [65] have all been studied as electrode materials for hybrid supercapacitor applications. A supercapacitor's stability, energy density, and power density are determined by electrode material properties, specific surface area, and pore sizes. The morphology of hybrid supercapacitors can be controlled: the specific surface area can be improved, and the pore sizes can be reduced. As a result of recent advancements in nanomaterials and charge storage methods, the performance of hybrid supercapacitors has increased significantly. Unique electrochemical capabilities, high processability, various redox reactions, and exact programmable hybrid supercapacitors compositions are some of the advantages over other materials [15, 19, 20, 66, 67]. The hybrid supercapacitor's ability to store energy, maintain stability, and charge at a high rate is heavily reliant on the active materials, which are only found in redox-active nanomaterials. While quick charge/discharge cycles can deposit reversible redox species on electrode surfaces and degrade structure, pure redox-active materials do not perform well in large-scale applications due to

their poor cyclic stability [68]. The limitations of redox-active materials have prompted a great deal of research. Hybrid supercapacitors can be supported on robust and better platforms thanks to the development of hybrid composite materials. The most logical way to combine carbon and redox-active nanomaterials in one system is to combine high power density and high energy density with suitable stability. There have already been developed a great number of hybrid composites using these active materials [69–72]. The sum of the performance of the various active components determines the supercapacitive performance of hybrid composites like these. Using porous electrode materials makes it possible for ion diffusion and storage; high electrical conductivity makes it simpler for the charge to move, and enhanced cyclic stability is achieved via the combination of high electrochemical and physical stability [9, 12, 19, 73].

6.3 Conclusions

The rise in popularity of supercapacitors can be attributed to the fact that they can be used in a wide variety of energy-related contexts. This chapter provides a straightforward summary of supercapacitors as well as a concise summary of current advancements in the field. It was highlighted how these supercapacitor structures could be separated into three distinct groups according to the way they store charge and then separated again according to the material utilized for the electrodes. There are three different kinds of capacitors: EDLCs, pseudocapacitors, and hybrid supercapacitors. The capacitance values of supercapacitors range from the picofarad to the microfarad, and they have the ability to store potential energy as electric charge. Supercapacitors were rated in farads, and values are regarded to be one thousand times higher than those associated with electrolytic capacitors. In addition, the energy density of the supercapacitor is greater than that of the capacitor, although it is not greater than that of the battery. However, due to the flexibility of supercapacitors, it was possible that they could be adapted to serve in certain roles for which electrochemical batteries were not a good fit. Supercapacitors have a few inherent qualities that make them suited for specialized roles as well as applications that complement the capabilities of the batteries. These roles and applications complement the strengths of the batteries. In particular, supercapacitors have a significant amount of potential for applications that require a combination of quick charging time, high power, long shelf life, and good cycle stability. The supercapacitor's behavior was investigated using various electrode materials, and its performance was improved as a result. Currently, scientists are concentrating their efforts on the ternary composite that has been published. Highly conductive electrodes exhibit a wide range of pore sizes and maintain a large number of charge/discharge cycles due to the introduction of novel redox-active and carbon-based nanomaterials. These are the essential components for the applications of supercapacitors. A large number of researchers from all around the world are working on improving the performance of supercapacitors by considering and proposing nanomaterials based on carbonaceous compounds and derivates of transition metals as ideal options. As potential active materials for use in real-world supercapacitor systems, conductive polymers and metallic complexes that are both inexpensive and easily accessible should receive significant research. Commercial-scale supercapacitors must also evaluate low-cost

current collectors (such as aluminum, carbon cloth, and stainless steel), electrolytes, inexpensive separators (such as polymeric membranes and ceramic sheets), and other affordable passive components. Various supercapacitors are classified according to the energy storage mechanism and electrode configurations, providing a unique pathway for the supercapacitor industry.

Acknowledgments

References

1 Y. Shao, M. F. El-Kady, J. Sun, Y. Li, Q. Zhang, M. Zhu, H. Wang, B. Dunn, R. B. Kaner, *Chem. Rev.* **2018**, *118*, 9233–9280.

2 M. Winter, R. J. Brodd, *Chem. Rev.* **2004**, *104*, 4245–4270.

3 S. S. Shah, M. A. Aziz, E. Cevik, M. Ali, S. T. Gunday, A. Bozkurt, Z. H. Yamani, *J. Energy Storage* **2022**, *56*, 105944.

4 S. M. A. Nayem, A. Ahmad, S. S. Shah, A. S. Alzahrani, A. J. S. Ahammad, M. A. Aziz, *Chem. Rec.* **2022**, e202200181. https://doi.org/10.1002/tcr.202200181.

5 S. S. Shah, S. M. A. Nayem, N. Sultana, A. J. S. Ahammad, M. A. Aziz, *ChemSusChem* **2022**, *15*, e202101282.

6 M. Yaseen, M. A. K. Khattak, M. Humayun, M. Usman, S. S. Shah, S. Bibi, B. S. U. Hasnain, S. M. Ahmad, A. Khan, N. Shah, A. A. Tahir, H. Ullah, *Energies* **2021**, *14*, 7779.

7 D. P. Dubal, O. Ayyad, V. Ruiz, P. Gomez-Romero, *Chem. Soc. Rev.* **2015**, *44*, 1777–1790.

8 F. Wang, X. Wu, X. Yuan, Z. Liu, Y. Zhang, L. Fu, Y. Zhu, Q. Zhou, Y. Wu, W. Huang, *Chem. Soc. Rev.* **2017**, *46*, 6816–6854.

9 G. Wang, L. Zhang, J. Zhang, *Chem. Soc. Rev.* **2012**, *41*, 797–828.

10 T. Islam, M. M. Hasan, S. S. Shah, M. R. Karim, F. S. Al-Mubaddel, M. H. Zahir, M. A. Dar, M. D. Hossain, M. A. Aziz, A. J. S. Ahammad, *J. Energy Storage* **2020**, *32*, 101908.

11 S. S. Shah, M. A. Aziz, W. Mahfoz, A.-R. Al-Betar, Conducting Polymers Based Nanocomposites for Supercapacitors in *Nanostructured Materials for Supercapacitors*, (Eds.: S. Thomas, A. B. Gueye, R. K. Gupta), Springer, Cham, **2022**, Chapter 22, pp. 485–511, Vol. *1*.

12 S. S. Shah, E. Cevik, M. A. Aziz, T. F. Qahtan, A. Bozkurt, Z. H. Yamani, *Synth. Met.* **2021**, *277*, 116765.

13 N. C. Deb Nath, S. S. Shah, M. A. A. Qasem, M. H. Zahir, M. A. Aziz, *ChemistrySelect* **2019**, *4*, 9079–9083.

14 M. A. Aziz, S. S. Shah, S. M. A. Nayem, M. N. Shaikh, A. S. Hakeem, I. A. Bakare, *J. Energy Storage* **2022**, *50*, 104278.

15 M. Ashraf, I. Khan, M. Usman, A. Khan, S. S. Shah, A. Z. Khan, K. Saeed, M. Yaseen, M. F. Ehsan, M. N. Tahir, N. Ullah, *Chem. Res. Toxicol.* **2020**, *33*, 1292–1311.

16 K. Hayat, S. S. Shah, S. Ali, S. K. Shah, Y. Iqbal, M. A. Aziz, *J. Mater. Sci. - Mater. Electron.* **2020**, *31*, 15859–15874.

17 A. Helal, S. S. Shah, M. Usman, M. Y. Khan, M. A. Aziz, M. Mizanur Rahman, *Chem. Rec.* **2022**, *22*, e202200055.

18 S. S. Shah, M. A. Aziz, A. K. Mohamedkhair, M. A. A. Qasem, A. S. Hakeem, M. K. Nazal, Z. H. Yamani, *J. Mater. Sci. - Mater. Electron.* **2019**, *30*, 16087–16098.

19 S. S. Shah, M. A. A. Qasem, R. Berni, C. Del Casino, G. Cai, S. Contal, I. Ahmad, K. S. Siddiqui, E. Gatti, S. Predieri, J.-F. Hausman, S. Cambier, G. Guerriero, M. A. Aziz, *Sci. Rep.* **2021**, *11*, 6945.

20 M. Usman, M. Humayun, S. S. Shah, H. Ullah, A. A. Tahir, A. Khan, H. Ullah, *Energies* **2021**, *14*, 2281.

21 M. M. Hasan, T. Islam, S. S. Shah, A. Awal, M. A. Aziz, A. J. S. Ahammad, *Chem. Rec.* **2022**, *22*, e202200041.

22 S. S. Shah, M. A. Aziz, Z. H. Yamani, *Chem. Rec.* **2022**, *22*, e202200018.

23 M. Ashraf, S. S. Shah, I. Khan, M. A. Aziz, N. Ullah, M. Khan, S. F. Adil, Z. Liaqat, M. Usman, W. Tremel, M. N. Tahir, *Chem. Eur. J.* **2021**, *27*, 6973–6984.

24 C. Lekakou, O. Moudam, F. Markoulidis, T. Andrews, J. Watts, G. Reed, *J. Nanotechnol.* **2011**, *2011*, 409382.

25 M. Rauf, S. S. Shah, S. K. Shah, S. N. A. Shah, T. U. Haq, J. Shah, A. Ullah, T. Ahmad, Y. Khan, M. A. Aziz, K. Hayat, *J. Saudi Chem. Soc.* **2022**, *26*, 101514.

26 S. S. Shah, H. T. Das, H. R. Barai, M. A. Aziz, *Polymers* **2022**, *14*, 270.

27 A. Daraghmeh, S. Hussain, A. U. Haq, I. Saadeddin, L. Servera, J. M. Ruiz, *J. Energy Storage* **2020**, *32*, 101798.

28 Y. K. Penke, P. Sinha, A. K. Yadav, J. Ramkumar, K. K. Kar, *Compos. B. Eng.* **2020**, *202*, 108431.

29 M. Daud, M. S. Kamal, F. Shehzad, M. A. Al-Harthi, *Carbon* **2016**, *104*, 241–252.

30 S. S. Shah, M. A. Aziz, M. Oyama, A.-R. F. Al-Betar, *Chem. Rec.* **2021**, *21*, 204–238.

31 S. S. Shah, M. N. Shaikh, M. Y. Khan, M. A. Alfasane, M. M. Rahman, M. A. Aziz, *Chem. Rec.* **2021**, *21*, 1631–1665.

32 L. L. Zhang, X. Zhao, *Chem. Soc. Rev.* **2009**, *38*, 2520–2531.

33 Y. N. Sudhakar, M. Selvakumar, D. K. Bhat, Biopolymer Electrolyte for Supercapacitor in *Biopolymer Electrolytes*, 1st ed., (Eds: Y. N. Sudhakar, M. Selvakumar, D. K. Bhat), Elsevier, **2018**, Chapter 3, pp. 53–116.

34 J. Liu, J. Wang, C. Xu, H. Jiang, C. Li, L. Zhang, J. Lin, Z. X. Shen, *Adv. Sci.* **2018**, *5*, 1700322.

35 D. Pavlov, P. Nikolov, *J. Power Sources* **2013**, *242*, 380–399.

36 V. Sharma, I. Singh, A. Chandra, *Sci. Rep.* **2018**, *8*, 1307.

37 L. G. H. Staaf, P. Lundgren, P. Enoksson, *Nano Energy* **2014**, *9*, 128–141.

38 K. Kraiwattanawong, *Arab. J. Chem.* **2022**, *15*, 103625.

39 A. Aziz, S. S. Shah, A. Kashem, *Chem. Rec.* **2020**, *20*, 1074–1098.

40 H. Huang, M. Niederberger, *Nanoscale* **2019**, *11*, 19225–19240.

41 L. Li, Z. Wu, S. Yuan, X.-B. Zhang, *Energy Environ. Sci.* **2014**, *7*, 2101–2122.

42 H. Li, M. Yu, F. Wang, P. Liu, Y. Liang, J. Xiao, C. Wang, Y. Tong, G. Yang, *Nat. Commun.* **2013**, *4*, 1894.

43 T. Liu, L. Finn, M. Yu, H. Wang, T. Zhai, X. Lu, Y. Tong, Y. Li, *Nano Lett.* **2014**, *14*, 2522–2527.

44 S. Trasatti, G. Buzzanca, *J. Electroanal. Chem. Interf. Electrochem.* **1971**, *29*, A1–A5.

45 J. W. Long, D. Bélanger, T. Brousse, W. Sugimoto, M. B. Sassin, O. Crosnier, *MRS Bull.* **2011**, *36*, 513–522.

46 M. Huang, F. Li, F. Dong, Y. X. Zhang, L. L. Zhang, *J. Mater. Chem. A* **2015**, *3*, 21380–21423.

47 K. Jost, G. Dion, Y. Gogotsi, *J. Mater. Chem. A* **2014**, *2*, 10776–10787.

48 B. E. Conway, *J. Electrochem. Soc.* **1991**, *138*, 1539–1548.

49 E. Herrero, L. J. Buller, H. D. Abruña, *Chem. Rev.* **2001**, *101*, 1897–1930.

50 V. Augustyn, J. Come, M. A. Lowe, J. W. Kim, P.-L. Taberna, S. H. Tolbert, H. D. Abruña, P. Simon, B. Dunn, *Nat. Mater.* **2013**, *12*, 518–522.

51 K. Subramani, N. Sudhan, R. Divya, M. Sathish, *RSC Adv.* **2017**, *7*, 6648–6659.

52 R. Wang, S. Wang, X. Peng, Y. Zhang, D. Jin, P. K. Chu, L. Zhang, *ACS Appl. Mater. Interfaces* **2017**, *9*, 32745–32755.

53 A. K. Mohamedkhair, M. A. Aziz, S. S. Shah, M. N. Shaikh, A. K. Jamil, M. A. A. Qasem, I. A. Buliyaminu, Z. H. Yamani, *Arab. J. Chem.* **2020**, *13*, 6161–6173.

54 T. Liu, L. Zhang, B. Cheng, J. Yu, *Adv. Energy Mater.* **2019**, *9*, 1803900.

55 J. Saravanan, M. Pannipara, A. G. Al-Sehemi, S. Talebi, V. Periasamy, S. S. Shah, M. A. Aziz, G. Gnana Kumar, *J. Mater. Sci. - Mater. Electron.* **2021**, *32*, 24775–24789.

56 B. Pal, S. Yang, S. Ramesh, V. Thangadurai, R. Jose, *Nanoscale Adv.* **2019**, *1*, 3807–3835.

57 D. Zhang, C. Tan, W. Zhang, W. Pan, Q. Wang, L. Li, *Molecules* **2022**, *27*, 716.

58 A. Noori, M. F. El-Kady, M. S. Rahmanifar, R. B. Kaner, M. F. Mousavi, *Chem. Soc. Rev.* **2019**, *48*, 1272–1341.

59 Z. Wu, L. Li, J.-m. Yan, X.-b. Zhang, *Adv. Sci.* **2017**, *4*, 1600382.

60 G. A. Safitri, K. Nueangnoraj, P. Sreearunothai, J. Manyam, *Curr. Appl. Sci. Technol.* **2020**, *20*, 124–135.

61 L.-Q. Mai, A. Minhas-Khan, X. Tian, K. M. Hercule, Y.-L. Zhao, X. Lin, X. Xu, *Nat. Commun.* **2013**, *4*, 2923.

62 P. Sinha, A. Yadav, A. Tyagi, P. Paik, H. Yokoi, A. K. Naskar, T. Kuila, K. K. Kar, *Carbon* **2020**, *168*, 419–438.

63 T. Cottineau, M. Toupin, T. Delahaye, T. Brousse, D. Bélanger, *Appl. Phys. A* **2006**, *82*, 599–606.

64 H. Li, Y. Gao, C. Wang, G. Yang, *Adv. Energy Mater.* **2015**, *5*, 1401767.

65 J. Kim, J. Lee, J. You, M.-S. Park, M. S. Al Hossain, Y. Yamauchi, J. H. Kim, *Mater. Horiz.* **2016**, *3*, 517–535.

66 M. D. Garba, M. Usman, S. Khan, F. Shehzad, A. Galadima, M. F. Ehsan, A. S. Ghanem, M. Humayun, *J. Environ. Chem. Eng.* **2021**, *9*, 104756.

67 M. Usman, *Membranes* **2022**, *12*, 507.

68 X. Zhang, Z. Xiao, X. Liu, P. Mei, Y. Yang, *Renew. Sust. Energ. Rev.* **2021**, *147*, 111247.

69 V. S. Prabhin, K. Jeyasubramanian, V. S. Benitha, P. Veluswamy, B. J. Cho, *Electrochim. Acta* **2020**, *330*, 135199.

70 S. Kaipannan, S. Marappan, *Sci. Rep.* **2019**, *9*, 1104.

71 D. Sangeetha, M. Selvakumar, *Appl. Surf. Sci.* **2018**, *453*, 132–140.

72 A. K. Nayak, A. K. Das, D. Pradhan, *ACS Sustain. Chem. Eng.* **2017**, *5*, 10128–10138.

73 I. Khan, N. Baig, S. Ali, M. Usman, S. A. Khan, K. Saeed, *Energy Storage Mater.* **2021**, *35*, 443–469.

Part 3

Biomass Derived Electrode Materials for Supercapacitors

7

Non-activated Carbon for Supercapacitor Electrodes

Md. Akib Hasan, Mohammad Anikur Rahman, and Md. Mominul Islam*

Department of Chemistry, University of Dhaka, Dhaka 1000, Bangladesh
* Corresponding author

7.1   Introduction

Supercapacitors are ultrafast electrochemical charge storage devices. There are two methods of supercapacitive charge accumulation: electrostatic and faradaic [1–4]. Electrostatic charge loading results from forming an electrical double layer (EDL) in the vicinity of the electrified electrode and electrolyte interface. The storage device using EDL is known as an electrochemical double-layer capacitor (EDLC). Predominantly, carbon-based materials exhibit an EDLC mechanism for storing charges [1–4]. High specific surface area (SSA), enormous electrical conductivity, low-cost, easy processability, electrochemical idleness, tailorable porosity, and environmental benignity render carbonaceous materials as ideal candidates for EDLCs [1–4].

Biomass-derived AC and non-AC have been tested for their compatibility for use as electrode material for supercapacitors [3–5]. non-AC is precisely how the carbonaceous material comes out after synthesis, i.e., the raw or crude carbonization product before any physical or chemical activations. Therefore, non-AC is the carbon synthesized without any chemical or physical activations that eliminate oxygenated groups in the biomass. The non-AC exhibits fewer functionalities and possesses more defects with lower electrical conductivity [3]. Some differences between the non-AC and AC are given in Table 7.1. The properties that are a prerequisite for a material to be employed as an electrode material for supercapacitors application, such as high porosity, high SSA, high capability of adsorption of charges etc., are less prevalent in non-AC compared to AC [6, 7].

It requires some sort of activation, namely chemical, physical, or both, to obtain AC from the initially synthesized carbonized product, i.e., non-AC. This activation does not ensure a 100% conversion to AC from non-AC; hence, there is a low yield percentage of AC in the obtained product. Moreover, there is an extra cost required for activation [7, 8]. Definitely, AC exhibits an excellent supercapacitive property described elsewhere [5]. This chapter mainly focuses on the charge-storing properties of non-AC derived from different biomass sources, as summarized in Figure 7.1. Simple synthesis, characterization, and application

Table 7.1 Some common features of non-ACs and ACs with their comparisons.

Characteristics	non-ACs	ACs
Nature	Carbon residue of dehydrated organic substrate	Carbon residue of dehydrated organic substrate that has been physically or chemically activated
Porosity	Porous	More porous than non-AC
Composition	~95% carbon with some of O, N, H etc.	~80–85% carbon with an appreciable amount of O, N, H etc.
Surface area	Lower SSA	Higher SSA
Surface charge	Less surface charge	More surface charge
Adsorption capacity	High	Very high
Preparation method	Simple and straightforward	Complicated
%Yield	High	Low
Cost	Low	High

as supercapacitors material of non-AC are described based on the available literature. A discussion on the mechanism of charge storage of non-AC-based supercapacitors is also given.

7.2 Synthesis of Non-activated Carbon

Non-AC can be derived from several organic precursors, mainly through heat treatment and dehydration, i.e., through the carbonization process. Preparation, characterization, and applications of various biomass-derived non-AC have been reported [9–11]. All of
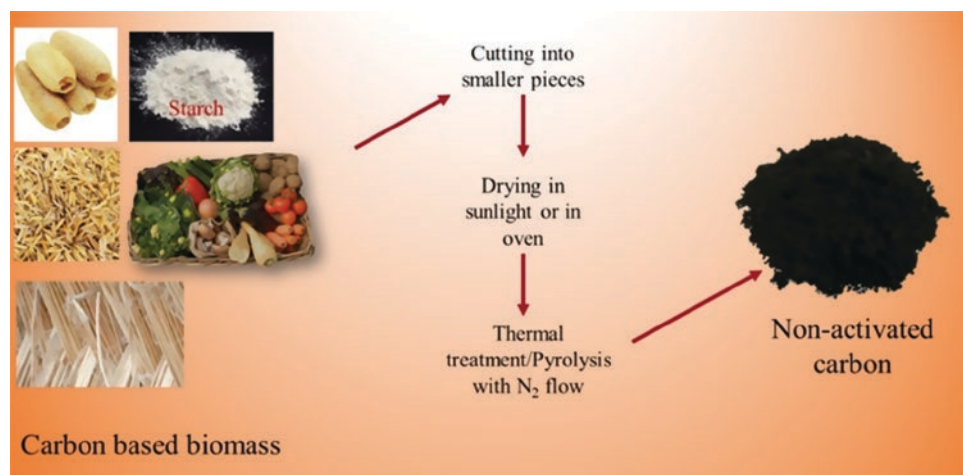
Figure 7.1 Thermal carbonization of biomass to form non-AC materials.
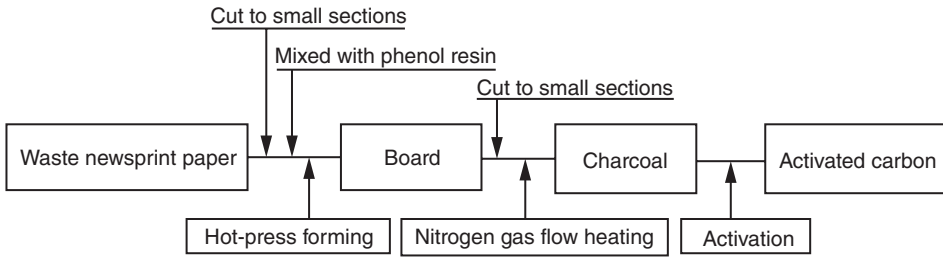
Figure 7.2 Method for manufacturing AC from waste newsprint paper. *Reproduced with permission [5]. Copyright 1999, Springer.*

Table 7.2 Synthetic procedures of non-AC derived from different biomass sources.

Precursor material	Procedure	Ref.
Starch	Carbonization at 200°C followed by heating at 750°C in N_2 atmosphere	[3]
Conocarpus wastes	Pyrolysis of the woody wastes	[12]
Areca nut shells	Pyrolysis followed by heating in N_2 atmosphere	[13]
Waste newsprint paper	Pyrolysis followed by heating in N_2 atmosphere	[5]
Wheat straw	Carbonization at 420°C for 120 min	[9]
Sakura flower stalks	Pyrolysis followed by heating in N_2 atmosphere	[10]
Banana	Carbonization at 180°C followed by heating at 750°C in Ar atmosphere	[14]
Pithophora polymorpha	Pyrolysis at 900°C in N_2 atmosphere	[15]
Albizia procera leaves	Pyrolysis at 850°C in N_2 atmosphere	[16]

them have identical synthetic routes. Waste organic materials are washed, dried, and then shredded into smaller pieces. These small pieces are then dried in the open air under sunlight or in an electrical oven at around 60°C to 80°C. The raw organic material is then dehydrated at elevated temperature in a muffle furnace or in the oven, usually in a nitrogen environment. Chemical or any sort of physical activation is absent in this case. A general route for synthesizing non-AC from various biomass sources is shown in Figure 7.1 and Table 7.2. A typical example of the synthesis of AC from waste newsprint paper is also illustrated in Figure 7.2.

7.3 Morphology and Surface Properties

Surface properties play a key role in dictating the performance of any carbon material for supercapacitor application [17]. Activation of carbonized materials results in the formation of a highly porous nanostructure with higher SSA that has homogeneously dispersed pores

and well-defined pore size distribution [6]. On the other hand, non-AC is less porous with a morphology of smaller SSA, randomly dispersed pores, and not well-defined pore size distribution [18]. In the field emission scanning electron microscopy (FESEM) of sugar-derived non-AC and AC in Figure 7.3(a, b), a highly porous and well-dispersed nanostructure of AC that has been achieved by the chemical activation of non-AC with KOH can be produced [3]. The numbers of micro- and mesopores observed in AC (Figure 7.3(c, d)) are higher than that of non-AC [12]. Thus, AC contains a more well-dispersed porous nanostructure than non-AC, which would result in higher SSA.

On activation, particle size decreases, rendering higher SSA with a concomitant increase in the number of pores (Figure 4) (4) that may facilitate the accumulation of charges, thus influencing specific capacitance (C_{sp}). Larger pores provide easily accessible sites for ions to be stored with a greater extent [13]. Figure 5 represents the N_2 adsorption-desorption isotherms, the relation between pore size and adsorbed pore volumes, and pore size distributions between non-AC and AC. non-AC exhibits type IV isotherms, indicating that a large distribution of pore sizes from micro to macropores are present [13].

SSA, pore volumes, and pore size of both carbons derived from areca nut shells are summarized in Table 7.3 [13]. non-AC has a C_{sp} of 45 F g^{-1}, while AC has 64 F g^{-1} studied by
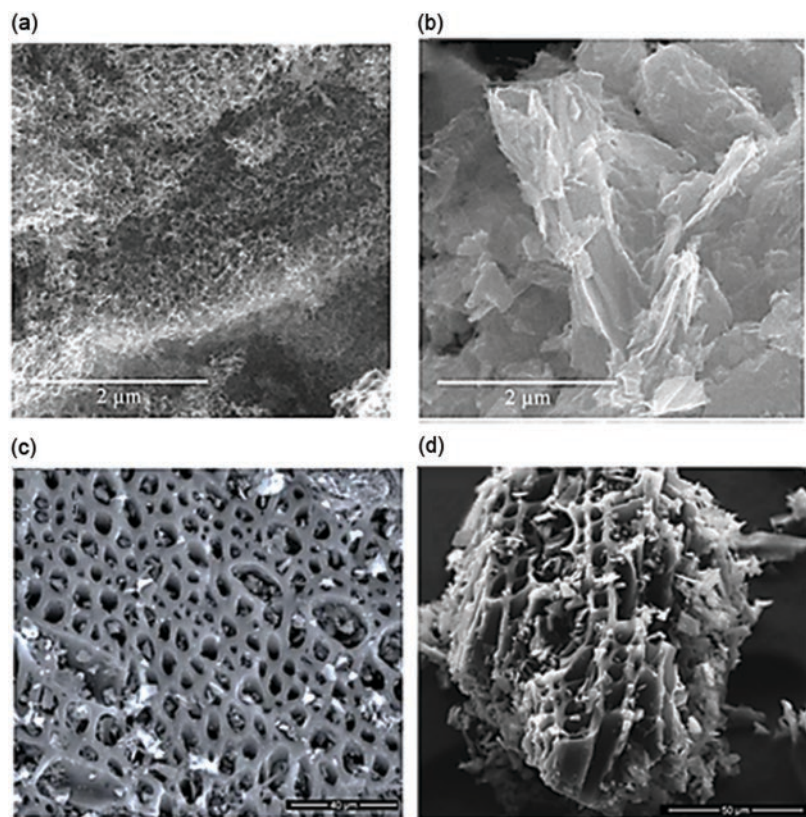
Figure 7.3 FESEM images of a) AC-sugar, b) non-AC-sugar. *Reproduced with permission [3]. Copyright 2017, Springer. SEM micrographs of c) ZnCl$_2$-AC, d) non-AC. Reproduced with permission [12]. Copyright 2016, Bioresources.*

(a)

(b)
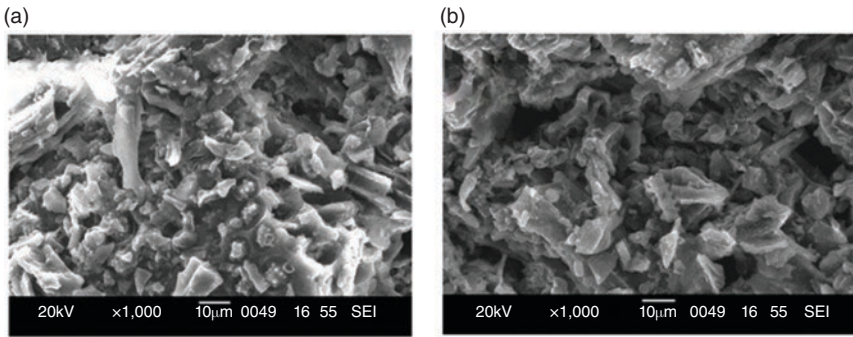
Figure 7.4 SEM images of a) non-AC and b) AC derived from areca nut shells. *Reproduced with permission [13]. Copyright 2013, NISCAIR-CSIR, India.*
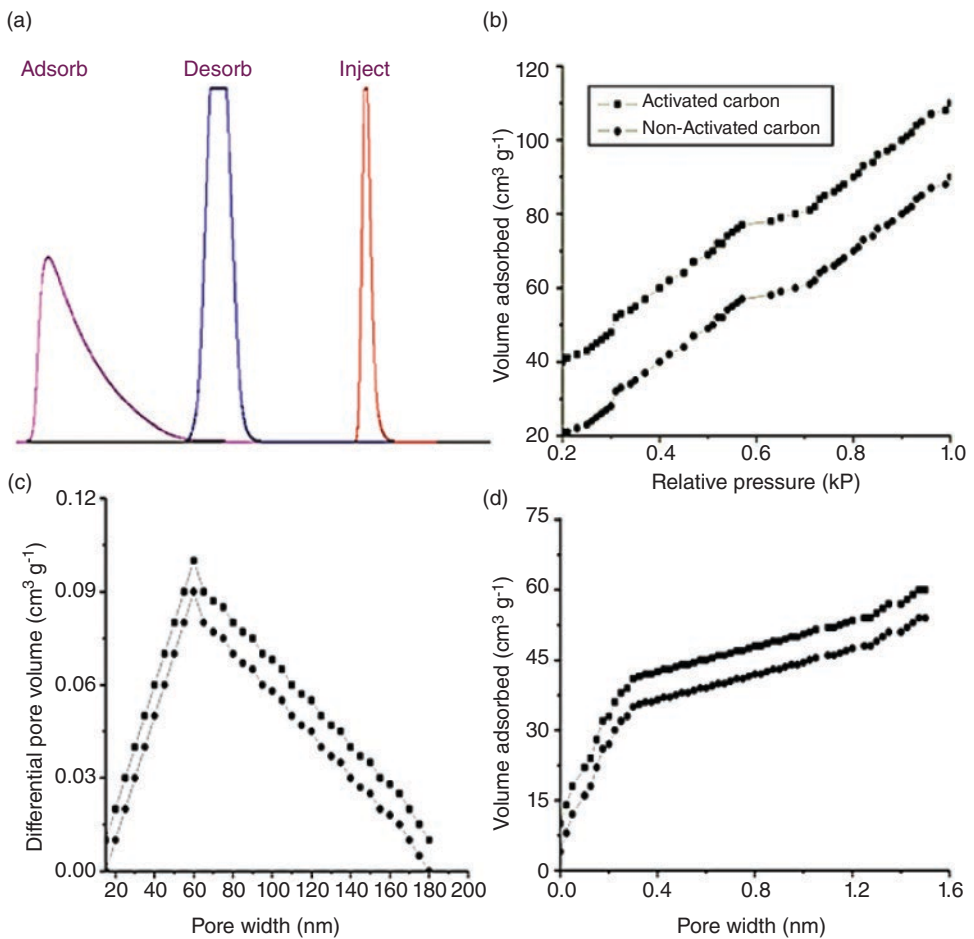
Figure 7.5 a) N$_2$ adsorption-desorption isotherms, b) pore size distribution, and (c and d) pore width versus volume absorbed of AC and non-AC derived from areca nut shells. *Reproduced with permission [13]. Copyright 2013, NISCAIR-CSIR, India.*

Table 7.3 Comparison of capacitances against surface parameters of AC and non-AC.

Sample	Surface area $(m^2 g^{-1})$	Macropore volume $(cm^3 g^{-1})$	Pore size (nm)	Micropore volume $(cm^3 g^{-1})$	Capacitance $(F g^{-1})$
AC	228	0.24	2.33	0.08	64
non-AC	192	0.20	1.88	0.06	45

Reproduced with permission [13]. Copyright 2013, NISCAIR-CSIR, India.

Table 7.4 Physico-chemical properties of AC and non-AC from sugar cane fibre.

Properties	AC	non-AC
pH	6.8	7.2
Bulk density $(g mL^{-1})$	0.081	0.069
Ash content %	5.92	5.72
Surface area $m^2 g^{-1}$	836	603
Surface charge $(mmol^+ g^{-1} C^{-1})$	1.62	0.81

Reproduced with permission [19]. Copyright 2017, AJOL.

applying an identical current density. It is noteworthy to mention that apart from SSA, the pore size is another major determining factor of C_{sp} of a supercapacitor material. Larger pores allow the hydrated ions of the electrolyte to enter the inner surface of the porous materials, resulting in higher capacitance.

Sugar cane fibre-derived AC and non-AC have been analyzed by Ikhuoria et al. [19] The properties of such carbons are compared in Table 7.4. Bulk density, ash content, surface area, surface charge, etc., increase tremendously. The accumulation of ions has been doubled on activation. This indicates a favourable improvement in charge storage.

The effects of activation of non-AC concerning the morphology and functional sites are depicted in Figure 7.6. Activation creates different functional groups and pores on the surface of carbon to form AC. However, the initial carbonized product, i.e., the non-AC, has less promising properties than AC as a supercapacitor material. This fact is reflected in the electrochemical behaviour discussed in the following section.

It has been considered that the biomass possessing naturally occurring inherent porous structure would produce porous non-AC [15]. non-AC has been prepared from the filaments with naturally occurring pores of *Pithophora polymorpha* via a direct pyrolysis without performing any chemical activation. The obtained non-AC is macro-, meso- and microporous in nature possessing the SSA of $113 m^2 g^{-1}$ and an average pore size of 5.5 nm [16]. Besides chemical activation, the doping of the non-AC with heteroatoms such as Mg, Si, P, S, Cl, Ca, Fe and N is another excellent approach (Figure 7.7) for enhancing SSA and charge storage capacity, C_{sp}. N-doped carbon nanostructures of non-AC have been
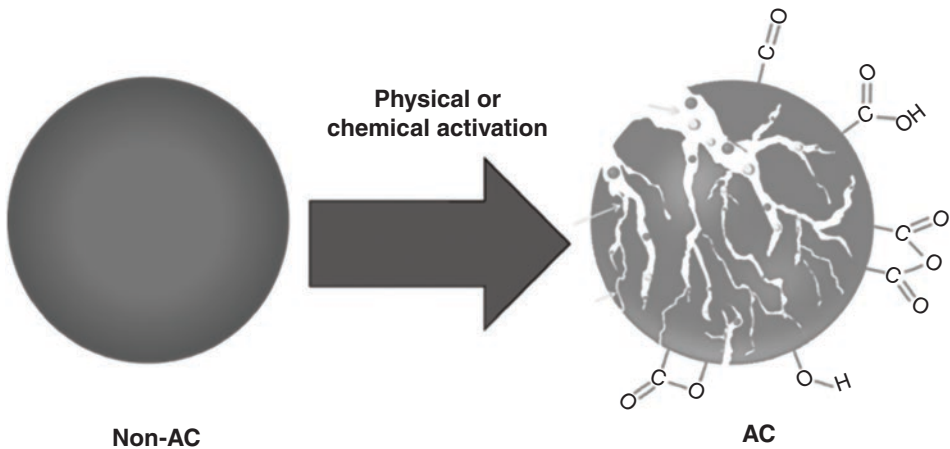
Figure 7.6 Effect of activation on the morphology and surface.
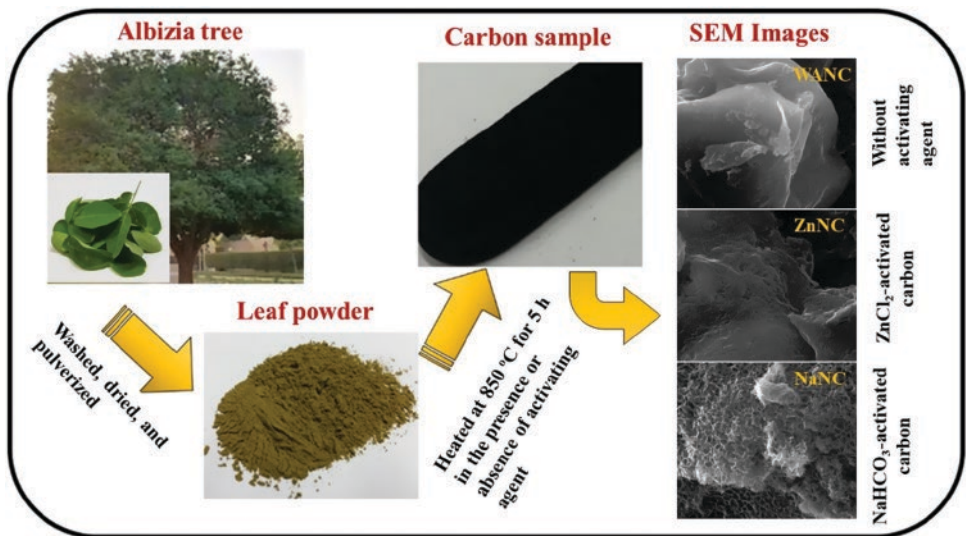
Figure 7.7 Preparation of carbons from *Albizia procera* leaves. *Reproduced with permission [16]. Copyright 2020, Elsevier.*

prepared from the leaves of the *Albizia* tree (nitrogen-doped carbon prepared without an activating agent (WANC)) with SSA of 322 m^2 g^{-1} [16]. Further activation of WANC with $NaHCO_3$ and $ZnCl_2$ has been proved to produce ACs NaNC and ZnNC, respectively, with higher SSA. However, the SSA of these carbons derived from the leaves of *Albizia* has been found to decrease in the order of NaNC > ZnNC > WANC. The presence of higher percent of graphitic carbon that has been identified with Raman and XPS techniques is considered to create porous nanostructures [16].

7.4 Charge Storage Performance

Structural and morphological studies suggest that non-AC would result in a lower C_{sp}. The charge storage capability of non-AC can be explored by electrochemical characterization with cyclic voltammetric, galvanostatic charge-discharge, and electrochemical impedance spectroscopic (EIS) measurements. Through these measurements, further insight into the contribution of the type of capacitance, namely EDLC and pseudocapacitance, resulted from double layer charging and faradaic process, respectively, to the total capacitance and hence the degree of electroactive group present on the active surface of the material can be understood.

In Figure 7.8(a), cyclic voltammograms (CVs) recorded typically for non-AC and AC are shown. The shape of these CVs is a nearly rectangular box, depicting EDLC. No redox peak is seen, so pseudocapacitance is absent. Analysis of CV allows estimating the value of C_{sp} from the area under the curve [20]. The area under the CV curve measured for non-AC is less than that of AC, indicating inferior charge storage capacity. The C_{sp} of non-AC is about
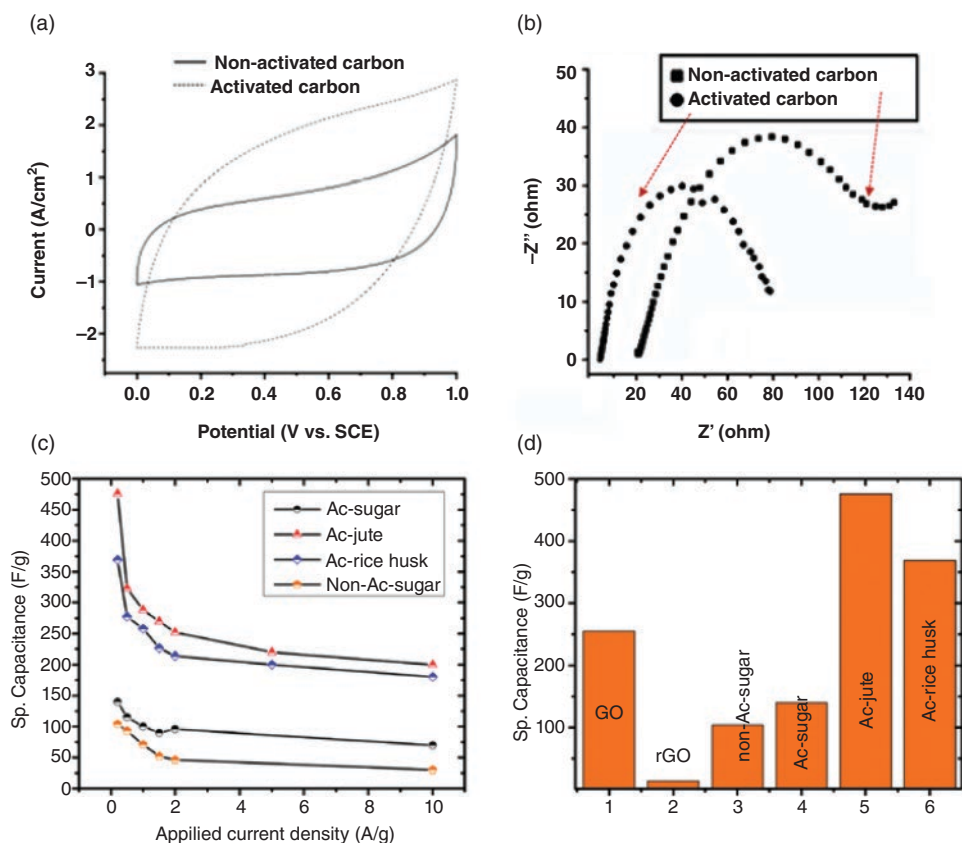
Figure 7.8 a) Comparison of CVs and b) Nyquist plots measured at stainless steel plate modified with Non-AC and AC materials in aqueous 0.1 M Na$_2$SO$_4$. *Reproduced with permission [13]. Copyright 2013 NISCAIR-CSIR, India. c) Variation of C$_{sp}$ as a function of applied current density and d) comparison of C$_{sp}$ of various carbon materials measured at a current density of 0.2 A g^{-1}. Reproduced with permission [3]. Copyright 2017, Springer.*

one-half of that obtained for AC. Lower SSA with a limited number of sizable pores, that act as charge storage sites, is responsible for the lower C_{sp} of non-AC.

EIS measurement is a powerful tool that assists in evaluating different parameters associated with electrochemical processes occurring at the electrified electrode–electrolyte interface, including equivalent series resistance (ESR) resulting from electrolyte resistance, electrode resistance, charge transfer resistance, and the charge storing capability of a material [21–33]. EIS studies of both non-AC and AC have been presented as examples. It is quite clear from the typical Nyquist plots shown in Figure 7.8(b) that the charge transfer resistance is higher for non-AC (130 Ω) compared to AC (80 Ω). This reveals that non-AC are not good conductors compared to AC [13].

A comparison of C_{sp} of non-AC with AC and those of other carbonaceous materials are displayed in Figure 7.8 (c) and Figure 7.8 (d), respectively. Non-AC exhibit C_{sp} of about 100 F g^{-1}, which is commonly low compared to graphene oxide (GO) and other ACs. This kind of mediocre performance restricts the commercial and practical uses of non-AC as an electrode material for application in supercapacitors [3]. N-doped carbon nanostructures of non-AC shows a EDL characteristic in storing charges (Figure 7.9). Electrochemical characterizations with CVs and GCDs reveal that the supercapacitive performances of non-AC, WANC, is poor compared to both ZnNC and NaNC as can be clearly seen in the CV and galvanostatic charging-discharging (GCD) responses. At a current density of 5 A g^{-1}, WANC demonstrates a C_{sp}
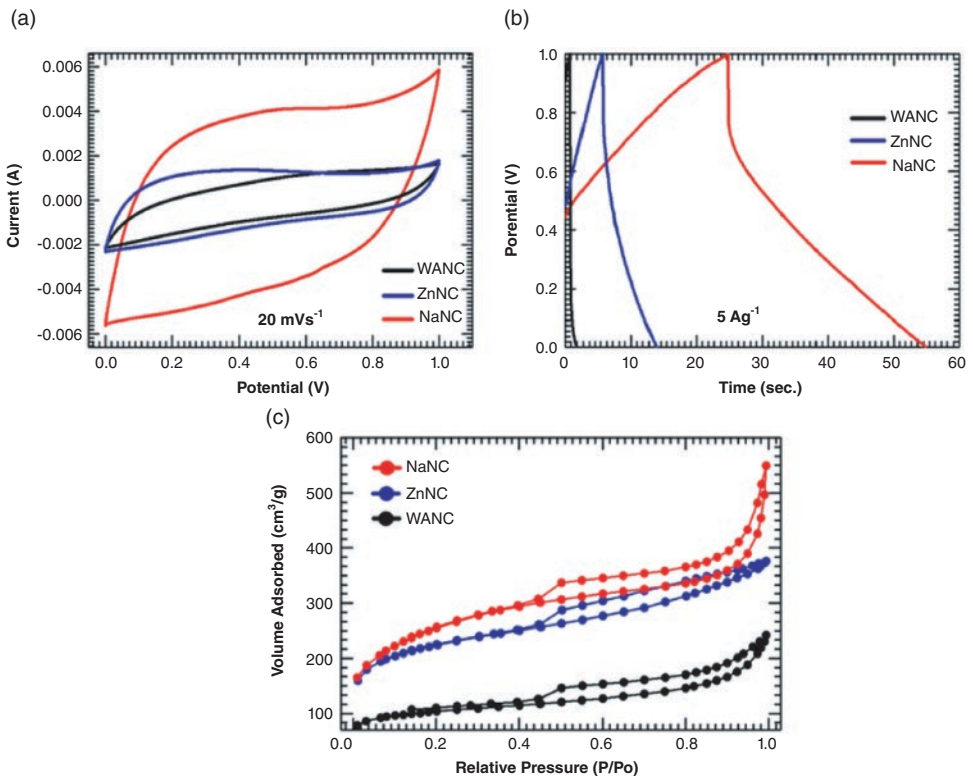
Figure 7.9 a) CV at scan rate of 20 mVs^{-1} and b) GCD measurements at current density of 5 Ag^{-1} of WANC, ZnNC, and NaNC. c) Nitrogen isothermal analysis for the WANC, ZnNC, and NaNC. *Reproduced with permission [16]. Copyright 2020, Elsevier.*

of 19.1 F g^{-1}, while the C_{sp} of ZnNC and NaNC are 30.3 and 166.7 F g^{-1}, respectively [21]. The relatively higher values of C_{sp} may ascribed to be resulted from the higher SSA of NaNC (910 m^2 g^{-1}) and ZnNC (777 m^2 g^{-1}) compared to WANC with SAA of 322 m^2 g^{-1} determined from BET results shown in Figure 7.9(c).

7.5 Charge Storage Mechanism

The electrochemical capacitors store electrical energy in the form of ions at the electrode–electrolyte interface in the form of EDL. The formation of a rigid EDL leads to higher charge storage, i.e., higher capacitance, since the diameter of the compact layer that is inversely proportional to the capacitance is very small, in the range of angstroms [34, 35]. Moreover, the surface morphology of electrodes like porosity and surface area greatly affects C_{sp}. For enhancing the EDL capacitance, a moderate pore size (>2 nm) is required for facile mobility and the insertion of individual electrolyte ions into the pores of the electrode [35]. The porous surface with a high surface area permits a large number of solvated ions to be adsorbed on the electrode surface to form a rigid EDL. These facts described well explain the observation of lower C_{sp} of non-AC than that of AC.

Further insight into the factors leading to the lower C_{sp} of non-AC may be clarified by consulting with the EDL formation in the vicinity of the electrode surface. Pictorial views of EDL formed at the non-AC and AC modified electrode–electrolytic solution interfaces are represented in Figure 7.10. The surface area and porosity of non-AC are less than AC,
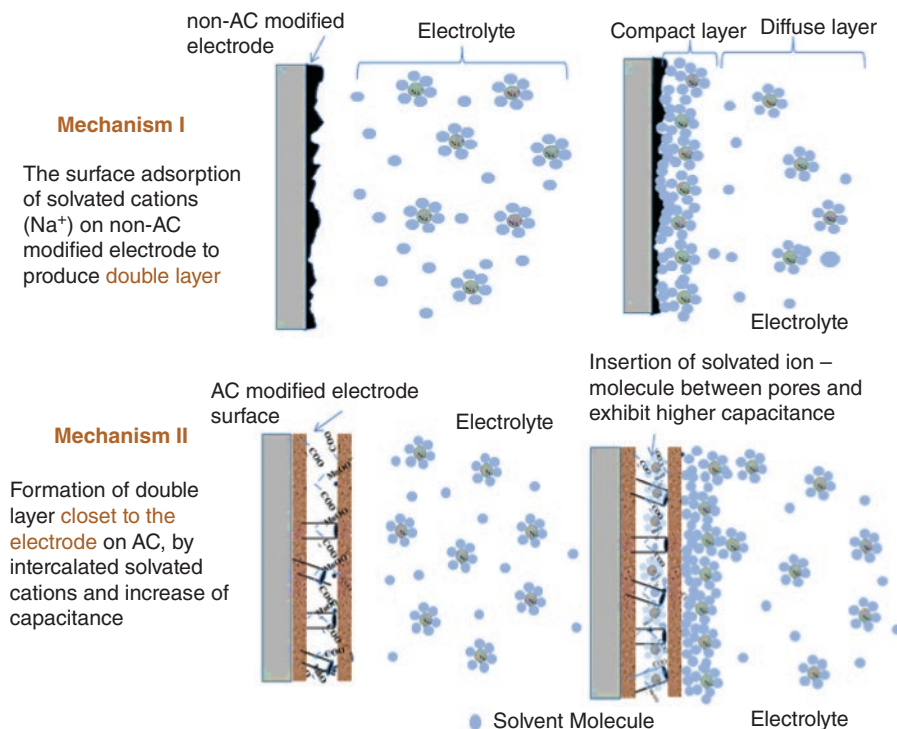
Figure 7.10   Presumptive charge storage mechanism of both AC and non-AC.

which is directly reflected in C_{sp} values as summarized in Table 7.3 and Figure 7.8. The introduction of porosity into AC during the activation processes of non-AC is associated with introducing oxygen-containing groups on the surface of AC. Pores of the AC give more access to the solvated ions to form a compact layer with respect to non-AC materials (Figure 7.10). The oxygen-containing functional group of AC makes the compact layer formation more rigid with the closest possible area at the electrode surface, which has a direct influence on increasing the capacitance.

As described above, among three N-doped carbon materials, NaNC is rated as the best electrode material for supercapacitor applications (see in Figure 7.9). It is remarkable to note that the sizable pores play a vital and pivotal role in charge storage [34, 35]. Doping of non-AC with heteroatoms increases the pore size to be macropore. NaNC has a higher micro/mesopore ratio than WANC, as evidenced by the fact that the average pore size of NaNC (2.8 nm) is larger than that of WANC (4.9 nm). Besides, the average pore size (1.5 nm) and a kind of hysteresis loop of ZnNC show that it has a combination of micro- and mesoporous structure [20]. However, these porosities match well with the hydrodynamic volume of common ions resulting in higher C_{sp}.

7.6 Concluding Remarks and Future Prospects

Preparation of non-AC materials from biomass is simple and can be easily carried out through pyrolysis without any physical and chemical activation. Ease of preparation, almost free of cost, and a huge abundance of precursors in nature over the globe make non-AC a cheap and environmentally friendly material of choice for multipurpose application. Low levels of oxygen-containing functionalities, surface area, and porosity that might be advantageous in other applications result in a lower charge storage capacity compared to AC. On the other hand, the interconnected structure of AC that is absent in non-AC creates small resistance and hence short diffusional pathways for ion transportation required for a good quality supercapacitor material. All these factors make the non-AC as less suitable materials for supercapacitor electrodes used commercially. Making composites of non-AC, cheap, and non-toxic material, with non-conductive materials possessing a high capacitive property, such as natural and synthetic polymers, oxides, and carbon dots, may be a new direction of future study [36–41].

Carbon-based materials are needed in supercapacitors to improve their surface area, conductivity, cycle life span, to introduce pores, and so on [42–44]. non-AC is a potential candidate for this very purpose because of its cheap costs, facile synthesis, non-toxicity, high thermal stability, electrochemical inertness, acid tolerance, etc. [45]. However, the commercial application of non-AC as supercapacitor materials is limited due to their poor performance. Generally, SSA of non-AC is low compared to other carbon-based materials. non-AC carbon is further ground/ball-milled to get nano-scaled non-AC which could be suitable for improving the supercapacitor performances [46, 47]. Proper selection of precursors and preparation methods may enhance the supercapacitive performance of non-ACs. Judicious selection of additives during synthesis is also crucial for improving the properties of non-ACs. Doping non-AC with heteroatoms like Mg, Si, N, B, S, P can substantially improve supercapacitor performance [15, 48]. Blending non-AC with other

high-performance supercapacitive materials like metal oxides, conductive polymers [15], and so on may assist in devising commercially viable low-cost supercapacitors.

Acknowledgements

Declaration of Competing Interest

The authors declare that they have no known competing financial interests or personal relationships that could have appeared to influence the work reported in this chapter.

References

  1 J. Wang, X. Zhang, Z. Li, Y. Ma, L. Ma, *J. Power Sources* **2020**, *451*, 227794.
  2 S. S. Shah, S. M. A. Nayem, N. Sultana, A. J. S. Ahammad, M. A. Aziz, *ChemSusChem* **2022**, *15*, e202101282.
  3 K. Ojha, B. Kumar, A. K. Ganguli, *J. Chem. Sci.* **2017**, *129*, 397–404.
  4 P. Ratajczak, M. E. Suss, F. Kaasik, F. Béguin, *Energy Storage Mater.* **2019**, *16*, 126–145.
  5 M. Shimada, H. Hamabe, T. Iida, K. Kawarada, T. Okayama, *J. Porous Mater.* **1999**, *6*, 191–196.
  6 M. Durai, M. Sivakumar, H. Chang, Y.-H. Ahn, M. Durai, *J. Mater. Sci. - Mater. Electron.* **2021**, *32*, 3487–3497.
  7 Z. Heidarinejad, M. H. Dehghani, M. Heidari, G. Javedan, I. Ali, M. Sillanpää, *Environ. Chem. Lett.* **2020**, *18*, 393–415.
  8 M. Sevilla, R. Mokaya, *Energy Environ. Sci.* **2014**, *7*, 1250–1280.
  9 X. Li, C. Han, X. Chen, C. Shi, *Microporous Mesoporous Mater.* **2010**, *131*, 303–309.
 10 F. Ma, S. Ding, H. Ren, Y. Liu, *RSC Adv.* **2019**, *9*, 2474–2483.
 11 S. Bilgen, *Renew. Sust. Energ. Rev.* **2014**, *38*, 890–902.
 12 A. H. El-Naggar, A. K. Alzhrani, M. Ahmad, A. R. Usman, D. Mohan, Y. S. Ok, M. I. Al-Wabel, *BioResources* **2016**, *11*, 1092–1107.
 13 M. Natalia, Y. Sudhakar, M. Selvakumar, *Indian J. Sci. Technol.* **2013**, *20*, 392–399.
 14 L. Wang, X. Li, J. Ma, Q. Wu, X. Duan, *Sustainable Energy* **2014**, *2*, 39–43.
 15 S. S. Shah, M. A. Alfasane, I. A. Bakare, M. A. Aziz, Z. H. Yamani, *J. Energy Storage* **2020**, *30*, 101562.
 16 A. K. Mohamedkhair, M. A. Aziz, S. S. Shah, M. N. Shaikh, A. K. Jamil, M. A. A. Qasem, I. A. Buliyaminu, Z. H. Yamani, *Arab. J. Chem.* **2020**, *13*, 6161–6173.
 17 E. Frackowiak, *Phys. Chem. Chem. Phys.* **2007**, *9*, 1774–1785.

18 F. H. Puspitasari, N. Sirimorok, U. Salamah, N. R. Sari, A. Maddu, A. Solikhin, *Fiber. Polym.* **2020**, *21*, 701–708.

19 E. Ikhuoria, O. Onojie, *Bull. Chem. Soc. Ethiop.* **2007**, *21, 151–156.*

20 S. Aderyani, P. Flouda, S. A. Shah, M. J. Green, J. L. Lutkenhaus, H. Ardebili, *Electrochim. Acta* **2021**, *390*, 138822.

21 S. S. Shah, M. A. Aziz, W. Mahfoz, A.-R. Al-Betar, Conducting Polymers Based Nanocomposites for Supercapacitors in *Nanostructured Materials for Supercapacitors*, (Eds: S. Thomas, A. B. Gueye, R. K. Gupta), Springer, Cham, **2022**, Chapter 22, pp. 485–511, Vol. *1*.

22 S. I. Basha, S. S. Shah, S. Ahmad, M. Maslehuddin, M. M. Al-Zahrani, M. A. Aziz, *Chem. Rec.* **2022**, https://doi.org/10.1002/tcr.202200134, e202200134.

23 R. Shakil, M. N. Shaikh, S. S. Shah, A. H. Reaz, C. K. Roy, A.-N. Chowdhury, M. A. Aziz, *Asian J. Org. Chem.* **2021**, *10*, 2220–2230.

24 S. S. Shah, M. A. Aziz, A.-R. Al-Betar, W. Mahfoz, *Arab. J. Chem.* **2022**, *15*, 104058.

25 M. Rauf, S. S. Shah, S. K. Shah, S. N. A. Shah, T. U. Haq, J. Shah, A. Ullah, T. Ahmad, Y. Khan, M. A. Aziz, K. Hayat, *J. Saudi Chem. Soc.* **2022**, *26*, 101514.

26 M. Ashraf, S. S. Shah, I. Khan, M. A. Aziz, N. Ullah, M. Khan, S. F. Adil, Z. Liaqat, M. Usman, W. Tremel, M. N. Tahir, *Chem. Eur. J.* **2021**, *27*, 6973–6984.

27 S. S. Shah, E. Cevik, M. A. Aziz, T. F. Qahtan, A. Bozkurt, Z. H. Yamani, *Synth. Met.* **2021**, *277*, 116765.

28 M. A. Aziz, S. S. Shah, S. M. A. Nayem, M. N. Shaikh, A. S. Hakeem, I. A. Bakare, *J. Energy Storage* **2022**, *50*, 104278.

29 C. K. Roy, S. S. Shah, A. H. Reaz, S. Sultana, A.-N. Chowdhury, S. H. Firoz, M. H. Zahir, M. A. A. Qasem, M. A. Aziz, *Chem. Asian J.* **2021**, *16*, 296–308.

30 M. M. Hasan, T. Islam, S. S. Shah, A. Awal, M. A. Aziz, A. J. S. Ahammad, *Chem. Rec.* **2022**, *22*, e202200041.

31 S. S. Shah, M. A. Aziz, Z. H. Yamani, *Chem. Rec.* **2022**, *22*, e202200018.

32 M. Yaseen, M. A. K. Khattak, M. Humayun, M. Usman, S. S. Shah, S. Bibi, B. S. U. Hasnain, S. M. Ahmad, A. Khan, N. Shah, A. A. Tahir, H. Ullah, *Energies* **2021**, *14*, 7779.

33 S. S. Shah, M. A. Aziz, E. Cevik, M. Ali, S. T. Gunday, A. Bozkurt, Z. H. Yamani, *J. Energy Storage* **2022**, *56*, 105944.

34 M. A. Hasan, M. M. Islam, M. A. B. H. Susan, M. M. Islam, *ECS Transactions* **2022**, *107*, 12435.

35 M. M. Islam, M. Y. A. Mollah, M. A. B. H. Susan, M. M. Islam, *RSC Adv* **2020**, *10*, 44884–44891.

36 M. M. Hasan, T. Islam, A. Imran, B. Alqahtani, S. S. Shah, W. Mahfoz, M. R. Karim, H. F. Alharbi, M. A. Aziz, A. J. S. Ahammad, *Electrochim. Acta* **2021**, *374*, 137968.

37 S. S. Shah, H. T. Das, H. R. Barai, M. A. Aziz, *Polymers* **2022**, *14*, 270.

38 M. Ashraf, I. Khan, M. Usman, A. Khan, S. S. Shah, A. Z. Khan, K. Saeed, M. Yaseen, M. F. Ehsan, M. N. Tahir, N. Ullah, *Chem. Res. Toxicol.* **2020**, *33*, 1292–1311.

39 A. Helal, S. S. Shah, M. Usman, M. Y. Khan, M. A. Aziz, M. Mizanur Rahman, *Chem. Rec.* **2022**, *22*, e202200055.

40 S. S. Shah, M. A. A. Qasem, R. Berni, C. Del Casino, G. Cai, S. Contal, I. Ahmad, K. S. Siddiqui, E. Gatti, S. Predieri, J.-F. Hausman, S. Cambier, G. Guerriero, M. A. Aziz, *Sci. Rep.* **2021**, *11*, 6945.

41 M. Usman, M. Humayun, S. S. Shah, H. Ullah, A. A. Tahir, A. Khan, H. Ullah, *Energies* **2021**, *14*, 2281.

42 A. J. S. Ahammad, P. R. Pal, S. S. Shah, T. Islam, M. Mahedi Hasan, M. A. A. Qasem, N. Odhikari, S. Sarker, D. M. Kim, M. A. Aziz, *J. Electroanal. Chem.* **2019**, *832*, 368–379.

43 T. Islam, M. M. Hasan, S. S. Shah, M. R. Karim, F. S. Al-Mubaddel, M. H. Zahir, M. A. Dar, M. D. Hossain, M. A. Aziz, A. J. S. Ahammad, *J. Energy Storage* **2020**, *32*, 101908.

44 J. Saravanan, M. Pannipara, A. G. Al-Sehemi, S. Talebi, V. Periasamy, S. S. Shah, M. A. Aziz, G. Gnana Kumar, *J. Mater. Sci. - Mater. Electron.* **2021**, *32*, 24775–24789.

45 R. Dubey, V. Guruviah, *Ionics* **2019**, *25*, 1419–1445.

46 S. I. Basha, M. A. Aziz, M. Maslehuddin, S. Ahmad, *Chem. Asian J.* **2021**, *16*, 3914–3930.

47 B. Haq, M. A. Aziz, D. Al Shehri, N. S. Muhammed, S. I. Basha, A. S. Hakeem, M. A. A. Qasem, M. Lardhi, S. Iglauer, *Nanomaterials* **2022**, *12*, 1245.

48 M. A. Haque, M. R. Akanda, D. Hossain, M. A. Haque, I. A. Buliyaminu, S. I. Basha, M. Oyama, M. A. Aziz, *Electroanal* **2020**, *32*, 528–535.

8

Carbon from Pre-Treated Biomass

Syeda Ramsha Ali, Mian Muhammad Faisal[†], and K.C. Sanal*

Universidad Autónoma de Nuevo León, UANL, Facultad de Ciencias Químicas, Av. Universidad, Cd. Universitaria, 66455 San Nicolás de los Garza, Nuevo León, México
*,[†] Corresponding author

8.1 Introduction

Activated carbon is a porous form of carbon developed with enhanced pore structure, pore volume, and excellent surface area and thus has a high adsorption capacity [1]. The activated carbons have gained tremendous research interest in different fields like lithium-ion batteries, sodium-ion batteries, and electrochemical supercapacitors owing to high specific surface areas of around 500–3000 $m^2\,g^{-1}$. They possess various pores, including macropores (>50 nm), mesopores (2–50 nm), and micropores (2 < nanometres (nm)) [2, 3]. Biowaste materials are the main source for producing efficient and high-performance activated carbon through physical or chemical activation [4]. The precursors used for activated carbon production from biowaste materials include sugarcane bagasse, jute sticks, banana leaves, peat soil, coffee beans, banana fibers, peanut shells, almond peel, cherry stone waste, orange peel, paper pulp, firewood, corncob, camellia shell, carrageenan, urea, tamarind fruit shell, eggshell, corncob residue, lignin, and oil palm [3, 5–18]. Physical and chemical means are used for the production of activated carbon, which means varying the conditions of pyrolysis, hydrothermal carbonization, and pre-treatments tunes the properties of porosity and surface area. To obtain the activated carbon, hot gases are utilized, followed by pyrolysis at different temperature ranges from 600 to 900°C for the physical reactivation, and 450 to 900°C in chemical reactivation where acids and bases or salts are used with the biomass [4]. The templated process can also be utilized for activated carbon production; this process was declared the best technique as it controls the surface area and pore size. This technique involves the infiltration within the pores of carbon material for any of the materials under investigation, followed by a polymerization process, and finally to get porous activated carbon template removal was performed [19]. Production of activated carbon is also possible through other less common methods. Deng et al. reported carbonization of molten salt of chitosan, which is 10 times heavier than zinc chloride while maintaining the temperature range of 400–700°C [2]. Furthermore, around 200,000 articles on carbon-based materials have been reported,

including articles on carbon nanotubes, activated carbon, graphene, graphite, fullerenes, carbon black, and carbon nanofibers.

8.2 Supercapacitor and Activated Carbon

Supercapacitors have been recognized as a latent energy storage system for a decade. The electrochemical capacitors, including ultracapacitors, supercapacitors, electric double layer capacitors (EDLCs), pseudocapacitors, power capacitors, etc., have attracted researchers' interest at a universal level due to their applications in energy storing fields. The supercapacitors lie between the conventional capacitors and battery technology when considering these technologies' power density and energy density [20–30]. They have numerous applications for electric vehicles, power backups, and electronics as they have a long cyclic life, high energy density, maintenance-free operation, environmental friendliness, and fast charging and discharging rate. The major research focus is on the supercapacitive material that can be utilized to form a capacitance link between the electrode and electrolyte interface. To approach this objective, carbon-based materials are utilized as the basic material for supercapacitors' numerous applications as they have a highly porous structure, large surface area, high conductivity, and better adsorption quality [31]. Theproperties of these carbon-based materials directly affect the electrochemical performance of the supercapacitors as they depend upon the material's surface chemistry, pore structure, and surface area. With a greater surface area, the surface chemistry and pore structure will be more suitable for the successful performance of supercapacitors. To attain this, carbons are pre-treated to get activated carbon with a good surface chemistry, sufficiently high surface area, and the desired pore volume [32]. Activated carbons have edge sites and surface functional groups that can help in specific surface area improvement, eventually enhancing the supercapacitors' electrochemical properties [33]. There are numerous pre-treatment methods to obtain activated carbons, which will be discussed later in this chapter.

8.2.1 Processes to Obtain Activated Carbon

The two major ways to synthesize activated carbon are via chemical methods or physical methods. These are not the only techniques reported for synthesizing activated carbon. Thermal activation in a nitrogen atmosphere and microwave irradiation is also reportedly used for the activation of carbon. A combination of physical and chemical processes has also been proposed to obtain hierarchical porous activated carbons [34]. The activation process will be briefly explained in this section, followed by pre-treatment techniques.

8.2.1.1 Carbonization

Carbonization (pyrolysis) is a process that is applied before the activation stage in which the original lignocelluloseexperiences heat treatment for carbon enrichment. In this process, the elements that have low molecular weight and are volatile are releasedfirst, and the aromatic and hydrogen gas are eliminated in the later. What remains is the carbonaceous skeleton. The porosity obtained in this process is very low, and it needs some activation to enhance the size of the pores and increase the surface area. The activation of

carbon is very critical; the carbonization parameters should be strictly controlled as the process controls the final yield. The most important parameters during carbonization are the temperature and the rate at which the material is heated, the inert environment, the rate at which the gas flows, and the time allowed for the treatment. In general, the carbonization temperature is kept higher than 600 °C; maintaining a higher temperature will reduce the chances of producing char. The maintenance of higher temperatures will increase carbon content and ash, which minimizes the volatile matter. Therefore, a higher temperature for the carbonization is recommended to obtain high quality but might compromise the yield [35, 36].

8.2.1.2 Chemical Activation

Chemical activation is a process in which two steps are carried out simultaneously by mixing a precursor with chemical activation agents, such as dehydrating agents and oxidants [36]. In this process, the raw materials from lignocellulose are directly treated with chemicals such as phosphoric acid (H_3PO_4), sulfuric acid (H_2SO_4), zinc chloride ($ZnCl_2$), nitric acid (HNO_3), sodium hydroxide (NaOH), potassium hydroxide (KOH), etc. Some chemicals like hydrogen peroxide (H_2O_2), potassium carbonate (K_2CO_3), formamide, calcium chloride have also been reported for use in activation. While performing this step, the ratio between the biomass and the activation agent is varied and optimized along with the reaction time and stirring to manage the formation of tar and some undesired products. The final product is then heated in the temperature range of 400–1000 °C under a controlled atmosphere, followed by washing with DI, ethanol, and methanol. Some gases like air, nitrogen, and argon are purged during carbonization to develop the production of internal porosity. These activation agents help to mature the internal porosity by dehydration and degradation of the actual structure of biomass. The pore size and surface area distribution can be determined by finding the ratio of precursor and activation agent. An activation agent like zinc chloride is recommended for promoting micropores in the biomass; the acid agent inhibits the micropores and promotes macro- and mesopores in the materials. In comparison, the alkaline agents are suitable for developing the micro- and mesopores in the precursor [35, 37, 38]. The activation agent has a key role in the surface area of the activated carbon; a detailed analysis has been added in Table 8.1, which summarizes different precursors with different activation agents along with the obtained surface area.

8.2.1.3 Physical Activation

Physical activation is a two-step process involving the carbonization of carbon-enriched materials followed by activation of the obtained yield with suitable activation agents at the required temperature in the presence of several oxidizing gases such as carbon dioxide, steam, air or a mixture of them. Physical activation can be carried out by carbonizing the precursor under an inert atmosphere and then subjecting the obtained carbon to controlled gasification at higher temperatures. The activation atmosphere is maintained with a high oxidizing agent like CO_2, or water steam or O_2, or a mixture of these at high temperatures. A detailed list of activated carbons obtained through this technique is listed in Table 8.2. In the specific case of steam gasification, the reaction followed is presented below:

Table 8.1 Different precursors for activated carbon with several chemical activation agents and the obtained surface area.

Precursor	Activation agent	Surface area (m²/g)	Precursor	Activation agent	Surface area (m²/g)
Sisal[39]	$ZnCl_2$	5	Banana[40]	KOH	2086
Oil palm shell[41]	KOH	1630	Tea waste[38]	K_2CO_3	1722
			Tea waste	H_3PO_4	1398
Peach stones[42]	$ZnCl_2$	1425	Coconut pith[43]	KOH	505
Orange peel[44]	H_3PO_4	1056	Coffee[45]	$ZnCl_2$	890
			Coffee	H_3PO_4	696
Hemp[46]	HNO_3	1250	Pomelo[47]	KOH	1533
Eucalyptus wood[48]	KOH	2000	Stem of date palm[49]	KOH	947
	NaOH	3167		H_3PO_4	1100
Peach stones[50]	H_3PO_4	1225	Sky fruit husk[51]	H_3PO_4	1211
Olive stones[52]	H_3PO_4	990	Grape seeds[53]	KOH	1860
Coir fibre[54]	H_3PO_4	540	Apple pulp[55]	H_3PO_4	1004
Phoenix dactyliferous[56]	H_3PO_4	1225	Date stones[57]	H_3PO_4	1100
Prosopis ruscifolia[58]	H_3PO_4	1638	Coconut shells	$H_2O_2/ZnCl_2$	2050
Pine[37]	K_2CO_3	1509	Peanut shells[59]	H_3PO_4	751
Tobacco[60]	HNO_3	1104	Potato waste[61]	$ZnCl_2$	1052
Starch-rich banana[62]	H_3PO_4	2068	Willow catkins[63]	KOH	1586
Soybean oil cake[64]	K_2CO_3	1353	Date pits[65]	$FeCl_2$	780
Olives stones[66]	$ZnCl_2$	1860	Peanut shell[67]	K_2CO_3/Fe_3O_4	1236
Apricot & peach stones[68]	H_3PO_4	1740	Flamboyant pods[69]	NaOH	2463
Olive stones[70]	KOH	587	Rice[72]	KOH	3263
Olive stones[71]	H_3PO_4	1014			

$$C + H_2O \rightarrow CO + H_2$$
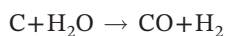
Two mechanisms in these equations are as follows:

(1) Oxygen exchange model

$$H_2O + C \leftrightarrow C(O) + H_2$$

$$C(O) \rightarrow C + CO$$
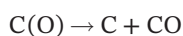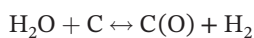
(2) Hydrogen inhibition

$$C + H_2O \rightarrow C(O) + H_2$$

$$C + H_2 \rightarrow C(H_2)$$
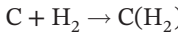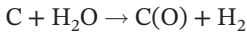
C here corresponds to the active site, C(O) denotes the complex of the oxygen surface, whereas $C(H_2)$ shows the amount of hydrogen absorbed. In each mechanism, water is adsorbed/disassociated into the active sites of carbon, with H_2 and CO generation. However, C(O) complexes are challenging to energetically eliminate from the surface [73]. Due to different physical activation, the surface area could be different; Table 8.2 elaborates on the role of physical activation agents in producing activated carbon.

Table 8.2 Precursor for activated carbon with different physical activation agents and the obtained surface area.

Precursor	Surface area (m^2/g)	Activation agent	Precursor	Activation agent	Surface area (m^2/g)
Hemp[74]	877	Steam	Almond shell, walnut shell, olive stone, almond tree pruning[75]	Steam	601
Flax,	776				792
Jute,	840				1080
coir	822				813
Droppings of chicken	1618	Thermal	Olive stone[76]	steam	950
Bamboo[34]	2169	Thermal	Palm shells[77]	CO_2	912
Rapeseed, Kenaf[78]	1352, 1036	CO_2	Almond shell[79]	CO_2	851
Kapok[80]	1474	CO_2	Olive stone[81]	CO_2	1355
Rice[83]	1122	Steam	Olive stones[82]	Steam	807
Nutshells[84]	485	CO_2	Peanut shells[85]	Steam	757
Palm kernel[86]	167	CO_2	Oil palm shells[87]	Thermal	988
Vine shoots[88]	1173	CO_2	Corn-starch[89]	Thermal	686
Finish wood[90]	590	CO_2	Sugar cane bagasse, Eucalyptus sawdust[91]	CO_2	260
Oil cake/walnut[92]	1207	CO_2			298
Cocoa shell[93]	558	CO_2	Cellulose[94]	Thermal	2602
Pistachio nut shells[95]	1014	CO_2	Grape pomace	Steam	266
			Grape stalks[96]	Steam	300
Rice[97]	1111	Steam			
Sunflower stem,	438	CO_2	Guava seeds,	80% CO_2, 20% H_2O	1201
walnut shells,	379		Tropical almond shells,		1029
olive stone[98]	438		Dinde stones[99]		1074
Crofton weed[100]	1036	CO_2	Date pits[101]	Steam	1467

8.3   Pre-treatment

Pre-treatment of lignocellulose is an essential step in converting biomass to fuels. It influences the efficiency of the subsequent saccharification (breaking down the complex carbohydrates) process. For thermo- and biochemical biomass conversion, pre-treatment is the essential step, which helps alter biomass structure. Pre-treatment is the major procedure to improve the characteristics of biomass so that it can be utilized as an efficient energy resource [102]. Heat is required for the pre-treatment, and the self-degradation property of lignocellulosic biomass can be controlled through aromatic and polymeric constituents. The inorganic elements and the heteroatoms in non-lignocellulosic biomass act as the catalyst and facilitate the decomposition process, resulting in the formation of carbon-based frameworks, with major changes in structures to enhance the performance of the pre-treated material [103]. The high cost of pre-treatment and the loss of major vital components during the pre-treatment process are the major concerns undergoing considerable research. Different approaches have been adopted and are still under examination to control the loss of vital components during pre-treatment with minimal cost. The pre-treatment step is crucial, specifically while tailoring with the biomass origin and applying it in biorefineries and the bio-conversion processes.

8.4   The Role of Pre-treatment

80% of the world's energy demand is fulfilled through non-renewable energy sources like oil, gases, and coal. Combustion of these non-renewable sources is continuously exhausting hazardous gases causing environmental pollution, which is an alarming situation for health safety. Society is undertaking a quest to explore renewable energy sources. In this regard, several green precursors from organic families, such as maize, palm oil, sugar cane, and starch, are investigated as carbon sources to produce energy. Hence, sustainable, renewable, and low-cost cellulosic biomass like waste materials, food waste, forestry waste, wood waste, agricultural waste, and other industrial wastes could be utilized for the production of energy [104, 105]. These lignocellulosic biomasses are composed of cellulose, hemicellulose, lignin, and minor amounts of extraneous components like soluble extractives in wood biomass, i.e., ketones, resins, fatty acids, isoprene alcohols, resin acids, phytosterols, insoluble inorganic extractives like starches, oxalates, carbonates, protein, etc., and phenols and ashes [106]. Various pre-treatment techniques have been reported to decompose the lignocellulosic structure to get a material from which to harvest biofuel and products. The key aim of the pre-treatment is to enhance the sugar yielding and alter the lignin structure. Due to this change, the surface area and porosity of the structure are increased. In the pre-treatment process, the lignin is first melted and then merged by cooling, which alters its characteristics [107]. Furthermore, the pre-treatment can cause degradation to the cellulose and hemicellulose structure. It is highly advised to avoid weak acids like formic acids, levulinic acid, acetic acid, and some furan derivates like 5-hydroxy-2methyl furfural and phenolic compounds that will affect the structure [108]. Different pre-treatment techniques have been reported, schematically illustrated in Figure 8.1. The final product's properties depend on the process followed for pre-treatment. An ideal pre-treatment is one
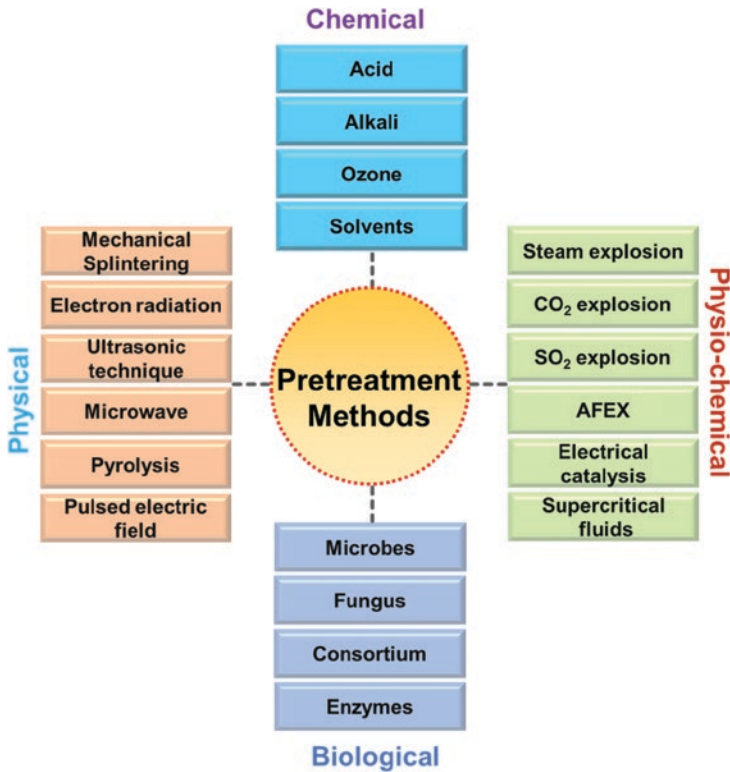
Figure 8.1 Diagram presenting the pre-treatment methods.

that is cost-effective, can easily limit the production of inhibitors, can enhance the sugar concentration for fermentation, and needs less energy [109]. Hence, a pre-treatment technique is favoured for increasing the sugar production from the cellulose of lignocellulosic biomass; this phenomenon can unveil the way for biofuel production [110]. In the next section, all the pre-treatment techniques will be discussed thoroughly, along with the effects and output of the final product.

8.5   Methods of Carbon Preparation via Pre-treatment for Supercapacitors

Among many methods, the physical pre-treatment method intends to decrease the particle size, increasing the activated carbon's surface area and pore size. There are several types of physical pre-treatment, some of which are presented in Figure 8.1. Commonly used physical pre-treatment methods for supercapacitors are mechanical splintering, high energy electron radiation, ultrasonic treatment, microwave treatment, pyrolysis treatment, pulsed electric field, and physical pre-treatments are comparatively less polluting and are facile. Still, they are expensive as they require high energy and power [111]. The requirement for more heat and high power consumption increases the cost of an overall process. Another

physical pre-treatment method is high energy radiation, which can be done by irradiating with different radiations like microwaves to activate the carbon to be utilized for supercapacitor applications [112]. Even though high-intensity radiation is a very effective process for pre-treatment, it still has a high cost, which is a bottleneck for industrial applications. It is also noted for the supercapacitor applications that if this process is combined with any of the chemical methods, it will be more efficient than when used on its own [113–116]. Ultrasonic treatment is another physical pre-treatment method, reported specifically for supercapacitor applications; that ultrasonic treatment can be used with the alkali treatment, which is a chemical pre-treatment (discussed later) and will show significant impact in breaking down hydrogen bonds that eventually reduce the crystalline structure [117–119]. The schematic presentation of the ultrasonic pre-treatment effect is presented in Figure 8.2. Enzymatic hydrolysis can also be improved using ultrasonic treatment by introducing ultrasound into the enzyme activity, increasing the transport of macromolecules [120–122].

The pyrolysis technique is another physical pre-treatment method, and it is divided into two parts pyrolysis and decomposition of water [123]. This technique is less common for the application of supercapacitors as it is time-consuming and requires harsh conditions to efficiently produce the end product. The pulsed electric field is an efficient physical pre-treatment method, as it disrupts the raw material's structure and reduces the complex molecules to simple aggregates [124]. This process has been utilized to apply supercapacitor devices with better performance by Heon Lee et al. in 2015 [125]. This process doesn't require any chemicals nor does it consume a lot of energy, so it is a comparatively better and environmentally friendly pre-treatment method [126].

Then we have the chemical pre-treatment methods that use organic and inorganic composites to dislocate the material's structure by interacting with the polymer inter- and intra- bonding. For chemical pre-treatment to occur, the material to be pre-treated is considered as recalcitrant in nature, due to the complex structure, crystalline nature, heterogeneity and the extent of lignification in the material [127]. For acid pre-treatment, different
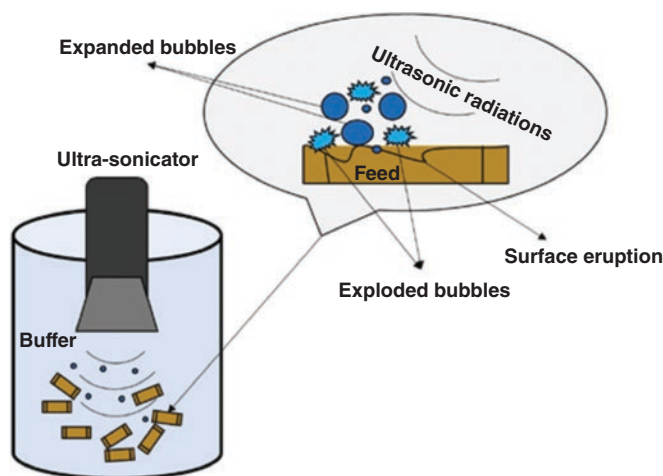
Figure 8.2 Schematic of ultrasonic pre-treatment.

acids are used, including nitric, sulfuric, phosphoric, hydrochloric, acetic, propionic and formic [128–131]. This method is most common for supercapacitor applications [132–134]. It is noted that organic acid pre-treatment gives better conversion results by enhancing the hydrolysis process [135]. The two types of acid pretreatment are dilution and concentration. In concentrated acid pre-treatment, the concentration of acid used is above 30% to hydrolyze complex carbon structures, but this process is slow, and many acids are highly corrosive and toxic. Dilute acid pre-treatment requires a concentration of acids up to 10%, which will act as a catalyst, the temperature and pressure needed for this pre-treatment to take place is 110–250 $^{\circ}$C and 10 atm, respectively [136]. However, this pre-treatment is rapid, and the acid also doesn't need to be recycled, but the high temperature and pressure demand shows degradation of products, which is the negative influence. Another chemical pre-treatment method includes alkali pre-treatment. This process is also very common for supercapacitor applications, as it is mostly combined with the physical pre-treatment methods to obtain the good results. The most commonly used alkaline solutions for pre-treatment are potassium, ammonium, sodium, and calcium hydroxides [137]. Alkali pre-treatment is performed at room temperature and atmospheric pressure with a number of days to complete the reaction and it degrades less sugar in comparison to acid pre-treatment [138, 139]. Ozone pre-treatment is another chemical pre-treatment method, which is also referred as oxidation pre-treatment. This process will take place easily at room temperature and pressure, but it still needs a massive quantity of ozone, which doesn't make it feasible economically and industrially. Likewise, wet oxidation method is the chemical reaction in water at high temperature and pressure. This reaction can be called as the ideal pre-treatment method for the activation of carbon to be applied for the supercapacitors, as it can improve the yield up to 70% [140–142]. Photocatalysis is the same as the wet oxidation method; only it reduces the duration of reaction without affecting the final product distribution. Solvent pre-treatment methods also belong to the chemical treatments group, including ionic liquids and organic solvents used for supercapacitor applications [143, 144]. Ionic liquids dissolve the cellulose and are more commonly known as green solvents because they are environment friendly and require very low temperature. These liquids are composed of small inorganic anions and large organic cations [145, 146].

The synergetic pre-treatment methods significantly improve the yield by optimizing the essential parameters. As the name suggests, the physio-chemical pre-treatment is a blend of physical-chemical techniques [147]. This method involves steam, CO_2 and SO_2 explosion, Ammonia Fibre Expansion (AFEX), electrical catalysis and supercritical fluid techniques. To date, the steam explosion method of physio-chemical pre-treatments is the most widely used for the creation of supercapacitors because this technique adopts a hydrothermal route [148, 149]. This pre-treatment method includes steam at a very high temperature maintained for several minutes during the hydrothermal process and the reactor ejects out the steam. The schematic presentation of hydrothermal pre-treatment is presented in Figure 8.3. The entire system is rapidly cooled by the reduced pressure of the liquid material and vapour outflow [150]. The high pressure plays the main role, as it pushes steam into the fibres and is released as air from the pores, causing the fracture. The mechanical forces and chemical reaction both take place during this pre-treatment. This pre-treatment technique is non-flammable, non-toxic and can be recovered after extraction [151, 152]. Likewise, the SO_2 explosion is technically the same as CO_2 explosion. However, it requires

sophisticated equipment and processes to degrade large amounts of acid, making it very expensive [153]. But among the various explosion methods, the SO_2 explosion is regarded as the most efficient, specifically on softwood materials.

AFEX is another physio-chemical pre-treatment method for supercapacitor devices, which involves the combined effect of alkali treatment and steam explosion [154–156]. The AFEX pre-treatment is processed in the presence of liquid ammonia (anhydrous) at a temperature of 100 °C while maintaining a pressure of 5.2 MPa. The pressure is released immediately along with the ammonia evaporation, which abruptly cools the ammonia, leading to the enhanced surface area for enzyme accessibility. AFEX pre-treatment is usually maintained for nearly half an hour, and the mass ratio of raw material to ammonia (liquid) is sustained at 1:1, until it was allowed to evaporate after the required time. [157, 158]. Ammonia in this procedure can be recycled as it is costly and volatile [136, 159]. Oxidation is a process to resolve the energy and environmental issues; electric catalyst is one of the physio-chemical pre-treatment methods [160]. Along with the oxidation property, no secondary pollutant is produced as a by-product, which grabs people's attention to this pre-treatment method. Another important pre-treatment method that has attracted attention is supercritical fluids, which include ionic liquids. The use of superfluids reported so far includes methanol, ethanol, butane, carbon dioxide, butane, iso-propanol, cyclohexane, acetone, and supercritical water [161–163]. Supercritical fluids own properties such as mild viscosity, high diffusivity, tuneable property, no phase separation, low density, modulate pressure and temperature, and the co-solvent choice is feasible and available [161, 164, 165]. The high temperature and pressure are the key parameters here, as they get into the closed pores of the raw material, enhancing the surface area for the enzymatic action and accessibility [163, 166].

8.6 Supercapacitor Applications of Pre-treated Biomass-based Carbon

As explained in the early sections, pre-treated carbon obtained from different biomasses through various techniques has been effectively applied for supercapacitor devices. An adequate search for the carbonaceous materials to be applied for the supercapacitor electrode material is going on. For this purpose, inexpensive, abundant and high-performance carbon materials obtained from sources that are renewable and non-toxic are needed to fulfil the demand of energy through supercapacitors in today's world. Extensive research has been carried out and reported using pre-treated carbon for supercapacitor applications. The most basic requirements for the high performance of supercapacitors include high energy density, high specific capacitance, and better cyclic life of the material. In 2016, tobacco rods were used to obtain the carbon. It was then applied to a supercapacitor which delivered 286.6 F g^{-1} of capacitance and 31.3 Wh kg^{-1} energy density, with a power density of 11.8 kW kg^{-1}. The device was assembled using this material and gives capacity retention of 96%, which shows the excellent stability of the material, which can be seen through the cyclic voltammetry (CV) and galvanostatic charge-discharge (GCD) curves presented in Figure 8.4a–b [167]. Another group reported using tobacco stems using KOH pre-treatment to activate this carbon. The surface area given through this material was
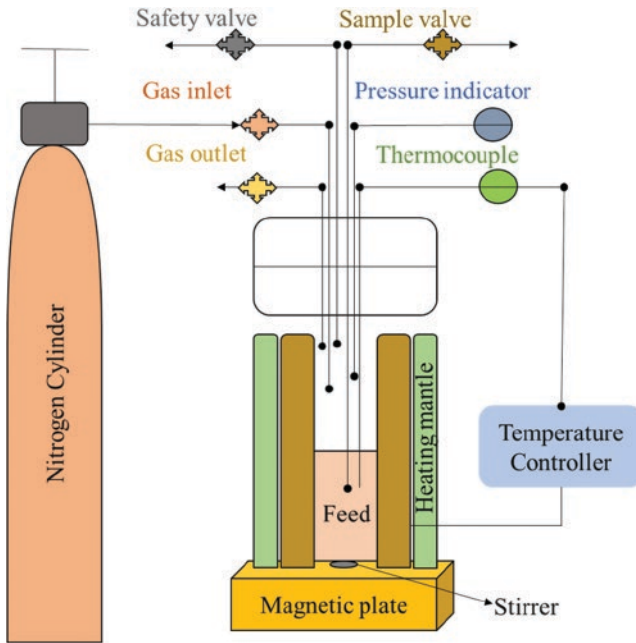
Figure 8.3 Hydrothermal pre-treatment method.

3326.7 $m^2\,g^{-1}$, and the specific capacitance of this material was 190 F g^{-1} [168]. In 2014, K. Fredi et al. reported using water hyacinth as a source of pre-treated carbon to be applied to supercapacitor applications. The carbon obtained through water hyacinth was activated through chemical and physical treatments. They reported the comparison of commercially available activated carbon and the synthesized through CV and GCD curves, as is presented in Figure 8.4c–d. The stability presented by this material after one thousand charge discharge cycles was ranging from 179.6–168.9 F g^{-1}, which reflects that the material sustains 94% of the initial capacitance after the stability test [169]. In 2013, P. Chao reported carbon synthesis from waste tea leaves that were pre-treated with KOH. This material displays above-average surface area with a 330 F g^{-1} specific capacitance value and 92% retentivity. The CV and GCD graphs obtained after pre-treatment are shown in Figure 8.4e–f [170]. Likewise, another group reported the carbon obtained from pistachio shells pre-treated with the combination of CO_2 and KOH, which deliver a 122 F g^{-1} of specific capacitance. The supercapacitor, through this material, reveals better specific capacitance retention, which is the sign of good stability, valuable reversible properties, and lower equivalent series resistance [171]. Kalpana et al. used recycled waste paper to obtain carbon and activate it through KOH as a pre-treatment for the supercapacitor electrode application. The electrochemical measurements were taken using CV and GCD, as are presented in Figure 8.4g–h, and found a specific capacity of 180 F g^{-1} [172].

In a short communication by Kim et al., activated carbon from bamboo was applied to the electrode of the supercapacitor. They examined the effect on specific capacitance by altering the temperature directly impacting the surface area. With the increase in temperature, the activated carbon's surface area increases, so the specific capacitance increases.
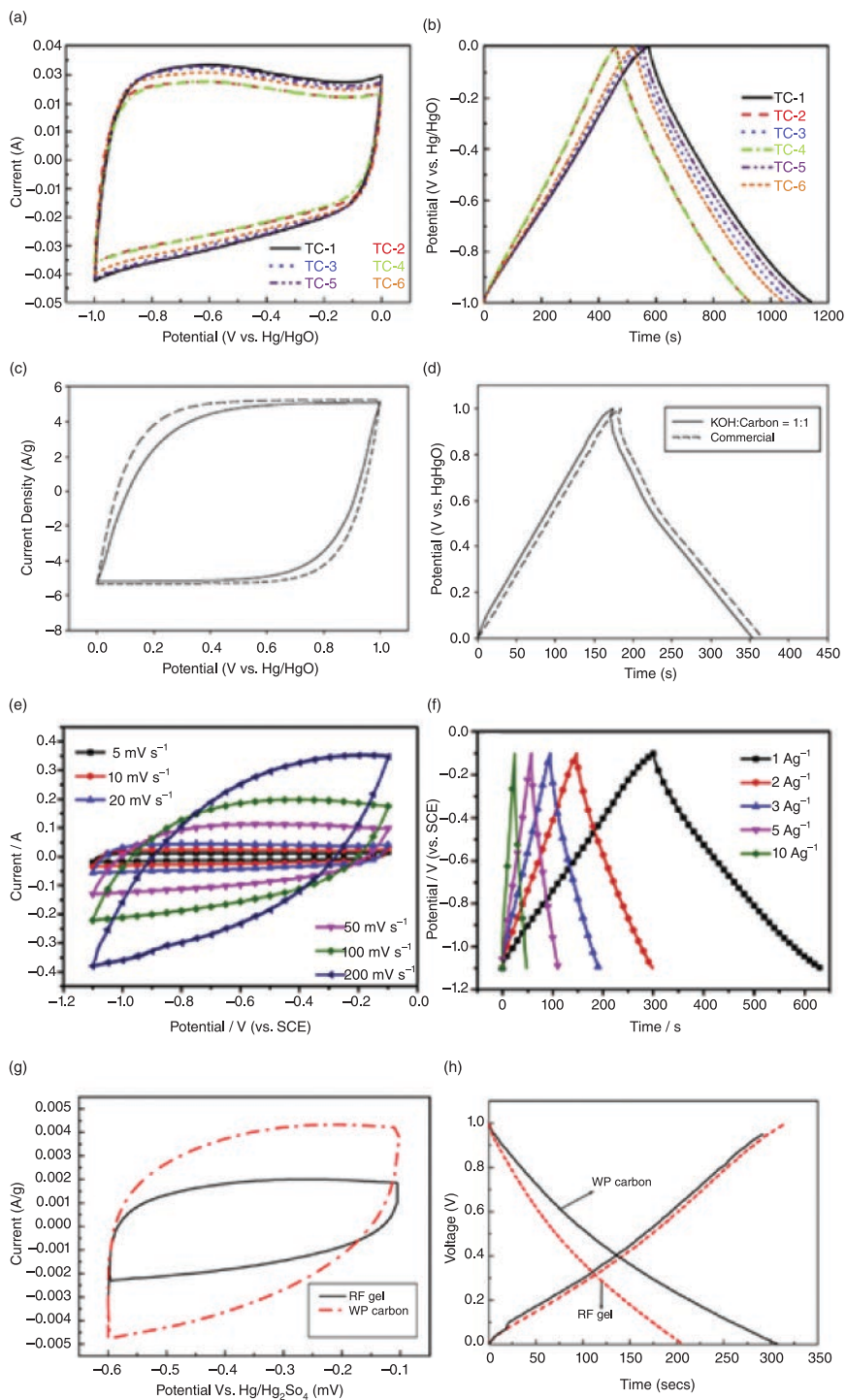
Figure 8.4 CV and GCD plots from pre-treated carbon obtained from (a–b) tobacco rods, (c–d) water hyacinth, (e–f) waste tea leaves, and (g–h) recycled waste paper. *Reproduced with permission* [167, 169, 170, 172]. *Copyright (Elsevier 2016, Elsevier 2015, Elsevier 2013, and Elsevier 2009).*

The maximum specific capacitance shown by the supercapacitor was 60 F g^{-1}, after activation at 900 °C for one hour. The increase in capacitance can also be deduced from the area under the CV plots, which shows that as temperature increases the area under the plot increases [173]. Another agricultural by-product, rice husk, has also been reported as having higher porosity and surface area carbon. The obtained carbon was activated through microwave heating, and the specific capacity value for this material was 245 F/g. It sustains this capacitance up to 95.1% even after one thousand charge-discharge cycles [174]. Moreover, in 2012 a Chinese group used celtuce leaves for synthesizing porous carbon and then activated it by pyrolysis via KOH treatment. The activated carbon was then utilized for supercapacitor electrode material that showed a 421 F g^{-1} of specific capacitance in three-electrode assembly. An excellent electrode material's performance can be depicted from cyclic voltammetry and galvanic charge-discharge plots at different scan rates and current density values, presented in Figure 8.5(a–b). A tremendous specific surface area was obtained for this activated carbon, around 3404 m^2/g, along with the 1.88 cm^3 g^{-1} pore volume [175]. In 2013, M. Chen and his coworkers published the use of cotton stalk to
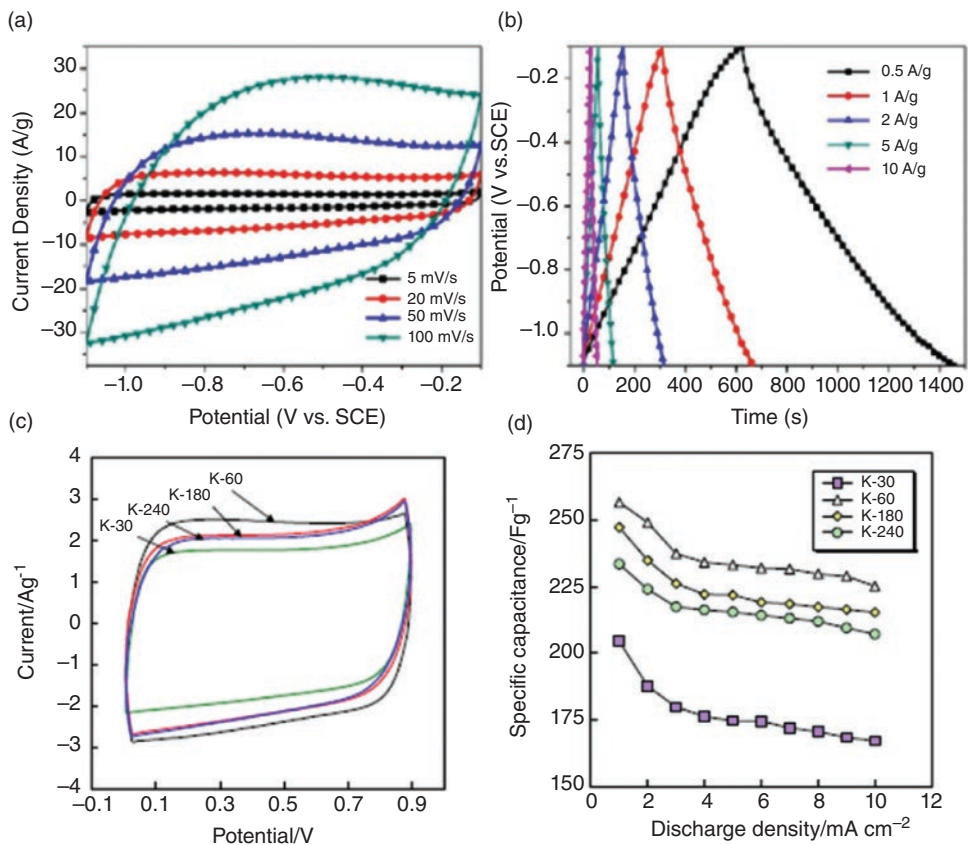
Figure 8.5 (a, b) CV and GCD graphs for the activated carbon obtained from celtuce leaves. *Reproduced with permission* [175]. *Copyright 2012, American Chemical Society.* (c, d) CV and specific capacity plots for the activated carbon obtained from the grains of corn. *Reproduced with permission* [177]. *Copyright 2008, Elsevier.*

prepare carbon and activated this carbon through chemical pre-treatment utilizing phosphoric acid. The obtained carbon gave the 1481 cm^2/g surface area and 0.0377 $cm^3 g^{-1}$ of pore vol ume, and its electrochemical energy storage potential was investigated to explore its application for supercapacitors. The specific capacitance yield by this material's electrode was 114 Fg^{-1}, making it suitable for the electric double-layer capacitor (EDLC), as it also retains a capacitance of up to 95.3% [176].

Furthermore, grains of corn had also been utilized to obtain carbon and had been pretreated before activation. One of the groups from Korea studied the optimization of activation time for the carbon obtained from corn grains. They successfully reported one hour's duration to be optimal for activating this carbon, which gives 257 $F g^{-1}$ of specific capacitance in addition to 2139 $m^2 g^{-1}$ surface area. The comparison of CV curves from 30 minutes to 240 minutes activation time is presented in Figure 8.5c, which depicts the higher area under the plot for the 60 minutes [177]. In Figure 8.5d, the specific capacitances obtained for all the samples at different current densities also show the higher specific capacity with the carbon, whose activation time is 60 minutes [177]. A lot more research has been going on pre-treated activated carbon that can be utilized for the application of supercapacitors. In light of all the discussions and studied materials based on the pretreatment technique, data has been tabulated in Table 8.3, elucidating the materials from which the carbon was obtained, and after applying the supercapacitors, the surface area of the activated carbon and specific capacitance values yielded.

Table 8.3 Materials through which activated carbon is obtained and their corresponding specific capacities and specific surface areas.

Material	Pretreatment method	Specific capacitance ($F g^{-1}$)	Specific surface area ($m^2 g^{-1}$)	Ref.
Tobacco rods	Hydrothermal	286.6	2115	[167]
Tobacco stem	KOH	190	3326.7	[168]
Water hyacinth	Physio-chemical	179.6	1020	[169]
Waste tea leaves	KOH	330.0	2841	[170]
Pistachio shells	KOH and CO_2	122	2145	[171]
Recycled waste paper	Physical (Steam)	180	416	[172]
Bamboo based	Physio-chemical	60	1025	[173]
Rice husk	Chemical ($ZnCl_2$)	243	1442	[174]
Celtuce leaves	Physio-Chemical	421	3404	[175]
Cotton stalk	Chemical (H_3PO_4)	114	1481 $cm^2 g^{-1}$	[176]
Corn grains	Chemical	257	2139	[177]
Coffee shells	Chemical ($ZnCl_2$)	150	842	[178]
Coffee beans	Chemical ($ZnCl_2$)	368	1019	[179]
Sugarcane bagasse	Chemical ($ZnCl_2$)	300	1788	[180]
Sunflower seeds	KOH	311	1163	[181]

8.7   Summary

The demand for storage devices has recently accelerated due to the power requirement of portable electronics, electric vehicles, and power tools. The supercapacitor is a critical member of the class of energy storage devices that mainly incorporates activated carbon and fulfils the power demands of several devices. The surface area and pore size of the activated carbon directly impact the performance of the supercapacitors, which can be enhanced through pre-treatment during the synthesis of the activated carbon. The pre-treatment step is significant for the pyrolysis of lignocellulose in biomass and converting it efficiently to activated carbon with high surface chemistry. Much research has been accomplished so far to improve the quality of activated carbon yielded using a pre-treatment process, which decomposes the complex structure of lignocellulose. The main factors related to the substrate that influence enzymatic hydrolysis are the removal of cellulose, hemicellulose, and lignin, which enhances the cellulose surface area and crystallinity. The critical parameters to be considered while selecting pretreatment methods are the method's efficiency, cost, and eco-friendly and facile operational process. Furthermore, the pre-treatment method must also be optimized through the combined effect of fermentation and saccharification. All these parameters, when appropriately optimized with appropriate conditions, will then will elucidate the effect of enzymolysis on the lignocellulose structure. Considerable research had been done on the different materials to obtain the carbon, which is then activated through different pre-treatment techniques. In this chapter, some of those materials have been tabulated along with their specific capacitance values, surface area, and stability discussion. Thus, the pre-treatment process can be applied for large-scale industrial applications to enhance the quality and efficiency of activated carbon produced from lignocellulose.

Acknowledgments

References

1   R. B. Galvão, A. A. da Silva Moretti, F. Fernandes, E. K. Kuroda, *Environ. Technol.* **2021**, *42*, 4179–4188.

2   X. Deng, B. Zhao, L. Zhu, Z. Shao, *Carbon* **2015**, *93*, 48–58.

3   S. S. Shah, E. Cevik, M. A. Aziz, T. F. Qahtan, A. Bozkurt, Z. H. Yamani, *Synth. Met.* **2021**, *277*, 116765.

4   A. Divyashree, G. Hegde, *RSC Adv.* **2015**, *5*, 88339–88352.

5   T. Islam, M. M. Hasan, S. S. Shah, M. R. Karim, F. S. Al-Mubaddel, M. H. Zahir, M. A. Dar, M. D. Hossain, M. A. Aziz, A. J. S. Ahammad, *J. Energy Storage* **2020**, *32*, 101908.

6   S. S. Shah, M. A. Alfasane, I. A. Bakare, M. A. Aziz, Z. H. Yamani, *J. Energy Storage* **2020**, *30*, 101562.

7 S. S. Shah, M. A. Aziz, E. Cevik, M. Ali, S. T. Gunday, A. Bozkurt, Z. H. Yamani, *J. Energy Storage* **2022**, *56*, 105944.

8 J. Saravanan, M. Pannipara, A. G. Al-Sehemi, S. Talebi, V. Periasamy, S. S. Shah, M. A. Aziz, G. Gnana Kumar, *J. Mater. Sci. Mater. Electron.* **2021**, *32*, 24775–24789.

9 S. S. Shah, M. A. Aziz, A. K. Mohamedkhair, M. A. A. Qasem, A. S. Hakeem, M. K. Nazal, Z. H. Yamani, *J. Mater. Sci. Mater. Electron.* **2019**, *30*, 16087–16098.

10 M. Rauf, S. S. Shah, S. K. Shah, S. N. A. Shah, T. U. Haq, J. Shah, A. Ullah, T. Ahmad, Y. Khan, M. A. Aziz, K. Hayat, *J. Saudi Chem. Soc.* **2022**, *26*, 101514.

11 A. J. S. Ahammad, N. Odhikari, S. S. Shah, M. M. Hasan, T. Islam, P. R. Pal, M. A. Ahmed Qasem, M. A. Aziz, *Nanoscale Adv.* **2019**, *1*, 613–626.

12 S. S. Shah, H. T. Das, H. R. Barai, M. A. Aziz, *Polymers* **2022**, *14*, 270.

13 S. S. Shah, M. A. A. Qasem, R. Berni, C. Del Casino, G. Cai, S. Contal, I. Ahmad, K. S. Siddiqui, E. Gatti, S. Predieri, J.-F. Hausman, S. Cambier, G. Guerriero, M. A. Aziz, *Sci. Rep.* **2021**, *11*, 6945.

14 S. M. Abu Nayem, S. S. Shah, S. B. Chaity, B. K. Biswas, B. Nahar, M. A. Aziz, M. Z. Hossain, *Arab. J. Chem.* **2022**, *15*, 104265.

15 S. S. Shah, M. N. Shaikh, M. Y. Khan, M. A. Alfasane, M. M. Rahman, M. A. Aziz, *Chem. Rec.* **2021**, *21*, 1631–1665.

16 S. S. Shah, H. Yang, M. Ashraf, M. A. A. Qasem, A. S. Hakeem, M. A. Aziz, *Chem. Asian J.* **2022**, *17*, e202200567.

17 A. J. S. Ahammad, P. R. Pal, S. S. Shah, T. Islam, M. Mahedi Hasan, M. A. A. Qasem, N. Odhikari, S. Sarker, D. M. Kim, M. A. Aziz, *J. Electroanal. Chem.* **2019**, *832*, 368–379.

18 M. R. Hasan, T. Islam, M. M. Hasan, A.-N. Chowdhury, A. J. S. Ahammad, A. H. Reaz, C. K. Roy, S. S. Shah, I. Al, M. A. Aziz, *J. Phys. Chem. Solids* **2022**, *165*, 110659.

19 C. O. Ania, V. Khomenko, E. Raymundo-Piñero, J. B. Parra, F. Beguin, *Adv. Funct. Mater.* **2007**, *17*, 1828–1836.

20 A. K. Mohamedkhair, M. A. Aziz, S. S. Shah, M. N. Shaikh, A. K. Jamil, M. A. A. Qasem, I. A. Buliyaminu, Z. H. Yamani, *Arab. J. Chem.* **2020**, *13*, 6161–6173.

21 S. S. Shah, M. A. Aziz, A.-R. Al-Betar, W. Mahfoz, *Arab. J. Chem.* **2022**, *15*, 104058.

22 R. Shakil, M. N. Shaikh, S. S. Shah, A. H. Reaz, C. K. Roy, A.-N. Chowdhury, M. A. Aziz, *Asian J. Org. Chem.* **2021**, *10*, 2220–2230.

23 M. M. Hasan, T. Islam, S. S. Shah, A. Awal, M. A. Aziz, A. J. S. Ahammad, *Chem. Rec.* **2022**, *22*, e202200041.

24 S. Islam, M. M. Mia, S. S. Shah, S. Naher, M. N. Shaikh, M. A. Aziz, A. J. S. Ahammad, *Chem. Rec.* **2022**, *22*, e202200013.

25 S. S. Shah, M. A. Aziz, Z. H. Yamani, *Chem. Rec.* **2022**, *22*, e202200018.

26 M. Ashraf, S. S. Shah, I. Khan, M. A. Aziz, N. Ullah, M. Khan, S. F. Adil, Z. Liaqat, M. Usman, W. Tremel, M. N. Tahir, *Chem. Eur. J.* **2021**, *27*, 6973–6984.

27 C. K. Roy, S. S. Shah, A. H. Reaz, S. Sultana, A.-N. Chowdhury, S. H. Firoz, M. H. Zahir, M. A. A. Qasem, M. A. Aziz, *Chem. Asian J.* **2021**, *16*, 296–308.

28 S. S. Shah, S. M. A. Nayem, N. Sultana, A. J. S. Ahammad, M. A. Aziz, *ChemSusChem* **2022**, *15*, e202101282.

29 M. Yaseen, M. A. K. Khattak, M. Humayun, M. Usman, S. S. Shah, S. Bibi, B. S. U. Hasnain, S. M. Ahmad, A. Khan, N. Shah, A. A. Tahir, H. Ullah, *Energies* **2021**, *14*, 7779.

30 S. S. Shah, M. A. Aziz, W. Mahfoz, A.-R. Al-Betar, Conducting Polymers Based Nanocomposites for Supercapacitors in *Nanostructured Materials for Supercapacitors*, (Eds. S. Thomas, A. B. Gueye, R. K. Gupta), Springer, Cham, **2022**, Chapter 22, pp. 485–511, vol. *1*.

31 Y. Zhang, H. Feng, X. Wu, L. Wang, A. Zhang, T. Xia, H. Dong, X. Li, L. Zhang, *Int. J. Hydrog. Energy* **2009**, *34*, 4889–4899.

32 M. Inagaki, H. Konno, O. Tanaike, *J. Power Sources* **2010**, *195*, 7880–7903.

33 T. Takamura, Y. Sato, Y. Sato, *J. Power Sources* **2011**, *196*, 5774–5778.

34 Y. Zhao, F. Fang, H.-M. Xiao, Q.-P. Feng, L.-Y. Xiong, S.-Y. Fu, *Chem. Eng. J.* **2015**, *270*, 528–534.

35 P. González-García, T. A. Centeno, E. Urones-Garrote, D. Ávila-Brande, L. C. Otero-Díaz, *Appl. Surf. Sci.* **2013**, *265*, 731–737.

36 O. Ioannidou, A. Zabaniotou, *Renew. Sust. Energ. Rev.* **2007**, *11*, 1966–2005.

37 M. Galhetas, A. S. Mestre, M. L. Pinto, I. Gulyurtlu, H. Lopes, A. P. Carvalho, *J. Colloid Interface Sci.* **2014**, *433*, 94–103.

38 I. I. Gurten, M. Ozmak, E. Yagmur, Z. Aktas, *Biomass Bioenerg.* **2012**, *37*, 73–81.

39 E. Unur, *Microporous Mesoporous Mater.* **2013**, *168*, 92–101.

40 R.-L. Liu, Y. Liu, X.-Y. Zhou, Z.-Q. Zhang, J. Zhang, F.-Q. Dang, *Bioresour. Technol.* **2014**, *154*, 138–147.

41 R. H. Hesas, A. Arami-Niya, W. M. A. W. Daud, J. Sahu, *J. Ind. Eng. Chem.* **2015**, *24*, 196–205.

42 A. Silvestre-Albero, M. Gonçalves, T. Itoh, K. Kaneko, M. Endo, M. Thommes, F. Rodríguez-Reinoso, J. Silvestre-Albero, *Carbon* **2012**, *50*, 66–72.

43 N. Saman, A. A. Aziz, K. Johari, S.-T. Song, H. Mat, *Process Saf. Environ. Prot.* **2015**, *96*, 33–42.

44 M. O. Guerrero-Pérez, J. M. Rosas, R. López-Medina, M. A. Bañares, J. Rodríguez-Mirasol, T. Cordero, *Catal. Commun.* **2011**, *12*, 989–992.

45 F. Boudrahem, F. Aissani-Benissad, H. Aït-Amar, *J. Environ. Manage.* **2009**, *90*, 3031–3039.

46 J. M. Rosas, R. Ruiz-Rosas, J. Rodríguez-Mirasol, T. Cordero, *Carbon* **2012**, *50*, 1523–1537.

47 J. Zhang, J. Xiang, Z. Dong, Y. Liu, Y. Wu, C. Xu, G. Du, *Electrochim. Acta* **2014**, *116*, 146–151.

48 M. Lillo-Ródenas, J. Marco-Lozar, D. Cazorla-Amorós, A. Linares-Solano, *J. Anal. Appl. Pyrolysis* **2007**, *80*, 166–174.

49 B. Jibril, O. Houache, R. Al-Maamari, B. Al-Rashidi, *J. Anal. Appl. Pyrolysis* **2008**, *83*, 151–156.

50 D. A. S. Maia, K. Sapag, J. P. Toso, R. H. López, D. C. Azevedo, C. L. Cavalcante, Jr, G. Zgrablich, *Microporous Mesoporous Mater.* **2010**, *134*, 181–188.

51 V. Njoku, M. A. Islam, M. Asif, B. Hameed, *Chem. Eng. J.* **2014**, *251*, 183–191.

52 F. J. García-Mateos, R. Ruiz-Rosas, M. D. Marqués, L. M. Cotoruelo, J. Rodríguez-Mirasol, T. Cordero, *Chem. Eng. J.* **2015**, *279*, 18–30.

53 B. Ruiz, E. Ruisánchez, R. Gil, N. Ferrera-Lorenzo, M. Lozano, E. Fuente, *Microporous Mesoporous Mater.* **2015**, *209*, 23–29.

54 J. S. Macedo, L. Otubo, O. P. Ferreira, I. de Fátima Gimenez, I. O. Mazali, L. S. Barreto, *Microporous Mesoporous Mater.* **2008**, *107*, 276–285.

55 F. Suarez-Garcia, A. Martinez-Alonso, J. Tascon, *J. Anal. Appl. Pyrolysis* **2002**, *62*, 93–109.

56 M. Danish, R. Hashim, M. M. Ibrahim, O. Sulaiman, *Biomass Bioenerg.* **2014**, *61*, 167–178.

57 S. Hazourli, M. Ziati, A. Hazourli, *Phys. Procedia* **2009**, *2*, 1039–1043.

58 D. Nabarlatz, J. de Celis, P. Bonelli, A. L. Cukierman, *J. Environ. Manage.* **2012**, *97*, 109–115.

59 M. Gueye, Y. Richardson, F. T. Kafack, J. Blin, *J. Environ. Chem. Eng.* **2014**, *2*, 273–281.

60 Y. Sha, J. Lou, S. Bai, D. Wu, B. Liu, Y. Ling, *Mater. Res. Bull.* **2015**, *64*, 327–332.

61 G. Ma, Q. Yang, K. Sun, H. Peng, F. Ran, X. Zhao, Z. Lei, *Bioresour. Technol.* **2015**, *197*, 137–142.

62 A. Romero-Anaya, A. Molina, P. Garcia, A. Ruiz-Colorado, A. Linares-Solano, C. S.-M. de Lecea, *Biomass Bioenerg.* **2011**, *35*, 1196–1204.

63 K. Wang, N. Zhao, S. Lei, R. Yan, X. Tian, J. Wang, Y. Song, D. Xu, Q. Guo, L. Liu, *Electrochim. Acta* **2015**, *166*, 1–11.

64 T. Tay, S. Ucar, S. Karagöz, *J. Hazard. Mater.* **2009**, *165*, 481–485.

65 S. K. Theydan, M. J. Ahmed, *J. Anal. Appl. Pyrolysis* **2012**, *97*, 116–122.

66 L. Temdrara, A. Khelifi, A. Addoun, N. Spahis, *Desalination* **2008**, *223*, 274–282.

67 S. Zhang, L. Tao, M. Jiang, G. Gou, Z. Zhou, *Mater. Lett.* **2015**, *157*, 281–284.

68 A. M. Puziy, O. I. Poddubnaya, A. Martínez-Alonso, F. Suárez-García, J. M. Tascón, *Carbon* **2005**, *43*, 2857–2868.

69 A. M. Vargas, A. L. Cazetta, C. A. Garcia, J. C. Moraes, E. M. Nogami, E. Lenzi, W. F. Costa, V. C. Almeida, *J. Environ. Manage.* **2011**, *92*, 178–184.

70 W. Djeridi, N. B. Mansour, A. Ouederni, P. Llewellyn, L. El Mir, *Int. J. Hydrog. Energy* **2015**, *40*, 13690–13701.

71 N. Moreno, A. Caballero, L. Hernán, J. Morales, *Carbon* **2014**, *70*, 241–248.

72 D. Liu, W. Zhang, H. Lin, Y. Li, H. Lu, Y. Wang, *J. Clean. Prod.* **2016**, *112*, 1190–1198.

73 F. Salvador, M. J. Sánchez-Montero, C. Izquierdo, *J. Phys. Chem. C* **2007**, *111*, 14011–14020.

74 A. R. Reed, P. T. Williams, *Int. J. Energy Res.* **2004**, *28*, 131–145.

75 J. González, S. Román, J. M. Encinar, G. Martínez, *J. Anal. Appl. Pyrolysis* **2009**, *85*, 134–141.

76 B. Tsyntsarski, I. Stoycheva, T. Tsoncheva, I. Genova, M. Dimitrov, B. Petrova, D. Paneva, Z. Cherkezova-Zheleva, T. Budinova, H. Kolev, *Fuel Process. Technol.* **2015**, *137*, 139–147.

77 S.-H. Jung, S.-J. Oh, -G.-G. Choi, J.-S. Kim, *J. Anal. Appl. Pyrolysis* **2014**, *109*, 123–131.

78 J. V. Nabais, J. Gomes, P. Carrott, C. Laginhas, S. Roman, *J. Hazard. Mater.* **2009**, *167*, 904–910.

79 P. Mourão, C. Laginhas, F. Custódio, J. V. Nabais, P. Carrott, M. R. Carrott, *Fuel Process. Technol.* **2011**, *92*, 241–246.

80 J. Li, D. H. Ng, P. Song, C. Kong, Y. Song, *Mater. Sci. Eng. B* **2015**, *194*, 1–8.

81 M. Guerrero-Pérez, M. Valero-Romero, S. Hernández, J. L. Nieto, J. Rodríguez-Mirasol, T. Cordero, *Catal. Today* **2012**, *195*, 155–161.

82 I. Ghouma, M. Jeguirim, S. Dorge, L. Limousy, C. M. Ghimbeu, A. Ouederni, *Comptes Rendus Chimie* **2015**, *18*, 63–74.

83 A. Amaya, N. Medero, N. Tancredi, H. Silva, C. Deiana, *Bioresour. Technol.* **2007**, *98*, 1635–1641.

84 C. Toles, W. Marshall, M. Johns, *Carbon* **1997**, *35*, 1407–1414.

85 K. Wilson, H. Yang, C. W. Seo, W. E. Marshall, *Bioresour. Technol.* **2006**, *97*, 2266–2270.

86 N. S. Nasri, U. D. Hamza, S. N. Ismail, M. M. Ahmed, R. Mohsin, *J. Clean. Prod.* **2014**, *71*, 148–157.

87 Q. Jia, A. C. Lua, *J. Anal. Appl. Pyrolysis* **2008**, *83*, 175–179.

88 J. V. Nabais, C. Laginhas, P. Carrott, M. R. Carrott, *J. Anal. Appl. Pyrolysis* **2010**, *87*, 8–13.

89 H. Lei, Y. Wang, J. Huo, *Microporous Mesoporous Mater.* **2015**, *210*, 39–45.

90 S. Kilpimaa, H. Runtti, T. Kangas, U. Lassi, T. Kuokkanen, *J. Ind. Eng. Chem.* **2015**, *21*, 1354–1364.

91 L. Giraldo-Gutiérrez, J. C. Moreno-Piraján, *J. Anal. Appl. Pyrolysis* **2008**, *81*, 278–284.

92 E. David, J. Kopac, *J. Anal. Appl. Pyrolysis* **2014**, *110*, 322–332.

93 R. G. Pereira, C. M. Veloso, N. M. da Silva, L. F. de Sousa, R. C. F. Bonomo, A. O. de Souza, M. O. da Guarda Souza, R. D. C. I. Fontan, *Fuel Process. Technol.* **2014**, *126*, 476–486.

94 C. Bommier, R. Xu, W. Wang, X. Wang, D. Wen, J. Lu, X. Ji, *Nano Energy* **2015**, *13*, 709–717.

95 T. Yang, A. C. Lua, *J. Colloid Interface Sci.* **2003**, *267*, 408–417.

96 F. Sardella, M. Gimenez, C. Navas, C. Morandi, C. Deiana, K. Sapag, *J. Environ. Chem. Eng.* **2015**, *3*, 253–260.

97 L. M. Petkovic, D. M. Ginosar, H. W. Rollins, K. C. Burch, C. Deiana, H. S. Silva, M. F. Sardella, D. Granados, *Int. J. Hydrog. Energy* **2009**, *34*, 4057–4064.

98 S. Roman, J. V. Nabais, B. Ledesma, J. González, C. Laginhas, M. Titirici, *Microporous Mesoporous Mater.* **2013**, *165*, 127–133.

99 L. Largitte, T. Brudey, T. Tant, P. C. Dumesnil, P. Lodewyckx, *Microporous Mesoporous Mater.* **2016**, *219*, 265–275.

100 Z.-Q. Zheng, H.-Y. Xia, C. Srinivasakannan, J.-H. Peng, L.-B. Zhang, *Chem. Eng. Process. Process Intensif.* **2014**, *82*, 1–8.

101 C. Bouchelta, M. S. Medjram, M. Zoubida, F. A. Chekkat, N. Ramdane, J.-P. Bellat, *J. Anal. Appl. Pyrolysis* **2012**, *94*, 215–222.

102 A. Anukam, S. Mamphweli, P. Reddy, E. Meyer, O. Okoh, *Renew. Sust. Energ. Rev.* **2016**, *66*, 775–801.

103 A. Anukam, S. Mamphweli, O. Okoh, P. Reddy, *Bioengineering* **2017**, *4*, 22.

104 S. R. Naqvi, S. Jamshaid, M. Naqvi, W. Farooq, M. B. K. Niazi, Z. Aman, M. Zubair, M. Ali, M. Shahbaz, A. Inayat, *Renew. Sust. Energ. Rev.* **2018**, *81*, 1247–1258.

105 A. S. Nair, H. Al-Battashi, A. Al-Akzawi, N. Annamalai, A. Gujarathi, S. Al-Bahry, G. S. Dhillon, N. Sivakumar, *Waste Manage.* **2018**, *79*, 491–500.

106 T. Kan, V. Strezov, T. J. Evans, *Renew. Sust. Energ. Rev.* **2016**, *57*, 1126–1140.

107 K. Karimi, M. J. Taherzadeh, *Bioresour. Technol.* **2016**, *200*, 1008–1018.

108 S. Behera, R. Arora, N. Nandhagopal, S. Kumar, *Renew. Sust. Energ. Rev.* **2014**, *36*, 91–106.

109 A. Gupta, J. P. Verma, *Renew. Sust. Energ. Rev.* **2015**, *41*, 550–567.

110 A. S. Nair, S. Al-Bahry, N. Gathergood, B. N. Tripathi, N. Sivakumar, *Renew. Energy* **2020**, *148*, 124–134.

111 Y. Hu, Y. Zhao, Y. Li, H. Li, H. Shao, L. Qu, *Electrochim. Acta* **2012**, *66*, 279–286.

112 D. Liu, X. Zhao, R. Su, Z. Hao, B. Jia, S. Li, L. Dong, *Processes* **2019**, *7*, 300.

113 V. R. Pallapolu, Y. Lee, R. J. Garlock, V. Balan, B. E. Dale, Y. Kim, N. S. Mosier, M. R. Ladisch, M. Falls, M. T. Holtzapple, *Bioresour. Technol.* **2011**, *102*, 11115–11120.

114 M. Ashraf, I. Khan, M. Usman, A. Khan, S. S. Shah, A. Z. Khan, K. Saeed, M. Yaseen, M. F. Ehsan, M. N. Tahir, N. Ullah, *Chem. Res. Toxicol.* **2020**, *33*, 1292–1311.

115 A. Helal, S. S. Shah, M. Usman, M. Y. Khan, M. A. Aziz, M. Mizanur Rahman, *Chem. Rec.* **2022**, *22*, e202200055.

116 M. Usman, M. Humayun, S. S. Shah, H. Ullah, A. A. Tahir, A. Khan, H. Ullah, *Energies* **2021**, *14*, 2281.

117 S. Zhang, Y. Su, S. Zhu, H. Zhang, Q. Zhang, *J. Anal. Appl. Pyrolysis* **2018**, *135*, 22–31.

118 C. Peng, S. Zhang, D. Jewell, G. Z. Chen, *Prog. Nat. Sci.* **2008**, *18*, 777–788.

119 W.-C. Chen, -C.-C. Hu, -C.-C. Wang, C.-K. Min, *J. Power Sources* **2004**, *125*, 292–298.

120 Y. Zhang, E. Fu, J. Liang, *Chem. Eng. Technol.* **2008**, *31*, 1510–1515.

121 N. Guo, M. Li, X. Sun, F. Wang, R. Yang, *Green Chem.* **2017**, *19*, 2595–2602.

122 Z. Liu, X. Wan, Q. Wang, D. Tian, J. Hu, M. Huang, F. Shen, Y. Zeng, *Renew. Sust. Energ. Rev.* **2021**, *150*, 111503.

123 F. Shafizadeh, Y.-Z. Lai, *Carbohydr. Res.* **1975**, *42*, 39–53.

124 A. Abraham, A. K. Mathew, H. Park, O. Choi, R. Sindhu, B. Parameswaran, A. Pandey, J. H. Park, B.-I. Sang, *Bioresour. Technol.* **2020**, *301*, 122725.

125 H. Lee, S. H. Park, S.-J. Kim, Y.-K. Park, B.-J. Kim, K.-H. An, S. J. Ki, S.-C. Jung, *Int. J. Hydrog. Energy* **2015**, *40*, 754–759.

126 C. Joannes, C. S. Sipaut, J. Dayou, S. M. Yasir, R. F. Mansa, *Int. J. Renew. Energy Res.* **2015**, *5*, 598–621.

127 G. Guerriero, J. F. Hausman, J. Strauss, H. Ertan, K. S. Siddiqui, *Eng. Life Sci.* **2016**, *16*, 1–16.

128 C. C. Geddes, J. Peterson, C. Roslander, G. Zacchi, M. Mullinnix, K. Shanmugam, L. Ingram, *Bioresour. Technol.* **2010**, *101*, 1851–1857.

129 P. M. Martínez, R. Bakker, P. Harmsen, H. Gruppen, M. Kabel, *Ind. Crops Prod.* **2015**, *64*, 88–96.

130 J. S. Pierre, L. Duran, A. van Heiningen, *J. Anal. Appl. Pyrolysis* **2015**, *113*, 591–598.

131 S. Aslanzadeh, A. Berg, M. J. Taherzadeh, I. S. Horváth, *Appl. Biochem. Biotechnol.* **2014**, *172*, 2998–3008.

132 K. M. Horax, S. Bao, M. Wang, Y. Li, *Chin. Chem. Lett.* **2017**, *28*, 2290–2294.

133 W. Li, Y. Ding, W. Zhang, Y. Shu, L. Zhang, F. Yang, Y. Shen, *J. Taiwan Inst. Chem. Eng.* **2016**, *64*, 166–172.

134 L. Fan, Z. Hou, T. Liu, X. Liang, A. Ivanets, K. Ma, X. Su, *J. Environ. Chem. Eng.* **2022**, *10*, 108256.

135 A. M. J. Kootstra, H. H. Beeftink, E. L. Scott, J. P. Sanders, *Biochem. Eng. J.* **2009**, *46*, 126–131.

136 M. J. Taherzadeh, K. Karimi, *Int. J. Mol. Sci.* **2008**, *9*, 1621–1651.

137 G. D. Saratale, M.-Y. Jung, M.-K. Oh, *Bioresour. Technol.* **2016**, *205*, 90–96.

138 E. B. Heggset, K. Syverud, K. Øyaas, *Biomass Bioenerg.* **2016**, *93*, 194–200.

139 Z. Yan, J. Li, S. Chang, T. Cui, Y. Jiang, M. Yu, L. Zhang, G. Zhao, P. Qi, S. Li, *Fuel* **2015**, *158*, 152–158.

140 C. Martín, M. H. Thomsen, H. Hauggaard-Nielsen, A. BelindaThomsen, *Bioresour. Technol.* **2008**, *99*, 8777–8782.

141 Y. Fu, X. Ding, J. Zhao, Z. Zheng, *Ultrason. Sonochem.* **2020**, *69*, 104921.

142 N. He, Q. Pan, Y. Liu, W. Gao, *ACS Appl. Mater. Interfaces* **2017**, *9*, 24568–24576.

143 G. Sima, L. Gan, L. Chang, Y. Cui, R. K. Kankala, *Microporous Mesoporous Mater.* **2021**, *323*, 111192.

144 W. Qian, X. Li, X. Zhu, Z. Hu, X. Zhang, G. Luo, H. Yao, *RSC Adv.* **2020**, *10*, 8172–8180.

145 A. A. Elgharbawy, M. Z. Alam, M. Moniruzzaman, M. Goto, *Biochem. Eng. J.* **2016**, *109*, 252–267.

146 J.-C. Plaquevent, J. Levillain, F. Guillen, C. Malhiac, A.-C. Gaumont, *Chem. Rev.* **2008**, *108*, 5035–5060.

147 V. Ashokkumar, R. Venkatkarthick, S. Jayashree, S. Chuetor, S. Dharmaraj, G. Kumar, W.-H. Chen, C. Ngamcharussrivichai, *Bioresour. Technol.* **2022**, *344*, 126195.

148 X. Li, D. Ding, Z. Liu, L. Hui, T. Guo, T. You, Y. Cao, Y. Zhao, *ChemElectroChem* **2022**, *9*, e202200035.

149 D. Ding, L. Ma, X. Li, Z. Liu, L. Hui, F. Zhang, Y. Zhao, *Materials* **2022**, *15*, 2741.

150 A. M. Borrero-López, C. Valencia, D. Ibarra, I. Ballesteros, J. M. Franco, *Int. J. Biol. Macromol.* **2021**, *195*, 412–423.

151 Y. Zheng, H. M. Lin, G. T. Tsao, *Biotechnol. Progr.* **1998**, *14*, 890–896.

152 K. Öhgren, R. Bura, J. Saddler, G. Zacchi, *Bioresour. Technol.* **2007**, *98*, 2503–2510.

153 N. Mosier, C. Wyman, B. Dale, R. Elander, Y. Lee, M. Holtzapple, M. Ladisch, *Bioresour. Technol.* **2005**, *96*, 673–686.

154 S. Mehta, S. Jha, H. Liang, *Renew. Sust. Energ. Rev.* **2020**, *134*, 110345.

155 J. Zhu, C. Yan, X. Zhang, C. Yang, M. Jiang, X. Zhang, *Prog. Energy Combust. Sci.* **2020**, *76*, 100788.

156 D. R. Lobato-Peralta, E. Duque-Brito, H. I. Villafan-Vidales, A. Longoria, P. Sebastian, A. K. Cuentas-Gallegos, C. A. Arancibia-Bulnes, P. U. Okoye, *J. Clean. Prod.* **2021**, *293*, 126123.

157 I. J. Bonner, D. N. Thompson, M. Plummer, M. Dee, J. S. Tumuluru, D. Pace, F. Teymouri, T. Campbell, B. Bals, *Drying Technol.* **2016**, *34*, 1319–1329.

158 S. Harun, V. Balan, M. S. Takriff, O. Hassan, J. Jahim, B. E. Dale, *Biotechnol. Biofuels* **2013**, *6*, 40.

159 N. Curreli, M. B. Fadda, A. Rescigno, A. C. Rinaldi, G. Soddu, F. Sollai, S. Vaccargiu, E. Sanjust, A. Rinaldi, *Process Biochem.* **1997**, *32*, 665–670.

160 Y. Ding, B. Du, X. Zhao, J. Zhu, D. Liu, *Bioresour. Technol.* **2017**, *228*, 279–289.

161 K. Alper, K. Tekin, S. Karagöz, *Biomass Convers. Biorefin.* **2019**, *9*, 669–680.

162 N. Montesantos, M. Maschietti, *Energies* **2020**, *13*, 1600.

163 J. K. C. N. Agutaya, R. Inoue, S. S. Vin Tsie, A. T. Quitain, J. de la Peña-garcía, H. Perez-Sanchez, M. Sasaki, T. Kida, *Ind. Eng. Chem. Res.* **2020**, *59*, 16527–16538.

164 W. J. Sagues, H. Bao, J. L. Nemenyi, Z. Tong, *ACS Sustain. Chem. Eng.* **2018**, *6*, 4958–4965.

165 N. Hao, K. Alper, K. Tekin, S. Karagoz, A. J. Ragauskas, *Bioresour. Technol.* **2019**, *288*, 121500.

166 W. Li, X.-A. Xie, J. Sun, D. Fan, X. Wei, *Green Chem. Lett. Rev.* **2019**, *12*, 299–309.

167 Y.-Q. Zhao, M. Lu, P.-Y. Tao, Y.-J. Zhang, X.-T. Gong, Z. Yang, G.-Q. Zhang, H.-L. Li, *J. Power Sources* **2016**, *307*, 391–400.

168 X. Xia, H. Liu, L. Shi, Y. He, *J. Mater. Eng. Perform.* **2012**, *21*, 1956–1961.

169 F. Kurniawan, M. Wongso, A. Ayucitra, F. E. Soetaredjo, A. E. Angkawijaya, Y.-H. Ju, S. Ismadji, *J. Taiwan Inst. Chem. Eng.* **2015**, *47*, 197–201.

170 C. Peng, X.-B. Yan, R.-T. Wang, J.-W. Lang, Y.-J. Ou, Q.-J. Xue, *Electrochim. Acta* **2013**, *87*, 401–408.

171 -C.-C. Hu, -C.-C. Wang, F.-C. Wu, R.-L. Tseng, *Electrochim. Acta* **2007**, *52*, 2498–2505.

172 D. Kalpana, S. Cho, S. Lee, Y. Lee, R. Misra, N. Renganathan, *J. Power Sources* **2009**, *190*, 587–591.

173 C. Kim, J.-W. Lee, J.-H. Kim, K.-S. Yang, *Korean J. Chem. Eng.* **2006**, *23*, 592–594.

174 X. He, P. Ling, M. Yu, X. Wang, X. Zhang, M. Zheng, *Electrochim. Acta* **2013**, *105*, 635–641.

175 R. Wang, P. Wang, X. Yan, J. Lang, C. Peng, Q. Xue, *ACS Appl. Mater. Interfaces* **2012**, *4*, 5800–5806.

176 M. Chen, X. Kang, T. Wumaier, J. Dou, B. Gao, Y. Han, G. Xu, Z. Liu, L. Zhang, *J. Solid State Electrochem.* **2013**, *17*, 1005–1012.

177 M. Balathanigaimani, W.-G. Shim, M.-J. Lee, C. Kim, J.-W. Lee, H. Moon, *Electrochem. Commun.* **2008**, *10*, 868–871.

178 M. Jisha, Y. J. Hwang, J. S. Shin, K. S. Nahm, T. P. Kumar, K. Karthikeyan, N. Dhanikaivelu, D. Kalpana, N. Renganathan, A. M. Stephan, *Mater. Chem. Phys.* **2009**, *115*, 33–39.

179 T. E. Rufford, D. Hulicova-Jurcakova, Z. Zhu, G. Q. Lu, *Electrochem. Commun.* **2008**, *10*, 1594–1597.

180 T. E. Rufford, D. Hulicova-Jurcakova, K. Khosla, Z. Zhu, G. Q. Lu, *J. Power Sources* **2010**, *195*, 912–918.

181 X. Li, W. Xing, S. Zhuo, J. Zhou, F. Li, S.-Z. Qiao, G.-Q. Lu, *Bioresour. Technol.* **2011**, *102*, 1118–1123.

9

Carbonate Salts-activated Carbon

Syed Shaheen Shah[1,2], Md. Abdul Aziz[1,3,*], Laiq Zada[4], Haroon Ur Rahman[5], Falak Niaz[6], and Khizar Hayat[5]

[1] *Interdisciplinary Research Center for Hydrogen and Energy Storage (IRC-HES), King Fahd University of Petroleum & Minerals, KFUPM Box 5040, Dhahran 31261, Saudi Arabia*
[2] *Physics Department, King Fahd University of Petroleum & Minerals, KFUPM Box 5047, Dhahran 31261, Saudi Arabia*
[3] *K. A. CARE Energy Research and Innovation Center, King Fahd University of Petroleum & Minerals, Dhahran, 31261, Saudi Arabia*
[4] *Department of Microbiology, Faculty of Biological Sciences, Quaid-i-Azam University, Islamabad, 45320, Pakistan*
[5] *Department of Physics Abdul Wali Khan University, Mardan, 23200, Khyber Pakhtunkhwa, Pakistan*
[6] *Materials Research Laboratory, Department of Physics, University of Peshawar, Peshawar 25120, Pakistan*
* Corresponding author

9.1 Introduction

Electrical energy storage is tough, particularly in light of rising energy use and dwindling nonrenewable energy sources. It is critical to build clean electrical energy storage systems that can efficiently store energy. Batteries and supercapacitors have the potential to solve the energy storage puzzle. At the same time, most supercapacitors use carbonaceous materials as electrodes and exhibit high specific capacitance and power density [1–4]. It is generally known that activated carbon (AC) is a porous substance with a large specific surface area that can be used to adsorb gases and solutes from aqueous solutions. As a result, it has been extensively employed for catalyst support, solvent recovery, organic pollutant removal from drinking water, gas separation, and supercapacitors [4–12]. The need for AC is increasing as environmental pollution becomes an increasingly critical issue: agriculture wastes such as tropical wood, coconut shells, *Syzygium cumini* leaves, sawdust, banana leaves, walnut shells, nettle fiber clone, almond shells, *Albizia procera* leaves, and jute sticks are some of the most often utilized materials in producing AC [3–6, 9, 11–18].

Electrode materials, key aspects of supercapacitor performance, have drawn much investigation. Carbonaceous materials, transition metals, and conductive polymers are utilized as electrodes [19–22]. In recent decades researchers have focused on developing green carbon compounds that can reduce agro-industrial waste. Based on multiple investigations of the synthesis and physiochemical properties of AC, its porous structure, high surface area, and chemical polarity rely on the precursor's materials and activation procedure [1, 23–29]. There is a growing focus on biomass precursors since they are more affordable, easily

accessible, renewable, physically porous, and ecologically benign than the fossil fuel-based precursors (petroleum and coal) used to generate the majority of commercial ACs. Agricultural waste biomass has recently received much interest due to its widespread availability and affordable price [30–32].

It has been demonstrated that chemical activation is an effective technique for obtaining ACs with high surface area and wide pores distribution. Despite its widespread use in the production of ACs, the process's complexity is underlined by the fact that little is known about the overall mechanism of chemical activation. In order to achieve porosity, chemical activation by alkalis often involves a solid-solid or solid-liquid process that involves the reduction of the hydroxide and the oxidation of the carbon. The chemicals NaOH, H_3PO_4, KOH, and $ZnCl_2$ are also often utilized. However, alkali hydroxides like NaOH and KOH are risky, costly, and caustic, and $ZnCl_2$ is harmful to the ecosystem and causes issues with waste management. As a result, a less harmful chemical is preferred; K_2CO_3, which is often used as a food additive, is neither dangerous nor harmful [33]. Figure 9.1 illustrates the activation mechanism of both alkaline and acidic activating agents, as well as the effects of activating agents on the physiochemical properties of AC. The diverse activation methods of activating agents can explain the differences in physiochemical features of the resulting AC [34]. It is important to understand the diverse activation mechanisms that result from different activating chemicals reacting with the cellulose, hemicellulose, and lignin in carbon precursors to develop more practical activation methods. The interaction with pore production, combination, expansion, and collapse results in AC's porous structure development [34]. Carbonate salts have seen widespread application in the process of making high-quality alternating AC for use in supercapacitor electrodes. Carbonate salts have a number of benefits, including the fact that they are a low-cost industrial byproduct readily available all over the world. Activation with carbonate salts allows for special morphology such as hierarchical and is composed of micro-, meso-, and macropores for easy penetration of the electrolyte, which shortens the path length and exhibits oxygen functional groups.

Using potassium hydroxide salt and acids like H_2SO_4 increases surface area and micropores. These activators affect the ecosystem. KOH is the most frequent activating agent; however, it has two drawbacks. KOH is highly corrosive at high temperatures,
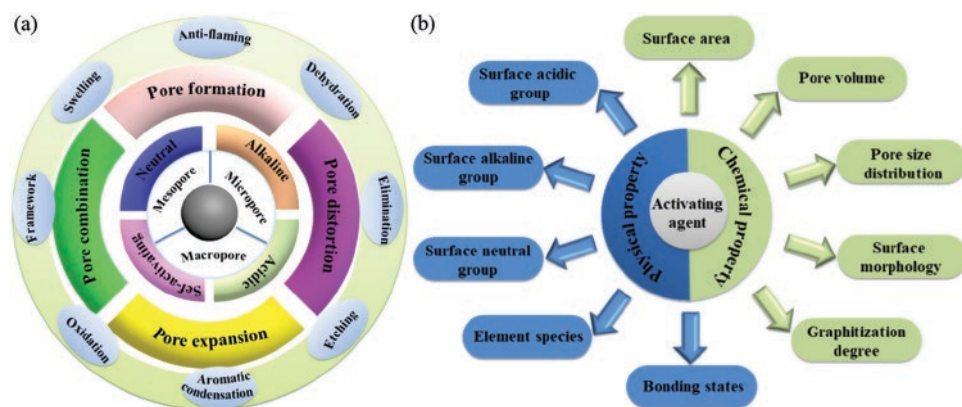
Figure 9.1 (a) The various ways that acidic and alkaline activating agents work. (b) The effect of the activating agent on the physical, chemical, and biological characteristics of the carbons produced. *Reproduced with permission [34]. Copyright 2020, Elsevier.*

damaging equipment, and pipes, and its remains can cause pollution when removed from AC. Acidic substances also harm the ecosystem, according to reports. Therefore, eco-friendly activators are recommended. Carbonate salts, such as K_2CO_3, $NaHCO_3$, and $KHCO_3$, are activating substances that are more ecologically friendly and attain the same porosity and surface area. They are non-toxic, cheap, and non-corrosive. K_2CO_3 decomposes into K, K_2O, CO_2, and CO around 600 to 800°C in an inert environment. The following equations (9.1–9.3) show the K_2CO_3 and AC gasification processes [35].

$$2C + K_2CO_3 \rightarrow 3CO + 2K \tag{9.1}$$

$$K_2CO_3 \rightarrow CO_2 + K_2O \tag{9.2}$$

$$2C + K_2O \rightarrow CO + 2K \tag{9.3}$$

These equations state that the reduction of K_2CO_3 under inert conditions to K, K_2O, CO_2, and CO causes porosity development after activation with K_2CO_3. The potassium chemical created after the activation stage enters the char matrix's interior structure, enlarges the current pores and produces new pores. Additionally, the cavities on the AC surface could be created from the areas occupied by the activating agent due to the evaporation of potassium carbonate. The channels formed by these cavities give the adsorbent molecules access to the AC's micro- and mesopores. Phenolic groups have a higher specificity than other groups on the K_2CO_3-ACs surface, and the amount of functionalized groups decreases as the activation temperature rises. Additionally, as the potassium carbonate concentration rises, the mesopores degrade, and the dehydration effect diminishes, which lowers the adsorption effectiveness. The AC's surface develops more microscopic pores as carbonization temperatures rise from 600 to 800°C. In this chapter, we have summarized the preparation of various biomass-derived AC via carbonate salt activation and their applications as electrode materials for supercapacitors.

9.2 Carbonate Salt AC Preparation

Carbonate salts are considered non-toxic and are mostly used as food additives [36]. There have been several reports on preparing ACs using carbonate salts. Hayashi et al. [37] prepared ACs from various nutshells with a high specific surface area by activating them with K_2CO_3. Onion husks were directly converted by Wang et al. [38] into 3D interconnected porous carbon frameworks using K_2CO_3 as an activation agent. Figure 9.2(a) displays the scheme for creating porous carbon from onion husks. First, onion husks were steeped in aqueous K_2CO_3 solutions at varied concentrations. The excess K_2CO_3 solution was filtered out, the K_2CO_3 was equally dispersed throughout the cells, and then the dried residues were carbonized at 800°C to create porous carbons. With this method, carbonization and activation can be conducted simultaneously to produce interconnected porous carbon frameworks, as opposed to traditional activation, which is often carried out with KOH and pre-carbonized samples or hydrochars. This method for synthesizing carbon compounds from onion husk seems to be both energy and money-efficient, and it might be scaled up for future industrialized manufacturing. The morphologies of the prepared items were examined using SEM and TEM tests. The produced carbon sample is composed of micrometer-sized ground with
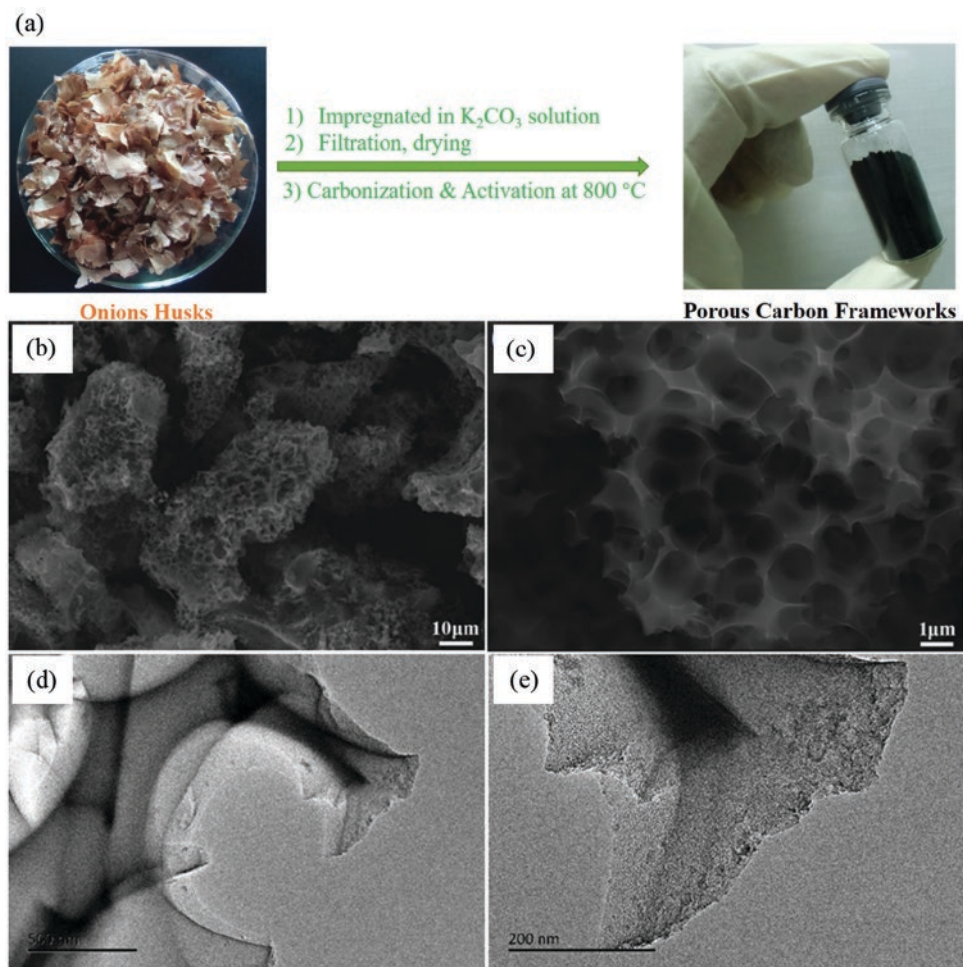
Figure 9.2 (a) Schematic representation for the onion husks-derived porous AC networks synthesis using K_2CO_3 as an activation agent. (b, c) SEM micrographs and (d, e) TEM images of the prepared onion husks derived porous carbon frameworks. *Reproduced with permission [38]. Copyright 2016, Elsevier.*

numerous open voids on the surface as a result of K^+ ions-induced etching at high temperature, as seen by the SEM micrographs [39], which self-assemble into 3D connected frameworks with random orientation from the cavities, as shown in Figure 9.2(b,c). It should be highlighted that these unique structures could not be formed if KOH or other biomass was utilized. TEM images (Figure 9.2(d, e)) show the continuous interconnected porous architectures of the obtained AC and the presence of many porous structures on the carbon skeletons. They found lamellar porous architectures of the porous carbon backbones. On the carbon surfaces of one sample, however, there are only a few macrospores because there was inadequate etching at lower K_2CO_3 concentrations. In contrast, the 3D interconnected frameworks in another carbon sample are partially collapsed, most likely due to severe etching of carbon at much higher K_2CO_3 concentration. The distinctive opened interconnecting

morphology differs significantly from that of several biomass-derived porous ACs and commercial ACs with a particle morphology. High-rate ion transport would benefit from the produced AC's continuous connected porous structure [40].

Yin et al. [41] demonstrated the extraction of value-added capacitive carbon from agricultural waste biomass using a single-step molten carbonate salt carbonization process. In order to generate high-performance capacitive carbon under ideal circumstances, the procedure is being researched. It was observed that an appropriate media for carbonizing diverse agricultural waste biomasses was a eutectic Na_2CO_3-K_2CO_3 melt. Due to the distinct catalytic characteristics and improved dissolution capabilities of this molten salt system, carbon compounds with high specific capacitance were produced. The reactor for carbonization consisted of a sealed stainless-steel tube filled with a 500 g salts-filled alumina crucible and pyrolyzed in a tube furnace. The Na_2CO_3-K_2CO_3 anhydrous salt was dried at 250°C without oxygen for 24 hours. N_2 was then used to purge the reactor, and it was then heated to operating temperature. After that, the leftover biomass (peanut shell) was carbonized. At first, the waste biomass was pre-dried for 12 hours at 140°C. Next, a nickel foam sheet was used to wrap the pre-dried waste biomass, which was then fastened to a stainless-steel rod. After being wrapped in salt, the waste biomass was then placed in the steel reactor, immersed in the molten salt, and held in the molten salt for one hour at a steady temperature. After being removed from the melt, in the reactor's headspace, the product was cooled using an environment of N_2. The product was taken out of the reactor, pulverized with an agate mortar and pestle to remove the absorbed salts, rinsed in water and 0.1 M HCl, and vacuum-dried for 10 hours at 100°C. The schematic representation for the synthesis of peanut shell-derived carbon is shown in Figure 9.3(A). Black AC was created during the peanut shells carbonization in molten Na_2CO_3-K_2CO_3. Figure 9.3(B-a,b) shows how XRD and EDS confirmed the structure and elements of amorphous carbon. The FESEM micrographs in Figure 9.3(B-c) demonstrate the sheet-type morphology of the carbon derived from peanut shells. The thickness of the carbon sheets, which ranged between 50 and 200 nm, was smooth and clean (Figure 9.3(B-d)). The TEM images in Figure 9.2(B-e,f) show that typical carbon thin and uniform sheets are visible. The HRTEM image of the carbon (Figure 9.3(B-g)) showed no lattice fringes, consistent with the XRD results that the AC is amorphous. In another study, Tang et al. [42] reported waste *Lentinus edodes* derived hierarchical porous carbon materials via a combined molten salt and hydrothermal technique for supercapacitor applications. Investigations were conducted into how the hydrothermal and molten salt treatment processes affected the surface composition, porosity, and morphology of the produced carbon product. It was demonstrated how the hydrothermal treatment process duration significantly influences the prepared carbon materials' porous structure distribution. During the hydrothermal process, numerous small pores are created; these pre-formed pores are essential for the subsequent molten salt activation process because they will later form into smaller micropores and larger mesopores. The obtained carbon was produced by hydrothermally treating the material for 24 hours and then activating it for 1 hour in molten Na_2CO_3-K_2CO_3. It generated hierarchical micro- and mesoporous structures and had a high specific surface area of 1144 m^2/g. Additionally, functional groups containing oxygen and nitrogen have been found on the carbon surface.

To prepare activated jute-derived hierarchical carbon nanosheets with a porous structure, Shah et al. [5] had chosen jute sticks as the biomass. One of the most important

(A)

(B)
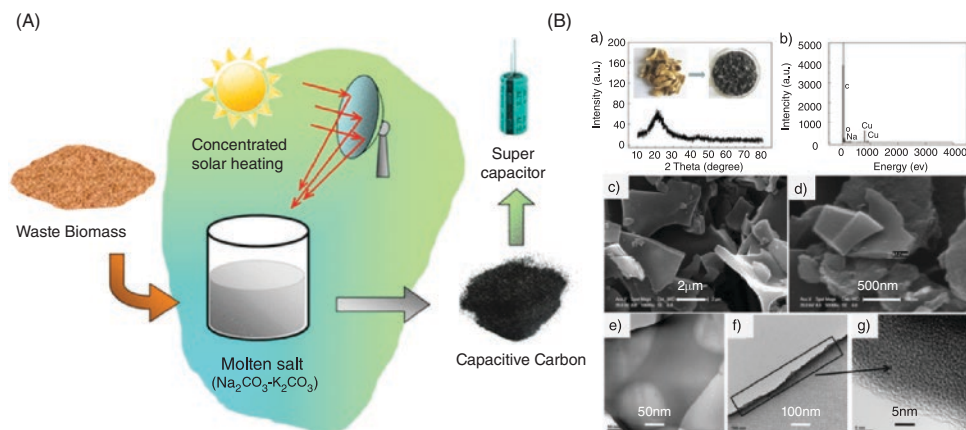
Figure 9.3 (A) Schematic representation for the synthesis of peanut shell-derived AC at 850 °C using Na_2CO_3-K_2CO_3 melt and (B) the corresponding various structural and morphological characteristics (a) XRD spectrum, (b) EDS pattern, (c, d) FESEM micrographs, (e, f) TEM micrographs, and (g) HRTEM image. *Reproduced with permission [41]. Copyright 2014, American Chemical Society.*

Figure 9.4 Schematic representation for synthesizing AC from jute sticks using $NaHCO_3$ as an activation agent. *Reproduced with permission [5]. Copyright 2021, Elsevier.*

historical plants is jute, which produces fiber with high commercial value, widely used to make industrial goods like carpet backing, decorative fabrics, and gunny bags. On the other hand, jute sticks, produced after the fiber is removed from the jute plant, typically have little commercial significance. They are either burned or allowed to decompose into the soil for household use. However, the chemical make-up of jute sticks includes carbon resources like hemicellulose, cellulose, and lignin. Therefore, converting them into carbon materials appropriate for supercapacitors and other important applications might be advantageous [3–5, 9, 12, 14, 43]. The schematic representation for synthesizing hierarchical AC nanosheets from jute sticks using $NaHCO_3$ as an activation agent is shown in Figure 9.4. The prepared jute-derived AC exhibited a substantial surface area of ~1100 m^2 g^{-1}. It has been proven simple and effective to prepare AC nanosheets using banana leaves as a precursor with a special mix of macro-, meso-, and micropores [10]. AC was prepared from banana leaves using K_2CO_3 as an activation agent, which exhibited a nanosheet type morphology and demonstrated a huge surface area of ~1469 m^2 g^{-1}. High-performance supercapacitors were made using the developed AC as electrode materials.

Li et al. [44] prepared AC from fallen leaves of *Fraxinus chinensis* using mixed KOH and K_2CO_3 activation agents. Characterizations showed that KOH produced most of the 3D
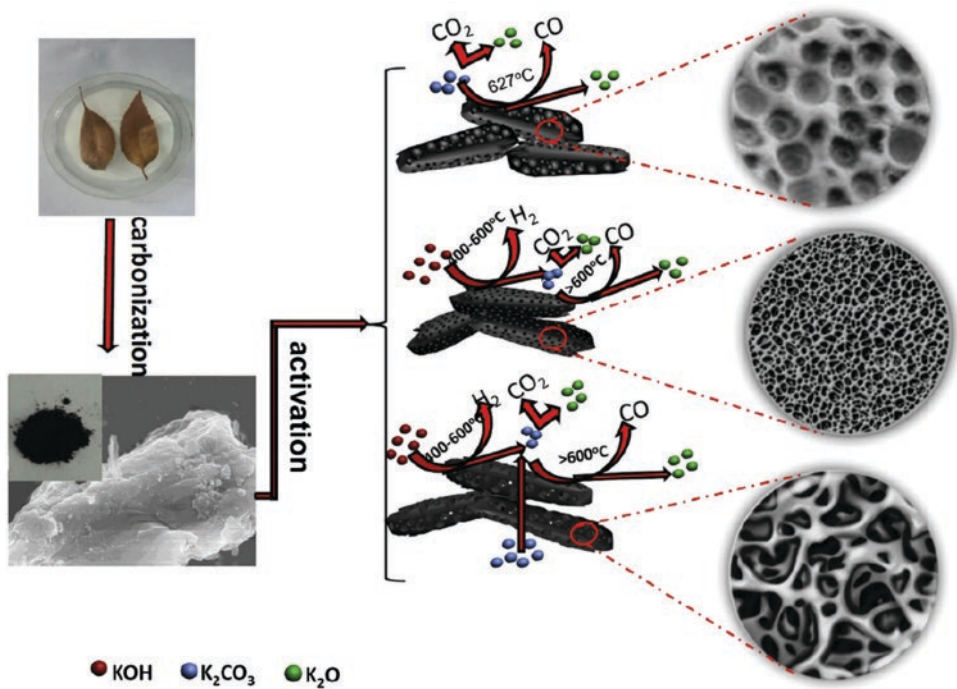
Figure 9.5 The activation process for the *Fraxinus chinensis* fallen leaves derived AC using KOH and/or K_2CO_3 as activation agents. *Reproduced with permission [44]. Copyright 2015, Elsevier.*

micropores, and K_2CO_3 produced most of the shallow meso- and/or macropores. In contrast, the pore size in the AC increases when KOH and K_2CO_3 are combined. The surface areas and hierarchical pore architectures are connected to the mass ratio of two activators. The reactions shown in equations (9.4–9.7) represent the general mechanism of chemical activation [44]. The activation process for the *Fraxinus chinensis* fallen leaves derived AC using KOH and/or K_2CO_3 as activation agents are shown in Figure 9.5.

$$C + 6KOH \leftrightarrow 2K_2CO_3 + 2K + 3H_2 \tag{9.4}$$

$$C + K_2CO_3 \leftrightarrow 2CO + K_2O \tag{9.5}$$

$$K_2CO_3 \leftrightarrow CO_2 + K_2O \tag{9.6}$$

$$CO_2 + 2K \leftrightarrow CO + K_2O \tag{9.7}$$
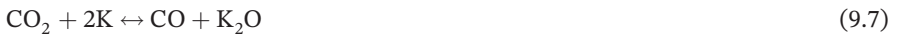
9.3 Carbonate salt-AC-based Supercapacitors Performance

Carbonate salt AC has been extensively used as the electrode material for supercapacitor electrode fabrication. Wang et al. [38] demonstrated the direct conversion of onion husks into AC frameworks with 3D interconnected porous structures for high-performance supercapacitors. The K_2CO_3 influenced 3D interconnected porous ACs-based symmetric

supercapacitor exhibited excellent electrochemical performance. It shows pure EDLC behavior as described by the CV curves and GCD profiles, shown in Figure 9.6(a, b). The symmetric supercapacitor exhibited a small IR-drop (Figure 9.6(c)), a large specific capacitance of around 188 Fg^{-1} at a current density of 1 A g^{-1} (Figure 9.6(d)), good cycling stability of around 93% capacitance retention for 2000 GCD cycles (Figure 9.6(e)), perfect Warburg impedance (Figure 9.6(f)), and high energy density of 47.6 $Wh\,kg^{-1}$ at a power density 675 W kg^{-1} in 1 M tetraethylammonium tetrafluoroborate salt (TEABF$_4$) solution with acetonitrile as the electrolyte. These findings show that K$_2$CO$_3$ activated 3D interconnected porous carbon frameworks are advantageous to demonstrate electrochemical capacitive behavior by speeding the kinetic process of ion diffusion in electrodes. This straightforward, effective, and template-free synthesis method shows great potential for the synthesis of novel porous carbons from renewable biomass sources for use in state-of-the-art energy storage technologies.

To lessen greenhouse gas emissions and air pollution from open burning, waste biomass can be converted to value-added carbon. A one-step molten salt carbonization technique was used by Yin et al. [41] to transform various waste biomasses to active ACs. The carbon materials are amorphous and have functional groups that contain oxygen on their surface when prepared. For the same type of waste biomass, carbon compounds produced in Na$_2$CO$_3$-K$_2$CO$_3$ melt have the largest specific surface area (408 $m^2\,g^{-1}$) and specific capacitance (160 Fg^{-1}) at 0.25 A g^{-1} current density (peanut shell). Temperatures greater than 700°C are required to generate capacitive carbon. Alkaline carbonate's high dissolving capacity helps produce high surface area carbon while reducing the carbon output from waste biomasses. The Na$_2$CO$_3$-K$_2$CO$_3$ melt yields the best capacitive carbon, according to the specific capacitance statistics. Carbon derived from peanut shell retains 95% of specific
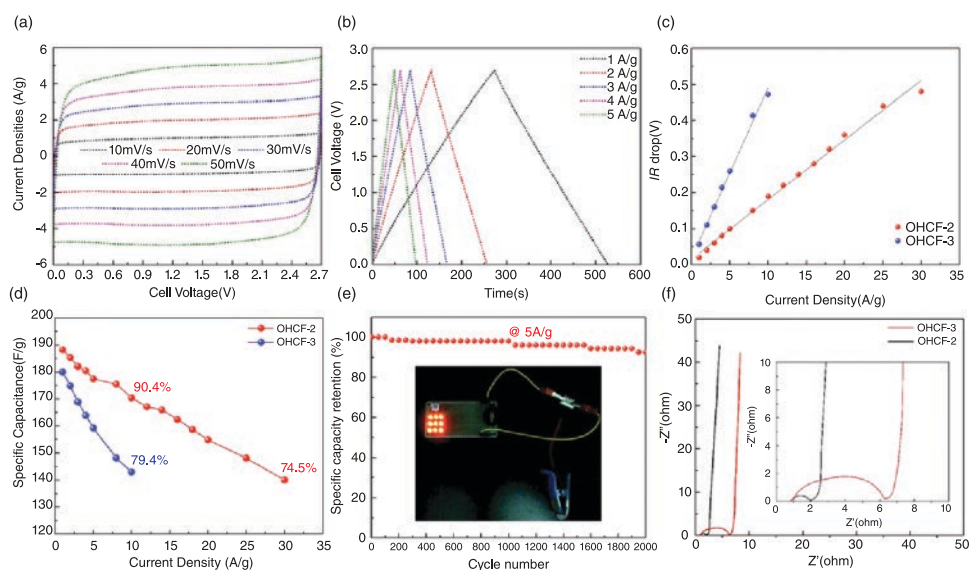
Figure 9.6 (a) CV curves, (b) GCD profiles, (c) IR-drop, (d) specific capacitances, (e) capacitance retention, and (f) Nyquist plots of the carbonate salt activated 3D interconnected porous carbon frameworks-based supercapacitor. *Reproduced with permission [38]. Copyright 2016, Elsevier.*

capacitance after 10000 GCD cycles. Furthermore, the rectangular form of CVs is indicative of a reliable double-layer capacitor even at a scan rate of $50 \, mV \, s^{-1}$ (Figure 9.7(a)). A good rate capability is demonstrated by the GCD profiles at various current densities, which reveal no statistically significant variation in specific capacitance for the carbon-based supercapacitor made from peanut shells (Figure 9.7(b)). The GCD profiles' symmetric properties reveal a minimal charge transfer resistance and dominant electrical conductance of the electrode. The Nyquist plot in Figure 9.7(c) indicates that the electrode has strong electrical conductivity by showing a semicircle in the high-frequency band followed by a straight line in the low-frequency range. A vertical line signifies that at lower frequencies, the electrode is more similar to an ideal capacitor. The supercapacitor that was reported had a power density of $125 \, W \, kg^{-1}$ and an energy density of $22 \, Wh \, kg^{-1}$. With this technique, waste biomass may be easily and sustainably converted into highly capacitive carbon, which can then be stored as carbon dioxide. In another report [42], the *Lentinus edodes*-derived AC using Na_2CO_3-K_2CO_3 melt-based supercapacitor exhibited a $389 \, Fg^{-1}$ high specific capacitance at $0.2 \, Ag^{-1}$ current density and a decent rate capacity with capacitance retention of ~$174 \, Fg^{-1}$ at a high current density of $20 \, A \, g^{-1}$ in aqueous electrolyte of $1 \, M \, H_2SO_4$. A good energy density of $45.69 \, Wh \, kg^{-1}$ at a power density of $100 \, W \, kg^{-1}$ was also provided by the built symmetric supercapacitor. It additionally displayed good cycling stability, holding 90% of the initial capacitance after 10000 GCD cycles.

The sustainable energy development of green carbon precursors and affordable activating agents has attracted significant attention regarding producing high-performance
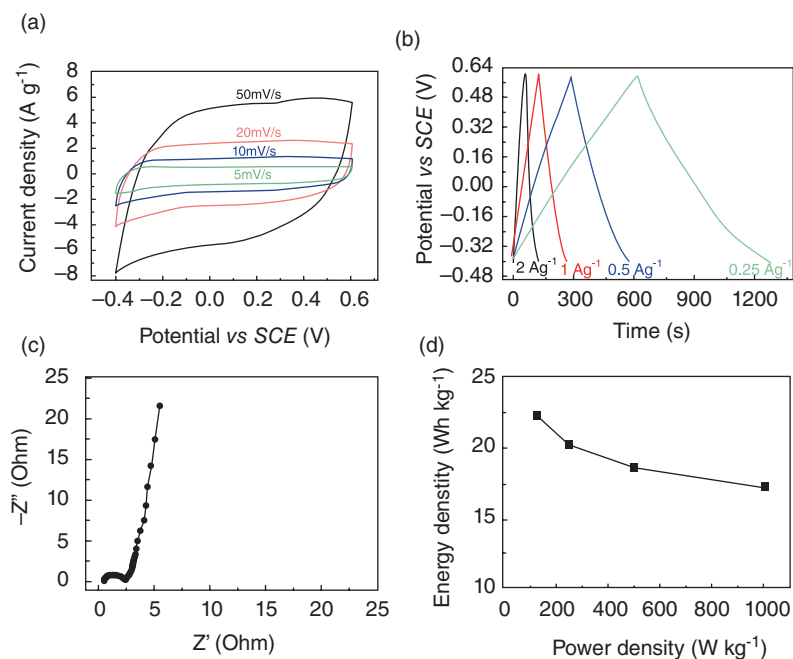
Figure 9.7 (a) CV curves, (b) GCD profiles, (c) Nyquist curve, and (d) Ragone plot of the calculated from the peanut shell derived carbon-based supercapacitor in $1 \, M \, H_2SO_4$ electrolyte. *Reproduced with permission [41]. Copyright 2014, American Chemical Society.*

electrodes for supercapacitors. Even though the most researched activation agents, like $ZnCl_2$ and KOH, produce porous carbon with a high surface area and a substantial capacity for charge storage, these activation agents have a poor carbon production yield and a high dosage utilization rate [45]. Demir et al. [45] described a different method of making porous carbons using NaOH, $Na_2S_2O_3$, Na_2CO_3, and K_2CO_3 as the appropriate activating agents. The performance of carbons prepared in this way, in terms of textural, morphological, and electrochemical characteristics, was compared. Additionally, these carbons produce exceptional electrochemical performance for use in supercapacitors. Likewise, Mohamedkhair et al. [11] reported the activating agents effect on the supercapacitor performance of carbon derived from *Albizia procera* leaves. Nitrogen-doped carbon nanostructured materials with improved electrochemical supercapacitance properties were prepared from *Albizia procera* leaves. The carbon materials were prepared by pyrolyzing the leaves at 850°C. The effects of utilizing various activation agents, such as $ZnCl_2$ and $NaHCO_3$, on the structural and textural characteristics, specific capacitance, surface functional groups, and surface area were investigated and compared. The $NaHCO_3$-activated nitrogen-doped carbon (NaNC) displayed a greater specific surface area (910 $m^2 g^{-1}$) in comparison to $ZnCl_2$-activated nitrogen-doped carbon (ZnNC) and nitrogen-doped carbon prepared without an activating agent (WANC). Overall, the BET and microscopic investigations showed that NaNC is fundamentally different from ZnNC and WANC in that it is composed of carbon nanosheets with macropores, mesopores, and a large number of micropores. Due to its distinctive characteristics, such as significant nitrogen concentrations, high specific surface area, and nanosheet-type morphology, NaNC exhibited a specific capacitance of 230 $F g^{-1}$ at 1.0 A g^{-1} current density, adequate energy and power densities, and exceptional charge-discharge stability. The schematic representation for carbon synthesis using various activation agents, their structural and morphological investigations, and the corresponding supercapacitor performance are shown in Figure 9.8. As electrode materials for electrochemical supercapacitors, Nath et al. [15] synthesized defective carbon nanosheets, which were obtained through the chemical activation of *Syzygium cumini* leaves using $NaHCO_3$ as an activation agent. A large specific surface area (1184.4 $m^2 g^{-1}$) and a sufficient number of oxygen-containing functional groups were present in the defective AC nanosheets. This resulted in the induction of enormous electroactive sites, which corresponded to a high specific capacitance of ~223 $F g^{-1}$ and greater durability. The use of inexpensive, ecologically benign, and electroactive carbon materials in energy-storage systems like supercapacitors and batteries has the potential to be very significant. Shrestha et al. [46] investigated on how activating chemicals affect the physical and electrochemical characteristics of AC electrodes made from *Shorea robusta* wood dust. The preparation of ACs, also known as AC-H_3PO_4, AC-KOH, and AC-Na_2CO_3, involved the use of three separate activating agents, i.e., H_3PO_4, KOH, and Na_2CO_3, respectively. The AC-H_3PO_4, AC-KOH, and AC-Na_2CO_3 were found to have surface areas of 1269.5, 280.6, and 58.9 $m^2 g^{-1}$, respectively. The supercapacitive performances AC electrodes were then assessed utilizing a three-electrode system in aqueous 6 M KOH employing CV, GCD, and EIS. The specific capacitance values at 1.0 A g^{-1} current density were 136.3, 42.2, and 59.1 Fg^{-1} for AC-H_3PO_4, AC-KOH, and AC-Na_2CO_3-electrodes, respectively.

There is a great demand for environmentally friendly synthesis methods that can produce porous ACs with the right structural characteristics for use as supercapacitor electrodes [47–49]. A more environmentally friendly substitute for the popular but destructive KOH is
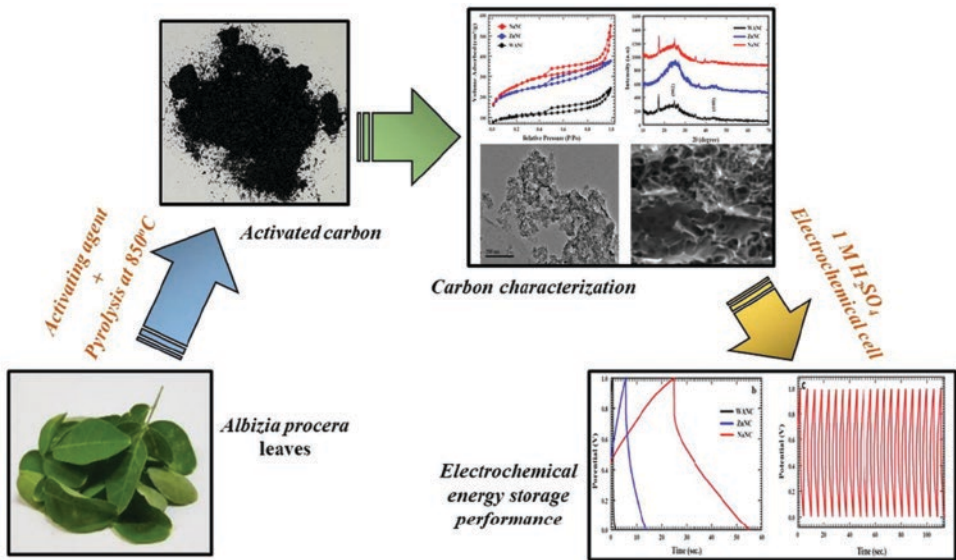
Figure 9.8 Schematic representation for carbon synthesis using various activation agents, their structural and morphological investigations, and the corresponding supercapacitor performance. *Reproduced with permission [11]. Copyright 2020, The Author(s). Published by Elsevier B.V. on behalf of King Saud University.*

suggested for synthesizing extremely porous carbons [50]. Products made from hydrochar are employed as carbon precursors. It has been demonstrated that utilizing a mildly alkaline potassium salt, such as potassium bicarbonate, is a highly effective way to increase porosity in hydrochar to make materials with large surface areas (> 2000 m^2 g^{-1}) and a controllable pore size distribution. Additionally, the yield of AC increased significantly by 10% when $KHCO_3$ was used in place of KOH, and hydrochar maintained its spherical morphology, which resulted in improved packing qualities and shorter ion diffusion distances. These characteristics resulted in a supercapacitor performance in a mixture of 1-ethyl-3-methylimidazolium tetrafluoroborate ($EMImBF_4$) and acetonitrile electrolyte, which can match or even outperform that of KOH-activated hydrochar. Effective energy storage depends on producing eco-friendly, inexpensive, high-performance supercapacitors with superior electrolytes and hierarchical porous electrodes. Shah et al. [5] compared the electrochemical performance of symmetric supercapacitors made from commercially available AC (ACE) and AC derived from jute sticks (JCE) using $NaHCO_3$ as an activation agent. They pyrolyzed jute sticks to create highly effective porous activated hierarchical carbon nanosheets. Devices for electrochemical double-layer supercapacitors were constructed using bioelectrolyte and the ACE and JCE-based electrodes, as shown in Figure 9.9. Due to the prepared JCE's low charge transfer resistance, the fabricated JCE-based supercapacitor exhibited a minor IR-drop when compared to the ACE-based supercapacitor. The findings demonstrated that at a 1.0 A g^{-1} current density, the JCE-based symmetric supercapacitor offers higher specific capacitance (142 F g^{-1}) than the ACE-based symmetric supercapacitor (20 F g^{-1}). The JAC-based supercapacitor exhibited excellent performance after 10000 GCD cycles and an energy density of 20 Wh kg^{-1} at a power density of 500 W kg^{-1}. The created
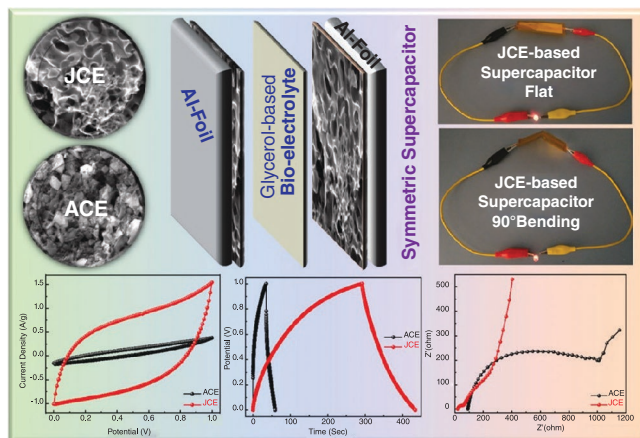
Figure 9.9 Development of symmetric supercapacitors using ACE and JCE and the corresponding electrochemical performance. *Reproduced with permission [5]. Copyright 2021, Elsevier.*

JCE-based supercapacitor also exhibits mechanical robustness in various bending positions. The reported research supported the idea that processed biowaste attains a strong potential as a material for storing energy. Roy et al. [10] showed how to easily and effectively develop hierarchical porous carbon called AC nanosheets. AC nanosheets were produced by simply heating banana leaves with K_2CO_3 in an inert atmosphere, which demonstrated a high specific surface area of 1459 $m^2 g^{-1}$. A two-electrode system was used to test the triggers of various electrolytes on the stability and performance of the AC nanosheet-based supercapacitors. In an ionic liquid electrolyte i.e., 1-butyl-3-methylimidazolium hexafluorophosphate [BMIM][PF$_6$], an organic electrolyte, i.e., tetraethylammonium tetrafluoroborate, and an aqueous electrolyte i.e., 0.5 M sodium sulfate, the specific capacitance values were 190, 114, and 55 F g^{-1}, respectively.

Hierarchically porous carbons have a significant surface area and a short ion transport channel as a result of the linked porous framework, which makes them excellent candidates for energy storage [51]. However, the majority of protocols heavily rely on soft-templating and nano-casting, which usually forbids the usage of specific raw materials and their industrial application. Building hierarchically porous carbons from crude biomass, widely available on the planet, using a straightforward one-pot method is still a significant challenge. Deng et al. [52] developed a technique to create hierarchically porous carbons with 3D hierarchical pores made up of macro-, meso-, and micropores that were inspired by the leavening in bread. Simply combining the biomass with $KHCO_3$ and heating it to a high temperature is the "leavening process". The hierarchically porous carbons produced also displayed a noticeably large specific area (1893 $m^2 g^{-1}$) in addition to the clearly defined hierarchical structure. It is noteworthy that the majority of biomass derivatives, such as starch, cellulose, glucose, chitin, bamboo, and rice straw can be processed using this "leavening" technique. The resulting hierarchically porous carbons demonstrated excellent electrochemical performance has a specific capacitance of ~250 F g^{-1} and nearly no capacitance loss after 10000 GCD cycles when evaluated as supercapacitor electrode materials in two-electrode test systems.

3D hierarchical porous carbon was successfully prepared with micro-, meso-, and macro pores by activating chestnut shells with $KHCO_3$ [53]. High specific surface area (~2300 $m^2 g^{-1}$) and high average pore volume (1.5 $cm^3 g^{-1}$) were obtained with the optimal $KHCO_3$ concentration, providing the electrode used in the three-electrode system with favorable electrochemical properties. A high specific electric capacity of 387 F g^{-1} was attained at 2 A g^{-1} current density. The electrochemical performances are astounding due to the hierarchical porous structure's high specific surface area and significant total pore volume. This indicates that the future of this hierarchically porous carbon created by activating it with $KHCO_3$ is more promising in terms of energy storage. By impregnating corncob with K_2CO_3 in various ratios, AC was prepared from a cheap and plentiful feedstock [32]. In order to create the electrodes for energy storage, the impregnated samples were activated at various temperatures (ranging from 500°C to 800°C). According to the findings, increasing the activation temperature and K_2CO_3 customized the AC's surface area (489–884 $m^2 g^{-1}$), morphology, and topography to propagate increased energy storage via a primarily EDLC process. The materials' capacitive performance at various temperatures is in the range of 650°C > 500°C > 800°C. Chemically created ACs based on leftover tea provedvery stable and reversible supercapacitor electrodes were created [54]. Despite having a smaller specific surface area, the AC created from waste tea by K_2CO_3 activation outperformed H_3PO_4 activation in an aqueous electrolyte in terms of supercapacitive performance. In aqueous electrolytes, K_2CO_3 activation led to a more uniform microporous structure, fewer surface oxygen groups, a lower internal resistance, and good electrochemical reversibility. Furthermore, a well-developed microporous design, which permits the ions to move smoothly within the porous structure, has a greater impact on the electrochemical performance than surface area and impacts capacitive performance. Various carbonate salts AC-based supercapacitors, previously reported in literature, are tabulated in Table 9.1.

9.4 Conclusions

Due to its low cost, straightforward synthesis process, and widespread availability, using AC in supercapacitors is a practical option. Physical, chemical, physiochemical, catalytic, and interface activation are among the common preparation techniques. Chemical activation stands out among them because of its low temperature for pyrolysis, rapid processing, high carbon output, large specific surface area, and controlled porous structure. A thorough analysis of the most important pore-forming step in AC utilizing various chemical activating agents (such as alkaline, acidic, neutral, and self-activating agents) has been conducted in light of a sizable body of pertinent published research from recent years. The performance of agricultural waste-based ACs made from different precursors but produced under the same conditions varies, emphasizing the effects of environmental factors, the preparation techniques, and the structure and composition of the agricultural waste precursors. Electrical conductivity, surface characteristics, and pore dispersion of electrodes all affect how well they function as capacitors. Because they have a small surface area, ultrasmall micropores considerably impact the capacitance of active carbons. Overall, the electrolyte system impacts how well energy cells work electrochemically.

Table 9.1 Carbonate salts AC-based supercapacitors, reported in the literature.

Biomass Source	Activation Agent	BET SSA ($m^2 g^{-1}$)	Morphology	Specific Capacitance ($F g^{-1}$) @ Current Density ($A g^{-1}$)	Electrolyte	Energy Density ($Wh kg^{-1}$) @ Power Density ($W kg^{-1}$)	Stability @ No. of Cycles	Ref.
Jute sticks	$NaHCO_3$	1100	Nanosheets	142 @ 1.0	Glycerol/KOH	20 @ 500	95 @ 10000	[5]
Banana leaves	K_2CO_3	1469	Nanosheets	190 @ 0.5	[BMIM][PF_6]	59 @ 750	90 @ 10000	[10]
Albizia procera leaves	$NaHCO_3$	910	Nanosheets	231 @ 1.0	1 M H_2SO_4	32 @ 625	97.3 @ 1000	[11]
Syzygium cumini leaves	$NaHCO_3$	1184.4	Defective nanosheets	222.3 @ 1.0	1 M H_2SO_4	…	94 @ 5000	[15]
Corncob	K_2CO_3	793	Sponge-like	322 @ 0.25	0.5 M H_2SO_4	9.9 @ 200	90 @ 10000	[32]
Onion husks	K_2CO_3	2571	Micrometer-sized ground with open cavities	188 @ 1.0	1 M $TEABF_4$	47.6 @ 675	93 @ 2000	[38]
Peanut shell	Na_2CO_3-K_2CO_3	408	Nanosheets	160 @ 0.25	1 M H_2SO_4	22 @ 125	95 @ 10000	[41]
Lentinus edodes	Na_2CO_3-K_2CO_3	1144	Nanosheets	398 @ 0.2	1 M H_2SO_4	45.69 @ 100	90 @ 10000	[42]
Fraxinus chinensis fallen leaves	KOH/K_2CO_3	2869	Fluffy fragment	242 @ 0.3	6 M KOH	33.9 @ 1080	100 @ 2000	[44]

Wood-dust of *Shorea robusta*	Na_2CO_3	58.9	Agglomerated particles	59.1 @ 1.0	6 M KOH	3.0 @ 99.6	96.9 @ 1000	[46]
α-D-Glucose	$KHCO_3$	2000	Spherical particles	270 @ 0.5	$EMImBF_4$	25 @ 19000	90 @ 4000	[50]
Bread leavening	$KHCO_3$	1893	Nanosheets	253 @ 0.5	6 M KOH	8.7 @ 500	96.5 @ 10000	[52]
Chestnut shells	$KHCO_3$	2298	Microfibers composed of nanosheets	387 @ 2.0	6 M KOH	...	98.68 @ 10000	[53]
Waste tea	K_2CO_3	1125	Rough surface with craters	203 @ 1.5 A/cm^2	1 M H_2SO_4	...	98 @ 400	[54]

Electrochemical qualities were altered more significantly than physiochemical features by changes in surface chemistry and adding certain surface functionalities to ACs. When creating high-quality AC for supercapacitor electrodes, carbonate salts are frequently employed. This chapter summarizes how different biomasses are used to make AC with carbonate salts as activation agents and how they can be used as electrode materials in supercapacitors. With the increasing demand for biomass-derived ACs, carbonate salts-based ACs will be efficiently used at the industrial level due to the low cost and availability of carbonate salts worldwide.

Acknowledgments

References

1 M. Yaseen, M. A. K. Khattak, M. Humayun, M. Usman, S. S. Shah, S. Bibi, B. S. U. Hasnain, S. M. Ahmad, A. Khan, N. Shah, A. A. Tahir, H. Ullah, *Energies* **2021**, *14*, 7779.

2 S. S. Shah, S. M. A. Nayem, N. Sultana, A. J. S. Ahammad, M. A. Aziz, *ChemSusChem* **2022**, *15*, e202101282.

3 S. S. Shah, M. N. Shaikh, M. Y. Khan, M. A. Alfasane, M. M. Rahman, M. A. Aziz, *Chem. Rec.* **2021**, *21*, 1631–1665.

4 A. Aziz, S. S. Shah, A. Kashem, *Chem. Rec.* **2020**, *20*, 1074–1098.

5 S. S. Shah, E. Cevik, M. A. Aziz, T. F. Qahtan, A. Bozkurt, Z. H. Yamani, *Synth. Met.* **2021**, *277*, 116765.

6 S. S. Shah, M. A. A. Qasem, R. Berni, C. Del Casino, G. Cai, S. Contal, I. Ahmad, K. S. Siddiqui, E. Gatti, S. Predieri, J.-F. Hausman, S. Cambier, G. Guerriero, M. A. Aziz, *Sci. Rep.* **2021**, *11*, 6945.

7 S. S. Shah, H. T. Das, H. R. Barai, M. A. Aziz, *Polymers* **2022**, *14*, 270.

8 A. J. S. Ahammad, N. Odhikari, S. S. Shah, M. M. Hasan, T. Islam, P. R. Pal, M. A. Ahmed Qasem, M. A. Aziz, *Nanoscale Adv.* **2019**, *1*, 613–626.

9 A. J. S. Ahammad, P. R. Pal, S. S. Shah, T. Islam, M. Mahedi Hasan, M. A. A. Qasem, N. Odhikari, S. Sarker, D. M. Kim, M. A. Aziz, *J. Electroanal. Chem.* **2019**, *832*, 368–379.

10 C. K. Roy, S. S. Shah, A. H. Reaz, S. Sultana, A.-N. Chowdhury, S. H. Firoz, M. H. Zahir, M. A. A. Qasem, M. A. Aziz, *Chem. Asian J.* **2021**, *16*, 296–308.

11 A. K. Mohamedkhair, M. A. Aziz, S. S. Shah, M. N. Shaikh, A. K. Jamil, M. A. A. Qasem, I. A. Buliyaminu, Z. H. Yamani, *Arab. J. Chem.* **2020**, *13*, 6161–6173.

12 S. M. Abu Nayem, S. S. Shah, S. B. Chaity, B. K. Biswas, B. Nahar, M. A. Aziz, M. Z. Hossain, *Arab. J. Chem.* **2022**, *15*, 104265.

13 M. A. Aziz, S. S. Shah, S. M. A. Nayem, M. N. Shaikh, A. S. Hakeem, I. A. Bakare, *J. Energy Storage* **2022**, *50*, 104278.

14 M. A. Aziz, S. S. Shah, S. Reza, A. S. Hakeem, W. Mahfoz, *Chem. Asian J.* **2022**, e202200869, https://doi.org/10.1002/asia.202200869.

15 N. C. Deb Nath, S. S. Shah, M. A. A. Qasem, M. H. Zahir, M. A. Aziz, *ChemistrySelect* **2019**, *4*, 9079–9083.

16 S. S. Shah, M. A. Aziz, A. K. Mohamedkhair, M. A. A. Qasem, A. S. Hakeem, M. K. Nazal, Z. H. Yamani, *J. Mater. Sci. Mater. Electron.* **2019**, *30*, 16087–16098.

17 I. A. Buliyaminu, M. A. Aziz, S. S. Shah, A. K. Mohamedkhair, Z. H. Yamani, *Arab. J. Chem.* **2020**, *13*, 4785–4796.

18 M. A. Aziz, S. S. Shah, Z. H. Yamani, *Manganese Oxide Nanoparticle Carbon Microparticle Electrocatalyst and Method of Making from Albizia Procera Leaf*, *U.S. Patents*, **2021**, *16/589,711*, US20210095384A1.

19 S. S. Shah, M. A. Alfasane, I. A. Bakare, M. A. Aziz, Z. H. Yamani, *J. Energy Storage* **2020**, *30*, 101562.

20 S. S. Shah, M. A. Aziz, A.-R. Al-Betar, W. Mahfoz, *Arab. J. Chem.* **2022**, *15*, 104058.

21 M. M. Hasan, T. Islam, S. S. Shah, A. Awal, M. A. Aziz, A. J. S. Ahammad, *Chem. Rec.* **2022**, *22*, e202200041.

22 S. S. Shah, M. A. Aziz, Z. H. Yamani, *Chem. Rec.* **2022**, *22*, e202200018.

23 M. Ashraf, I. Khan, M. Usman, A. Khan, S. S. Shah, A. Z. Khan, K. Saeed, M. Yaseen, M. F. Ehsan, M. N. Tahir, N. Ullah, *Chem. Res. Toxicol.* **2020**, *33*, 1292–1311.

24 M. Ashraf, S. S. Shah, I. Khan, M. A. Aziz, N. Ullah, M. Khan, S. F. Adil, Z. Liaqat, M. Usman, W. Tremel, M. N. Tahir, *Chem. Eur. J.* **2021**, *27*, 6973–6984.

25 A. Helal, S. S. Shah, M. Usman, M. Y. Khan, M. A. Aziz, M. Mizanur Rahman, *Chem. Rec.* **2022**, *22*, e202200055.

26 M. Rauf, S. S. Shah, S. K. Shah, S. N. A. Shah, T. U. Haq, J. Shah, A. Ullah, T. Ahmad, Y. Khan, M. A. Aziz, K. Hayat, *J. Saudi Chem. Soc.* **2022**, *26*, 101514.

27 S. S. Shah, M. A. Aziz, E. Cevik, M. Ali, S. T. Gunday, A. Bozkurt, Z. H. Yamani, *J. Energy Storage* **2022**, *56*, 105944.

28 S. S. Shah, M. A. Aziz, W. Mahfoz, A.-R. Al-Betar, Conducting Polymers Based Nano-composites for Supercapacitors in *Nanostructured Materials for Supercapacitors*, (Eds: S. Thomas, A. B. Gueye, R. K. Gupta), Springer, Cham, **2022**, Chapter 22, pp. 485–511, Vol. *1*.

29 M. Usman, M. Humayun, S. S. Shah, H. Ullah, A. A. Tahir, A. Khan, H. Ullah, *Energies* **2021**, *14*, 2281.

30 A. M. Abioye, F. N. Ani, *Renew. Sust. Energ. Rev.* **2015**, *52*, 1282–1293.

31 H. Lu, X. S. Zhao, *Sustain. Energy Fuels* **2017**, *1*, 1265–1281.

32 R. D. Ortiz-Olivares, D. R. Lobato-Peralta, D. M. Arias, J. A. Okolie, A. K. Cuentas-Gallegos, P. J. Sebastian, A. R. Mayer, P. U. Okoye, *J. Energy Storage* **2022**, *55*, 105447.

33 D. Adinata, W. M. A. Wan Daud, M. K. Aroua, *Bioresour. Technol.* **2007**, *98*, 145–149.

34 Y. Gao, Q. Yue, B. Gao, A. Li, *Sci. Total Environ.* **2020**, *746*, 141094.

35 Z. Heidarinejad, M. H. Dehghani, M. Heidari, G. Javedan, I. Ali, M. Sillanpää, *Environ. Chem. Lett.* **2020**, *18*, 393–415.

36 J. A. Nieto, L. Soriano-Romaní, L. Tomás-Cobos, L. Sharma, T. Budde, *Food Chem.* **2021**, *348*, 128740.

37 J. I. Hayashi, T. Horikawa, I. Takeda, K. Muroyama, F. N. Ani, *Carbon* **2002**, *40*, 2381–2386.

38 D. Wang, S. Liu, G. Fang, G. Geng, J. Ma, *Electrochim. Acta* **2016**, *216*, 405–411.

39 J. Wang, S. Kaskel, *J. Mater. Chem.* **2012**, *22*, 23710–23725.

40 A. Bello, F. Barzegar, D. Momodu, J. Dangbegnon, F. Taghizadeh, N. Manyala, *Electrochim. Acta* **2015**, *151*, 386–392.

41 H. Yin, B. Lu, Y. Xu, D. Tang, X. Mao, W. Xiao, D. Wang, A. N. Alshawabkeh, *Environ. Sci. Technol.* **2014**, *48*, 8101–8108.

42 D. Tang, Y. Luo, W. Lei, Q. Xiang, W. Ren, W. Song, K. Chen, J. Sun, *Appl. Surf. Sci.* **2018**, *462*, 862–871.

43 M. R. Hasan, T. Islam, M. M. Hasan, A.-N. Chowdhury, A. J. S. Ahammad, A. H. Reaz, C. K. Roy, S. S. Shah, I. Al, M. A. Aziz, *J. Phys. Chem. Solids* **2022**, *165*, 110659.

44 Y.-T. Li, Y.-T. Pi, L.-M. Lu, S.-H. Xu, T.-Z. Ren, *J. Power Sources* **2015**, *299*, 519–528.

45 M. Demir, M. Doguscu, *ChemistrySelect* **2022**, *7*, e202104295.

46 D. Shrestha, A. Rajbhandari, *Heliyon* **2021**, *7*, e07917.

47 T. Islam, M. M. Hasan, S. S. Shah, M. R. Karim, F. S. Al-Mubaddel, M. H. Zahir, M. A. Dar, M. D. Hossain, M. A. Aziz, A. J. S. Ahammad, *J. Energy Storage* **2020**, *32*, 101908.

48 J. Saravanan, M. Pannipara, A. G. Al-Sehemi, S. Talebi, V. Periasamy, S. S. Shah, M. A. Aziz, G. Gnana Kumar, *J. Mater. Sci. Mater. Electron.* **2021**, *32*, 24775–24789.

49 R. Shakil, M. N. Shaikh, S. S. Shah, A. H. Reaz, C. K. Roy, A.-N. Chowdhury, M. A. Aziz, *Asian J. Org. Chem.* **2021**, *10*, 2220–2230.

50 M. Sevilla, A. B. Fuertes, *ChemSusChem* **2016**, *9*, 1880–1888.

51 M. Daud, M. S. Kamal, F. Shehzad, M. A. Al-Harthi, *Carbon* **2016**, *104*, 241–252.

52 J. Deng, T. Xiong, F. Xu, M. Li, C. Han, Y. Gong, H. Wang, Y. Wang, *Green Chem.* **2015**, *17*, 4053–4060.

53 P. Hong, X. Liu, X. Zhang, S. Peng, Z. Wang, Y. Yang, R. Zhao, Y. Wang, *Int. J. Energy Res.* **2020**, *44*, 988–999.

54 I. I. G. Inal, S. M. Holmes, A. Banford, Z. Aktas, *Appl. Surf. Sci.* **2015**, *357*, 696–703.

10

KOH/NaOH-activated Carbon

Nasrin Siraj Lopa[1], Biswa Nath Bhadra[2], Nazmul Abedin Khan[3], Serge Zhuiykov[1,*], and Md. Mahbubur Rahman[4,*]

[1] *Center for Environmental & Energy Research, Ghent University Global Campus, 119-5 Songdomunhwa-ro, Yeonsu-gu, Incheon 21985, South Korea*

[2] *International Center for Materials Nanoarchitectonics (WPI-MANA), National Institute for Materials Science (NIMS), 1-1 Namiki, Tsukuba 305-0044, Ibaraki, Japan*

[3] *Department of Mathematical and Physical Sciences, East West University, Dhaka 1212, Bangladesh*

[4] *Department of Applied Chemistry, Konkuk University, Chungju 27478, South Korea*

* Corresponding authors

10.1 Introduction

Electrochemical supercapacitors (ESCs) are energy storage devices and are broadly recognized due to their in-between energy density (E_d) between the battery and conventional dielectric capacitors and high-power density (P_d) [1–3]. ESCs exhibit long cycle life, a wide range of operational temperatures, good reversibility, and high safety [4, 5]. Based on the principles of the charge storage mechanism, ESCs can be categorized mainly as electric double-layer capacitors (EDLCs) and pseudocapacitors [6]. In EDLCs, energy is stored by the adsorption/desorption of electrolyte ions in a non-Faradaic process, while in pseudocapacitors, energy is stored by a Faradaic process that occurs at the electrode surface [7]. For EDLCs, carbon-based materials (e.g., activated carbon (AC), graphene, carbon nanotubes, and graphitic carbon nitride) are used as common electrode materials. In contrast, the transition metal-oxides (TMOs) (e.g., RuO_2, MnO_2, Cu_xO, TiO_2, and NiO_x) and conducting polymers (CPs) are the potential electrode materials for the development of pseudocapacitors [8–12].

Among the carbon materials, for the development of high-performance EDLC-type ESCs, research interests have focused on the development of AC materials (also called activated charcoal) from a wide variety of agricultural waste biomass including coffee beans, rice husk, sunflower seed shell, coffee endocarp, *Camellia oleifera* shell, bamboo species, apricot shell, cassava peel waste, sugarcane bagasse, rubberwood sawdust, palm kernel shell, jute stick, wood, anthracite, date seeds, coconut, corncob, bitumen charcoal, lignite, and peat [13–15]. The ACs are superior to other porous materials because of their

robust pore architecture, high porosity (wide range in pore diameter), high specific surface area, and ample pore functionalities for the intercalation/deintercalation of electrolyte ions [16]. Depending on the carbonization conditions and the activator, the carbon content in AC could be approximately 40–90 wt.% [17, 18]. Additionally, ACs contain carboxyl (–COOH), carbonyl (C=O), phenolic, lactonic, pyrrolic, and pyridinic functional groups, along with various heteroatoms (S, O, N) within the porous framework, which are presumed to be the active sites for various chemical interactions in adsorption, catalysis, sensing or so on [19–22]. These improved physical and chemical properties of AC continually expanded its applications for ESCs, water treatment, desalination, gas and air purification, CO_2 adsorption, catalysis, battery, solar cells, pharmaceuticals, etc., as shown in Figure 10.1 [23–31].

The performance of ACs in ESCs, as well as other technologies, is highly dependent on the carbonization conditions and activation methods (e.g., physical, chemical, electrochemical, microwave, ultrasound, and plasma methods) used to prepare them from the different precursors such as woody biomass, herbaceous and agricultural waste, aquatic biomass, fibers, grass, starch, and coal [32]. Specifically, the physical, chemical, and electrochemical characteristics of the chemically prepared ACs are highly dependent on the type of activation agents (e.g., NaOH, KOH, $ZnCl_2$, K_2CO_3, H_3PO_4, $FeCl_3$, CO_2, steam, N_2, O_3, O_2) and preparation methods [32–34]. Additionally, selecting biomass precursors is crucial for manufacturing high-quality ACs [35]. Thus, a systematic study is necessary to conclude the production of ACs for high-performance ESCs. This chapter discusses the properties of ACs and their performance in ESCs, synthesized from various biomass using KOH/NaOH as activation agents.
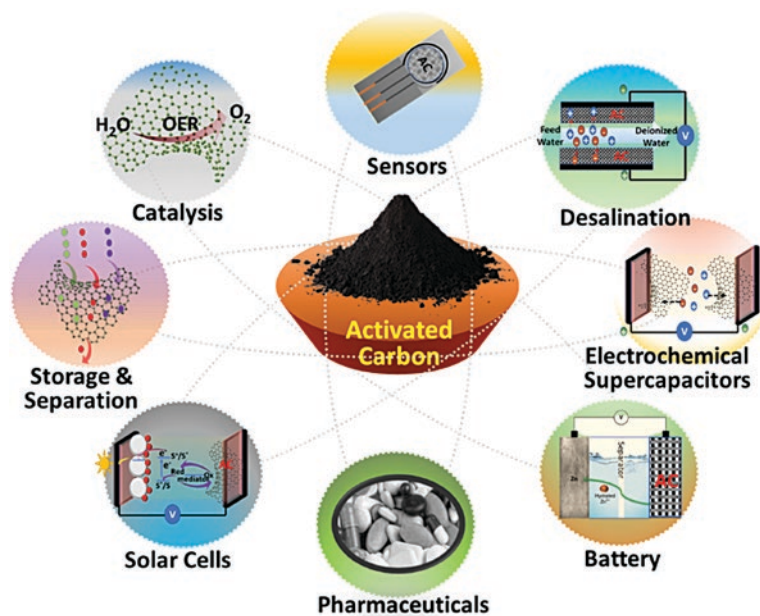
Figure 10.1 Wide range applications of activated carbons.

10.2 Basics of Activated Carbon

In the 1950s, Rosalind Franklin first described the structure of carbons produced by the pyrolysis of organic materials with two distinct classes: graphitizing and non-graphitizing [36]. In graphitizing, carbon units are almost parallel, and the links between the adjacent carbon units are assumed to be weak (Figure 10.2a). In contrast, non-graphitizing carbons and/or ACs are based on a small graphitic crystallite joined together by cross-links in a disordered manner (Figure 10.2b) [36, 37]. However, Franklin did not explain the bonding type of these cross-links. Later on, it was hypothesized that this cross-link might consist of sp^3-bonded carbon atoms domains [38, 39]. Further analyses of non-graphitizing carbon using neutron diffraction studies revealed that non-graphitizing carbon cross-links consist entirely of sp^2-bonded carbon atoms [40]. Recent studies suggested that non-graphitizing carbon structure is related to that of the fullerenes, consisting of curved fragments with pentagonal and other non-hexagonal rings along with hexagons [41].

10.3 Preparation of Activated Carbon from Biomass

Activation is usually performed (i) to boost up surface area, (ii) to tune the pore diameter (from nano to macro sizes), (iii) to impart new functionalities such as –COOH, –C=O, phenolic, and –OH groups, and (iv) to increase carbon content (wt.%) via eliminating some heteroatoms [34]. For the ACs preparation, biochar (BC) is initially synthesized from biomass either via carbonization at the temperature range of 400 to 850 °C under the inert atmosphere or via hydrothermal carbonization at 130 to 250 °C using a hydrothermal reactor [15, 42]. The BC is subsequently activated; and referred to as AC. The most common activation methods include physical activation, chemical activation, combined physical and chemical activation, thermal activation, microwave activation, ultrasound activation, plasma activation, and electrochemical activation. Figure 10.3 depicts biomass carbonization and various activation methods to produce ACs. The following section briefly discusses the chemical activation of BC, derived from biomass.

(a) (b)
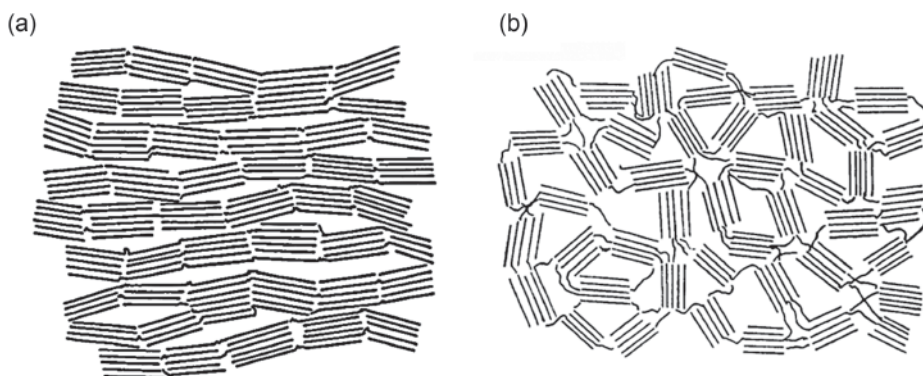
Figure 10.2 Structure of (a) graphitizing and (b) non-graphitizing carbons. *Reproduced with permission [36]. Copyright 1951, The Royal Society (UK).*
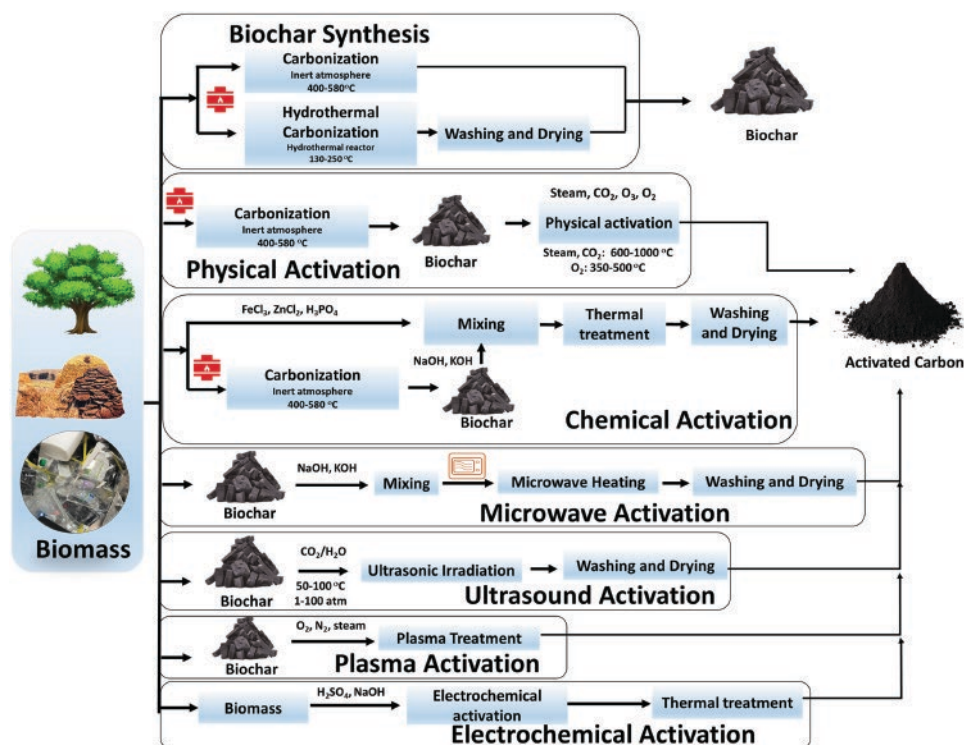
Figure 10.3 Synthesis of biochar and activated carbon from biomass.

10.3.1 Chemical Activation

Chemical activation, also known as wet oxidation of BC for AC production, offers the advantages of kinetic-controlled chemical reactions [32]. In the chemical activation process, the biomass precursors and/or BCs are mixed with activating agents such as NaOH, KOH, $ZnCl_2$, K_2CO_3, H_3PO_4, and $FeCl_3$ via wet or dry techniques [32, 34]. Subsequently, chemical activation is executed in which the carbonization and activation are carried out simultaneously at the temperature range of 300–950 °C [32, 34]. Based on the chemical properties of chemical activators, chemical activation can be classified as *acidic, basic*, and *neutral* activation. In contrast to physical activation, chemical activation facilitates the deep penetration of activators into the carbon structure, which results in a better porous structure with a high surface area [32, 34]. Noteworthy, chemical activation under suitable conditions remarkably increases carbon's surface area/pore volume via the carbon reduction (or carbon consumption) process, which converts the small pores into bigger ones. The main disadvantages of the chemical activation method are time and energy-consumption and require expensive post-activation washing of the carbons for removing the residual reactants and inorganic residues (ash) produced from the precursor during the activation process. Table 10.1 summarizes the production of ACs from the different biomasses by chemical activation methods, while the details of the basic activation method using KOH and NaOH are discussed in section 10.3.2.

Table 10.1 Acid and salt activation of biomass for the synthesis of ACs.

Biomass	Carbonization conditions		Activation conditions			Surface area, S_{BET} (m^2 g^{-1})	Yield (%)	Ref.
	T_c (°C)	Time (h)	Activators	T_a (°C)	Time (h)			
Acacia fumosa seed	–	–	HCl	450	6	–	–	[43]
Acacia mangium	500	2	H$_3$PO$_4$	–	–	1038.77	–	[44]
Acacia mangium	–	–	H$_3$PO$_4$	500	0.75	1767	–	[45]
Acacia nilotica sawdust	–	–	H$_3$PO$_4$	900	1	1701	–	[46]
Argan nutshell	500	1	H$_3$PO$_4$	700	1	1372	–	[47]
Chestnut oak shells	–	–	H$_3$PO$_4$	450	–	–	38.12	[48]
Waste sludge and bagasse	800	0.5	HNO$_3$	–	–	806.	–	[49]
Acacia mangium	–	–	CaO	500	2	65.33	–	[44]
Acacia mangium	500	2	ZnCl$_2$	–	-	957.47		[44]
Acacia nilotica	–	–	ZnCl$_2$	600	5	403	–	[50]
Shorea robusta sawdust	–	–	Na$_2$CO$_3$	400	3	10.45	–	[51]
Pistachio wood wastes	–	–	NH$_4$NO$_3$	800	2	1448		[52]
Waste tea	–	–	C$_2$H$_3$O$_2$K	800	2	845	27.9	[53]
Rice straw	–	–	N$_2$H$_9$PO$_4$	700	1	1154	41.1	[53]
Date pits	–	–	FeCl$_3$	700	1	780	47	[54]
Paper mill sludge	–	–	K$_2$CO$_3$	800	2.5	1583	3.4	[55]
Hide waste	–	–	K$_2$SiO$_3$	700	1	1804.37	–	[56]
Corn cob	–	–	ZnCl$_2$	500	–	1400	–	[57]
Dry okra waste	–	–	ZnCl$_2$	500	1	1044	–	[46]
Cocoa shell	110	24	ZnCl$_2$	500	0.6	–	–	[58]

10.3.2 Chemical Activation Using KOH/NaOH

Generally, chemical activation of carbonaceous materials is preferable over physical activation due to its short process time, kinetic-controlled chemical reactions, and lower activation temperature [32]. The AC prepared via the chemical activation method exhibited a high surface area and porosity. The following sections highlight the fundamentals, limitations, and implications of KOH and NaOH activation methods for producing biomass-derived AC.

10.3.2.1 KOH Activation
In recent years, KOH activator has been used extensively for manufacturing low-cost AC with a large amount of micropores, high specific surface area, and enriched –OH

functional groups on the carbon surface [32, 34]. The production of AC using KOH and other chemical activators can be demonstrated either in one-step or two-step methods [59, 60]. In a one-step process, pyrolysis/activation below the boiling point of KOH (1327°C) is executed simultaneously by impregnating KOH with the desired impregnation ratio into the selected carbonaceous precursor, while in the two-step method, activation consists of biomass precursor carbonization followed by impregnation of the resulting BC with KOH for the activation process [34]. Regardless of activation steps, the textural properties of ACs are highly dependent on biomass precursors' properties and chemical compositions. For example, Oginni et al. reported that the AC prepared from Kanlow Switchgrass by one-step and two-step KOH activation method showed a surface area of 1271.66 and 599.19 $m^2 \, g^{-1}$, respectively, which is evident in the scanning electron microscopic (SEM) images of the resulting ACs (Figure 10.4) [59]. In another report, Basta et al. demonstrated that the AC produced from raw rice straw exhibited a surface area of 1917 and 657 $m^2 \, g^{-1}$, respectively, for the two-step and one-step methods [60]. Irrespective of the activation steps, the KOH activation results in a higher carbon reduction. Consequently, the yield (carbon content) of the resultant AC usually remains lower compared to the other chemical activators, such as $ZnCl_2$ and H_3PO_4 [59]. This could be attributed to the pore development in the AC structures that accelerate the loss of carbon induced by the K intercalation into the carbon network [61]. During carbonization, the KOH activator eliminates the water present in the precursor by forming tar, which could block the carbon pores. Upon carbonization, the corresponding primary chemical reactions (Equations 10.1–10.4) and secondary reactions (Equation 10.5) are presented as follows [32, 34]:

$$2KOH \rightarrow K_2O + H_2O \tag{10.1}$$

$$C + 2KOH \rightarrow 2K + H_2 + CO_2 \tag{10.2}$$

$$C + 2KOH \rightarrow 2K + H_2O + CO \tag{10.3}$$

$$K_2O + CO_2 \rightarrow K_2CO_3 \tag{10.4}$$

$$H_2O + C + 2KOH \rightarrow K_2CO_3 + H_2 \tag{10.5}$$

(a)   (b)
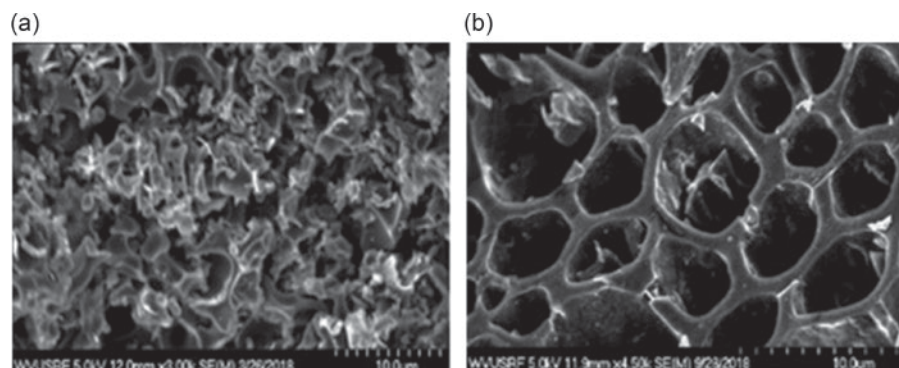
Figure 10.4 Scanning electron microscopic images of ACs prepared from Kanlow Switchgrass by (a) one-step and (b) two-step method. *Reproduced with permission [59]. Copyright 2019, Elsevier.*

During the activation, the creation of metallic K and its intercalation into the carbon matrix can induce an expansion of the gaps between the carbon-atom layers. Thus, both mesopores and micropores are formed into the carbon network. In contrast, the produced K_2CO_3 can be eliminated during carbonization with the production of CO_2 gas, which also partly contributes to the development of the pore in the AC. Thus, the mechanism of KOH activation of BC can be described as presented in Figure 10.5 [62], where the KOH is dehydrated to K_2O at the beginning of the carbonization process (step 1: dehydration process). In step 2, the produced K_2O is reduced to metallic K and intercalated into the carbon layers, which induces the structural expansion of the carbon layers. Next, (step 3) K was oxidized by the production of K_2O and then the hydration of K_2O (step 4).

Table 10.2 summarizes the properties of recently synthesized ACs, prepared from the various biomass precursors using a KOH activator. It can be clearly seen that the source of
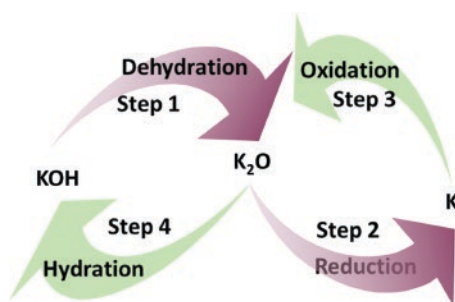
Figure 10.5 Mechanism of KOH activation. *Redrawn from ref. [62] Copyright 2016, Elsevier.*

Table 10.2 Textural characteristics of ACs prepared from various biomass precursors using KOH activator.

Biomass precursors	T (°C)	t (h)	Surface area, S_{BET} (m^2 g^{-1})	Pore size (nm)/pore volume (cm^3 g^{-1})	Yield (%)	Ref.
Jatoba fruits	500	2	2794	1.74/–	–	[63]
Schima wallichii	700	1	1,005.71	–/0.491	18.84	[64]
Augarcane bagasse	700	1	709.3	6.6/0.31	–	[65]
Sorghum stem	800	2	948.6	3.12/0.55	–	[66]
Sorghum root	800	2	168.1	4.48/0.13	–	[66]
Giant miscanthus	900	1	2212	–/0.99	–	[67]
Corn stalk	900	1	2434	–/1.22	–	[67]
Wheat stalk	900	1	2327	–/1.10	–	[67]
Oak wood	800	1	1662	2.60/0.791	13.0– 21.7	[68]
Date seeds	900	1	912.32	–/0.67	>10	[69]
Corn stover	800	3	956	6.9/–	–	[70]
Rice straw	800	1	1554	–/0.930	13.5	[71]
Coconut shell	850	2	1026	–/0.576	–	[72]
Silkworm cocoon waste	800	3	2797	–/1.735	21.7	[73]

biomass and the carbonization temperature significantly controlled the properties of ACs, such as surface area, pore volume, and pore diameter. Further, it is evident that the yield of carbon production through the KOH activation is relatively low (about 22%) compared to the H_3PO_4 and $FeCl_3$ activators (Table 10.1). However, KOH improves the physicochemical properties of ACs. The drawbacks of KOH is that it is toxic and detrimental to humans and the environment. Thus, exploring suitable other environmentally friendly and low-cost chemicals as an alternative to KOH is required without affecting the functional and textural characteristics ACs.

10.3.2.2 NaOH Activation

Similar to the KOH activator, NaOH has also been widely used as an effective activator for the production of ACs with a large number of micropores, high specific surface area, and abundant –OH functional groups [33, 35]. This can be achieved by treating the selected carbonaceous precursor, and/or BC, with NaOH with the desired impregnation ratio via one-step and/or two-step methods [74]. In a one-step process, carbonization and activation of biomass are performed concurrently below the boiling temperature of NaOH (1388°C) by impregnating with NaOH. While in the two-step method, activation involves the carbonization of precursors followed by the impregnation of the corresponding BC with NaOH for the activation process. The following Equations (10.6–10.8) depict the plausible mechanism for producing ACs through NaOH [75].

$$6NaOH + 2C \rightarrow 2Na + 2Na_2CO_3 + 3H_2 \tag{10.6}$$

$$Na_2CO_3 \rightarrow Na_2O + CO_2 \tag{10.7}$$

$$2Na + CO_2 \rightarrow Na_2O + CO \tag{10.8}$$
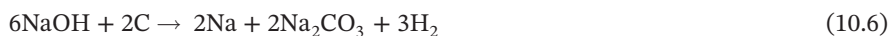
It can be concluded that the formation of micropores on the NaOH-assisted ACs is responsible for releasing the different gaseous species (CO, CO_2, and H_2). The Na metal intercalation into the carbon networks is also responsible for the creation of micropores within the ACs. Finally, the residual NaOH as well as other compounds generated by carbonization, are evaporated from the ACs and form a rugged surface with improved porosity.

Both textural properties and chemical functionalities of produced ACs depend highly on the precursor's source and its chemical composition, the amount of NaOH, and the activation steps (one-step or two-step). For example, Zhang et al. studied the textural properties of ACs, prepared from corn cob (CC), wheat bran (WB), rice husk (RH), and soybean shell (SS) with varying NaOH amounts via the one-step method [75]. It can be observed that the NaOH dosage ratio significantly controls the surface area of ACs prepared this way (Figure 10.6a), and at the optimized ratios of NaOH (1:4 (m/m) for CC, WB, SS, and 1:3 (m/m) for RH) induced the surface area of 2381, 2532, 2786, and 2628 $m^2\,g^{-1}$ for CC-, WB-, RH- and SS-derived ACs, respectively. This is evident in the N_2 adsorption-desorption isotherms (Figure 10.6b) and the corresponding SEM images of the samples (Figure 10.6(c-f)). Alteration in the ACs surface area by varying the biomass precursors with similar NaOH dosage could be attributed to the fact that the different precursors contain dissimilar amounts of ash, and the high ash content precursors consumed less NaOH and exhibited a larger surface area. In another report, Wanprakhon et al. investigated the textural properties of AC derived from the longan seeds with NaOH activator by both one-step and two-step
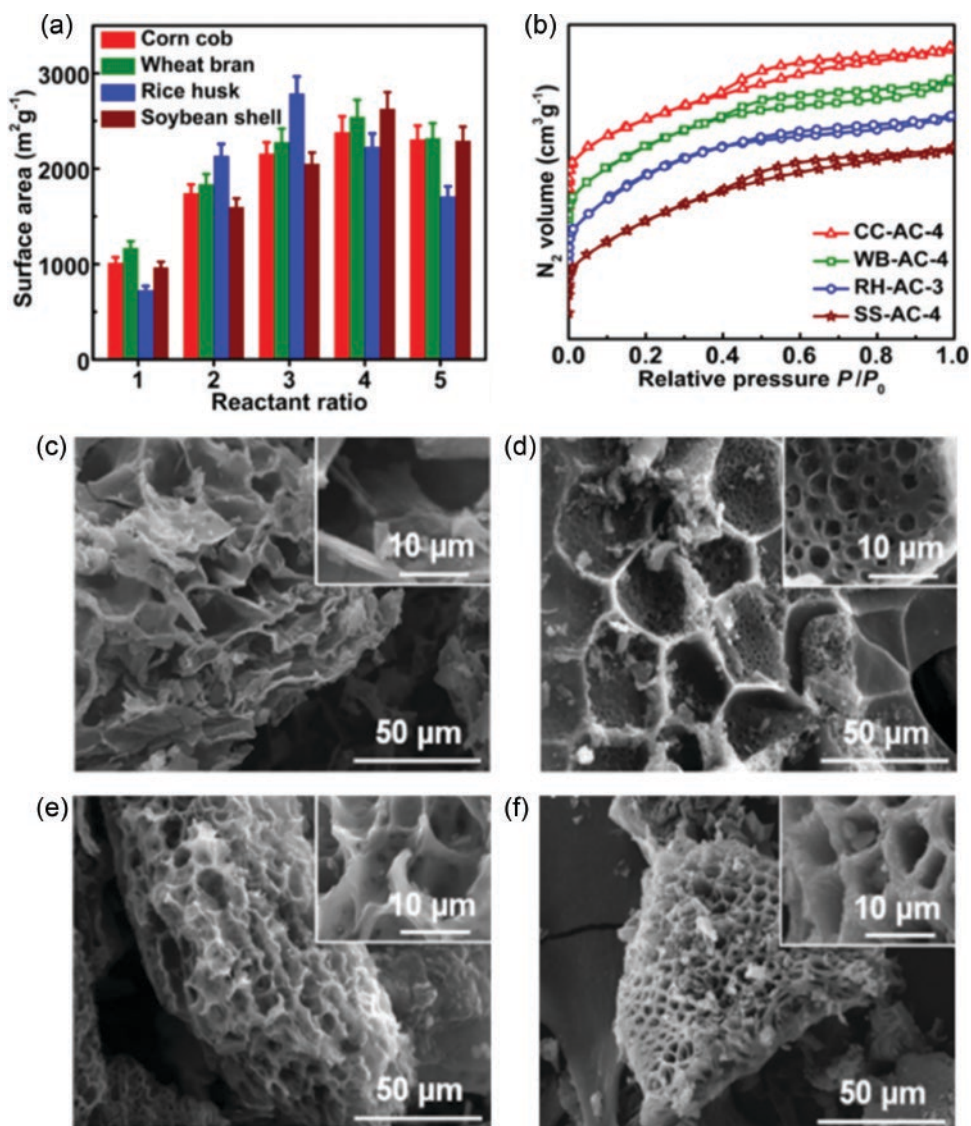
Figure 10.6 (a) Variation of the surface area of ACs prepared from CC, WB, RH and SS biomass precursors with varying NaOH: precursors ratios. (b) N_2 adsorption-desorption isotherms of the optimized ACs prepared from the precursors and their corresponding SEM images: (c) CC-AC, (d) WB-AC, (e) RH-AC and (f) SS-AC. *Adapted with permission from ref. [75] Copyright 2020, Elsevier.*

activation methods [74]. The ACs prepared by the two-step process showed better textural properties compared to the one-step process, and the corresponding surface area of the prepared ACs was 975.18 and 605.13 $m^2\ g^{-1}$, respectively. Although the NaOH activation method displayed a high surface area compared to other chemical activators (Table 10.3 and Table 10.1), such as CaO, Na_2CO_3, and $C_2H_3O_2K$, the specific surface area and porosity of ACs prepared through NaOH activation are less compared to the ACs produced via KOH

Table 10.3 Textural characteristics of AC prepared from various biomass precursors using NaOH activator.

Biomass precursors	Temperature (°C)	Time (h)	Surface area, S_{BET} (m^2 g^{-1})	pore size (nm)/pore volume (cm^3 g^{-1})	Yield (%)	Ref.
Rattan furniture wastes	600	1	1135	0.355/0.44	–	[77]
Rice husk	850	2	429.82	–/0.29	–	[78]
Rice husk	800	1	2681	–/1.4016	–	[79]
Rice husk	800	3	1828	–	–	[80]
Corncob	780	1	2474	4.2/0.949	–	[81]
Coconut shell	700	1.5	2825	2.27/1.498	18.80	[82]
Leucaena leucocephala	800	1.5	776	–	–	[83]
Date press cake	650	1.5	2025.9	–	26.2	[84]
Plum kernel	780	1	1887	2.2/1.049	–	[76]

activation. This is mainly due to the occurrence of a vigorous gasification reaction of carbon or BC with NaOH activator (Equation 10.9) [76], which decreases the porosity and accessible area in ACs.

$$4NaOH + C \rightarrow 4Na + CO_2 + 2H_2O \tag{10.9}$$

10.4 KOH and NaOH Assisted Activated Carbon for ESCs

The E_d of ESC is proportional to its C_s and the square of the operating voltage, according to the equation $E = \frac{1}{2}C_s V^2$ [85–89]. C_s relies on the type, architecture, and textural properties of electrode materials, while voltage (V) depends on electrolytes and the textural properties of the electrode materials. Thus, designing the electrode materials architecture and tuning the textural properties are considered the best approaches to enhance the C_s of ACs in ESC applications [90]. This is because ACs containing an interconnected network of macro-, meso- and micropores facilitate the rapid infiltration of electrolytes and improve the rate of electrolyte ions intercalation/deintercalation, thereby enhancing C_s and the rate capability when applied in ECS [91, 92]. A large number of reports are available on the ACs applications for ESCs (as summarized in Table 10.4), produced via KOH activation. This is because the KOH activation method can substantially tune the textural properties of ACs and improve the capacitive performance of ESCs.

From Table 10.4, it can be seen that the surface area and the capacitive performance of ACs vary with different precursors. This is because different biomass precursors contain different chemical compositions and have different properties, which affect the textural properties and the electrochemical performance [93–101]. Furthermore, the activation methods and the chemical activator types can also tune the textural properties as well as

Table 10.4 Specific capacitance, surface area, and energy density of ACs prepared by KOH activation for ESCs application.

Precursors	Surface area, S_{BET} (m^2 g^{-1})	C_s (F g^{-1})	E_d (Wh kg^{-1})	Electrolyte	Ref.
Hazelnut shells	3469	338	16.42	KOH	[93]
Oak seeds	2896	552	262.7	H$_2$SO$_4$	[94]
Tobacco waste	1875.5	356.4	10.4	KOH	[95]
Lignin	3033.88	214.03	–	KOH	[96]
Sargassum	2928.78	481	16.68 W h	KOH	[97]
Bagasse	1,861	134	–	KOH	[98]
Cluster stalks	2,662	95	–	KOH	[98]
Desmostachya bipinnata	738.56	218	19.3	KOH	[99]
Argan seed shells	2062	355	–	H$_2$SO$_4$	[100]
Corn grains	3199	257	–	KOH	[101]

the electrochemical performance of ACs. For example, Roldán et al. [102] prepared ACs from coke using KOH and NaOH activators with varying carbonization temperatures. The ACs prepared under similar carbonization conditions (700 °C) exhibited a much higher surface area (1480 m^2 g^{-1}) and improved capacitive performance for KOH activation compared to the NaOH activation with the surface area of 922 m^2 g^{-1} (Figure 10.7). This is due to the development of highly microporous structures with refined oxygen functionalities in ACs upon KOH activation compared to NaOH activation. In another report, Hoang et al. [103] prepared ACs from rice husks using KOH and NaOH activators, revealing a higher C_s value for AC prepared by KOH than the AC produced using NaOH. Generally, the ACs produced through KOH from biomass demonstrated much higher capacitive performance (Table 10.4) compared to the ACs prepared using other activators such as ZnCl$_2$ [104, 105], H$_3$PO$_4$ [106], and HNO$_3$ [107]. However, further comprehensive investigation of the ACs electrochemical performance from the same biomass precursor and under similar experimental conditions by using KOH and other chemical activators is necessary in order to get chemical and physical insights of the materials.

Compared to the KOH-assisted ACs for ESCs applications, the NaOH-assisted ACs have been investigated less. This is because activation with KOH generally shows better results than NaOH in terms of surface area, chemical functionalities, and electrochemical performance [102]. Few reports are available on the ACs preparation from biomass using NaOH activator for ESCs application, as summarized in Table 10.5. Nevertheless, the ACs created from biomass with NaOH exhibited much better electrochemical performance compared to the ACs produced by the physical activation method. For example, Alhebshi et al. [108] compared the ESC performance of ACs derived from date palm fronds, prepared by NaOH activator and physical activation by CO$_2$[108]. Results showed that the ACs assembled by using NaOH showed much higher surface area (1011 m^2 g^{-1}) and C_s (125.9 F g^{-1}), while these values for physically activated AC were 603.5 m^2 g^{-1} and 56.8 F g^{-1}, as presented in Figure 10.8. In contrast, H$_3$PO$_4$ activator-based AC derived from the rubberwood wastes
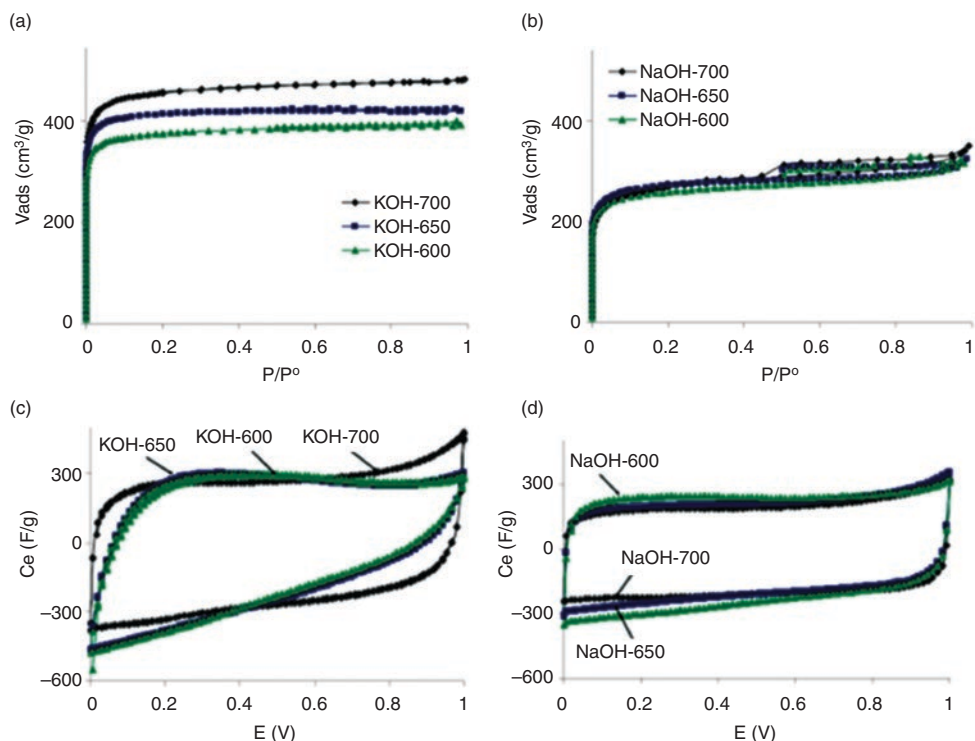
Figure 10.7 N_2 adsorption-isotherms of ACs activated with (a) KOH and (b) NaOH, and cyclic voltammograms in a two-electrode system for (c) KOH and (d) NaOH-ACs. *Reprinted with permission from ref. [102] Copyright 2010, American Chemical Society.*

Table 10.5 Specific capacitance, surface area, and energy density of ACs prepared by NaOH activation for ESCs application.

Precursors	Surface area, S_{BET} ($m^2\,g^{-1}$)	C_s ($F\,g^{-1}$)	E_d (Wh kg^{-1})	Electrolyte	Ref.
Date palm fronds	1011	125.9	–	H_2SO_4	[108]
Rubberwood wastes	429	69	–	H_2SO_4	[109]
Apricot shell	2074	339	–	KOH	[110]
Rice husk	2681	172.3	–	K_2SO_4	[79]
Sunflower stalks	2658	207	18.4	H_2SO_4	[111]

showed improved capacitive performance ($C_s = 129\ F\,g^{-1}$) and high surface area (605–693 $m^2\,g^{-1}$) compared to the NaOH activator-based AC with the C_s value of 69 $F\,g^{-1}$ and the surface area of 429 $F\,g^{-1}$ [109]. This significantly low electrochemical performance of AC derived from the rubberwood wastes and NaOH activation could be ascribed to the lower AC surface, which restricts the infiltration of electrolytes and limits the rate of electrolyte ions intercalation/deintercalation into the AC. In another report, Xu et al. developed ACs using NaOH activator from the apricot shell that exhibited a much higher surface area

(a)

(b)

(c)

(d)
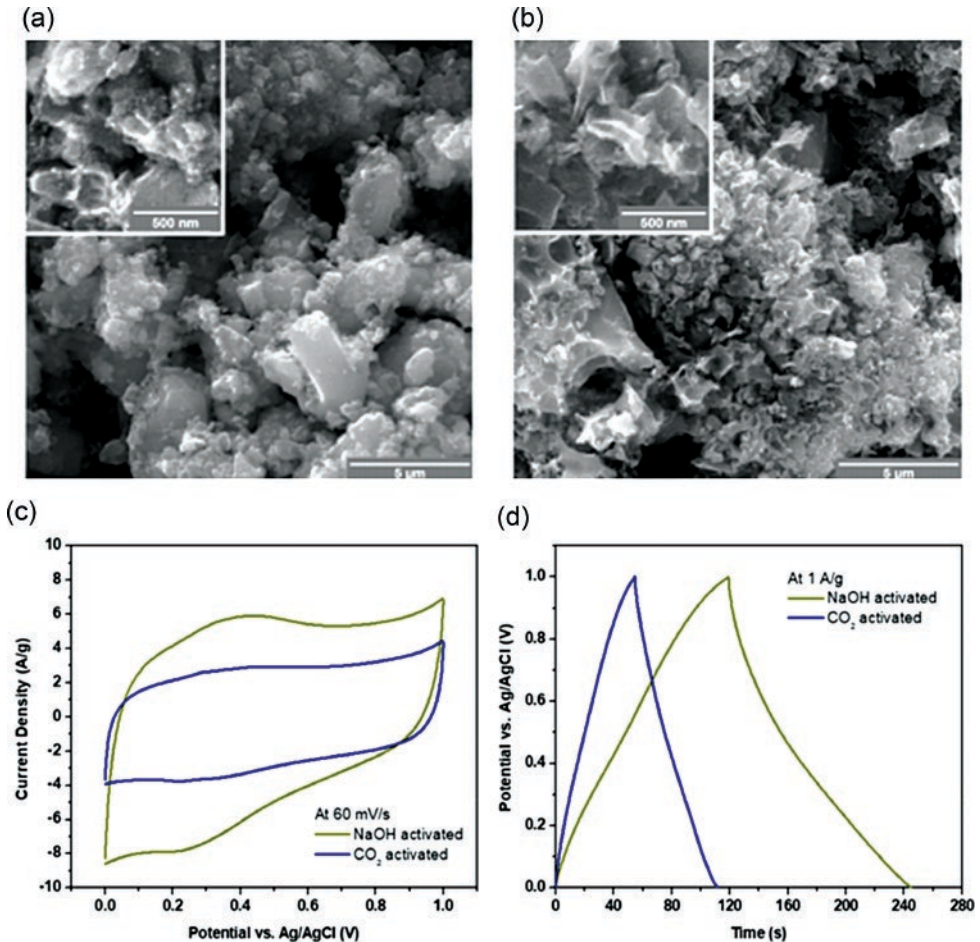
Figure 10.8   SEM images of ACs prepared from date palm fronds by (a) physical activation using CO_2 and (b) chemical activation using NaOH. (c) Cyclic voltammetry curve at 60 mV/s (d) and galvanostatic charge-discharge plot at 1 A/g for the as-prepared ESC based on CO_2 and NaOH-assisted ACs. *Adapted from ref. [108] Copyright 2022, MDPI.*

(2074 $m^2 g^{-1}$); concurrently, the AC-based ESC delivered significantly high C_s (339 F/g^{-1}) [110]. Therefore, it can be concluded that for developing high-performance ESCs based on AC composed of the NaOH activator, the choice of biomass precursor is crucial, and comparative performance analysis of ACs created from the different biomass sources using NaOH as the activator for ESC is necessary.

10.5   Conclusions

This chapter discusses the synthesis of ACs from biomass using KOH and NaOH activators and application of ACs for ESCs. A brief discussion on the structural characteristics of ACs and the synthesis methods of ACs from biomass are also presented. Although

KOH is toxic and detrimental to humans and the environment, among the alkaline chemical activators, KOH is widely used for producing ACs from biomass with many micropores, high specific surface area, and abundant –OH functional group. Accordingly, the KOH-assisted ACs-modified electrodes deliver high electrochemical performance when applied in ESCs compared to the ACs prepared by other chemical activators. Even though the NaOH activator is cheaper, more environmentally friendly, and less toxic than KOH, the ACs developed thought the NaOH activation have been investigated less for use in ESCs applications. This is mainly due to the reduced textural and chemical functionalities of ACs arranged by the NaOH activation compared to the ACs prepared through KOH activation. Nevertheless, the ESCs performance of the NaOH-assisted ACs is much better than physical (CO_2) activation-based ACs, and their textural and chemical functionalities are highly dependent on the chemical compositions of biomass. Therefore, further development of the NaOH-assisted ACs by selecting a suitable biomass precursor and the performance analyses in the ESCs is necessary. The authors are confident that this book chapter can guide the researchers in understanding the fundamentals of ACs, chemical activation methods, and the stepwise development of the KOH and NaOH-assisted ACs as electrode materials for ESCs.

Acknowledgments

References

1 J. Zhao, A. F. Burke, *J. Energy Chem.* **2021**, *59*, 276–291.

2 H. R. Barai, N. S. Lopa, F. Ahmed, N. A. Khan, S. A. Ansari, S. W. Joo, M. M. Rahman, *ACS Omega* **2020**, *5*, 22356–22366.

3 H. R. Barai, M. M. Rahman, S. W. Joo, *Electrochim. Acta* **2017**, *253*, 563–571.

4 S. A. Ansari, N. A. Khan, Z. Hasan, A. A. Shaikh, F. K. Ferdousi, H. R. Barai, N. S. Lopa, M. M. Rahman, *Sust. Energy Fuels.* **2020**, *4*, 2480–2490.

5 H. R. Barai, M. M. Rahman, S. W. Joo, *J. Power Sources* **2017**, *372*, 227–234.

6 S. S. Shah, S. M. A. Nayem, N. Sultana, A. J. S. Ahammad, M. A. Aziz, *ChemSusChem* **2022**, *15*, e202101282.

7 H. R. Barai, M. M. Rahman, M. Adeel, S. W. Joo, *Mater. Res. Bull.* **2022**, *148*, 111678.

8 P. Sharma, T. S. Bhatti, *Energy Convers. Manag.* **2010**, *51*, 2901–2912.

9 M. Ashraf, S. S. Shah, I. Khan, M. A. Aziz, N. Ullah, M. Khan, S. F. Adil, Z. Liaqat, M. Usman, W. Tremel, M. N. Tahir, *Chem. Eur. J.* **2021**, *27*, 6973–6984.

10 S. S. Shah, M. A. Alfasane, I. A. Bakare, M. A. Aziz, Z. H. Yamani, *J. Energy Storage* **2020**, *30*, 101562.

11 C. Zhong, Y. Deng, W. Hu, J. Qiao, L. Zhang, J. Zhang, *Chem. Soc. Rev.* **2015**, *44*, 7484–7539.

12 J. Wang, S. Dong, B. Ding, Y. Wang, X. Hao, H. Dou, Y. Xia, X. Zhang, *Natl. Sci. Rev.* **2017**, *4*, 71–90.

13 S. Ghosh, R. Santhosh, S. Jenifer, V. Raghavan, G. Jacob, K. Nanaji, P. Kollu, S. K. Jeong, A. N. Grace, *Sci. Rep.* **2019**, *9*, 16315.

14 S. S. Shah, M. A. Aziz, E. Cevik, M. Ali, S. T. Gunday, A. Bozkurt, Z. H. Yamani, *J. Energy Storage* **2022**, *56*, 105944.

15 S. S. Shah, H. T. Das, H. R. Barai, M. A. Aziz, *Polymers* **2022**, *14*, 270.

16 N. M. Nor, L. L. Chung, L. K. Teong, A. R. Mohamed, *J. Environ. Chem. Eng.* **2013**, *1*, 658–666.

17 X. Cui, F. Jia, Y. Chen, J. Gan, *Ecotoxicology* **2011**, *20*, 1277–1285.

18 N. Khadhri, M. E. K. Saad, M. B. Mosbah, Y. Moussaoui, *J. Environ. Chem. Eng.* **2019**, *7*, 102775.

19 J. Ouyang, L. Zhou, Z. Liu, J. Y. Y. Heng, W. Chen, *Sep. Purif. Technol.* **2020**, *253*, 117536.

20 S. S. Shah, M. A. Aziz, *Bangladesh J. Plant Taxon.* **2020**, *27*, 467–478.

21 M. R. Akanda, A. Bibi, M. A. Aziz, *ChemistrySelect* **2021**, *6*, 6714–6732.

22 S. A. Hira, M. Yusuf, D. Annas, H. S. Hui, K. H. Park, *Processes* **2020**, *8*, 926.

23 K. Konieczny, G. Klomfas, *Desalination* **2002**, *147*, 109–116.

24 S. Wong, N. Ngadi, I. M. Inuwa, O. Hassan, *J. Clean. Prod.* **2018**, *175*, 361–375.

25 S. S. Shah, M. A. A. Qasem, R. Berni, C. Del Casino, G. Cai, S. Contal, I. Ahmad, K. S. Siddiqui, E. Gatti, S. Predieri, J.-F. Hausman, S. Cambier, G. Guerriero, M. A. Aziz, *Sci. Rep.* **2021**, *11*, 6945.

26 M. S. Shafeeyan, W. M. A. W. Daud, A. Houshmand, A. Shamiri, *J. Anal. Appl. Pyrolysis* **2010**, *89*, 143–151.

27 S. S. Shah, M. N. Shaikh, M. Y. Khan, M. A. Alfasane, M. M. Rahman, M. A. Aziz, *Chem. Rec.* **2021**, *21*, 1631–1665.

28 H. Jüntgen, *Fuel* **1986**, *65*, 1436–1446.

29 M. Bora, D. Bhattacharjya, B. K. Saikia, *Energy Fuels* **2021**, *35*, 18285–18307.

30 K. D. M. S. P. K. Kumarasinghe, G. R. A. Kumara, R. M. G. Rajapakse, D. N. Liyanage, K. Tennakone, *Org. Electron.* **2019**, *71*, 93–97.

31 L. S. Rocha, D. Pereira, É. Sousa, M. Otero, V. I. Esteves, V. Calisto, *Sci. Total Environ.* **2020**, *718*, 137272.

32 Z. Heidarinejad, M. H. Dehghani, M. Heidari, G. Javedan, I. Ali, M. Sillanpää, *Environ. Chem. Lett.* **2020**, *18*, 393–415.

33 T. S. Hui, M. A. A. Zaini, *Carbon Lett* **2015**, *16*, 275–280.

34 B. Sajjadi, W.-Y. Chen, N. O. Egiebor, *Rev. Chem. Eng.* **2018**, *35*, 735–776.

35 A. M. Abioye, F. N. Ani, *Renew. Sust. Energy Rev.* **2015**, *52*, 1282–1293.

36 R. E. Franklin, *Proc. R. Soc. A* **1951**, *209*, 196–218.

37 D. B. Schuepfer, F. Badaczewski, J. M. Guerra-Castro, D. M. Hofmann, C. Heiliger, B. Smarsly, P. J. Klar, *Carbon* **2020**, *161*, 359–372.

38 S. Ergun, V. H. Tiensuu, *Acta Crystallogr.* **1959**, *12*, 1050–1051.

39 S. Ergun, L. E. Alexander, *Nature* **1962**, *195*, 765–767.

40 D. F. R. Mildner, J. M. Carpenter, *J. Non-Cryst. Solid* **1982**, *47*, 391–402.

41 P. J. F. Harris, Z. Liu, K. Suenaga, *J. Phys. Condens. Matter.* **2008**, *20*, 362201.

42 Y. X. Gan, *C* **2021**, *7*, 39.

43 M. Kumar, R. Tamilarasan, *J. Environ. Chem. Eng.* **2013**, *1*, 1108–1116.

44 M. Danish, R. Hashim, M. N. M. Ibrahim, M. Rafatullah, T. Ahmad, O. Sulaiman, *BioResources* **2011**, *8*, 3019–3033.

45 M. Danish, R. Hashim, M. N. M. Ibrahim, M. Rafatullah, T. Ahmad, O. Sulaiman, *Wood Sci. Technol.* **2014**, *48*, 1085–1105.

46 T. B. Gupta, D. H. Lataye, *J. Hazard. Toxic Radioac. Waste* **2017**, *21*, 04017013.

47 M. Zbair, K. Ainassaari, A. Drif, S. Ojala, M. Bottlinger, M. Pirila, R. L. Keiski, M. Bensitel, R. Brahmi, *Environ. Sci. Pollut. Res.* **2018**, *25*, 1869–1882.

48 L. Niazi, A. Lashanizadegan, H. Sharififard, *J. Clean. Prod.* **2018**, *185*, 554–561.

49 Y. Bian, Q. Yuan, G. Zhu, B. Ren, A. Hursthouse, P. Zhang, *Int. J. Polym. Sci. 2018* **2018**, 1–17.

50 B. Dass, P. Jha, *Artic. Int. J. Chem. Tech. Res.* **2015**, *8*, 269–279.

51 D. Shrestha, G. Gyawali, A. R. Rajbhandari, *J. Hazard. Mater.* **2009**, *165*, 481–485.

52 S. A. Sajjadi, A. Mohammadzadeh, H. N. Tran, I. Anastopoulos, G. L. Dotto, Z. R. Lopicic, S. Sivamani, A. Rahmani-Sani, A. Ivanets, A. Hosseini-Bandegharaei, *J. Environ. Manag.* **2018**, *223*, 1001–1009.

53 M. J. Ahmed, *J. Environ. Chem. Eng.* **2016**, *4*, 89–99.

54 S. K. Theydan, M. J. Ahmed, *J. Anal. Appl. Pyrol.* **2012**, *97*, 116–122.

55 G. Jaria, C. P. Silva, J. A. B. P. Oliveira, S. M. Santos, M. V. Gil, M. Otero, V. Calisto, V. I. Esteves, *J. Hazard. Mater.* **2019**, *370*, 212–218.

56 J. Kong, R. Gu, J. Yuan, W. Liu, J. Wu, Z. Fei, Q. Yue, *Ecotoxicol. Environ. Saf.* **2018**, *156*, 294–300.

57 J. M. Dias, M. C. M. Alvim-Ferraz, M. F. Almeida, J. Rivera-Utrilla, M. Sanchez-Polo, *J. Environ. Manag.* **2007**, *85*, 833–846.

58 M. I. Din, S. Ashraf, A. Intisar, *Sci. Prog.* **2017**, *100*, 299–312.

59 O. Oginni, K. Singh, G. Oporto, B. Dawson-Andoh, L. McDonald, E. Sabolsky, *Bioresour. Technol. Rep.* **2019**, *7*, 100266.

60 A. H. Basta, V. Fierro, H. El-Saied, A. Celzard, *Bioresour. Technol.* **2009**, *100*, 3941–3947.

61 M. J. Ahmed, S. K. Theydan, *J. Anal. Appl. Pyrolysis* **2014**, *105*, 199–208.

62 H. Tounsadi, A. Khalidi, M. Farnane, M. Abdennouri, N. Barka, *Process Saf. Environ. Prot.* **2016**, *102*, 710–723.

63 L. Spessato, K. C. Bedin, A. L. Cazetta, I. P. A. F. Souza, V. A. Duarte, L. H. S. Crespo, M. C. Silva, R. M. Pontes, V. C. Almeida, *J. Hazard. Mater.* **2019**, *371*, 499–505.

64 P. C. Bhomick, A. Supong, R. Karmaker, M. Baruah, C. Pongener, D. Sinha, *Korean J. Chem. Eng.* **2019**, *36*, 551–562.

65 A. H. Jawad, A. S. Abdulhameed, N. N. Bahrudin, N. N. M. F. Huma, S. N. Surip, S. S. A. Syed-Hassan, E. Yousif, S. Sabar, *Water Sci. Technol.* **2021**, *84*, 1858–1872.

66 J. Hou, Y. Liu, S. Wen, W. Li, R. Liao, L. Wang, *ACS Omega* **2020**, *5*, 13548–13556.

67 J. Han, J. H. Lee, K. C. Roh, *J. Electrochem. Sci. Technol.* **2018**, *9*, 157–162.

68 O. Bag, K. Tekin, S. Karagoz, *Fuller. Nanotub. Carbon Nanostructures* **2020**, *28*, 1030–1037.

69 A. E. Ogungbenro, D. V. Quang, K. A. Al-Ali, L. F. Vega, M. R. M. Abu-Zahra, *J. Environ. Chem. Eng.* **2020**, *8*, 104257.

70 M. Gale, T. Nguyen, M. Moreno, K. L. Gilliard-AbdulAziz, *ACS Omega* **2021**, *6*, 10224–10233.

71 A. Basta, V. Fierro, H. El-Saied, A. Celzard, *Bioresour. Technol.* **2009**, *100*, 3941–3947.

72 A. T. M. Din, B. Hameed, A. L. Ahmad, *J. Hazard. Mater.* **2009**, *161*, 1522–1529.

73 J. Li, D. H. L. Ng, P. Song, C. Kong, Y. Song, P. Yang, *Biomass Bioenergy* **2015**, *75*, 189–200.

74 S. Wanprakhon, P. Sukcharoen, S. Krongchai, *J. Mater. Sci. Appl. Energy* **2022**, *11*, 9–15.

75 Y. Zhang, X. Song, P. Zhang, H. Gao, C. Ou, X. Kong, *Chemosphere* **2020**, *245*, 125587.

76 R.-L. Tseng, *J. Hazard. Mater.* **2007**, *147*, 1020–1027.

77 M. A. Islam, M. J. Ahmed, W. A. Khanday, M. Asif, B. H. Hameed, *Ecotoxicol. Environ. Saf.* **2017**, *138*, 279–285.

78 M. J. Saad, C. C. Hua, S. Misran, S. Zakaria, M. Saiful Sajab, M. H. A. Rahman, *Sains Malays.* **2020**, *49*, 2261–2267.

79 K. L. Vann, T. T. L. Thi, *Prog. Nat. Sci. Mater. Int.* **2014**, *24*, 191–198.

80 A. F. Hassan, A. M. Youssef, *Carbon Lett.* **2014**, *15*, 57–66.

81 R.-L. Tseng, *J. Colloid Interface Sci.* **2006**, *303*, 494–502.

82 A. L. Cazetta, A. M. M. Vargas, E. M. Nogami, M. H. Kunita, M. R. Guilherme, A. C. Martins, T. L. Silva, J. C. G. Moraes, V. C. Almeida, *Chem. Eng. J.* **2011**, *174*, 117–125.

83 W. M. H. W. Ibrahim, M. H. M. Amini, N. S. Sulaiman, W. R. W. A. Kadir, *Appl. Water Sci.* **2021**, *11*, 1.

84 S. Norouzi, M. Heidari, V. Alipour, O. Rahmanian, M. Fazlzadeh, F. Mohammadi-moghadam, H. Nourmoradi, B. Goudarzi, K. Dindarloo, *Bioresour. Technol.* **2018**, *258*, 48–56.

85 N. S. Lopa, M. K. Akbari, S. Zhuiykov, *Electrochim. Acta.* **2022**, *434*, 141322.

86 H. R. Barai, M. M. Rahman, N. S. Lopa, P. Barai, S. W. Joo, *J. Electrochem. Soc.* **2020**, *167*, 126516.

87 H. R. Barai, N. S. Lopa, P. Barai, M. M. Rahman, A. K. Sarker, S. W. Joo, *J. Mater. Sci. Mater. Electron.* **2019**, *30*, 21269–21277.

88 H. R. Barai, M. M. Rahman, M. Roy, P. Barai, S. W. Joo, *Mater. Sci. Semicond. Process.* **2019**, *90*, 245–251.

89 H. R. Baraia, M. M. Rahman, A. Rahim, S. W. Joo, *J. Ind. Eng. Chem.* **2019**, *79*, 115–123.

90 T. Wang, S. Hu, D. Wu, W. Zhao, W. Yu, M. Wang, J. Xu, J. Zhang, *J. Mater. Chem. A* **2021**, *9*, 11839–11852.

91 N. Guo, W. Luo, R. Guo, D. Qiu, Z. Zhao, L. Wang, D. Jia, J. Guo, *J. Alloy. Compd.* **2020**, *834*, 155115.

92 X. Yang, Y. Li, P. Zhang, L. Sun, X. Ren, H. Mi, *Carbon* **2020**, *157*, 70–79.

93 Y. Liu, P. Liu, L. Li, S. Wang, Z. Pan, C. Song, T. Wang, *J. Electroanal. Chem.* **2021**, *903*, 115828.

94 S. A. Borghei, M. H. Zare, M. Ahmadi, M. H. Sadeghi, A. Marjani, S. Shirazian, M. Ghadiri, *Arab. J. Chem.* **2021**, *14*, 102958.

95 Z. Huang, C. Qin, J. Wang, L. Cao, Z. Ma, Q. Yuan, Z. Lin, P. Zhang, *Materials* **2021**, *14*, 1714.

96 L. Wang, X. Feng, X. Li, H. Wang, J. Wu, H. Ma, J. Zhou, *J. Mater. Res. Technol.* **2022**, *16*, 570–580.

97 F. Guo, Y. Zhan, X. Jia, H. Zhou, S. Liang, L. Qian, *New J. Chem.* **2021**, *45*, 15514–15524.

98 L. Alcaraz, A. Adán-Más, P. Arévalo-Cid, M. de Fatima Montemor, F. A. López, *Front. Chem.* **2020**, *8*, 686.

99 G. K. Gupta, P. Sagar, S. K. Pandey, M. Srivastava, A. K. Singh, J. Singh, A. Srivastava, S. K. Srivastava, A. Srivastava, *Nanoscale Res. Lett.* **2021**, *16*, 85.

100 A. Elmouwahidi, Z. Zapata-Benabithe, F. Carrasco-Marin, C. Moreno-Castilla, *Bioresour. Technol.* **2012**, *111*, 185–190.

101 M. S. Balathanigaimani, W. G. Shim, M. J. Lee, C. Kim, J. W. Lee, H. Moon, *Electrochem. Commun.* **2008**, *10*, 868–871.

102 S. Roldán, I. Villar, V. Ruiz, C. Blanco, M. Granda, R. Menendez, R. Santamaria, *Energy Fuels* **2010**, *24*, 3422–3428.

103 K. L. Vana, T. L. T. Thua, H. N. T. Thua, H. V. Hoang, *Russ. J. Electrochem.* **2019**, *55*, 900–907.

104 C. Wang, T. Liu, *J. Alloy Compd.* **2017**, *696*, 42–50.

105 E. Taer, T. E. Sugianti, Apriwandi, A. S. Rini, U. Malik, R. Taslim, *J. Phys. Conf. Ser.* **2021**, *2049*, 012007.

106 T. K. Trinh, T. Tsubota, S. Takahashi, N. T. Mai, M. N. Nguyen, N. H. Nguyen, *Sci. Rep.* **2020**, *10*, 19974.

107 Y.-R. Nian, H. Teng, *J. Electrochem. Soc.* **2002**, *149*, A1008–A1014.

108 N. A. Alhebshi, N. Salah, H. Hussain, Y. N. Salah, J. Yin, *Nanomaterials* **2022**, *12*, 122.

109 U. Thubsuang, S. Laebang, N. Manmuanpom, S. Wongkasemjit, T. Chaisuwan, *J. Mater. Sci.* **2017**, *52*, 6837–6855.

110 B. Xu, Y. Chen, G. Wei, G. Cao, H. Zhang, Y. Yang, *Mater. Chem. Phys.* **2010**, *124*, 504–509.

111 A. Yürüm, *Hacettepe J. Biol. Chem.* **2019**, *47*, 235–247.

11

Chloride Salt-activated Carbon for Supercapacitors

Eman Gul[1], Syed Adil Shah[2], and Syed Niaz Ali Shah[3],*

[1] *Institute of Chemical Sciences, University of Peshawar, Peshawar Pakistan*
[2] *National Laboratory of Solid-States Microstructures, Department of Physics, Nanjing University, Nanjing China*
[3] *Center for Integrative Petroleum Research, King Fahad University of Petroleum and Minerals, Dhahran, Saudi Arabia*
* Corresponding author

11.1   Introduction

The excessive usage of non-renewable energy resources and the consequential creation of greenhouse gases is the most alarming issue in the rapidly growing world. The energy crisis is a significant bottleneck in meeting the world's energy requirements [1]. To meet the need for energy requirements and to protect the world from the life-threatening effects of greenhouse gases, researchers are working on a serious note to address this problem by utilizing environmentally-sound sustainable energies like wind, solar, and biomass [2]. Because of their high power density, quick charge-discharge, and long lifetime, supercapacitors (SC) are the most commonly used type of energy storage in a variety of applications, including medical applications, consumer electronics, pure electric vehicles (PEVs), and hybrid electric vehicles (HEVs) [3, 4]. The power source, polarized electrode, collector, Helmholtz double layer, electrolyte with negative and positive ions, and separator are the key components of a supercapacitor. Supercapacitors use electrostatic forces to store electric charges at the electrode–electrolyte interface [5]. Carbon materials are commonly used as an electrode in supercapacitors due to their properties like high surface area, high electrical conductivity, and better thermal stabilities [6]. Electrical double-layer capacitance (EDLC) is the storage mechanism in supercapacitors [7].

To advance commercialization of supercapacitors, cost-effective biomass waste is vital. Andrew Burke's studies show that in a carbon-based supercapacitor, 60% of supercapacitor cost is due to carbon, where 0.1 cent/F is due to the electrode material. In contrast, only around 0.001cent/F is due to biochar-derived electrode material. Hence, using biomass-derived carbonaceous material can reduce the cost for large supercapacitor applications and increase associated revenues [8, 9]. Also, supercapacitors derived from biomass have almost the same capacitance as conventional supercapacitors.

Over the last few years, much work has been done in studying carbonaceous materials due to their tremendous electrochemical storage of energy [10, 11]. Carbon exists in many

allotropic forms and structures, and its different dimensionality from 0 to 3D makes it suitable for supercapacitors [12]. Carbon has an amphoteric nature which enables the usage of its electrochemical properties from donor to acceptor state [13]. Carbon materials are not harmful [14].

Most of the electrodes are prepared from carbonaceous materials due to their cost-effectiveness, easy availability, and ease of handling. Carbonaceous materials are stable in alkali and alkaline solutions [15] and operate effectively at a broad temperature range. For electrochemical applications, the electrode–electrolyte interface is largely determined by the materials used to synthesize it. These materials can be synthesized with a high surface area and precisely controlled pore size and volume via various physical and chemical activation techniques [16].

Many chemical agents have been used to activate carbonaceous materials, such as some acids, bases, and salts. Chloride salts are much used as chemical agents for activating carbon materials due to their easy availability, cheapness, and eco-friendliness. For example, Xiang *et al.* prepared an activated carbon electrode for supercapacitors from polyaniline by using $ZnCl_2$ as activating agent [17]. Among carbon materials, activated carbon is widely used, as the activating agents utilized for them are cost-effective, and their synthesis method is relatively simple. In the following sections we will discuss biomass-derived activated carbon materials, using chloride salts as activation agents, which have been used as electrode materials for supercapacitors.

11.2 Biomass-derived Carbon Materials for Supercapacitors

In electrical double-layer capacitance (EDLC), the electrode surface area is the most important aspect [18]. Different carbonaceous materials are given in the literature as electrode materials. Among them, active carbons have shown to have remarkable properties [19–21]. It is well known that carbonaceous materials have a high surface area compared to metal oxides, phosphides, and sulfides [22–24]. Activated carbons often have increased porosity, chemical, and thermal stability, packing density, and surface area. Biomass is plant and animal-derived organic material that can be utilized as an energy source [25, 26]. Figure 11.1 shows the conversion of different biomasses into carbon materials for their application in supercapacitors [27]. Activated carbons (AC) utilized as electrodes for supercapacitors are usually acquired from renewable resources, biowastes, neem leaves, jute sticks, banana leaves, sawdust, bamboo, coconut shell, and seaweeds [28–39].

Various biomasses, such as coconut shells, pitch, coal, tea leaves, polymers, cellulose, etc., are used to synthesize activated carbon [40, 41]. Biomass has been broadly explored as a carbon source due to its large quantity, cheapness, and easy accessibility compared to other sources. Biomass can be converted to conducting carbonaceous materials, which is a cost-effective and resourceful way of recycling biomasses [30, 34, 42–45]. Although certain carbon materials, like carbon nanotubes (CNTs) and graphene, have high capacitance, they are prohibitively expensive due to difficult production procedures and insufficient precursors, limiting the viability of large-scale use. Although carbon is broadly employed, it has the limitation of specific capacitance compared to conducting polymers and metal oxides [46, 47].
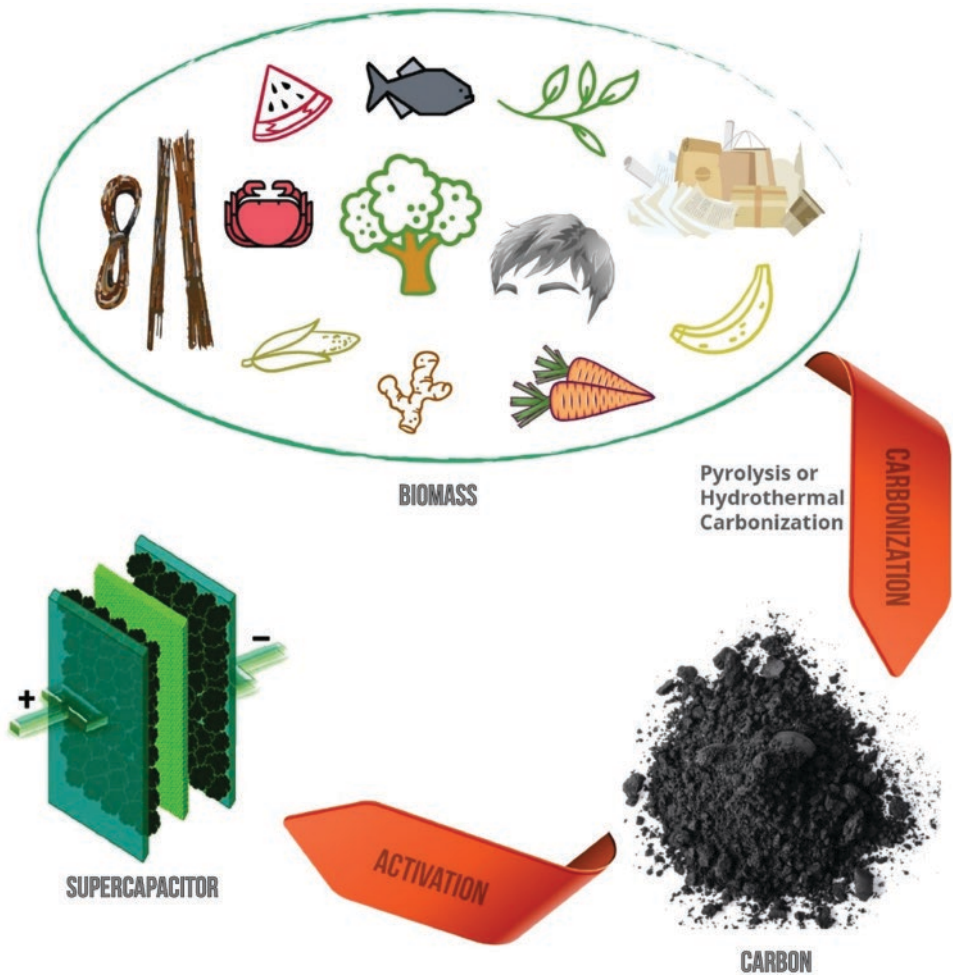
Figure 11.1 Conversion of different biomasses into carbon materials for their application in supercapacitors.

11.3 Methods of Converting Biomass to Carbon for Supercapacitors

Different methods can be employed to derive carbon from biomass, such as pyrolysis and hydrothermal carbonization, followed by its activation [48]. The detail of this can be seen in Figure 11.2a. Optimizing parameters, i.e., temperature, pressure, chemicals involved, and time for synthesizing carbon materials, can enhance its surface area, porosity, and morphology.

Biomass pyrolysis is executed in an inert or low oxygen level atmosphere at high temperatures [31, 33, 36, 37, 45, 49–51]. This method can produce porous carbon with a large pore volume and a high surface area [20, 52]. Studies have shown that pyrolysis can produce carbon with enhanced properties without activating them. B'eguin *et al.* demonstrated
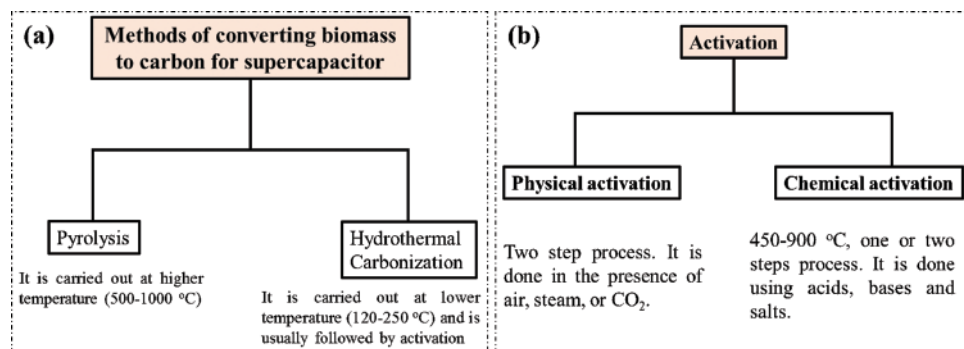
Figure 11.2 (a) The biomass conversion methods. (b) Different methods of activation of carbonaceous materials.

a carbonaceous electrode with an enhanced surface area for SC derived from waste sea-weeds without activation [53–56]. The factors such as temperature, particle size, and the catalyst used influence the product obtained [57].

Hydrothermal carbonization (HC) is a thermochemical process that is applied to derive carbon materials from biomass. HC is carried out at low temperatures, usually between 120 and 250 °C, under pressure in an aqueous environment [58], with or without the assistance of a catalyst [59]. It is similar to the natural coalification of biomass, but the reaction rate is fast compared to coalification [60]. Many factors influence HC, like temperature, precursor concentration, residence time, and catalyst. The application of HC for the derivation of biomass into carbonaceous materials has gained substantial interest for numerous uses, such as catalysis [61, 62], CO_2 capture [63, 64], and energy storage [65, 66]. The carbonaceous product obtained from the HC process is called "hydrochar", which is rich in oxygen-containing groups [67]. The product obtained from HC is poor in porosity with low surface area, so activation of the surface of carbon material after HC is necessary [68–70].

11.4 Improving the Specific Capacitance Performance of Carbon Materials

The effective surface area of the electrode materials determines the supercapacitors' capacity to store charges and their specific capacitance.This section describes increasing the surface area of electrode materials by improving their porous structure via physical and chemical methods. The process of making carbon active by making materials porous and improving surface area is called "activation of carbon" and the carbon is called "activated carbon" (AC). The activation of carbon can be done both by physical and chemical means to obtain biomass-derived ACs, as can be seen in Figure 11.2b [71]. Physical activation is less complicated and less harmful to the environment but requires a high temperature. Chemical activation is currently the most popular method due to its many advantages. These include a lower activation temperature, faster activation time, higher yield, larger surface area, and well-developed pores. The chemical activation method has

some disadvantages, including the necessity of water cleansing after activation to remove contaminants produced during the process and subsequent management of the polluted water [72, 73].

The activating strategies, such as physical or chemical methods, make it difficult to construct the special architecture of carbon materials such as carbon nanosheets or networks [74]. Preparing 2D carbon materials by 2D space-confined method [75] or CVD or template method can be costly and not environmentally friendly [76]. Therefore, the molten salt activation method is becoming the common approach for synthesizing 2D carbon materials [77, 78].

The physical activation or thermal activation of carbon materials typically happens at high temperatures (700 to 1100 °C) in the presence of carbon dioxide or water steam to form porous structures internally and externally. During the activation of carbon materials initially, the pore opens, clogged by excessive carbon atoms and other heteroatoms. In the second stage the carbon in the elementary crystals reacts with oxidative gas at the surface to generate gaseous oxides. In the final stage the existing micropores are continually enlarged, and the walls between adjacent micropores entirely collapse to generate larger pores [79, 80].

Chemical activation happens at a slightly low temperature along with the use of activating agents such as KOH, $ZnCl_2$, NH_3, $NaNO_3$, etc. Washing the carbon after activation is necessary to remove residual reactants (also known as ash) that come from the carbon precursors or have been introduced during activation [81]. Kim *et al.* produced carbon using walnut shells as a raw material [82]. The produced carbon was activated by using $ZnCl_2$ as an activating agent through a chemical activation method.

According to the International Union of Pure and Applied Chemistry (IUPAC), pore sizes can be grouped as macroporous (>50 nm), mesoporous (2–50 nm), and microporous (<2 nm) [83]. Pore size distribution is a key characteristic of charged ion adsorption. Nowadays, there is much interest in carbon as an electrode material as it can be turned into a form with a high surface area with improved porous structures [84, 85]. Increasing surface area and improving the porous structure of carbon organic materials is generally stated as "activation" and the resulting materials are called activated carbons [86]. Chars, for example, have a very small pore size and a structure composed of primary crystallites with a significant number of interstices between them, the majority of which are filled with "disorganized" carbon residues (tars) that block the pores.

Activation clears these pores and can additionally produce extra porosity. Changing the carbonaceous organic materials and activation parameters such as time, temperature, and gaseous environment can govern the subsequent porosity, the nature of the internal surfaces, and pore-size distribution. Carbonaceous materials can be activated by two general methods, i.e., thermal activation and chemical activation. Carbon electrode materials having a porous structure, a high specific surface area (SSA), and an optimum pore size distribution are proven to have greater capacitance at high current densities [87, 88]. Many studies have shown that the micropores are the most active in the double-layer formation process while decreasing the rate of ion transport to some degree [89]. Mesopores minimize ion diffusion resistance, while macropores aid in establishing ion buffering reservoirs, hence reducing ion transit distance after electrolyte penetration. Numerous studies have been conducted on the combinations of different pore size distributions and pore volumes [90].

Figure 11.3 Synthesis of biomass-derived hierarchically porous carbon materials. *Reproduced with permission [93]. Copyright 2020, Elsevier.*

The combined effects of multiple porous morphologies can enhance charge transfer and an ion diffusion process. As a result, making electrodes from such materials allows for ion transport affinity and excellent capacitance of SCs. Furthermore, the linked mesopores minimize low resistance ion diffusion pathways at the surface of the inner pore, and the large space of macropores can enhance the potential electrostatic adsorption area, enhancing SC rate capacity [91]. Moreover, the hierarchically macroporous and mesoporous combinations not only allow free ion contact to the inner or outer surface of materials and transport across channels, which is satisfactory for the diffusion of electrolyte and electrochemical reactions, but also offer a large specific surface area for high mass loading of the electroactive materials. It's worth noting that charges are stored in nanopores that are conducive to confinement [92, 93]. The synthesis of biomass-derived hierarchically porous carbon materials is shown in Figure 11.3. Methods to manufacture spongy materials are vital for maximizing the electrochemical performance of SCs [91]. Furthermore, because of their unique mechanical, electrical, and thermal conductivity properties, numerous micro/nanoscale materials have become standard electrode materials [94–100].

11.5 Chloride Salt-activated Carbon

In this section, chloride salt-activated carbon materials for supercapacitors will be discussed. The main properties, synthesis methods, and electrochemical properties will be presented for each chloride salt-activated carbon. AC has also been extensively utilized in supercapacitors because of its low cost, large specific surface area, and relatively good electrical property, making it feasible to commercialize. Various activating agents have been reported in the literature, such as $ZnCl_2$, KOH, NaOH, and H_3PO_4, among others, for producing porous carbon materials.

11.5.1 Preparation and Electrochemical Performance of Biomass-derived Activated Carbon Using Chloride-based Activation Agents

The properties of biomass-derived carbon, i.e., porosity type, specific surface area (SSA), and morphology, depend on the activating agent used. Numerous activating agents have been utilized, and each type develops diverse sorts of morphologies with different pore sizes due to their different activating mechanisms. Other activation agents like KOH or H_3PO_4 are very strong acids and bases. The handling of these materials needs precautionary measures as these materials are corrosive, which increases the steps in the preparation. Also, these harsh agents can dissolve the organic part of biomass, making the activation process difficult. Chloride salts-activated carbonaceous materials, have been given much attention in recent years. The use of chloride salt has some advantages over other typically used chemical activating agents. For example, it has easy availability, low cost, and is environmentally benign. Table 11.1 shows the effect of different activating agents on the electrochemical properties of SC.

Table 11.1 The effect of various activating agents on the structural and electrochemical properties of carbon generated from biomass.

Raw material	Activation agent	Pore Size $(cm^3 g^{-1})$	Surface area $(m^2 g^{-1})$	Specific capacitance $(F g^{-1})$	Current Density $(A g^{-1})$	Ref.
Rotten carrot	$ZnCl_2$	-	-	135.5	1	[105]
Cotton	$ZnCl_2$	1.23	1990	240	1	[107]
1H-Benzotriazole (BTA)	$ZnCl_2$	-	1228	332	0.5	[108]
4-(4-nitrophenylazo) resorcinol	$ZnCl_2$	0.54	891.1	431.5	1	[110]
Rapeseed dregs	$ZnCl_2$	-	1416.966	170.5	1	[111]
Ginkgo leaf	$CaCl_2/KCl$	-	-	150.4	0.05	[117]
Walnut shells	KCl	-	1958	233.7	0.1	[115]
Mung bean	$CaCl_2$ + urea	-	-	300.5	1	[121]
Java kapok tree shell	(NaCl: KCl) (1: 1)	0.439	1260	169	1	[116]
Waste coffee grounds	$FeCl_3$	-	846	57	-	[113]
Moringa oleifera stem	$ZnCl_2$: $FeCl_3$ (1:3)	2.3	2250	283	0.5	[119]
Coconut shell	$ZnCl_2$	1.21	1874	268	1	[112]
Peanut shells	$FeCl_3/MgCl_2$	-	1401.4	247	1	[122]
Lithium chloride-doped polyaniline	PAni-LiCl	-	-	471	1	[123]
polyaniline-doped lithium chloride	PANI-LiCl$_6$	-	-	388	1	[124]
Kapok flower	HCl	-	1904	286.8	0.5	[125]
Tree residues	$HNO_3:H_2SO_4 = 1:3$	-	616	24	0.25	[126]
Wood sawdust and tannicacid	$KCl + Na_2S_2O_3$	2.3	2650	200	-	[118]

11.5.1.1 Zinc Chloride

Zinc chloride ($ZnCl_2$) is a neutral type of activating agent. $ZnCl_2$ is used as a dehydrating agent to encourage carbon material condensation processes and to prevent the production of tar and the gasification of carbon atoms, which results in materials with greater carbon contents. The parameters, surface area, pore size, and pore volume, which impact the electrochemical performance of SC, can be optimized by carbonization temperature and the $ZnCl_2$ concentration.

To eliminate the water content from the lignocellulose skeleton, $ZnCl_2$ is employed as a dehydrating agent. This produces mainly micro- and mesoporous AC with no loss in carbon amount [101–104]. Ahmad *et al.* describe the amalgamation of porous AC generated from rotting carrots using a chemical activation process using $ZnCl_2$ as an activating agent at a variable temperature under an inert environment (Figure 11.4a) [105, 106]. The electrochemical performance of prepared AC was explored using the AC as an electrode in different electrolyte solutions named Cell#1, Cell#2, and Cell#3. It was observed that the prepared activated carbon-based electrode, i.e., Cell #3, has the highest specific capacitance ($135.5\,F\,g^{-1}$ at $10\,mHz$), specific energy ($29.1\,Wh\,kg^{-1}$ at $2.2\,A\,g^{-1}$), and specific power ($142.5\,kW\,kg^{-1}$ at $2.2\,A\,g^{-1}$) in the ionic liquid-based electrolyte. Cell #3 also has the highest specific energy ($29.1\,Wh\,kg^{-1}$ at $2.2\,A\,g^{-1}$) (Figure 11.4b). Results showed the suitability of prepared electrode material in the application of energy storage devices.

Sun *et al.* utilized cotton as biomass for which they derived porous carbon materials [107]. They used MgO and $ZnCl_2$ as templating and activating agents, respectively. Cotton carbon absorbs MgO from cellulose fibers that have absorbed a solution of $Mg(NO_3)_2$, then

(a)

(b)
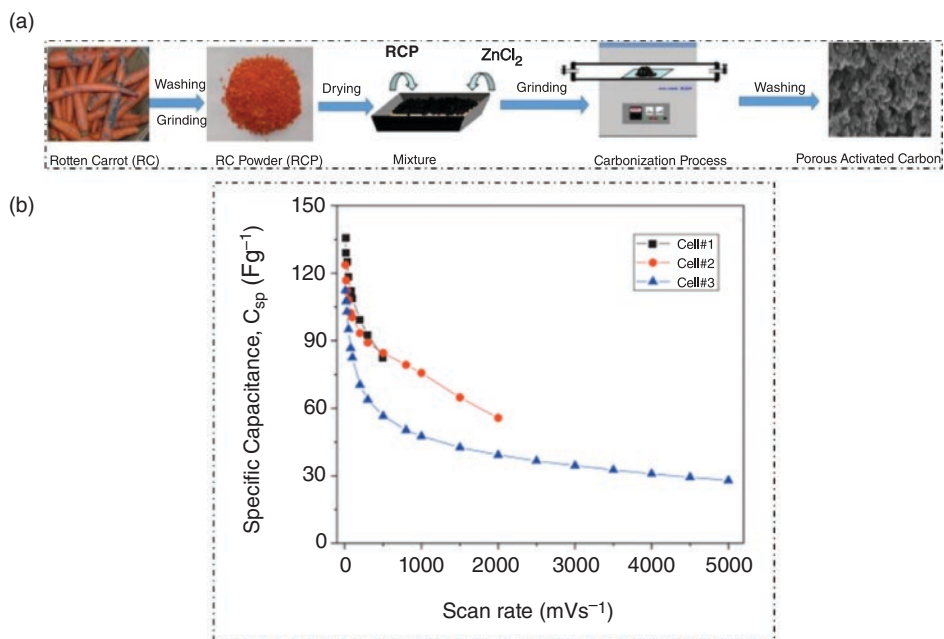
Figure 11.4 (a) Schematic for preparing activated carbon from rotten carrots. (b) Specific capacitance versus scan rate of prepared AC electrode. *Reproduced with permission [105]. Copyright 2018, Elsevier.*

undergoes dehydration and calcination to create porosity. A low-priced, high-specific surface-area porous carbon material can be created from biomass by acid leaching of the MgO. During the activation process, the hydrogen and oxygen in the raw material are liberated as water vapor thanks to $ZnCl_2$ dehydroxylation and dehydration properties. Also, activation involves the conversion of $ZnCl_2$ to ZnO. When acid is used to wash the produced material, the ZnO particles are removed, and the resulting voids increase the material's porosity. The findings of the research indicate that the activated carbon material manufactured by using MgO as the template and $ZnCl_2$ as the activating agent has a specific surface area that can reach up to $1990\,m^2g^{-1}$. The results show a capacitance of $240\,Fg^{-1}$ and a current density of $1\,Ag^{-1}$ in the three-electrode system test. The specific capacitance at $20\,Ag^{-1}$ is $173\,Fg^{-1}$, and the capacitance retention rate is 71%. Additional testing was conducted in 6M KOH aqueous solution and 1M Na_2SO_4 aqueous solution on the built symmetric supercapacitors. The alkaline system has an energy density of $5.7\,Whkg^{-1}$. A neutral electrolyte has an energy density of $12.5\,Whkg^{-1}$ and a cycle stability of 89% [107].

Chen *et al.* use a straightforward method to produce porous carbon materials with a high concentration of nitrogen [108]. This is accomplished by heating 1H-Benzotriazole (BTA) as a carbon precursor with $ZnCl_2$ as the activating agent at temperatures ranging from 600 to 800 °C for two hours in an environment containing nitrogen gas. $ZnCl_2$ has the ability to convert more organics to carbon as a result of its dehydration, whereas pure BTA degrades completely even when exposed to inert gas at temperatures as low as 270 °C. The NC-2–700 sample that was created has a nitrogen concentration of up to 10.27 weight percent and a high specific surface area ($1228\,m^2g^{-1}$). With a specific capacitance of $332\,Fg^{-1}$ at a current density of $0.5\,Ag^{-1}$, N-doped carbon is an excellent electrochemical material, and it also has excellent cycle stability, retaining 96.5% of its initial specific capacitance even after 5000 cycles at $1\,Ag^{-1}$. In addition, the NC-2–700 sample symmetric ultra-capacitor demonstrates a maximum power density of $375\,Wkg^{-1}$ and a maximum energy density of $12.94\,Whkg^{-1}$ when measured at a current density of $1\,Ag^{-1}$. Even at a high current density of $10\,Ag^{-1}$, the NC2–700/NC-2-700 supercapacitor provides $5.43\,Whkg^{-1}$ of energy storage or $3750\,Wkg^{-1}$ of power. These experimental results verify the potential of high-nitrogen-content porous carbon materials as electrodes for supercapacitors [108].

Shrestha *et al.* create Areca catechu nut (ACN)-derived nanoporous carbon materials (NCMs) with improved electrochemical supercapacitance capabilities [109]. The impact of activating agents $ZnCl_2$ and others on the surface functional groups, electrochemical super capacitance capabilities, and textural characteristics were carefully studied. They discovered that several kinds of nanoporous carbon materials synthesized from ACN were produced depending on the sort of activating agents utilized. They studied the supercapacitive properties of the prepared sample by cyclic voltammetry and chronopotentiometry. The charge-discharge profile of $ZnCl_2$-activated NCM was studied by chronopotentiometry at a fixed current density of $1\,Ag^{-1}$. The prepared material shows better charge/discharge over 5000 cycles with 91% capacity retention.

Zhang *et al.* showed that 4-(4-nitrophenylazo)resorcinol, sodium 5-[(4-nitrophenyl)azo] salicylate, and tartrazine were used to create nitrogen-containing nanoporous carbon materials using a generic yet effective $ZnCl_2$ activation approach [110]. It was shown that the activation temperature and mass ratio of the carbon/nitrogen precursors to the $ZnCl_2$ activating agent has significant effects on the carbon structures and the resulting capacitive behaviors. Samples of carbon created in this work have an amorphous structure. Named

carbon-1#, this activated carbon sample was produced by heating 4-(4-nitrophenylazo)res-orcinol in $ZnCl_2$ at 900 °C. It has the highest nitrogen concentration, 5.96%, and the highest porosity, 891.1 m^2 g^{-1} on the BET surface area scale and 0.54 cm^3/g for its total pore volume. Because of this, the carbon-1# sample offers the best specific capacitances of 431.5 Fg^{-1} at a current density of 1 A g^{-1} and the best long-term cycle stability of 97.16% even after 10,000 charges and discharges. The current $ZnCl_2$ activation method is expected to enable the synthesis of novel carbon compounds with significant porosities and excellent electrochemical properties for supercapacitor applications.

Kang *et al.* manufactured hierarchically porous and heteroatom-doped ACs using rapeseed dregs (RDs) as a novel carbon source by activating $ZnCl_2$ at varied high temperatures in a tube furnace [111]. The RD-derived ACs have up to 1416.966 m^2 g^{-1} specific surface area. The tests showed that activated carbons generated through RD had high specific capacitances of 170.5 and 153.2 Fg^{-1} in 1 M H_2SO_4 and 1 M Et_4NBF_4/AN, respectively, at a scan rate of 5 mV s^{-1}. Additionally, the RD-derived ACs exhibit respectable long-term cycling stability, and after 6400 cycles at a high current density of 1 A g^{-1}, more than 90% of the original capacity was still present [111].

Sun *et al.* prepare porous graphene-like nanosheets (PGNS) from coconut shells having properties of low resistance and small ion transport paths which can be appropriate for SCs application [112]. $ZnCl_2$ was used as the activating agent. The prepared PGNS possess a high specific surface area of 1874 m^2 g^{-1} and a high pore volume of 1.21 cm^3 g^{-1}. The PGNS possess good electrochemical properties for SCs application. PGNS, as additions, have a high specific capacitance of 268 Fg^{-1} at 1 A g^{-1}. Moreover, after 5000 cycles, PGNS have higher cycle endurance and Coulombic efficiency of over 99.5%. At high power density, an energy density of up to 54.7 Wh kg^{-1} has been achieved (Figure 11.5a, b). Electrochemical impedance (EIS) confirms the electron mobility behavior of the prepared sample. Figure 11.6 shows the Nyquist plots of PGNS-3–900, activated carbon AC-900, and
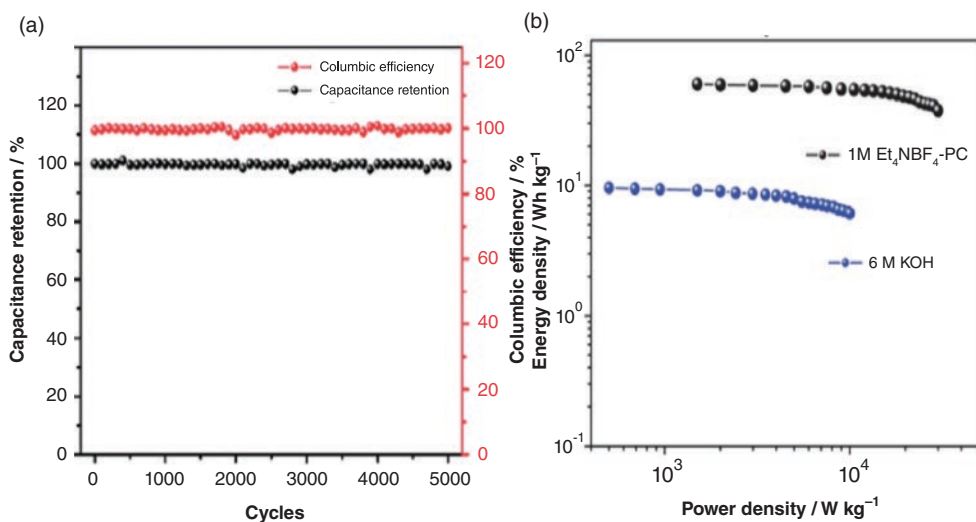
Figure 11.5 (a) the cyclic stability and Coulombic efficiency of PGNS; (b) Ragone diagram shows the corresponding power and energy densities. *Reproduced with permission [112]. Copyright 2013, Royal Society of Chemistry.*

Figure 11.6 A comparison of PGNS-3–900, AC-900, and GC-900 in an EIS plot. *Reproduced with permission [112]. Copyright 2013, Royal Society of Chemistry.*
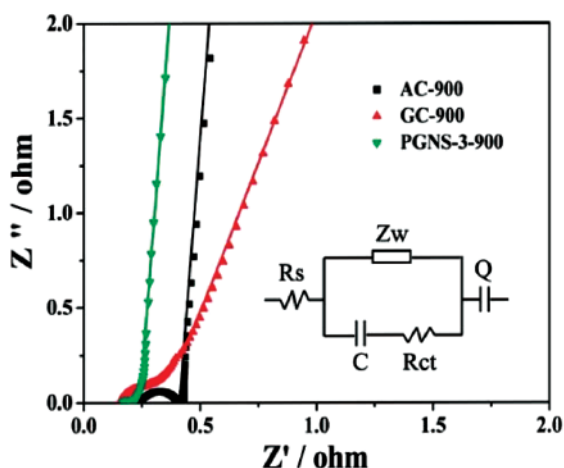
graphitization catalyst GC-900. The Nyquist plot on the low-frequency region showed a straight line for PGNS-3–900. The vertical line indicates the behavior of the supercapacitor, like a perfect capacitor. So, in comparison to the other two electrodes, PGNS-3–900 showed a much straighter line with an angle of nearly 90 °C, which shows good capacitance behavior of the electrode. The Warburg region of the PGNS-3–900-based electrode is smaller in comparison to other electrodes. The semi-circle of PGNS-3–900 is smaller, indicating low ion transport resistance. The equivalent circuit shows the appropriate conductivity of PGNS-3–900 (Figure 11.6).

11.5.1.2 Iron Chloride (FeCl$_3$) and Magnesium Chloride (MgCl$_2$)

Rufford *et al.* [113] fabricated carbon electrodes from waste coffee grounds. They drenched coffee grounds with FeCl$_3$ and MgCl$_2$ and then treated at 900 °C. The resulting carbon was characterized with different spectroscopic techniques and then compared with ZnCl$_2$ treated carbon obtained from coffee grounds. ZnCl$_2$ and FeCl$_3$ activated carbons show higher surface area, i.e., 977 and 846 m^2/g, respectively, when compared to MgCl$_2$. The electrode fabricated with FeCl$_3$-activated carbon shows a specific capacitance of 57 F g^{-1}. Their results show that FeCl$_3$-activated carbon gives stable charge cycles and, as a result, can be used as an alternative to ZnCl$_2$ to prepare activated carbons electrodes for SC from biomasses. Gunasekaran *et al.* showed that iron salt activated plays a vital role in forming activated carbon from the biomass [114].

11.5.1.3 Potassium Chloride (KCl)

Yuhe *et al.* synthesized KCl-activated carbon derived from walnut shells. Around 900 °C, CO$_2$ activation of biochar with a KCl template yielded AC with a significant specific surface area (1958 m^2 g^{-1}) [115]. At a current density of 0.1 A g^{-1}, the specific capacitance was found to be 245.0 F g^{-1} in an electrolyte containing 6 mol/L of KOH. This value decreased from 245.0 to 233.7 F g^{-1} at 0.1 A g^{-1} after 4000 cycles (at 0.1, 0.5, 1.0, and 5.0 A g^{-1} for 1000 cycles, respectively), resulting in a capacitance retention ratio of 95.4%. It also had extremely strong cyclic stability. Kumar et al. prepare nanoporous carbon from kapok shells using melted NaCl:KCl (1:1) as activating agent (Figure 11.7a). The surface area of the prepared

material is reported as $1260\,m^2\,g^{-1}$, and the specific capacitance is $169\,F\,g^{-1}$ with 97% capacitance retention after 10,000 cycles at $1\,A\,g^{-1}$ [116].

Zhang *et al.* prepared N/S co-doped porous carbon nanosheets (PCNS) from ginkgo leaves utilizing $CaCl_2$/KCl molten salt as an activation agent (Figure 11.7b) [117]. The ecologically friendly activation agents $CaCl_2$/KCl improve the pore volume and morphologies of the carbonaceous materials. Temperature is also one of the factors affecting the activation of carbon. The electrochemical properties of PCNS were checked at 700, 800, and 900 °C temperatures. The manufactured carbon electrode, 0.75PCNS$_{800}$, has good cycling performance with a capacity retention of 94.2% after 10,000 charge-discharge cycles at $1\,A\,g^{-1}$. Additionally, the constructed carbon electrode has an extraordinary specific capacitance of $150.4\,F\,g^{-1}$ when charged at $0.05\,A\,g^{-1}$ (Figure 11.7c). This easy and ecologically welcoming activation process offers a new way to fabricate N, S-doped, 2-D porous carbonaceous nanosheets for advanced energy storage devices.
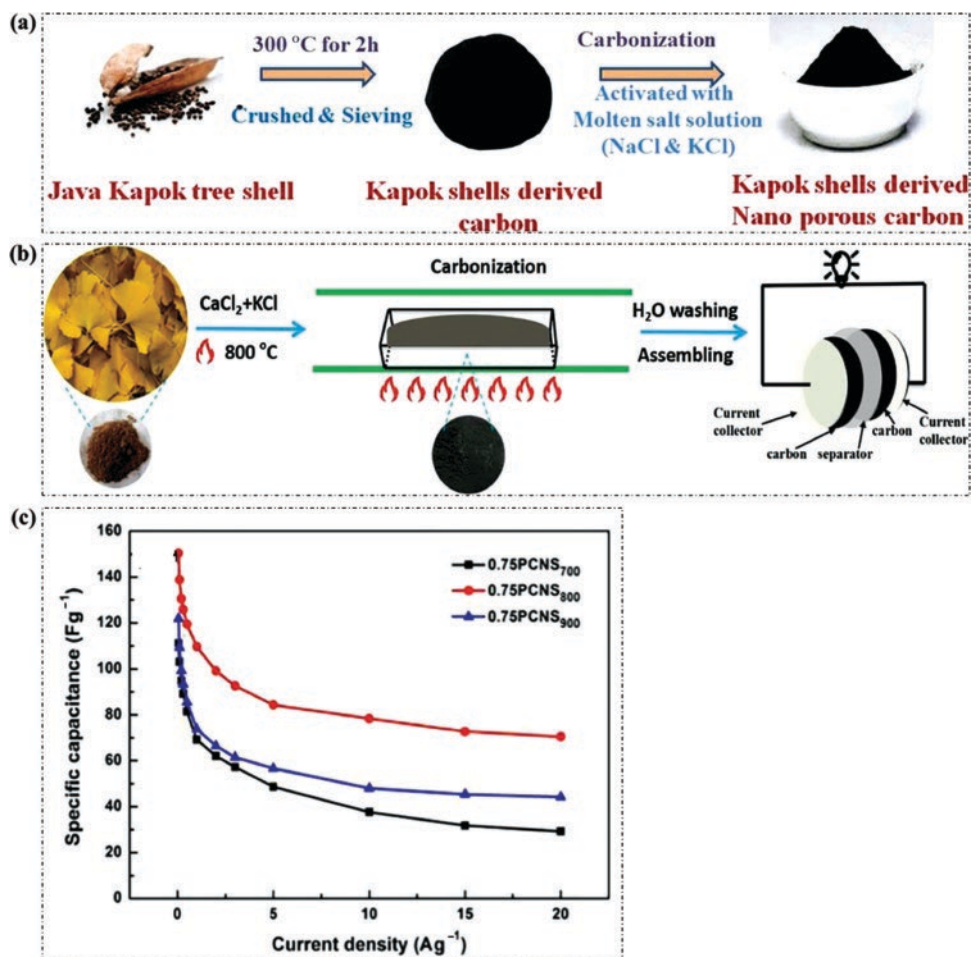
Figure 11.7 (a) Schematic illustration of kapok shell-derived nanoporous carbon formation. *Reproduced with permission* [116]. Copyright 2018, Elsevier. (b) Schematic for the synthesis of porous carbon by molten metal chloride salt. (c) The specific capacitance of all three samples when subjected to varying current densities. *Reproduced with permission [117]. Copyright 2021, Elsevier.*

According to Sevilla *et al.*, by using sodium thiosulfate as the activating agent and KCl as the confinement medium for the activation reaction, high-surface-area carbons can be produced in an environmentally acceptable way from biomass-based resources like wood sawdust and tannic acid [118]. Depending on the amount of activating agent used, these porous carbons can have BET surface areas as high as $2650 \, m^2 g^{-1}$, pore volumes as large as $2.3 \, cm^3 g^{-1}$, and porosity that mixes micro- and mesopores in varying proportions. These carbons are also notable because they are S-doped (containing between 2 and 6 wt.% S) and possess good electrical conductivities (with values ranging from 2.5 to 4.5 Scm^{-1}). These carbon compounds are very promising as electrodes for use in supercapacitors because of their desirable characteristics. Extensive testing in a wide range of electrolytes (including H_2SO_4, $TEABF_4$/AN, and EMImTFSI) at commercial mass loadings reveals high specific capacitances (up to $200 \, Fg^{-1}$ in aqueous, organic, and ionic liquid electrolytes, respectively) and excellent stability under cycling and floating modes.

11.5.1.4 Zinc Chloride ($ZnCl_2$) and Iron Chloride ($FeCl_3$)

Cai *et al.* prepare hierarchically porous carbon nanosheets (PCNS) by single-step pyrolysis method from *Morinaga oleifera* (MOS) [119]. $ZnCl_2$ and $FeCl_3$ were used as activating agents. It is known that $ZnCl_2$ produces porosity, and $FeCl_3$ can result in nanosheets of carbon materials [120]. MOS was mixed with $ZnCl_2$ and $FeCl_3$ at a ratio of 1:3, heated at 800 °C for 2 hr, and then washed and dried. The synthesized materials possess a high specific surface area and porosity, and doping with N and O improves the electrochemical properties for SCs. The different concentrations of $FeCl_3$ (0, 1.0, 2.0, 3.0 M) were used to produce porous carbon nanosheets, which were denoted as PCNS-0, PCNS-1, PCNS-2, and PCNS-3, respectively. The electrochemical performance of the synthesized materials in 6.0M KOH as an electrolyte is shown in Figure 11.8. Among all, the PCNS-2 represents the highest capacitance. Cyclic voltammetric (CV) curves of PCNS-2 at different scan rates show well-rate performance even at $200 \, mVs^{-1}$. In comparison to other samples, PCNS-2 exhibits a superior capacitance of $283 \, Fg^{-1}$ and 72% retention of the initial capacitance. The PCNS-2's capacity to withstand repeated charges and discharges at a high current density of $20 \, Ag^{-1}$ for 20,000 cycles was measured using the GCD test (Figure 11.8). It is possible that after 20,000 charge/discharge cycles, the capacitance of PCNS-2 falls somewhat but remains constant at 95%. At 99%, initial capacitance and coulombic efficiency can be steady, showing exceptional stability and reversibility.

11.5.1.5 Calcium Chloride ($CaCl_2$)

Zhong *et al.* utilized chemical activation with calcium chloride and urea to turn mung bean flour into N-doped porous carbons for use in the preparation of products [121]. The substrate and preparation temperature variations significantly influenced the graphitization, porosity, specific surface area, and surface chemical composition of the porous carbons. The best sample was created by heating mung bean flour, urea, and $CaCl_2$ to 800 °C. It had great specific capacitance ($247.2 \, Fg^{-1}$ at $2 \, mVs^{-1}$ and $300.5 \, Fg^{-1}$ at $1 \, Ag^{-1}$), great rate performance ($178.6 \, Fg^{-1}$ at 200 and $225 \, Fg^{-1}$ at $100 \, Ag^{-1}$), and great durability (93.2 and 97.5% capacitance retention after 10000 cyclic voltammograms and 2000 galvanostatic charge/discharge, respectively) in 6M KOH. According to structure-performance connections, the
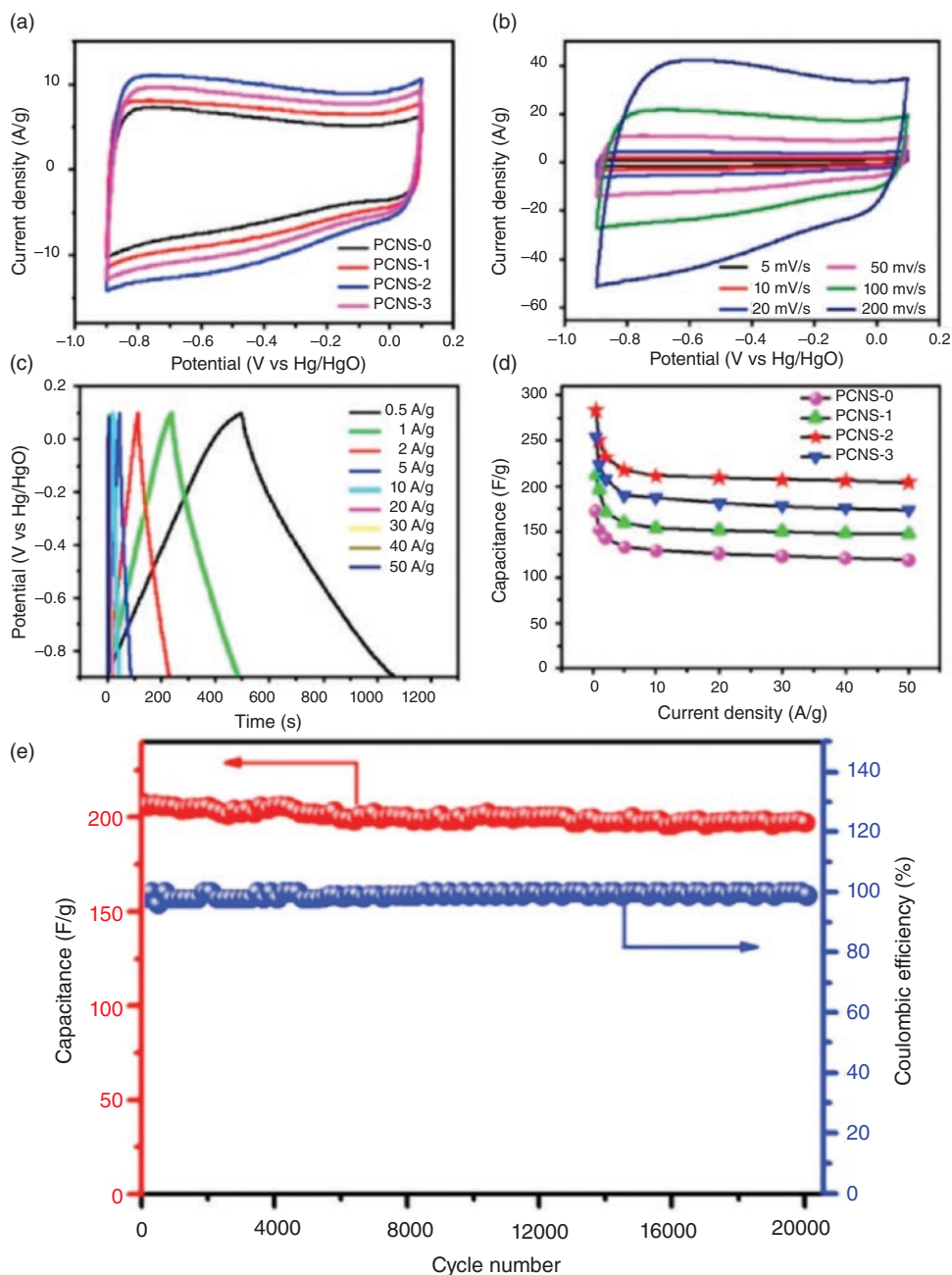
Figure 11.8 (a) The corresponding CV curves for the prepared PCNS. (b) CV curves of PCNS-2 at various scan rates. (c) The PCNS-2 GCD curves at different current densities. (d) The capacitance retention of PCNS in a variety of different current densities. (e) The PCNS-2's capacity to maintain its long-term cycling stability across 20,000 charge/discharge cycles when subjected to a high current density of 20 Ag^{-1}. *Reproduced with permission [119]. Copyright 2017, Elsevier.*

high carbonation, abundant porosities, and doped-N are to credit for this sample's exceptional specific capacitance.

11.5.1.6 Bimetallic Chloride Salts

Guo *et al.* generated biomass-derived activated carbons from peanut shells (PS) for use in supercapacitors [122]. They devised a one-step bimetallic activation technique that combines the activation efficacy of different activating agents ($FeCl_3$/$ZnCl_2$, $FeCl_3$/$MgCl_2$, and $ZnCl_2$/$MgCl_2$) with the etching effect of CO_2. The injecting of $ZnCl_2$ and $FeCl_3$ formed a large number of micropores during the activation of biomass, which can supply ion adsorption sites. $MgCl_2$ enhanced the creation of mesoporous structures, which aids in the transfer of electrolyte ions. Before activating the AC, the PS was rinsed, dried out, and powdered, passing through a 100-mesh sieve. The activated carbon samples were produced by combining PS with a variety of activating agents in a ratio of 2: 1 (activator: PS). After this, the mixture was activated at varying temperatures (700, 800, and 900 °C) and in the presence
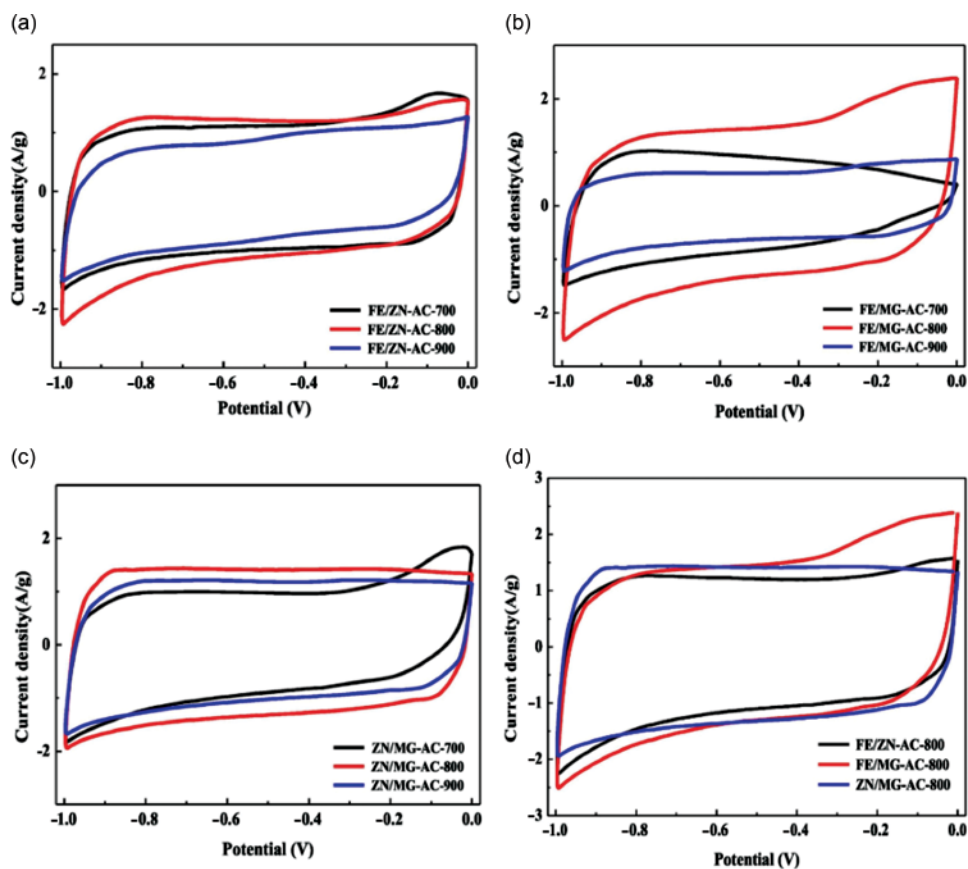
Figure 11.9 CV curves of (a) Fe/Zn-AC-*y*, (b) Fe/Mg-AC-*y* and (c) Zn/Mg-AC-*y* at a scan rate of 10 mVs^{-1} (y = activation temperature); (d) CV curves of *x*-AC-800 at the scan rate of 10 mVs^{-1} (AC = bimetallic). *Reproduced with permission [122]. Copyright 2019, Elsevier.*

(a)

(b)
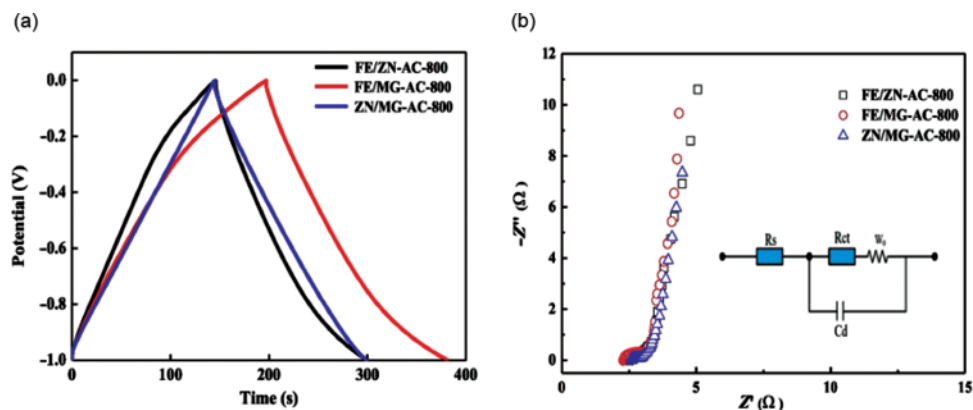
Figure 11.10 (a) GCD plot of Fe/Zn-AC-800, Fe/Mg-Ac-800, and Zn/Mg-Ac-800 electrodes at $1\,Ag^{-1}$; (b) EIS of Fe/Zn-AC-800, Fe/Mg-Ac-800 and Zn/Mg-Ac-800 electrodes over a frequency range of 0.01 Hz to 100 kHz. *Reproduced with permission [122]. Copyright 2019, Elsevier.*

of carbon dioxide. After preparation, the samples were dried and heated in a tube furnace under the CO_2 atmosphere. Figure 11.9a–c shows the CV curves of different activation temperatures at which activated carbon electrodes were prepared at a scan rate of $10\,mVs^{-1}$ in Na_2SO_4 electrolyte. All three electrodes show good CV curves; however, the current response was weak. Enhancing the activation temperature to 800 °C increases the area covered by the CV curves, signifying their good capacitance performance. However, the area of CV curves decreases for an increase in temperature to 900 °C. The CV curves of the electrodes formed at the activation temperature of 800 °C revealed the greatest surrounding regions for all three bimetallic activators, signifying that 800 °C was a favorable activation temperature at which activated carbons with larger specific capacitance. The CV curves of all three electrodes at 800 °C were examined to explore the influence of activation agents on the electrochemical supercapacitor behavior of the electrode materials made in this way, Figure 11.9d. The fact that each of the three CV curves maintains a form that is essentially rectangular throughout a given voltage range of 1 to 0 V is suggestive of the high electrochemical reversibility of the substances. When used as electrode material, Fe/Mg-AC-800 demonstrates a maximum specific capacitance of $247.28\,Fg^{-1}$ when subjected to a current density of $1\,Ag^{-1}$. EIS measurements were performed for the three samples in the frequency range of 0.01 to 100 kHz to assess further the electrochemical characteristics (Figure 11.10a,b). In the low-frequency region of each EIS plot, you'll find a straight line, and in the high-frequency region, you'll find a semi-circle. The Fe/Mg-AC-800 sample exhibited the least vertical deviation compared to the other three samples.

11.6 Conclusions and Future Perspective

Because of its availability, cheapness, and cleanliness factors biomass can be utilized to synthesize valuable carbonaceous materials as SC electrode materials. Parameters of prepared carbon materials such as high conductivity, surface area, porosity, and morphologies make biomass suitable for energy storage properties, particularly in electric double-layer

capacitors. Carbon materials resulting from pyrolysis and hydrothermal carbonization of biomasses need to be activated before their application through physical and chemical methods. The chemical activation method is widely used to activate carbon and facilitate porous structures. Various activating agents are employed for the activation of carbon. Using chloride salts as an activating agent has many advantages, as they are less hazardous, cost-effective, and easily available in nature.

Production of the world's plant biomass is estimated to be around 10^{11} tons per year. These plant biomasses are considered promising resources to produce carbonaceous materials in the future. Converting biomass into useful carbon materials will be cost-effective and provide new ways to cope with advanced, challenging energy storage devices and deal with waste management.

Chloride salt-activated carbon for supercapacitors has gained attention in recent years. These activating agents are easily available, environmentally friendly, and cost-effective and they can be easily removed during the washing of carbon materials. However, this acidic and basic activating agent can be corrosive, and it can be difficult to handle. These harsh reagents can also dissolve the organic matter of biomass. Chloride salts used as activating agents produce activated carbon with a large specific area, and porous size, which greatly influences EDLC properties.

Acknowledgment

References

1 J. Xue, T. Wu, Y. Dai, Y. Xia, *Chem. Rev.* **2019**, *119*, 5298–5415.

2 Y. Zheng, Z. Li, S. Feng, M. Lucas, G. Wu, Y. Li, C. Li, G. Jiang, *Renew. Sust. Energ. Rev.* **2010**, *14*, 3132–3139.

3 W. Raza, F. Ali, N. Raza, Y. Luo, K.-H. Kim, J. Yang, S. Kumar, A. Mehmood, E. E. Kwon, *Nano Energy* **2018**, *52*, 441–473.

4 S. Mohapatra, A. Acharya, G. Roy, *Lat. Am. J. Phys. Educ.* **2012**, *6*, 380–384.

5 A. K. Samantara, S. Ratha,Components of supercapacitor In: *Materials Development for Active/Passive Components of a Supercapacitor*, **2018**, Springer, pp. 11–39.

6 E. Frackowiak, F. Béguin, *Carbon.* **2001**, *39*, 937–950.

7 G. Wang, L. Zhang, J. Zhang, *Chem. Soc. Rev.* **2012**, *41*, 797–828.

8 J. Jiang, L. Zhang, X. Wang, N. Holm, K. Rajagopalan, F. Chen, S. Ma, *Electrochim. Acta.* **2013**, *113*, 481–489.

9 J. Yoder, S. Galinato, D. Granatstein, M. Garcia-Pérez, *Biomass Bioenerg.* **2011**, *35*, 1851–1862.

10 M. Wu, J. Liao, L. Yu, R. Lv, P. Li, W. Sun, R. Tan, X. Duan, L. Zhang, F. Li, *Chem. Asian J.* **2020**, *15*, 995–1013.

11 X. Deng, J. Li, L. Ma, J. Sha, N. Zhao, *Mater. Chem. Front.* **2019**, *3*, 2221–2245.

12 G. Lota, K. Fic, E. Frackowiak, *Energy Environ. Sci.* **2011**, *4*, 1592–1605.

13 J. Zhang, X. S. Zhao, *ChemSusChem* **2012**, *5*, 818–841.

14 A. Divyashree, G. Hegde, *RSC Adv.* **2015**, *5*, 88339–88352.

15 P. Lodewyckx, T. Rufford, J. Zhu, D. Hulicova-Jurcakova, *Green Carbon Materials: Advances and Applications*, **2014**, p. 235.

16 C. Ania, V. Khomenko, *Adv. Funct. Mater.* **2007**, *17*, 1828.

17 X. Xiang, E. Liu, Z. Huang, H. Shen, Y. Tian, C. Xiao, J. Yang, Z. Mao, *J. Solid State Electrochem.* **2011**, *15*, 2667–2674.

18 B. K. Deka, A. Hazarika, J. Kim, Y. B. Park, H. W. Park, *Int. J. Energy Res.* **2017**, *41*, 1397–1411.

19 A. Nisar, E. Gul, G. Rahman, Y. Wu, T. H. Bokhari, A. U. Rahman, A. Zafar, Z. Rana, A. Shah, S. Hussain, *New J. Chem.* **2022**, *46*, 16280–16288.

20 Y. Zhai, Y. Dou, D. Zhao, P. F. Fulvio, R. T. Mayes, S. Dai, *Adv. Mater.* **2011**, *23*, 4828–4850.

21 S. He, L. Chen, C. Xie, H. Hu, S. Chen, M. Hanif, H. Hou, *J. Power Sources* **2013**, *243*, 880–886.

22 J. Xia, N. Zhang, S. Chong, Y. Chen, C. Sun, *Green Chem.* **2018**, *20*, 694–700.

23 Y. Zhang, S. Yu, G. Lou, Y. Shen, H. Chen, Z. Shen, S. Zhao, J. Zhang, S. Chai, Q. Zou, *J. Mater. Sci.* **2017**, *52*, 11201–11228.

24 H. Chen, S. Zhou, L. Wu, *ACS Appl. Mater. Interfaces* **2014**, *6*, 8621–8630.

25 L. Zhang, Z. Liu, G. Cui, L. Chen, *Prog. Polym. Sci.* **2015**, *43*, 136–164.

26 A. M. Abioye, F. N. Ani, *Renew. Sust. Energ. Rev.* **2015**, *52*, 1282–1293.

27 R. B. Marichi, V. Sahu, R. K. Sharma, G. Singh, *Handbook of ecomaterials*, **2017**, 1–26.

28 M. Danish, R. Hashim, M. M. Ibrahim, M. Rafatullah, T. Ahmad, O. Sulaiman, *BioResources* **2011**, *6*, 3019–3033.

29 C. Lekakou, O. Moudam, F. Markoulidis, T. Andrews, J. Watts, G. Reed, *J. Nanotechnol.* **2011**, *2011*, 409382.

30 N. C. Deb Nath, S. S. Shah, M. A. A. Qasem, M. H. Zahir, M. A. Aziz, *ChemistrySelect* **2019**, *4*, 9079–9083.

31 C. K. Roy, S. S. Shah, A. H. Reaz, S. Sultana, A.-N. Chowdhury, S. H. Firoz, M. H. Zahir, M. A. A. Qasem, M. A. Aziz, *Chem. Asian J.* **2021**, *16*, 296–308.

32 S. M. Abu Nayem, S. S. Shah, S. B. Chaity, B. K. Biswas, B. Nahar, M. A. Aziz, M. Z. Hossain, *Arab. J. Chem.* **2022**, *15*, 104265.

33 A. J. S. Ahammad, P. R. Pal, S. S. Shah, T. Islam, M. Mahedi Hasan, M. A. A. Qasem, N. Odhikari, S. Sarker, D. M. Kim, M. A. Aziz, *J. Electroanal. Chem.* **2019**, *832*, 368–379.

34 A. Aziz, S. S. Shah, A. Kashem, *Chem. Rec.* **2020**, *20*, 1074–1098.

35 M. R. Hasan, T. Islam, M. M. Hasan, A.-N. Chowdhury, A. J. S. Ahammad, A. H. Reaz, C. K. Roy, S. S. Shah, I. Al, M. A. Aziz, *J. Phys. Chem. Solids* **2022**, *165*, 110659.

36 S. S. Shah, M. A. Aziz, E. Cevik, M. Ali, S. T. Gunday, A. Bozkurt, Z. H. Yamani, *J. Energy Storage* **2022**, *56*, 105944.

37 S. S. Shah, E. Cevik, M. A. Aziz, T. F. Qahtan, A. Bozkurt, Z. H. Yamani, *Synth. Met.* **2021**, *277*, 116765.

38 S. S. Shah, M. N. Shaikh, M. Y. Khan, M. A. Alfasane, M. M. Rahman, M. A. Aziz, *Chem. Rec.* **2021**, *21*, 1631–1665.

39 S. S. Shah, H. Yang, M. Ashraf, M. A. A. Qasem, A. S. Hakeem, M. A. Aziz, *Chem. Asian J.* **2022**, *17*, e202200567.

40 Z. Bi, Q. Kong, Y. Cao, G. Sun, F. Su, X. Wei, X. Li, A. Ahmad, L. Xie, C.-M. Chen, *J. Mater. Chem. A* **2019**, *7*, 16028–16045.

41 L. Wang, L. Xie, H. Wang, H. Ma, J. Zhou, *Colloids Surf. A Physicochem. Eng. Asp.* **2022**, *637*, 128257.

42 M. A. Aziz, S. S. Shah, S. M. A. Nayem, M. N. Shaikh, A. S. Hakeem, I. A. Bakare, *J. Energy Storage* **2022**, *50*, 104278.

43 A. K. Mohamedkhair, M. A. Aziz, S. S. Shah, M. N. Shaikh, A. K. Jamil, M. A. A. Qasem, I. A. Buliyaminu, Z. H. Yamani, *Arab. J. Chem.* **2020**, *13*, 6161–6173.

44 S. S. Shah, M. A. Aziz, Z. H. Yamani, *Chem. Rec.* **2022**, *22*, e202200018.

45 S. S. Shah, M. A. A. Qasem, R. Berni, C. Del Casino, G. Cai, S. Contal, I. Ahmad, K. S. Siddiqui, E. Gatti, S. Predieri, J.-F. Hausman, S. Cambier, G. Guerriero, M. A. Aziz, *Sci. Rep.* **2021**, *11*, 6945.

46 C. Zhang, J. Hu, J. Cong, Y. Zhao, W. Shen, H. Toyoda, M. Nagatsu, Y. Meng, *J. Power Sources* **2011**, *196*, 5386–5393.

47 L. Jiang, Z. Ren, S. Chen, Q. Zhang, X. Lu, H. Zhang, G. Wan, *Sci. Rep.* **2018**, *8*, 1–9.

48 X. Hou, T. Peng, J. Cheng, Q. Yu, R. Luo, Y. Lu, X. Liu, J.-K. Kim, J. He, Y. Luo, *Nano Res.* **2017**, *10*, 2570–2583.

49 T. Islam, M. M. Hasan, S. S. Shah, M. R. Karim, F. S. Al-Mubaddel, M. H. Zahir, M. A. Dar, M. D. Hossain, M. A. Aziz, A. J. S. Ahammad, *J. Energy Storage* **2020**, *32*, 101908.

50 J. Saravanan, M. Pannipara, A. G. Al-Sehemi, S. Talebi, V. Periasamy, S. S. Shah, M. A. Aziz, G. Gnana Kumar, *J. Mater. Sci. Mater. Electron.* **2021**, *32*, 24775–24789.

51 R. Shakil, M. N. Shaikh, S. S. Shah, A. H. Reaz, C. K. Roy, A.-N. Chowdhury, M. A. Aziz, *Asian J. Org. Chem.* **2021**, *10*, 2220–2230.

52 K. László, A. Bóta, L. G. Nagy, *Carbon* **2000**, *38*, 1965–1976.

53 Y. Ren, Q. Xu, J. Zhang, H. Yang, B. Wang, D. Yang, J. Hu, Z. Liu, *ACS Appl. Mater. Interfaces* **2014**, *6*, 9689–9697.

54 M. Biswal, A. Banerjee, M. Deo, S. Ogale, *Energy Environ. Sci.* **2013**, *6*, 1249–1259.

55 Z. Li, W. Lv, C. Zhang, B. Li, F. Kang, Q.-H. Yang, *Carbon* **2015**, *92*, 11–14.

56 D. Puthusseri, V. Aravindan, S. Madhavi, S. Ogale, *Energy Environ. Sci.* **2014**, *7*, 728–735.

57 R. Saidur, E. A. Abdelaziz, A. Demirbas, M. S. Hossain, S. Mekhilef, *Renew. Sust. Energ. Rev.* **2011**, *15*, 2262–2289.

58 M.-M. Titirici, R. J. White, C. Falco, M. Sevilla, *Energy Environ. Sci.* **2012**, *5*, 6796–6822.

59 H. Wang, Z. Li, D. Mitlin, *ChemElectroChem* **2014**, *1*, 332–337.

60 K. Qian, A. Kumar, H. Zhang, D. Bellmer, R. Huhnke. Recent advances in utilization of biochar, *Renew. Sustain. Energy Rev.* **2015**, *42*, 1055–1064.

61 M.-M. Titirici, M. Antonietti, A. Thomas, *Chem. Mater.* **2006**, *18*, 3808–3812.

62 R. Demir-Cakan, P. Makowski, M. Antonietti, F. Goettmann, M.-M. Titirici, *Catal. Today* **2010**, *150*, 115–118.

63 M. Sevilla, J. A. Maciá-Agulló, A. B. Fuertes, *Biomass Bioenerg* **2011**, *35*, 3152–3159.

64 M. Sevilla, A. B. Fuertes, *Energy Environ. Sci.* **2011**, *4*, 1765–1771.

65 L. Zhao, N. Baccile, S. Gross, Y. Zhang, W. Wei, Y. Sun, M. Antonietti, M.-M. Titirici, *Carbon* **2010**, *48*, 3778–3787.

66 J. Yang, L.-S. Tang, L. Bai, R.-Y. Bao, Z.-Y. Liu, B.-H. Xie, M.-B. Yang, W. Yang, *Mater. Horiz.* **2019**, *6*, 250–273.

67 A. Jain, R. Balasubramanian, M. Srinivasan, *Chem. Eng. J.* **2016**, *283*, 789–805.

68 L. Wei, M. Sevilla, A. B. Fuertes, R. Mokaya, G. Yushin, *Adv. Energy Mater.* **2011**, *1*, 356–361.

69 L. Zhao, *Adv. Mater.* **2010**, *22*, 5202.

70 C. Ruan, K. Ai, L. Lu, *RSC Adv.* **2014**, *4*, 30887–30895.

71 M. Rauf, S. S. Shah, S. K. Shah, S. N. A. Shah, T. U. Haq, J. Shah, A. Ullah, T. Ahmad, Y. Khan, M. A. Aziz, K. Hayat, *J. Saudi Chem. Soc.* **2022**, *26*, 101514.

72 J. Wang, S. Kaskel, *J. Mater. Chem.* **2012**, *22*, 23710–23725.

73 M. Choi, R. Ryoo, *J. Mater. Chem.* **2007**, *17*, 4204–4209.

74 Z. Yu, X. Wang, X. Song, Y. Liu, J. Qiu, *Carbon* **2015**, *95*, 852–860.

75 X. Che, J. Yang, S. Liu, M. Wang, S. He, J. Qiu, *Ind. Eng. Chem. Res.* **2022**, *61*, 8908–8917.

76 Y. Qiao, R. Han, Y. Pang, Z. Lu, J. Zhao, X. Cheng, H. Zhang, Z. Yang, S. Yang, Y. Liu, *J. Mater. Chem. A* **2019**, *7*, 11400–11407.

77 W. Zhang, R. Cheng, Z. Wang, Y. Ma, S. Ran, Y. Lv, L. Ma, *J. Mater. Sci. Mater. Electron.* **2020**, *31*, 22498–22511.

78 X. Liu, C. Giordano, M. Antonietti, *Small* **2014**, *10*, 193–200.

79 Y.-M. Fan, Y. Liu, X. Liu, Y. Liu, L.-Z. Fan, *Electrochim. Acta* **2017**, *249*, 1–8.

80 C. Wang, Y. V. Kaneti, Y. Bando, J. Lin, C. Liu, J. Li, Y. Yamauchi, *Mater. Horiz.* **2018**, *5*, 394–407.

81 X. Qiu, X. Zhang, L.-Z. Fan, *J. Mater. Chem.* **2018**, *6*, 16186–16195.

82 J.-W. Kim, M.-H. Sohn, D.-S. Kim, S.-M. Sohn, Y.-S. Kwon, *J. Hazard. Mater.* **2001**, *85*, 301–315.

83 A. G. Pandolfo, A. F. Hollenkamp, *J. Power Sources.* **2006**, *157*, 11–27.

84 K. S. Sing, *Pure Appl. Chem.* **1985**, *57*, 603–619.

85 E. Fitzer, K.-H. Kochling, H. Boehm, H. Marsh, *Pure Appl. Chem.* **1995**, *67*, 473–506.

86 H. Marsh, F. R. Reinoso, *Activated Carbon*. Elsevier, Amsterdam **2006**.

87 H.-F. Ju, W.-L. Song, L.-Z. Fan, *J. Mater. Chem. A* **2014**, *2*, 10895–10903.

88 A. Stein, Z. Wang, M. A. Fierke, *Adv. Mater.* **2009**, *21*, 265–293.

89 Y. Wang, S. Su, L. Cai, B. Qiu, C. Yang, X. Tao, Y. Chai, *Energy Storage Mater.* **2019**, *20*, 315–323.

90 Y. Chen, Z. Xiao, Y. Liu, L.-Z. Fan, *J. Mater. Chem. A* **2017**, *5*, 24178–24184.

91 S. He, R. Zhang, C. Zhang, M. Liu, X. Gao, J. Ju, L. Li, W. Chen, *J. Power Sources* **2015**, *299*, 408–416.

92 G. S. D. Reis, H. P. D. Oliveira, S. H. Larsson, M. Thyrel, E. Claudio Lima, *Nanomaterials* **2021**, *11*, 424.

93 G. Gou, F. Huang, M. Jiang, J. Li, Z. Zhou, *Renew. Energy.* **2020**, *149*, 208–216.

94 A. J. S. Ahammad, N. Odhikari, S. S. Shah, M. M. Hasan, T. Islam, P. R. Pal, M. A. Ahmed Qasem, M. A. Aziz, *Nanoscale Adv.* **2019**, *1*, 613–626.

95 M. A. Aziz, S. S. Shah, Z. H. Yamani, *Manganese oxide nanoparticle carbon microparticle electrocatalyst and method of making from albizia procera leaf*, *U.S. Patents*, **2021**, *16/589,711*, US20210095384A1.

96 S. S. Shah, M. A. Alfasane, I. A. Bakare, M. A. Aziz, Z. H. Yamani, *J. Energy Storage.* **2020**, *30*, 101562.

97 S. S. Shah, M. A. Aziz, *Bangladesh J. Plant Taxon.* **2020**, *27*, 467–478.

98 S. S. Shah, H. T. Das, H. R. Barai, M. A. Aziz, *Polymers* **2022**, *14*, 270.

99 M. Usman, M. Humayun, S. S. Shah, H. Ullah, A. A. Tahir, A. Khan, H. Ullah, *Energies* **2021**, *14*, 2281.

100 M. Yaseen, M. A. K. Khattak, M. Humayun, M. Usman, S. S. Shah, S. Bibi, B. S. U. Hasnain, S. M. Ahmad, A. Khan, N. Shah, A. A. Tahir, H. Ullah, *Energies* **2021**, *14*, 7779.

101 S. Murali, D. R. Dreyer, P. Valle-Vigon, M. D. Stoller, Y. Zhu, C. Morales, A. B. Fuertes, C. W. Bielawski, R. S. Ruoff, *Phys. Chem. Chem. Phys.* **2011**, *13*, 2652–2655.

102 T. E. Rufford, D. Hulicova-Jurcakova, K. Khosla, Z. Zhu, G. Q. Lu, *J. Power Sources* **2010**, *195*, 912–918.

103 T. E. Rufford, D. Hulicova-Jurcakova, Z. Zhu, G. Q. Lu, *Electrochem. Commun.* **2008**, *10*, 1594–1597.

104 J. Zhang, L. Gong, K. Sun, J. Jiang, X. Zhang, *J. Solid State Electrochem.* **2012**, *16*, 2179–2186.

105 S. Ahmed, A. Ahmed, M. Rafat, *J. Saudi Chem. Soc.* **2018**, *22*, 993–1002.

106 Y.-H. Chiu, L.-Y. Lin, *J. Taiwan Inst. Chem. Eng.* **2019**, *101*, 177–185.

107 Q. Sun, T. Jiang, G. Zhao, J. Shi, *Int. J. Electrochem. Sci.* **2019**, *14*, 1–14.

108 H. Chen, H. Wei, N. Fu, W. Qian, Y. Liu, H. Lin, S. Han, *J. Mater. Sci.* **2018**, *53*, 2669–2684.

109 L. K. Shrestha, R. G. Shrestha, S. Joshi, R. Rajbhandari, N. Shrestha, M. P. Adhikari, R. R. Pradhananga, K. Ariga, *J. Inorg. Organomet. Polym. Mater.* **2017**, *27*, 48–56.

110 Z. J. Zhang, C. Dong, X. Y. Ding, Y. K. Xia, *J. Alloys Compd.* **2015**, *636*, 275–281.

111 X. Kang, H. Zhu, C. Wang, K. Sun, J. Yin, *J. Colloid Interface Sci.* **2018**, *509*, 369–383.

112 L. Sun, C. Tian, M. Li, X. Meng, L. Wang, R. Wang, J. Yin, H. Fu, *J. Mater. Chem. A* **2013**, *1*, 6462–6470.

113 T. E. Rufford, D. Hulicova-Jurcakova, Z. Zhu, G. Q. Lu, *J. Mater. Res.* **2010**, *25*, 1451–1459.

114 S. S. Gunasekaran, S. K. Elumalali, T. K. Kumaresan, R. Meganathan, A. Ashok, V. Pawar, K. Vediappan, G. Ramasamy, S. Z. Karazhanov, K. Raman, R. Subashchandra Bose, *Mater. Lett.* **2018**, *218*, 165–168.

115 Y. Cao, X. Wang, Z. Gu, Q. Fan, W. Gibbons, V. Gadhamshetty, N. Ai, G. Zeng, *J. Power Sources* **2018**, *384*, 360–366.

116 K. T. Kumar, G. S. Sundari, E. S. Kumar, A. Ashwini, M. Ramya, P. Varsha, R. Kalaivani, M. S. Andikkadu, V. Kumaran, R. Gnanamuthu, *Mater. Lett.* **2018**, *218*, 181–184.

117 W. Zhang, M. Lin, R. Cheng, L. Li, Y. Sun, S. Ran, Y. Lv, L. Ma, *Diamond Relat. Mater.* **2021**, *113*, 108278.

118 M. Sevilla, N. Diez, G. A. Ferrero, A. B. Fuertes, *Energy Storage Mater.* **2019**, *18*, 356–365.

119 Y. Cai, Y. Luo, H. Dong, X. Zhao, Y. Xiao, Y. Liang, H. Hu, Y. Liu, M. Zheng, *J. Power Sources* **2017**, *353*, 260–269.

120 A. Ōya, H. Marsh, *J. Mater. Sci.* **1982**, *17*, 309–322.

121 G. Zhong, H. Xie, Z. Xu, S. Xu, S. Xu, Z. Cai, X. Fu, W. Liao, R. Miao, *ChemistrySelect* **2019**, *4*, 3432–3439.

122 F. Guo, X. Jiang, X. Jia, S. Liang, L. Qian, Z. Rao, *J. Electroanal. Chem.* **2019**, *844*, 105–115.

123 J. Dominic, T. David, A. Vanaja, G. Muralidharan, N. Maheswari, K. S. Kumar, *Appl. Surf. Sci.* **2018**, *460*, 40–47.

124 D. Jesuraj, D. Thanasamy, M. Gopalan, J. W. Joseph, S. K. K. Kannan, *Mater. Chem. Phys.* **2022**, *285*, 126109.

125 L.-H. Zheng, M.-H. Chen, S.-X. Liang, Q.-F. Lü, *Diamond Relat. Mater.* **2021**, *113*, 108267.

126 A. Jain, M. Ghosh, M. Krajewski, S. Kurungot, M. Michalska, *J. Energy Storage* **2021**, *34*, 102178.

12

CO$_2$-activated Carbon

Salman Farsi[1], Thuhin Kumar Dey[2], Mushfiqur Rahman[1], and Mamun Jamal[3,*]

[1] *Department of Materials Science & Engineering, Khulna University of Engineering & Technology, Khulna 9203, Bangladesh*
[2] *Department of Leather Engineering, Khulna University of Engineering & Technology, Khulna 9203, Bangladesh*
[3] *Department of Chemistry, Khulna University of Engineering & Technology, Khulna 9203, Bangladesh*
* *Corresponding author*

12.1 Introduction

The production of activated carbon (AC) from natural sources such as waste biomass, ligno-cellulosic biomass, and various biological sources has grown in popularity in recent years. Simultaneously, applying such bio-based activated carbon as supercapacitor electrode materials is becoming of interest to the research community [1, 2]. A summary of recent developments, along with critical analysis, is provided here. Because of their widespread availability and low cost, bio-materials are considered potential precursors for the fabrication of AC. AC is defined as an amorphous carbonaceous material with higher porosity that can be competitively produced for various commercial products [3–5]. However, the physiochemical properties of AC, such as pore structure, specific surface area, and chemical polarity, are primarily determined by the precursor material composition and activation process [6]. Fabricating activated carbon-based electrodes from waste biomass is also helping to alleviate waste disposal concerns in agro-based industries. Several articles published in the last decade focused on fabricating biomass-oriented AC for use as a supercapacitor electrode [7, 8]. Essentially, climate change and the depletion of fossil fuels are compelling society to consider green energy sources commercially for various purposes. As a result, hydro, solar, and wind energy have surpassed petroleum as superior alternatives. Simultaneously, the production of electric vehicles is now the primary focus of automobile manufacturers, while developing an efficient energy storage system remains a major concern [9, 10]. The raw composition of electrode materials in supercapacitors continues to be the most appealing aspect to the research community [11–19].

Both hydrothermal and thermochemical pathways are conventionally employed to fabricate AC from natural biomass. Particularly, in a one-step thermochemical process, biomass is converted into porous carbon material through heating at 600–900°C [3]. The whole process is carried out under an inert atmosphere in the presence of a chemical activating agent, steam,

or CO$_2$ [3, 20]. In a two-step thermochemical process, pyrolysis is carried out to convert the biomass into biochar, followed by a physical or chemical activation process. Specifically, CO$_2$ activation is a physical activation process based on controlled biochar gasification in the presence of CO$_2$ at temperatures between 800–1000°C. The research found that smaller-sized micropore-activated carbons exhibit a larger capacitance, while CO$_2$-activated carbon possesses a higher number of mesopores along with larger pore size. This happens due to the limited accessibility of larger CO$_2$ molecules into micropores [6]. Moreover, compared with chemical activation like KOH activation, CO$_2$ activation causes a higher degree of graphitization oriented with multilayer domains and graphene sheets stacking parallel in the structure of the porous carbons[6, 19, 21–23]. In general, CO$_2$ activation demands lower temperature and tend to form a wider pore size distribution [24]. Research on CO$_2$-based physical activation of biomass is relatively less often investigated than commonly used chemical activation.

Until now, commercial-graded AC has been primarily derived from petroleum and coal-based precursors, which are both costly and unfriendly to the environment [25]. As a result, the emphasis has shifted to biomass precursors in order to make AC more affordable, widely available, renewable, structurally porous, and environmentally friendly [25–30]. This chapter highlights an in-depth analysis of CO$_2$-activated-AC fabrication from biomass-based precursors and direct biomass-derived AC for use in energy storage applications. Furthermore, our conclusions and recommendations are noted in order to identify future research gaps to advance AC-based energy storage to the next level.

12.2 Roles of CO$_2$ – Functions of Activated Carbon

The transformation of carbon into CO$_2$-activated carbon by building up novel carbon-based nanostructure can produce two positives: (i) reduction of a greenhouse gas atmospheric CO$_2$ and (ii) formation of potential carbon materials with maximum electrochemical performance [31]. Today, global warming is a huge problem due to the frequent emission of CO$_2$ into the atmosphere [32]. But commercial utilization of this pernicious gas can greatly reduce the environmental strain. CO$_2$ is capable of participating directly or indirectly in the formation of AC and carbon extraction from biological substances can be converted into AC with a higher surface area and pore interconnected natural network, which occurs due to the transportation of nutritional elements within bio-plants. In addition, such extracted AC can also be functionalized via catalytic agents or CO$_2$ as an activation agent [33]. Consequently, a large volume of CO$_2$ will be required for this reaction, and it's quite possible to supply this gas from atmospheric air or different biological sources [22, 34–39].

The major concern for such an activation process is using compatible activation agents. Various activating agents are frequently employed to fabricate porous activated carbon, including KOH, HCl, H$_3$PO$_4$, ZnCl$_2$, and steam, followed by the utilization of AC as electrodes for supercapacitors [4, 5, 40, 41]. Keppetipola et al. [40] particularly considered fabricating activated carbon coconut shell biomass by utilizing H$_2$O and steam, respectively. The authors also highlighted the two routes of the working mechanism: (i) coconut shells being dried and burned in a closed chamber to make charcoal powder. Later the powder was heated again at 900 ºC for 20 min and immediately quenched with distilled water to activate it, and (ii) the activation process was performed by heating charcoal powder at 900 ºC in a furnace for 1 to 2 hours with a continuous steam flow. Then immediately quenched with distilled water to make it activated (Figure 12.1).
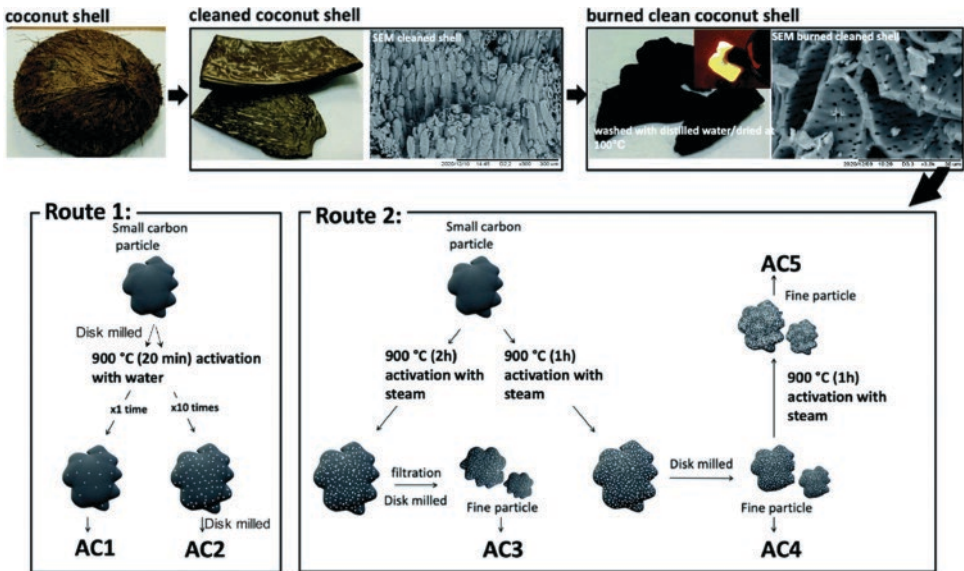
Figure 12.1 Preparation methods of activated carbon (AC1-AC5) using coconut shells as the precursor. The final products were prepared according to the activation routes using distilled water quenching or steam as an activation agent. *Reproduced with permission* [40]. *Reproduced under the terms of the CC BY-NC 3.0 license. Copyright 2021, Keppetipola et al.*

Abd et al. [42] showed details on the selective adsorption of CO$_2$ in AC based on molecular sieving impact. In this work, authors explain how CO$_2$ plays a critical role in activating carbon to meet the demands of carbon electrodes in energy storage systems. CO$_2$ functions can be classified into several synthetic processes for the production of porous activated carbon:

 i) The conversion of carbon into CO$_2$-AC by chemical activation process from biological precursors (Figure 12.2).
 ii) CO$_2$ can easily impinge into porous AC during activation from natural air.
 iii) CO$_2$ from the gaseous environment is used in the physical activation process.

AC plays two major roles in energy storage systems: (a) ensuring maximum surface area and porosity, and (b) ion transition spaces with excellent super-capacitive performances and cyclic stability. As a result, AC is widely available in various energy storage devices such as fuel cells, supercapacitors, and batteries [43–47]. In such cases, biological sources such as sweet potato starch can be converted to AC using the various synthetic approaches depicted in Figure 12.3 [48].

This is a real world scenario and mechanism of formation of the AC from biomass or bio-plants using the CO$_2$ activation process. In detail, starch is extracted from natural sweet potato, and further gelatinization and hydrothermal processes convert it into powder black carbon. Finally, CO$_2$ was used as an activating agent to produce activated carbon for supercapacitor applications. AC has a high surface area and excellent adsorption performance; hence adsorption of CO$_2$ into AC easily impinges for a proper activation process. The primary consideration in selecting an AC-based adsorbent for CO$_2$ adsorption is that the pore diameter of the adsorbent must be rational with the kinetic diameter of the CO$_2$ molecule. According
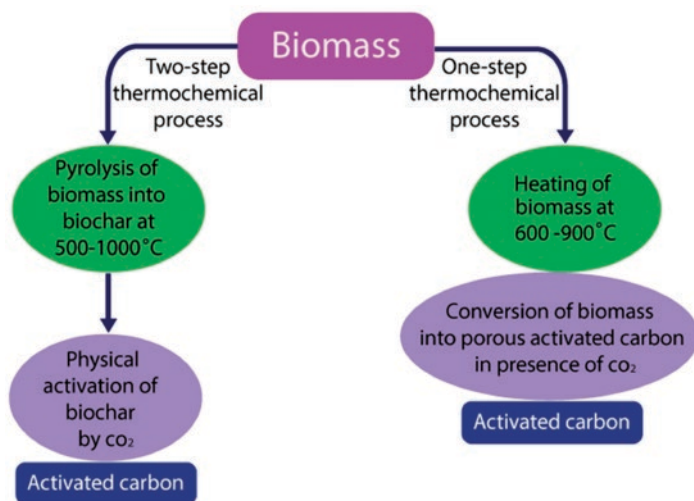
Figure 12.2 Mechanism of the CO$_2$ activation of porous carbon from biomass.
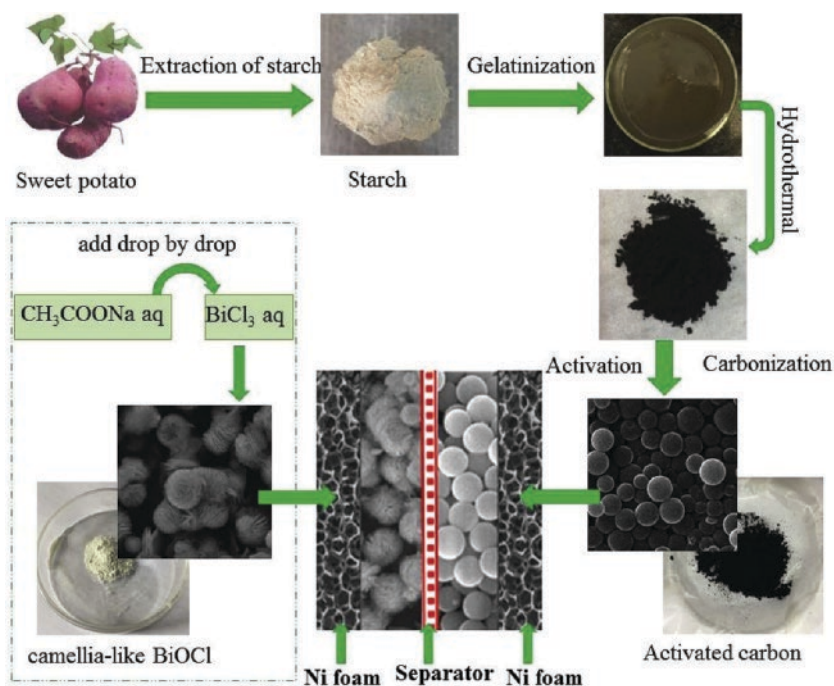
Figure 12.3 Schematic illustration for synthesizing activated carbon from starch and fabrication of supercapacitor device. *Reproduced with permission* [48]. *Copyright 2018, Elsevier.*

to this viewpoint, proper design and fabrication of AC can improve CO$_2$ adsorption performance and selectivity for further activation of retained carbon via CO$_2$ activating power [49].

In general, the classification of AC-based adsorbents is determined by their activation pathways. Physical activation and chemical activation are the two main approaches used.

It is possible to tune both the shape and texture of adsorbents during physical activation and achieve a surface area of around 2000 m^2 g^{-1} [50]. On the other hand, chemical activation controlled both the porosity and surface area of the adsorbent [51]. Currently, AC-based adsorbents have proven to be highly viable for adsorbing various gases based on size and shape [52]. As a result, it is clear that gas molecules can migrate through pores if their kinetic diameters are compatible with adsorbent pores (Figure 12.4) [53]. Wilcox et al. [54] supported this claim by reporting that matching the pore diameter to the CO_2 molecule will never allow the CO_2 molecules to escape from the adsorbent surface. Pore sizes less than 1 nm are highly compatible with CO_2 adsorption at atmospheric temperature and pressure and this structure aids in the retention of CO_2 molecules in adsorbent pore walls [55]. Aside from retaining CO_2 molecules, such pore size can also ensure the desired selectivity of CO_2 molecules in the case of a mixture of nitrogen (N_2) and CO_2 by inhibiting N_2 flow into the pore wall [56]. On the other hand, small porosity has a lower adsorption capacity because the pore size is close to the kinetic diameter (0.33 nm) of a CO_2 molecule [57]. However, pore sizes smaller than 1 nm are ineffective for CO_2 uptake at low pressure and it would be impossible to achieve a dense pack of CO_2 molecules in such a case [58].

12.3 Routes for Synthesis of Activated Carbon

The synthesis of activated carbon is critical for obtaining high performance and is a new frontier in super-capacitance materials [6, 10]. Figure 12.4 demonstrates that CO_2 and carbon extracted from biomass can play an important role in forming activated carbon, which has two common functions: super-capacitive application and CO_2 adsorption. The relationship
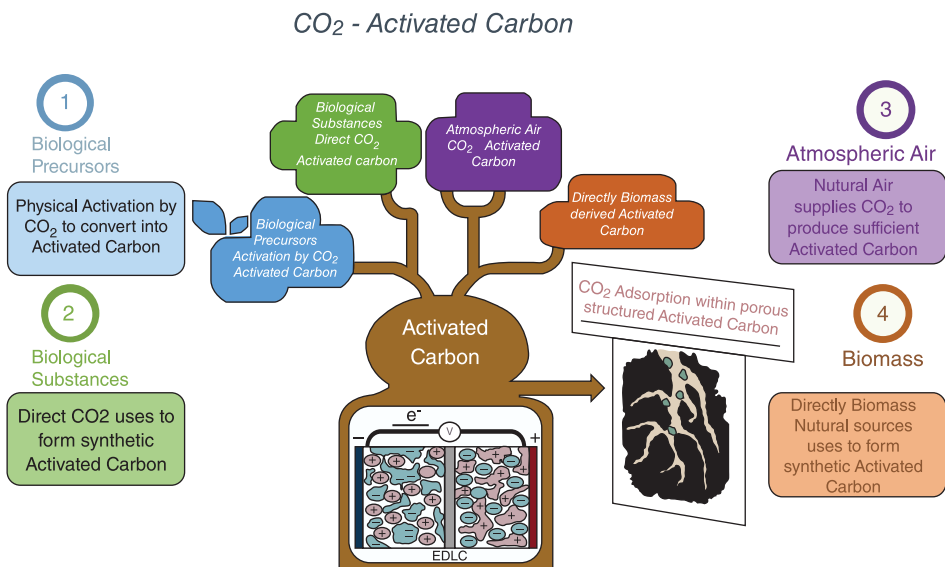
Figure 12.4 Synthesis routes for activated carbon with CO_2 interrelationship and its applicable paths within energy reservoir systems and adsorption process by functionalizing it for cyclic production purposes.

between these two features can be deduced as four major chemical interrelationships capable of having excellent super-capacitive performances and noticeable CO_2 adsorption or capture phenomena. This chain process can produce available carbon materials at a low cost and in abundance, reducing greenhouse gas (i.e., CO_2) and environmental pollution, making the atmosphere safe to breathe and saving animal and plant life [23, 59–62].

In this chapter, we summariz the activation roles of CO_2 of the biomass extracted carbon and the use of activated carbon for energy storage applications and CO_2 reservation to manufacture further activated carbon from or by CO_2 as the main raw component. Although our primary focus is carbon extraction from biomass substances, a minor discussion is presented on direct conversion into AC, or direct CO_2 used as a raw material from biological or environmental sources. Adsorption of CO_2 is also discussed here because a huge volume of CO_2 is needed during the activation process and raw usage. AC has a high adsorption capability of CO_2, so during the activation AC can play an important role as a supplier and enhancer of the CO_2 activation process. Using this cyclic process, we can reduce CO_2 levels in our environment and use it both as a primary or secondary ingredient in forming activated carbon, which has multifunctional activity and can also capture CO_2 from the atmosphere. That is, a chain of CO_2 reduction processes will be carried out through the formation and functionalization of activated carbon and energy storage devices.

12.4 Biological Precursors – Activation by CO₂-activated Carbon

Coconut husk is used to fabricate AC-based electrodes via physical and chemical activation in the presence of CO_2 as an activating agent (Figure 12.5) [63]. Firstly, low temperatures (<500 °C) and an inert atmosphere or limited air are used to make powdered carbon from bio-precursor such as coconut husk. Secondly, high temperature is applied in the presence of CO_2. Specifically, CO_2 was introduced as a potential activator during physical activation
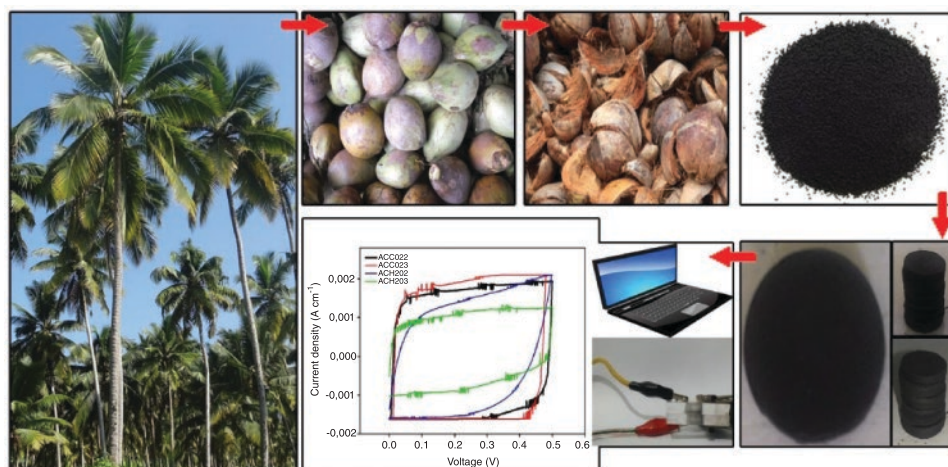
Figure 12.5 Preparation process of the activated carbon electrodes from coconut husk. *Reproduced with permission* [63]. *Reproduced under the terms of the CC BY 4.0 license. Copyright 2018, Taer et al.*

at temperatures ranging from 750 to 900 °C. During the chemical activation of a coconut husk-based adsorbent, potassium hydroxide was considered as another activator [63].Miao Yu et al. [64] presented a low-cost method for producing porous carbon by utilizing cattail biomass. The carbon was then activated in the presence of CO_2, eliminating the need for any chemicals. Finally, the result showed that the carbon activated with CO_2 had a specific surface area of about 441.12 $m^2 g^{-1}$. In addition, the AC was also capable of adsorbing malachite green dye (Figure 12.6). At the same time, this porous activated carbon could function as electrochemical supercapacitors, with a capacitance of 126.5 F g^{-1} and a current density of 0.5 A g^{-1} in the presence of a 6 M KOH solution.

Gunasekaran et al. [65] created porous carbon from hemp fibre (HFPC) by carbonizing it at a lower temperature and then activating it physically in the presence of CO_2. Carbon was then used in a high-performance solid-state supercapacitor. HFPC-30 material was formed during activation and consists of interconnected networking of pores (both meso and macro) with a surface area of 1060 $m^2 g^{-1}$. This property facilitated rapid ion transfer and efficient interactions between electrode and electrolyte. Furthermore, HFPC-30 demonstrated exceptional half-cell capacitance of 600 F g^{-1} at 1 A g^{-1}. During the experiment, they built a supercapacitor that can deliver 2V and retains 85% of capacitance even after 10,000 cycles.

Jiang et al. [66] investigated biomass-based porous carbon, in which lignocellulose was transformed into hierarchical porous carbon in the presence of CO_2. During this activation process, the physical activation method was used. It is worth noting that engineered porosity in carbon material was achieved in addition to biomass's inherent porosity. This property of porous carbon makes it more suitable for supercapacitors in terms of ion storage and transportation. Furthermore, the available functional groups had a significant influence on the performance of the supercapacitor. Similarly, Taer et al. [67] created biomass-based activated carbon from sawdust of rubber wood. The activation was completed in the presence of CO_2, and the temperature was adjusted between 700 and 1000 °C. The prepared carbon pellet appeared to be supercapacitor compatible. Wang et al. [68] investigated potential bottlenecks
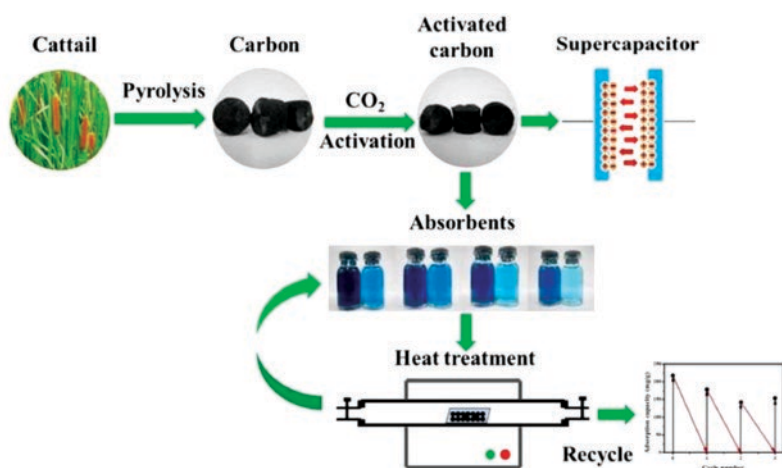
Figure 12.6 CO_2-activated porous carbon derived from cattail biomass for removal of malachite green dye and application as supercapacitors. *Reproduced with permission* [64]. *Copyright 2017, Elsevier.*
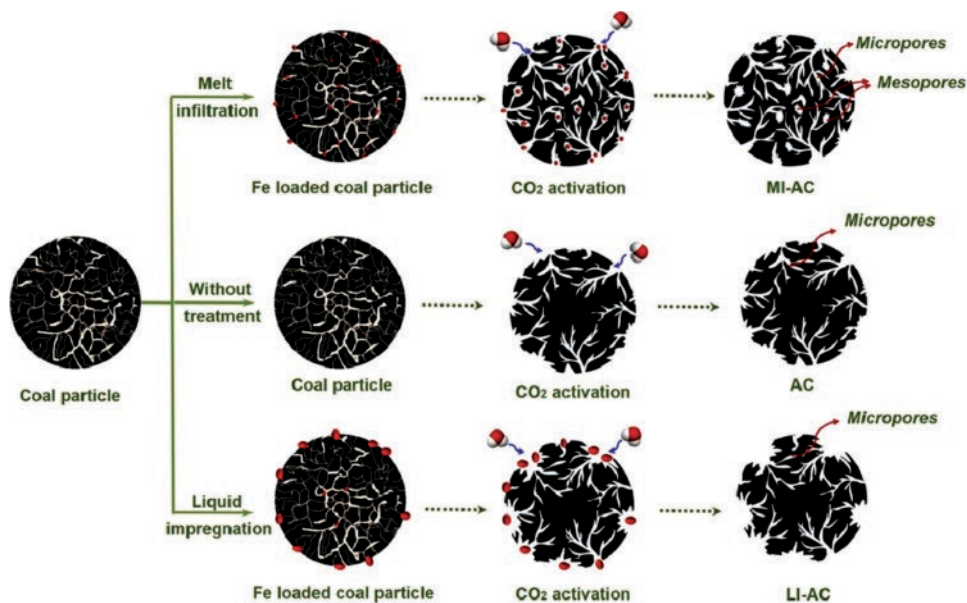
Figure 12.7 A schematic illustration of the porosity development mechanism via various strategies. *Reproduced with permission* [68]. *Copyright 2018, Elsevier.*

in traditional AC preparation methods (physical and chemical activation). To make activated carbons they developed a simple and adjustable melt infiltration technique that was aided by CO_2 activation. A low dose of iron (III) chloride can be used to introduce metal precursors into coal or biomass during the preparation of highly-porous activated carbon (Figure 12.7). Murugan Vinayagam et al. [69] investigated two types of biomass for the first time: *Chrysopogon zizanioides* roots (CZR) and *Syzygium cumini* fruit shells (SCFS). They advocated a straightforward approach to producing porous AC by considering the physical activation process. More specifically, the AC fabrication method was divided into two steps. First, carbonization was completed at 700 °C in the presence of nitrogen. Second, complete CO_2 activation at 700 °C, again in the presence of nitrogen. At 200 W kg^{-1} power density, the resulting AC was capable of delivering a maximum energy density of 16.72 Wh kg^{-1} (CZR-AC) and 27.22 Wh kg^{-1} (SCFS-AC) and this stability was maintained over 5000 cycles.

Zhu et al. [70] created AC from waste poly-acrylonitrile fibers by carbonizing them and then activating them with CO_2. Then, thermal and chemical treatments were used to host functional groups on the surface of the AC. A significant capacitance of 214 F g^{-1} was confirmed at a current density of 0.5 mA/cm^2 due to the presence of optimized pore structure and surface functional groups.

12.5 Conclusion and Future Perspective

The preparation procedures, reaction conditions, effects of biological waste precursor structure and composition all significantly impact the performance of biomass-based AC. The capacitive performances of AC-based electrodes were found to be dependent not only

on the AC's surface area, but also on pore structure and distribution, electrical conductivity, and surface functionalities. Furthermore, ultra-small micropores discovered in low surface area active carbons have significantly contributed to the capacitance observed in those carbons. Overall, it was discovered that the electrolyte system influenced the energy cells' electrochemical performance. Massive research efforts are currently focused on developing low-cost active carbon electrodes with high capacitance and low resistance.

Despite the fact that there have been few publications in this field, the results obtained thus far are promising. As a result, more research is required into the performance of CO_2-activated carbon electrodesand also to design nanostructured materials which could significantly improve the existing energy and power capabilities of electric double-layer capacitors. A thorough understanding of the interrelationship between pore size, surface area, surface chemistry, electrochemical capacitor performance, and the CO_2-based activation process is also required. In addition, to achieve superior CO_2 capture from gas mixtures such as flue gas or biogas, a new design of activated carbon materials that can withstand corrosive environments is urgently required. Also, there is a need to develop optimized electrolyte systems with higher conductivity at room temperature and the ability to operate at higher voltages required for future generations of supercapacitors. An in-depth analysis should be carried out to understand the effects of electrolytes on physical properties, molecular interactions, and supercapacitor performance.

Acknowledgements

References

1 S. Najib, E. Erdem, *Nanoscale Adv.* **2019**, *1*, 2817–2827.

2 N. A. Rashidi, S. Yusup, *J. Energy Storage* **2020**, *32*, 101757.

3 A. Aziz, S. S. Shah, A. Kashem, *Chem. Rec.* **2020**, *20*, 1074–1098.

4 S. S. Shah, S. M. A. Nayem, N. Sultana, A. J. S. Ahammad, M. A. Aziz, *ChemSusChem* **2022**, *15*, e202101282.

5 S. S. Shah, M. N. Shaikh, M. Y. Khan, M. A. Alfasane, M. M. Rahman, M. A. Aziz, *Chem. Rec.* **2021**, *21*, 1631–1665.

6 P. González-García, T. A. Centeno, E. Urones-Garrote, D. Ávila-Brande, L. C. Otero-Díaz, *Appl. Surf. Sci.* **2013**, *265*, 731–737.

7 A. M. Abioye, F. N. Ani, *Renew. Sust. Energ. Rev.* **2015**, *52*, 1282–1293.

8 K. Wang, N. Zhao, S. Lei, R. Yan, X. Tian, J. Wang, Y. Song, D. Xu, Q. Guo, L. Liu, *Electrochim. Acta* **2015**, *166*, 1–11.

9 P. Simon, Y. Gogotsi, *Nat. Mater.* **2008**, *7*, 845–854.

10 D. Pech, M. Brunet, H. Durou, P. Huang, V. Mochalin, Y. Gogotsi, P.-L. Taberna, P. Simon, *Nat. Nanotechnol.* **2010**, *5*, 651–654.

11 H. Tran Thi Dieu, K. Charoensook, H.-C. Tai, Y.-T. Lin, -Y.-Y. Li, *J. Porous Mater.* **2021**, *28*, 9–18.

12 Z. Li, Z. Xu, X. Tan, H. Wang, C. M. B. Holt, T. Stephenson, B. C. Olsen, D. Mitlin, *Energy Environ. Sci.* **2013**, *6*, 871–878.

13 A. Alabadi, X. Yang, Z. Dong, Z. Li, B. Tan, *J. Mater. Chem. A* **2014**, *2*, 11697–11705.

14 S. M. Abu Nayem, S. S. Shah, S. B. Chaity, B. K. Biswas, B. Nahar, M. A. Aziz, M. Z. Hossain, *Arab. J. Chem.* **2022**, *15*, 104265.

15 A. J. S. Ahammad, P. R. Pal, S. S. Shah, T. Islam, M. Mahedi Hasan, M. A. A. Qasem, N. Odhikari, S. Sarker, D. M. Kim, M. A. Aziz, *J. Electroanal. Chem.* **2019**, *832*, 368–379.

16 M. A. Aziz, S. S. Shah, S. Reza, A. S. Hakeem, W. Mahfoz, *Chem. Asian J.* **2022**, https://doi.org/10.1002/asia.202200869, e202200869. Accessed February 2023.

17 M. R. Hasan, T. Islam, M. M. Hasan, A.-N. Chowdhury, A. J. S. Ahammad, A. H. Reaz, C. K. Roy, S. S. Shah, I. Al, M. A. Aziz, *J. Phys. Chem. Solids* **2022**, *165*, 110659.

18 S. S. Shah, M. A. Aziz, E. Cevik, M. Ali, S. T. Gunday, A. Bozkurt, Z. H. Yamani, *J. Energy Storage* **2022**, *56*, 105944.

19 S. S. Shah, H. Yang, M. Ashraf, M. A. A. Qasem, A. S. Hakeem, M. A. Aziz, *Chem. Asian J.* **2022**, *17*, e202200567.

20 J. A. Maciá-Agulló, B. C. Moore, D. Cazorla-Amorós, A. Linares-Solano, *Carbon* **2004**, *42*, 1367–1370.

21 M. Daud, M. S. Kamal, F. Shehzad, M. A. Al-Harthi, *Carbon* **2016**, *104*, 241–252.

22 M. D. Garba, M. Usman, S. Khan, F. Shehzad, A. Galadima, M. F. Ehsan, A. S. Ghanem, M. Humayun, *J. Environ. Chem. Eng.* **2021**, *9*, 104756.

23 M. Ashraf, S. S. Shah, I. Khan, M. A. Aziz, N. Ullah, M. Khan, S. F. Adil, Z. Liaqat, M. Usman, W. Tremel, M. N. Tahir, *Chem. Eur. J.* **2021**, *27*, 6973–6984.

24 R. Farma, M. Deraman, A. Awitdrus, I. A. Talib, E. Taer, N. H. Basri, J. G. Manjunatha, M. M. Ishak, B. N. M. Dollah, S. A. Hashmi, *Bioresour. Technol.* **2013**, *132*, 254–261.

25 S. S. Shah, E. Cevik, M. A. Aziz, T. F. Qahtan, A. Bozkurt, Z. H. Yamani, *Synth. Met.* **2021**, *277*, 116765.

26 -M.-M. Titirici, R. J. White, C. Falco, M. Sevilla, *Energy Environ. Sci.* **2012**, *5*, 6796–6822.

27 M. Yaseen, M. A. K. Khattak, M. Humayun, M. Usman, S. S. Shah, S. Bibi, B. S. U. Hasnain, S. M. Ahmad, A. Khan, N. Shah, A. A. Tahir, H. Ullah, *Energies* **2021**, *14*, 7779.

28 S. S. Shah, M. A. Aziz, Z. H. Yamani, *Chem. Rec.* **2022**, *22*, e202200018.

29 S. S. Shah, M. A. A. Qasem, R. Berni, C. Del Casino, G. Cai, S. Contal, I. Ahmad, K. S. Siddiqui, E. Gatti, S. Predieri, J.-F. Hausman, S. Cambier, G. Guerriero, M. A. Aziz, *Sci. Rep.* **2021**, *11*, 6945.

30 S. S. Shah, H. T. Das, H. R. Barai, M. A. Aziz, *Polymers* **2022**, *14*, 270.

31 C. Li, X. Zhang, K. Wang, F. Su, C.-M. Chen, F. Liu, Z.-S. Wu, Y. Ma, *J. Energy Chem.* **2021**, *54*, 352–367.

32 G. Crabtree, *Nature* **2015**, *526*, S92–S92.

33 Y. Zhang, S.-J. Park, *Carbon* **2017**, *122*, 287–297.

34 Z. Zhang, S.-Y. Pan, H. Li, J. Cai, A. G. Olabi, E. J. Anthony, V. Manovic, *Renew. Sust. Energ. Rev.* **2020**, *125*, 109799.

35 I. U. Din, M. Usman, S. Khan, A. Helal, M. A. Alotaibi, A. I. Alharthi, G. Centi, *J. CO2 Util.* **2021**, *43*, 101361.

36 M. Usman, M. Humayun, S. S. Shah, H. Ullah, A. A. Tahir, A. Khan, H. Ullah, *Energies* **2021**, *14*, 2281.

37 M. Usman, *Membranes* **2022**, *12*, 507.

38 M. Usman, M. Humayun, M. D. Garba, L. Ullah, Z. Zeb, A. Helal, M. H. Suliman, B. Y. Alfaifi, N. Iqbal, M. Abdinejad, A. A. Tahir, H. Ullah, *Nanomaterials* **2021**, *11*, 2029.

39 M. Usman, A. S. Ghanem, S. Niaz Ali Shah, M. D. Garba, M. Yusuf Khan, S. Khan, M. Humayun, A. Laeeq Khan, *Chem. Rec.* **2022**, *22*, e202200039.

40 N. M. Keppetipola, M. Dissanayake, P. Dissanayake, B. Karunarathne, M. A. Dourges, D. Talaga, L. Servant, C. Olivier, T. Toupance, S. Uchida, K. Tennakone, G. R. A. Kumara, L. Cojocaru, *RSC Adv.* **2021**, *11*, 2854–2865.

41 M. M. Hasan, T. Islam, S. S. Shah, A. Awal, M. A. Aziz, A. J. S. Ahammad, *Chem. Rec.* **2022**, *22*, e202200041.

42 A. A. Abd, M. R. Othman, J. Kim, *Environ. Sci. Pollut. Res.* **2021**, *28*, 43329–43364.

43 J. L. Goldfarb, G. Dou, M. Salari, M. W. Grinstaff, *ACS Sustain. Chem. Eng.* **2017**, *5*, 3046–3054.

44 S. M. Abu Nayem, A. Ahmad, S. S. Shah, A. Saeed Alzahrani, A. J. Saleh Ahammad, M. A. Aziz, *Chem. Rec.* **2022**, https://doi.org/10.1002/tcr.202200181, e202200181. Accessed February 2023.

45 M. M. Faisal, S. R. Ali, S. S. Shah, M. W. Iqbal, S. Pushpan, M. A. Aziz, N. P. Aguilar, M. M. Alcalá Rodríguez, S. L. Loredo, K. C. Sanal, *Ceram. Int.* **2022**, *48*, 28565–28577.

46 S. S. Shah, M. A. Alfasane, I. A. Bakare, M. A. Aziz, Z. H. Yamani, *J. Energy Storage* **2020**, *30*, 101562.

47 M. A. Aziz, S. S. Shah, S. M. A. Nayem, M. N. Shaikh, A. S. Hakeem, I. A. Bakare, *J. Energy Storage* **2022**, *50*, 104278.

48 W. Hong, L. Wang, K. Liu, X. Han, Y. Zhou, P. Gao, R. Ding, E. Liu, *J. Alloys Compd.* **2018**, *746*, 292–300.

49 T. K. Kim, M. P. Suh, *Chem. Commun.* **2011**, *47*, 4258–4260.

50 Z. Yang, R. Gleisner, D. H. Mann, J. Xu, J. Jiang, J. Y. Zhu, *Polymers* **2020**, *12*, 2829.

51 S. M. Manocha, *Sadhana* **2003**, *28*, 335–348.

52 A. E. Creamer, B. Gao, *Environ. Sci. Technol.* **2016**, *50*, 7276–7289.

53 M. E. Casco, M. Martínez-Escandell, J. Silvestre-Albero, F. Rodríguez-Reinoso, *Carbon* **2014**, *67*, 230–235.

54 J. Wilcox, R. Haghpanah, E. C. Rupp, J. He, K. Lee, *Annu. Rev. Chem. Biomol. Eng.* **2014**, *5*, 479–505.

55 Z. Chen, S. Deng, H. Wei, B. Wang, J. Huang, G. Yu, *Front. Environ. Sci. Eng.* **2013**, *7*, 326–340.

56 H. Yuan, Z. Zhang, Y. Mi, F. Ye, W. Liu, J. Kuan, X. Jiang, Y. Luo, *Energy Fuel* **2020**, *34*, 8316–8324.

57 S. Deng, B. Hu, T. Chen, B. Wang, J. Huang, Y. Wang, G. Yu, *Adsorption* **2015**, *21*, 125–133.

58 H. Wei, S. Deng, B. Hu, Z. Chen, B. Wang, J. Huang, G. Yu, *ChemSusChem* **2012**, *5*, 2354–2360.

59 M. Ashraf, I. Khan, M. Usman, A. Khan, S. S. Shah, A. Z. Khan, K. Saeed, M. Yaseen, M. F. Ehsan, M. N. Tahir, N. Ullah, *Chem. Res. Toxicol.* **2020**, *33*, 1292–1311.

60 A. Helal, S. S. Shah, M. Usman, M. Y. Khan, M. A. Aziz, M. Mizanur Rahman, *Chem. Rec.* **2022**, *22*, e202200055.

61 M. Rauf, S. S. Shah, S. K. Shah, S. N. A. Shah, T. U. Haq, J. Shah, A. Ullah, T. Ahmad, Y. Khan, M. A. Aziz, K. Hayat, *J. Saudi Chem. Soc.* **2022**, *26*, 101514.

62 S. S. Shah, M. A. Aziz, W. Mahfoz, A.-R. Al-Betar, Conducting Polymers Based Nanocomposites for Supercapacitors in *Nanostructured Materials for Supercapacitors*, (Eds. S. Thomas, A. B. Gueye, R. K. Gupta), Springer, Cham, **2022**, Chapter 22, 485–511, vol. *1*.

63 E. Taer, R. Taslim, A. Putri, A. Apriwandi, A. Agustino, *Int. J. Electrochem. Sci.* **2018**, *13*, 12072–12084.

64 M. Yu, Y. Han, J. Li, L. Wang, *Chem. Eng. J.* **2017**, *317*, 493–502.

65 S. S. Gunasekaran, S. Badhulika, *Energy Storage* **2022**, https://doi.org/10.1002/est2.404, e404. Accessed February 2023.

66 C. Jiang, G. A. Yakaboylu, T. Yumak, J. W. Zondlo, E. M. Sabolsky, J. Wang, *Renew. Energy* **2020**, *155*, 38–52.

67 E. Taer, M. Deraman, I. A. Talib, A. A. Umar, M. Oyama, R. M. Yunus, *Curr. Appl. Phys.* **2010**, *10*, 1071–1075.

68 L. Wang, F. Sun, J. Gao, X. Pi, T. Pei, Z. Qie, G. Zhao, Y. Qin, *J. Taiwan Inst. Chem. Eng.* **2018**, *91*, 588–596.

69 M. Vinayagam, R. Suresh Babu, A. Sivasamy, A. L. Ferreira de Barros, *Biomass Bioenerg.* **2020**, *143*, 105838.

70 K. Zhu, Y. Wang, J. A. Tang, S. Guo, Z. Gao, Y. Wei, G. Chen, Y. Gao, *Mater. Chem. Front.* **2017**, *1*, 958–966.

13

Steam-activated Carbon for Supercapacitors

Madhusudan Roy[1] and Hasi Rani Barai[2],*

[1] Department of Physics, National Taiwan University, Taipei, Taiwan
[2] Department of Mechanical Engineering, School of Mechanical and IT Engineering, Yeungnam University, Gyeongsan 38541, Republic of Korea
* Corresponding author

13.1 Introduction

To understand steam-AC first we need to understand activated carbon (AC). AC, sometimes entitled activated charcoal, is a certain pattern of carbon utilized for air and water filtration with several contaminants. ACs are prepared so that the synthesized materials will have a lot of small pores with relatively larger pore volumes, and a relatively large amount of materials can adsorb. The ACs are used for several purposes, e.g., purifying liquids and gases [1, 2], and preparation of storage devices, including supercapacitors [3–11]. Based on the target application, ACs are prepared using different methods and from different materials.

ACs are used for different purposes such as in industrial processes, medical science, analytical study, environmental science, agricultural purposes, purification of alcoholic beverages, manufacturing supercapacitors, energy storage devices, storing fuels, purifying gas and chemicals, removing mercury, food additives, and caring for skin. The ACs can be synthesized or prepared from carbonaceous materials like bamboo, coconut husks, jute sticks, willow peat, wood, and coir, and lignite from coal and petroleum pitches [12–21]. As the purpose of use and raw materials differ, scientists prepare ACs using different techniques. Some of them are quite expensive, complicated, and time-consuming; some of them are very simple and very fast. Among them, steam-AC is a very environmentally friendly, cheap, easy and fast process for synthesizing AC. The steam-activation mechanism can be explained as the creation and development of pores in carbonaceous substances via minor oxidation caused by the passing of hot steam over it. At higher temperatures (700–800 °C), generally, water reacts with carbon to produce $CO + H_2$. So, carbon is oxidized, very narrow holes/pores are created, increasing with time, and the materials are considered AC. This chapter will discuss steam-AC's different aspects and their applications in supercapacitors.

From when modern society was revolutionized with industry, humans experienced fast technological progress and uncontrolled population increase, rapidly adding the necessity for more foodstuffs and energy [22, 23]. Up to now, above 85% of the entire power required is supplied by hydrocarbon deposits, like char, petroleum, and natural gases [24]. Due to the steady rise in worldwide energy use, fossil fuel storage is decreasing fast, and energy generation from a more accessible way will be a challenge [22]. Along with this, the generation of energy from fossil fuels creates a lot of CO_2 and some additional greenhouse gases that are ultimately culpable for increasing the temperature of the atmosphere and oceans and will be responsible for many circumstances associated with environmental problems [24, 25].

In the last 30–40 years, the reduction of non-renewable energy sources and related environmental difficulties stimulated scientists' awareness and helped people investigate environmentally sustainable and renewable energy [26]. Using many energy sources is commonly influenced by unpredictable external conditions like climate or geological changes [26]. To ensure the uninterrupted and steady harvest of this reusable, long-lasting power, the progress and investigation into better quality, energy-storing systems attracted the scientists and environmental protection agencies of several countries. Electrochemical energy-storing processes and systems can add to and support the energy requirements of the world [26, 27]. Some major and widely used battery devices are made of lithium-ion, lead-acid, Ni-H$_2$, fuel cells, metal-air, Na-ion, Ni-Cd, supercapacitors, and H$_2$O depletion schemes, along with emergent energy-storing devices, like as Al-ion, Mg-ion, Zn-ion, and other H$_2$O-based metal ion batteries have also received attention from several scientists [23, 28–30]. The electrochemical energy storing techniques can improve capacity and support the faster acceptance of transferrable electrical parts and static energy generation plants [28]. Recently, the electrical energy-storing mechanism genertaed great interest from scientists and became a widely studied topic in the academic community and commercial manufacturing world [29].

Supercapacitors are unable to be used on their own; rather, they are connected to other apparatuses for increasing total capacity along with the lifetime of energy-storing apparatuses to gain maximum workability [31]. However, the specific capacity for supercapacitors is quite large, which can rise up to ten times or more than the regular Pb-acid batteries [31]. At a higher power level, the supercapacitors exhibit more precise energy than the batteries [32]. Also, supercapacitors can be applied in handy power sources as they have a quicker charging speed. Supercapacitors can be implemented at a wider range of temperatures (-40 to 80 °C), whereas traditional batteries can be used only in a concise range of temperatures [33, 34].

Most of the time, electrode materials do not react during discharge. So, the lifetime for supercapacitors can be longer [34] than that in simple batteries because the electrode materials of batteries decompose during discharge. Based on these special properties, the supercapacitors represent very high ability and value in the upcoming energy systems.

Due to the regular developments of electronic instruments, the use and progress of supercapacitors has become a barrier. As shown in the Ragone plots (Figure 13.1) energy and power densities for batteries and supercapacitors are quite different. Batteries offer energy densities among 150–500 Wh kg^{-1} [31, 34, 35]; however, the power density value shows a lower value due to the slower movement of electrons rather than the faster transfer of ions. To keep the larger energy output of batteries, the discharge time needs to be very long, 10–60 minutes or greater. In comparison to this, electric double-layer capacitors with
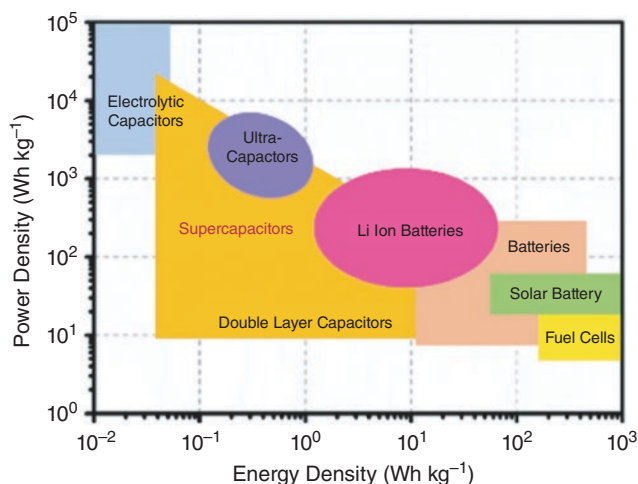
Figure 13.1 Ragone plots of various energy storage systems. *Reproduced with permission* [43]. *Copyright 2014, Royal Society of Chemistry.*

larger power density can fully discharge the energy within 10 seconds. The yield powers are around 10–20 kWkg^{-1} [23, 25, 26, 35]. If the supercapacitor discharge time is increased, the energy density can't be increased more than 30 Whkg^{-1} [35]. The electrode material plays a crucial role in supercapacitors. The study of the creation and modification of electrode materials to overcome the limits of utilization predictions of supercapacitors will show tremendous application to manufacturing advanced energy storing arrangements.

Among the various energy-storing materials, carbon has huge advantages over many others, such as availability, affordable cost, consistent chemical characteristics, larger specific surface area (SA), relatively easier to regulate the porous pattern and surface characteristics, etc [36]. Therefore, electrode materials made of carbon are the most studied and highly developed for supercapacitors [30, 37]. The actual performance of a carbon-based supercapacitor is very much interrelated with the chemical and physical characteristics of the source materials. The porosity, specific SA, the density of electrodes, and conductivity of supercapacitors made from carbon need to be adjusted to find the optimum condition [22, 38]. Major electrode materials made of carbon are porous carbon, graphene, carbon nanotubes, carbon nanofibers, and/or their combinations [39–41]. Among them, porous carbon and graphene are mostly studied due to their better performance than the performance of the others. However, there have been a lot of difficulties in manufacturing and successful energy-storing. For example, chemical vapour deposition creates graphene, which creates environmental problems and is unsustainable [42].

Porous carbon synthesized from graphite and petroleum is not renewable and is contaminative, and requires unenvironmentally-friendly methods to prepare them [44]. Therefore, scientists are trying to find an appropriate, environmentally clean, and cost-effective path for manufacturing a sequence of carbon electrode substances to solve the many difficulties that have to be faced. Biomass, including renewable harvests or animals, can be considered environmentally clean raw materials for preparing materials for the

electrode to be used in supercapacitors. Electrode materials prepared from biomass create permeable and layered shapes following a simple method [45]. Many studies are presently going on to prepare electrode materials from renewable biomass. It is considered that the carbon in trees, plants, and aquatic bodies, can be used economically. Worldwide crop production per annum is around 146 billion tons [46], and domestic and wild agricultural wastage is around 1014 kg [47]. That is a severe problem for the environment. Therefore, if the biomasses can be used to prepare AC it reduces the waste [48].

13.2 Supercapacitors

Supercapacitors or ultracapacitors are capacitors having large capacitance values and lower voltage limits compared to many other capacitors. Normally the supercapacitor is able to accumulate 10 to 100 times higher energy than other capacitors. The charge of rechargeable batteries depends on the control of ions diffusion, which determines the rate of charging-discharging of lithium-ion batteries [49–56]. As supercapacitors have larger power capacity, wider cycling stability relative to lithium-ion batteries, and improved energy density relative to dielectric capacitors, they are generally acknowledged as good replacements for batteries for high power-requiring applications [57–59]. Based on their charge storing method, supercapacitors can be divided into two broad groups: electrical double-layer capacitors (EDLC) and pseudo-capacitors. The value of the specific capacitance of a supercapacitor defines the electrical charge stored. The specific capacitance can be represented as gravimetric capacitance, areal capacitance, and volume capacitance. Previously, carbon materials like graphene, active carbons, carbon nanotubes, and nanofibers have been used for electrical double-layer capacitors. However, having a larger distinct SA, a lot of openings, improved conductivity, and carbon materials impacts power performance and cycling stability. Again, due to being less harmful to nature, less expensive, highly available in nature, renewable resource-based substances can be vastly utilized for the preparation of supercapacitor electrodes corresponding to a sustainable growth. Actually, these types of biomaterials are available around us in different forms, just like as a particular portion of a tree (shaddock peel, bamboo, petals, etc.), some substances found in vertebrates or insects (silk, crab shell, honeycomb, etc.), and significant metabolites alike cellulose, starch, etc [60].

13.3 Preparation of Activated Carbon

The manufacture of AC involves two main steps: carbonization and activation that are can be performed discretely or in a combination of two steps. The carbonization of a source occurs within a temperature range of 400–850 °C without the presence of oxygen [61]. Activation can be explained as transforming carbonaceous substances into AC using heat in an incinerator or microwaves in a regulated environment and temperature [61]. Typically, activation is done in either a physical or chemical process. Steam activation belongs to the class of physical activation. For physical activation, some oxidizing gases such as steam, air, CO_2, or a combination of the mentioned gas mixtures are used within

the temperature range of of 600–900 °C [61]. The selection of activating gases depends on the type of raw materials because different activating agents will behave differently from different sources [62]. The creation of more pores is directly related to the increase in surface space and opening volume, and is the main activity of the activator. The amount of carbon released relies on the value of temperature, the continuation of burning, the flow of gas, and the category of the furnace. Examples of steam-ACs are corncob, ashes obtained from bagasse, macadamia nut shell, rice husk, sawdust, etc [62], date stones, bean pods, coconut shells, apple pulp, olive stones, etc [63]. jatropha hull, coconut shells [64].

13.4 Activated Carbon from Biomass

To create AC from biomass [12], two main processes are applied: carbonization and activation. Carbonization is achieved by heating biomass to an upper temperature inside an oven generating biochar. At this level, the volatile components are removed by thermal decomposition. There are some common parameters to control the quality of the carbonization: heating temperature, heating rate, flow rate of N_2 gas, and the time of the operation. The active SA of biochar is lower than 300 m^2g^{-1} [65], and the level of adsorption at this stage is quite low; therefore, the activation process is very important for the expansion of volume and size and SA of the pores [66]. After that, the poorly organized carbons are removed when microporous structures are prepared. In the final stage, the available openings are expanded into a larger diameter by igniting the walls within the pores, increasing the intervening opening and macro-porosity and decreasing the size of the micropores. Depending on the activation process, the removal the remaining deposited substances in the biochar may be done before or after the carbonization, which will increase the porosity and larger SAs for the ACs [67]. The selections of the carbonization parameters are essential because they determine the quality of the final product [68]. Among them, the parameters are carbonization temperature, heating rate, amount and flow rate of inert gas, and holding time, as depicted in Figure 13.2.

Normally, extra resilient substances are removed at a higher temperature, and the amount of rigid carbon and ash composition increases. However, the amount of biochar yield decreases with increasing temperature [70]. The reduction in yield is due to the break down of primary and secondary biomass and biochar at a higher temperature. However, higher temperature creates better-quality biochar [71]. It has been observed in several types of
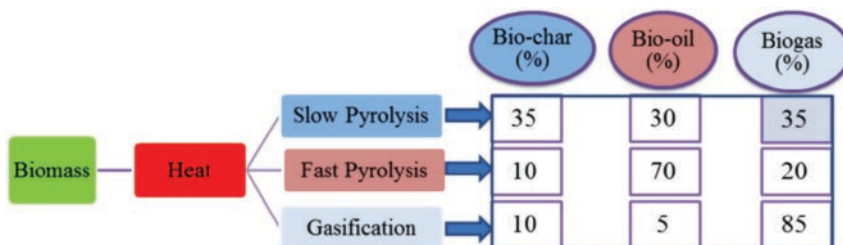
Figure 13.2 Thermochemical conversion of biomass into bio-oil, biochar, and gases. *Reproduced with permission* [69]. *Copyright 2014, Elsevier.*

research that the two-step activation creates better textural properties and qualities. ACs produced via the physiochemical process produce well-developed and evenly distributed pore structures [72]. The highest adsorption capacity of 114.8 mg/g of AC was produced from tropical almond shells synthesized by the activation of a mixture of CO_2 and steam [73].

To prepare steam-AC, carbonization is carried out at 500 °C, when initial oxidation occurs. The process generates a lot of heat, like burning some oxygen fuel, which is an exothermic process. Therefore, it is necessary to control the temperature precisely. The process begins at 150 °C, gradually increasing to 500 °C at the carbonization phase. Table 13.1 represents the reactions for solid or gas reactions, including the amount of energy required or released. The pores created at this level are relatively small. Therefore, the adsorption is too low. However, it does not have any volatile substances. At this stage, we need to find some way to increase the pore size and number of pores. One of the best ways to do that is to activate using steam at around 1000 °C. The overall process is exothermic (formation of carbon dioxide from carbon). It can create a lot of additional energy, which can be reused to generate steam or can be supplied to some energy storage system.

Different kilns and reaction furnaces are utilized for carbonization and activation. Rotary, multi-heart furnaces and fluidized bed reactors are among them. One of the easiest ways to do that is simply bending the kiln to a few degrees, adding water at a controlled rate along with the flow of nitrogen around the temperature of 750 °C. A controllable pump is used, which can control the flow of water. For that purpose, a bubble saturator can be used, which is relatively cheap, and it is possible to control the saturation level by keeping the bubbler in a temperature-controlled bath. Every drop will move towards the hotter area of the furnace and convert into steam, which will interact with the carbon to convert into AC. Next, we will discuss examples of how some research groups prepared steam-AC from different raw materials and their specific applications.

For the physical activation, mainly steam or CO_2 are used because both of them can react with carbon. Sometimes oxygen can be used for the activation. But the steam or CO_2 activation efficiency is relatively high; the maximum SA can be 1000 m^2/g or higher. Steam is a better activator than CO_2 or oxygen [12]. Water molecules are smaller than carbon dioxide molecules, and H_2O molecules can distribute easily within the openings of biochar compared to carbon dioxide [74]. So, steam can react faster to produce more pores in biochar than carbon dioxide [75]. It has been reported that steam reacts at least four times faster with carbon around the activation temperature than CO_2 [65]. So the steam activation can

Table 13.1 The reactions occurring for solid/gas reactions.

Gas / solid reactions or Gas / gas reactions	Endothermic / exothermic	ΔH / kJ mol^{-1}
C(graphite, solid) + H_2O(g) → CO(g) + H_2(g)	Endothermic	130
C(graphite, solid) + CO_2(g) → 2 CO(g)	Endothermic	171
C(graphite, solid) + ½ O_2(g) → CO(g)	Exothermic	−111
C(graphite, solid) + O_2(g) → CO_2(g)	Exothermic	−393
CO(g) + ½ O_2(g) → CO_2(g)	Exothermic	−283
H_2(g) + ½ O_2(g) → H_2O(g)	Exothermic	−241

reach the maximum SA in a shorter period than CO_2 [76]. At a standard heating rate, the CO_2 develops advanced opening beyond the elevating of thinner pores. Also, steam activation widens the micropores into mesopores or macropores, and allows wider pore distribution for the ACs [70]. At a higher activation rate, a higher percentage of mesoporous and microporous structures are found for steam activation and CO_2 activation, respectively [65].

13.4.1 Steam-activated Carbon from Almond, Pistachio, and Walnut Shells

Steam-AC from three separate horticultural wastage substances, almond shells, pistachio shells, and walnut shells, was synthesized and optimized using the best method of activation [14]. First, the raw materials are collected, cleaned with deionized H_2O, and heated in a furnace at around 80 °C. Then the heated shells are ground in a rotary machine for half an hour, and regular shaped granules are separated by passing through a mesh 20. The classified particles are cleaned two more times with deionized water and heated in the furnace for six hours at 70 °C. The chemical composition of the samples is represented in Figure 13.3. After that, each sample is taken into a special crucible, placed into an atmospheric furnace, N_2 gas
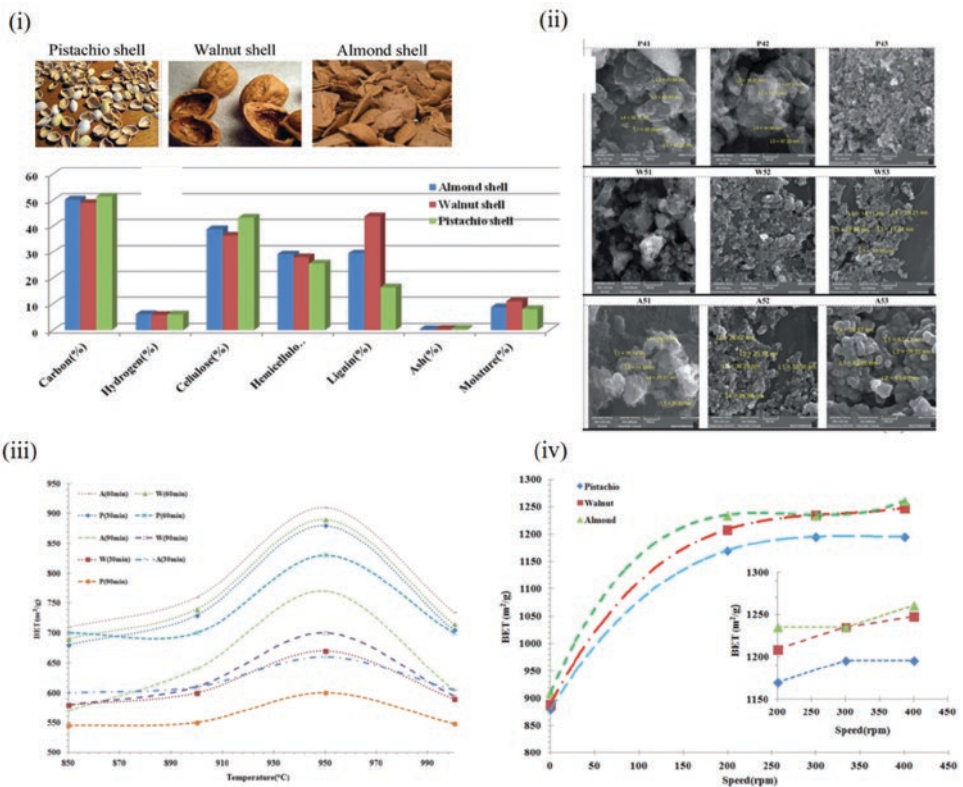
Figure 13.3 (i) Elemental composition of walnut (W), pistachio (P), and almond (A) shells samples used for the preparation of AC (ii) FESEM image of crushed activated nano-carbons after planetary ball mill (iii) Specific SA test results and temperature changes (after vibration milling). (iv) Results and changes of specific SA testing of samples after milling. *Reproduced with permission* [14]. *Copyright 2020, Royal Society of Chemistry.*

is added, and the sample is heated to around 600 °C for 60 minutes. It was then allowed to cool to ambient temperature by reducing by 10 °C min^{-1}. During the process, 150 cm^3 min^{-1} of N$_2$ gas was supplied to make the system inert. After the carbonization process, the particles are heated at 850–1000 °C temperature to activate it by increasing the temperature to 3 °C min^{-1} and continuous steam flow at 130 cm^3 min^{-1}, varying the retention time at different temperatures. During the activation process, the pores created during carbonization increase in size, which increases the active SA. The retention time is another important factor for the activation because, at the early stage of activation, the inorganic materials are removed, aromatic structures are created, and micropores developed at the end of the activation process.

The FESEM image of crushed activated nano-carbons after the planetary ball mill is shown in Figure 13.3(ii). The size of the particles just after the vibrating mill is too large, 5–20 μm, rather than being at the nano-scale. Therefore, it is confirmed that only the vibrating mill cannot create AC. So, intermediate planetary milling with higher energy was utilized, which converted the source into a porous structure that is visible in the SEM image. The porous structure allows the steam to penetrate and improve the quality of AC. Under the experimental conditions, AC obtained from walnut shell gives the best structure, size, and morphology as seen in Figure 13.3(ii)-(iv)[14]. The average size of the different raw materials were 50–100 nm. After 1 hour of carbonization at 600 °C using a N$_2$ environment and activated using steam at 950 °C for 0.5 hr for pistachio shell and 1 hour for walnut shell and almond shell, the BET SA obtained was 1196 (pistachio shell), 1261 (walnut shell), and 1248 (almond shell) m^2/g of AC [14].

13.4.2 Steam-activated Carbon from Coconut Charcoal or Coconut Shell

First, the char is prepared by heating the coconut shell or coconut charcoal to produce the char. Then the char is heated to a greater temperature at around 925–985 °C in a kiln with steam but no oxygen. During the activation process, all the volatile compounds present in the char or coal are removed, and carbon atoms from layer by layer of the char are peeled off, enhancing the available pores and keeping the carbon skeleton almost unchanged. The reaction between C + steam produces H$_2$ gas and CO gas. Once the CO gases are taken off, it takes away carbon atoms, and the weight of the AC reduces to almost one-third of the char, which has been phrased as *"less is more"* where the number of carbons are less, producing more internal spaces. In the next step, the hot activated charcoal is cooled down to remove the soluble ash by washing it with water or acid. Actually, it takes a lot of water to wash out; therefore, it is better to use some acid first to wash the acid-soluble contents, then wash several times with water to remove the acid content. During this washing procedure, some by-products can be collected, which can be called charcoal vinegar, and it can be processed into table vinegar.

AC was manufactured using coconut shells applying steam for activation and used to test the supercapacitor's energy storage capacity [77]. Figure 13.4(i) shows the preparation methodologies of AC from coconut shells. Two different routes were followed, and the ultimate products were synthesized based on the methods shown and activated with steam. Figure 13.4(ii) shows the pore size dissemination of the prepared ACs, which shows that the width of the pores are quite homogenous, and most of the samples show unique width except the last samples. Figure 13.4(iii) depicts the Ragone diagram contrasting the supercapacitor's power density and specific energy with AC5 electrodes and references.
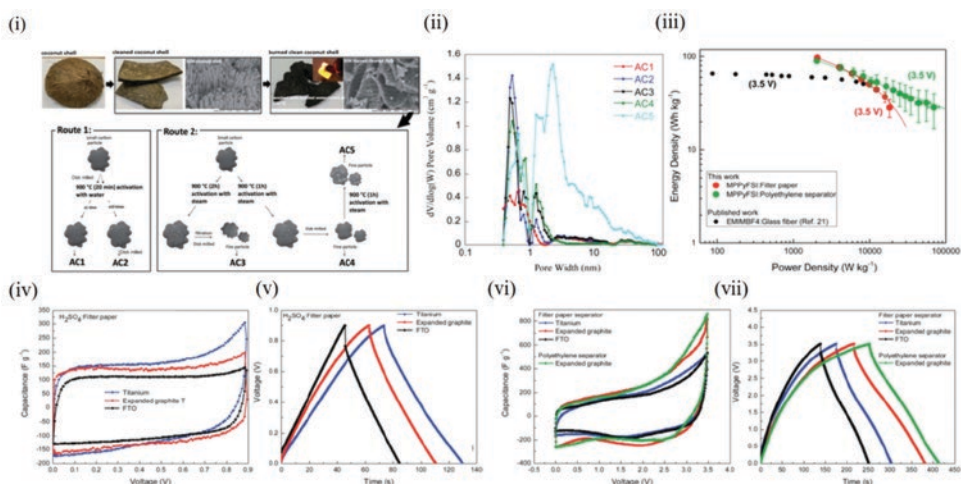
Figure 13.4 (i) Steam AC from coconut shells, (ii) pore size distribution, (iii) Ragone plot. The contrast of power density and specific energy of the supercapacitor with AC5 electrodes and references. Electrochemical characterization of supercapacitors based on AC5 (iv) CV curves at 5 mV s^{-1} (v) CD curves at 0.5 A g^{-1}. Electrochemical categorization of non-volatile supercapacitors with AC5 electrodes (vi) CV curves at 5 mV s^{-1}, (vii) CD curves at 1 Ag^{-1}. *Reproduced with permission* [77]. *Copyright 2021, Royal Society of Chemistry.*

By comparing the filter paper divider, the part with the polyethylene divider gives higher power and energy management capacity at a current density of 30 Ag^{-1}. Electrochemical categorization of supercapacitors based on AC5 represented as CV and CD patterns in Figure 13.4(iv) and Figure 13.4(v) at 5 mV/s at 0.5 A/g, respectively, and CV curves at 5 mV s^{-1} (v) CD curves at 0.5 A g^{-1}. Figure 13.4(vi, vii) shows the electrochemical characterization of non-volatile supercapacitors with AC5 electrodes (vi) CV graph at 5 mV s^{-1}, (vii) CD pattern at 1 A g-1. Figure 13.4(vi) and 4(vii) respectively. The XRD, Raman, conductivity, SEM analysis, N$_2$ gas adsorption capacity, and TGA-MS analysis reflect the synthesized AC and show graphitic character with a larger SA and higher pore volume. The ACs are used to prepare electrodes that show a BET SA of 1998 m^2/g, with a high capacitance value of 132.3 F/g in an aqueous electrolyte (1.5 M H$_2$SO$_4$). The AC synthesized with coconut shells and an ionic liquid represents an exceptional energy-storing capacity and energy-power control capacity of 219.4 F/g with a specific energy of 92.1 Wh/kg while the power density of 2046.9 W/kg at 1 A /g. It indicates an ultra-high value of 30 A/g representing the wider potential and power-related use. As reported by Keppetipola et al [77], this is the maximum value of energy-power handling capacity of an ionic liquid-based supercapacitor prepared from coconut shells.

13.4.3 Steam-activated Carbon from *Eucalyptus* Wood Chips

Figure 13.5a-f shows the AC production system from *Eucalyptus* wood chips, and Figure 13.5(g-j) shows the scanning electron microscopic study of dried *Eucalyptus* raw wood chips, activated at 500 °C, 600 °C, and 700 °C [78]. Actually, this method was used to steam-activate carbon materials on a large scale. First, *Eucalyptus* wood chips without bark and
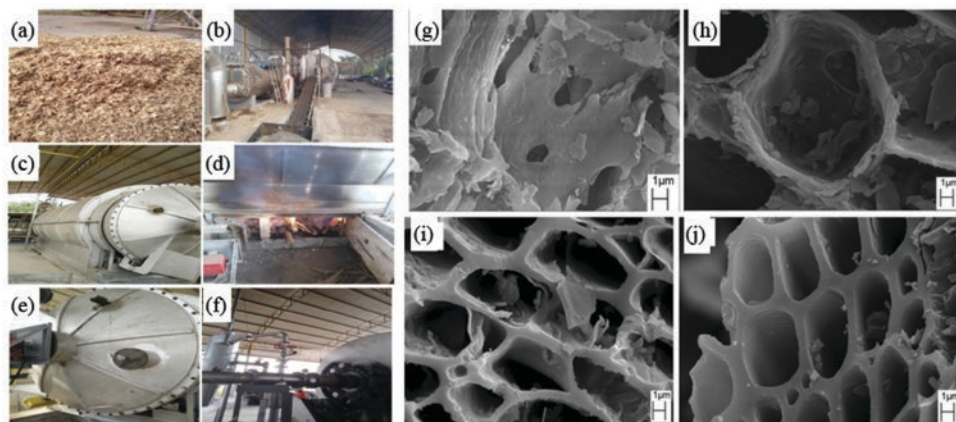
Figure 13.5 AC production system from *Eucalyptus* wood in set periodic revolving furnace (a) *Eucalyptus* logs chips being dehydrated using sunlight, (b) conveyor belt, (c) rotary kiln, (d) wood stove, (e) thermocouples, and (f) pipe vent (25 mm diameter). Scanning electron microscopic study of (g) dried *Eucalyptus* raw wood chips, activated at (h) 500 °C, (i) 600 °C, and (j) 700 °C. *Reproduced with permission* [78]. *Reproduced under the terms of the CC BY 4.0 license. Copyright 2021, Mopoung et al. published by nature.*

having a regular dimension (2.5 × 3.75 × 0.5 cm) were collected from a wood factory and dried in the sun. 2000 kg of the dried chips was taken to a rotary kiln. After that, the wood chips were burned, setting fire in an oven below the rotary kiln while the kiln was rotated continuously at a rate of 0.25 rpm. The temperatures were monitored back and forth, setting up thermocouples. The heating was increased slowly in steps of 2.5 °C per minute until the required temperature was attained. At this stage, steam was constantly applied from a boiler to activate the carbon to the kiln at 3 bar steam pressure for two hours. An almost equal amount of steam to the raw wood chips was added (a 1:1 mass proportion for water vapour and fresh logs chips). The gases obtained from the pyrolysis inside the kiln are transferred out of the system using an exhaust pipe. Once the steam activation took place for two hours, the oven and the kiln were turned off and allowed to reduce the temperature for the whole night to normal temperature. The cooled AC substances were taken out of the furnace and used for further study. Using this method, they obtained around 22–32% of the wood chips were converted into stem-AC with an absorptivity of 518–737 mg I_2 / per g [78]. The ACs' BET SA and micropore volume were estimated as 427–870 m^2/g and 0.1–0.2 cm^3/g.

13.4.4 Steam-activated Carbon from Malt Bagasse

Figure 13.6 shows the N_2 adsorption and desorption isotherms at 77 K, and pore size distribution. It also shows SEMs of malt bagasse precursor, and steam-AC [79]. Figure 13.6 shows that at lower relative pressure, more N_2 is adsorbed, which shows the presence of more micropores. The pore diameter is quite homogenous, with the maximum particle pore diameter around 4 nm. The local beer industry collected the fresh malt bagasse to prepare the steam-AC. The raw bagasse was dried in a stove at 100 °C for about 24 hours
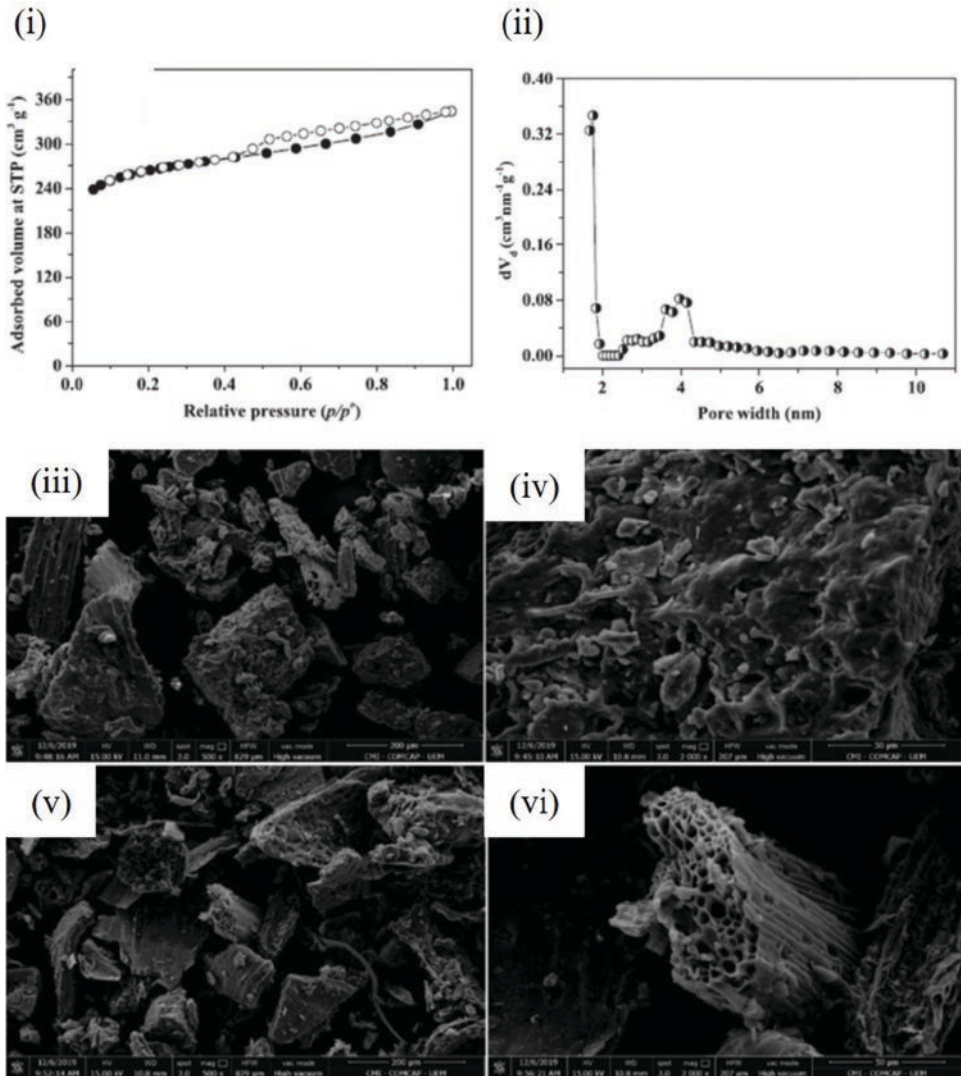
Figure 13.6 (i) N$_2$ adsorption and desorption isotherms at 77 K (ii) pore size distribution. SEM of malt bagasse precursor (iii-iv) and steam-AC (v-vi). *Reproduced with permission* [79]. *Copyright 2021, Elsevier.*

and grounded. Different parameters, like moisture content, volatile substance, rigid carbon contents, etc., were measured to get an idea as to which extension needs to be heated for further processing. The major factors for preparing AC were adjusted by combined strategy and feedback surface policy: temperature, pressure, and heating time. The steam flow rate was kept parallel to the flow of N$_2$ as carrier gas. The steam used for the process was created with the help of a round bottom flask positioned on a hot plate. As the synthesis was on a laboratory scale, around five grams of previously dried malt bagasse were taken in a covered ceramic vessel and heated in a muffle incinerator. The heat was raised gradually by 10 °C per minute in two distinct steps. First, the carbonization was performed by passing

100 cm^3 min^{-1} of nitrogen gas around a temperature of 500 °C for about two hours. Then, the activation step was performed from 600–735 °C at a steam pressure of 187–53 cm^3 min^{-1} for about 60–120 min. From the variation of different parameters for the manufacture of steam-AC from malt bagasse, they found that the optimum conditions for the process are 841 °C, 82-min steam flow of 164 cm^3 min^{-1}, and that gives the BET SA of 917 m^2 g^{-1}, and yield 9.45% [79]. They tested the adsorption of the optimized AC with the adsorption capacity of 199.7 mg g^{-1} at 55 °C for the food dye sunset yellow.

13.4.5 Steam-activated Carbon from *Artocarpus integer* Biowaste

To prepare the steam-AC from *Artocarpus integer* (AI) biowaste, first the raw material, AI biowaste, is cleaned and removed the carpel fibers. Then it was autoclaved to make it free from microbes and dried in air for one day beforehand, heating in a furnace for 48 h at 70 °C. The dried substances are blended and separated using an 18 mesh (1 mm). A tubular oven and a temperature controller were used for the pyrolysis and steam activation. Fifteen grams of powdered biowaste were taken in a porcelain ceramic pot and heated in a furnace, and highly pure N$_2$ was passed at an amount of 25 cm^3 min^{-1} up to 10 min. Next, the cracking was performed at around 600–950 °C by increasing the temperature to about 10 °C / min and passing nitrogen gas at a rate of 100 cm^3 min^{-1} for about 20–140 min. Direct pyrolysis steam activation was applied for the creation of Eco-ACs. The biochar obtained from the incineration of the biowastage at 700 °C for 1 hour was warmed with flowing nitrogen of 20 cm^3 min^{-1} and raised the temperature to about 10 °C min^{-1} to gain the desired temperature. At this stage, steam was introduced instead of N$_2$ gas after the targeted steam activation temperature was obtained. The water vapor level was created by adding deionized H$_2$O by 5 ml min^{-1} to a warm quartz hose using a peristaltic push. The temperature of the furnace was kept constant while flowing stream to the system for the desired time. Then it was gradually cooled down to the normal temperature by flowing nitrogen. The unwanted volatile materials were removed from the furnace, through nitrogen gas. The cooled ACs cleaned by washing with 0.1 M HCl at a proportion of 100:1 of HCl and carbon, w/w. After that, to wash away the excess HCl, it was cleaned with distilled H$_2$O and warmed up to 70 °C. Figure 13.7(i-viii) shows the scanning electron microscopic image of biochar (carbonized at 700 °C for 60 min) collected before steam-gasification and Eco-ACs prepared under optimum pyrolysis (700 °C; 1 hour) and steam-gasification (750 °C; 1 hour) situations. Pore size spreading lines of Eco-AC prepared at optimized situations (700 °C; 1 hour) and steam-gasification (750 °C; 60 min) [2]. From Figure 13.7, it is clear that the active SA for particles before activation is very low, while after activation, it has increased to a significant level. That is explained by the dimensions of pore distribution represented in Figure 13.7(ix-x).

13.4.6 Activated Carbon from Bamboo

First, the bamboo raw materials were collected, cut into smaller pieces, cleaned using fresh H$_2$O, and heated into an airtight furnace up to 150 °C for about 24 hours. The heated samples were carbonized for 60 minutes at a temperature of 1000 °C and ball-milled to convert into powder of an average diameter of 40 mm. The powdered samples are washed with 3M HCl to discard ash-like substances. Then the acid-washed samples are activated by
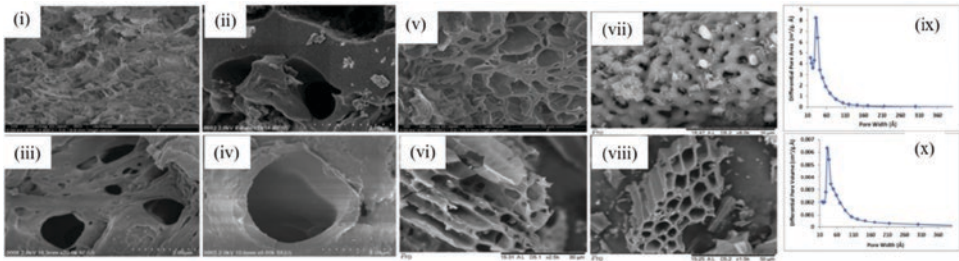
Figure 13.7 SEM of (i) biochar (carbonized at 700 °C for 1 hour) taken just before steam-gasification and (ii)–(viii) Eco-ACs synthesized at optimized condition (700 °C; 1 hour) and steam-gasification (750 °C; 1 hour) parameters. Scattering of pore size of Eco-AC prepared at optimized condition (700 °C; 1 hour) (ix) and steam-gasification (750 °C; 1 hour) (x). *Reproduced with permission* [2]. *Copyright 2018, Elsevier.*
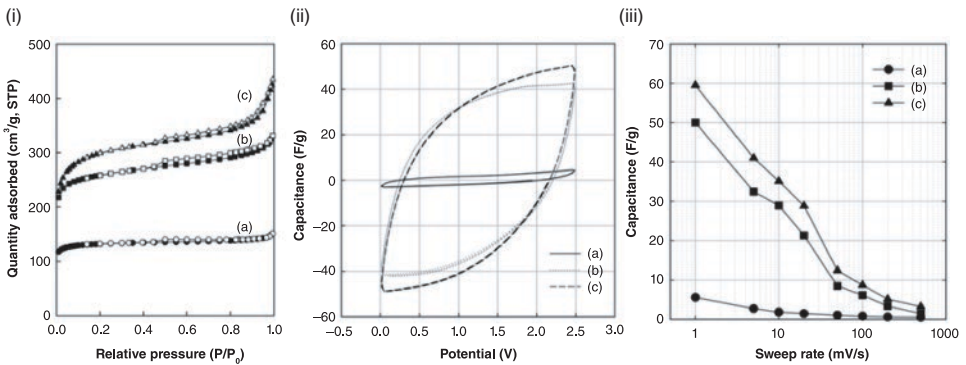
Figure 13.8 (i) N_2 adsorption isotherms at 77 K for AC prepared from bamboo (a) 700 °C, (b) 800 °C, and (c) 900 °C. (ii) CV at three different temperatures. (a) 700 °C, (b) 800 °C, and (c) 900 °C in 1M TEA electrolyte at 5 mV/s sweep rate. (iii) Dependence of specific capacitances on the sweep rate for raw materials activated at several temperatures: (a) 700 °C, (b) 800 °C, and (c) 900 °C. *Reproduced with permission* [80]. *Copyright 2006, Springer.*

supplying 30 vol % of steam using the N_2 gas carrier at 700, 800, and 900 °C for about an hour. Figure 13.8(i) shows the N_2 adsorption isotherms at 77 K for the ACs obtained from bamboo according to the mentioned mechanism at 700, 800, and 900 °C [80]. The BET equation has obtained the pore's specific SA, size, and distributions. The graph shows that the greater the activating temperature, the more N_2 adsorption is possible. The adsorption pattern is a type I with a little hysteresis effect. Figure 13.8(ii) shows the corresponding cyclic voltammogram (CV) of the bamboo-based AC electrode supercapacitor in the window of 0–2.5 V. From Figure 13.8, it is obvious that the anode and cathode are steady in a liquid solution of TEA within the potential window. The generated electricity increases as the activation temperature goes up. The sample which has been activated at a higher temperature (900 °C) shows higher capacitance because of the larger specific SA than the sample activated at lower temperatures (700 or 800 °C). Figure 13.8(iii) displays the specific capacitance at several sweep rates at several activation temperatures. Figure 13.8(iii) clearly shows that the specific capacitance reduces due to the increased sweep rate. Ions

block the entry of micropores so that specific capacitance reduces. The specific capacitance and SAs of the AC 5–60 Fg^{-1} and 445–1025 m^2g^{-1} at different activation temperatures. The AC prepared at 900 °C for one hour shows the maximum capacitance and specific SA.

13.4.7 Steam-activated Carbon Using Fir Wood and Pistachio Shell

Four different types of ACs with a similar specific SA of ~1050 m^2/g have been prepared using fir wood and pistachio shell by activation with steam or KOH to justify the impact of pore shape and type of electrolyte on the capacitive features for supercapacitors [81]. The fir wood or pistachio shell was heated to 110 °C for 24 hours. After that, the heated samples are kept in an airtight porcelain furnace and warmed slowly by increasing 5 °C min^{-1} upto 550 °C. Water vapor at a 3 cm^3 min^{-1} rate was blown for 3 h for fir wood and 2 h for pistachio shells. Then the heated samples were carbonized at 550 °C without oxygen by increasing the heat at the same rate. After the carbonization process, the furnace was heated to 900 °C (for 5 h) and 890 °C (for 3 h) for fir wood and pistachio shell, along with flowing steam at 3 cm^3 min^{-1}. Then the carbons were ground, cleaned by applying distilled H_2O, and dried. At the end, the dried particles are sieved through a 0.12–0.2 mm pore size sieve. To prepare the electrode out of the ACs, the prepared AC has been blended at a ratio of 2:1 (AC to PVDF) (wt.%) polyvinylidene fluoride (PVDF) for 0.5 h and N-methyl-2-pyrrolidone (NMP) was added drop by drop into the mixture and ground to create a slurry. The prepared slurry was spread over a pre-treated graphite substrate and dried in an airtight furnace at 50 °C overnight.

The dimensions of the graphite substrate are 1cm × 1cm × 0.3cm, and ahead of making the layer with ACs, is first roughened using very fine SiC paper, cleaned with CH_3COCH_3 and H_2O, then sculpted in a 0.1M hydrochloric acid solution at ~ca. 25 °C for 10 min, and lastly washed with H_2O in a sonicator. About 1 cm^2 of the pre-treated graphite electrode was exposed, and the rest of the parts were shielded with polytetrafluorene ethylene (PTFE) coatings.

For the steam activation, the adsorption and desorption pattern is identical at the lower relative pressure, while a hysteretic loop is visible for higher relative pressure (P/P_0 > 0.5). However, the adsorption-desorption isotherm for KOH-ACs represents the pattern of Type-I pattern. The pattern observed reflects that the spread of the pore size distribution and shape depends on the activation and precursor materials. Figure 13.9i shows the pore size distributions of W-H_2O-AC, P-H_2O-AC, WKOH-AC, and P-KOH-AC. A peak occurs at a pore diameter of < 2 nm, and a second peak is found between 3.5–4.5 nm for the steam-ACs, meaning the steam activation creates pores of two distributions, micropores and mesopores. The proportions within the SA of micropores with the entire specific SA are greater than those of steam-ACs. From this observation, we can say that the activation with KOH produces more carbons full of micropores and the H_2O vapor activation technique favors growing the outer SA.

Figure 13.9(ii) shows the CV performance of W-H_2O-AC, P-H_2O-AC, W-KOH-AC, and P-KOH-AC observed at 20 mVs^{-1} in 1.0 M $NaNO_3$. Two-layers' charge/discharge governs the energy-storing procedure of these electrodes. All the CV patterns are rectangular except for noticeable redox currents happening together with positive and negative sweeps during the study. From the i-E curve, it is clear that $NaNO_3$ is an important electrolyte for applying EDLC for steam and KOH-ACs. Both show good capacitive performance despite pore structures, and distributions differ. Again, as the voltammetric charges for forward and reverse sweeps are close to each other, the charge/discharge pattern is expected to be highly
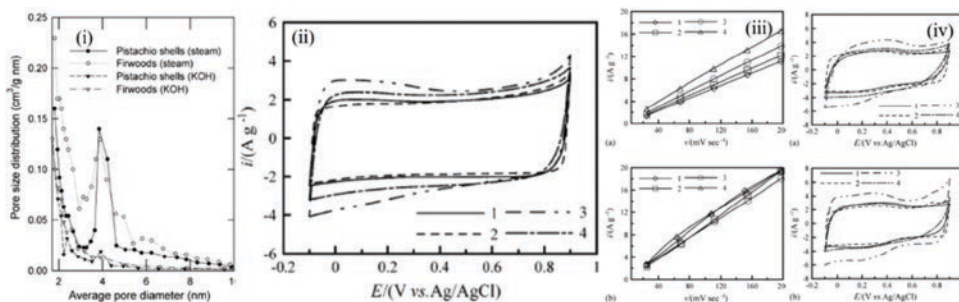
Figure 13.9 (i) Pore size distribution of different ACs prepared from pistachio (P) shells and fir woods (W) activated with steam (H_2O) and KOH. (ii) Cyclo voltammetric pattern of (1) W-H_2O-AC, (2) P-H_2O-AC, (3) W-KOH- AC, and (4) P-KOH-AC obtained for 20 mVs^{-1} in 1.0M $NaNO_3$. (iii) Dependence of CV currents for (a) W-H_2O-AC and (b) W-KOH-AC for the scan rate of cyclic voltammetry, where currents have been observed at (1) 0.2, (2) 0.4, (3) 0.6, and (4) 0.8V on the positive sweeps of CVs in 1M $NaNO_3$. (iv) CVs of (1) W-H_2O-AC, (2) P-H_2O-AC, (3) W-KOH- AC, and (4) P-KOH-AC measured at 20 mVs^{-1} in (a) 1M HNO_3 and (b) 0.5M H_2SO_4. *Reproduced with permission* [81]. *Copyright 2005, Elsevier.*

reversible in $NaNO_3$, which makes the ACs for the ability to use in the EDLCs. Figure 13.9 (iii) shows how CV current depends on the scan rate for W-H_2O-AC and W-KOHAC for different potentials in 1M $NaNO_3$, representing the two-layer charging /discharging currents. It is believed that the ACs inserted electrodes in 1.0 M $NaNO_3$ show very high power characteristics, which is very important for the supercapacitor electrode material. Also, the steam-AC shows the redox characteristics in acidic electrolytes [81, 82]. Figure 13.9(iv) shows the CV of W-H_2O-AC, P-H_2O-AC, W-KOH-AC, and P-KOH-AC monitored at 20 mV/s in 1.0 M HNO_3 and 0.5 MH_2SO_4, respectively. CV current determined for HNO_3 is greater compared to $NaNO_3$ for any specific AC due to the increment of the accessible SA of ACs in acidic electrolytes. However, the CV curves tend to distort from a rectangular shape due to the application of acidic electrolyte, but non-acidic electrolyte gives the capacitive curve. This is because an acidic electrolyte medium creates an electric double layer, increasing the partially accessible surface, which delays the transfer of solvated ions under a medium scan rate (20 mVs^{-1}). The specific capacitance of all ACs mentioned here have relatively higher values (180–85 F/g measured at 10 mV/s) using different electrolytes compared to some other ACs reported earlier, like 80 F/g (specific SA = 1200 m^2/g) [83], 60–125 F/g (the specific SA from 1200 to 2315 m^2/g) [84], 28–100 F/g (the specific SA from 1223 to 2571 m^2 g^{-1}) [85], and 90 Fg^{-1} (specific SA = 1500 m^2/g) [86]. Table 13.2 illustrates steam activated carbon from different biomasses and their BET surface area at different temperatures and retention times.

13.5 Applications of Steam-activated Carbon

Based on the dimension, shape, and number of micropores or mesopores, pore size, and volumes, the characteristics of AC change quite a lot. These parameters depend on the raw materials, manufacturing conditions, oxidizing technique, carbonization process, activation method, time of activation, temperature, etc. Based on the ACs' physical and chemical properties, they are used for different purposes. One of the most important applications is

Table 13.2 Steam ACs from different biomass and their corresponding BET SA.

Biomass	Applied temperature (°C)	Retention time (min)	BET SSA (m^2/g)	Ref.
Date pits	800	60	702	[87]
Rice husk	850	105	1180	[88]
Date palm tree fronds	577	30	1094	[88]
Industrial pre-treated cork	800	60	750	[89]
Camellia oleifera	820	-	1076	[90]
Oil palm EFB	-	-	720	[65]
Bamboo waste scraps	800–900	-	990–1099	[91]
Pistachio nut shells	850	20	2596	[92]
Bulgarian peach stones	1123	60	1258	[93]
Rubber seed shell	820	60	878	[94]
Apricot stones	800	60	712	[95]
Coconut shell	900	120	1926	[96]
Coconut shell	900	30	901	[96]
Tropical almond shell	850	-	1074	[73]
Guava seeds	850	-	1201	[73]
Dinde stones	850	-	1029	[73]
Artocarpus integer	750	60	852.63	[2]
Almond shell	850	30	601	[97]
Walnut shell	850	30	792	[97]
Pistachio shell	950	30	1196	[14]
Almond shell	950	60	1261	[14]
Walnut shell	950	60	1248	[14]
Coconut shells	200	30–90	228	[98]
Black liquor lignin	725	40	310	[99, 100]
Bamboo waste	850	120	363	[100]
Cherry stone	800	30	367	[101]

to prepare the electrode material. As the active SA and pore volume of the ACs are relatively larger than many other materials, the charging-discharging capacity and performances of ACs are higher than many other materials. Also, the cost of the AC materials is much cheaper than many other available suitable materials for making electrodes. Steam-ACs are preferable over chemical activation to manufacture electrode materials because producing chemical-AC uses more contaminates than steam-ACs. To prepare an electrode with high purity of materials used for manufacture is considered one of the most important factors. Naturally, steam-AC materials are prefered. Again, most of the volatile components present in the char are removed and washed away during steam activation. Therefore, no unexpected material will interfere during the charging and discharging of an electrochemical

cycle. Among some other applications of steam-ACs are industrial purposes, medical science, analytical study, environmental science, agricultural purpose, purification of alcoholic beverages, preparation electrodes, storing fuels, purifying gas, purifying chemicals, removing mercury, as some food additives, to care for skin and many more.

13.6 Design of AC Electrodes made from Biomass

To prepare a high-quality supercapacitor, very high-quality electrode materials are required. Highly adsorptive carbon materials are among the most used substances for electrodes, specifically porous materials obtained from biomass [102]. The extraordinary property of carbon materials leads to the quality of the supercapacitors. For the best output of a supercapacitor, rational design and preparation of the carbonaceous substances are essential. Though much research in different laboratories worldwide has shown excellent results, supercapacitors need to be adjusted and controlled to get the best output. In most cases, the following four parameters are critical to designing and improving the porous carbon materials for supercapacitors.

13.6.1 Hierarchical Porosity

Figure 13.10 (a) shows the types of pore and 13.10(b) shows the ion dispersion form. The larger the specific SA of the porous carbon materials the larger the electrode/electrolyte edge, which is directly associated with the higher adsorption of ions [103, 104]. The distribution, structure, and connectivity of the pores influences the electrochemical activity by altering the transport of the ions. Traditionally, it is thought that the larger the specific SA, the better the material performs as an electrode material [103]. Larger specific SA shows more charge accumulation capacity [104]. But, experimentally it has been shown that having wider pore size distribution does not allow more electrolyte ions to enter into smaller holes, and the transport of ions reduces, making the supercapacitor's quality poor [27, 103]. So, it is very much required to have an appropriate process for opening the carbon substances pores to get the optimized capacitance out of the supercapacitor. It was observed that the optimum capacitance and energy density could be obtained if ions can be selected that are similar in size to the pores of the derived materials, and the size of the hole, < 1 nm, gives the best capacitance [27]. Therefore, a higher energy-storing capacity can be obtained by adjusting the pore. However, micropores (< 2 nm) – and mesopores (2–50 nm), and macropores (> 50 nm) play a different roles in the activity of the supercapacitors [105, 106].

13.6.2 Graphitization

Higher conductivity lowers the internal resistance, stimulating the charge transmission and construction steadiness and ensuring excellent rate performance, power density, and cyclic stability [107]. If the conductivity is higher, the degree of graphitization is expected to be higher [107]. To get the best electrochemical activity, one must select the optimum condition within specific SA, configuration, functional groups, and amount of graphitization. These days, higher-temperature cracking and graphitization by catalysis are two
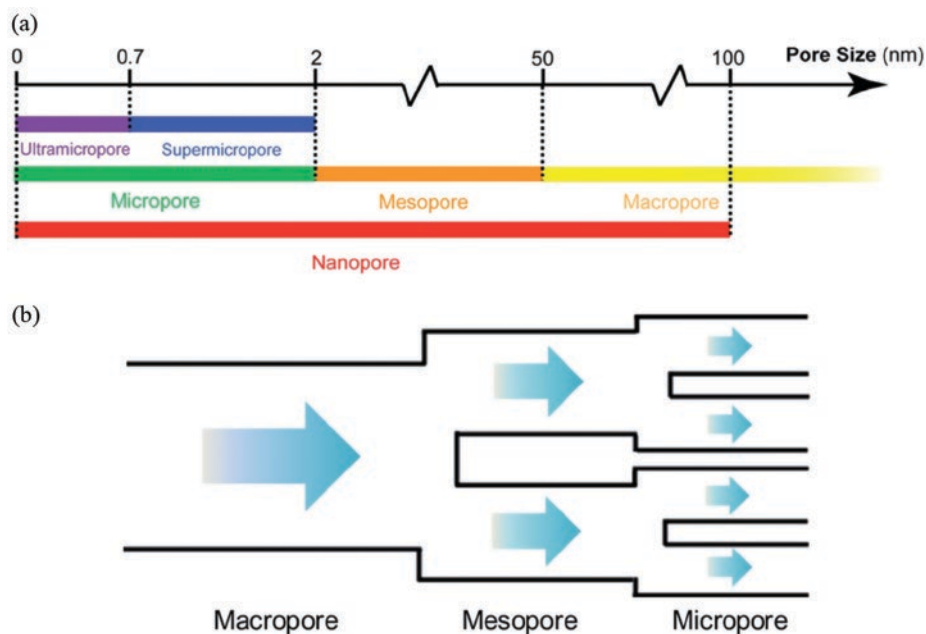
Figure 13.10 (a) Classification of pores and (b) graphics for ion dispersion form with the hierarchical porous configuration. *Reproduced with permission* [105]. *Copyright 2017, Royal Society of Chemistry.*

major ideas in order to prepare high-quality graphitic structures from biomass [108]. Higher temperature is better for carbonization because conjugated sp^2 bonds are created at that temperature. But, ultrahigh temperature (~2500 °C) is not suitable because the pores and functional groups can collapse at such a temperature and reduce the specific SA [108]. Again, if the carbonization is performed at ultrahigh temperature, the structure becomes very hard to modify in any other form. At the same time, higher temperature consumes a lot of energy which is goes against the green energy theme.

13.6.3 Phase or Surface Modification

Research has shown that functional groups on the surface or doping different atoms considerably alters the carbon materials [107]. Replacement of carbon with some other atom can easily compromise the intrinsic activity, which represents higher usability [109], because the dopant alters the symmetric π-π conjugation, and the band gap is altered, leading to the energy storing capacity [110]. In addition, a forward and reverse redox system can be introduced disturbing the rate and periodic activity, which progresses the capacitance. Extrinsic carbon doped with heteroatom can be obtained from biomass by choosing more heteroatom-containing raw materials, elemental dopants, or doping after the handling. N is used mostly for that which is responsible for allowing the electroactive core to increase the conducting ability, exterior polarity, and capacity to spread on a carbon surface by generating faults and changing the outermost orbit of the carbon by improving the electrical reactivity [60]. It has been found that carbon obtained from grape marc had a

significantly higher level of N doping (2.04%), a very high SA (2221.4 m^2g^{-1}), and a high-quality pore configuration that gives 446 Fg^{-1} at 0.5 A g^{-1} in 1 M H_2SO_4 [111].

13.6.4 Composites

Combining porous carbon obtained from biomass with other forms of carbon like CNT, carbon micro-tubes, graphene, or some pseudocapacitance substances can enhance the electrochemical property [36, 102]. The final product has a hierarchical spongy form and pollen-derived carbon microspheres, which can work as hollow bars for inhibiting the accumulation of graphene nanoplates. The adjusted combination showed elevated specific capacitance (420 F g^{-1} at 1 A g^{-1}), higher performing activity (280 F g^{-1} at 20 A g^{-1}) with better periodic steadiness (94% of capacitance afterward 10000 periods) [112]. Intrinsic porous carbon materials have relatively lower energy density than supercapacitors, which cannot satisfy modern requirements. Adding pseudocapacitance substances like an oxygenated compound of d-block elements or their hydroxides and conductive polymers can increase the energy density of supercapacitors for reversible Faraday reactions and the electrode–electrolyte edge [113]. The adsorption of ions can attain greater capacity and energy density. But, some defects like lower specific SA, lower intrinsic conductivity, and larger destruction on the structure while cycling can reduce the ion/electron transport a lot and reduce the cycle life [114]. Therefore, mixing pseudocapacitance materials with the porous carbon material obtained from biomass can be very helpful in recovering the problem. The carbon with high porosity has a very large specific SA, so it can accommodate pseudocapacitance substances to enhance the electrically active regions [114]. The solid structure of the porous carbon obtained from biomass buffers the mechanical stress due to the Faraday reaction of the mock capacitive materials due to recurring charging/discharging, and meaningfully increases the periodic stability of the composites [113]. So, biomass-derived carbon nanostructure shows boosted capacity, very high performance rate, energy and power density, and periodic stability.

13.7 Conclusions

Applications of AC range from personal to industrial scale including as supercapacitor and activation of carbon become critical research in recent years. There are two significant ways of activation of carbon; physical activation (e.g., steam activation) and chemical activation. Chemical activation requires several chemicals, which increases the cost and can cause environmental pollution. However, steam activation is possible with steam only without using any other chemicals. Therefore, steam activation is considered one of the most popular methods to activate the carbon as obtained from different sources like biomass, agricultural wastes, coconut shell, or any coal-based carbon. After activation of carbon, the pore size, active SA, pore volume, and the number of pores increase rapidly, which is very effective for the adsorption-desorption of ions or other molecules. Therefore, the use of steam to activate carbon from biomass to prepare highly effective supercapacitors, energy storage devices, and many more is widespread. Steam activation proceeds mainly in two steps: carbonization at a relatively lower temperature and activation by flowing steam

at a controlled rate at a higher temperature. Steam activation makes the carbon skeleton more stable and increases the pore size and volume, increasing the BET SA and capacitance. In addition, the electrode prepared with the steam-AC shows much charging/discharging stability, making the steam-AC better electrode material. Among the studied ACs presented here, the maximum BET SA was obtained at 2596 m^2/g for pistachio nut shells (activated with steam at 850 °C for 20 minutes), followed by 1926 m^2/g for coconut shells activated with steam at 900 °C for 120 minutes. Therefore, steam activation with 800–1000 °C is a better range for working while the time range is uncertain. Thus, much research is required to estimate the best retention time for steam activation. The pore size and pore volume of the mentioned ACs are relatively large so they are a suitable candidate for producing high-capacity supercapacitors and energy storage devices.

Acknowledgments

References

1 A. Patel, D. Sharma, P. Kharkar, D. Mehta, *Int. J. Eng. Sci. Technol.* **2019**, *3*, 63–66.

2 G. Selvaraju, N. K. A. Bakar, *J. Taiwan Inst. Chem. Eng.* **2018**, *93*, 414–426.

3 A. K. Mohamedkhair, M. A. Aziz, S. S. Shah, M. N. Shaikh, A. K. Jamil, M. A. A. Qasem, I. A. Buliyaminu, Z. H. Yamani, *Arab. J. Chem.* **2020**, *13*, 6161–6173.

4 M. Ashraf, S. S. Shah, I. Khan, M. A. Aziz, N. Ullah, M. Khan, S. F. Adil, Z. Liaqat, M. Usman, W. Tremel, M. N. Tahir, *Chem. Eur. J.* **2021**, *27*, 6973–6984.

5 M. Yaseen, M. A. K. Khattak, M. Humayun, M. Usman, S. S. Shah, S. Bibi, B. S. U. Hasnain, S. M. Ahmad, A. Khan, N. Shah, A. A. Tahir, H. Ullah, *Energies* **2021**, *14*, 7779.

6 M. Rauf, S. S. Shah, S. K. Shah, S. N. A. Shah, T. U. Haq, J. Shah, A. Ullah, T. Ahmad, Y. Khan, M. A. Aziz, K. Hayat, *J. Saudi Chem. Soc.* **2022**, *26*, 101514.

7 T. Islam, M. M. Hasan, S. S. Shah, M. R. Karim, F. S. Al-Mubaddel, M. H. Zahir, M. A. Dar, M. D. Hossain, M. A. Aziz, A. J. S. Ahammad, *J. Energy Storage* **2020**, *32*, 101908.

8 S. S. Shah, E. Cevik, M. A. Aziz, T. F. Qahtan, A. Bozkurt, Z. H. Yamani, *Synth. Met.* **2021**, *277*, 116765.

9 S. S. Shah, S. M. A. Nayem, N. Sultana, A. J. S. Ahammad, M. A. Aziz, *ChemSusChem* **2022**, *15*, e202101282.

10 S. S. Shah, M. A. Aziz, Z. H. Yamani, *Chem. Rec.* **2022**, *22*, e202200018.

11 M. M. Hasan, T. Islam, S. S. Shah, A. Awal, M. A. Aziz, A. J. S. Ahammad, *Chem. Rec.* **2022**, *22*, e202200041.

12 M. S. Reza, C. S. Yun, S. Afroze, N. Radenahmad, M. S. A. Bakar, R. Saidur, J. Taweekun, A. K. Azad, *Arab J. Basic Appl. Sci.* **2020**, *27*, 208–238.

13 M. J. Lázaro, M. E. Gálvez, S. Artal, J. M. Palacios, R. Moliner, *J. Anal. Appl. Pyrolysis* **2007**, *78*, 301–315.

14 M. A. Nazem, M. H. Zare, S. Shirazian, *RSC Adv.* **2020**, *10*, 1463–1475.

15 A. J. S. Ahammad, P. R. Pal, S. S. Shah, T. Islam, M. Mahedi Hasan, M. A. A. Qasem, N. Odhikari, S. Sarker, D. M. Kim, M. A. Aziz, *J. Electroanal. Chem.* **2019**, *832*, 368–379.

16 A. Aziz, S. S. Shah, A. Kashem, *Chem. Rec.* **2020**, *20*, 1074–1098.

17 S. S. Shah, M. N. Shaikh, M. Y. Khan, M. A. Alfasane, M. M. Rahman, M. A. Aziz, *Chem. Rec.* **2021**, *21*, 1631–1665.

18 S. M. Abu Nayem, S. S. Shah, S. B. Chaity, B. K. Biswas, B. Nahar, M. A. Aziz, M. Z. Hossain, *Arab. J. Chem.* **2022**, *15*, 104265.

19 S. S. Shah, M. A. Aziz, E. Cevik, M. Ali, S. T. Gunday, A. Bozkurt, Z. H. Yamani, *J. Energy Storage* **2022**, *56*, 105944.

20 M. R. Hasan, T. Islam, M. M. Hasan, A.-N. Chowdhury, A. J. S. Ahammad, A. H. Reaz, C. K. Roy, S. S. Shah, I. Al, M. A. Aziz, *J. Phys. Chem. Solids* **2022**, *165*, 110659.

21 M. A. Aziz, S. S. Shah, S. Reza, A. S. Hakeem, W. Mahfoz, *Chem. Asian J.* **2022**, e202200869, https://doi.org/10.1002/asia.202200869. Accessed February 2023.

22 P. Simon, Y. Gogotsi, *Nat. Mater.* **2008**, *7*, 845–854.

23 M. Salanne, B. Rotenberg, K. Naoi, K. Kaneko, P. L. Taberna, C. P. Grey, B. Dunn, P. Simon, *Nat. Energy* **2016**, *1*, 16070.

24 Z. Lin, E. Goikolea, A. Balducci, K. Naoi, P.-L. Taberna, M. Salanne, G. Yushin, P. Simon, *Mater. Today* **2018**, *21*, 419–436.

25 D. Liu, K. Ni, J. Ye, J. Xie, Y. Zhu, L. Song, *Adv. Mater.* **2018**, *30*, e1802104.

26 Z. Yang, J. Ren, Z. Zhang, X. Chen, G. Guan, L. Qiu, Y. Zhang, H. Peng, *Chem. Rev.* **2015**, *115*, 5159–5223.

27 J. Chmiola, G. Yushin, Y. Gogotsi, C. Portet, P. Simon, P.-L. Taberna, *Science* **2006**, *313*, 1760–1763.

28 B. Li, J. Zheng, H. Zhang, L. Jin, D. Yang, H. Lv, C. Shen, A. Shellikeri, Y. Zheng, R. Gong, J. P. Zheng, C. Zhang, *Adv. Mater.* **2018**, *30*, e1705670.

29 B. Cai, V. Sayevich, N. Gaponik, A. Eychmüller, *Adv. Mater.* **2018**, *30*, 1707518.

30 H. Jiang, P. S. Lee, C. Li, *Energy Environ. Sci.* **2013**, *6*, 41–53.

31 S. Kumar, G. Saeed, L. Zhu, K. N. Hui, N. H. Kim, J. H. Lee, *Chem. Eng. J.* **2021**, *403*, 126352.

32 J. R. Miller, P. Simon, *Science* **2008**, *321*, 651–652.

33 J. Xu, N. Yuan, J. M. Razal, Y. Zheng, X. Zhou, J. Ding, K. Cho, S. Ge, R. Zhang, Y. Gogotsi, R. H. Baughman, *Energy Storage Mater.* **2019**, *22*, 323–329.

34 F. Lai, J. Feng, R. Yan, G.-C. Wang, M. Antonietti, M. Oschatz, *Adv. Funct. Mater.* **2018**, *28*, 1801298.

35 A. Muzaffar, M. B. Ahamed, K. Deshmukh, J. Thirumalai, *Renew. Sust. Energ. Rev.* **2019**, *101*, 123–145.

36 Z. Li, D. Guo, Y. Liu, H. Wang, L. Wang, *Chem. Eng. J.* **2020**, *397*, 125418.

37 L. L. Zhang, X. Zhao, *Chem. Soc. Rev.* **2009**, *38*, 2520–2531.

38 W. Li, J. Liu, D. Zhao, *Nat. Rev. Mater.* **2016**, *1*, 16023.

39 D.-W. Wang, F. Li, M. Liu, G. Q. Lu, H.-M. Cheng, *Angew. Chem. Int. Ed.* **2008**, *47*, 373–376.

40 F. Ma, D. Ma, G. Wu, W. Geng, J. Shao, S. Song, J. Wan, J. Qiu, *Chem. Commun.* **2016**, *52*, 6673–6676.

41 F. Zhang, T. Liu, G. Hou, T. Kou, L. Yue, R. Guan, Y. Li, *Nano Res.* **2016**, *9*, 2875–2888.

42 H. Yang, S. Ye, J. Zhou, T. Liang, *Front. Chem.* **2019**, *7*, 274.

43 L. Sun, Y. Gong, D. Li, C. Pan, *Green Chem.* **2022**, *24*, 3864–3894.

44 K. S. Kim, Y. Zhao, H. Jang, S. Y. Lee, J. M. Kim, K. S. Kim, J.-H. Ahn, P. Kim, J.-Y. Choi, B. H. Hong, *Nature* **2009**, *457*, 706–710.

45 C. K. Ranaweera, P. K. Kahol, M. Ghimire, S. R. Mishra, R. K. Gupta, *C* **2017**, *3*, 25.

46 F. Abnisa, W. M. A. Wan Daud, *Energy Convers. Manage.* **2014**, *87*, 71–85.

47 S. Gillet, M. Aguedo, L. Petitjean, A. R. C. Morais, A. M. da Costa Lopes, R. M. Łukasik, P. T. Anastas, *Green Chem.* **2017**, *19*, 4200–4233.

48 B. Zhang, Y. Jiang, R. Balasubramanian, *J. Mater. Chem. A* **2021**, *9*, 24759–24802.

49 Y. Wang, Y. Xia, *Adv. Mater.* **2013**, *25*, 5336–5342.

50 S. S. Shah, M. A. Aziz, A.-R. Al-Betar, W. Mahfoz, *Arab. J. Chem.* **2022**, *15*, 104058.

51 R. Shakil, M. N. Shaikh, S. S. Shah, A. H. Reaz, C. K. Roy, A.-N. Chowdhury, M. A. Aziz, *Asian J. Org. Chem.* **2021**, *10*, 2220–2230.

52 N. C. Deb Nath, S. S. Shah, M. A. A. Qasem, M. H. Zahir, M. A. Aziz, *ChemistrySelect* **2019**, *4*, 9079–9083.

53 M. A. Aziz, S. S. Shah, S. M. A. Nayem, M. N. Shaikh, A. S. Hakeem, I. A. Bakare, *J. Energy Storage* **2022**, *50*, 104278.

54 S. S. Shah, M. A. Alfasane, I. A. Bakare, M. A. Aziz, Z. H. Yamani, *J. Energy Storage* **2020**, *30*, 101562.

55 S. S. Shah, M. A. Aziz, W. Mahfoz, A.-R. Al-Betar, Conducting Polymers Based Nanocomposites for Supercapacitors in *Nanostructured Materials for Supercapacitors*, (Eds. S. Thomas, A. B. Gueye, R. K. Gupta), Springer, Cham, **2022**, Chapter 22, 485–511, vol. 1.

56 S. S. Shah, H. T. Das, H. R. Barai, M. A. Aziz, *Polymers* **2022**, *14*, 270.

57 H. R. Barai, M. M. Rahman, M. Roy, P. Barai, S. W. Joo, *Mat. Sci. Semicon. Process.* **2019**, *90*, 245–251.

58 H. R. Barai, P. Barai, M. Roy, S. W. Joo, *Energy Fuel* **2021**, *35*, 16870–16881.

59 P. Simon, Y. Gogotsi, B. Dunn, *Science* **2014**, *343*, 1210–1211.

60 Y. Wang, Q. Qu, S. Gao, G. Tang, K. Liu, S. He, C. Huang, *Carbon* **2019**, *155*, 706–726.

61 A. M. Abioye, F. N. Ani, *Renew. Sust. Energ. Rev.* **2015**, *52*, 1282–1293.

62 A. Aworn, P. Thiravetyan, W. Nakbanpote, *J. Anal. Appl. Pyrolysis* **2008**, *82*, 279–285.

63 B. Cagnon, X. Py, A. Guillot, F. Stoeckli, G. Chambat, *Bioresour. Technol.* **2009**, *100*, 292–298.

64 D. Xin-hui, C. Srinivasakannan, P. Jin-hui, Z. Li-bo, Z. Zheng-yong, *Biomass Bioenerg.* **2011**, *35*, 3920–3926.

65 N. A. Rashidi, S. Yusup, *Chem. Eng. J.* **2017**, *314*, 277–290.

66 X. Yang, Y. Wan, Y. Zheng, F. He, Z. Yu, J. Huang, H. Wang, Y. S. Ok, Y. Jiang, B. Gao, *Chem. Eng. J.* **2019**, *366*, 608–621.

67 K. S. Ukanwa, K. Patchigolla, R. Sakrabani, E. Anthony, S. Mandavgane, *Sustainability* **2019**, *11*, 6204.

68 V. Dhyani, T. Bhaskar, *Renew. Energy* **2018**, *129*, 695–716.

69 D. Mohan, A. Sarswat, Y. S. Ok, C. U. Pittman, *Bioresour. Technol.* **2014**, *160*, 191–202.

70 P. González-García, *Renew. Sust. Energ. Rev.* **2018**, *82*, 1393–1414.

71 M. S. Reza, S. N. Islam, S. Afroze, M. S. Abu Bakar, R. S. Sukri, S. Rahman, A. K. Azad, *Energy Ecol. Environ.* **2020**, *5*, 118–133.

72 A. Arami-Niya, W. M. A. Wan Daud, F. S. Mjalli, F. Abnisa, M. S. Shafeeyan, *Chem. Eng. Res. Des.* **2012**, *90*, 776–784.

73 L. Largitte, T. Brudey, T. Tant, P. C. Dumesnil, P. Lodewyckx, *Microporous Mesoporous Mater.* **2016**, *219*, 265–275.

74 H. H. Rafsanjani, H. Kamandari, H. Najjarzadeh, *Iran. J. Chem. Eng.* **2013**, *10*, 27–38.

75 J. Alvarez, G. Lopez, M. Amutio, J. Bilbao, M. Olazar, *Ind. Eng. Chem. Res.* **2015**, *54*, 7241–7250.

76 S. Wong, N. Ngadi, I. M. Inuwa, O. Hassan, *J. Clean. Prod.* **2018**, *175*, 361–375.

77 N. M. Keppetipola, M. Dissanayake, P. Dissanayake, B. Karunarathne, M. A. Dourges, D. Talaga, L. Servant, C. Olivier, T. Toupance, S. Uchida, K. Tennakone, G. R. A. Kumara, L. Cojocaru, *RSC Adv.* **2021**, *11*, 2854–2865.

78 S. Mopoung, N. Dejang, *Sci. Rep.* **2021**, *11*, 13948.

79 G. K. P. Lopes, H. G. Zanella, L. Spessato, A. Ronix, P. Viero, J. M. Fonseca, J. T. C. Yokoyama, A. L. Cazetta, V. C. Almeida, *Arab. J. Chem.* **2021**, *14*, 103001.

80 C. Kim, J.-W. Lee, J.-H. Kim, K.-S. Yang, *Korean J. Chem. Eng.* **2006**, *23*, 592–594.

81 F.-C. Wu, R.-L. Tseng, -C.-C. Hu, -C.-C. Wang, *J. Power Sources* **2005**, *144*, 302–309.

82 F.-C. Wu, R.-L. Tseng, -C.-C. Hu, -C.-C. Wang, *J. Power Sources* **2004**, *138*, 351–359.

83 L. Bonnefoi, P. Simon, J. F. Fauvarque, C. Sarrazin, A. Dugast, *J. Power Sources* **1999**, *79*, 37–42.

84 J. Gamby, P. L. Taberna, P. Simon, J. F. Fauvarque, M. Chesneau, *J. Power Sources* **2001**, *101*, 109–116.

85 D. Qu, H. Shi, *J. Power Sources* **1998**, *74*, 99–107.

86 A. Lewandowski, M. Zajder, E. Frąckowiak, F. Béguin, *Electrochim. Acta* **2001**, *46*, 2777–2780.

87 M. J. Ahmed, *Process Saf. Environ. Prot.* **2016**, *102*, 168–182.

88 E. Menya, P. W. Olupot, H. Storz, M. Lubwama, Y. Kiros, *Chem. Eng. Res. Des.* **2018**, *129*, 271–296.

89 A. S. Mestre, R. A. Pires, I. Aroso, E. M. Fernandes, M. L. Pinto, R. L. Reis, M. A. Andrade, J. Pires, S. P. Silva, A. P. Carvalho, *Chem. Eng. J.* **2014**, *253*, 408–417.

90 H. S. Min, M. Abbas, R. Kanthasamy, H. Abdul Aziz, C. C. Tay, *Ideal International E-publication Pvt. Ltd* **2017**, *1*, 1–85.

91 L. Dong, W. Liu, Y. Yu, L. A. Hou, P. Gu, G. Chen, *Sci. Total Environ.* **2019**, *647*, 1359–1367.

92 A. Niksiar, B. Nasernejad, *Biomass Bioenerg.* **2017**, *106*, 43–50.

93 T. Tsoncheva, A. Mileva, B. Tsyntsarski, D. Paneva, I. Spassova, D. Kovacheva, N. Velinov, D. Karashanova, B. Georgieva, N. Petrov, *Biomass Bioenerg.* **2018**, *109*, 135–146.

94 K. Sun, J. C. Jiang, *Biomass Bioenerg.* **2010**, *34*, 539–544.

95 Ç. D. Şentorun-Shalaby, M. G. Uçak-Astarlıoğˇlu, L. Artok, Ç. Sarıcı, *Microporous Mesoporous Mater.* **2006**, *88*, 126–134.

96 W. Ao, J. Fu, X. Mao, Q. Kang, C. Ran, Y. Liu, H. Zhang, Z. Gao, J. Li, G. Liu, J. Dai, *Renew. Sust. Energ. Rev.* **2018**, *92*, 958–979.

97 J. González, S. Román, J. M. Encinar, G. Martínez, *J. Anal. Appl. Pyrolysis* **2009**, *85*, 134–141.

98 J. Mi, X.-R. Wang, R.-J. Fan, W.-H. Qu, W.-C. Li, *Energy Fuel* **2012**, *26*, 5321–5329.

99 J. Kazmierczak-Razna, P. Nowicki, M. Wiśniewska, A. Nosal-Wiercińska, R. Pietrzak, *J. Taiwan Inst. Chem. Eng.* **2017**, *80*, 1006–1013.

100 Y.-J. Zhang, Z.-J. Xing, Z.-K. Duan, M. Li, Y. Wang, *Appl. Surf. Sci.* **2014**, *315*, 279–286.

101 P. Nowicki, J. Kazmierczak, R. Pietrzak, *Powder Technol.* **2015**, *269*, 312–319.

102 Z. Bi, Q. Kong, Y. Cao, G. Sun, F. Su, X. Wei, X. Li, A. Ahmad, L. Xie, C.-M. Chen, *J. Mater. Chem. A* **2019**, *7*, 16028–16045.

103 Y. Wang, Y. Song, Y. Xia, *Chem. Soc. Rev.* **2016**, *45*, 5925–5950.

104 E. Frackowiak, *Phys. Chem. Chem. Phys.* **2007**, *9*, 1774–1785.

105 T. Liu, F. Zhang, Y. Song, Y. Li, *J. Mater. Chem. A* **2017**, *5*, 17705–17733.

106 L. Xie, F. Su, L. Xie, X. Guo, Z. Wang, Q. Kong, G. Sun, A. Ahmad, X. Li, Z. Yi, C. Chen, *Mater. Chem. Front.* **2020**, *4*, 2610–2634.

107 J. Wang, P. Nie, B. Ding, S. Dong, X. Hao, H. Dou, X. Zhang, *J. Mater. Chem. A* **2017**, *5*, 2411–2428.

108 Q. Chen, X. Tan, Y. Liu, S. Liu, M. Li, Y. Gu, P. Zhang, S. Ye, Z. Yang, Y. Yang, *J. Mater. Chem. A* **2020**, *8*, 5773–5811.

109 S. Zhou, L. Zhou, Y. Zhang, J. Sun, J. Wen, Y. Yuan, *J. Mater. Chem. A* **2019**, *7*, 4217–4229.

110 H. Zhu, X. Gan, A. McCreary, R. Lv, Z. Lin, M. Terrones, *Nano Today* **2020**, *30*, 100829.

111 J. Zhang, H. Chen, J. Bai, M. Xu, C. Luo, L. Yang, L. Bai, D. Wei, W. Wang, H. Yang, *J. Alloys Compd.* **2021**, *854*, 157207.

112 L. Cao, H. Li, X. Liu, S. Liu, L. Zhang, W. Xu, H. Yang, H. Hou, S. He, Y. Zhao, S. Jiang, *J. Colloid Interface Sci.* **2021**, *599*, 443–452.

113 L. Lyu, K.-D. Seong, D. Ko, J. Choi, C. Lee, T. Hwang, Y. Cho, X. Jin, W. Zhang, H. Pang, Y. Piao, *Mater. Chem. Front.* **2019**, *3*, 2543–2570.

114 P. Veerakumar, A. Sangili, S. Manavalan, P. Thanasekaran, K.-C. Lin, *Ind. Eng. Chem. Res.* **2020**, *59*, 6347–6374.

14

Biomass-Derived Hard Carbon for Supercapacitors

Himadri Tanaya Das[1,], Swapnamoy Dutta[2], Muhammad Usman[3], T. Elango Balaji[4], and Nigamananda Das[4]*

[1] Centre of Excellence for Advance Materials and Applications, Utkal University, Bhubaneswar 751004, Odisha, India
[2] Bredesen Center for Interdisciplinary Research and Graduate Education, University of Tennessee, Knoxville, TN, 37996, USA
[3] Interdisciplinary Research Center for Hydrogen and Energy Storage (IRC-HES), King Fahd University of Petroleum and Minerals (KFUPM), Dhahran 31261, Saudi Arabia
[4] Department of Chemistry, Utkal University, Bhubaneswar 751004, Odisha, India
* Corresponding author

14.1   Introduction

Environmental pollution around the globe has rapidly increased due to the unrestricted utilization of natural sources, and it keeps damaging the lives of every earthly organism. So, in this hour of need, renewable energies usch as wind and solar energy is likely to play the most crucial role in alleviating such harmful impacts and serving as promising energy sources for the future. However, the stability and efficiency of these energy technologies are of great concern and are being extensively investigated to increase their durability [1]. Besides focusing on alternative energy sources, researchers have explored a variety of energy storage devices to maximize the usage of these energy resources. Storage devices such as batteries and supercapacitors have been widely examined to enhance their energy storage capabilities. Using supercapacitors, efficacious characteristics like excellent power density, swift charge/discharge rate and longer cycle life were observed, which is why supercapacitors are considered a potential energy storage device [2]. Experimenting with supercapacitors with different types of electrode material and electrolytes has resulted in various electrochemical performance outcomes, creating a novel scope of research. Out of the tested materials, carbonaceous materials are one of the most examined and feasible ones. They contribute to different supercapacitors components, making these materials more attractive. To derive or prepare these carbonaceous materials, macromolecule polymer [3, 4], graphite oxide [5], micromolecule organics, etc., are the frequently used precursors. Compared to these precursors, biomass is considered an easily available and much cheaper candidate for deriving carbonaceous materials. Using these biomass materials is beneficial in terms of waste recycling as well. Among various carbonaceous materials used in energy storage devices [6], hard carbon has been recently regarded as a suitable choice compared to other carbonaceous materials. Figure 14.1 shows various carbonaceous materials derived from different biomasses. However, CNTs and graphene are carbon materials that give a superior performance but demand additional cost and complex preparation techniques.
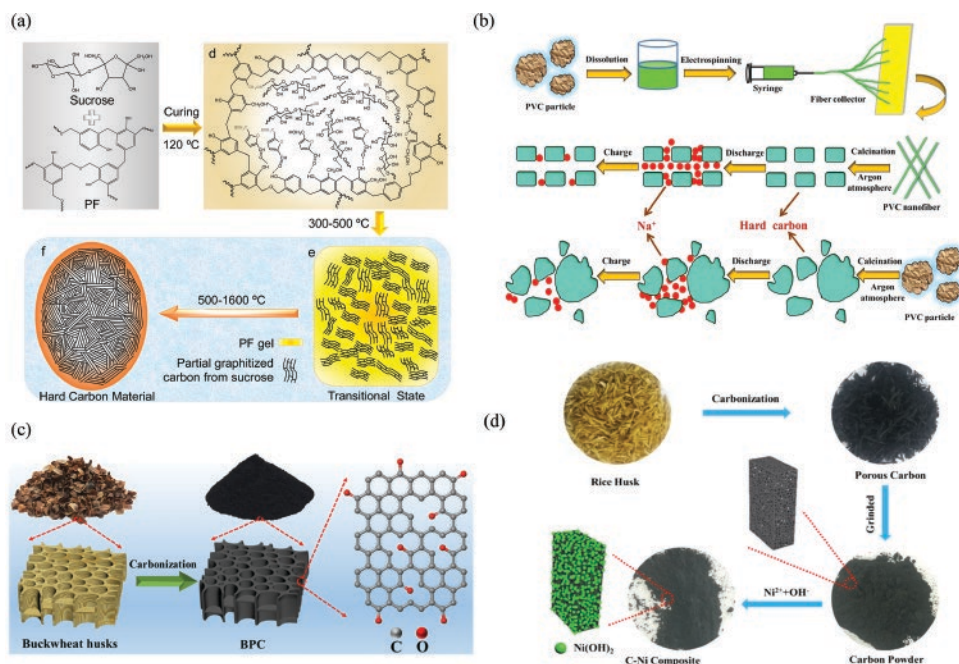
Figure 14.1 a) Proposed formation mechanism of hard carbon materials for sucrose/PF precursors toward the extremely low surface area. b) Schematic diagram of synthesis routes and Na$^+$ storage behaviors of hard carbon samples as anode materials for Na-ion batteries, c) Preparation scheme of BPC, d) Schematics of the preparation of the C–Ni composite materials. *Reproduced with permission* [7–10]. *Copyrights (2017, H. Zhang, Published by ACS) (2015, Y. Bai, Published by ACS) (2020, C. Chen, Published by ACS) (2020, J. Cai, Published by ACS).*

Researchers have reported efficient usage of hard carbons in sodium-ion batteries in the past few years. However, recent studies confirmed its usage in supercapacitors as well [11]. Hard carbon is comprised of randomly and closely attached single-layer carbon atoms, which are highly irregular and disordered, and it is also tough to graphitize. Earlier preparation was mostly done using epoxy resin, phenolic resin-like polymers, and a pyrolysis process [12]. But in recent studies, biomass has been considered a suitable choice to derive hard carbons. Already studies have shown the preparation of hard carbons using different biomass sources like lotus stems, soybean roots, rice husks, silk, puffed rice, and popcorn and their utilization as electrodes for supercapacitors [13–19]. A few examples of hard carbon derived from different sources and their synthesis has shown in Figure 14.2.

This chapter will particularly discuss biomass-derived hard carbon and its usage in supercapacitors. The electrodes produced with hard carbons have resulted in safer operation, longer cycle life, superior capacity, and higher rate performance [24]. Along with highlighting the positive aspects of employing hard carbons, its drawbacks, such as inadequate packing density, large irreversible capacity, and hysteresis in the voltage levels, will also be emphasized, which might help future researchers to understand and find approaches to prevent those pitfalls via modifications.
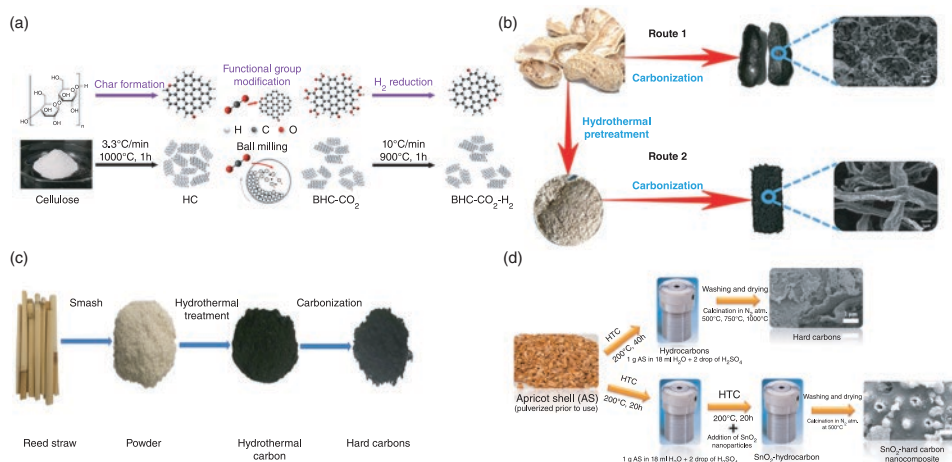
Figure 14.2 a) Preparation and microstructure of samples HC, BHC-CO$_2$, and BHC-CO$_2$-H$_2$, b) schematic of the synthesis routes of PSDHCs-X samples, c) schematic representation of the synthesis of hard carbon from reed straw, and d) schematic representation of the apricot shell-derived hard carbon materials and SnO$_2$ hard carbon nanocomposite structures. *Reproduced with permission* [20–23]. *Copyrights (2019, H. Wang, Published by ACS) (2019, X. Ren, Published by Elsevier) (2018, J. Wang, Published by Elsevier) (2019, E. Demir, Published by Elsevier).*

14.2 Biomass-derived Hard Carbons

The term hard carbon is primarily used to indicate its mechanical hardness and structural complexity. This type of carbon material does not get graphitized even at higher temperature levels (>3000 °C). In other words, we can say that these hard carbon materials are composed of curved graphene sheets. Under higher temperatures, these cannot be flattened or unfolded to convert the graphite stacking structures [25]. Also, covalent C–O–C bonds are significantly responsible for their inability to graphitize and for their mechanical hardness. Dahn et al. [26] first presented the developed "falling cards" model, which became useful in understanding structural sketches for hard carbons. This model clearly explains that this structure consists of small graphene sheets, nanopores, and amorphous regions with defects. Apart from these characteristics, hard carbons also possess randomly oriented intricate crystalline structures and textures and have different structures (micro/meso/macro) with varying stacking and pores [27]. Large interlayer spacing and more nanopores are mainly created due to this amalgamation of disordered structures and crystallinity. As a result, the structures of hard carbons can afford enhanced storage sites and improved charge diffusion pathways. Studies revealed that the interlayer spacings of hard carbon mostly vary between 3.6–4.0 Å, and paralleled layers of graphitic domains are observed to be in turbostratic, curved, or bent shapes [28]. Different hard carbon morphologies are mentioned in the literature, such as twisted, non-planar, buckled, spherical, wire-like, or porous [25, 29, 30]. Precursors such as biomass or pure organic compounds generally use chemical or thermal techniques to obtain hard carbons for electrochemical application. The conversion mechanism mainly involves the complex carbonization process, which includes concurrent reaction processes, like dehydrogenation, condensation,

hydrogen transfer, and isomerization. An important activity that needs to be emphasized is that during the carbonization process precursors having higher oxygen content are useful in forming better cross-linking regions or curved layers in the hard carbon structures, which in turn completely ensures the non-graphitize ability of the hard carbons. Here, another observable point is that the converted hard carbon has almost analogous morphological structures, but with low bulk density compared to the parent material. In the next sections, we will explain more about the formation of electrodes using hard carbons with suitable illustrations.

14.3 Biomass-derived Hard Carbon Electrodes in Supercapacitors

An electrode is a vital segment of the electrochemical device, which is very capable of conducting electrons or transferring the Faradic charge. In the case of supercapacitor devices, the electrode materials are majorly responsible for determining the charge-storing ability and capacitive performance. So, improving the electrode materials can easily enhance the performance outcome of supercapacitors. Recent studies have shown that enhancing electrode factors like morphology modification of electrode materials, improvement in electrochemically active sites, and manipulating pore size and shape can lead to the electrochemical performance of supercapacitors [31–33]. Supercapacitor electrodes are generally expected to exhibit a few crucial characteristics such as high specific surface area, improved chemical and thermal stability, corrosion resistance, suitable surface wettability, and high electrical conductivity [34–36]. Nanostructured carbon-based materials (such as activated carbon materials, carbon gels, graphene, carbon nanotubes), transition metal oxides/hydroxides-based materials (such as ruthenium oxide, manganese dioxide, nickel oxide/hydroxide, vanadium pentoxide, etc.), conducting polymer-based material (polyaniline, polypyrrole, etc.) are the frequently used electrode materials for supercapacitors. However, several newly developed 2-dimensional and 3-dimensional materials are being used as electrodes in recent studies, which have widened the scope for further exploration [37].

Carbon materials possess greater potential as supercapacitor electrodes due to their characteristics such as enhanced conductivity, better stability (both thermal and chemical), and the opportunity to modify the textural properties. Over the years, researchers have been putting a few specific aspects on carbon-based electrodes, such as surface chemistry modification, pore size adjustments and formation of materials with higher surface area. These explorations have resulted in the development of numerous carbon materials of various sizes and shapes. In recent trends, rice/rice stem, algae, jujun grass, jute sticks, and sugar cane bagasse [33, 38–45] biomass materials have been considered promising sustainable precursors to developing carbon nanomaterials. Interestingly, the morphology of the different biomass-derived hard carbons is different, as seen in SEM images given in Figure 14.3. The electrochemical performances are governed by the derived morphology, porosity, or distribution of the electrode [2]. Apart from being carbon-rich, these biomass materials also offer the presence of Si, Na, Ca, Mg, and K like minerals, which play a vital role in energy storage [42, 46]. However, the number of mineral elements, structural characteristics and the chemical composition are different in every individual species.
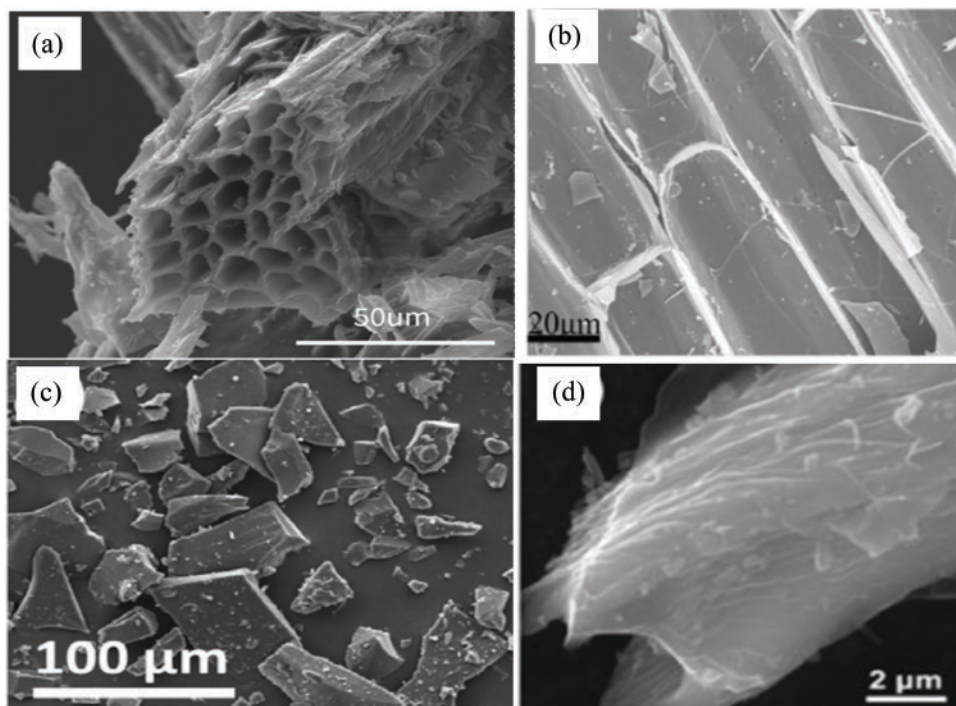
Figure 14.3 a) SEM pictures of poplar wood-derived hard carbon (PHC1400), b) SEM images of dandelion-derived biomass carbon, c) SEM images of sucrose-derived hard carbon, d) SEM images of renewable paper-derived hard carbon. *Reproduced with permission* [50–53]. *Copyrights (2019, Y. Zheng, Published by Elsevier) (2017, C. Wang, Published by Elsevier) (2015, W. Luo, Published by ACS) (2020, L. Pei, Published by Elsevier).*

Lately, an increasing scope of utilization of hard carbon as an electrode material has been observed in studies. Hard carbon has a highly disordered and irregular structural configuration, containing randomly and closely attached single-layer carbon atoms. Due to abundant micropores and expanded carbon inter-plane space, hard carbon can offer plenty of active sites that facilitate fast charge insertion/extraction surface reaction. As a result, it exhibits robust rate performance and the ability to store high charges [47]. Primarily, hard carbons were considered an effective choice for sodium-ion batteries because of efficient charge/discharge cycling [11]. Mainly epoxy resin, phenolic resin-like polymer materials are pyrolyzed to prepare hard carbon [12, 48, 49].

For instance, J. Ni et al. [54] utilized phenolic resin to prepare hard carbon at 1100 °C via pyrolysis. Afterward, the prepared hard carbon was used as a negative electrode in a supercapacitor setup, where activated carbon was added as the positive electrode. The supercapacitor exhibits specific capacitance fluctuating between 20.7 to 21.5 $F g^{-1}$, which was comparatively more than the supercapacitor constructed by the author formed using both electrodes made of activated carbon ($12\,F g^{-1}$). Moreover, it was observed that 90% of initial capacitance was retained using a hard carbon/activated carbon supercapacitor setup after 3000 cycles at a current density of $200\,mA g^{-1}$. In recent reports, biomass has been described as a good source for deriving hard carbon. For example, Ghosh S. et al. [55]

used biomass materials such as corn cob, banana stems, and potato starch to derive hard carbon by using them as supercapacitor electrodes individually. The authors employed three major steps – dehydration, porogenic stage, and pyrolysis – to prepare hard carbon. Furthermore, the banana stem sample was treated with potassium hydroxide and phosphoric acid to form separate samples. The prepared electrodes exhibited a different range of specific capacitance values, 479.23, 309.81, 202.11, and 99.9 Fg^{-1} for potassium hydroxide activated banana stem, corn-cob derived, phosphoric acid treated banana stem, and potato starch derived hard carbons. The electrode made with potassium hydroxide-activated banana stem has shown the highest efficiency, almost 72.88%, after 6000 cycles, and this result indicates good performance stability. Moreover, the potassium hydroxide-treated sample showed the highest columbic efficiency (47%) after the 100th cycle [55]. Hard carbon derived from oak wood has also shown promising electrochemical activity when used in organic supercapacitors. It has exhibited almost similar conductivity to artificial graphite [56]. Bio-derived or bio-based hard carbon aerogels are another great choices for various applications, as they exhibit mechanical strength and structural stability [57]. But at the same time, they have depicted inadequate electrical conductivity and restricted compressive strength (<300 kPa) due to having inherent interfacial issues, and this limits its further usage [58, 59]. Though, Ding et al. [60] came up with an effective solution, as the author used thiourea and self-assembling bacterial cellulose and carbonized them to prepare robust and ultra-elastic hard carbon aerogels for supercapacitor applications. These unique hard carbon aerogels have shown enhanced electrical conductivity ($23\,Sm^{-1}$) and remarkable areal capacitance ($0.97\,Fcm^{-2}$). Additionally, it displayed higher rate capability (at $20\,Ag^{-1}$, capacitance retention is 86%) and improved cyclic stability.

However, because of biomass's inherent robust microstructure, tuning the derived, hard carbon's structure became difficult. So, to make further improvements, studies have focused on forming composite using hard carbons. Dong et al. [61] prepared porous carbon nanosheets/hard carbon composite via grafting porous carbon nanosheets onto the hard carbons derived from rice husk to upgrade the functionality. The main purpose of grafting carbon nanosheets with leaf-like units was to enhance the approachable surface area of derived hard carbon for ion adsorption and to create abundant small pores for better ion movement during electrochemical activity. Hence conductivity was improved as well as supercapacitor performance. The composite electrodes prepared with different ratios of KOH were used in the supercapacitor setup individually, out of which 8 g KOH depicted the most efficient performance. That particular sample exhibited an outstanding rate capability of $189\,Fg^{-1}$ at a current density of $50\,Ag^{-1}$, a specific capacitance of $315\,Fg^{-1}$ at a current density of 0.1 A g^{-1}, and after 10000 cycles, capacity retention was found to be 95.8% with superb cycle stability. Additionally, the highest energy density was $10.9\,WhKg^{-1}$ at a power density of $52.6\,WKg^{-1}$ [61].

Other than that, N/O dual-doped hierarchical porous hard carbon and N/O-doped hard carbon electrodes have improved electronic conductivity, better reversible capacity, and excellent cycling stability [62, 63]. Huang et al. [62] prepared natural N/O co-doped hard carbon material via carbonizing mango seed shuck using a temperature range of 900–1300 °C. The material prepared in this way was used as an anode and activated carbon as a cathode in the potassium-ion hybrid capacitors setup. The fabricated hybrid capacitor has

exhibited a power density of $2000\,W\,kg^{-1}$ and an energy density of $68\ Wh\,kg^{-1}$ with improved cycling stability (after 500 cycles and at $0.1\,A\,g^{-1}$, 93.5% capacity retention was observed). Additionally initial reversible capacity of the fabricated device was $186.3\,mA\,h\,g^{-1}$. In actuality, N/O doping helped enhance the cyclability and rate capability of the electrode. In another study, H. Wu et al. [64] prepared composite electrodes using sodium iron silicate and H-N-doped hard carbon nanospheres [62]. The hybrid composite was prepared via the sol-gel procedure employing ferrous gluconate as a template and carbon source. Similar to the previous study, the author also aimed to create a fast charge (Na^+ ions and electron) transport pathway, which is why sodium iron silicate nanosheets were uniformly anchored in the mesoporous network structure of hard carbon nanospheres coating to form the hybrid electrode for supercapacitor. The electrode exhibited long-term cycling stability (after the 3300 cycles, 73.8% capacity retention) as well as high initial discharge capacity ($218.4\,mA\,h\,g^{-1}$ at current density of $276\ mA\,h\,g^{-1}$). Owing to the unique mesoporous carbon-coated structural characteristics, the hybrid electrode depicted an excellent energy density of $331.99\,Wh\,kg^{-1}$ and a power density of $2431.87\,W\,kg^{-1}$ within the working voltage range of 1.5−4.6 V [64]. The combination of hard carbon nanoparticles and carbon nanotubes has also shown potential energy storage applications [65]. However, this electrode has been used only for sodium-based batteries until now, and will hopefully be workable for supercapacitors as well.

14.4 Compatible Electrolytes for Biomass-derived Hard Carbon in Supercapacitors

Similar to the electrodes, electrolytes are also an essential element of the energy storage device. Its purpose is primarily to balance and effectively transfer the charges between the cathode and anode and to provide ionic conductivity. In past decades, electrolytes were explored and upgraded to serve better electrochemical performance and raise safety measures. The chemical and physical properties of electrolytes are greatly affected by rate performance, power density, specific capacity, cyclability, etc., like electrochemical performance parameters. Additionally, electrolyte and electrode interaction also has a crucial role in supercapacitor device performance as it strongly affects the internal structure of active materials and the electrode and electrolyte interface state. To design an electrolyte, one must control a few factors: electrolyte conductivity, salt concentration, solvent constituents, and electrochemical and thermal stability. Additionally, a recent article highlighted that energy density could be greatly improved by increasing the voltage window width of the electrolyte [66]. Various electrolytes are generally used in supercapacitors, such as liquid electrolytes, solid-state or quasi-solid-state electrolytes, and redox-active electrolytes and are implemented per the device fabrication requirements [67, 68].

In the literature, no studies are available that compare the hard carbon electrodes using a different set of electrolytes as a comparison. Still, as the trend is increasing recently, surely researchers will consider evaluating similar biomass-derived electrodes with various electrolytes. Nevertheless, here we will mention the electrolytes used in existing studies where biomass-derived hard carbon or composite hard carbon electrodes are utilized.

Dong et al. used a 6 M potassium hydroxide electrolyte (KOH) where rice husk-derived composite hard carbon material was employed as an electrode [61]. Likewise, S. Ghosh et al. also used the same type and amount (6 M KOH) of electrolytes where hard carbon was produced using different biomass, which shows excellent EDLC behavior with the symmetric triangle charge discharge shows less IR drop and high discharge time (Figure 14.4 c and d) [55].

In another study, where the hard carbon electrode was used, the electrolyte was 1 mol l^{-1} lithium hexafluorophosphate ($LiPF_6$) in ethylene carbonate (EC)/dimethyl carbonate (DMC) [54]. Here the ratio of DMC and EC was 3:1 (by volume). Using the volume ratio of DMC: EC as 1:1, 0.8 M potassium hexafluorophosphate (KPF_6) has also been used as electrolytes where mango seed shuck-derived nitrogen and oxygen dual-doped hard carbon was utilized as electrode [62]. While using sodium iron silicate/H-N-doped hard carbon composite electrode, H. Wu *et al.* used 1 M sodium perchlorate ($NaClO_4$) solution in ethylene carbonate (EC)/propylene carbonate (PC)/fluoroethylene carbonate (FEC) as the electrolyte. Here the ratio of PC and EC was 3:1 (by volume), with 5% FEC. From the CV curve (Figure 14.4 a) we can observe that varying ratio doesn't affect the redox actvity rather increased the conductivity. The material exhibits high specific capacity of 138.1 mAh g^{-1} at 0.1 C rate (Figure 14.4 b) [64]. An aqueous solution of sulfuric acid (H_2SO_4) is also a capable candidate for hard carbon electrode supercapacitor setup [56]. In conclusion, a very important factor observed in existing reports about the hard carbon and the utilized electrolyte is that carbon has random and irregular pores, due to which electrolyte and electrode interaction differs depending on the pore structure and accessibility by the electrolytes [54].

14.5 Pros and Cons of Application of Biomass-derived Hard Carbon in Supercapacitors

We have already discussed that hard carbon is extensively being explored as electrode material in a supercapacitor, and biomass as a potential source of hard carbon is getting a lot of attention. Due to having rapid kinetics feature, hard carbon is sufficiently useful for supercapacitor applications. However, its torturous and slender pore structures have created inadequate electrochemical performance issues. Due to its random pores and inner-pore configuration, ion transfer or diffusion was restricted [69]. This formation of pores and randomly oriented nano-graphite domains in bulk hard carbon seemed unable to access the electrolyte ions due to electrostatic shielding. Finally, electrochemical activity is confined [61]. But still, the hard carbon structure seemed to differ depending on the biomass used or the temperature used for carbonization. For example, hard carbon prepared with only 950 °C temperature has shown lower specific capacitance, but the same sample treated with KOH has exhibited better electrochemical device performance [61]. Like KOH, phosphoric acid-treated biomass (banana stem) derived hard carbons have also been proven a promising choice for supercapacitor application. In the same study, different types of biomass, such as corn cobs, potato starch, and banana stem, are employed, and structural and morphological parameters, such as interlayer distance, surface structure, porosity, etc., vary [55]. Apart from these, utilization of dopant or making composite using bio-derived hard carbon also enhanced device performance parameters such as rate
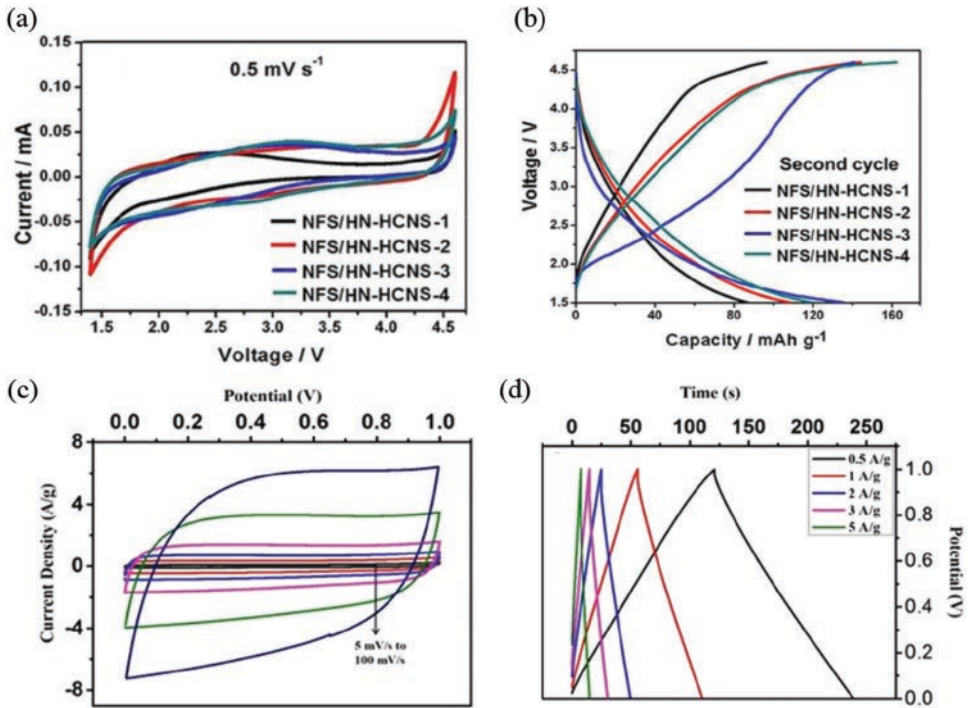
Figure 14.4 a) CV curves at 0.5 mV s-1 vs. Na/Na⁺ in the voltage range of 1.4–4.6 V, b) the second charge and discharge profiles at 0.1C, c) cyclic voltammetry of KHC-based device at different scan rates from 1 mV/s to 100 mV/s, d) galvanostatic charge/discharge curves measured at various current values in 6 M KOH solution. *Reproduced with permission* [55, 64]. *Copyright 2020, H. Wu, (Published by Elsevier) 2019, S. Ghosh, (Published by Springer Nature).*

performance, reversible capacity, cycle stability, etc. [62, 64, 70]. These reports focus on various aspects of using hard carbon in a supercapacitor. However, it still needs to explore more diversely for comparative evaluation to understand it more closely and make further optimization to make this commercially viable. Biomass to hard carbon will serve as an efficient choice for energy device applications and offers a great opportunity to reduce biomass wastage and to make waste biomass usable for valuable purposes.

14.6 Conclusions

Presently, researchers are exploring different types of materials in energy storage and conversion technologies to achieve maximum efficiency and make a commercial approach using them. Hard carbon is one of those options, and the practical scope of deriving these materials using biomass makes it more fascinating. The feasibility of utilizing hard-carbon materials has been discussed above with respective examples. We have illustrated the basic structural configurations and their electrochemical performance outcomes when devised in supercapacitor setups. Additionally, presently faced drawbacks and their possible

preventing measures have also been discussed, which will help the readers process more ideas for further advancements or modifications. However, beneficial characteristics of using hard carbons, such as better cycling performance, superior specific capacity, and better rate capability, have been explained concerning their supercapacitor device setup and their specific selection of other components (like electrolyte, electrode materials, etc.) used in the device. Finally, it can be concluded that biomass-derived hard carbon looks promising as an electrode material. Further improvement or modification can effectively boost its functionality, enhancing electrochemical activity and commercial-scale application.

References

1 M. Melikoglu, *Renew. Sust. Energ. Rev.* **2017**, *72*, 146–153.

2 T. E. Balaji, H. Tanaya Das, T. Maiyalagan, *ChemElectroChem* **2021**, *8*, 1723–1746.

3 X. Wei, S. Wan, S. Gao, *Nano Energy* **2016**, *28*, 206–215.

4 S. Xiong, J. Fan, Y. Wang, J. Zhu, J. Yu, Z. Hu, *J. Mater. Chem. A* **2017**, *5*, 18242–18252.

5 J. Yan, Q. Wang, T. Wei, L. Jiang, M. Zhang, X. Jing, Z. Fan, *ACS Nano* **2014**, *8*, 4720–4729.

6 X. Sun, L. Lin, L. Sun, J. Zhang, D. Rui, J. Li, M. Wang, C. Tan, N. Kang, D. Wei, H. Q. Xu, H. Peng, Z. Liu, *Small* **2018**, *14*, 1702916.

7 H. Zhang, H. Ming, W. Zhang, G. Cao, Y. Yang, *ACS Appl. Mater. Interfaces* **2017**, *9*, 23766–23774.

8 Y. Bai, Z. Wang, C. Wu, R. Xu, F. Wu, Y. Liu, H. Li, Y. Li, J. Lu, K. Amine, *ACS Appl. Mater. Interfaces* **2015**, *7*, 5598–5604.

9 C. Chen, Y. Huang, Y. Zhu, Z. Zhang, Z. Guang, Z. Meng, P. Liu, *ACS Sustain. Chem. Eng.* **2020**, *8*, 1497–1506.

10 J. Cai, D. Zhang, W.-P. Ding, -Z.-Z. Zhu, G.-Z. Wang, J.-R. He, H.-B. Wang, P. Fei, T.-L. Si, *ACS Omega* **2020**, *5*, 29896–29902.

11 X. Dou, I. Hasa, D. Saurel, C. Vaalma, L. Wu, D. Buchholz, D. Bresser, S. Komaba, S. Passerini, *Mater. Today* **2019**, *23*, 87–104.

12 H. Azuma, H. Imoto, S. I. Yamada, K. Sekai, *J. Power Sources* **1999**, *81-82*, 1–7.

13 Y. Zhang, S. Liu, X. Zheng, X. Wang, Y. Xu, H. Tang, F. Kang, Q.-H. Yang, J. Luo, *Adv. Funct. Mater.* **2017**, *27*, 1604687.

14 N. Guo, M. Li, Y. Wang, X. Sun, F. Wang, R. Yang, *ACS Appl. Mater. Interfaces* **2016**, *8*, 33626–33634.

15 Y. Liang, C. Yang, H. Dong, W. Li, H. Hu, Y. Xiao, M. Zheng, Y. Liu, *ACS Sustain. Chem. Eng.* **2017**, *5*, 7111–7117.

16 J. Hou, C. Cao, F. Idrees, X. Ma, *ACS Nano* **2015**, *9*, 2556–2564.

17 J. Hou, K. Jiang, M. Tahir, X. Wu, F. Idrees, M. Shen, C. Cao, *J. Power Sources* **2017**, *371*, 148–155.

18 J. Hou, K. Jiang, R. Wei, M. Tahir, X. Wu, M. Shen, X. Wang, C. Cao, *ACS Appl. Mater. Interfaces* **2017**, *9*, 30626–30634.

19 C. Chen, D. Yu, G. Zhao, L. Sun, Y. Sun, K. Leng, M. Yu, Y. Sun, *RSC Adv.* **2017**, *7*, 34488–34496.

20 X. Ren, S.-D. Xu, S. Liu, L. Chen, D. Zhang, L. Qiu, *J. Electroanal. Chem.* **2019**, *841*, 63–72.

21 J. Wang, L. Yan, Q. Ren, L. Fan, F. Zhang, Z. Shi, *Electrochim. Acta* **2018**, *291*, 188–196.

22 E. Demir, M. Aydin, A. A. Arie, R. Demir-Cakan, *J. Alloys Compd.* **2019**, *788*, 1093–1102.

23 H. Wang, F. Sun, Z. Qu, K. Wang, L. Wang, X. Pi, J. Gao, G. Zhao, *ACS Sustain. Chem. Eng.* **2019**, *7*, 18554–18565.

24 J.-L. Liu, J. Wang, -Y.-Y. Xia, *Electrochim. Acta* **2011**, *56*, 7392–7396.

25 S. S. Shah, H. Yang, M. Ashraf, M. A. A. Qasem, A. S. Hakeem, M. A. Aziz, *Chem. Asian J.* **2022**, *17*, e202200567.

26 J. R. Dahn, W. Xing, Y. Gao, *Carbon* **1997**, *35*, 825–830.

27 A. Manthiram, *Materials Aspects: An Overview in Lithium Batteries: Science and Technology*, (Eds. G.-A. Nazri, G. Pistoia), Springer US, Boston, MA, **2003**, pp. 3–41, 10.1007/978-0-387-92675-9_1.

28 L.-F. Zhao, Z. Hu, W.-H. Lai, Y. Tao, J. Peng, Z.-C. Miao, Y.-X. Wang, S.-L. Chou, H.-K. Liu, S.-X. Dou, *Adv. Energy Mater.* **2021**, *11*, 2002704.

29 S. Islam, S. S. Shah, S. Naher, M. A. Ehsan, M. A. Aziz, A. J. S. Ahammad, *Chem. Asian J.* **2021**, *16*, 3516–3543.

30 P. J. F. Harris, *Crit. Rev. Solid State Mater. Sci.* **2005**, *30*, 235–253.

31 L. L. Zhang, X. Zhao, *Chem. Soc. Rev.* **2009**, *38*, 2520–2531.

32 M. Sevilla, R. Mokaya, *Energy Environ. Sci.* **2014**, *7*, 1250–1280.

33 S. S. Shah, M. A. Aziz, E. Cevik, M. Ali, S. T. Gunday, A. Bozkurt, Z. H. Yamani, *J. Energy Storage* **2022**, *56*, 105944.

34 S. S. Shah, H. T. Das, H. R. Barai, M. A. Aziz, *Polymers* **2022**, *14*, 270.

35 S. S. Shah, M. A. Alfasane, I. A. Bakare, M. A. Aziz, Z. H. Yamani, *J. Energy Storage* **2020**, *30*, 101562.

36 M. Yaseen, M. A. K. Khattak, M. Humayun, M. Usman, S. S. Shah, S. Bibi, B. S. U. Hasnain, S. M. Ahmad, A. Khan, N. Shah, A. A. Tahir, H. Ullah, *Energies* **2021**, *14*, 7779.

37 P. Forouzandeh, V. Kumaravel, S. C. Pillai, *Catalysts* **2020**, *10*, 969.

38 Y. Zhong, X. Xia, S. Deng, J. Zhan, R. Fang, Y. Xia, X. Wang, Q. Zhang, J. Tu, *Adv. Energy Mater.* **2018**, *8*, 1701110.

39 S. E. M. Pourhosseini, O. Norouzi, P. Salimi, H. R. Naderi, *ACS Sustain. Chem. Eng.* **2018**, *6*, 4746–4758.

40 A. Aziz, S. S. Shah, A. Kashem, *Chem. Rec.* **2020**, *20*, 1074–1098.

41 K. Zou, Y. Deng, J. Chen, Y. Qian, Y. Yang, Y. Li, G. Chen, *J. Power Sources* **2018**, *378*, 579–588.

42 M. A. Aziz, S. S. Shah, S. M. A. Nayem, M. N. Shaikh, A. S. Hakeem, I. A. Bakare, *J. Energy Storage* **2022**, *50*, 104278.

43 M. R. Hasan, T. Islam, M. M. Hasan, A.-N. Chowdhury, A. J. S. Ahammad, A. H. Reaz, C. K. Roy, S. S. Shah, I. Al, M. A. Aziz, *J. Phys. Chem. Solids* **2022**, *165*, 110659.

44 S. S. Shah, E. Cevik, M. A. Aziz, T. F. Qahtan, A. Bozkurt, Z. H. Yamani, *Synth. Met.* **2021**, *277*, 116765.

45 S. S. Shah, M. N. Shaikh, M. Y. Khan, M. A. Alfasane, M. M. Rahman, M. A. Aziz, *Chem. Rec.* **2021**, *21*, 1631–1665.

46 D. Kang, Q. Liu, J. Gu, Y. Su, W. Zhang, D. Zhang, *ACS Nano* **2015**, *9*, 11225–11233.

47 A. G. Pandolfo, A. F. Hollenkamp, *J. Power Sources* **2006**, *157*, 11–27.

48 Y. Liu, J. S. Xue, T. Zheng, J. R. Dahn, *Carbon* **1996**, *34*, 193–200.

49 J. R. Dahn, T. Zheng, Y. Liu, J. S. Xue, *Science* **1995**, *270*, 590–593.

50 Y. Zheng, Y. Lu, X. Qi, Y. Wang, L. Mu, Y. Li, Q. Ma, J. Li, Y.-S. Hu, *Energy Storage Mater.* **2019**, *18*, 269–279.

51 W. Luo, C. Bommier, Z. Jian, X. Li, R. Carter, S. Vail, Y. Lu, -J.-J. Lee, X. Ji, *ACS Appl. Mater. Interfaces* **2015**, *7*, 2626–2631.

52 L. Pei, L. Yang, H. Cao, P. Liu, M. Zhao, B. Xu, J. Guo, *Electrochim. Acta* **2020**, *364*, 137313.

53 C. Wang, J. Huang, H. Qi, L. Cao, Z. Xu, Y. Cheng, X. Zhao, J. Li, *J. Power Sources* **2017**, *358*, 85–92.

54 J. Ni, Y. Huang, L. Gao, *J. Power Sources* **2013**, *223*, 306–311.

55 S. Ghosh, R. Santhosh, S. Jeniffer, V. Raghavan, G. Jacob, K. Nanaji, P. Kollu, S. K. Jeong, A. N. Grace, *Sci. Rep.* **2019**, *9*, 16315.

56 Y. Katsuyama, Y. Nakayasu, K. Oizumi, Y. Fujihara, H. Kobayashi, I. Honma, *Adv. Sustain. Syst.* **2019**, *3*, 1900083.

57 Z.-L. Yu, S. Xin, Y. You, L. Yu, Y. Lin, D.-W. Xu, C. Qiao, Z.-H. Huang, N. Yang, S.-H. Yu, J. B. Goodenough, *J. Am. Chem. Soc.* **2016**, *138*, 14915–14922.

58 X. Zhang, J. Zhao, X. He, Q. Li, C. Ao, T. Xia, W. Zhang, C. Lu, Y. Deng, *Carbon* **2018**, *127*, 236–244.

59 X. Xu, J. Zhou, D. H. Nagaraju, L. Jiang, V. R. Marinov, G. Lubineau, H. N. Alshareef, M. Oh, *Adv. Funct. Mater.* **2015**, *25*, 3193–3202.

60 C. Ding, L. Huang, X. Yan, F. Dunne, S. Hong, J. Lan, Y. Yu, W.-H. Zhong, X. Yang, *Adv. Funct. Mater.* **2020**, *30*, 1907486.

61 S. Dong, X. He, H. Zhang, X. Xie, M. Yu, C. Yu, N. Xiao, J. Qiu, *J. Mater. Chem. A* **2018**, *6*, 15954–15960.

62 F. Huang, W. Liu, Q. Wang, F. Wang, Q. Yao, D. Yan, H. Xu, B. Y. Xia, J. Deng, *Electrochim. Acta* **2020**, *354*, 136701.

63 J. Yang, Z. Ju, Y. Jiang, Z. Xing, B. Xi, J. Feng, S. Xiong, *Adv. Mater.* **2018**, *30*, 1700104.

64 H. Wu, Y. Zhang, X. Zhang, K. San Hui, J. Zhu, W. He, *J. Alloys Compd.* **2020**, *842*, 155797.

65 Y. Rangom, R. R. Gaddam, T. T. Duignan, X. S. Zhao, *ACS Appl. Mater. Interfaces* **2019**, *11*, 34796–34804.

66 B. K. Saikia, S. M. Benoy, M. Bora, J. Tamuly, M. Pandey, D. Bhattacharya, *Fuel* **2020**, *282*, 118796.

67 H. T. Das, K. Mahendraprabhu, T. Maiyalagan, P. Elumalai, *Sci. Rep.* **2017**, *7*, 15342.

68 R. Shakil, M. N. Shaikh, S. S. Shah, A. H. Reaz, C. K. Roy, A.-N. Chowdhury, M. A. Aziz, *Asian J. Org. Chem.* **2021**, *10*, 2220–2230.

69 J. Yang, H. Wu, M. Zhu, W. Ren, Y. Lin, H. Chen, F. Pan, *Nano Energy* **2017**, *33*, 453–461.

70 J. Jiang, Y. Zhang, Z. Li, Y. An, Q. Zhu, Y. Xu, S. Zang, H. Dou, X. Zhang, *J. Colloid Interface Sci.* **2020**, *567*, 75–83.

15

Carbon Nanofibers

Nasrin Sultana[1], Ahtisham Anjum[2], S. M. Abu Nayem[1], Syed Shaheen Shah[2,4]
Md. Hasan Zahir[3], A. J. Saleh Ahammad[1,], and Md. Abdul Aziz[4,5,*]*

[1] *Department of Chemistry, Jagannath University, Dhaka 1100, Bangladesh*
[2] *Physics Department, King Fahd University of Petroleum & Minerals, KFUPM Box 5047, Dhahran 31261, Saudi Arabia*
[3] *Interdisciplinary Research Center for Renewable Energy and Power Systems (IRC-REPS), King Fahd University of Petroleum & Minerals, Dhahran 31261, Saudi Arabia*
[4] *Interdisciplinary Research Center for Hydrogen and Energy Storage (IRC-HES), King Fahd University of Petroleum & Minerals, Dhahran 31261, Saudi Arabia*
[5] *K.A. CARE Energy Research and Innovation Center, King Fahd University of Petroleum & Minerals, Dhahran 31261, Saudi Arabia*
* Corresponding authors

15.1 Introduction

Carbon-based materials are commonly used as electrode materials for supercapacitors because of their unique chemical and physical properties, i.e., easy processability, controllable porosity, inert electrochemistry, good conductivity and high thermal stability [1, 2]. The versatile physical appearances of carbon materials such as powder, sheet, aerogel, tube, composite, monolith and fiber are also advantageous and desirable for preparing a high-performance supercapacitor [1, 3]. The charge storage mechanism of carbon-based electrode material is the adsorption of electrolytes across the electrode–electrolyte interface. The most promising material for use as an electrode in supercapacitors is carbon nanofiber (also known as CNF) due to its high surface area, flexibility, unique structure, good modulus of elasticity, high electrical conductivity, and homogenous porosity [4, 5]. One-dimensional CNFs with interconnected three-dimensional mesoporous morphology provide a suitable platform to incorporate foreign material for high-performance supercapacitors [4, 6, 7]. The tunable surface functionality of CNFs elevates the electrode performance by increasing the conductivity and introducing pseudocapacitive performance [8]. However, most CNFs are synthesized from high-cost and non-renewable resources such as poly(vinyl alcohol), poly pyrrole, and polyacrylonitrile. Thus, their use is still limited to lab-scale research [9]. Biomass is an abundant natural resource that has the potential to be a base for CNFs [5]. Biomass is the most significant source of carbon present as lignocellulose compounds, including cellulose, lignin and hemicellulose [10]. The components of plant biomass (hemicellulose, cellulose, plant protein, lignin, plant lipids) provide a fundamental skeletal structure and considerable numbers of functional groups for the carbons [11]. In

addition, cellulose's hydrophilic nature simplifies the ion diffusion process into nanofiber pores [5]. Furthermore, after cellulose, lignin comprises the second largest amount of biopolymer, found as a by-product in large quanities in the paper and pulp industry [12]. Biomass-derived CNFs have carbon-based material's fundamental chemical and physical properties, like heat resistance, good chemical inertia, and high conductivity [3]. Also, oxygen-containing functional groups such as –OH, –COOH and others on the biomass-derived carbon's surface, to a certain extent, make the CNFs appropriate for supercapacitor electrode materials[3]. This chapter comprehensively discusses the synthesis and development of biomass-based CNFs for high-performance supercapacitors.

15.2   Biomass-derived CNFs as Electrode Material for Supercapacitors

The electrode material used in a supercapacitor has a significant role in determining the device's electrochemical performance. It has been proved that the physical and chemical properties of controlled electrodes affects the charge storage efficiency of supercapacitors [13]. CNFs extracted from biomass provide modification facilities with low-cost renewable precursors, enhanced ion mobility and faster diffusion rate. The charge storage property of CNFs can be enlarged through activation, porosity incorporation, heteroatom doping and composite formation. In such a case, the modified electrode changes the charge storage mechanism.

15.2.1   Carbon Nanofibers

CNFs are considered promising electrode materials for supercapacitors in the energy storage field, especially for wearable devices. Biomass-based organic polymers such as cellulose, lignocellulose and lignin are used to synthesize CNFs and are regarded as a partial or total alternative to synthetic polymers for electrospun CNFs. A study on biomass-derived CNFs shows the potential charge storage property of CNFs being used as electrode material. Chen et al. [14] reported an esterification modified electrospun technique for preparing the CNFs from biomass: CNFs from whole lignocellulosic biomass acetylated sugarcane bagasse and polyacrylonitrile (PAN, as blending agent) without activating chemicals or pore-forming agents followed by carbonization. In addition, CNFs obtained from the esterification of lignin precursors show higher electrochemical performance in charge storage performance than the CNFs obtained from original lignin precursors [15]. The sugarcane bagasse-derived CNFs possessed abundant meso and microporosity, resulting in good BET surface area value of 450.0 $m^2 g^{-1}$ and thereby showing high charge storage performance with $S_c = 289.50$ Fg^{-1} and areal capacitance of $(\Xi = 64.20 \, \mu F \, cm^{-2})$. The symmetric system prepared with the sugarcane bagasse-derived CNFs also showed power density $(P_d = 1.260 \, kW \, kg^{-1})$ and high energy density $(E_d = 56.0 \, Wh \, kg^{-1})$ with good cyclic stability (5000 cycles at a current of 2.0 Ag^{-1}) and a high capacitance retention rate (111.80%). However, different biomass-derived CNFs show different responses as the organic polymers or CNFs precursors obtained from different biomasses don't have a similar chemical structure. Therefore, the selection of biomass precursors is quite important in preparing high-performance CNFs for supercapacitor electrode material. The mechanism and

electrochemical performance of lignin-based CNFs obtained from different plant species precursors were unlocked by Du et al. [16] who also gave clear guidance in the case of biomass-based precursors selection. Here, three different types of typical lignin were extracted from softwood (pine, PE), hardwood (poplar, PR), and grass (corn stalk, CS) materials and used to prepare CNFs. In addition, the three types of lignin contain different structural units (*p*-hydroxyphenyl unit (H), guaiacyl units (G), and/or syringyl units (S)). Lignin-based CNFs were prepared by electrospinning, where PAN was the blending agent and followed by peroxidation and carbonization. In a comparison of the electrochemical performance of the three types of lignin-based CNFs, poplar lignin-based CNFs showed a greater specific surface area of 1062.50 $m^2\,g^{-1}$, larger $S_c = 349.2\,Fg^{-1}$ and higher tensile strength of 35.31 MPa. Even in a two-electrode system with symmetric assembly, poplar lignin-based CNFs, when tested in an aqueous electrolyte containing Na_2SO_4, CNFs showed an excellent $E_d = 39.60\,Wh\,kg^{-1}$ when subjected to a $P_d = 5.0\,kW\,kg^{-1}$

They also displayed exceptional cycling stability, having a value of 90.51% after 5000 cycles. The findings demonstrated that lignin derived from hardwoods, specifically poplar, was an excellent choice for an eco-friendly raw material for lignin-based CNFs. Analyzing the connection between the structure of various lignins and the behaviour of lignin-based CNFs allowed researchers to better understand the process by which different plant species affect the electrochemical performance of these materials. This was done by focusing on the lignins themselves. In general, it was noted that the performance of lignin-derived CNFs was better when the molecular weight was higher, more -O-4 aryl ether linkages and S units were present, fewer –COOH groups were present, and the polydispersity was smaller. Among all lignin-based CNFs, poplar lignin contained these superior functionalities and therefore high performance was observed.

15.2.2   Activated CNFs

Biomass precursors have a complex hierarchical structure, which allows the freestanding formation of conductive CNFs after simple activation [5, 17]. Activation of carbon material introduces high porosity and enlarges the specific surface area. Generally, the activation is carried out either physically (in air, steam or CO_2) or chemically using activation agents [18]. Physically activated cellulosic biomass gives activated CNFs, which showed a high specific surface area and appropriate surface porosity [19]. High electrochemical performances, i.e., high $S_c = 240.80\,Fg^{-1}$ (in 6.0 M KOH electrolyte) and excellent reversibility and rate capability were observed using the physically activated CNFs. Chemically activated electrospinning CNF mats prepared from lignin biomass showed highly densified carbon electrodes (0.10 to 0.60 $g\,cm^{-3}$) where NaOH was used as the activating agent to ensure microporosity [20]. Therefore, a high surface area was maintained even after densification, which is beneficial for electrochemical double-layer capacitors. Shi et al. showed that activated CNFs prepared from a mixture of biomass (industrial hemp straw) and PAN showed higher charge storage performance than the CNFs obtained from synthetic organic polymer PAN [21]. The activated CNFs obtained from biomass were found to have a high surface area, strong electro-conductivity, and outstanding electrochemical performance. The activated CNFs as electrode material showed $S_c = 244.80\,Fg^{-1}$ at a $j = 1.0\,Ag^{-1}$, and the specific capacitance reached 219.0 Fg^{-1} at $j = 10.0\,Ag^{-1}$. After being charged and

discharged 3000 times in a 6 M KOH solution using a three-electrode setup, activated CNFs showed a specific capacitance retention rate of 96.0% (at $2.0\,A\,g^{-1}$).

15.2.3 Heteroatom Doped CNFs

The existence of heteroatoms (such as O, N, S and P) is beneficial for the electrochemical properties of biomass-derived CNFs electrodes [9]. N-doped CNFs derived from bacterial cellulose combined with a reduced graphene oxide (RGO) sheet form an efficient electrode material for supercapacitors [22]. Here, N doping increased the electrode material's wettability and increased the speed of the transportation and diffusion of electrolyte ions. The N-doped carbon nanofiber networks showed enhanced specific capacitance, improved rate capability and exceptional cycling performance (100% retentions after 20,000 cycles). On the other hand, N and S co-doped CNFs based electrodes were prepared from a lignin biomass precursor where graphene was used to immobilize the S and N by capturing NH_3, HCN, and SO_2 released during carbonization and activation of lignin and PAN [23].

The supercapacitor fabricated with the N, S self-doped graphene-modified CNFs displayed a high $S_c = 267.32\,Fg^{-1}$, a long cycling life, high $P_d = 0.493\,kW\,kg^{-1}$, and exhibited a $E_d = 9.28$ Wh kg^{-1}. Improved performance of heteroatom doped CNFs based flexible electrode inspired Li et al. [24] to further modify the morphology of CNFs to enhance the charge storage capacity. However, the limited mass transfer of electrolyte ions through the one-dimensional carbon material reduces the performance of charge storage and energy conversion. Therefore, the introduction of multifunctional pores on the surface of CNFs can enhance the active surface for electrolyte ions adsorption. Li et al. [24] reported a new method for preparing high-performance electrode material by incorporating multimodal porosity in seaweed-derived CNFs (PCNFs) and then activating with NH_3 for N-doping (N-PCNFs). In addition, heteroatoms helped to enlarge the charge storage performance by introducing pseudocapacitance. Figure 15.1A-D shows the morphology and elemental composition of the mesoporous N-PCNFs. Figure 15.1E-H demonstrates the CV as well as the GCD measurement. N atom incorporation in PCNF showed a significant enhancement in the rectangular shape of the CV curve (Figure 15.1F), and the highest discharging time (Figure 15.1G) was achieved for N-PCNF-600 (annealed at 600 °C), which offered higher capacity for charge storage.

15.2.4 Hierarchical Hollow Porous CNFs

Solid structural CNFs generally expose the outer surface for ion adsorption. On the other hand, hollow CNFs provide a better two-dimensional active flat surface for charge storage, increase the permeability of electrolyte ions through the hollow structure of the electrode and shorten the diffusion path for ions. Hence high capacitance performance can be achieved by hierarchical hollow porous structural electrodes. The complex microstructure of biomass often helps to have high porosity in carbon material.

Wang et al. [25] synthesized hollow activated carbon nanofibers (HACF) of the three different types using biomass from willow catkins (WC), pitch-based hollow fibers and phenolis. These hollow fibers were investigated from multiple angles, looking at their shape, pore structure, surface, electrochemical capabilities and chemical content. HACFs that are produced from WCs have the potential to serve as good electrode materials for electrochemical energy storage devices on account of their high hollowness, low cost, and eco-friendly
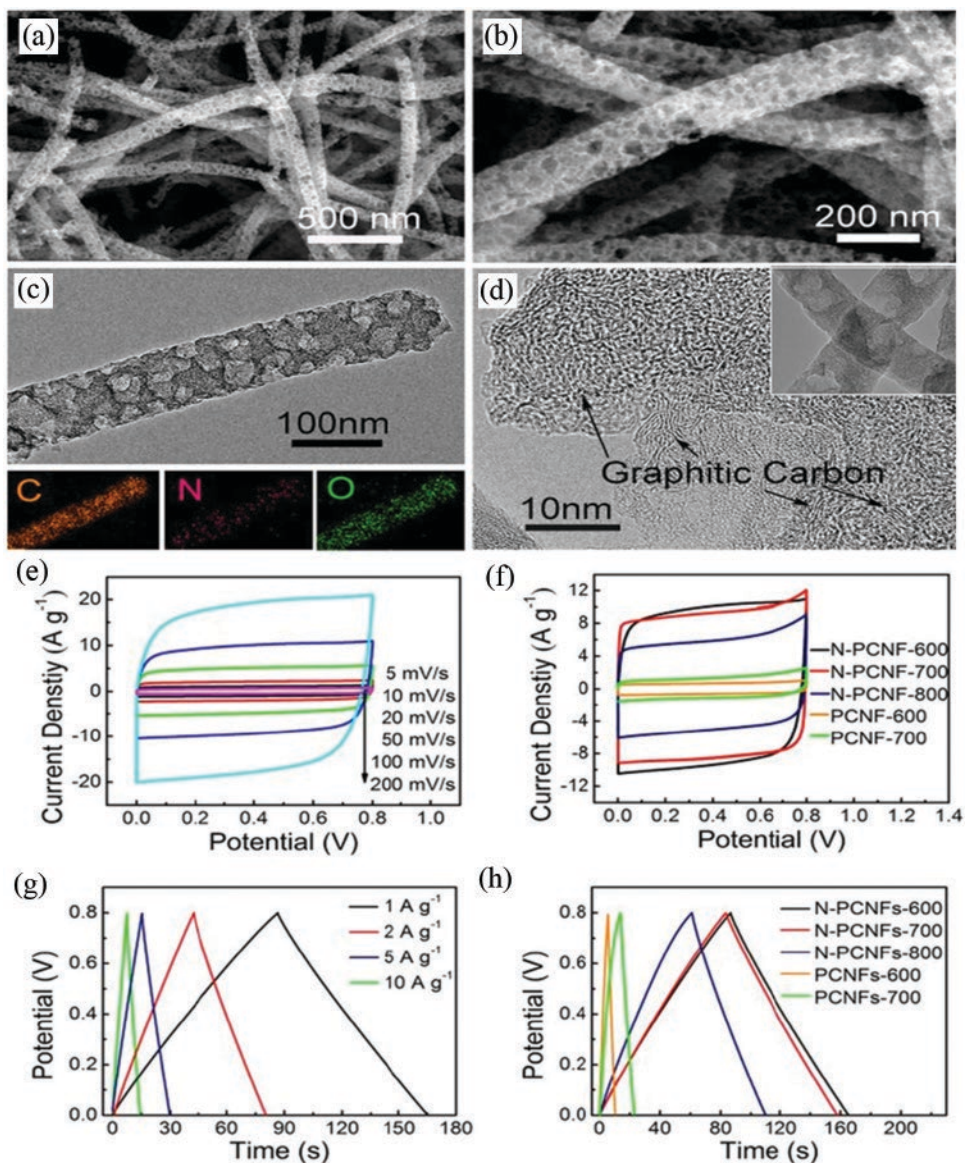
Figure 15.1 (A and B) Scanning electron microscopic images of the N-doped porous graphitic carbon nanofibers-600 material. (C) TEM image at low magnification, as well as TEM-EDS (energy-dispersive spectroscopy) elemental mapping and (D) transmission electron microscopy image of N-doped porous graphitic carbon nanofibers-600 captured by a TEM operating at high magnification. (E) CV of N-doped porous graphitic carbon nanofibers-600 SCs measured between 0.0 and 0.80 volts in a solution containing 6.0 M KOH while using a variety of scan rates. (F) CV curves of various PCNF and N-doped porous graphitic carbon nanofibers-600 compounds were scanned at a rate of 100 mVs^{-1} in a solution that contained 6.0 M KOH. (G) N-doped porous graphitic carbon nanofibers-600 galvanostatic charge and discharge (GCD) curves were measured over a wide range of current densities. (H) GCD curves at 1.0 Ag^{-1} for various PCNF and N-PCNF are displayed. *Reproduced with permission [24]. Copyright 2015, American Chemical Society.*

nature. Compared to melt-pinned hollow fibers, willow-HACFs are better for fabricating electrode materials due to their low cost, renewability and the particularly high-hollow tubular structure of naturally occurring biomass WCs. The willow-HACFs have excellent electrochemical properties due to the combination of EDLCs and pseudocapacitance. The willow-HACFs feature a substantial amount of surface heteroatom-doped functional groups (2.390 wt.% N and 16.410 wt.% O species) and a high microporous specific surface area (1067.0 m^2 g^{-1}). The pore size distribution is more concentrated at 0.7~1.2 nm. Electrochemical studies showed that the HACFs produced from WCs possess a high specific capacitance of 333.0 Fg^{-1} at a current rate of 0.10 Ag^{-1} and had 62.70% of a large rate capability with retention (209.0 Fg^{-1} at 10.0 Ag^{-1}). When HACFs derived from WCs-based electrodes are used in symmetric supercapacitor devices, HACFs produced from WCs provide a maximum $E_d \approx 8.80$ Wh kg^{-1} at a $P_d = 0.050$ kW kg^{-1} and good cycling performance, with 95.50% retention over 3000 cycles at 5.0 Ag^{-1} in 6 M KOH aqueous electrolytes. The supercapacitor device has exceptional electrochemical performance, which makes it a good candidate for application in a high-performance electrochemical energy system [25]. Figure 15.2 shows an illustration of the manufacture of HACFs obtained from willow catkins and the corresponding scanning electron microscopic images.
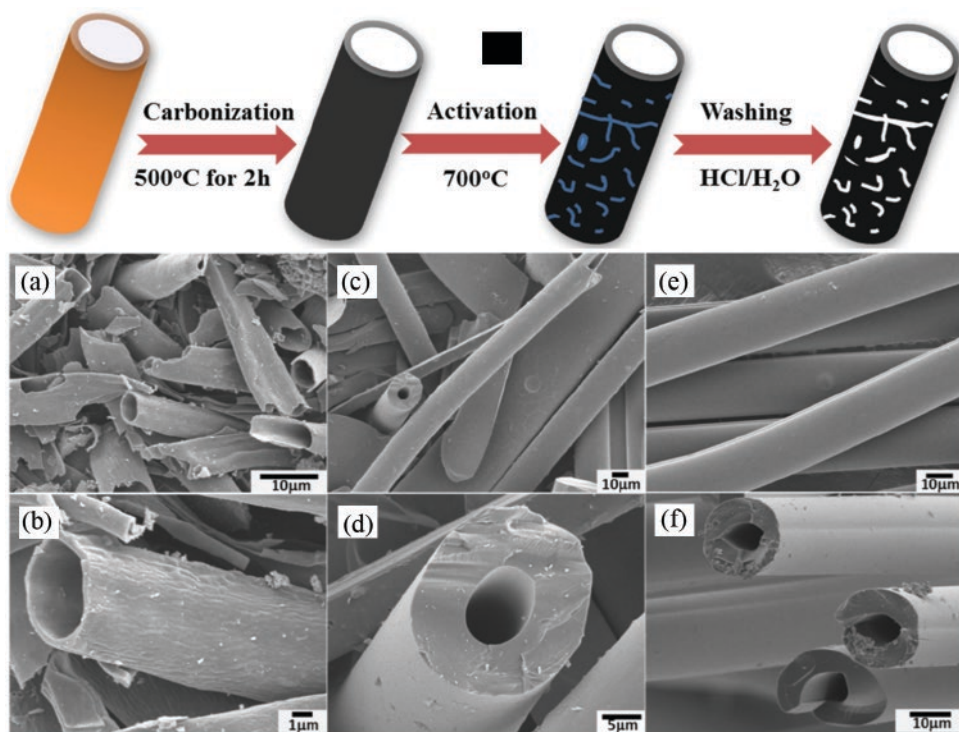
Figure 15.2 An illustration of the manufacture of HACFs obtained from willow catkins according. (a, b) Scanning electron microscopic images of willow-HACFs, (c, d) scanning electron microscopic images of phenolic-HACFs, (e, f) scanning electron microscopic images of pitch-HACFs. *Reproduced with permission [25]. Copyright 2017, Elsevier.*

Ma et al. [26] synthesized biomass-derived activated carbon hollow fibres (ACHF) at different carbonization temperatures (600 °C, 700 °C and 800 °C) using wood waste to prepare high-performance electrode material for supercapacitors. For a comparative study, commercial wood charcoal (WC) was mixed with ACHF in liquefication before electrospinning to prepare WC-modified ACHF (WC-ACHF). Carbonization of the WC-ACHF was also done at 600 °C, 700 °C and 800 °C. The WC-ACHF showed large inner and outer porosity due to effective contraction between ACHF and WC. High-extent porosity demonstrates an exceptional $S_c = 295 Fg^{-1}$ at 0.5 A g^{-1}, which was measured for WC-ACHF-800. This specific capacitance remained as high as 218 F g^{-1} even when the current density is 20.0 A g^{-1} (214 F g^{-1} at the current rate of 20.0 A g^{-1} observed for ACHF-800). Modifying AHCF with WC showed an excellent capacitance retention rate of 73.80% at the current rate of 20 A g^{-1}. At 500 W kg^{-1} power density, a symmetrically assembled WC-ACHF-800 two-electrode system achieved an energy density of 7.80 Wh kg^{-1}, and when the power density was increased up to 10.0 kW kg^{-1}, the energy density was 5.20 Wh kg^{-1}.

15.2.5 Transition Metal or a Metal Oxide Containing CNFs

Significant effort has been made to produce a supercapacitor with a high energy density. Biomass-derived CNFs are used to effectively elevate the double-layer charge storage capacitance property. A freestanding three-dimensional network of CNFs accelerates electrolyte accessibility and shortens the path to the active sites. The CNFs have a hierarchical structure, increasing the specific capacitance and, as a result, the power density. Nevertheless, low energy density continues to be a problem that has to be studied. Transition metals or metal oxides are considered active pseudocapacitive materials that store energy through redox reactions resulting in high energy density.

A metal or metal oxide composite and CNFs add a new charge storage mechanism (redox center) to double-layer capacitance and enhance the specific capacitance. Literature study shows transition metal compounds such as oxide, sulfide and hydroxide have been used to enlarge the electrochemical performance of biomass-based CNFs [26–29]. Changing the surface chemistry of biomass-derived CNFs with such metal compounds helps develop an electrode material for high-performance supercapacitors. In addition, a biomass-derived organic polymer such as cellulose provides a three-dimensional web to anchor metals or metal oxides. Long et al. used bacterial cellulose as both a carbon precursor and a template to prepare a nanofibrous carbon network (c-BP) by carbonization with polyaniline [28]. The deposition of MnO_2 on the c-BP showed a larger CV curve and higher specific capacitance for c-BP/MnO_2 than a single MnO_2 electrode.

Sun et al. [30] synthesized manganese dioxide (MnO_2) nanosheets that were formed on multichannel carbon nanofibers containing amorphous cobalt oxide (CoMCNFs@MnO_2) by using electrospinning technology, then carbonization and a straightforward chemical bath deposition. The resulting CoMCNFs@MnO_2 composites exhibit flexible characteristics, which have the potential to serve as freestanding electrodes in supercapacitors. This one-of-a-kind structure offers a variety of benefits, such as embedding amorphous cobalt oxide (CoO), which encourages the growth of surface MnO_2 nanosheets; hierarchical MnO_2 nanosheets, increase the exposure of active spots and speed up OH-movements as well as forming a structure consisting of 1D multichannel carbon nanofibers, which makes it possible to transport ions over shorter distances. It is interesting to note that flexible

composite films could be used as electrode materials for supercapacitors even if they stand independently. Because of this, CoMCNFs@MnO$_2$-2.50 displays a $S_c = 265.0\,Fg^{-1}$ at $0.50\,Ag^{-1}$, which is more than the capacitances displayed by their counterparts (135.0 and $143.0\,Fg^{-1}$ at $0.50\,Ag^{-1}$ for MCNFs@MnO$_2$ and CoMCNFs, respectively). And after 10,000 cycles, the CoMCNFs@MnO$_2$-2.50 specific capacitance was still 98.70 %. Importantly, the electrospinning carbon nanofibers (CNFs) and CoMCNFs@MnO$_2$-2.50 form an asymmetric supercapacitor (ASC) with a high $E_d = 19.270\,Wh\,kg^{-1}$ and a $P_d = 0.21751\,kW\,kg^{-1}$ at $0.30\,Ag^{-1}$ and a remarkable cycle ability of capacitance retention of 94.90% after 10000 cycles. As a result, their work presents a promising method for creating high-performance flexible electrode materials for application in future generations of wearable energy storage gadgets [30]. Figure 15.3 presents XRD patterns, cyclic voltammetry curves, galvanostatic discharge curves, and specific capacitances of the fabricated electrodes. Figure 15.4 shows the asymmetric supercapacitors performance.

15.3 Preparation of CNFs

Biomass-based CNFs can be synthesized using chemical vapour deposition, electrospinning, pyrolysis, and hydrothermal techniques.
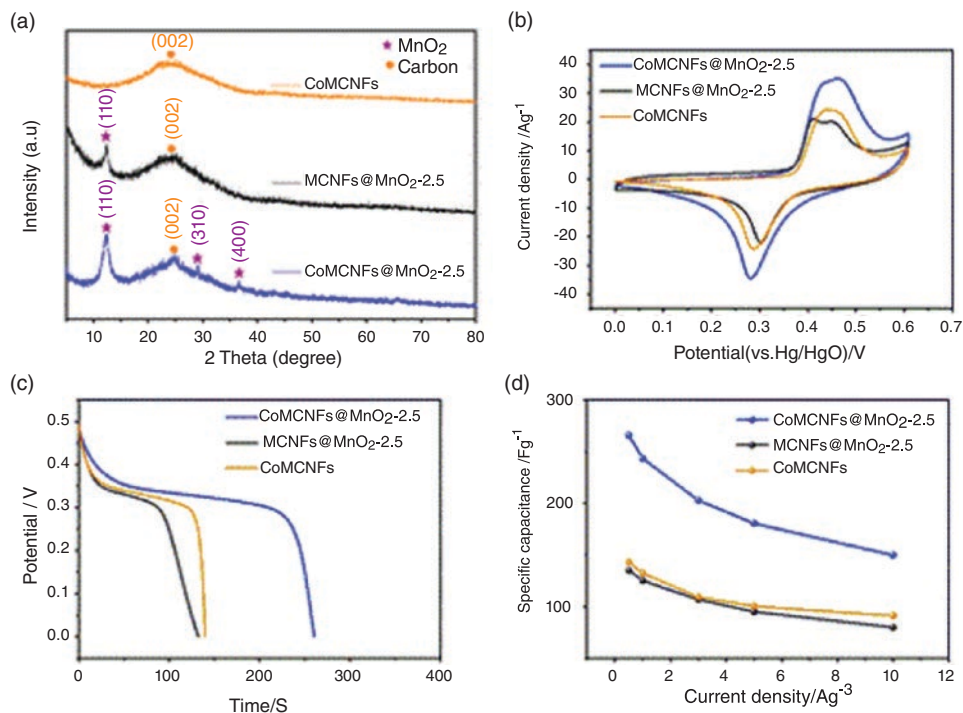
Figure 15.3 (a) XRD patterns, (b) cyclic voltammetry curves at a scan rate of 50.0 mVs^{-1}, (c) curves of the galvanostatic discharge at a given current density ($j = 0.50\,Ag^{-1}$), (d) specific capacitance (S_c) at different current densities. *Reproduced with permission [30]. Copyright 2019, American Chemical Society.*
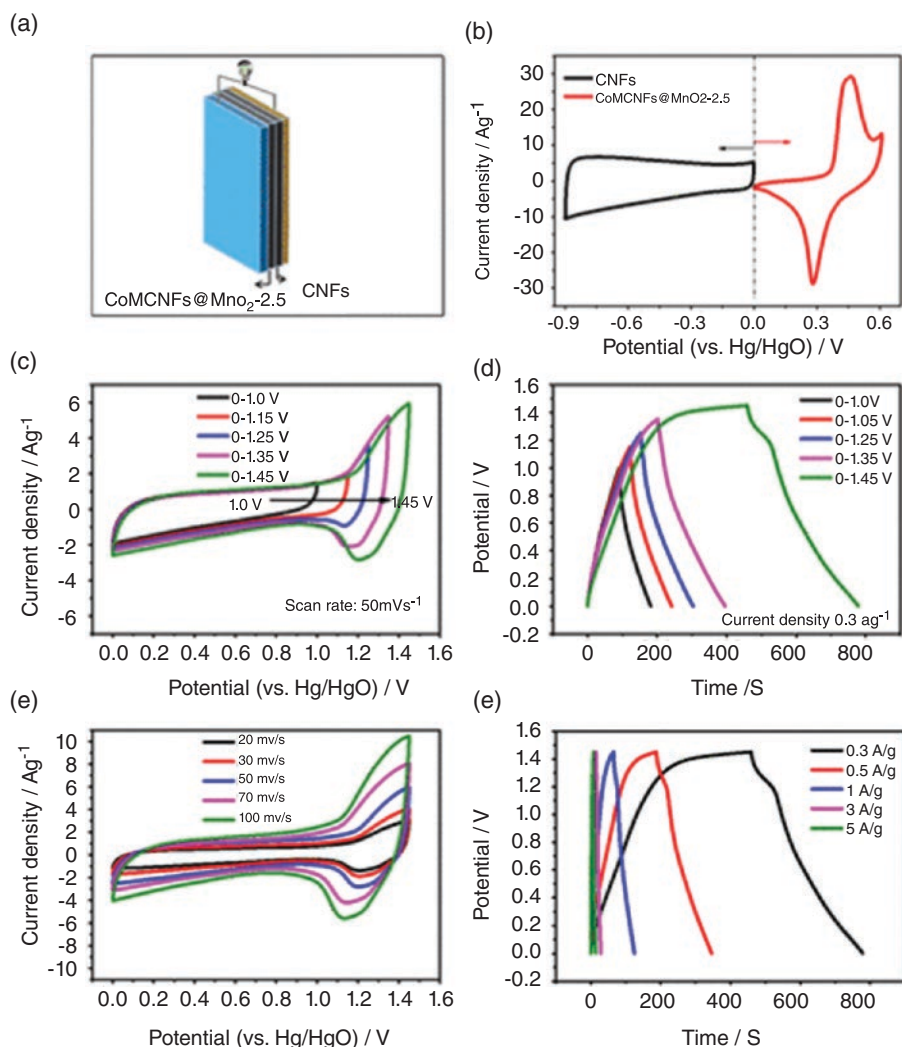
Figure 15.4 (a) The asymmetric supercapacitors based on CoMCNFs@MnO$_2$-2.5 and CNFs are depicted schematically above. (b) CoMCNFs@MnO$_2$-2.5 and CNFs cyclic voltammetry curves scan at 50.0 mV s^{-1}. (c) Asymmetric supercapacitors cyclic voltammetry curves measured at a scan rate of 50.0 mV s^{-1} over a potential range of 1.0 to 1.45 V, (d) from 1.0 to 1.45 V at 0.30 Ag^{-1}, GCD curves of the ASCs, (e) ASCs cyclic voltammetry curves at scan rates between 20 and 100 mV s^{-1}, and (f) asymmetric supercapacitors galvanostatic charge-discharge curves for current densities between 0.30 and 5 Ag^{-1}. *Reproduced with permission [30]. Copyright 2019, American Chemical Society.*

15.3.1 Chemical Vapour Deposition

The chemical vapour deposition (CVD) method is effective for manufacturing high-quality carbon nanofiber with complete control over its thickness and uniformity [31]. This method uses a quartz tube reactor, quartz boat, metal catalyst, and N$_2$, He, H$_2$ or Ar, etc., as carrier gas and stabilizer [31–33]. Along with biomass-derived activated carbon, low molecular hydrocarbons (acetone, ethylene etc.) are also carbon precursors for CVD [31].

A high temperature (500–700 °C) is maintained during the CNFs formation, where CNFs start forming over a metal catalyst placed in a quartz boat. The metal catalyst governs the shape of the CNFs. Figure 15.5A shows the CVD simple instrumentation. Sari et al. [34] prepared CNFs using activated carbon (AC) derived from banana peel and acetylene as a carbon source and Ni as a metal catalyst. Figure 15.5B, D show SEM images of CNFs made from banana peel using the CVD technique at temperatures of 600 °C and 700 °C, respectively. Chen et al. also synthesized CNFs/AC composite through the CVD method [32]. They made AC from palm kernel shell (AC-P), wheat straw (AC-W) and coconut (AC-C) and placed them in a vertical fixed bed microreactor, and a mixture of ethylene and hydrogen (the ratio 1:1) was introduced into the reactor where a high temperature of 700 °C was maintained for two hours to prepare the CNFs composite.

15.3.2 Electrospinning

Electrospinning is an effective and versatile technique to prepare ultrathin fiber [36–42]. This method is extensively used to prepare CNFs with very low diameters (< 100 nm) [43]. The basic setup of electrospinning includes a syringe pump, a high-voltage power supply (AC or DC current), a spinneret (usually a hypodermic needle with a blunt tip), and a conductive collector [44]. Synthesis of CNFs from biomass by electrospinning can be divided into four steps; i) pretreatment of biomass; ii) prepare a polymeric solution; iii) nanofibers (also called precursor fibers) formation through electrospinning; and iv) stabilization and carbonization. The schematic representation for the basic setup of the electrospinning process is shown in Figure 15.6.

This process mainly involves an electrohydrodynamic process in which a melt solution or liquid is electrified to produce a jet that is then stretched and elongated to generate fibers. During electrospinning, polymeric solution or melt of biomass precursor is poured into the reservoir and connected with a high voltage power supply [45]. Surface tension causes the melt to be extruded from the spinneret during the electrospinning process, which results in the generation of a pendant droplet. In the presence of an electric field, the droplet is forced into the shape of a Taylor cone by the repulsive interaction between surface charges with the same sign. This results in the emission of a charged jet [46]. Finally, the charged jet is directed towards a grounded target where the jet is collected as
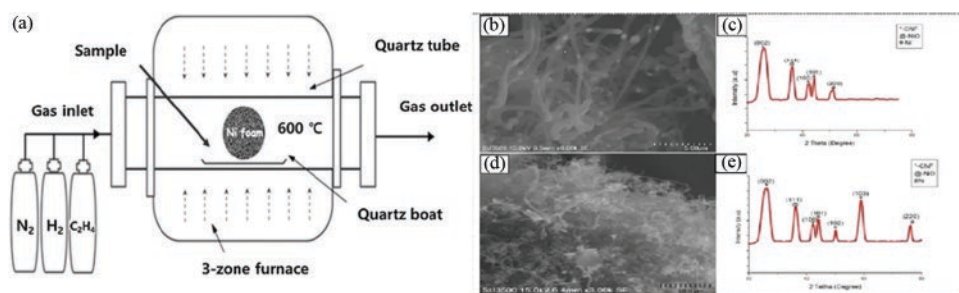
Figure 15.5 (A) Schematic diagram of experimental apparatus used in CVD. *Reproduced with permission [35]. Copyright 2018, Elsevier.* (B, C) SEM image and XRD pattern of CNF produced at temperature 600 °C; (D, E) SEM image and XRD pattern of CNF produced at temperature 700 °C. *Reproduced with permission [34]. Copyright 2019, Elsevier.*
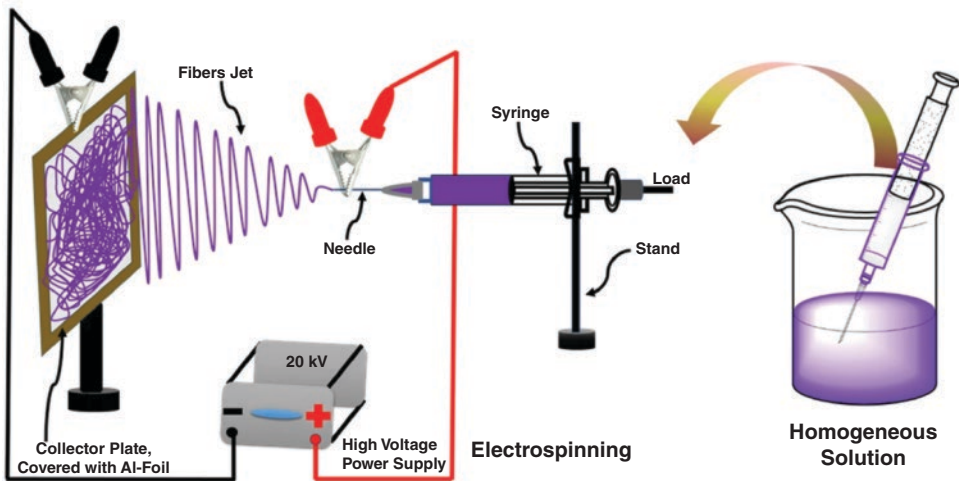
Figure 15.6 Schematic representation of the basic setup of the electrospinning process. *Reproduced with permission [38]. Copyright 2020, Springer.*

a nonwoven interconnected web of small, thin and long nanofiber fiber. During this time, solvent elongation, instability and evaporation occur as the jet reaches the collector [47]. The collected web was then dried to stabilize and carbonized (with or without activation) to prepare CNFs from biomass. Several working parameters, such as solution flow rate, applied voltage and distance between nozzle and collector, influence the diameter of the CNFs. Polymers such as polyvinyl alcohol are frequently utilized to elevate the viscosity of fiber precursor solutions and enhance their capacity to spin [23]. Dai et al. [23] used lignin (corn stalk residues) to prepare N, and S co-doped graphene (GN) modified lignin/ PAN-based carbon nanofiber (ACNFs) by employing electrospinning followed by carbonization and activation. Systematic synthesis of the CNFs from corn stalk residues is shown in Figure 15.7.

15.3.3 Pyrolysis

Pyrolysis treatment is a simple process usually carried out at high temperatures [48–51]. This method consists of carbonization and activation of the biomass precursors. Activation is carried out either physically or chemically (using chemical activating agents such as KOH, and NaOH). In the case of physical activation, carbonization and activation are carried out simultaneously. Alkaline compounds as activating agents facilitate the conversion of lignocellulose of biomass into carbon fiber. Residence time and temperature have significant effects on the electrochemical property of the carbonized material. Pyrolysis under an inert argon environment at 700 °C temperature has produced CNFs from bacterial cellulose with a diameter as low as 20 nm and a density of 4 mg cm^{-3} [52]. Such a study demonstrates pyrolysis is an effective method to prepare high-performance CNFs for use in supercapacitors. Zhang et al. reported microwave pyrolysis of pine nut shells with microwave irradiation to prepare hollow CNFs with a diameter of about 400 nm and 1400–5000 nm length [53].
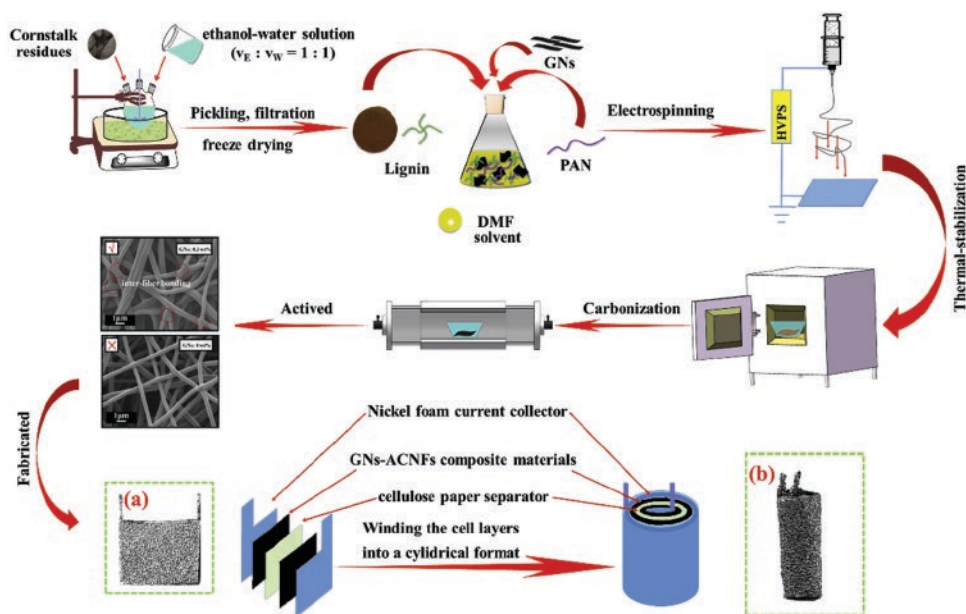
Figure 15.7 Schematic representation of the preparation GNs-N-S co-doped activated lignin-based CNFs for supercapacitor by electrospinning method. *Reproduced with permission [23]. Copyright 2019, Elsevier.*

15.3.4 Hydrothermal Treatment

In the hydrothermal method, biomass conversion is done thermochemically at high pressure (2 MPa–10 MPa) in an autoclave [54–56]. Water is a commonly used solvent in this treatment. Water turns into a supercritical form at a temperature above boiling point and 1.0 MPa pressure. The comparatively lower temperature within the range of 180–300 °C is applied during the hydrothermal method [54]. However, this process requires a low heating temperature but take a long time and uses more electrical energy than pyrolysis and electrospinning methods. Golmohammadi and Amiri [57] synthesized CNFs by hydrothermal treatment of *Typha domingensis* biomass at 200 °C for 2 h. During the heating treatment precursor of Ni and Co was used to prepare a composite of nanofiber, which showed extremely high specific capacitance of 1770 Fg^{-1} at 1.0 Ag^{-1}. Hydrothermal treatment of bacterial cellulose for 12 h at 180 °C provided a lower diameter (10 – 20 nm) containing three-dimensional interconnected nanofiber. It ensured homogenous incorporation of heteroatom (i.e., N) on the bacteria cellulose-derived CNFs [27]. Therefore, hydrothermal-treated CNFs showed better charge storage performance than pyrolysis-treated CNFs.

15.4 Biomass-derived CNFs in Symmetric Supercapacitors

Symmetric supercapacitors contain the same material in their positive and negative electrodes. Consequently, to get a high energy density, it is necessary to make an appropriate choice of electrode material [2, 51, 58–61]. Biomass-derived CNFs have potential use to fabricate electrode material for high-energy-density supercapacitors. A simple modification of

precursors or change in composition can significantly change charge storage performance. Lemongrass leaf waste showed a potential raw material for preparing interconnected porous activated CNFs for high-performance symmetric supercapacitors [62]. At first, activated carbon was prepared from lemongrass leave using $ZnCl_2$ as an activator, and lastly, the porous activated CNFs were prepared by carbonization (600 °C in N_2 gas) and physical activation at 800 °C in CO_2. Optimization of $ZnCl_2$ concentration was done based on the electrochemical performance and morphological study of the porous activated CNFs. The activated porous CNFs in optimum condition (0.7M $ZnCl_2$) showed the appearance of hierarchical pores and nanofiber pores, which resulted in a high specific surface area of 1694 m^2 g^{-1}. Hence high charge storage performance was observed in the symmetric cell with a $P_d = 0.1283$ kW kg^{-1} and $E_d = 35.6$ Wh kg^{-1}. Cao et al. reported high-performance electrode material with poplar lignin and cellulose acetate-derived CNFs, which achieved a high $E_d = 30.20$ Wh kg^{-1} when keeping a $P_d = 0.40$ kW kg^{-1} in a symmetric system [63]. Here the phosphating process was carried out to modify lignin and cellulose acetate to prepare the fiber precursors. Zhu et al. [64] introduced an effective process using lignin with high molecular weight and lower heterogeneity which is conducive to reducing the carbon weight loss of precursor fibers. Modifying lignin extracted from cornstalk by refining with isophorone diisocyanate and fractionation increased lignin's molecular weight and resulted in high-performed CNFs.Such modification and fractionation maintained the morphology of nanofiber and significantly enlarged the surface area (2042.86 m^2 g^{-1}) and charge storage capacity (442.2 Fg^{-1}). A supercapacitor that was made by using modified lignin-based CNFs demonstrated a high $E_d = 37.10$ Wh kg^{-1} while having a $P_d = 0.40$ kWkg^{-1}. Chen et al. used bacterial cellulose-derived self-doped CNFs (N-CNFs) as electrodes to achieve high-performance symmetric supercapacitors [65]. N-doped CNFs showed high ($S_c = 224$ Fg^{-1} at a current rate of 0.5 Ag^{-1}) as the heteroatom introduced pseudocapacitance property. More than one heteroatom in CNFs also enhances the active electrolyte ions' active sites, thereby improving the charge storage capacity. N and S co-doped CNFs with graphene nanosheet (GN) showed ultra-high $S_c = 267.32$ Fg^{-1}, and energy density of the symmetric supercapacitor increases by four to 9.28 Wh kg^{-1} after graphene addition [23]. Figure 15.8 shows the voltammetric performance of activated N, S-doped GN-CNFs (ACNF) in 6 mol L^{-1} KOH. At low frequencies, the Nyquist plot displays a slope of approximately 80^0 for all ACNF supercapacitors. This indicates that electrolyte ions diffuse quickly.

15.5 Biomass-derived CNFs in Asymmetric Supercapacitors

An asymmetric supercapacitor contains two electrodes made of different compounds, and in which the anode of a capacitor-type electrode serves as the power source. In contrast, the cathode of a battery-type Faradaic electrode serves as the energy source [2, 55, 66–68]. In the case of a symmetric supercapacitor, the operating voltage is often limited to less than 1.0 voltage in an aqueous electrolyte because of the thermodynamic breakdown potential of water molecules. The asymmetric arrangement can extend the potential working window since dissimilar electrodes can combine their operating voltage [69]. As a result, various potential windows of dissimilar electrodes can be exploited in asymmetric supercapacitors, resulting in a high energy density and specific capacitance. This is how asymmetric supercapacitors obtain greater energy density than symmetric supercapacitors. In asymmetric
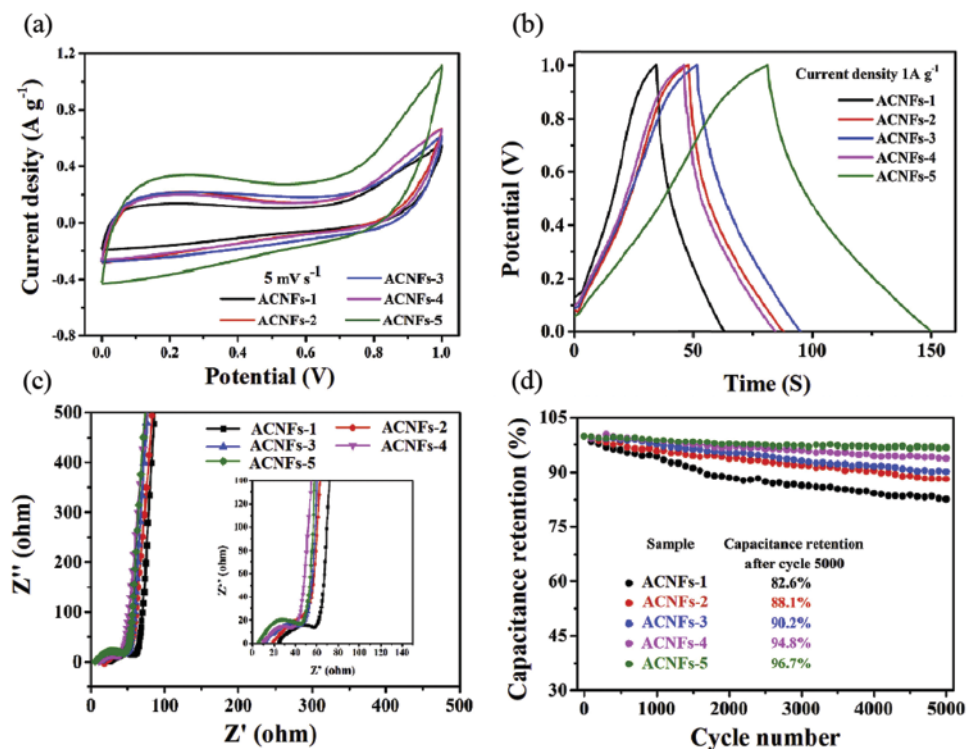
Figure 15.8 (a) CV curves of all electrodes of various supercapacitors at 5.0 mV s^{-1}. (b) GCD curves of all electrodes of various supercapacitors measured at a j = 1.0 Ag^{-1}. (c–d) Nyquist plots of all electrodes as well as their cycle stability. *Reproduced with permission [23]. Copyright 2019, Elsevier.*

supercapacitors, the positive electrode material is often metal oxide or conducting polymer. These capacitors demonstrate a pseudocapacitive charge storage mechanism [70]. On the other hand, carbon-based material shows a double-layer charge storage mechanism or electrochemical double-layer capacitance and can be used as a negative electrode. The surface tuning property of CNFs makes it a promising material to be used in asymmetric supercapacitors [71, 72]. Metal or metal oxide and polymer incorporation in CNFs alters charge storage mechanisms and are effectively used as positive electrodes to enhance energy density. Bacterial cellulose is a widely used biomass precursor to prepare CNFs web. Lai et al. [73] synthesized N-doped CNFs (CBC-N) through carbonization polyaniline and bacterial cellulose and used the result as negative electrodes. Further modification of CBC-N with ultrathin nickel-cobalt layered double hydroxide (Ni-Co LDH) nanosheets resulted in CBC-N@LDH composite electrode, which demonstrated high S_c = 1949.5 F g^{-1} at 1.0 Ag^{-1} in three electrode systems. The elevated property of the composite CBC-N@LDH made it suitable to use it as a positive electrode.

Huang et al. [74] fabricated MnO$_2$ nanosheets using a polycarbonate (PTCE) membrane as the template for the one-pot hydrothermal process that was used to construct the porous nanotubes composed of MnO$_2$ nanosheets. The one-of-a-kind mesopore materials (having diameter of 2–50 nm) in nanotubular structure allowed for fast ion transport, and the ultrathin MnO$_2$ nanosheet shortened the paths that ions took as they diffused through the

material, providing a high level of material utilization. Figure 15.9a shows the schematic representation of asymmetric supercapacitors. The operating voltage of the asymmetric charge storage device increased up to 2V, as shown in Figure 15.9b,c, and the GCD curve preserved a nearly symmetric nature even at high voltage (Figure 15.9d). Table 15.1 shows
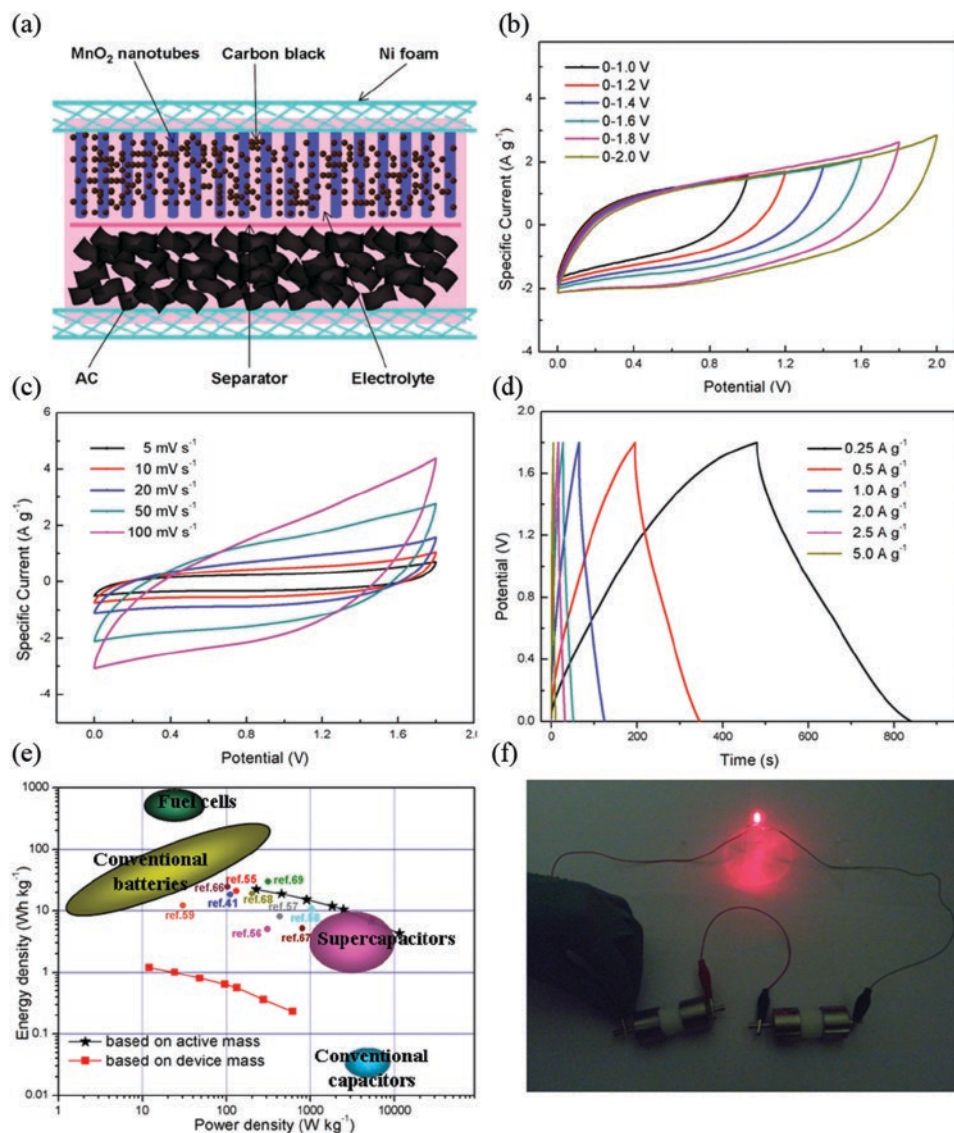
Figure 15.9 (a) An illustration of the ASC setup in the form of a schematic. (b) CV curves of manganese dioxide (MnO_2) nanosheets-built nanotubes/AG ASC recorded at various potential windows at a scan rate of 50.0 mV s^{-1}. (c) The ASC's CV curves were measured at different scan rates between 0 and 1.8.0 V. (d) GCD curves with varied current densities. (e) E_d vs. P_d of the MnO_2 nanotubes//AG ASCs in a Ragone plot for conventional batteries, fuel cells, ultracapacitors and conventional capacitors. (f) A digital representation of a red light-emitting diode (LED), which was illuminated by a MnO_2 nanotubes/AG device. *Reproduced with permission [74]. Reproduced under the terms of the CC BY-NC-ND 3.0 license. Copyright 2014, Huang et al., Springer.*

Table 15.1 Biomass-derived CNFs electrode in asymmetric supercapacitor.

Source	Negative electrode	Positive electrode	Energy density (E_d(Wh kg^{-1})	Power density (P_d (W kg^{-1})	Ref.
Bacterial cellulose	p-BC/N	p -BC@MnO$_2$	32.91	284.63×10^3	[27]
Bacterial pellicles	a-CBP	c-BP/MnO$_2$	63	227	[28]
Bacterial cellulose	CNFs	Ni$_3$S$_2$/CNFs	25.8	425	[29]
Typha domingensis	Vulcan XC-72R (VC)	NFKP/Ni-Co	101	25.6×10^3	[57]
Bacterial cellulose	CBC-N	CBC-N@LDH	36.3	800.2	[73]

the use of biomass-derived CNFs as positive and negative electrodes to prepare high-energy density asymmetric supercapacitors. Nanotubes can alter their diameter and thickness by adjusting the membrane's pore size and chemical composition. As an electrode material for the supercapacitor, porous MnO$_2$ nanotubes were utilized. In a system with three electrodes, the specific capacitance was measured to be 365.0 F g^{-1} at a current density of 0.250 A g^{-1}, and the capacitance retained 90.40% of its initial value after 3000 cycles. An asymmetric superconductor that utilized porous manganese dioxide (MO$_2$) nanotubes and activated graphene acted as a positive (+) electrode for MnO$_2$ and as a negative (-) electrode for graphene respectively produced an $E_d = 22.50$ Wh kg^{-1} and a maximum value of $P_d = 146.20$ kW kg^{-1}. These values were higher than those that were reported for another MnO$_2$ nanostructures. Figure 15.9d displays the GCD curves for various current densities. The time required to charge or discharge the capacitor is roughly reflected in the potentials of the charge-discharge lines, according to a fast I–V response, excellent capacitive characteristics and a minimal equivalent series resistance (ESR). At a current density of $j = 0.250$ A g^{-1}, the discharge curve slope showed that the asymmetric supercapacitor had A gravimetric capacitance (Ct) of 50.0 F g^{-1} based on the total mass of active materials in the two electrodes system.

Based on the entire weight of the electrodes (i.e., the mass of MnO$_2$ + activated graphene (AG)), a maximum gravimetric $E_d = 22.50$ Wh kg^{-1} and had a maximum gravimetric value of $P_d = 146.20$ kW kg^{-1} were obtained, as shown in Figure 15.9e. To achieve an even more significant improvement in the energy density of the supercapacitors based on MnO$_2$ nanotubes, an intelligent hybrid architecture can be designed based on mesoporous MnO$_2$ nanotubes with conductive supports or other metal oxides/hydroxides. Based on the total electrode density (i.e., a mass of MnO$_2$ + AG + Ni foam), the asymmetric supercapacitor device was able to attain a volumetric value of $E_d = 7.20$ Wh L^{-1} and $P_d = 46.80$ kW L^{-1}. The efficiency of the asymmetric cell after it had been completely packaged was also calculated. There was a maximum practicable gravimetric $E_d = 1.20$ Wh kg^{-1} ($P_d = 7.50$ kW kg^{-1}) and volumetric energy density = 5.0 Wh L^{-1} for the compact device (highest $P_d = 31.50$ kW L^{-1}). They were able to successfully light up a red LED using a prototype device (Figure 15.9f). In addition, after being charged for 27.0 s at 1.80 V, the LED stayed on for almost 120.0 seconds. It was clear from these findings that our MnO$_2$ nanotubes/AG asymmetric supercapacitor

technology has potential in real-world settings. According to the findings, the mesoporous MnO_2 nanotubes have an excellent prospect for developing electrochemically stable super-capacitors for practical applications. These one-of-a-kind MnO_2 nanotubes constructed from nanosheets may also find use in a wide variety of disciplines, such as gas sensors and the treatment of dye wastewater. In addition, the suggested synthetic process would make it possible to explore new avenues for developing high-performance supercapacitors utilizing transition metal oxides [74].

15.6   Conclusions

Nowadays, due to their renewability, flexibility and abundant resource biomass precursors have become a popular choice in the fabrication of electrode material. Though many studies have been conducted on the application of supercapacitors information about biomass-based CNFs in a supercapacitor is limited. CNFs with unique surface morphology, freestanding 3D structure, and high mechanical strength make it possible to prepare a flexible supercapacitor. But biomass-derived CNFs suffer from proper analysis and investigation. Different biomass-derived CNFs have different charge storage properties, and variation in the structural component of the biomass precursors is observed. Therefore, to get effective CNFs from biomass resources, the biology of the biomass precursors should be well understood. In addition, every part of biomass doesn't contribute to CNFs structure formation. To get carbon-containing CNFs, carbon precursor needs to isolate from the biomass. However, the densification of CNFs can enhance the carbon content, reducing the porosity inside the CNFs. As a result, the specific surface area can be drastically reduced, creating a barrier for the diffusion of ions. Flexibility in modifying surface morphology and surface chemistry of biomass-derived CNFs makes them desirable candidates for high-performing supercapacitors. Change in surface chemistry of CNFs with appropriate components gives a facile opportunity to prepare different electrodes for high energy density supercapacitors. In addition, the three-dimensional matrix of CNFs act as the anchor to an additional component. Modification on the surface morphology of CNFs also enlarges the active sites for charge storage and thereby enhances the specific capacitance of EDLC.

Acknowledgements

References

1 L. L. Zhang, X. Zhao, *Chem. Soc. Rev.* **2009**, *38*, 2520–2531.
2 S. S. Shah, S. M. A. Nayem, N. Sultana, A. J. S. Ahammad, M. A. Aziz, *ChemSusChem* **2022**, *15*, e202101282.

3 W. Yang, Z. Shi, H. Guo, J. Guo, X. Lei, L. Yue, *Int. J. Electrochem. Sci.* **2017**, *12*, 5587–5597.

4 S. Ghosh, W. D. Yong, E. M. Jin, S. R. Polaki, S. M. Jeong, H. Jun, *Korean J. Chem. Eng.* **2019**, *36*, 312–320.

5 E. Taer, R. Taslim, Apriwandi, Agustino, *AIP Conf. Proc.* **2020**, *2219*, 020001.

6 C. H. Kim, B.-H. Kim, *J. Power Sources* **2015**, *274*, 512–520.

7 E. Samuel, B. Joshi, H. S. Jo, Y. I. Kim, S. An, M. T. Swihart, J. M. Yun, K. H. Kim, S. S. Yoon, *Chem. Eng. J.* **2017**, *328*, 776–784.

8 J. Jang, J. Bae, M. Choi, S.-H. Yoon, *Carbon* **2005**, *43*, 2730–2736.

9 D. Xuan, J. Liu, D. Wang, Z. Lu, Q. Liu, Y. Liu, S. Li, Z. Zheng, *Energy Fuel.* **2021**, *35*, 796–805.

10 S. Rangabhashiyam, P. Balasubramanian, *Ind. Crops Prod.* **2019**, *128*, 405–423.

11 Apriwandi, Agustino, E. Taer, R. Taslim, *J. Phys. Conf. Ser.* **2020**, *1655*, 012007.

12 S. I. Yun, S. H. Kim, D. W. Kim, Y. A. Kim, B.-H. Kim, *Carbon* **2019**, *149*, 637–645.

13 L. Wannasen, W. Mongkolthanaruk, E. Swatsitang, P. Pavasant, S. Pinitsoontorn, *Nanomaterials* **2021**, *11*, 2015.

14 W. Chen, H. Wang, W. Lan, D. Li, A. Zhang, C. Liu, *Ind. Crops Prod.* **2021**, *170*, 113700.

15 Z. Dai, P.-G. Ren, W. He, X. Hou, F. Ren, Q. Zhang, Y.-L. Jin, *Renew. Energy* **2020**, *162*, 613–623.

16 B. Du, H. Zhu, L. Chai, J. Cheng, X. Wang, X. Chen, J. Zhou, R.-C. Sun, *Ind. Crops Prod.* **2021**, *170*, 113745.

17 Y. Liu, Z. Shi, Y. Gao, W. An, Z. Cao, J. Liu, *ACS Appl. Mater. Interfaces* **2016**, *8*, 28283–28290.

18 Z. Gao, Y. Zhang, N. Song, X. Li, *Mater. Res. Lett.* **2017**, *5*, 69–88.

19 M. Vinayagam, R. S. Babu, A. Sivasamy, A. L. Ferreira de Barros, *Biomass Bioenerg.* **2020**, *143*, 105838.

20 S. Hérou, J. J. Bailey, M. Kok, P. Schlee, R. Jervis, D. J. L. Brett, P. R. Shearing, M. C. Ribadeneyra, M. Titirici, *Adv. Sci.* **2021**, *8*, 2100016.

21 G. Shi, C. Liu, G. Wang, X. Chen, L. Li, X. Jiang, P. Zhang, Y. Dong, S. Jia, H. Tian, Y. Liu, Z. Wang, Q. Zhang, H. Zhang, *Ionics* **2019**, *25*, 1805–1812.

22 L. Ma, R. Liu, H. Niu, M. Zhao, Y. Huang, *Compos. Sci. Technol.* **2016**, *137*, 87–93.

23 Z. Dai, P.-G. Ren, Y.-L. Jin, H. Zhang, F. Ren, Q. Zhang, *J. Power Sources* **2019**, *437*, 226937.

24 D. Li, C. Lv, L. Liu, Y. Xia, X. She, S. Guo, D. Yang, *ACS Cent. Sci.* **2015**, *1*, 261–269.

25 K. Wang, Y. Song, R. Yan, N. Zhao, X. Tian, X. Li, Q. Guo, Z. Liu, *Appl. Surf. Sci.* **2017**, *394*, 569–577.

26 X. Ma, C. Ding, D. Li, M. Wu, Y. Yu, *Cellulose* **2018**, *25*, 4743–4755.

27 L. F. Chen, Z. H. Huang, H. W. Liang, Q. F. Guan, S. H. Yu, *Adv. Mater.* **2013**, *25*, 4746–4752.

28 C. Long, D. Qi, T. Wei, J. Yan, L. Jiang, Z. Fan, *Adv. Funct. Mater.* **2014**, *24*, 3953–3961.

29 W. Yu, W. Lin, X. Shao, Z. Hu, R. Li, D. Yuan, *J. Power Sources* **2014**, *272*, 137–143.

30 X. Sun, T. Xu, J. Bai, C. Li, *ACS Appl. Energy Mater.* **2019**, *2*, 8675–8684.

31 Z. Xue, Q. Xiong, C. Zou, H. Chi, X. Hu, Z. Ji, *Mater. Res. Bull.* **2021**, *133*, 111049.

32 X.-W. Chen, O. Timpe, S. B. A. Hamid, R. Schlögl, D. S. Su, *Carbon* **2009**, *47*, 340–343.

33 E. Jang, H.-K. Park, J.-H. Choi, C.-S. Lee, *Bull. Korean Chem. Soc.* **2015**, *36*, 1452–1459.

34 S. N. Sari, A. Melati, *Mat. Today: Proc.* **2019**, *13*, 165–168.

35 J.-Y. Choi, Y. Hyun, H.-K. Park, C.-S. Lee, *J. Ind. Eng. Chem.* **2018**, *68*, 161–167.

36 K. Hayat, S. S. Shah, M. Yousaf, M. J. Iqbal, M. Ali, S. Ali, M. Ajmal, Y. Iqbal, *Mater. Sci. Semicond. Process.* **2016**, *41*, 364–369.

37 J. Saravanan, M. Pannipara, A. G. Al-Sehemi, S. Talebi, V. Periasamy, S. S. Shah, M. A. Aziz, G. Gnana Kumar, *J. Mater. Sci. - Mater. Electron.* **2021**, *32*, 24775–24789.

38 K. Hayat, S. S. Shah, S. Ali, S. K. Shah, Y. Iqbal, M. A. Aziz, *J. Mater. Sci. - Mater. Electron.* **2020**, *31*, 15859–15874.

39 S. S. Shah, K. Hayat, S. Ali, K. Rasool, Y. Iqbal, *Mater. Sci. Semicond. Process.* **2019**, *90*, 65–71.

40 F. Wahed, S. S. Shah, K. Hayat, S. K. Shah, M. A. Aziz, *J. Mater. Sci.* **2022**, *57*, 8828–8844.

41 M. A. Aziz, S. S. Shah, M. A. J. Mazumder, M. Oyama, A.-R. Al-Betar, *Chem. Asian J.* **2021**, *16*, 1570–1583.

42 J. Saravanan, A. Vignesh, S. S. Shah, M. A. Aziz, M. Pannipara, A. G. Al-Sehemi, S.-M. Phang, F.-L. Ng, B. A. A. Abdul, G. G. kumar, *Res. Chem. Intermed.* **2022**, *48*, 101–116.

43 J. A. Matthews, G. E. Wnek, D. G. Simpson, G. L. Bowlin, *Biomacromolecules* **2002**, *3*, 232–238.

44 X. Yu, C. Pei, W. Chen, L. Feng, *Electrochim. Acta* **2018**, *272*, 119.

45 C. Ma, Z. Li, J. Li, Q. Fan, L. Wu, J. Shi, Y. Song, *Appl. Surf. Sci.* **2018**, *456*, 568–576.

46 J. Xue, T. Wu, Y. Dai, Y. Xia, *Chem. Rev.* **2019**, *119*, 5298–5415.

47 Z.-M. Huang, Y.-Z. Zhang, M. Kotaki, S. Ramakrishna, *Compos. Sci. Technol.* **2003**, *63*, 2223–2253.

48 S. S. Shah, M. A. Aziz, E. Cevik, M. Ali, S. T. Gunday, A. Bozkurt, Z. H. Yamani, *J. Energy Storage* **2022**, *56*, 105944.

49 S. S. Shah, M. N. Shaikh, M. Y. Khan, M. A. Alfasane, M. M. Rahman, M. A. Aziz, *Chem. Rec.* **2021**, *21*, 1631–1665.

50 A. Aziz, S. S. Shah, A. Kashem, *Chem. Rec.* **2020**, *20*, 1074–1098.

51 S. S. Shah, E. Cevik, M. A. Aziz, T. F. Qahtan, A. Bozkurt, Z. H. Yamani, *Synth. Met.* **2021**, *277*, 116765.

52 Z. Y. Wu, C. Li, H. W. Liang, J. F. Chen, S. H. Yu, *Angew. Chem.* **2013**, *125*, 2997–3001.

53 J. Zhang, A. Tahmasebi, J. E. Omoriyekomwan, J. Yu, *J. Anal. Appl. Pyrolysis* **2018**, *130*, 142–148.

54 S. Nizamuddin, H. A. Baloch, G. J. Griffin, N. M. Mubarak, A. W. Bhutto, R. Abro, S. A. Mazari, B. S. Ali, *Renew. Sust. Energ. Rev.* **2017**, *73*, 1289–1299.

55 M. Ashraf, S. S. Shah, I. Khan, M. A. Aziz, N. Ullah, M. Khan, S. F. Adil, Z. Liaqat, M. Usman, W. Tremel, M. N. Tahir, *Chem. Eur. J.* **2021**, *27*, 6973–6984.

56 M. M. Faisal, S. R. Ali, S. S. Shah, M. W. Iqbal, S. Pushpan, M. A. Aziz, N. P. Aguilar, M. M. Alcalá Rodríguez, S. L. Loredo, K. C. Sanal, *Ceram. Int.* **2022**, *48*, 28565–28577.

57 F. Golmohammadi, M. Amiri, *J. Mater. Sci. - Mater. Electron.* **2020**, *31*, 2269–2279.

58 M. Yaseen, M. A. K. Khattak, M. Humayun, M. Usman, S. S. Shah, S. Bibi, B. S. U. Hasnain, S. M. Ahmad, A. Khan, N. Shah, A. A. Tahir, H. Ullah, *Energies* **2021**, *14*, 7779.

59 S. S. Shah, M. A. Aziz, Z. H. Yamani, *Chem. Rec.* **2022**, *22*, e202200018.

60 M. M. Hasan, T. Islam, S. S. Shah, A. Awal, M. A. Aziz, A. J. S. Ahammad, *Chem. Rec.* **2022**, *22*, e202200041.

61 M. A. Ehsan, S. S. Shah, S. I. Basha, A. S. Hakeem, M. A. Aziz, *Chem. Rec* **2022**, *22*, e202100278.

62 E. Taer, N. Y. Effendi, R. Taslim, A. Apriwandi, *J. Mater. Res. Technol.* **2022**, *19*, 4721–4732.

63 Q. Cao, Y. Zhang, J. Chen, M. Zhu, C. Yang, H. Guo, Y. Song, Y. Li, J. Zhou, *Ind. Crops Prod.* **2020**, *148*, 112181.

64 M. Zhu, Q. Yan, Y. Xue, Y. Yan, K. Zhu, K. Ye, J. Yan, D. Cao, H. Xie, G. Wang, *ACS Sustain. Chem. Eng.* **2022**, *10*, 279–287.

65 H. Chen, T. Liu, J. Mou, W. Zhang, Z. Jiang, J. Liu, J. Huang, M. Liu, *Nano Energy* **2019**, *63*, 103836.

66 A. Helal, S. S. Shah, M. Usman, M. Y. Khan, M. A. Aziz, M. Mizanur Rahman, *Chem. Rec.* **2022**, *22*, e202200055.

67 M. Rauf, S. S. Shah, S. K. Shah, S. N. A. Shah, T. U. Haq, J. Shah, A. Ullah, T. Ahmad, Y. Khan, M. A. Aziz, K. Hayat, *J. Saudi Chem. Soc.* **2022**, *26*, 101514.

68 S. S. Shah, H. T. Das, H. R. Barai, M. A. Aziz, *Polymers* **2022**, *14*, 270.

69 S. S. Shah, M. A. Alfasane, I. A. Bakare, M. A. Aziz, Z. H. Yamani, *J. Energy Storage* **2020**, *30*, 101562.

70 C.-H. Wang, H.-C. Hsu, J.-H. Hu, *J. Power Sources* **2014**, *249*, 1–8.

71 Z. Tang, C. H. Tang, H. Gong, *Adv. Funct. Mater.* **2012**, *22*, 1272–1278.

72 F. Wang, S. Xiao, Y. Hou, C. Hu, L. Liu, Y. Wu, *RSC Adv.* **2013**, *3*, 13059–13084.

73 F. Lai, Y.-E. Miao, L. Zuo, H. Lu, Y. Huang, T. Liu, *Small* **2016**, *12*, 3235–3244.

74 M. Huang, Y. Zhang, F. Li, L. Zhang, R. S. Ruoff, Z. Wen, Q. Liu, *Sci. Rep.* **2014**, *4*, 3878.

16

Biomass-Derived Graphene-Based Supercapacitors

Nafeesa Sarfraz[1], Ibrahim Khan[1],*, and Abdulmajeed H. Hendi[2]

[1] *School of Chemical Engineering & Materials Science, Chung-Ang University, 84 Heukseok-ro, Dongjak-gu, Seoul 06974, Republic of Korea*
[2] *Physics Department, King Fahd University of Petroleum and Minerals, Dhahran, 31261, Saudi Arabia*
* *Corresponding author*

16.1   Introduction

Graphene is an ultrathin two-dimensional (2D) sheet structure of graphite composed of carbon atoms (atomic crystal) that possess excellent thermal conductivity, optical transparency, and chemical, mechanical, electrochemical, and electrical properties. Due to these properties, graphene can be used in various fields, e.g., nanoelectronics and energy-storage devices [1, 2]. Graphene is composed of multiple benzene rings connected in a two-dimensional arrangement. Like benzene, the carbon atoms in the structure of graphene are sp2 hybridized, and their 2pz electrons are involved in π bonding. Thus, one could expect the same reactive behavior from graphene as is seen with benzene, e.g., free radical [3, 4] and cycloaddition [5, 6] involving various –C=C– double bond reactions. However, the π electron conjugation differs in both cases because graphene is a semimetal with a zero band-gap, whereas benzene possesses a large HOMO-LUMO gap. The π electron cloud in the graphene is immensely delocalized in the plane, making the graphene unable to react chemically, i.e., totally inert [7, 8]. To make the graphene chemically active (so all its carbon atoms are accessible) [9], several methods can be used, e.g., sp2 hybridized carbon atoms can be turned into sp3 hybridization in new 2D material by using the covalent chemistry approach. Through a same approach, creating a new 2D superlattice and modification of the energy band structure of graphene is possible to make it suitable for energy conversion and storage devices [8]. Moreover, graphene-metal nanoparticles (NPs) composites can be developed to be applied in next-generation conversion and storage devices. This approach practically enables the electronic-level study of the interaction between graphene and other materials used in nanocomposites. Alternatively, defects can be introduced in graphene structures to tune their physicochemical properties. Also, based on the source, high-quality graphene can be achieved. Naturally occurring biomass is the most attractive source for producing graphene and its oxide forms. The biomass-derived carbon materials usually have a high surface area and improved electrochemical charge storage characteristics [10–12]. Lastly, the conversion of 2D structure graphene into partially

three-dimensional (3D) graphene-based macrostructures can induce electrochemical robustness and improved electro-kinetics [13–15].

16.2   The Properties and Background of Graphene

The technique through which graphene was synthesized for the first time from a 3D graphite crystal is named the "Scotch tape" method (micromechanical cleavage) (Figure 16.1a). Adhesive tape was applied on the top layer of graphite, which removed the layer with
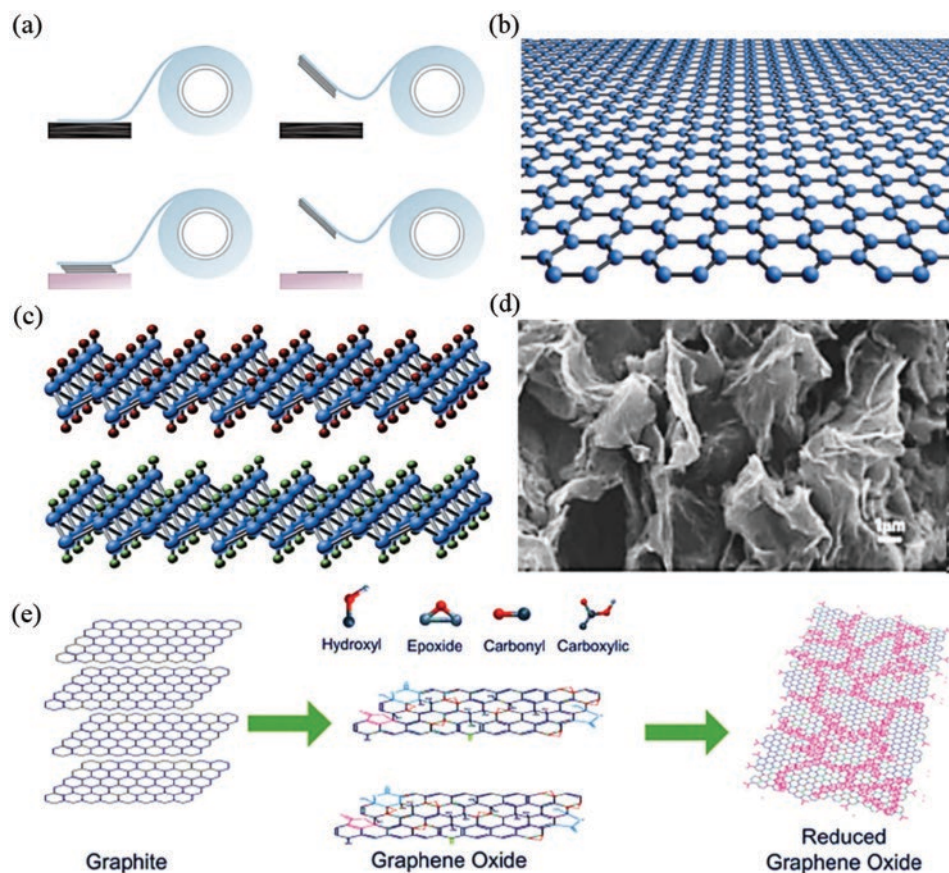
Figure 16.1   (a) Scotch tape method to produce graphene: (Top) adhesive tape is used to cleave the first few layers of graphite from a bulk crystal of the material. (Bottom) left: the tape with graphitic flakes is passed against the substrate of choice. Right: some flakes stay on the substrate even when removing the tape. (b) Arrangement of carbon atoms in the crystal structure of graphene (honeycomb lattice). (c) Blue: chemical modifications of graphene by adding hydrogen (top) and fluorine (bottom) to sp2 hybridized carbon atom. (Carbon atoms, red: hydrogen atoms, and green: fluorine atoms). *Reproduced with permission* [24]. *Copyright 2021, American Physical Society*. (d) SEM image of thermally expanded and reduced graphite oxide leading to conductive graphene sheets in wrinkled morphology. *Reproduced with permission* [29]. *Copyright 2009, Wiley*. (e) Modification of graphite to graphene oxide and reduced graphene oxide. *Reproduced with permission* [21]. *Copyright 2012, Elsevier*.

graphite crystallites. That layer was pressed against a substrate (of choice). Due to the stronger bottom graphene layer/substrate adhesion, the graphene layer was transferred to the substrate, producing extremely high-quality crystallites. This simple method can be applied to any surface with appropriate adhesion to graphene. The fabricated graphene was a 2D sheet of the flat crystalline form of carbon atoms with sp^2 hybridization with a hexagonal lattice structure, as shown in Figure 16.1b. The sp^2 hybridization also counts for their facile chemical modification, e.g., fluorination in Figure 16.1c. Physically, the bond length of C–C in graphene structure is about 0.142 nm with an atomic thickness of 0.345 nm. It is stronger than steel, with a strength of ~0.4 GPa. Young's modulus of 500 GPa suggests its elasticity is more than rubber [16]. Another aspect that gives makes graphene unique is its mechanical characteristics. Graphene is considered the thinnest fabric as it can be deformed mechanically, stretched, compressed, folded, rippled, and even torn into pieces [17, 18]. These mechanical properties give rise to excellent robustness in the electronic structure of graphene. Graphene is exceedingly stiff, with zero effective mass and high thermal conductivity. It shows excellent mobility for charge carriers and is impermeable to gases. Optical transparency is another interesting aspect of graphene [19, 20]. Morphologically, graphene exists in thin sheets, as shown in Figure 16.1d. The thin layer is expected to create wrinkles, further enhancing the surface area of graphene and its electrochemical and adsorption characteristics. Chemically, the sp^2 hybridization of carbon atoms in graphene allows it to form three strong sigma bonds and a single pi bond. Therefore, graphene is a semimetal with zero overlaps and a good conductor of electricity compared to diamond, which has an sp^3 hybridized carbon atom making it an insulator. The vulnerable nature of the sp^2 hybridized carbon atom helps explore new ideas to create 2D crystals of graphene derivative with variable hybridization, i.e., sp^3 most commonly, by attaching a new group or species to the carbon atoms in graphene structure. This led to the fabrication of new materials like graphene oxide, reduced graphene oxide, graphene nanocomposites, etc. Figure 16.1e shows graphite modification to graphene oxide and reduced graphene oxide [21].

Crystallographically ordered modifications that have been achieved chemically include graphene (structural modification of graphene where a hydrogen atom is bonded to each of the sp2 hybridized carbon atoms) [22] and fluorographene, as shown in Figure 16.1c. [23] Unlike graphene, both modification products exhibit a large electronic bandgap which does not allow the electrons to jump from valence to the conduction band. That is why both derivatives of graphene are insulators. Even then, they are high crystallographic products and much more stable at ambient temperature. This makes graphene a good conductor of electricity with zero band gaps.

In contrast, graphene (chemical modification of graphene) is an insulator with a large bandgap, making it an exciting prospect for scientists to explore the other derivatives to fill the gap of electrical conduction between graphene and graphene layers by tunning the bandgap range [24]. Edge and surface modification of graphene via patterning strategy can also enhance their physicochemical properties. However, these modifications are not easy to achieve because of the high energy barriers arising due to the van der Waals forces and interlayer conjugation between single graphene layers in the multilayer model. Unlike traditional 2D crystals, graphene is more exposed to form arched edges, which show folding [25]. The functionalization of this arched structure is more complicated

than layered geometry. Apart from these tricky aspects, graphene's covalent functionalization and transparency are crucial for smart windows and touchscreen applications. The surface chemistry of graphene is particularly important in controlling the adhesion properties of graphene as it directly influences the adhesion of graphene films to polymer or glass surfaces. Also, surface chemistry decides the cyclic lifetime and capacitance of supercapacitor electrodes. Functional groups bonded on the surface of graphene can control the cytotoxicity and biocompatibility of graphene. The mechanical and thermal properties of graphene (nanocomposite) can be maximized by covalently bonding it to the polymer matrix [26].

Graphene can also impart various modifications when combined with other materials. For example, when mixed with a non-conductive polymer matrix, it reduces the electrical resistivity of the host polymer by integrating its conductivity [27]. Therefore, the conductive graphene sheets play the role of the conductive bridge within electrically resistive polymers. When graphite oxide was expanded thermally at $1000\,^{\circ}C$ under a reduced graphene oxide, the functionalization of graphene occurred along with the reduction of single-layer graphene oxide (SLGO) to single-layer graphene (SLG) [28]. This reduction caused the aromatic nature of bonding to be restored by removing oxygen, improving the electrical conductivity due to the π-electrons delocalization across the surface of the 2D graphene sheet. These two operations, i.e., thermal expansion and reduction of graphite oxide, led to the wrinkled morphology of conductive graphene sheets, as shown in Figure 16.1d. The wrinkled morphology of graphene is found to be exceptionally good for charge storage applications. When these wrinkled graphene sheets were hybridized with polyvinylidene fluoride (a non-conductive polymer), the latter turned conductive due to the conductive pathways that are provided by wrinkled graphene [29].

When forces of different magnitudes are applied to the surface of graphene in various diverse ways, the surface is affected by the processing conditions and chemistry of graphene-based reactions resulting in the deformation and stabilization of both 2D and 3D graphene sheets. Graphene can be folded on receiving external stimuli, e.g., thermal induction [30], stress on the edges of the graphene sheet, external load across the whole sheet [31, 32], evaporation of solvent from the surface of graphene [33], and freeze drying [34]. In the case of thermal induction, numerous factors play their role in folding the graphene sheet. These factors include size, functionality, aspect ratio of the graphene system, and the external environment in which the graphene system lies. By increasing the aspect ratio, the greater will be the deformation of the graphene structure away from planar geometry. As an example, stress applied on the edges of graphene nanoribbons can result in scrolling [31]. These demonstrations suggest that graphene can be effectively tuned for various electrochemical applications.

16.3 Biomass-derived Synthesis of Graphene

Biomass is a naturally occurring source of carbon-based materials with low-cost, natural abundance, and environmentally friendly characteristics. The biomass is composed mainly of lignin, hemicelluloses, and cellulose [35, 36]. The carbon can be extracted from biomass in various ways, such as simple pyrolysis and pyrolysis with chemical and

physical treatments. The biomass-derived precursors usually produce carbon products cheaply. Pyrolysis (an inert thermal decomposition of biomass at 450–650 °C) and high-temperature carbonization (thermal decomposition of biomass in the presence of water) are the two well-known processes that produce novel carbon-based materials from biomass (Figure 16.2) [37]. Besides these, gasification and liquefaction are other methods that can be used to obtain various carbon products. The main carbon products include char, charcoal, carbon black, and graphite. Once carbon precursors are extracted from biomass, they can be selectively transformed into graphene and derivatives. The primary biomass sources include fungi, plant remains, naturally occurring polymers/plastics, food wastes, etc. For example, the jute plant is one of the best carbon precursors that can be carbonized to carbon and graphitic sources. Nanaji et al. crushed the jute stick and activated it with KOH at high carbonizing temperatures to achieve the black jute carbon [38]. After further chemical treatment, the carbon black is converted into a highly porous graphene sheet that can be used for various electrochemical applications (Figure 16.2).

The scheme in Figure 16.3a, shows various top-down and bottom-up techniques to process the carbon precursors into graphene-based materials [40]. In general, these synthesis methods can be classified into top-down and bottom-up approaches (Figure 16.3b). In the top-down approach, the graphene is synthesized from graphite by breaking the stacked layers of graphite into single, bi, and few layers of graphene, while in the bottom-up approach, the graphene is synthesized from the atomic-sized carbon-containing precursors. Even though some of the top-down approaches are scalable and produce high-quality products, defective graphene sheets cannot be avoided due to the separation of the source layers. For the bottom-up approaches, the produced graphene sheets are almost defect-free with a high surface area, but the production cost in some methods is often high. Synthesis approaches such as microchemical cleavage (exfoliation) [41], chemical reduction of graphite oxide [42], pulsed laser deposition [43], and ion sputtering [44] are examples of graphene synthesis by top-down approaches. The bottom-up approaches include epitaxial growth [21], chemical vapor deposition [45], pyrolysis [46], and ion implantation [47].
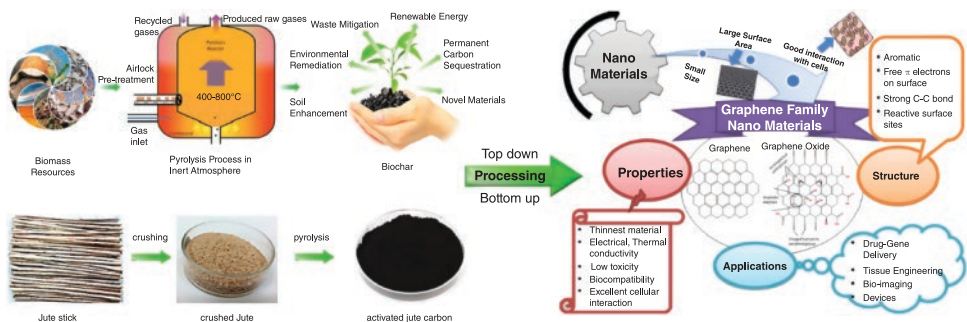
Figure 16.2 Schematic illustration of graphene-based material synthesis from biomass and their properties and application. *Reproduced with permissions* [37–39]. *Copyright, Elsevier 2018, American Chemical Society 2018, and Elsevier 2014.*
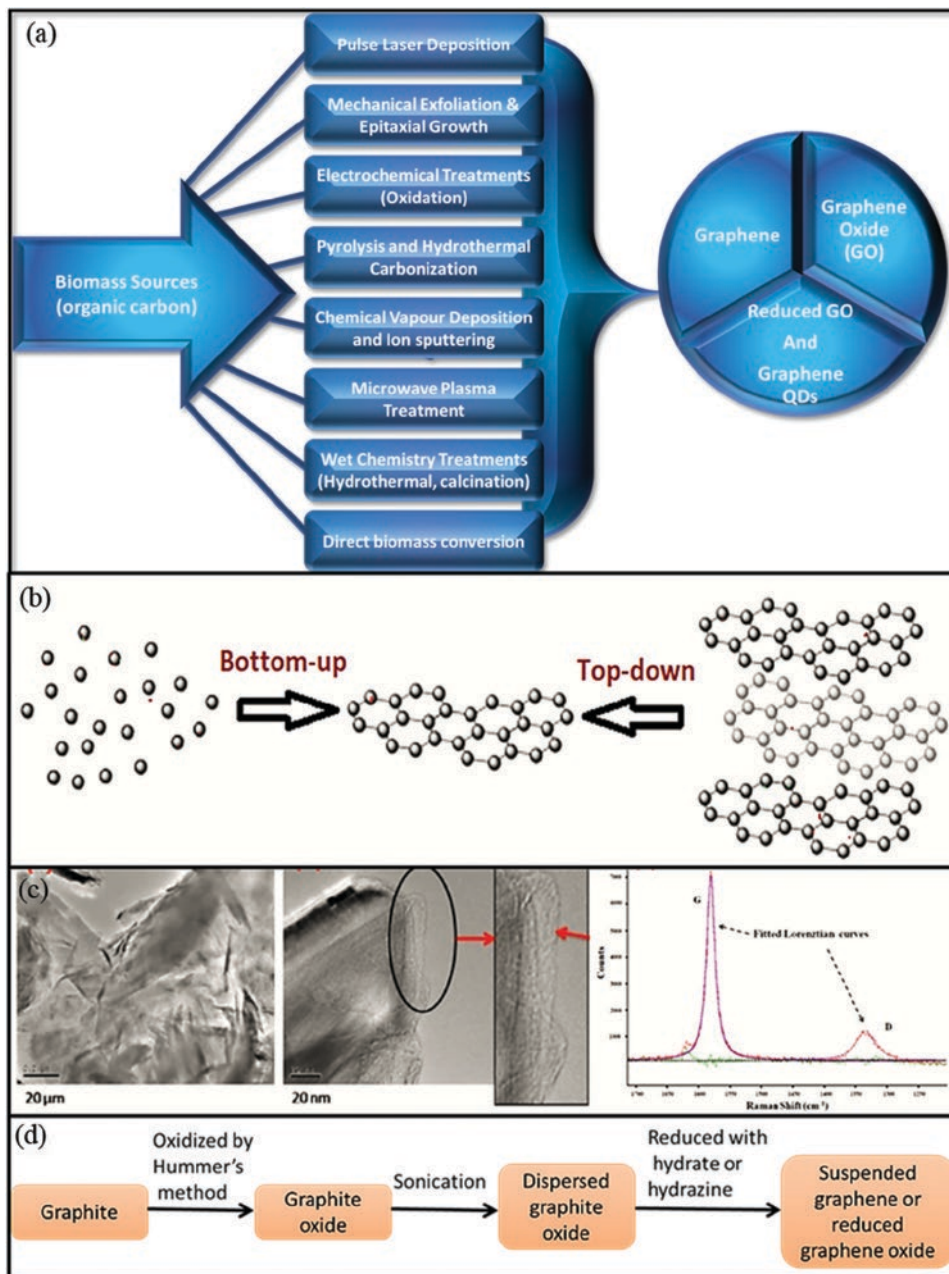
Figure 16.3 (a) Schematic representation of the pyrolysis process and benefits of the biochar obtained, (b) synthesis methods of graphene, (c) TEM images with ultrasonic oscillation (left) graphene comprising a few layers, (middle) edge of graphene sheet with clear grain boundaries, and (right) Raman spectroscopy spectrum. (d) Synthesis of graphene from graphite by Hummer's method. *Reproduced with permission* [48]. *Reproduced under the terms of the CC BY 2.0 license. Copyright 2011, Jayasena et al.*

16.3.1 Top-down Methods

16.3.1.1 Mechanical Cleaving (Exfoliation)

The mechanical exfoliation technique involves repeated cleaving of graphite by adhesive tape to obtain different graphene layers (mono, bi, and few-layers), which can be identified by Raman spectroscopy or atomic force microscopy. K. S. Novosolev first used this technique in 2004. In 2011, B. Jayasena *et al.* employed advanced machinery with an ultra-sharp single-crystal diamond wedge assisted by ultrasonic oscillations for fabricating a few graphene layers from graphite [48]. The results showed that a few graphene layers were obtained with ultrasonic oscillations, as shown in Figure 16.3c. As can be seen, the obtained graphene sheets are crumpled, and the grain boundaries are clearly observed. Moreover, the Raman microscopy study confirmed that graphene sheets were obtained, and the defects in the sheets obtained with oscillations have fewer defects than those obtained without oscillations. In addition to the reduced defects in the obtained graphene, this technique saves time and labor costs. Nevertheless, mechanical exfoliation techniques need further improvement to obtain high-purity, defect-free, and scalable graphene for feasible commercial applications.

16.3.1.2 Chemical Reduction of Graphite Oxide

Chemical reduction methods are widely used for graphene synthesis because they are time-saving, scalable in production, and adaptable to various applications [42]. These methods involve the oxidation of graphite using concentrated acids and strong oxidants. Among these methods, Hummer's method is the most popular technique for large-scale synthesis (Figure 16.3d). The method involves the oxidation of graphite to obtain graphene oxide within a few hours by dissolving $NaNO_3$ and $KMnO_4$ in concentrated H_2SO_4. Then, the obtained graphene oxide is dispersed by sonication, and finally, it is reduced to graphene upon treatment with hydrazine or hydrate, as schematically shown in Figure 16.3d. Such a method is easy and time-saving, but it has some drawbacks, including the low production yield, residual nitrate, and the toxicity of the generated NO_2 and N_2O_4 gases. Therefore, various strategies have been developed to overcome such drawbacks, including i) eliminating $NaNO_3$ from the synthesis method, ii) increasing the amount of $KMnO_4$ rather than $NaNO_3$, and iii) using K_2FeO_4 instead of $KMnO_4$ while $NaNO_3$ is removed [49]. In 2010, Marcano *et al.* [50] succeeded in modifying Hummer's method to obtain a high production yield with a controlled temperature by increasing the amount of $KMnO_4$ and H_2SO_4 rather than $NaNO_3$. Another strategy for modifying Hummer's method was proposed by Peng *et al.* [51] in 2015. In such a strategy, the authors employed K_2FeO_4 as an oxidizing agent instead of $KMnO_4$ and successfully obtained single-layer graphene oxide at room temperature.

16.3.1.3 Pulsed Laser Deposition

The working principle of the pulsed laser deposition (PLD) technique can be summarized as follows. In a vacuum chamber, a laser beam is directed at the desired target (for graphene synthesis, carbon-based material such as graphite). As the laser beam strikes the target, an energetic plasma containing ions and atoms is created and then deposited on the

substrate mounted in front of the target. The quality of the deposited material depends on several experimental parameters such as substrate temperature and crystallinity, target-to-substrate distance nature and pressure of the environment, and laser parameters such as pulse duration, wavelength, and repetition time. The kinetic energy of the ablated species has up to a few KeV, enabling deposition of thin layers at relatively low temperatures compared to other techniques.

The first study on graphene synthesis by the PLD technique was reported by Cappelli *et al.* in 2005 [52]. In their study, Nd:YAG laser operating in the near IR with the following parameters: pulse width t = 7 ns, repetition rate ν = 10 Hz, λ = 532 nm, fluence φ ~7 J cm^{-2}, and deposition time = 15 minwas used. The target was 99 % pure graphite, and the deposition was performed on Si <100> substrates at room temperature to 900 °C. Since then, many studies have reported graphene synthesis by the PLD. In 2017, Dong et al. [53] reported synthesizing large-area, few-layer graphene sheets by femtosecond PLD with low defects and good electrical properties. The product was obtained at a relative temperature of 500 °C and showed good electrical properties. The authors attributed the obtained product's quality to the double-layer Ni catalyst.

16.3.1.4 Ion Sputtering

In a sputtering system, argon is ionized employing electromagnetic excitation or direct current, resulting in the creation of Ar^+ ions plasma, which is then accelerated and directed toward a solid target (carbon material anode in this case). As the Ar^+ ions strike the target, target atoms are ejected and deposited on a substrate (the cathode), forming a coating. In a recent study [44], graphene was successfully synthesized on Si (100) by copper cathode target using high-power impulse reactive magnetron sputtering. The number of graphene layers can be tuned with the separation distance between the precursor and magnetron and the synthesis temperature. The defects density in the obtained product decreased, while the graphene crystallite size increased with the synthesis temperature. Moreover, the product's morphology, shape, and size can be determined by the distance between the substrate and the magnetron cathode target surface, synthesis time, and grid bias voltage.

16.3.2 Bottom-up Methods

16.3.2.1 Epitaxial Growth

Epitaxial growth grows a thin crystalline film in a particular orientation. The underlying crystal determines the orientation of the grown crystalline layers. Many studies reported graphene synthesis by the epitaxial growth method [21, 54, 55]. As depicted in Figure 16.4a, graphene can be synthesized by the thermal decomposition of hexagonal silicon carbide (SiC) substrate in a vacuum or inert environment [21]. Upon annealing silicon (Si) to sublimate (Si melting point = 1100 °C), it evaporates and leaves excessive C atoms on the surface, which aggregate to form a graphitic layer [54]. Such a process is known as the epitaxial growth of graphene on SiC. Nevertheless, it was noticed that graphene obtained by this method lacks homogeneity. Moreover, the method is expensive because of the energy-intensive process [56, 57].
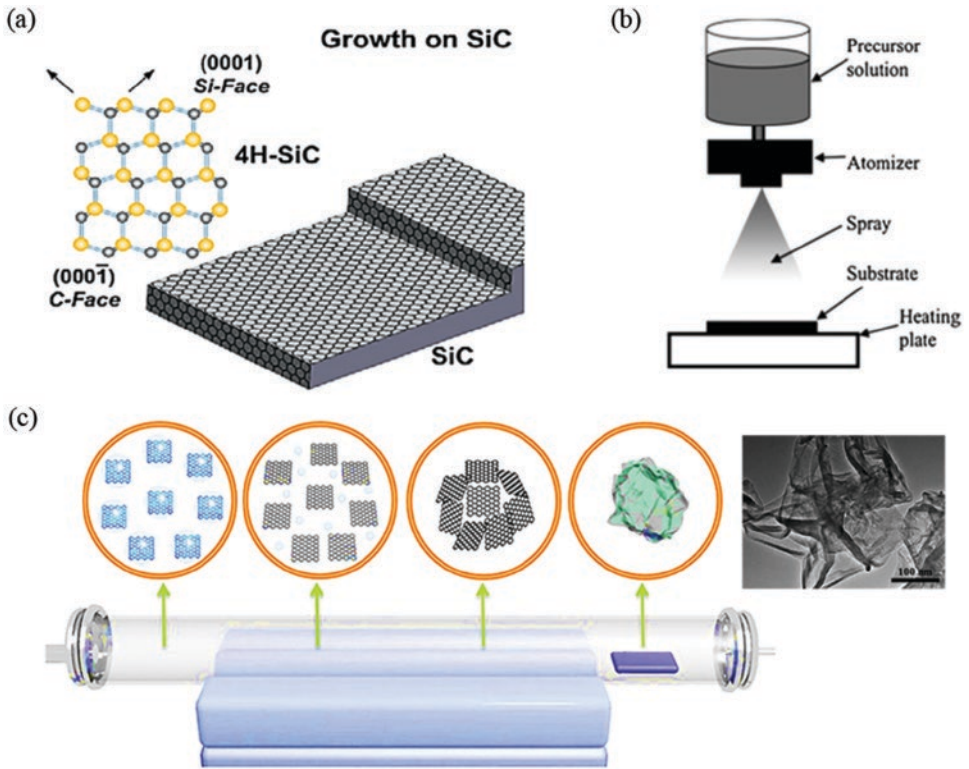
Figure 16.4 (a) Growth on SiC. Gold and grey spheres represent Si and C atoms, respectively. At elevated temperature, Si atoms evaporate (arrows), leaving a carbon-rich surface that forms graphene sheets. *Reproduced with permission* [21]. *Copyright 2012, Elsevier.* (b) A schematic of spray pyrolysis setup. *Reproduced with permission* [63]. *Copyright 2019, Elsevier.* (c) Schematic diagram of the crumpled reduced graphene oxide formation with TEM image. *Reprodued with permission* [65]. *Copyright 2018, Elsevier.*

16.3.2.2 Chemical Vapor Deposition

In the chemical vapour deposition (CVD) method, different hydrocarbon gases such as ethylene, methane, hexane, and biomass materials are decomposed to grow graphene layers on a metallic substrate such as nickel or copper film in temperatures 650–1000 °C [45, 58]. The carbon precursor dissociates into free carbon and hydrogen atoms as it touches the hot surface of the metal substrate. Subsequently, the carbon atoms diffuse through the metal substrate surface, forming a graphene sheet upon reaching the carbon solubility [59, 60]. It has been reported that CVD can obtain high-quality graphene with low defects and a large surface area. Nevertheless, CVD has some drawbacks, such as high production cost, further processing to remove residue catalyst and transfer of the product to other substrates [56]. Therefore, researchers have attempted to overcome such drawbacks by optimizing the synthesis temperatures and ambient pressures [61]. Kalita et al. successfully synthesized graphene at 450 °C using surface wave plasma-enhanced CVD (PECVD) as an example of these attempts. Such a strategy lowered the synthesis temperature and deposition time (< 5 min) and subsequently enhanced the process's overall synthesis and scalability [62].

16.3.2.3 Spray Pyrolysis

Spray pyrolysis is a process in which a thin film can be deposited by spraying a solution containing a precursor onto a hot substrate, where the precursor decomposes to form the desired material. A typical spray pyrolysis setup is shown in Figure 16.4b. Compared with other techniques for the deposition of thin films, this method has several advantages. Such as its open atmosphere process, adjustability during the deposition, accessibility for observing the deposition procedure, and the capability to prepare favorable multilayer films for fabricating functionally graded layers [63]. One of the spray pyrolysis strategies is the nebulized spray pyrolysis technique, which was first used by Illakkiya *et al.* [64] to obtain thin graphene layers. The nebulization produced uniform and fine droplets of the sprayed graphene dispersion. The design of the nebulizer employed a baffle for producing homogeneous and fine droplets of the sprayed graphene solution and so thin homogeneous films. Ultrasonic spray pyrolysis (USP) is another technique characterized by cost-effectivity and adaptability based on an aerosol process for depositing nanostructured thin films. In the USP technique, the dispersion of the precursor into droplets is induced by ultrasonic waves [63]. Gao et al. [65] employed USP to obtain crumpled graphene nanostructures for photodetection applications. The formation of the crumpled graphene nanostructures comprising ethanol evaporation, thermal reduction of graphene oxide aerosol droplets, and film evolution on any substrates placed five cm away from the furnace, is shown in Figure 16.4c.

16.3.2.4 Ion Implantation

Ion implantation is a technique by which ions of the desired material can be implanted into another solid material to a depth of several microns. One of the advantages of this technique is that the thickness of the implanted material can be controlled by the energy of the ions, implanted dose, and annealing temperature. This technique has demonstrated the synthesis of graphene with controlled layer-by-layer thickness. [47, 66] A precise carbon dose was implanted into polycrystalline Ni film, and subsequent heat treatment was conducted to enable graphene growth on the Ni film [66]. The effect of annealing and quenching on the thickness of the graphene layers implanted in Ni film was investigated. The results showed that the graphene out-diffusion from the Ni film decreases with annealing followed by quenching. Annealing up to $900\,^{\circ}$C led to the dissolving of all the implanted carbon dose ($\sim$16 $\times$ 10^{15} cm^{-2} corresponding to $\sim$ four graphene layers) in the Ni film. However, a slight decrease in temperature to $750\,^{\circ}$C evolves carbon solubility in Ni film from (16 $\times$ 10^{15} cm^{-2} to 8 $\times$ 10^{15} cm^{-2}), which corresponds to $\sim$ two graphene layers. Furthermore, rapid quenching from $750\,^{\circ}$C resulted in trapping the residual carbon inside the Ni. Consequently, even though such a technique enables controlling the amount of the precipitated carbon at a high annealing temperature, the details of the kinetics of carbon out-diffusion from Ni at moderate to low temperatures are not well known.

16.4 Biomass-derived Graphene-based Supercapacitors

As mentioned earlier, graphene is a demanding material to use in electrochemical applications due to its exceptional characteristics. The tuned sp^2-sp^3 hybridized carbon mono- and multi-layered graphene provide much scope for charge storage and generation

applications, respectively. The biomass-derived graphene possesses unique characteristics such as large surface area, electrochemically enhanced, and mechanical robustness. Biomass-derived graphene-based supercapacitors have been explored widely, and a few case studies are provided below.

The morphology of the electrode always influences the electrochemical outcome of charge storage devices. Biomass-derived graphene predominantly exists in a sheet form. However, those sheets can be wrinkled or coiled to increase the surface area and other physicochemical characteristics that influence the overall device capacitance. With a large surface area, three-dimensional (3D) graphene was produced by sequential transforming glucose-based polymers via carbonization (Figure 16.5a, b). The product possessed macroporous carbons with thin graphene-based carbon walls. The physicochemical activation of this product led to micro- and mesoporous structures, selectively with a Brunauer-Emmett-Teller (BET) surface area of $3,657\ \mathrm{m^2 g^{-1}}$. This product held a high specific capacitance of $175\ \mathrm{F\,g^{-1}}$ in ionic liquid electrolytes due to its enormous surface area, hierarchical pore structure, and elevated graphitization degree. The hierarchical 3D
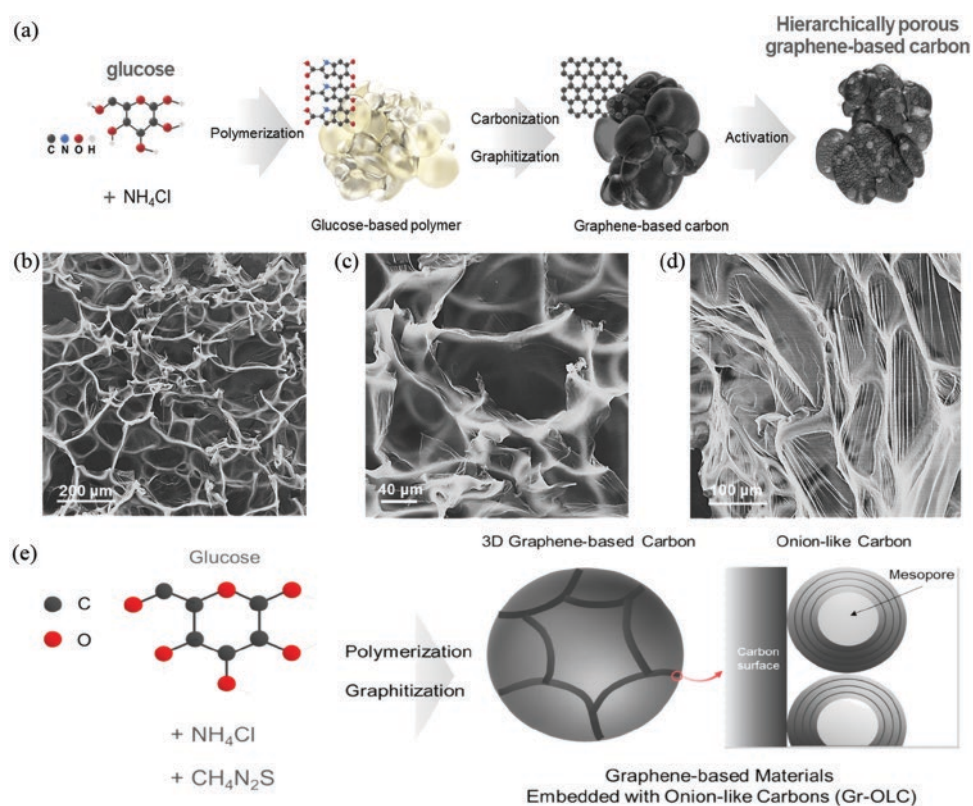
Figure 16.5 (a) Extraction of graphene-based carbon from glucose-based polymer. (b-d) SEM images of activated biomass-derived graphene-based carbons at different magnifications. *Reproduced with permission* [67]. *Reproduced under the terms of the CC BY 4.0 license. Copyright 2018, Jung et al.* (e) Schematic illustration of biomass-derived graphene-based carbons embedded with onion-like carbons. *Reproduced with permission* [68]. *Copyright 2022, IOPscience.*

graphene-based supercapacitor yielded energy and power densities of 74 Wh kg^{-1} and 408 kW kg^{-1}, respectively [67]. The results were highly comparable with relevant biomass-derived supercapacitors, as provided in Figure 16.6a.

In a related study by the same group, hierarchically porous graphene embedded with onion-shaped carbons is efficient for superior supercapacitance. The precursor for this large surface product consisted of a mixture of glucose, ammonium chloride, and thiourea. At 64 A g^{-1}, this carbon demonstrated a high specific capacitance of 140 F g^{-1} due to high surface area, interconnected carbon networks (embedded within onion-like carbons), and hierarchical pore distribution. The highly interconnected carbon channels and pore structures facilitated transport of ions. Hence, charge carriers produce an exceptionally high-power density of 1,737 kW kg^{-1}. Moreover, the capacitance ability is intact for a more extended period of time with minimal capacitive loss [68].

Activating biomass-derived graphene is essential in enhancing the device's capacitance. KOH, KOH-CO$_2$, FeCl$_3$, HAc-H$_2$O$_2$, NaCl-KCl, etc., have been used for activation purposes. The selection of activating agents is usually influenced by the nature of biomass sources from which carbon material is derived and the morphology of the final product [69]. For instance, the eggplant-derived graphene sheets obtained via freeze-drying followed by activation with KOH and carbonization (700–1100 °C) exhibited excellent capacitance activity. It is revealed in this study that the carbonization temperature helps control the overall porosity of the sheets and, ultimately, the capacitance activity. When these materials were tested in a three-electrode system having 1 M H$_2$SO$_4$ electrolyte, the CV retained their rectangular shape within a potential window of 0.0 to 1.0 V at different scan rates. It was found that mesoporous graphene sheets obtained at 800 °C showed superior EDLC behaviour with 390 F g^{-1} capacitance at 1 A g^{-1} current density due to facile ion accessibility [70].

Combining graphene with selective capacitance materials enhanced capacitive abilities within charge storage devices. The biomass-derived graphene is excellent in this case as it can provide a large surface area for hybrid material, hence making the combining reaction
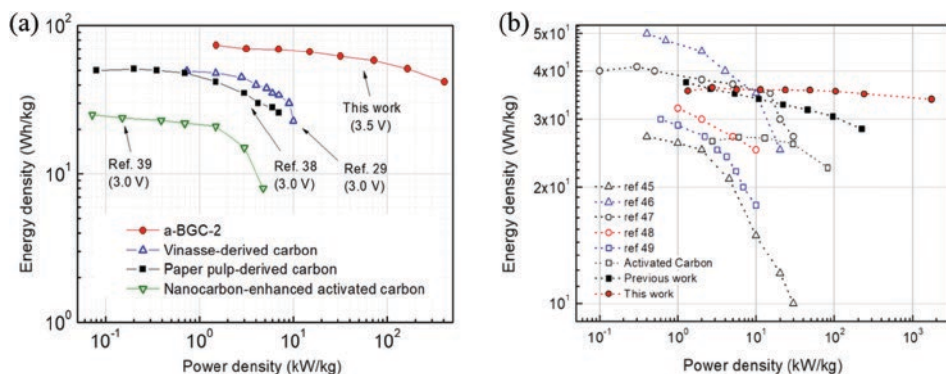
Figure 16.6 Comparative Ragone plots and comparison of power densities with available literature of (a) activated biomass-derived graphene-based carbons supercapacitor. *Reproduced with permission* [67]. *Reproduced under the terms of the CC BY 4.0 license. Copyright 2018, Jung et al.* (b) Graphene-based embedded in onion-like carbon. *Reproduced with permission* [68]. *Copyright 2022, IOPscience.*

more facile. Different biomass-derived graphene-based heterostructures and nanocomposites have been tested to achieve improved capacitive performance. For example, flower-like biomass-derived silver-decorated graphene electrodes were prepared by the CVD method. It was revealed that 800 °C is a suitable temperature to achieve a product with a large number of active sites and showed a maximum capacitance of 93.5 F g^{-1} [71]. Similarly, high-performance biomass (extracted from *Typha domingensis* from Kermanshah, Iran,) derived 3D-graphene/nickel-aluminium LDH composite was manufactured (Figure 16.7A,B). This material was utilized as a cathode in a supercapacitor. A specific capacitance of 1390 F g^{-1} is achieved at 1 A g^{-1}, with excellent cycling stability (92% capacitance retention after 5000 cycles). In the asymmetric setup against a Vulcan XC-72R (negative electrode), maximum energy and power density of 173 Wh kg^{-1} and 28.8 kW kg^{-1} were recovered. The exceptional performance of composite electrodes can be attributed to the combining characteristics of biomass-derived graphene's surface area and the electro-kinetics of LDH [72].

Similarly, high-energy storage supercapacitors can be fabricated by compositing porous biomass-derived material with graphene. For example, a porous carbon derived from *Typha domingensis* was combined with graphene to produce a hierarchical porous carbon graphene composite with high porosity and capacitance. When testing the fabricated carbon composite as an electrode in a two-electrode cell against a Vulcan XC-72R as the
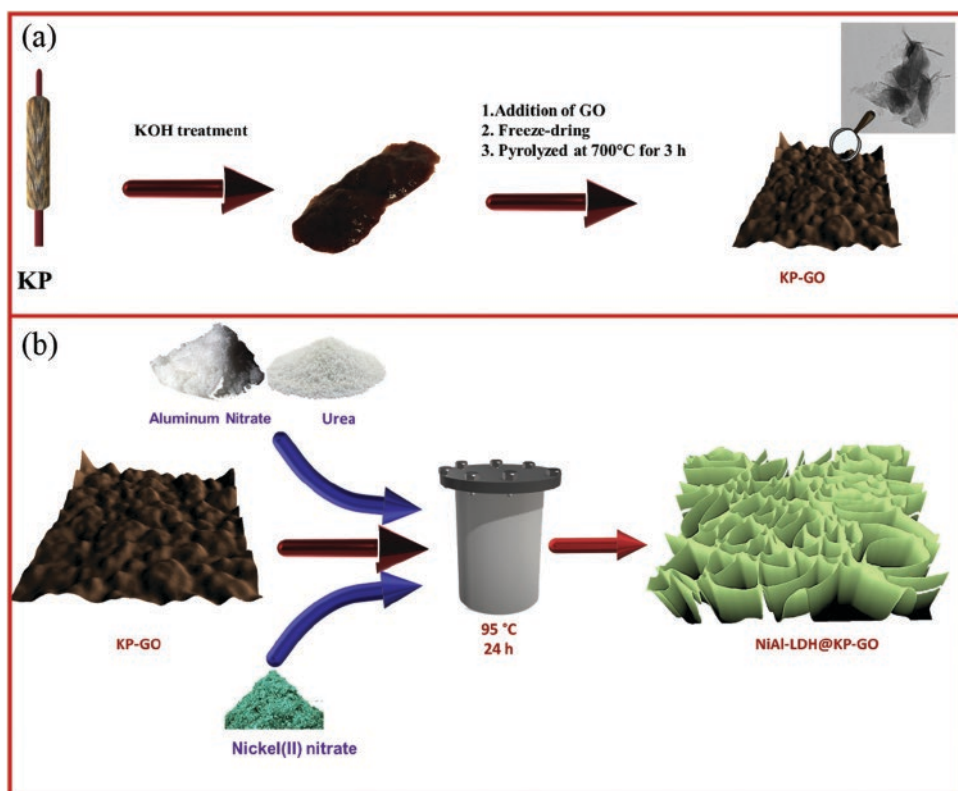
Figure 16.7 Synthesis schemes of (A) bare KP-GO and (B) NiAl-LDH@KP-GO composite. *Reproduced with permission* [72]. *Copyright 2020, Elsevier* [72].

negative electrode, in 6 M KOH as an electrolyte, the fabricated electrode showed a specific capacitance of 277.5 F g^{-1} with more than 94% of the initial specific capacitance after 5000 cycles of successive charge/discharge. Such results illustrate that the graphene/biomass-derived porous carbon materials composite is a promising material for electrochemical energy storage devices [73].

The properties and performance of biomass-derived graphene-based supercapacitors were also found to be improved by optimizing the activation temperature. For example, amorphous carbon synthesized from jute stick-based biowaste was converted into a stable graphene-like network with a high specific surface area of 2396 m^2 g^{-1} and highly ordered graphitic sp^2 carbon at activation temperature in the range of 800–1000 °C. It can be seen in Figure 16.8 that the carbonizing temperature offered significant morphological changes, which led to their electrochemical performance control. For the supercapacitor applications, the activated jute stick carbon performance showed a high specific capacitance of 282 F g^{-1} with good capacitance retention of 70% at high current rates compared to the non-activated jute stick carbon [38].
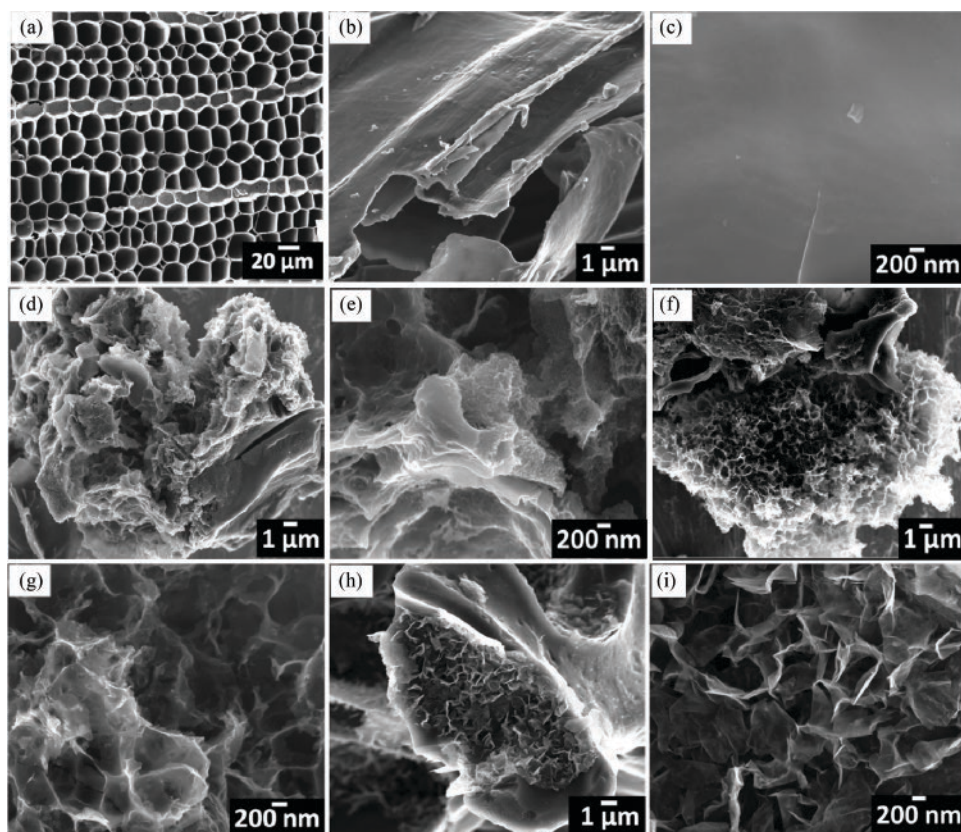
Figure 16.8 Morphologies of carbonized jute stick-derived nanoporous carbon; (A) cross section of jute, (B, C) not activated, (D, E) activated at 800 °C (F, G) activated at 900 °C, and (H, I) activated at 1000 °C. *Reproduced with permission* [38]. *Copyright 2018, American Chemical Society.*

In a similar study, graphene-like activated carbon nanostructures synthesized from jute exhibited higher specific capacitance than the non-activated carbons [74]. Galvanostatic charge-discharge cycles showed a time decrease with the current density increase. It was found that maximum charge/discharge is obtained at 0.2 A g^{-1} in the case of activated carbon from jute. Additionally, the calculated specific capacitance at 0.2 A g^{-1} was 476 F g^{-1}, which can be attributed to the larger surface area and porosity of jute-derived carbon compared with other biomass products.

Extracting carbon sources from biomass and their conversion to graphene involves multiple reaction steps (usually high-temperature processes). Therefore, structural defects (intrinsic) are inevitable, influencing the electrical, structural, mechanical, and thermal properties. The π-bonds in derived graphene are responsible for capacitance properties, which are influenced by the defects as they cause bond ordering or may add extra energy states with dangling bonds. These variables could act as charge accumulation centers and improve the overall capacitance. Another kind of defect is extrinsic, in which some foreign impurity is added to the structure of graphene. The heteroatom insertion within biomass-derived graphene is an alternative to using expensive composite materials for enhanced performance. Heteroatom doping can endow graphene with improved physicochemical, optical, electromagnetic, and structural properties [75]. High-capacitance electrochemical supercapacitors were fabricated from biomass-derived few-layer graphene nanosheets from the ginger root. Suitable heteroatom contents of potassium (1.14%), magnesium (0.34%), and phosphorous (0.34%) enhanced the specific capacitance of the device. In a three-electrode cell configuration, the fabricated capacitors demonstrated good EDLC behavior. It can be concluded from CV profiling that the capacitance is maintained up to a high scan rate, i.e., 200 mV s^{-1}. Perfect isosceles triangle shapes in the GCD curves determined that a negligible resistance existed at different current densities, which increased the capacitance behavior of biomass-derived few-layers graphene capacitors. The capacitance reached 70 F g^{-1} at 0.1 A g^{-1}. The fabricated electrodes demonstrated excellent stability up to 3500 cycles (acquired at 2 A g^{-1}) with 93.3% capacitance retention. Finally, a Ragone plot exhibited a reasonable energy density of 9.67 W h kg^{-1} with a power density of 200 W kg^{-1} [76]. These measurements emulate the excellent efficiency of ginger-derived capacitors at a larger scale.

Further electrochemical capacitance can be enhanced by doping with heteroatoms such as H, N, B, P, F, and S. Moreover, doping can also change the surface wettability, change the electrical conductivity, accelerate the charge transfer, introduce pseudocapacitance, and facilitate the electrode–electrolyte interface reactions [77]. Taking oxygen doping as a representative example, it is found that oxygen enrichment can enhance the surface wettability and ions accessibility, thus establishing extra pseudocapacitance. The graphene derived from elm seeds has an oxygen-rich porous structure (oxygen content = 32.95 %) [78]. Similarly, carbon-based precursors from *Camellia oleifera* have oxygen-rich functional groups (C/O = 1.66) after microwave-assisted carbonization and KOH activation [79]. These materials demonstrated exceptional super capacitance activities and can be considered suitable precursors for oxygen-doped graphene synthesis.

On the other hand, nitrogen doping improves electrical features by increasing the electroactive sites. It also polarizes the structure by disturbing the valence electron of carbon within bio-derived graphene. Graphene derived from nitrogen-rich biomass sources such as pine pollen, pine needle, spirulina platensis, Juncus, coronarium, chitosan, bamboo fungus, and porcine bladders tends to be self-doped with nitrogen easily. Nonetheless, it needs

Table 16.1 Capacitance performance of biomass-derived graphene electrodes for supercapacitors.

Biomass materials	Temperature (°C)	Activation agents	Electrolyte	Specific capacitance (F g^{-1})	Current density (A g^{-1})
Bamboo bagasse [80]	800	KOH-iron	6M KOH	173.2	1
Corn stalk [81]	1100	$K_4[Fe(CN)_6]$	6M KOH	213	1
Sugarcane bagasse [82]	800	KOH	1M H_2SO_4	280	1
Ginger [76]	800	No activation	1M H_2SO_4	390	1
Cellulose [83]	1100	No activation	6 KOH	132	1
Camellia oleifera shell [79]	800	KOH	6M KOH	251	0.5
Elm seeds [78]	500	KOH solution	6M KOH	501	0.5
Onion peels [71]	600 to 800	–	1M H_2SO_4	93.5	1
Ginger roots [76]	600 to 900	Self-activated	1M H_2SO_4	390	1
Glucose-based polymers [67]	1100	CO_2, KOH	Ionic liquid (EMIM-TFSI/AN)	175	1
Orange-peel [84]	800	KOH	6M KOH	425	0.5
Tobacco stalk [85]	850	KOH	6M KOH	281.3	1

further treatments to improve the device's nitrogen contents and overall capacitance [77]. Table 16.1 has provided a few representative examples of biomass-derived supercapacitors with operating conditions and efficiencies in terms of capacitance.

16.5 Conclusions

The examples presented reveal that biomass-derived carbon materials, especially graphene, can be emphasized due to their superior charge-discharge characteristics, commercial and economic values, and abundant availability of biomass sources. Future research should emphasize new biomass sources, including alternative species of plants, animals, and microbes. Much progress has been made on the plant-derived biomass for carbon extractions. The cheaper biomass sources, such as jute plant-derived carbons [35, 86], could offer good alternatives to assemble highly stable and more powerful energy devices. However, this trend needs to be more directed toward the plant's derived carbon materials to explore the unfolding characteristics of those products. However, more work is required to make a comparative assessment of plant-derived and animal-derived graphene-based supercapacitors. Another aspect for the future is using advanced carbonizing machinery that could control the thermodynamical parameters to advance the yield and purity of carbon materials for more efficient performance. Lastly, the impact on the environmentshould be considered as converting biomass materials into various carbon-based products usually requires high temperature burning that can lead to CO_2 emission.

Acknowledgments

References

1 L. Qiu, D. Li, H.-M. Cheng, *ACS Nano* **2018**, *12*, 5085–5092.

2 X. Wang, G. Shi, *Phys. Chem. Chem. Phys.* **2015**, *17*, 28484–28504.

3 W. H. Lee, J. W. Suk, H. Chou, J. Lee, Y. Hao, Y. Wu, R. Piner, D. Akinwande, K. S. Kim, R. S. Ruoff, *Nano Lett.* **2012**, *12*, 2374–2378.

4 H. Liu, S. Ryu, Z. Chen, M. L. Steigerwald, C. Nuckolls, L. E. Brus, *J. Am. Chem. Soc.* **2009**, *131*, 17099–17101.

5 V. Georgakilas, A. B. Bourlinos, R. Zboril, T. A. Steriotis, P. Dallas, A. K. Stubos, C. Trapalis, *Chem. Commun.* **2010**, *46*, 1766–1768.

6 L. H. Liu, G. Zorn, D. G. Castner, R. Solanki, M. M. Lerner, M. Yan, *J. Mater. Chem.* **2010**, *20*, 5041–5046.

7 S. Gayathri, P. Jayabal, M. Kottaisamy, V. Ramakrishnan, *AIP Adv.* **2014**, *4*, 027116.

8 L. Liao, H. Peng, Z. Liu, *J. Am. Chem. Soc.* **2014**, *136*, 12194–12200. https://pubs.acs.org/doi/10.1021/acs.chemrev.2c00602

9 E. Bekyarova, M. E. Itkis, P. Ramesh, C. Berger, M. Sprinkle, W. A. de Heer, R. C. Haddon, *J. Am. Chem. Soc.* **2009**, *131*, 1336–1337.

10 S. S. Shah, M. N. Shaikh, M. Y. Khan, M. A. Alfasane, M. M. Rahman, M. A. Aziz, *Chem. Rec.* **2021**, *21*, 1631–1665.

11 S. S. Shah, E. Cevik, M. A. Aziz, T. F. Qahtan, A. Bozkurt, Z. H. Yamani, *Synth. Met.* **2021**, *277*, 116765.

12 S. S. Shah, M. A. A. Qasem, R. Berni, C. Del Casino, G. Cai, S. Contal, I. Ahmad, K. S. Siddiqui, E. Gatti, S. Predieri, J. F. Hausman, S. Cambier, G. Guerriero, M. A. Aziz, *Sci. Rep.* **2021**, *11*, 6945.

13 C. Li, G. Shi, *Nanoscale* **2012**, *4*, 5549–5563.

14 Z. Tang, S. Shen, J. Zhuang, X. Wang, *Angew. Chemie - Int. Ed.* **2010**, *49*, 4603–4607.

15 Y. Shen, Q. Fang, B. Chen, *Environ. Sci. Technol.* **2015**, *49*, 67–84.

16 A. K. Geim, K. S. Novoselov, *Nat. Mater. 2007 63* **2007**, *6*, 183–191.

17 W. Bao, F. Miao, Z. Chen, H. Zhang, W. Jang, C. Dames, C. N. Lau, *Nat. Nanotechnol. 2009 49* **2009**, *4*, 562–566.

18 D. Sen, K. S. Novoselov, P. M. Reis, M. J. Buehler, *Small* **2010**, *6*, 1108–1116.

19 D. E. Sheehy, J. Schmalian, *Phys. Rev. B - Condens. Matter Mater. Phys.* **2009**, *80*, 193411.

20 D. G. Papageorgiou, I. A. Kinloch, R. J. Young, *Prog. Mater. Sci.* **2017**, *90*, 75–127.

21 F. Bonaccorso, A. Lombardo, T. Hasan, Z. Sun, L. Colombo, A. C. Ferrari, *Mater. Today* **2012**, *15*, 564–589.

22 D. C. Elias, R. R. Nair, T. M. G. Mohiuddin, S. V. Morozov, P. Blake, M. P. Halsall, A. C. Ferrari, D. W. Boukhvalov, M. I. Katsnelson, A. K. Geim, K. S. Novoselov, *Science* **2009**, *323*, 610–613.

23 F. Withers, M. Dubois, A. K. Savchenko, *Phys. Rev. B - Condens. Matter Mater. Phys.* **2010**, *82*, 073403.

24 K. S. Novoselov, *Angew. Chemie Int. Ed.* **2011**, *50*, 6986–7002.

25 S. V. Rotkin, Y. Gogotsi, *Mater. Res. Innov.* **2002**, *5*, 191–200.

26 Y. Gogotsi, *J. Phys. Chem. Lett.* **2011**, *2*, 2509–2510.

27 H. C. Schniepp, J. L. Li, M. J. McAllister, H. Sai, M. Herrera-Alonson, D. H. Adamson, R. K. Prud'homme, R. Car, D. A. Seville, I. A. Aksay, *J. Phys. Chem. B* **2006**, *110*, 8535–8539.

28 C. Vallés, J. David Núñez, A. M. Benito, W. K. Maser, *Carbon* **2012**, *50*, 835–844.

29 S. Ansari, E. P. Giannelis, *J. Polym. Sci. Part B Polym. Phys.* **2009**, *47*, 888–897.

30 Z. Xu, M. J. Buehler, *ACS Nano* **2010**, *4*, 3869–3876.

31 V. B. Shenoy, C. D. Reddy, A. Ramasubramaniam, Y. W. Zhang, *Phys. Rev. Lett.* **2008**, *101*, 245501.

32 X. Meng, M. Li, Z. Kang, X. Zhang, J. Xiao, *J. Phys. D. Appl. Phys.* **2013**, *46*, 055308.

33 N. Patra, B. Wang, P. Král, *Nano Lett.* **2009**, *9*, 3766–3771.

34 H. Ham, T. Van Khai, N.-H. Park, D. S. So, J.-W. Lee, H. G. Na, Y. J. Kwon, H. Y. Cho, H. W. Kim, *Nanotechnology* **2014**, *25*, 235601.

35 A. Aziz, S. S. Shah, A. Kashem, *Chem. Rec.* **2020**, *20*, 1074–1098.

36 M. A. Aziz, S. S. Shah, S. M. A. Nayem, M. N. Shaikh, A. S. Hakeem, I. A. Bakare, *J. Energy Storage* **2022**, *50*, 104278.

37 A. Abbas, L. T. Mariana, A. N. Phan, *Carbon* **2018**, *140*, 77–99.

38 K. Nanaji, V. Upadhyayula, T. N. Rao, S. Anandan, *ACS Sustain. Chem. Eng.* **2019**, *7*, 2516–2529.

39 S. Goenka, V. Sant, S. Sant, *J. Control. Release* **2014**, *173*, 75–88.

40 J. K. Saha, A. Dutta, *Waste Biomass Valorization* **2022**, *13*, 1385–1429.

41 K. S. Novoselov, A. K. Geim, S. V. Morozov, D. Jiang, Y. Zhang, S. V. Dubonos, I. V. Grigorieva, A. A. Firsov, *Science* **2004**, *306*, 666–669.

42 S. Park, R. S. Ruoff, *Nat. Nanotechnol.* **2009**, *4*, 217–224.

43 Y. Bleu, F. Bourquard, V. Gartiser, A. S. Loir, B. Caja-Munoz, J. Avila, V. Barnier, F. Garrelie, C. Donnet, *Mater. Chem. Phys.* **2019**, *238*, 121905.

44 V. Stankus, A. Vasiliauskas, A. Guobienė, M. Andrulevičius, Š. Meškinis, *Surf. Coatings Technol.* **2022**, *437*, 128361.

45 J. Campos-Delgado, A. R. Botello-Méndez, G. Algara-Siller, B. Hackens, T. Pardoen, U. Kaiser, M. S. Dresselhaus, J. C. Charlier, J. P. Raskin, *Chem. Phys. Lett.* **2013**, *584*, 142–146.

46 L. F. Gorup, L. H. Amorin, E. R. Camargo, T. Sequinel, F. H. Cincotto, G. Biasotto, N. Ramesar, F. D. A. La Porta, *Nanosensors for Smart Cities*, Elsevier, **2020**, 9–30.

47 S. Garaj, W. Hubbard, J. A. Golovchenko, *Appl. Phys. Lett.* **2010**, *97*, 183103.

48 B. Jayasena, S. Subbiah, *Nanoscale Res. Lett.* **2011**, *6*, 95.

49 H. Yu, B. Zhang, C. Bulin, R. Li, R. Xing, *Sci. Rep.* **2016**, *6*, 36143.

50 D. C. Marcano, D. V. Kosynkin, J. M. Berlin, A. Sinitskii, Z. Sun, A. Slesarev, L. B. Alemany, W. Lu, J. M. Tour, *ACS Nano* **2010**, *4*, 4806–4814.

51 L. Peng, Z. Xu, Z. Liu, Y. Wei, H. Sun, Z. Li, X. Zhao, C. Gao, *Nat. Commun.* **2015**, *6*, 5716.

52 E. Cappelli, S. Orlando, M. Servidori, C. Scilletta, *Appl. Surf. Sci.* **2007**, *254*, 1273–1278.

53 X. Dong, S. Liu, H. Song, P. Gu, *J. Mater. Sci.* **2017**, *52*, 2060–2065.

54 N. Mishra, J. Boeckl, N. Motta, F. Iacopi, *Phys. Status Solidi* **2016**, *213*, 2277–2289.

55 W. Norimatsu, M. Kusunoki, *Phys. Chem. Chem. Phys.* **2014**, *16*, 3501–3511.

56 B. Gupta, M. Notarianni, N. Mishra, M. Shafiei, F. Iacopi, N. Motta, *Carbon* **2014**, *68*, 563–572.

57 C. Riedl, C. Coletti, U. Starke, *J. Phys. D. Appl. Phys.* **2010**, *43*, 374009.

58 B. H. Min, D. W. Kim, K. H. Kim, H. O. Choi, S. W. Jang, H. T. Jung, *Carbon* **2014**, *80*, 446–452.

59 D. A. C. Brownson, C. E. Banks, *Phys. Chem. Chem. Phys.* **2012**, *14*, 8264–8281.

60 X. J. Lee, L. Y. Lee, L. P. Y. Foo, K. W. Tan, D. G. Hassell, *J. Environ. Sci. (China)* **2012**, *24*, 1559–1568.

61 J. Jang, M. Son, S. Chung, K. Kim, C. Cho, B. H. Lee, M.-H. Ham, *Sci. Rep.* **2015**, *5*, 17955.

62 V. Singh, D. Joung, L. Zhai, S. Das, S. I. Khondaker, S. Seal, *Prog. Mater. Sci.* **2011**, *56*, 1178–1271.

63 S. Rahemi Ardekani, A. Sabour Rouh Aghdam, M. Nazari, A. Bayat, E. Yazdani, E. Saievar-Iranizad, *J. Anal. Appl. Pyrolysis* **2019**, *141*, 104631.

64 J. T. Illakkiya, P. U. Rajalakshmi, R. Oommen, *Surf. Coatings Technol.* **2016**, *307*, 65–72.

65 Z. Gao, Z. Jin, Q. Ji, Y. Tang, J. Kong, L. Zhang, Y. Li, *Carbon* **2018**, *128*, 117–124.

66 L. Baraton, Z. He, C. S. Lee, J. L. Maurice, C. S. Cojocaru, A. F. Gourgues-Lorenzon, Y. H. Lee, D. Pribat, *Nanotechnology* **2011**, *22*, 085601.

67 S. H. Jung, Y. Myung, B. N. Kim, I. G. Kim, I.-K.-K. You, T. Y. Kim, *Sci. Rep.* **2018**, *8*, 1915.

68 A. S. Jung, P. T. Huong, S. Sahani, K. M. Tripathi, B. J. Park, Y. H. Han, T. Kim, *J. Electrochem. Soc.* **2022**, *169*, 010509.

69 S. A. Sawant, A. V. Patil, M. R. Waikar, A. S. Rasal, S. D. Dhas, A. V. Moholkar, R. S. Vhatkar, R. G. Sonkawade, *J. Energy Storage* **2022**, *51*, 104445.

70 Z. Li, W. Lv, C. Zhang, B. Li, F. Kang, Q. H. Yang, *Carbon* **2015**, *92*, 11–14.

71 R. Bhujel, S. Rai, K. Baruah, U. Deka, J. Biswas, B. P. Swain, *Sci. Rep.* **2019**, *9*, 19725.

72 F. Golmohammadi, M. Amiri, *Int. J. Hydrogen Energy* **2020**, *45*, 15578–15588.

73 M. Amiri, F. Golmohammadi, *J. Electroanal. Chem.* **2019**, *849*, 113388.

74 K. Ojha, B. Kumar, A. K. Ganguli, *J. Chem. Sci.* **2017**, *129*, 397–404.

75 X. Wang, G. Sun, P. Routh, D. H. Kim, W. Huang, P. Chen, *Chem. Soc. Rev.* **2014**, *43*, 7067–7098.

76 A. Gopalakrishnan, C. Y. Kong, S. Badhulika, *New J. Chem.* **2019**, *43*, 1186–1194.

77 X. Luo, S. Chen, T. Hu, Y. Chen, F. Li, *SusMat* **2021**, *1*, 211–240.

78 D. Guo, X. Song, B. Li, L. Tan, H. Ma, H. Pang, X. Wang, L. Zhang, D. Chu, *J. Electroanal. Chem.* **2019**, *855*, 113349.

79 J. Liang, T. Qu, X. Kun, Y. Zhang, S. Chen, Y. C. Cao, M. Xie, X. Guo, *Appl. Surf. Sci.* **2018**, *436*, 934–940.

80 S. S. Gunasekaran, S. K. Elumalali, T. K. Kumaresan, R. Meganathan, A. Ashok, V. Pawar, K. Vediappan, G. Ramasamy, S. Z. Karazhanov, K. Raman, R. Subashchandra Bose, *Mater. Lett.* **2018**, *218*, 165–168.

81 L. Wang, G. Mu, C. Tian, L. Sun, W. Zhou, P. Yu, J. Yin, H. Fu, *ChemSusChem* **2013**, *6*, 880–889.

82 M. Wahid, D. Puthusseri, D. Phase, S. Ogale, *Energy Fuels* **2014**, *28*, 4233–4240.

83 C. Bommier, R. Xu, W. Wang, X. Wang, D. Wen, J. Lu, X. Ji, *Nano Energy* **2015**, *13*, 709–717.

84 C. Karaman, O. Karaman, N. Atar, M. L. Yola, *Phys. Chem. Chem. Phys.* **2021**, *23*, 12807–12821.

85 Q. Yuan, Z. Ma, J. Chen, Z. Huang, Z. Fang, P. Zhang, Z. Lin, J. Cui, *Polym 2020, Vol. 12, Page 1982* **2020**, *12*, 1982.

86 S. S. Shah, H. Yang, M. Ashraf, M. A. A. Qasem, A. S. Hakeem, M. A. Aziz, *Chem. – An Asian J.* **2022**, *17*, e202200567.

17

Biomass-derived N-doped Carbon for Electrochemical Supercapacitors

Syed Niaz Ali Shah[1,], Eman Gul[2], Narayan Chandra Deb Nath[3,*], and Guodong Du[3]*

[1] Center for Integrative Petroleum Research, King Fahd University of Petroleum and Minerals, Dhahran 31262, Saudi Arabia
[2] Institute of Chemical Sciences, University of Peshawar, 25120, Pakistan
[3] Department of Chemistry, University of North Dakota, Grand Forks, North Dakota 58202, United States
* Corresponding authors

17.1 Introduction

The synthesis of carbon-based materials from non-renewable fossil feedstock resources like coal and oil generally requires harsh reaction conditions [1–3] and is considered an environmentally unfriendly and economically unviable method [4, 5]. Therefore, developing environment-friendly, sustainable, and cost-effective methods for synthesizing various carbon materials is considered a crucial topic in different research fields [6, 7]. The manufacturing of functional carbon-based porous materials, including heteroatoms-doped porous carbons and value-added fuels from a naturally abundant source of biomass, is a robust alternative to fossil feedstocks because of its environment-friendly and renewable nature [8–10]. The preparation of a variety of N-doped porous carbons (NPCs) with different morphologies and nanostructures from the biomass has shown better benefits and suitability, which established itself as the best, most benign, and environment-friendly method [11, 12].

There is a lot of interest in using carbon materials obtained from biomass as electrodes for energy storage devices (Figure 17.1) due to their versatility as raw materials, low environmental impact, and high commercial value [13]. Naturally, the most abundant source of biomass is lignocellulose. Hemicellulose, cellulose, and lignin are the main components of the lignocellulose biomass. The significant source of lignocellulose biomass is agricultural wastes, e.g., rice husk, wheat straw, cotton stalk, bamboo shoots, and bagasse [14–16]. The synthesis of porous carbons by pyrolysis of agricultural crop wastes is the best and most efficient utilization of raw biomass and can reduce air pollution [17–19]. The other important agricultural sources are algae, soybean residue, chitosan, and shrimp shells, which are studied extensively to synthesize NPCs because of the high abundance of carbon and nitrogen. The porous carbons are mostly synthesized from biomass by the methods such as hydrothermal carbonization (HTC), activation, and pyrolysis. Some of the advantages

Figure 17.1 Biomass-derived carbon is used as an electrode material for energy storage devices. *Reproduced with permission* [13]. *Copyright 2017, Royal Society of Chemistry.*

of synthesizing the porous carbons are a high thermally, chemically stable, large Brunauer-Emmett-Teller (BET) specific surface area ($500-3000\,m^2g^{-1}$), and cost-effective availability. However, the porous carbons suffer from poor electrical conductivity due to having a lower degree of graphitization [20]. Therefore, the incorporation of heteroatoms, including nitrogen (N), oxygen (O), phosphorous (P), and boron (B) in the carbon framework considerably increases the capacitance compared with pristine carbon due to the significant increase in electrical conductivity and electroactive sites. The presence of the heteroatoms can change carbon's crystalline and electronic structure by improving the electron donor properties, which increase the pseudocapacitive behaviors [19, 21]. The incorporation of N enhances the number of active sites for ion adsorption, improving electrocatalytic activity. The doping carbon with N could facilitate the electron transfer abilities in the carbon backbone, leading to high selectivity in alcohol oxidation to aldehyde. There are lots of opportunities to tune NPC's pore size, doping content, and specific surface easily, which could affect the electron transfer activity or electroactive sites for the performance of electrochemical devices, suggesting that its synthetic method would be a very significant study area due to its variable characteristics and wide range of uses [22–29]. N-doping is a great way to enhance porous carbons' physicochemical characteristics and energy storage capacities. NPCs also have a distinct surface area and a variable pore size. Because of its customizable characteristics and wide range of uses, the N content could easily be adjusted, indicating that the synthesis of NPCs is an interesting research area. N-doping is a great method for enhancing the physicochemical characteristics and energy-storage capacities of porous carbons [30, 31].

Incorporating N-dopants into a carbon framework is simple since carbon and nitrogen atoms have nearly identical radii of 0.77 and 0.74 angstroms, respectively [32–34]. However, nitrogen has a higher electronegativity (3.04) than carbon does (2.55), which causes a shift in the electrical makeup of the carbon network. N-doping contributes extra electrons, leading to surface basicity, which boosts catalytic activity in the electrochemical process. N exists in several forms, including pyridine-N-oxide (N-x), pyrrolic (N-5), pyridinic (N-6), and quaternary N/graphitic N (N-Q). Compared to the high price of Pt/C catalysts, NPCs are a far more economical choice. Therefore, a lot of effort was put into synthesizing nitrogen-doped carbon (NC) with different amounts of N and different N functions for electrochemical energy storage applications. Additionally serving as lithium-ion batteries and supercapacitors (SCs) electrode materials, the NCs are beneficial as catalysts for the generation of the hydrogen evolution process (HER) and oxygen reduction reaction (ORR) [35, 36].

When N-doping is present in a supercapacitor, Faradaic interactions between the ions in the electrolyte increase capacitance via a pseudocapacitive effect [37–39]. Using NPC has many benefits over porous carbon. To give just one example, consider adding elements like N, which improves wettability and hydrophilicity. The introduction of reductive N entities on the surface of porous carbon, generated by the doping procedure, allows energy to be stored

in the form of pseudocapacitance or electrocatalytic sites. N-doping significantly increases the capacitive performance by (a) disturbing the carbon surface's electric neutrality, which causes delocalization of the adjacent carbon atoms' electrons and increases the amount of adsorption on the surface, so enhancing the electrocatalytic activity, (b) increasing electrocatalytic activity, sp2 carbon's electrical structure is altered through the introduction of defects, and (c) by boosting the energy storage catalyst's conductivity [33, 40, 41]. Changing the N precursors or constituents allowed for fine-tuning of the N-functionalities, with the strongest activity coming from N functional groups located near the graphitic layer edges. In addition, PCNs that have N doped into them are more affordable, last longer, and are better for the planet. Recent research has shown that heteroatom self-doping, which does not require the addition of any extra N-precursors, greatly aids in enhancing a material's surface properties, electrical properties, and pseudo-capacitive properties. The pyrolysis of the N-precursor leads to the homogenous allocation of heteroatoms in the bulk carbon, which influences the structures and morphologies of PCNs. Therefore, the microporosity and surface characteristics of porous C can be easily controlled by selecting the appropriate containing N-precursor and the weight ratio of C to N-precursor [42, 43].

17.2   Synthesis Methods for N-doped Porous Carbons

To produce NPCs, numerous effective ways have been investigated. Corrosive NH_3 was reported as the N source at high temperatures in many NPCs synthesis processes. To get over this problem, biomass was used as a source of renewable carbon and N precursors in NC synthesis [44]. It is challenging to regulate the physicochemical features (porous structure, N-type, and N-content) of NCs made from low-cost materials like biomass. Carbon and nitrogen precursors generated from biomass are carbohydrates with amino-functional groups like glucosamine and chitosan. Additionally, N-containing compounds like amino acids or proteins are used. Despite their widespread use in the production of NCs, biomass was favored as a source of N and carbon precursors due to its status as a renewable, sustainable resource and abundance. The following is a comprehensive breakdown of the several NC synthesis techniques available.

17.2.1   Hydrothermal Carbonization

For decades, scientists have relied on hydrothermal carbonization (HTC) as a reliable technique for creating carbon-based compounds. Using peat as the carbon source in the HTC initially produced a lot of carbon monoxide [17]. In this way, a carbonaceous residue is produced that is similar to coal. At the turn of the 21st century, the HTC technique was rediscovered and used to produce carbon microspheres from monosaccharides. By heating biomass as a carbon feedstock in a closed system with water at low temperatures (180–250 °C) a solid product is produced rather than gases. In light of this, further study with diverse carbon sources is required to investigate the true applicability of the HTC method at a big scale (lignin, cellulose, glucose, and chitin). A thorough characterization is required to tackle the underlying chemistry of this complicated process. High-temperature HTC, and low-temperature HTC, are two examples of how the HTC technique can be broken down into subcategories. While the high-temperature HTC process often happened

at temperatures over 250 °C [45], the low-temperature HTC process typically ensued at temperatures below 250 °C. In recent years, the high-temperature HTC approach has been widely used for NC synthesis [46].

Chitosan and glucosamine generated from biomass were mostly employed for NC synthesis because of their high N content. According to Zhao et al. NCs can be synthesized using a green, sustainable approach under mild reaction circumstances [47]. Hydrothermal treatment at 180 °C was used to produce chitosan and D(+)-glucosamine hydrochloride from biomass. Both carbohydrates are rich in nitrogen and carbon. These materials were calcined at 750 °C in an N_2 environment to obtain N-containing carbon from chitosan and glucosamine. According to the results of the elemental analysis, chitosan-derived NC has more carbon (59 wt%) and nitrogen (9 wt%) than pure chitosan (32.8 wt%). However, the sample of NC produced from glucosamine and glucose contains around 6.8 wt% nitrogen and 65 wt% carbon. In contrast to the unchanged N concentration, the increasing carbon content during HTC suggests that hydrogen and oxygen were lost during the dehydration of carbohydrates. Hydrothermal treatment at 180 °C (12 h) was initially done on splits of flowers from *Typha orientalis* to create carbonaceous hydrogel, which was then used to manufacture this NC nanosheet (Figure 17.2). To wash away any remaining soluble contaminants, the produced carbonaceous hydrogel was submerged in water on multiple occasions. The NC nanosheet was formed after the material was freeze dried for 24 hours, then annealed with NH_3 at 800 °C for 2 h at a heating and cooling rate of 5 °C per minute. Additionally, it increased total pore volume from 0.36 to 0.52 cm³/g while decreasing micropore volume from 0.27 to 0.16 cm³/g [48, 49]. The hydrothermal method has been used to synthesize carbon nanomaterials using amino acids as precursors [50–53]. The precursor greatly influences the N content of the
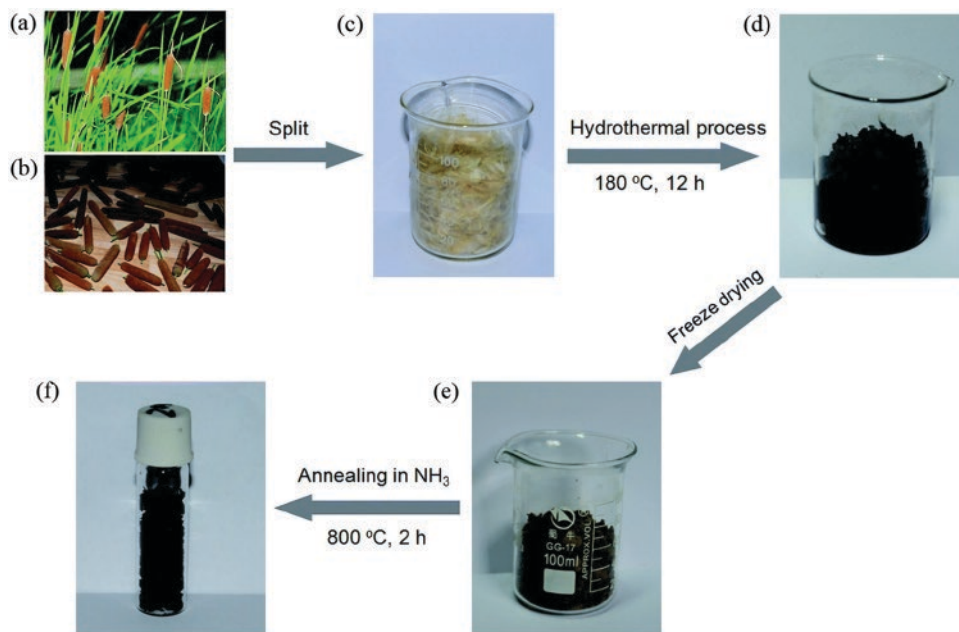
Figure 17.2 Schematic for the hydrothermal synthesis of biomass-derived NPC materials. *Reproduced with permission* [48]. *Copyright 2014, Royal Society of Chemistry.*

synthesized carbon materials. By using 5-aminotetrazole as a precursor in a hydrothermal way, very high N-content carbon nanomaterials have been synthesized [54].

17.2.2 Pyrolysis

Since the combustion of 1,6-hexanediol results in the formation of hazardous oxides of N, which are corrosive to metals and tissue, it is essential to make use of environmentally acceptable precursors in the NC preparation. Lee et al. described versatile synthesis techniques for hierarchically porous carbon (HPCs) derived from bioethanol lignin and Kraft alkaline lignin [55]. Both potassium hydroxide and sodium hydroxide were required to extract the HPC from bioethanol lignin. Only micropores emerged when KOH was added, and nothing else. Based on the results of this research, using KOH in conjunction with NaOH to create pores results in a eutectic mixture of NaOH and KOH. The existence of inherent NaOH in Kraft alkaline lignin allows for preparing HPC even with just KOH addition. It follows that N-containing biomass can be used in conjunction with the addition of NaOH or KOH to create N-doped HPC. Using pyrolysis of Kraft lignin, Liu et al. demonstrated the production of O, N, and S co-doped hierarchical porous carbon (ONS-HPCs) (Figure 17.3) [56]. Under an N_2 environment, the Kraft lignin was pyrolyzed directly at 400 °C for one hour. The temperature was then raised to 600 °C or more for another hour. To remove any remaining inorganic contaminants from the black solid that was formed after pyrolysis, it was washed in an HCl solution. Interestingly, the impurities in Kraft lignin (Na_2CO_3 Na_2SO_4, NaCl, and KCl) are essential to creating proes in hierarchical carbons. They demonstrated that Na_2SO_4 reacts with carbon during carbonization to yield Na_2CO_3, which then acts as an activating agent for hierarchical pores. Samples pyrolyzed at 600 °C had a smaller BET-specific surface area ($338\,m^2g^{-1}$), while those pyrolyzed at 800 °C had a much larger BET-specific surface area, $1307\,m^2g^{-1}$. When subjected to SC application
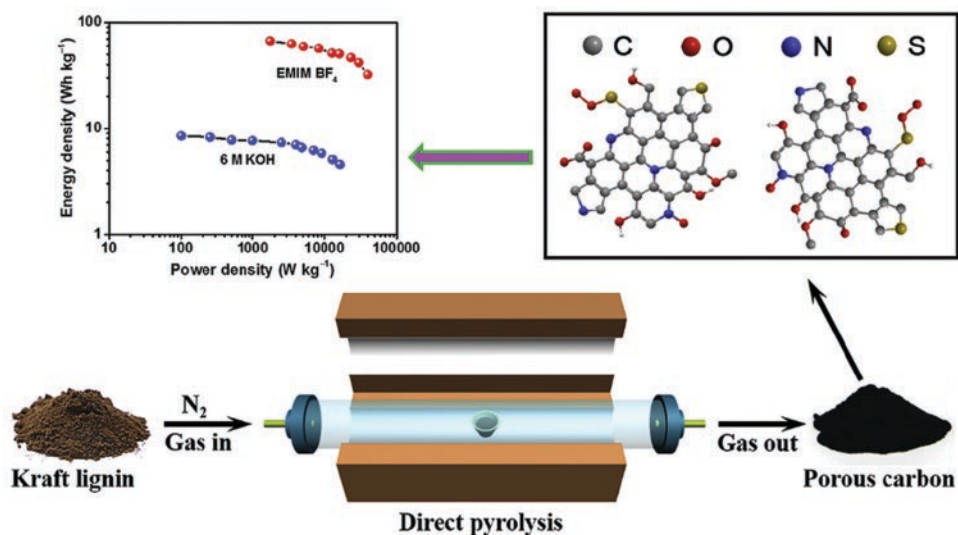
Figure 17.3 Pyrolytic conversion of Kraft lignin to porous carbon. *Reproduced with permission* [56]. *Copyright 2019, Elsevier.*

at 0.2 A g^{-1} in 6 M KOH, the ONS-HPC electrode displayed a superior specific capacitance (244.5 F g^{-1}). These findings demonstrated the successful use of lignin in synthesizing heteroatom-doped HPCs with good characteristics, including greater specific surface area, 3D framework, and heteroatom doping of diverse types. Further research is needed to investigate the feasibility of large-scale electrode manufacture for energy storage devices and catalytic applications, even if lignin may be transformed into an extremely active electrode material utilizing a easy method.

Wei et al. showed how to synthesize N-doped hierarchical porous carbon (N-HPC) from wheat straw [57]. N-HPC is synthesized by combining 1.5 grams of dried wheat straw, 1.5 grams of melamine, and 1.5 grams of CaCl$_2$ in 25 mL of ethylene glycol while stirring the mixture at 90 °C (2 h). To obtain a solid combination, the solution was cooked in a vacuum oven at 110 °C. The resulting solid was further calcined for two hours at 600–800 °C in a nitrogen environment. The material was cleaned with 1.5 M HCl and Millipore water before being dried at 70 °C for 24 hours in a vacuum to extract N-HPC.

17.2.3   Template Directed Synthesis

Since the porosity and N content of NC tend to decrease after pyrolysis, it has been proposed that different techniques be used to create them, like sol-gel, chemical/physical activation, and templating synthesis. The ability to generate ordered porous NCs via the template-directed synthesis process has led to its widespread implementation utilizing biomass as the starting material. Well-ordered pore NCs with appropriate physicochemical properties were synthesized utilizing a template-directed approach. During carbonization, the template aids in the formation of pores and promotes structural ordering. The template-directed HTC technique was recently employed to synthesize NC nanofiber aerogels (Figure 17.4) [58]. To create NC aerogel with enhanced electrical conductivity, tellurium nanowires were used as templates, and the N supply was a carbohydrate-containing N, i.e., glucosamine. This type of synthesis has the benefit of electrospinning in that fiber diameters can be adjusted during the synthesis process. Tellurium nanofibers, which are utilized to guide the formation of carbon nanofibers, are more expensive than alternative methods. To overcome this problem, you can use a template made of cheap materials like cellulose nanofiber or inorganic nanowires. High porosity and conductivity were achieved by activating with CO$_2$ at elevated temperatures. This NC nanofiber displayed promising electrocatalytic activity in SCs and other contexts. Liu et al. described the production of 3D-NPC
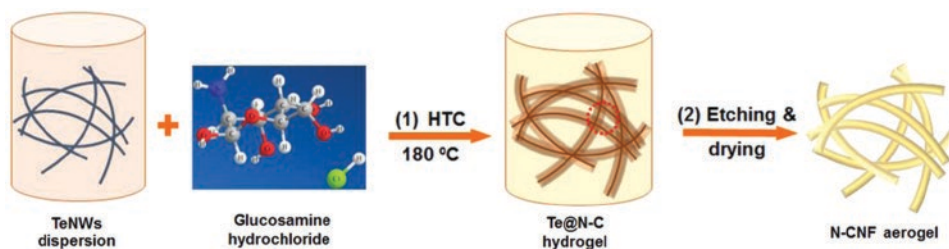
Figure 17.4   Template-directed hydrothermal carbonization method for the preparation of carbon materials. *Reproduced with permission* [58]. *Copyright 2016, Elsevier.*

exploiting carbon nanodots extracted from shrimp shells for energy conversion reactions [59]. 3D-NPCs were made with HTC and template-assisted pyrolysis. Shrimp-shell generated N-doped nanoparticles are tiny (1.5–5 nm in size) and rich in functional groups of N and O. The Stöber technique was used to create a mold out of silica spheres (200 nm in diameter). N-CNs@SiO_2 is a composite material that combines N-CNs with silica spheres and evaporates the mixture. Additionally, 3D-NPC is formed when the acquired N-CNs@SiO_2 was pyrolyzed, then acid etched. The 3D-NPC created through pyrolysis treatment at 800 °C was equivalent to the Pt/C catalyst in terms of catalytic activity and durability for oxygen reduction (ORR). High methanol tolerance in alkaline media was observed with the 3D-NPC electrocatalyst, which was better than that of standard Pt/C electrocatalyst.

17.2.4 Activation

NCs can be produced from biomass through chemical, physical, or combined activation processes (Figure 17.5) [4]. A physical activating agent such as CO_2, air, or steam is necessary for a more tangible activation. NaOH, KOH, $ZnCl_2$, $KHCO_3$, K_2CO_3, H_3PO_4, and $AlCl_3$ are only some of the chemical activation agents that can be used in the chemical activation process [60–62]. The exothermic interaction of carbon with the O existing in the air is problematic for physical activation because it makes it harder to control the reaction, which in turn causes burning and reduces the carbon output. Due to oxygen's higher activity and lower activation energy compared to CO_2 and steam, using air makes the process cost-effective. Several different chemicals, including KOH, H_3PO_4, and $ZnCl_2$, are utilized in chemical activation. While H_3PO_4 and $ZnCl_2$ carry out the dehydration reaction, KOH serves as the oxidizing agent. Chemical activation often involves heating carbon precursors with activating chemicals at temperatures between 400 and 900 °C. The activation agent enhances the surface area and porosity due to the compound's multifaceted actions and synergistic effects, such as the expansion of the carbon lattice and chemical activation
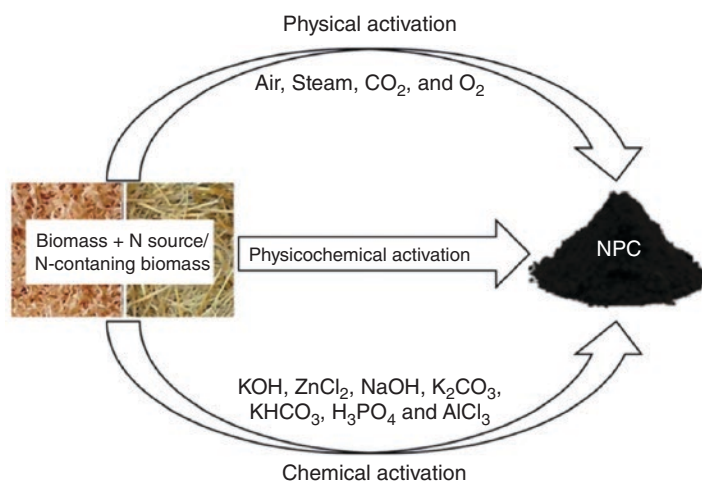
Figure 17.5 Schematic showing the activation of NPCs through different methods. *Reproduced with permission* [4]. *Copyright 2021, Royal Society of Chemistry.*

caused by metallic intercalation [63]. Since $ZnCl_2$ micropores are uniform in size due to the presence of its hydrates or a smaller size, it is preferable to H_3PO_4 activation agents, which induce heterogeneity in the micro-porosity [64]. KOH is an oxidizing chemical that converts carbon to carbonate ($6KOH + 2C \rightarrow 2K + 3H_2 + 2K_2CO_3$), which in turn etches the carbon structure to create pores. Decomposing K_2CO_3 into CO_2 through gasification at temperatures above 700 °C also creates porosity [65, 66].

When the temperature is raised above the optimum range, the material's porosity decreases due to the structure collapsing or the material shrinking [67–70]. When compared to other activating agents, KOH activation provides a greater pore volume and larger surface area [71–73]. As a bonus, the activating agent KOH offers a fine pore size distribution that may be adjusted by varying activation conditions (time, temperature, and amount of KOH). Soybean residue was used by Ferrero et al. to synthesize NC via HTC and KOH activation [74]. Protein-rich soybean pulp was defatted for use in HTC treatment and KOH activation. The resulting NC demonstrates excellent capacitive function in an aqueous electrolyte and a high BET-specific surface area (SBET = $2130 m^2 g^{-1}$ for 800 °C). Rana et al. demonstrated the creation of soybean-derived NCs through activation with NaOH tracked by pyrolysis for SC, ORR, and CO_2 capture applications [75]. This N-doped catalyst made from soybeans has a $1072 m^2 g^{-1}$ SBET and worked admirably in SC applications.

17.2.5 Direct and Post-synthesis

Alternative methods for producing NC include layer separation growth, chemical vapor deposition (CVD), and arch discharge. The term "direct synthesis" describes these techniques [76, 77]. However, thermal annealing, bombardment, and solution treatment are all examples of post-synthesis techniques [78]. Functionalization of NPCs has received a lot of attention lately to enhance their features for use in the real world. Porosity-inducing temperatures vary with carbon precursor and activation agent.

17.3 Supercapacitive Performance of Biomass-derived N-doped Carbon Materials Capacitive Performance

Recently, different nanomaterials have been used for supercapacitance performance [79]. Among them, nitrogen-doped carbon (NCs) generated from biomass have become popular electrode materials for SCs [60]. Doping a carbon electrode with different heteroatoms (O, N, P, S, and B) increases its specific capacitance without diminishing its long cycle life or high rate capacity [80, 81]. The current significant problem with SCs is their inferior energy density ($10 Wh kg^{-1}$) in comparison to Li-ion batteries ($180 Wh kg^{-1}$). The development of active electrodes and innovative electrolytes that can function across a wide voltage range has received a lot of attention in an effort to increase the energy density of SCs. As reported by Qian et al., micro/mesoporous carbon extracted from human hair (HMC) was shown to have an excellent charge storage capacity, with a specific capacitance of $340 Fg^{-1}$ at $1 Ag^{-1}$ current density [82]. A rise in activation temperature from 700 to 800 °C results in a rise in surface area and pore volume, dramatically altering the material's porosity. The increased surface area and smaller pore size distribution aid in charge storage. The hysteresis loop

from P/Po = 0.4 to 0.8 demonstrated that micropore and mesopore development occurred in the HMC-900. The HMC-900 catalyst was quite stable; after 20,000 cycles in 6 M KOH, its specific capacitance was still almost 98% as high as when it was first used.

In organic and ionic liquid (IL) electrolytes, Shao et al. used meso- and macroporous nitrogen-doped hierarchically porous carbon (NHPCs) produced from cow bone for high-energy, ultrafast SCs [83]. The generated NHPCs have a superior specific area of $2203\,m^2g^{-1}$ and noticeable meso- and macroporosity as a result of KOH activation and hydroxyapatite in the cattle bone. The capacitive performance of these NHPC electrocatalysts, produced from bovine bone, was exceptional in a 1.0 M $EMIMBF_4$ IL solution ($240\,Fg^{-1}$ at $5\,Ag^{-1}$). When used as SCs in an aqueous electrolyte, this N-doped microporous carbon showed impressive capacitive performance in gravimetric volumetric units (Li_2SO_4 and H_2SO_4). The voltage window was expanded up to 1.7 V in Li_2SO_4, but it was only 1.1 V in H_2SO_4, indicating a 50% increase in the amount of energy that could be saved in Li_2SO_4 compared to the H_2SO_4 electrolyte. The findings indicated that the O and N moieties each contributed to the pseudo-capacitance event. Greater temperatures (800 °C) made NC better suitable for higher rates, whereas lower temperatures (600 °C) made NC better suited for SCs with lower discharge rates ($5\,Ag^{-1}$). Because of its heteroatoms and porous structure, the NC produced from waste shrimp shells performed exceptionally well in Li-ion batteries and SCs.

Hydrothermal synthesis using mild conditions and low temperatures allowed the creation of N-doped nanoporous carbon from pyrolyzed bacterial cellulose. The prepared N-doped carbon nanoporous exhibited enhanced electrochemical performances in terms of specific capacity, energy density, and power. It also demonstrated a 3D network nanostructure with co-adjacent nanowires of 10–20 nm and numerous interconnecting pores.

By electrospinning a cellulose acetate solution and then subjecting it to deacetylation and pyrolysis, Jie Cai et al. were able to create nitrogen-functionalized carbon nanostructures [84]. Promising rate capability and non-kinetic restricted performance were observed in the resulting electrode, with a specific capacitance of $241.4\,Fg^{-1}$ at $1\,Ag^{-1}$ and capacitance retention of 84.1% even at $10\,Ag^{-1}$, making it a good candidate for use in high-power supercapacitors. Biomass carbons are very structure-, intrinsic-, conformation-, and intermolecular-configuration-dependent in terms of their yield, microstructure, and heteroatom doping. Biochar's qualities can be improved with a deeper understanding of the molecular and elemental characteristics of biomass precursors. High oxygen content in biomass leads to a poor yield, while a high nitrogen content in biomass leads to NC with superior electrochemical characteristics. Plant-based biomass with high N and lignin concentrations and low cellulose and O content provides high-performance carbon composites with high yield, controllable defects, high graphitization degree, and high conductivity, much like chitin biomass with high N content does. The biomass must have the following characteristics to produce high-quality porous carbons: (a) a high concentration of thermally stable, cross-linked, high molecular weight biomacromolecules like lignin; (b) a low concentration of low-molecular-weight aliphatic compounds; and (c) low O and high N for N self-doping of carbons [85]. Microporosity and nanosheet production during KOH activation can be modulated by adjusting the activation temperature, duration, and the activating agent-to-biomass precursor mass ratio. Understanding the fundamental principles is essential to obtaining effective feedstocks for solving future energy and environmental concerns, but improving performance is the primary obstacle [86].

Total pore volume is $0.93\,cm^3g^{-1}$ for N-PCNs and $0.92\,cm^3g^{-1}$ for N&S-PCNs, demonstrating their high surface areas [87]. Whereas 4.14 at.% of N can be found in N-PCNs, 4.62 at.% of N, and 2.56 at.% of S can be found in N&S-PCN. N&S co-doped PCNs are a useful electrode material for SCs because they have a high specific capacitance of 298 Fg-1 and a minimal capacitance loss after 10,000 cycles. The doping of a single heteroatom (N) typically improves just one aspect of a material's capabilities; the synergistic effect of co-doping (S and N) has been demonstrated to boost the performance of carbon materials in general.

The pomelo mesocarp-derived N-PCNs exhibit a porous architecture and a strong N-doping (9.12 wt.%) in addition to their huge surface area ($974.6\,m^2g^{-1}$), total pore volume ($0.69\,cm^3g^{-1}$), average pore size (2.9 nm), and interconnected sheet-like morphology. Using CV and GCD, researchers have analyzed the electrochemical characteristics of N-PCNs [88]. The GCD curves display isosceles triangle-like shapes and are highly symmetrical at different current densities (0.5–$20\,Ag^{-1}$), indicating excellent electrochemical reversibility of these electrodes, in contrast to the CV curves, which maintain a stable rectangular shape at various scan rates, indicating excellent rate capability. The SC displays exceptional rate capability, a specific capacitance of $245\,Fg^{-1}$, superior specific energy (14.7 Whkg-1) and power density (90 Wkg-1), and excellent cycle stability as the electrode. The excellent electrochemical performance of N-PCNs results from their highly porous interconnected structure and high N-doping of carbon nanosheets.

17.3.1 Silk

Metal salts ($ZnCl_2$ and $FeCl_3$) were found during the search for renewable carbon sources; they regenerate silk fibroin from natural silk and construct NHPC nanosheets (N-PCNs) by activating/graphitization of silk. Silk, which has a lamellar multi-layered structure, was activated by a metal salt and graphitized to produce N-PCNs. The resultant nanosheet shape has a 15–30 nm thickness and a continuous 2D porous network [89]. Due to the reduced number of diffusion channels afforded by the nanosheet topology, mass transport at the interface is facilitated for charge/discharge reactions, and ion transport is straightforward. Nanopores serve as ion-active sites, with graphene layers providing a conductive channel for fast electron transfer and intercalation sites.

Quaternary-N (73%) and pyridinic-N (27%), both of which increase the electronic conductivity of carbons that are essential for electrodes, are present in large amounts in the deconvolved N1s XPS spectrum. N-PCNs have a large enough electrode–electrolyte interface ($2494\,m^2/g$) to allow for the buildup of ions or charge, and they also have a large enough number of active sites. N_2 adsorption isotherm calculations reveal continuously distributed pores between 2 and 100 nm, with a linear fall with pore diameter. Micropores are clustered around 0.59 and 1.29 nm. The average pore size of micro-, meso-, and macropores is 4.6 nm, which is perfect for high-speed performance and energy storage. The electrocatalytic conductivity and activity were improved by the presence of defects in the nanosheets and strong N-doping (4.7 wt.%). The partly graphitic PCN structure with electrochemically active defects is doped with electron-rich heteroatoms (N), which increases the number of accessible active sites. N-PCNs' strong performance results from several interrelated factors working in concert: the nanosheet architecture shortens the distance an ion must travel to reach the electrode, the wide surface area offers an efficient transport path, and the porous structure increases the flow of electrolytes between the electrode and ions. In

addition to their enhanced performance for SCs, these N-PCNs are predicted to exhibit strong ORR execution because of their advantageous electrochemical characteristics.

17.3.2 Potato Starch

Potato starch and urea were employed as carbon and N precursors, respectively, and graphene oxide (GO) was used as a structural guiding agent to create 2D N-doped ultrathin PCNs. Composites of GO with carbon species derived from biomass have been shown to improve electrochemical performance, and GO's presence in PCNs aids in nanosheet production and charge (electrons and electrolyte ions) transmission [90]. Additionally, the GO concentration is linked to the pore architectures and N species positions on the surface of carbon nanosheets, both of which influence electrochemical performance. To generate N-PCNs from potato starch, samples with a GO mass ratio of 0 (NC), 1 (NCNS-1), 3 (NCNS-3), and 5 (NCNS-5) were made (Figure 17.6) [90]. The NCNS-3 sample, which has a nanosheet design with linked pores, was provided a 2D template for the activation of biomass by GO. The EDL capacitance of PCNs was increased by the presence of sheet-like structures (5 nm thick) and by the abundance of pores in nanosheets. N content at the surface was approximately 4–5%, according to XPS analyses, and the C and O contents are also evenly distributed.

The better electrochemical performance was associated with a greater pyridinic-to-pyrrolic-N ratio, and the relative abundance of various N species is seen in the N 1 s spectrum as bands attributable to pyridinic-, pyrrolic-, and graphitic-N. An increase in N content after adding graphene shows that it prevents N loss during chemical activation. A pore size of 0.6 nm and a surface area of 600–800 m^2/g are ideal for SC electrodes [90]. Galvanostatic charging patterns are used to calculate specific capacitance; NCNS-3 has the maximum capacitance at 305 Fg^{-1}. Graphene enhances cycling stability, as evidenced by a rise in capacitance retention from 90 to 95%. Because of their good cycling stability and improved rate capability, these ultrathin 2D PCNs derived from biomass are well-suited for use in energy storage devices.

17.3.3 Sugar Cane Bagasse

As a free and accessible renewable agricultural waste byproduct, sugar cane bagasse makes for a useful carbon precursor for synthesizing carbon electrodes for SCs in a way that is both straightforward and environmentally friendly. Carbonization, activation, and N-doping all occur simultaneously using KOH as the activating agent and urea as the N
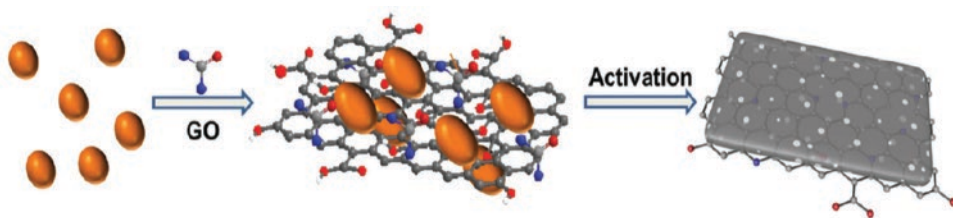
Figure 17.6 Schematic for the preparation of potato starch-derived NPC materials. *Reproduced with permission* [90]. *Copyright 2019, Royal Society of Chemistry.*

precursor [91]. The electrochemical performance was improved because urea boosts the surface area and pore size and delivers a porous network and extensive layer stacking of NC is visible in the morphology. Rich micropores with a partially graphite-like structure, ultrathin nanosheets, meso- and macropores, and an increased specific capacitance are all features of N-doped PCNs. With a high surface area of $2905.4\,m^2g^{-1}$ and a total pore volume of $2.05\,cm^3g^{-1}$, it also exhibits favorable properties for charge storage and ion diffusions in SCs. The N-content was 1.70% (according to XPS), and 2.63% (according to elemental analysis), and a higher fraction of nitrogen at the graphite edge improves pseudocapacitance for SCs [91]. Self-doping of nitrogen in PCNs using biomass was evaluated utilizing a three-electrode assembly, which revealed a high energy and power density, as well as strong cycle stability, as well as a specific capacitance of 301.9 (alkaline), 350.8 (acidic), and $259.5\,Fg^{-1}$ (neutral) at $1\,Ag^{-1}$.

17.3.4 Peanut Skin

Another biomass waste, peanut skin, which is rich in cellulose fibers, was used to create PCNs by graphitizing at 700–900 °C and activating it with $ZnCl_2$, and the sample that resulted from this showed to contain N and S [92]. Nanosheet morphology has been observed through morphological analyses. The sample that was carbonized at 900 °C has a porous nanosheet structure with a high degree of interconnection typical of materials with a sheet-like structure. The elemental analysis confirms that the desirable heteroatoms S (0.26 wt.%) and N (0.84 wt.%) were also present along with the expected C, H, and O. XPS confirms the presence of N in the carbon network as pyridinic-, pyrrolic-, and graphitic-N species, suggesting that the high O-content (20.25 wt.%) may be useful for providing pseudocapacitance via Faradaic charge-transfer processes. According to the Raman findings, the number of fault sites increased from 700 to 900 °C as the graphitization temperature was raised. The Type IV isotherm found in N_2 adsorption/desorption studies at 77 K is consistent with the pore size distribution, showing the existence of micro- and mesoporosities. The quick transit of ions is made possible by the large surface area ($859\,m^2$), and small pore volume ($0.43\,cm^3$) of the sample prepared at 900 °C. The high specific capacitance of $148\,Fg^{-1}$ in 6.0 M KOH was attributed to the existence of S and N, and the wide surface area is responsible for the sample's long-term durability, as evaluated by electrochemical performance with different electrolytes [92]. Further, as a metal-free electrocatalyst, the S and N co-doped samples exhibit impressive ORR performance. Another study used the simultaneous carbonization and activation technique to create PCNs from peanut skin [93]. The nanosheets made have a disordered structure with a micro-, meso- and macroporous network and have dimensions as small as 20 nm in thickness and as large as $2700\,m^2/g$ in surface area, making them ideal for electrocatalytic uses.

17.3.5 Pigskin

Dried pigskin, is a natural feedstock that contains C (48%), O (28%), N (14%), S (0.16%) and H (6%), and was used to make O and N co-doped porous carbon nanosheets (PCNs), which were used in SCs with superior energy and power densities [94]. After being cleaned and dried, raw pigskin was carbonized at 600 °C under N_2 for two hours before being activated with KOH at 600 °C to 900 °C under N_2 for 3.5 hours. After washing the powder with HCl

and DI water, O and N-doped activated carbon was formed by drying it at 80 °C [94]. Pigskin collagen fibers provide a macroscopic disordered network structure that changes into carbon sheets after being carbonized and activated. These carbon sheets have certain macropores that shorten the electrolyte diffusion path to the interior surface [25, 29, 79, 95–109]. In addition to their excellent electrical conductivity, PCNs also exhibit a porous amorphous microstructure. Elemental analysis revealed that there was oxygen and nitrogen at concentrations of 3.3 wt.% and 2.9 wt.%, respectively, on the surface of the carbon. Samples activated at 800 °C were found to have the highest surface area (3337 m^2/g) and total pore volume (2.06 cm^3/g), while samples activated at 600 °C contained the most mesopores and abundant micropores (0.6–0.9 nm), making them the most useful for EDLCs and demonstrating that the activation temperature might be used to regulate porosity. Pigskin-derived activated carbon contains N-H and C-N species, and Fourier Transform Infrared (FTIR) spectroscopy studies demonstrate that, at increasing temperatures, adsorption peaks containing heteroatoms (O, N, and H) grow weaker. Deconvolution of the N 1 s spectra revealed the presence of four distinct N-species, and XPS measurements show that both N and O may be found on the carbon surface at temperatures ranging from 600 to 900 °C. The three types of N-caused pseudocapacitance found near the margins of the graphite plane are pyridinic-N, pyrrolic-N, and pyridine-N. The roughly rectangular shape of the CV curves of samples made at various temperatures reveals the predominant EDLC nature. At the same time, the pseudocapacitance caused by O and N doping on the carbon surface is visible as a broad hump at -0.4 V. Higher temperatures are associated with less N and O doping, which causes less of a hump. At 600 °C, the sample has the highest capacitance (547 F g^{-1}) because it has the most micropores and the most O and N. The capacitance enhancement depends more on the pore size distribution and O and N content, and less on the surface area. Pigskin has thus proven to be a reliable source of nitrogenous precursors for producing N self-doped PCNs for SCs.

17.3.6 Eggplant

Eggplant carbonization as a C and N precursor created porous carbon with a sheet-like microstructure [110]. A sheet-like porous structure was achieved by carbonizing the eggplant for three hours at varying carbonization temperatures (Figure 17.7). As the carbonization temperature determines the resulting microstructure, carbon materials are highly amenable to manipulation. Because of its inherent sheet-like structure at the micro-scale, dried eggplant was used as a carbon precursor. Since decomposition of organics was complete by 700 °C, no morphological change is seen in porous carbon sheets from 700–1000 °C. After being subjected to carbonization, the thick sheets of eggplant turn into loose and thin sheets with 100–200 nm thickness, and the TEM picture displays an interlinked network of pores ranging in size from 40–60 nm. This mass loss was recognized to the decomposition of organic materials between 200 and 400 °C, while carbonization occurs at 700 °C based on the size of the exothermic peak at that temperature. At 1100 °C, the partial gasification of carbon results in the collapse of micropores, which results in some small pores (1–3 nm) becoming larger pores. Samples produced at 900 °C yield the highest SBET (950 m^2/g), mostly attributable to the presence of micropores. The XPS N1s spectrum, which also boosts conductivity and high-rate performance, revealed the N content (0.88 wt.%) as well as the presence of pyrrolic-N and quaternary-N. Thus, using eggplant as biomass and a N
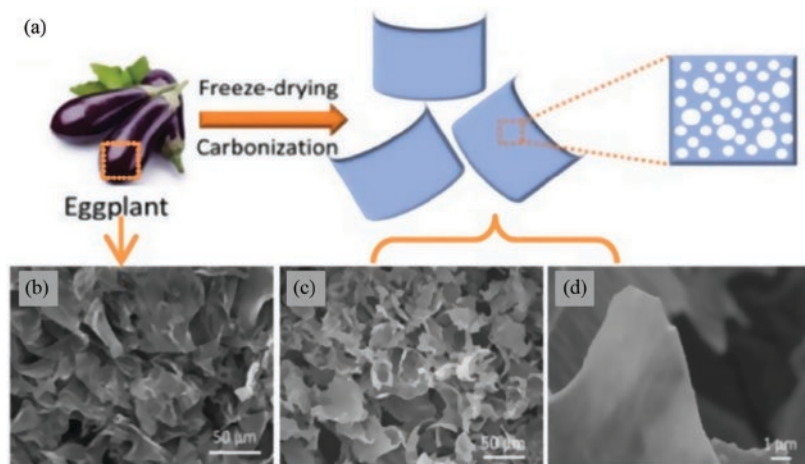
Figure 17.7 Preparation of NPC from eggplant. *Reproduced with permission* [110]. *Copyright 2015, Elsevier.*

precursor, one-step carbonization was used to create a thin carbon sheet with N-doping and porous structure. The material is gaining popularity as an electrode for SCs because of its high conductivity and low specific capacitance (121 Fg^{-1}). The latter results from the shorter path taken by ions as they diffuse through the material.

17.3.7 Clover

Fresh clover stem biomass has been used as a source of carbon and nitrogen, and a single-step carbonization procedure has been used to synthesize PCNs with a large surface area, hierarchical pore structure, and 2.55 wt.% nitrogen for use as electrodes in SCs [111]. Clover stems were heated at 80 °C (a) in air, and (b) under N_2 flow for three hours at a rate of 10 °C/min, then letting it cool naturally to room temperature, washed multiple times with HCl and water, and dried for 12 hours at 60 °C. At the same time and under the same conditions, a control sample was made without any KCl. When PCNs are made from fresh clover stems in the air using a straightforward KCl salt-sealing method, the use of pricey inert gas is avoided. The PCN has a large surface area and an interconnected, hierarchically porous (micro to macro) structure because of O traces in the molten salt. This provides enough active storage sites and routes for quick ion diffusion [111]. The air, molten KCl, and water in the clover stem all contribute to the hierarchical structure of the PCN. KCl can permeate the substructure of the precursor and mix equally when there is water present and the temperature is higher. As biomass was carbonized, its tissues changed from possessing sp3 C-X (X: C, O, and H) bonds to maintaining aromatic sp2 C-C bonds, thereby generating a carbon structural skeleton. Since the molten salt serves as a template for the transition from layer to sheet structure, it allows for forming numerous micro- and mesopores on the carbon sheets. The formation of 2D carbon sheets with meso- to micro-sized pores results from the precipitation of KCl after the temperature falls below the melting point. Though the surface area was drastically reduced when inert N_2 was used instead of air, no KCl was used, and dried clover stems are utilized in the preparation process [111].

Clover stems appear to have a multilayer structure, as seen in FESEM pictures, with thin walls serving as a prelude to the development of carbon sheets. Micropores and mesopores are both present in the 2D carbon sheets. The 2D hierarchical N-doped PCNs possessed large surface areas ($2244 \, m^2g^{-1}$), large pore volumes ($1.440 \, cm^3g^{-1}$), a large number of micro/meso pores, and many active sites, and straightforward transport pathways for rapid ion transfer. Since molten salt was essential for carbonization and pore creation, keeping the temperature below the melting point of KCl could prevent the salt from being lost as vapor. The 2.55 wt% N doping, which is in turn due to the plentiful N existing in the biomass precursor, is what caused the high pseudocapacitance, electrochemical reactivity, and conductivity of the electrode. The reversible oxidation/reduction of the O-comprising group was also credited with contributing to the material's high specific capacitance of $420 \, Fg^{-1}$. Making N-doped PCNs from biomass was a quick, cheap, and efficient process with a better specific capacitance of $420 \, Fg^{-1}$, a higher energy density of $58.4 \, Wh \, kg^{-1}$, good cycling stability, and 99.4% capacitance retention even after 30,000 cycles. The material's remarkable electrochemical performance was attributed to its large surface area, N-doping, porous sheet shape, many pores, and reversible oxidation/reduction of O-comprising functionalities.

17.3.8 Potato Waste Residue

To create NPC, Ma et al. used potato waste residue [112]. Porous carbon doped with nitrogen can be broken down into different-sized pores. Supercapacitors can be put to practical use if they meet two crucial criteria: they have a high capacitance property and are inexpensive. To create a low-cost NPC with a high specific capacitance, potato waste residue (PWR) was employed as the carbon source, melamine as the N doping agent, and $ZnCl_2$ as the activating agent. NC produced at 700 °C had a surface area of $1052 \, m^2g^{-1}$, and it was observed to have a specific capacitance of up to $255 \, Fg^{-1}$ when utilized as electrode material in 2 M KOH electrolyte. The electrode materials are also exceptionally cycleable with a 93.7% coulombic efficiency at a current density of $5 \, Ag^{-1}$ for 5000 cycles. Due to the electrode porosity, the impedance spectra exhibit a distorted semicircle at high frequencies and a linear component at low frequencies due to the diffusion-controlled doping and undoping of ions resulting from Warburg behavior (Figure 17.8b). The high-frequency intercept in the semicircle with the real axis is represented by the ohmic resistance derived from the electrolyte and the contact between the current collector and the active material. It is the result of combining the contact resistance at the interface between the active material and the current collector, the resistance of the electrolyte solution, and the resistance of the carbon material itself. The equivalent series resistance (ESR) for the N-PCs-700 was 4.2 X as a consequence, suggesting that the carbon sample had low resistance and superb electrical characteristics (Figure 17.8).

17.3.9 Albizia Plant Leaves

Mohamedkhair et al. successfully manufactured NC from *Albizia* plant leaves with and without the activating chemicals ($NaHCO_3$, $ZnCl_2$) [101]. N-doped carbon materials synthesized with water as the activating agent (WANC), $NaHCO_3$ as the activating agent (NaNC), and $ZnCl_2$ as the activating agent (ZnNC) were all given specific names. The NaNC was discovered to have a surface area that was three times more than non-activated carbon. The specific capacitance of both untreated and activated carbon was examined
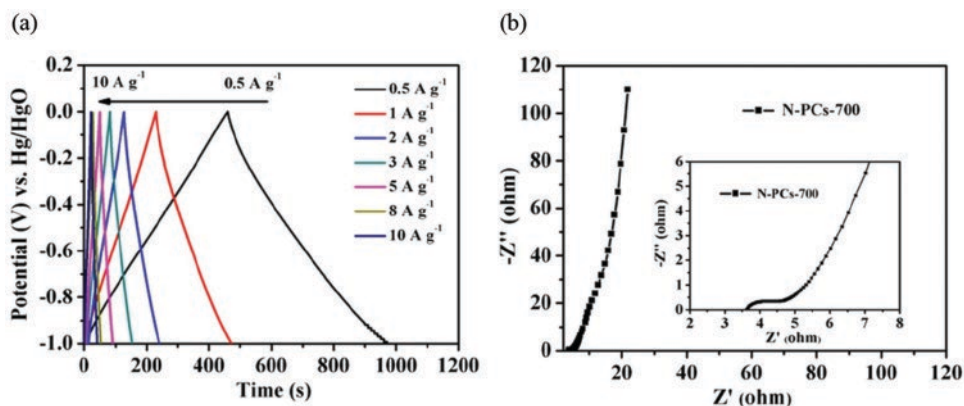
Figure 17.8 (a) GCD curves of N-PCs-700 at different current densities. (b) EIS plot for N-PCs-700 electrode. *Reproduced with permission* [112]. *Copyright 2015, Elsevier.*

using CV and GCD measurements. Because of its superior surface area, macroporosity, nitrogen concentration, and sheet-type morphology, activated carbon NaNC displayed the highest specific capacitance among the carbon samples. At an applied current density of $5\,Ag^{-1}$, NaNC has the most significant specific capacitance of any electrode, measuring $166.7\,Fg^{-1}$. The activated carbon NaNC also showed exceptional energy and power densities and extremely great charging-discharging cycle stability (97.3% held after 1000 cycles), in addition to its exceptional supercapacitance efficiency (Figure 17.9).

17.3.10 Mung Bean Flour

Zhong et al. prepared NPC from mung bean flour using calcium chloride and urea as chemical activators [113]. The surface chemistry, porosity, specific surface area, and graphitization of the NPC were significantly influenced by changing the precursor and preparation temperatures. The optimal sample was prepared at 800 °C using a mixture of mung
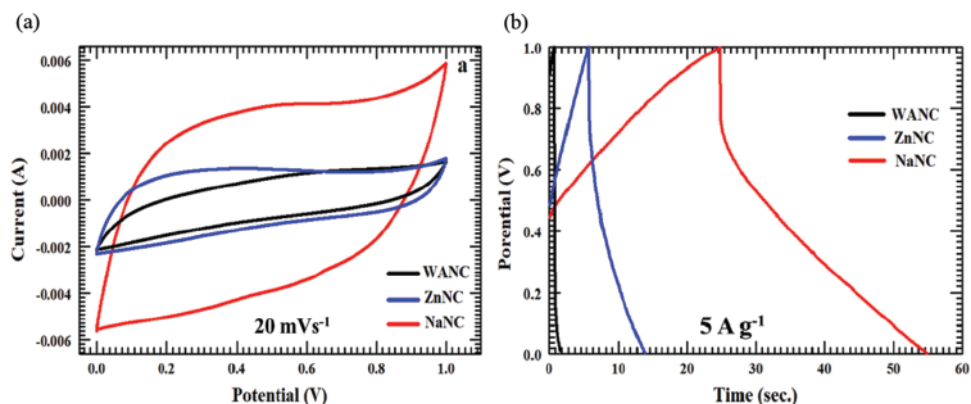
Figure 17.9 (a) CV of WANC, ZnNC, and NaNC at 20 mVs^{-1} scan rate. (b) GCD curves at a current density of 5 Ag^{-1} of WANC, ZnNC, and NaNC. *Reproduced with permission* [101]. *Copyright 2020, Elsevier.*

bean flour, urea, and $CaCl_2$. It displayed a remarkable specific capacitance of 247.2 Fg^{-1} at 2 mVs^{-1} and 300.5 Fg^{-1} at 1 Ag^{-1}. It also displayed excellent rate performance of 178.6 Fg^{-1} at 200 and 225 Fg^{-1} at 100 Ag^{-1} and good durability of 93.2 and 97.5% capacitance retention after 10000 cyclic voltammetric measurements and 2000 galvanostatic charge/discharge cycles, respectively. The structure-performance connections show that the high carbonation, abundant doped-N, and abundant porosities in this sample are what contribute to its good specific capacitance.

17.3.11 Orange Peel

Ahmed et al. described research on N-doped activated carbon (NAC) using leftover orange peel as a carbon source, KOH as an activating agent, and melamine as a N dopant [114]. The produced NAC materials offered a high surface area (1577 m^2g^{-1}), pore volume (0.87 cm^3g^{-1}), and have porous structure. Such beneficial characteristics of NAC show that it is a good electrode for supercapacitors. Utilizing conventional electrochemical techniques, the NAC material's electrochemical performance in a 6 M KOH solution was assessed. At a current load of 0.7 Ag-1, the synthesized NAC exhibited high specific capacitance (168 Fg^{-1}), specific power (2334.3 Wkg^{-1}), and specific energy (23.3 $Wh kg^{-1}$). The increased surface area and accessibility of N functionalities in the NAC are likely the causes of its superior electrochemical performance. Thus, NAC is a prospective electrode material for supercapacitors due to its porous structure and nitrogen-doping properties (Figure 17.10).

17.3.12 Eucalyptus Tree Leaves

Mondal et al. prepared NPC nanosheets by simply mixing the *Eucalyptus* leaves powder with $KHCO_3$ and subsequent carbonization [115]. NPC nanosheets were produced and used as electrode materials for supercapacitors and lithium-ion batteries, with a superior specific surface area of 2133 m^2/g. The NPC nanosheet electrode demonstrated excellent
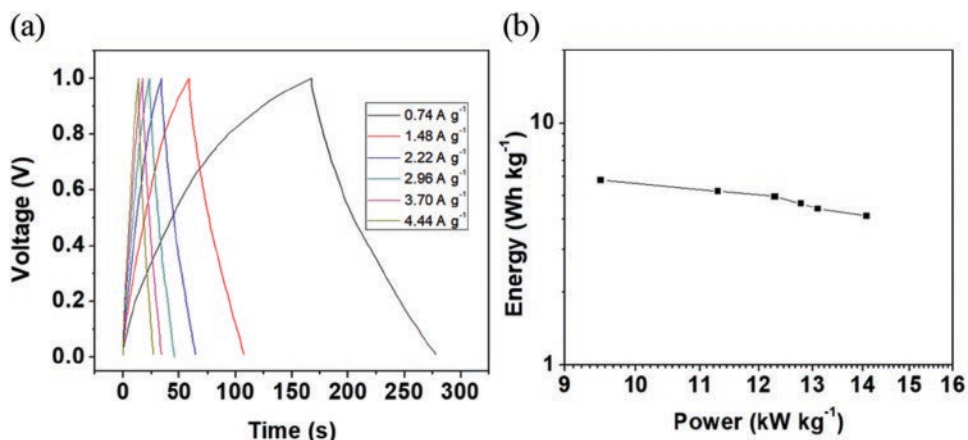
Figure 17.10 (a) GCD plots of prepared electrodes of current load at a constant potential. (b) Ragone plot for the prepared electrode. *Reproduced with permission* [114]. *Reproduced under the term CC-BY 3.0. Copyright 2018, Ahmed et al.*

cycling stability over 15000 cycles and a supercapacitance of 372 Fg^{-1} at 500 mAg^{-1} current density in aqueous electrolyte for supercapacitor applications. The nanosheet electrode exhibited sustained cycling performance and a specific capacitance of 71 Fg^{-1} in organic electrolytes. The prepared NPC nanosheets showed a high specific capacity, good rate capability, and stable cycling performance when employed as the anode material for lithium-ion batteries. The enormous specific surface area, N doping effects, and porous nanosheet structure are responsible for the astonishing electrochemical performances in lithium-ion batteries and supercapacitors. The method offers a new way to use biomass-derived materials for affordable energy storage systems.

17.3.13 Waste Shrimp Shells

Mondal et al. describe NPC from waste shrimp shells and its use in two different energy storage systems [116]. It is an auspicious material for both supercapacitors and lithium-ion batteries due to its distinctive porosity structure and the existence of heteroatoms (N, O). The manufactured porous carbon-based supercapacitors have a specific capacitance of 239 Fg^{-1} at 0.5 Ag^{-1} current density in a 6 M KOH electrolyte. Despite 5000 charge-discharge cycles, the specific capacitance retention remains 99.4%, indicating exceptional cycling stability. The high specific surface area, porous structure, and N doping impact could be responsible for the improved electrochemical performances for energy storage (Figure 17.11).

17.3.14 Waste Particleboard

By chemically activating waste particleboard with KOH in a variable ratio, Shang et al. were able to create NAC from waste particleboard [117]. The weight ratio of KOH/carbonization considerably impacts the NAC's porosity and N content. The specific surface area rises from 1498 to 1826 m2g-1 when the weight ratio of KOH/carbonization goes from two to five, although the N concentration falls from 2.86 to 1.32 wt.%. This NAC
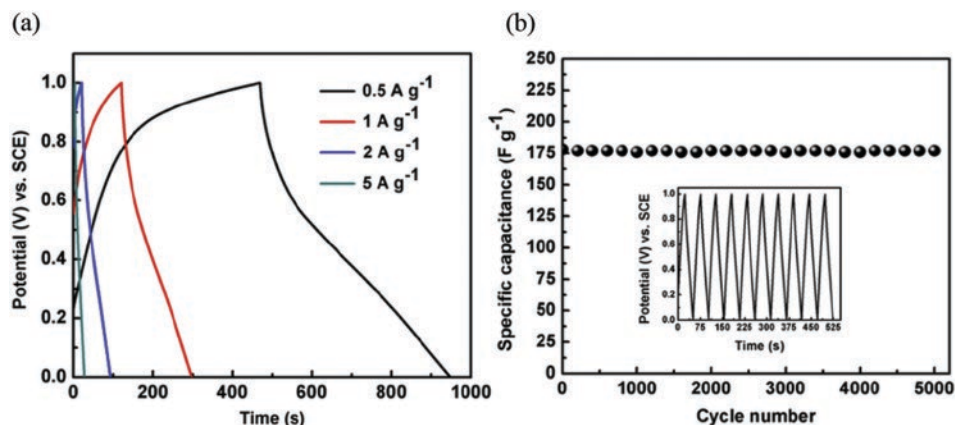
Figure 17.11 (a) Plots of the GCD at various current densities for the prepared electrode. (b) Cycle life at 1 A g^{-1} current density; inset, GCD for the first 10 cycles at 2 A g^{-1} current density. *Reproduced with permission* [116]. *Copyright 2017, Elsevier.*

was evaluated as an electrode material in a two-electrode symmetric supercapacitor device with a 7 M KOH electrolyte. They were shown to have superior specific capacitance, great retention, and long-term functioning at high current densities. The NAC with the greatest specific capacitance, 263 F g^{-1} at 0.05 A g^{-1}, was discovered to have been produced with a modest KOH/carbonization weight ratio of three. Double-layer capacitance and pseudocapacitance both contributed to the specific capacitance of this carbon. The nitrogen concentration (2.38 wt.%) and specific surface area (1758 m^2 g^{-1}) of this carbon are both balanced. It also showed outstanding rate capability (228 F g^{-1} at 10 A g^{-1}) and cycling stability (over 95% capacitance retention over 3000 cycles). This made it a favorable electrode material for supercapacitors.

17.3.15 *Broussonetia papyrifera*

Wei et al. synthesized NPC materials utilizing the stem bark of *Broussonetia papyrifera* (BP) as the biomass precursor via a facile approach [118]. First, a KOH solution based on the water was used to treat the BP stem bark hydrothermally. The hydrothermal product was dried and filtered, then immediately exposed to simultaneous pyrolysis and activation, producing NPC materials. The obtained NPC exhibited a superior surface area of 1212 m^2 g^{-1} and an average pore size of 3.8 nm. Due to the synergistic impact of O, N-doped species, this porous carbon exhibits exceptional capacitance performance (320 Fg^{-1} at 0.5 Ag^{-1}), decent rate capacitive performance, and superb cycling stability, suggesting a great potential for supercapacitors (Figure 17.12).

17.3.16 Almond

The protein-rich bitter almond can serve as a source for in-situ N-doping due to its 5% amygdalin component that contains nitrogen [119]. Almonds are natural products. The almonds were soaked in water overnight, and the next day the milk was made by combining ground almonds with polymethyl methacrylate (PMMA) and KOH and heating the mixture to 80 °C while stirring. The samples contain a 100 nm thick-walled macroporous structure resembling a 3D honeycomb. The honeycomb was produced from a carbon sheet with a curled edge. The synergistic impact between KOH and PMMA was vital to morphological development. In-situ KOH activation may contribute to the high surface area (1877.8 m^2), pore volume (0.67), and mean pore size (0.5–2.0 nm) of the sample prepared at 800 °C, which contains 80% micropores. The N is derived from the protein in almonds, and the 1% N in the sample was predominantly made up of pyridinic-N (44.7%), pyrrolic-N (23.7%), and graphitic-N (12.7%) species. Pseudocapacitance comes from pyridinic-N and pyrrolic-N, while higher electrical conductivity comes
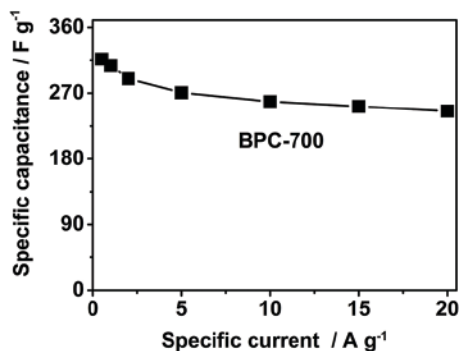
Figure 17.12 The GC curves of the electrode created from *Broussonetia papyrifera* at 0.5–20 Ag^{-1}. *Reproduced with permission* [118]. *Copyright 2015, Elsevier.*

from graphitic-N. Having a good specific capacitance of 228 Fg^{-1} and outstanding rate execution, carbon benefits from oxygen groups at its surface that increase its wettability. Numerous other biomass sources have also been used to create carbon nanosheets, such as amaranth [120], soybean milk [121], corn stalk [122], silkworm [123], starch [124], pistachio nutshells [125], gelatin [126], dried elm samara [127], okara [128], and pine nutshells [129].

17.4   Conclusion

We discussed the most recent research on the synthesis of NPCs resulting from various biomass materials, as well as their N-doping via traditional (using NH_3 and urea as N-precursors) and green (consuming the same biomass as C and N-precursors) approaches for energy technologies, particularly as electrodes in supercapacitors. Environmentally unfriendly practices are used for synthesizing NPCs, including the use of harsh chemicals and a template. An emerging green technique that is being used for the synthesis of NPCs is the usage of biomass (waste/residue/byproduct) as a C precursor and an N precursor. Because of their high surface area, layered structure, large aspect ratio, and good stability, two-dimensional (2D) porous carbon nanomaterials (PCN) are advantageous for electrochemical applications, as is their 2D geometry, which is compatible with the design of ultrathin electrodes for use in miniature energy devices. Since the shape, pore size distribution, porosity, and chemical composition of 2D N-doped PCNs determine their attributes, the porosity may be easily regulated during synthesis to achieve the maximum electrocatalytic activity. Pore size distribution and surface area may also be improved during carbonization and activation. To conclude, with the right kind of biomass and an easy synthesis procedure, PCNs with the desired porosity might be created. While other heteroatoms are useful, N is by far the most prevalent and widely used and modulating the electrochemical characteristics of PCNs for use in a broad range of energy applications frequently involves the introduction of heteroatoms into the carbon matrix, where they play an essential role. The self-doped green technique is an environmentally preferable method of N-doping since it uses the same biomass for both the C and N (or heteroatom) precursors. Therefore, the energy crisis, environmental pollution, and global warming could all be helped by synthesizing NPCs using a green approach for energy applications.

Acknowledgment

References

1 F. Barzegar, A. Bello, D. Momodu, M. J. Madito, J. Dangbegnon, N. Manyala, *J. Power Sources* **2016**, *309*, 245–253.

2 Y. Lei, M. Gan, L. Ma, M. Jin, X. Zhang, G. Fu, P. Yang, M. Yan, *Ceram. Int.* **2017**, *43*, 6502–6510.

3 W. Qiao, S.-H. Yoon, I. Mochida, *Energy Fuel* **2006**, *20*, 1680–1684.

4 B. M. Matsagar, R.-X. Yang, S. Dutta, Y. S. Ok, K. C. W. Wu, *J. Mater. Chem. A.* **2021**, *9*, 3703–3728.

5 E. Gul, G. Rahman, Y. Wu, T. H. Bokhari, A. u. Rahman, A. Zafar, Z. Rana, A. Shah, S. Hussain, K. Maaz, S. Karim, S. Javaid, H. Sun, M. Ahmad, G. Xiang, A. Nisar, *New J. Chem.* **2022**, *46*, 16280–16288.

6 S. Gu, X. Kang, L. Wang, E. Lichtfouse, C. Wang, *Environ. Chem. Lett.* **2019**, *17*, 629–654.

7 R.-Z. Wang, D.-L. Huang, Y.-G. Liu, C. Zhang, C. Lai, X. Wang, G.-M. Zeng, X.-M. Gong, A. Duan, Q. Zhang, *Chem. Eng. J.* **2019**, *371*, 380–403.

8 L. Chen, F. Li, Y. Wei, G. Li, K. Shen, H.-J. He, *Environ. Chem. Lett.* **2019**, *17*, 589–594.

9 C. Sassoye, C. Laberty, H. Le Khanh, S. Cassaignon, C. Boissiere, M. Antonietti, C. Sanchez, *Adv. Funct. Mater.* **2009**, *19*, 1922–1929.

10 V. Augustyn, P. Simon, B. Dunn, *Energy Environ. Sci.* **2014**, *7*, 1597–1614.

11 Y. Wang, H. Xuan, G. Lin, F. Wang, Z. Chen, X. Dong, *J. Power Sources* **2016**, *319*, 262–270.

12 H. Peng, G. Ma, K. Sun, Z. Zhang, Q. Yang, F. Ran, Z. Lei, *J. Mater. Chem. A* **2015**, *3*, 13210–13214.

13 J. Wang, P. Nie, B. Ding, S. Dong, X. Hao, H. Dou, X. Zhang, *J. Mater. Chem. A* **2017**, *5*, 2411–2428.

14 S. Kassaye, K. K. Pant, S. Jain, *Fuel Process. Technol.* **2016**, *148*, 289–294.

15 Y. Ma, W. Tan, J. Wang, J. Xu, K. Wang, J. Jiang, *J. Bioresour. Bioprod.* **2020**, *5*, 114–123.

16 X. Chen, J. Zhang, B. Zhang, S. Dong, X. Guo, X. Mu, B. Fei, *Sci. Rep.* **2017**, *7*, 1–11.

17 -M.-M. Titirici, R. J. White, N. Brun, V. L. Budarin, D. S. Su, F. del Monte, J. H. Clark, M. J. MacLachlan, *Chem. Soc. Rev.* **2015**, *44*, 250–290.

18 R. Saidur, E. A. Abdelaziz, A. Demirbas, M. S. Hossain, S. Mekhilef, *Renew. Sust. Energ. Rev.* **2011**, *15*, 2262–2289.

19 Z. Bi, Q. Kong, Y. Cao, G. Sun, F. Su, X. Wei, X. Li, A. Ahmad, L. Xie, C.-M. Chen, *J. Mater. Chem. A* **2019**, *7*, 16028–16045.

20 B. M. Matsagar, T.-C. Kang, Z.-Y. Wang, T. Yoshikawa, Y. Nakasaka, T. Masuda, L.-C. Chuang, K. C.-W. Wu, *React. Chem. Eng.* **2019**, *4*, 618–626.

21 J. Niu, J. Guan, M. Dou, Z. Zhang, J. Kong, F. Wang, *ACS Appl. Energy Mater.* **2020**, *3*, 2478–2489.

22 M. Ashraf, I. Khan, M. Usman, A. Khan, S. S. Shah, A. Z. Khan, K. Saeed, M. Yaseen, M. F. Ehsan, M. N. Tahir, N. Ullah, *Chem. Res. Toxicol.* **2020**, *33*, 1292–1311.

23 S. S. Shah, M. A. Aziz, *Bangladesh J. Plant Taxon.* **2020**, *27*, 467–478.

24 S. S. Shah, M. A. Aziz, M. Oyama, A.-R. F. Al-Betar, *Chem. Rec.* **2021**, *21*, 204–238.

25 S. S. Shah, M. A. Aziz, Z. H. Yamani, *Chem. Rec.* **2022**, *22*, e202200018.

26 S. S. Shah, S. M. A. Nayem, N. Sultana, A. J. S. Ahammad, M. A. Aziz, *ChemSusChem* **2022**, *15*, e202101282.

27 S. S. Shah, M. N. Shaikh, M. Y. Khan, M. A. Alfasane, M. M. Rahman, M. A. Aziz, *Chem. Rec.* **2021**, *21*, 1631–1665.

28 M. Usman, M. Humayun, S. S. Shah, H. Ullah, A. A. Tahir, A. Khan, H. Ullah, *Energies* **2021**, *14*, 2281.

29 M. Yaseen, M. A. K. Khattak, M. Humayun, M. Usman, S. S. Shah, S. Bibi, B. S. U. Hasnain, S. M. Ahmad, A. Khan, N. Shah, A. A. Tahir, H. Ullah, *Energies* **2021**, *14*, 7779.

30 L. Yan, J. Yu, J. Houston, N. Flores, H. Luo, *Green Energy Environ.* **2017**, *2*, 84–99.

31 S.-I. Fujita, H. Yoshida, M. Arai, *C* **2017**, *3*, 31.

32 Q. Lv, W. Si, J. He, L. Sun, C. Zhang, N. Wang, Z. Yang, X. Li, X. Wang, W. Deng, *Nat. Commun.* **2018**, *9*, 1–11.

33 K. Gong, F. Du, Z. Xia, M. Durstock, L. Dai, *Science* **2009**, *323*, 760–764.

34 J. Zhang, Z. Zhao, Z. Xia, L. Dai, *Nat. Nanotechnol.* **2015**, *10*, 444–452.

35 D. Guo, R. Shibuya, C. Akiba, S. Saji, T. Kondo, J. Nakamura, *Science* **2016**, *351*, 361–365.

36 K. Sakaushi, A. Lyalin, S. Tominaka, T. Taketsugu, K. Uosaki, *ACS Nano* **2017**, *11*, 1770–1779.

37 K. Jurewicz, K. Babeł, A. Ziółkowski, H. Wachowska, M. Kozłowski, *Fuel Process. Technol.* **2002**, *77*, 191–198.

38 K. Jurewicz, K. Babeł, A. Źiółkowski, H. Wachowska, *Electrochim. Acta.* **2003**, *48*, 1491–1498.

39 K. Jurewicz, C. Vix-Guterl, E. Frackowiak, S. Saadallah, M. Reda, J. Parmentier, J. Patarin, F. Béguin, *J. Phys. Chem. Solids* **2004**, *65*, 287–293.

40 N. Daems, X. Sheng, I. F. Vankelecom, P. P. Pescarmona, *J. Mater. Chem. A* **2014**, *2*, 4085–4110.

41 H. Wang, T. Maiyalagan, X. Wang, *ACS Catal.* **2012**, *2*, 781–794.

42 D. Yu, E. Nagelli, F. Du, L. Dai, *J. Phys. Chem. Lett.* **2010**, *1*, 2165–2173.

43 S. Barton, M. Evans, E. Halliop, J. MacDonald, *Carbon* **1997**, *35*, 1361–1366.

44 Z. Li, L. Zhang, B. S. Amirkhiz, X. Tan, Z. Xu, H. Wang, B. C. Olsen, C. M. Holt, D. Mitlin, *Adv. Energy Mater.* **2012**, *2*, 431–437.

45 L. Yu, C. Falco, J. Weber, R. J. White, J. Y. Howe, -M.-M. Titirici, *Langmuir* **2012**, *28*, 12373–12383.

46 M. Sevilla, A. B. Fuertes, *Mater. Chem. Phys.* **2009**, *113*, 208–214.

47 L. Zhao, N. Baccile, S. Gross, Y. Zhang, W. Wei, Y. Sun, M. Antonietti, -M.-M. Titirici, *Carbon* **2010**, *48*, 3778–3787.

48 P. Chen, L.-K. Wang, G. Wang, M.-R. Gao, J. Ge, W.-J. Yuan, Y.-H. Shen, A.-J. Xie, S.-H. Yu, *Energy Environ. Sci.* **2014**, *7*, 4095–4103.

49 S. S. Sekhon, J.-S. Park, *Chem. Eng. J.* **2021**, *425*, 129017.

50 S. N. A. Shah, X. Dou, M. Khan, K. Uchiyama, J.-M. Lin, *Talanta* **2019**, *196*, 370–375.

51 S. N. A. Shah, H. Li, J.-M. Lin, *Talanta* **2016**, *153*, 23–30.

52 S. N. A. Shah, J.-M. Lin, *Adv. Colloid Interface Sci.* **2017**, *241*, 24–36.

53 S. N. A. Shah, L. Lin, Y. Zheng, D. Zhang, J.-M. Lin, *Phys. Chem. Chem. Phys.* **2017**, *19*, 21604–21611.

54 Y. Zheng, D. Zhang, S. N. A. Shah, H. Li, J.-M. Lin, *Chem. Commun.* **2017**, *53*, 5657–5660.

55 D.-W. Lee, M.-H. Jin, J.-H. Park, Y.-J. Lee, Y.-C. Choi, *ACS Sustain. Chem. Eng.* **2018**, *6*, 10454–10462.

56 L. Fangyan, W. Zixing, Z. Haitao, J. Long, C. Xiang, G. Bingni, H. Haichao, Y. Weiqing, *Carbon* **2019**, *149*, 105–116.

57 W. Liu, J. Mei, G. Liu, Q. Kou, T. Yi, S. Xiao, *ACS Sustain. Chem. Eng.* **2018**, *6*, 11595–11605.

58 L.-T. Song, Z.-Y. Wu, H.-W. Liang, F. Zhou, Z.-Y. Yu, L. Xu, Z. Pan, S.-H. Yu, *Nano Energy* **2016**, *19*, 117–127.

59 R. Liu, H. Zhang, S. Liu, X. Zhang, T. Wu, X. Ge, Y. Zang, H. Zhao, G. Wang, *Phys. Chem. Chem. Phys.* **2016**, *18*, 4095–4101.

60 H. Lu, X. S. Zhao, *Sustain. Energy Fuels* **2017**, *1*, 1265–1281.

61 D. Lozano-Castello, J. Calo, D. Cazorla-Amorós, A. Linares-Solano, *Carbon* **2007**, *45*, 2529–2536.

62 X. Fan, L. Zhang, G. Zhang, Z. Shu, J. Shi, *Carbon* **2013**, *61*, 423–430.

63 J. Wang, S. Kaskel, *J. Mater. Chem.* **2012**, *22*, 23710–23725.

64 M. Molina-Sabio, F. Rodrıguez-Reinoso, *Colloids Surf. A Physicochem. Eng. Asp.* **2004**, *241*, 15–25.

65 C. Guan, K. Wang, C. Yang, X. Zhao, *Microporous Mesoporous Mater* **2009**, *118*, 503–507.

66 M. J. Bleda-Martínez, J. A. Maciá-Agulló, D. Lozano-Castelló, E. Morallon, D. Cazorla-Amorós, A. Linares-Solano, *Carbon* **2005**, *43*, 2677–2684.

67 M. Sevilla, R. Mokaya, *Energy Environ. Sci.* **2014**, *7*, 1250–1280.

68 A. S. Marriott, A. J. Hunt, E. Bergström, J. Thomas-Oates, J. H. Clark, *J. Anal. Appl. Pyrolysis* **2016**, *121*, 62–66.

69 W. Suliman, J. B. Harsh, N. I. Abu-Lail, A.-M. Fortuna, I. Dallmeyer, M. Garcia-Perez, *Biomass Bioenerg.* **2016**, *84*, 37–48.

70 F. Suárez-Garcıa, A. Martınez-Alonso, J. D. Tascón, *J. Anal. Appl. Pyrolysis* **2002**, *63*, 283–301.

71 P. Eletskii, V. Yakovlev, V. Fenelonov, V. Parmon, *Kinet. Catal.* **2008**, *49*, 708–719.

72 M. Sevilla, A. B. Fuertes, R. Mokaya, *Energy Environ. Sci.* **2011**, *4*, 1400–1410.

73 J. C. Moreno-Piraján, L. Giraldo, *J. Anal. Appl. Pyrolysis* **2010**, *87*, 288–290.

74 G. Ferrero, A. Fuertes, M. Sevilla, *Sci. Rep.* **2015**, *5*, 1–13.

75 M. Rana, K. Subramani, M. Sathish, U. K. Gautam, *Carbon* **2017**, *114*, 679–689.

76 L. Qu, Y. Liu, J.-B. Baek, L. Dai, *ACS Nano* **2010**, *4*, 1321–1326.

77 Y.-F. Lu, S.-T. Lo, J.-C. Lin, W. Zhang, J.-Y. Lu, F.-H. Liu, C.-M. Tseng, Y.-H. Lee, C.-T. Liang, L.-J. Li, *ACS Nano* **2013**, *7*, 6522–6532.

78 V. B. Parambhath, R. Nagar, S. Ramaprabhu, *Langmuir* **2012**, *28*, 7826–7833.

79 M. Rauf, S. S. Shah, S. K. Shah, S. N. A. Shah, T. U. Haq, J. Shah, A. Ullah, T. Ahmad, Y. Khan, M. A. Aziz, K. Hayat, *J. Saudi Chem. Soc.* **2022**, *26*, 101514.

80 Y. Zhu, M. Chen, W. Zhao, C. Wang, *Carbon* **2018**, *140*, 404–412.

81 Z. Ling, Z. Wang, M. Zhang, C. Yu, G. Wang, Y. Dong, S. Liu, Y. Wang, J. Qiu, *Adv. Funct. Mater.* **2016**, *26*, 111–119.

82 W. Qian, F. Sun, Y. Xu, L. Qiu, C. Liu, S. Wang, F. Yan, *Energy Environ. Sci.* **2014**, *7*, 379–386.

83 R. Shao, J. Niu, J. Liang, M. Liu, Z. Zhang, M. Dou, Y. Huang, F. Wang, *ACS Appl. Mater. Interfaces* **2017**, *9*, 42797–42805.

84 J. Cai, H. Niu, H. Wang, H. Shao, J. Fang, J. He, H. Xiong, C. Ma, T. Lin, *J. Power Sources* **2016**, *324*, 302–308.

85 Y. Liu, J. Chen, B. Cui, P. Yin, C. Zhang, *C* **2018**, *4*, 53.

86 Z. Gao, Y. Zhang, N. Song, X. Li, *Mater. Res. Lett.* **2017**, *5*, 69–88.

87 Y. Li, G. Wang, T. Wei, Z. Fan, P. Yan, *Nano Energy* **2016**, *19*, 165–175.

88 N. J. Vickers, *Curr. Biol.* **2017**, *27*, R713–R715.

89 J. Hou, C. Cao, F. Idrees, X. Ma, *ACS Nano* **2015**, *9*, 2556–2564.

90 X. Zhang, Q. Fan, N. Qu, H. Yang, M. Wang, A. Liu, J. Yang, *Nanoscale* **2019**, *11*, 8588–8596.

91 K. Zou, Y. Deng, J. Chen, Y. Qian, Y. Yang, Y. Li, G. Chen, *J. Power Sources* **2018**, *378*, 579–588.

92 V. Veeramani, G. Raghavi, S.-M. Chen, R. Madhu, M. Sivakumar, D. Tashima, C.-T. Hung, S.-B. Liu, *Nano Express* **2020**, *1*, 010036.

93 H. Wang, D. Mitlin, J. Ding, Z. Li, K. Cui, *J. Mater. Chem. A* **2016**, *4*, 5149–5158.

94 Y. Wang, R. Yang, Y. Wei, Z. Zhao, M. Li, *RSC Adv.* **2014**, *4*, 45318–45324.

95 M. Ashraf, S. S. Shah, I. Khan, M. A. Aziz, N. Ullah, M. Khan, S. F. Adil, Z. Liaqat, M. Usman, W. Tremel, M. N. Tahir, *Chem. Eur. J.* **2021**, *27*, 6973–6984.

96 M. A. Aziz, S. S. Shah, S. M. A. Nayem, M. N. Shaikh, A. S. Hakeem, I. A. Bakare, *J. Energy Storage* **2022**, *50*, 104278.

97 N. C. Deb Nath, S. S. Shah, M. A. A. Qasem, M. H. Zahir, M. A. Aziz, *Chem. Select* **2019**, *4*, 9079–9083.

98 M. M. Hasan, T. Islam, S. S. Shah, A. Awal, M. A. Aziz, A. J. S. Ahammad, *Chem. Rec.* **2022**, *22*, e202200041.

99 S. Islam, M. M. Mia, S. S. Shah, S. Naher, M. N. Shaikh, M. A. Aziz, A. J. S. Ahammad, *Chem. Rec.* **2022**, *22*, e202200013.

100 T. Islam, M. M. Hasan, S. S. Shah, M. R. Karim, F. S. Al-Mubaddel, M. H. Zahir, M. A. Dar, M. D. Hossain, M. A. Aziz, A. J. S. Ahammad, *J. Energy Storage* **2020**, *32*, 101908.

101 A. K. Mohamedkhair, M. A. Aziz, S. S. Shah, M. N. Shaikh, A. K. Jamil, M. A. A. Qasem, I. A. Buliyaminu, Z. H. Yamani, *Arab. J. Chem.* **2020**, *13*, 6161–6173.

102 C. K. Roy, S. S. Shah, A. H. Reaz, S. Sultana, A.-N. Chowdhury, S. H. Firoz, M. H. Zahir, M. A. A. Qasem, M. A. Aziz, *Chem. Asian J.* **2021**, *16*, 296–308.

103 S. S. Shah, M. A. Alfasane, I. A. Bakare, M. A. Aziz, Z. H. Yamani, *J. Energy Storage* **2020**, *30*, 101562.

104 S. S. Shah, M. A. Aziz, A.-R. Al-Betar, W. Mahfoz, *Arab. J. Chem.* **2022**, *15*, 104058.

105 S. S. Shah, M. A. Aziz, E. Cevik, M. Ali, S. T. Gunday, A. Bozkurt, Z. H. Yamani, *J. Energy Storage* **2022**, *56*, 105944.

106 S. S. Shah, M. A. Aziz, W. Mahfoz, A.-R. Al-Betar, Conducting Polymers Based Nanocomposites for Supercapacitors in *Nanostructured Materials for Supercapacitors*, (Eds.: S. Thomas, A. B. Gueye, R. K. Gupta), Springer, Cham, **2022**, Chapter 22, pp. 485–511, Vol. *1*.

107 S. S. Shah, E. Cevik, M. A. Aziz, T. F. Qahtan, A. Bozkurt, Z. H. Yamani, *Synth. Met.* **2021**, *277*, 116765.

108 S. S. Shah, H. T. Das, H. R. Barai, M. A. Aziz, *Polymers* **2022**, *14*, 270.

109 R. Shakil, M. N. Shaikh, S. S. Shah, A. H. Reaz, C. K. Roy, A.-N. Chowdhury, M. A. Aziz, *Asian J. Org. Chem.* **2021**, *10*, 2220–2230.

110 Z. Li, W. Lv, C. Zhang, B. Li, F. Kang, Q.-H. Yang, *Carbon* **2015**, *92*, 11–14.

111 C. Wang, D. Wu, H. Wang, Z. Gao, F. Xu, K. Jiang, *J. Power Sources* **2017**, *363*, 375–383.

112 G. Ma, Q. Yang, K. Sun, H. Peng, F. Ran, X. Zhao, Z. Lei, *Bioresour. Technol.* **2015**, *197*, 137–142.

113 G. Zhong, H. Xie, Z. Xu, S. Xu, S. Xu, Z. Cai, X. Fu, W. Liao, R. Miao, *Chem. Select* **2019**, *4*, 3432–3439.

114 S. Ahmed, M. Rafat, A. Ahmed, *Adv. Nat. Sci: Nanosci. Nanotechnol.* **2018**, *9*, 035008.

115 A. K. Mondal, K. Kretschmer, Y. Zhao, H. Liu, C. Wang, B. Sun, G. Wang, *Chem. Eur. J.* **2017**, *23*, 3683–3690.

116 A. K. Mondal, K. Kretschmer, Y. Zhao, H. Liu, H. Fan, G. Wang, *Microporous Mesoporous Mater.* **2017**, *246*, 72–80.

117 T. Shang, J. Zhang, F. Fan, X. Jin, *RSC Adv.* **2015**, *5*, 50843–50850.

118 T. Wei, X. Wei, Y. Gao, H. Li, *Electrochim. Acta* **2015**, *169*, 186–194.

119 F. Zeng, Z. Li, X. Li, J. Wang, Z. Kong, Y. Sun, Z. Liu, H. Feng, *Appl. Surf. Sci.* **2019**, *467*, 229–235.

120 S. Gao, K. Geng, H. Liu, X. Wei, M. Zhang, P. Wang, J. Wang, *Energy Environ. Sci.* **2015**, *8*, 221–229.

121 M. Chen, D. Yu, X. Zheng, X. Dong, *J. Energy Storage* **2019**, *21*, 105–112.

122 L. Wang, G. Mu, C. Tian, L. Sun, W. Zhou, P. Yu, J. Yin, H. Fu, *ChemSusChem* **2013**, *6*, 880–889.

123 S. Lei, L. Chen, W. Zhou, P. Deng, Y. Liu, L. Fei, W. Lu, Y. Xiao, B. Cheng, *J. Power Sources* **2018**, *379*, 74–83.

124 T. Wu, G. Wang, Q. Dong, F. Zhan, X. Zhang, S. Li, H. Qiao, J. Qiu, *Environ. Sci. Technol.* **2017**, *51*, 9244–9251.

125 J. Xu, Q. Gao, Y. Zhang, Y. Tan, W. Tian, L. Zhu, L. Jiang, *Sci. Rep.* **2014**, *4*, 5545.

126 H. Fan, W. Shen, *ACS Sustain. Chem. Eng.* **2016**, *4*, 1328–1337.

127 C. Chen, D. Yu, G. Zhao, B. Du, W. Tang, L. Sun, Y. Sun, F. Besenbacher, M. Yu, *Nano Energy* **2016**, *27*, 377–389.

128 T. Yang, T. Qian, M. Wang, X. Shen, N. Xu, Z. Sun, C. Yan, *Adv. Mater.* **2016**, *28*, 539–545.

129 L. Guan, L. Pan, T. Peng, C. Gao, W. Zhao, Z. Yang, H. Hu, M. Wu, *ACS Sustain. Chem. Eng.* **2019**, *7*, 8405–8412.

18

Biomass Based S-doped Carbon for Supercapacitor Application

S. M. Abu Nayem[1], Santa Islam[1], Syed Shaheen Shah[2,3], Nasrin Sultana[1], Wael Mahfoz[4], A. J. Saleh Ahammad[1,*], and Md. Abdul Aziz[2,5,*]

[1] Department of Chemistry, Jagannath University, Dhaka 1100, Bangladesh
[2] Interdisciplinary Research Center for Hydrogen and Energy Storage (IRC-HES), King Fahd University of Petroleum & Minerals, Dhahran 31261, Saudi Arabia
[3] Physics Department, King Fahd University of Petroleum & Minerals, KFUPM Box 5047, Dhahran 31261, Saudi Arabia
[4] Chemistry Department, King Fahd University of Petroleum and Minerals, Dhahran 31261, Saudi Arabia
[5] K. A. CARE Energy Research and Innovation Center, King Fahd University of Petroleum & Minerals, Dhahran, 31261, Saudi Arabia
* Corresponding authors

18.1   Introduction

With an increasing population and a fast-growing economy, global energy consumption has reached an alarming level, threatening the sustainability of living standards. This is due to the rapid depletion of fossil fuels (coal, oil, and gas) and also causing smog and haze, severe environmental pollution, and global warming, which in turn affects the health of everyone [1–4]. In response to these problems, tremendous efforts have been devoted to reducing fossil fuel consumption and providing a clean and sustainable energy supply with a convenient energy storage system worldwide [5, 6]. The widely accepted energy storage system, such as batteries, can not fulfill the demand of both high power and energy density application. However, supercapacitors offer the virtues of wide functional temperature ranges, more energy per unit mass/volume, remarkable power density, fast charging and discharging rate, extended service life, and minimal pollution compared to other energy storage technologies [7–9]. Mostly, the cost of the electrode materials decides the ultimate cost of a supercapacitor; hence, developing cost-effective and high-performance electrode materials is critical [10–12]. Because of its low cost, tunable surface features, high Coulombic efficiency, broad working temperature, porous design, and outstanding mechanical strength, carbon-based electrode material has been dubbed "the most used electrode materials for supercapacitors" in the literature [13–16].

Biomass is one of the most renewable carbon sources on the planet, with greater advantages compared to other materials, such as low cost, unique structure, environmental friendliness, and compatibility. It is widely used in supercapacitor electrode materials and sensors, water treatment, dye-sensitized solar cells, and other applications [6, 17–19]. Supercapacitors constructed of carbon material typically use the electrical chemical double-layer (ECDL)

capacitance approach. As a result, there is a loss in specific capacitance, a lack of energy density, and a constrained power supply [20, 21]. To achieve great capacitive performance, the pure carbon material should be changed to boost the energy density. Enlarging the working potential window or raising the specific capacitance value can both help to enhance energy density [22, 23]. One of the most recent areas of focus has been the development of pseudocapacitive electrode materials. Heteroatom doping is one of the most successful techniques for increasing the specific capacitance of the electrode material, which is based on the principle of fast-redox reactions at electrode surface areas or inside nanodomains, [12, 23]. Different heteroatoms such as oxygen (O), nitrogen (N), fluorine (F), silicon (Si), chlorine (Cl), boron, and others can be doped into carbon matrix, which results in high specific capacitance [23, 24]. Sulphur (S) doping technology has become an efficient method to boost the performance of carbon-based electrode material due to its easily polarizable nature, wider bandgap and unpaired electron of S, n-type character, and most importantly, pseudocapacitive behavior of S-containing groups in the electrode materials [25–27]. S doping also forms an electron dense area on the carbon surface, altering the chemical characteristics of carbon-based electrode materials, resulting in increased capacitance, wettability, and electrical conductivity [23, 24, 28]. In this chapter, we will look at how to make several types of S-doped carbon as electrode materials and their applicability in supercapacitors.

18.2 Synthetic Pathway of S-doped Carbon

The preparation of electrode materials is crucial in respect of obtaining efficient and marketable supercapacitor systems. Various methods have been used in the literature to manufacture biomass-based S-doped carbon. In this section, we will go through various S-doped carbon production methods. Along with other meaningful preparation methods, namely solvothermal, sol-gel, electrochemical, microwave-assisted synthesis, the classic S-doped carbon material production technique comprises the carbonization and activation of a combination of carbon source precursor and S source precursor. [28] In general, the carbon source precursor and sulfur source precursor are combined and carbonized at high temperatures before being activated to produce S-doped carbon in this two-step process (the carbonization and activation processes can be executed either way round, i.e., first carbonization then activation or first activation then carbonization). [29] Various types of biomass have been used as carbon sources in the literature, including egg yolk, [30] oak nutshells, [31] *Borassus flabellifer* flower, [32] glucose, [33] a solid residue contained in olive mill wastewater (OMW) that is primarily composed of the seed, mesocarp, exocarp, and small parts of olive stones, [34] and so on. The S-containing sources including sublimed sulfur, [33] Na_2SO_3, [35] sulfur, [36] thiourea, [32] and Mohr's salt ($Fe(NH_4)_2(SO_4)_2 \cdot 6H_2O$), [37] etc. are reported in the literature. To manufacture S-doped activated carbon, Raj et al. [32] employed *Borassus flabellifer* (palm male flower) as a carbon source and thiourea as a S source (Figure 18.1A). They began by washing, drying, and grinding black-colored charcoal particles made from raw palm male flowers. The obtained black-colored charcoal was then impregnated with an activating agent (KOH at 20 and 30 wt.%) and combined with a doping agent (thiourea) before carbonization for one hour at various temperatures (400, 500, and 600 °C) to produce S-doped activated carbon. Their sample exhibited a BET surface area ranging from 13.263 (20 wt.% KOH) to 474.99 m^2g^{-1} (30 wt.% KOH) of type I/IV
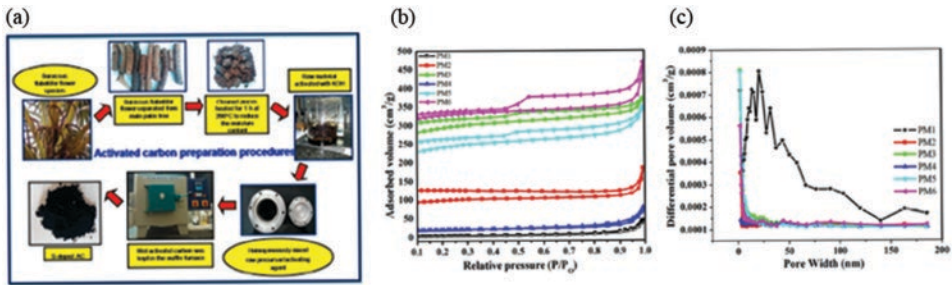
Figure 18.1 (A) Schematic illustration of synthetic pathways for preparing a highly porous S-doped carbon with *Borassus flabellifer* flower as starting materials. (B) Nitrogen adsorption-desorption isotherm and (C) pore-size distributions of the doped activated carbon. *Reproduced with permission* [32]. *Copyright 2019, Elsevier.*

mixed adsorption/desorption isotherms (Figure 18.1B, 18.1C). The sheet-like porous morphology was evidenced by elemental mapping analysis.

Elmouwahidi and colleagues [34] first created activated carbon (AC) from OMW by carbonizing it at 450 °C, then activating it with KOH at 60 °C for 12 hours, and then 840°C for two hours. The produced activated carbon was then heat treated with thioglycolic acid (temperature up to 120 °C for 24 hours) to produce S-doped activated carbon. After drying the obtained material was termed original activated carbon (AOW). Sulfur content on the external surface by x-ray photoemission spectroscopy (XPS). XP spectra were obtained with an ESCA 5701 (Physical Electronics) device. Survey and multi-region spectra were recorded at C1s, O1s, and S2p photoelectron peak. Characteristic XPS survey data and electrochemical investigations are shown in Figure 18.2. In addition, the manufacture of S-doped carbon in a single-step procedure via carbonization and activation has been described in the literature. In this procedure, carbon-based material is obtained from coffee grinds, KOH as an activating agent, and $MgSO_4$ as an S source. To create S-doped carbon, a 4:4:1 mass ratio combination of these three precursors followed the calcination process at 800 °C for 1 hour in the furnace under an argon environment, followed by hydrochloric acid washing, filtering, and subsequent drying. In the study, S-doped carbon was shown to have superior hydrophilic properties to undoped carbon. Later on new hydrophilic groups (C-SO_x-C) on the surface and bulk phase of S-doped carbon were ascribed. [38] The carbon precursor and the activating agent should have a high mass ratio in these typical carbonization and activation processes. There is a lack of consistent pore size distribution, % of heteroatom, and mesopore in the produced product. As a result, new synthetic strategies must be developed in order to manage pore size, increase the number of heteroatoms, and, most significantly, boost capacitance. [39] In this case, as a carbon source, pine needles were used. In contrast, potassium thioacetate as an activating agent, and S source were combined in a 2:1 ratio and pyrolyzed for 1 hour at 700, 800, and 900 °C under Ar protection. The pyrolyzed sample was acid-washed and dried for 12 hours at 80 °C to get S-doped 3D porous carbon. FESEM images confirmed abundant holes and fragments on the surface of these 3D particles. Furthermore, the XRD pattern revealed amorphous carbon for the (002) and (101) planes at 21° and 45°, respectively, with more significant defect at 900 °C. The disorders were also confirmed by Raman analysis. [39]
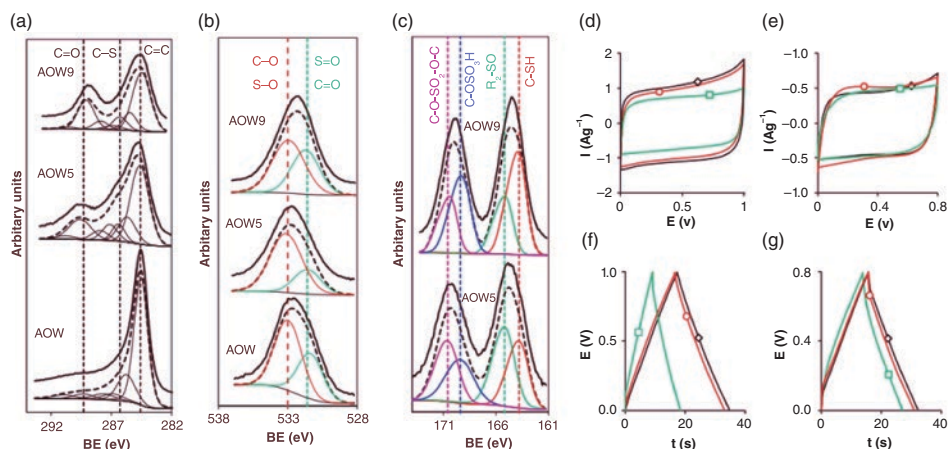
Figure 18.2 Deconvolution of C1s (a) O1s (b) and S2p (c) high-resolution XPS survey data. Cyclic voltammograms at 20.0 mV s^{-1} for samples AOW, AOW5, AOW9: (d) H$_2$SO$_4$ 1 M and (e) KOH 6 M. GCDS in (f) H$_2$SO$_4$ 1 M at 3 A g^{-1} and (g) KOH 6 M 1 A g^{-1} for samples AOW, AOW5, AOW9. *Reproduced with permission* [34]. *Copyright 2018, Elsevier.*

Carbonization of calcined magnesium sulfate whiskers with sucrose under Ar flow for one hour at 600 °C yielded a high S content. [40] The S in the fiber-like S-doped mesoporous carbons (SMCs) framework is mostly coupled via a C-S-C bond, as shown by XPS. A cyclic voltammetry (CV) study was employed to assess the electrochemical performance of the synthesized S-doped carbon material (Figure 18.3). For all electrode materials, an approximately rectangular shape with no prominent redox peak was found, indicating a pseudo-constant rate throughout the potential window and increasing capacitance with the rise of S %.

S-doped carbon-based hybrid (CSiO$_2$) was created in another study by hydrothermal carbonization of bamboo leaves, followed by thioglycolic acid mixing and controlled solvothermal treatment. The hydrothermal carbonization process begins with impurity removal from water at 210 °C for 12 hours, and then treating acid washing at 600 °C with a heating rate of 2 °C min^{-1} under N$_2$ pressure, and finally carbonization of the acid-washed dry product was performed. A controlled solvothermal treatment of carbonized product and thioglycolic acid solution in ethanol solvent for 24 hours at 120 °C yielded the desired result. As validated by SEM, TEM, and SAED patterns, the obtained S-doped carbon has a 3D porous structure with a non-crystalline condition. [41]

Because of its environmental friendliness, simplicity, and great stability, the direct laser writing procedure was also employed to manufacture S-doped carbon for an effective high-performance all-solid-state graphene-based microsupercapacitor (MSC) (Figure 18.4). In this synthesis, lignin and polyethersulfone were utilized as carbon and S sources, respectively, and the different power of an epilog CO$_2$ laser (10.6 m) was used. During preparation, they first created a lignin-polyethersulfone (L-P) film by combining lignin and polyethersulfone in dimethylformamide (DMF) solution and drying it overnight at 80 °C. The resulting lignin-polyethersulfone film was then scribed at different laser power levels with an epilog CO$_2$ laser to produce S-doped porous three-dimensional (3D) graphene materials (LIG). According to Raman analysis, the ratio of D and G bands is lower for the obtained S-doped porous 3D graphene when the intensity of laser light is 15% of its original value, suggesting high-quality graphene with the largest crystallite size was formed. [42]
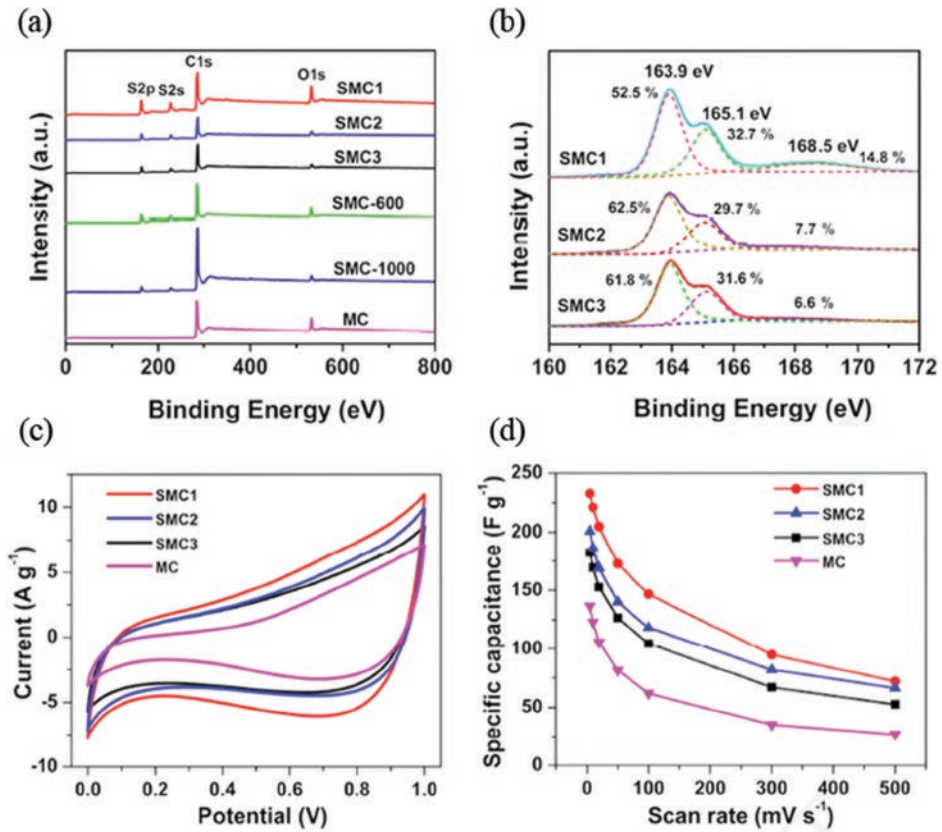
Figure 18.3 (A) XPS survey spectra of mesoporous carbon (MC) and SMCs. (B) S2p spectra of SMCs. (C) CV curves of the porous carbons at a scan rate of 50 mVs^{-1}. (D) Specific capacitances of MC and SMCs at different scan rates. *Reproduced with permission* [40]. *Copyright 2014, Elsevier.*
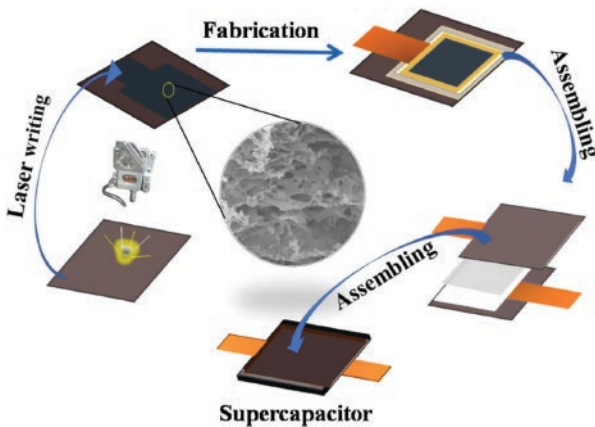
Figure 18.4 Schematic illustration of the synthesis procedure of L-P LIG MSC. *Reproduced with permission* [42]. *Copyright 2021, Elsevier.*

In another study, S-doped carbon nanoparticles were created using cow margarine, sulfur powder, and carbon disulfide as a precursor using flame pyrolysis. This manufactured sample contains 6.27% S, according to EDX analysis. [43] Due to the use of a hazardous chemical as an S source, the manufacture of S-doped carbon by combining carbon and S source is not ecologically friendly. As a result, preparing S-doped carbon from a single source rather than two is more important for the environment. Sulfonated lignin, [44] sodium lignosulfonate, [45, 46] calcium lignosulfonate, [47] red algae-produced carrageenan-Fe hydrogel, [48] and other carbon and sulfur precursors have been employed. Tian et al. [46] for example, generated a self-doped three-dimensional (3D) interconnected S-doped porous carbon (S-PC) from biowaste sodium lignosulfonate by employing a carbonization and activation process. In contrast, a carbon and a sulfur precursor, sodium lignosulfonate were used.

First, they made a solution of sodium lignosulfonate and KOH activating agent and dried it for 10 hours in a porcelain boat at 110 °C to evaporate deionized water. To get S-doped porous carbon, they washed and then dried at 80 °C for 24 hours in an oven; the dried product was carbonized under N_2 atmosphere at 900 °C for three hours at a heating rate of 5 °C min^{-1}. The interconnected porous structure of their synthesized S-doped porous carbon was verified by TEM examination. Raman and XRD analysis were performed to confirm the presence of disordered carbon (Figure 18.5). The same group produced S-doped porous carbon using
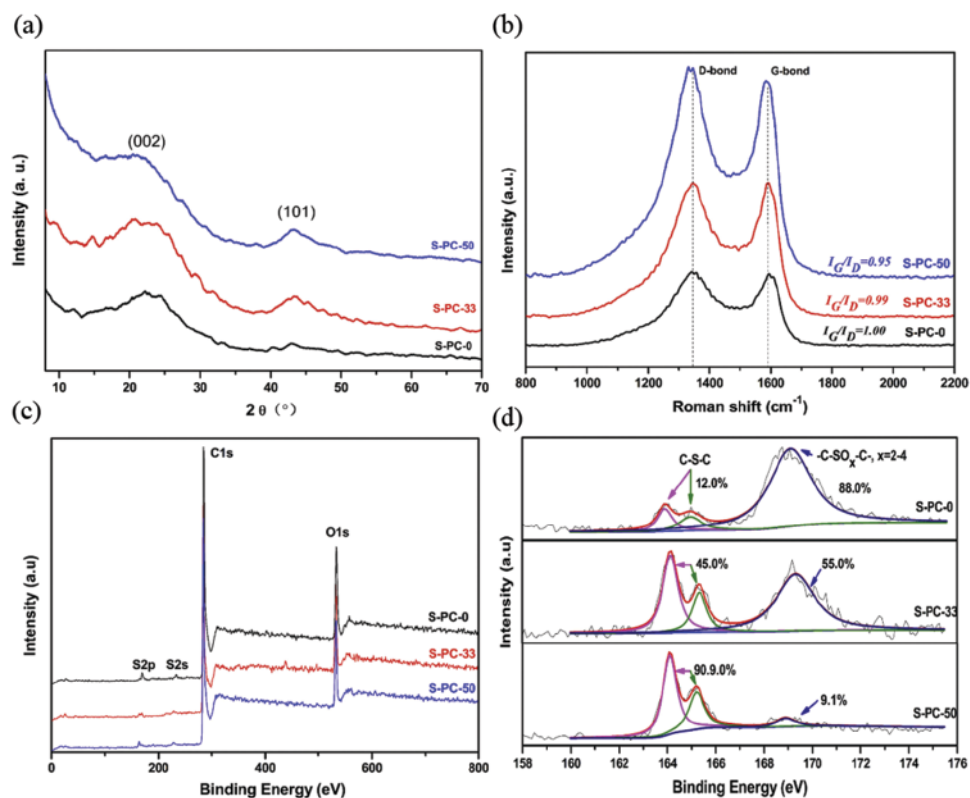
Figure 18.5 (a) XRD patterns, (b) Raman spectra of the S-PC samples, (c) the total XPS spectra, and (d) higher-resolution S_{2p} spectra of all the S-PC samples. *Reproduced with permission* [46]. *Copyright 2017, Elsevier.*

sodium lignosulfonate as a carbon and sulfur sources and using easy template method. They made a homogenous solution by combining tetraethyl orthosilicate, sodium lignosulfonate, and sulfuric acid then dried it for 48 hours at 40 °C and pre-carbonized it for six hours at 100 and 160 °C. Carbonizing the above-mentioned dried product at 700–900 °C in the presence of N_2 atmosphere for three hours and then carrying out etching with excess HF and drying at 105 °C overnight yielded S-doped porous carbon. The ratio of G band to D band at 900 °C carbonization temperature was 1.11, indicating the synthesis of graphitic sp^2 carbon at high carbonization temperature. [45] In another paper, Ji and colleagues [49] synthesized a single precursor source by combining glucose, $SnCl_4.5H_2O$, and thiourea using a microwave-hydro-thermal method. They then calcined the precursor to obtain porous S-doped carbon. The microwave-hydrothermal approach resulted in the formation of SnS and doped S in the carbon matrix. The calcination-induced evaporation of SnS resulted in porous S-doped carbon.

18.3   Super-capacitive Mechanism of S-doped Carbon

Pure biomass-based carbon or pristine carbon shows a lack of energy density and exhibits lower specific capacitance. Therefore, enhancing energy density and specific capacitance is a challenging issue. A doping strategy can be followed to enhance the capacitive perfor-mance to solve this problem. Liu et al. [50] conducted density functional theory and found that doping improves the affinity and ionic adsorption of carbon surfaces. Sulfur, similar to the heteroatom's oxygen, nitrogen, and phosphorus, has an affinity to enhance carbon material's specific capacitance. This can be attributed to the slight difference in the elec-tronegativity (EN) of S (2.58) and carbon (C) (2.55). Consequently, charge transfer in the C-S bond occurs, which is effective for supercapacitor performance. It changes the electron density of the carbon surface. Furthermore, by upsetting the electron density balance and giving varied bond angles and lengths, biomass-based carbon material's electronic struc-ture may be changed by adding S-containing groups to form active redox sites. [51] The S doping also improves carbon wettability and polarity (sulfur shifts the charge on surround-ing carbon atoms to a more positive charge), all of which are critical for charge transfer and EDLC charge storage efficiency. [52] Deng et al. [44] generated self-doped multi-porous lignin-based biocarbon from lignin biomass using a simple sulfonation-aided sacrificial template approach. They used various analytical techniques to characterize their sample. They discovered that the produced carbon contains sulfonate groups responsible for the carbon matrix's fault structure. XPS research verified the existence of thiophene S, which signifies C-S-C groups, and C-S-O, oxygenated C-S functionalities. They discovered a 3149 m^2g^{-1} BET surface area. The produced electrode material had strong reversibility and an excellent specific capacitance of 213 Fg^{-1} in 6 M KOH electrolyte when the current den-sity was 0.5 Ag^{-1}, whereas the undoped carbon capacitance was 132 Fg^{-1} at the same cur-rent density. They hypothesized a possible mechanism based on this characterization data. The large levels of oxygenated C-S-C functional groups increased the pseudocapacitance of carbon material owing to Faradaic redox processes. They improved the material's stability by inhibiting further oxidation across a wide potential range. In addition, the electron-rich C-S-C moieties produced a substantial shift of the Fermi level to the valence band, which leads to in a more polarized surface and better wettability of the carbon surface, as well as improved electrolyte transfer into the carbon material's well-connected pores. As a result,

the capacitance was higher than the undoped one due to the oxygen containing S dopant. Therefore, due to having a difference in electronegativity between S and C, S-doped carbon materials caused enhanced charge storage capability at the electrode–electrolyte interface compared with undoped carbon, through the acceleration of electron transfer from highest occupied molecular orbital (HOMO) to lowest unoccupied molecular orbital (LUMO) of respective species.

18.4 Application of S-doped Carbon

S doping can be achieved in two ways: external and self-doping, and each technique has a specific effect on super capacitive application. There have been some reports based on external doping. To create sulfonated porous carbon nanosheets, Gopalakrishnan et al. [31] employed acid hydrothermal carbonization and a KOH activation technique. They used two and three-electrode systems to evaluate the capacitance performance of the produced sulfonated porous carbon nanosheets. The produced material demonstrated a remarkable specific capacitance of 398 Fg^{-1} at 0.4 Ag^{-1} in a three-electrode system, with 98.5% capacitance retention for 10000 charge-discharge cycles at a current density of 3 Ag^{-1} in a two-electrode system. Li and colleagues [30] generated S-doped carbon from KOH-pretreated egg yolks, followed by carbonization at 700, 800, and 900 °C. They discovered the maximum specific capacitance of 287.66 Fg^{-1} at a current density of 0.5 Ag^{-1} in a 6M KOH at 800 °C. At a current density of 20 Ag^{-1}, the electrode material kept its specific capacitance of 220.37 Fg^{-1}. Yaglikci et al. [29] used discarded tea to make S-doped activated carbon by microwave pretreatment with H_3PO_4 followed by chemical activation in another study. Compared to undoped carbon, their developed S-doped carbon as an electrode material for supercapacitor application showed a 62% increase in specific capacitance in KOH and a 38% increase in the H_2SO_4 electrolyte solution. These findings suggested that KOH has a higher penetrating ability than H_2SO_4. Wang and his colleagues [37] used Mohr's salt as a template, S source, and co-activator to produce S-doped hierarchical carbon frameworks with spruce bark powder as carbon source simply termed as S-HPCFs-x (x refers the amount of KOH). They refined the amount of KOH used in electrode material fabrication and discovered that 3g of KOH served as a good activating agent for supercapacitive performance of S-HPCFs-3. They measured capacitance in both aqueous (KOH) and ionic liquid (1-ethyl-3-methylimidazolium tetrafluoroborate, $EMImBF_4$) electrolytes and found that the results were consistent. The developed electrode material was able to power the LED light for seven minutes at a current density of 1 Ag^{-1} (Figure 18.6).

Another study compared the supercapacitive performance of S-doped electrode materials in both aqueous and organic electrolytes. [33] As a symmetric capacitor, the S-doped nanoporous carbon (S-NCS) sphere produced from sublimed S and glucose displayed good capacitive performance in KOH, Na_2SO_4, and $LiPF_6$ electrolyte medium. The specific energy of the prepared doped carbon was 53.5 $Whkg^{-1}$ at 74.2 Wkg^{-1} in 1.0M $LiPF_6$ EC/DEC and 24.0 $Whkg^{-1}$ at 45.0 Wkg^{-1} in 1.0 M Na_2SO_4 (Figure 18.7). Desa and colleagues [35] used durian peels and Na_2SO_4 to create S-doped carbon material, then tuned the activation temperature to get super capacitive performance. They discovered that their manufactured doped carbon had the maximum capacitance value of 183 Fg^{-1} at 700 °C at 5 mVs^{-1} scan rate. Chen et al. [36] synthesized S-doped activated carbon from banana peel and
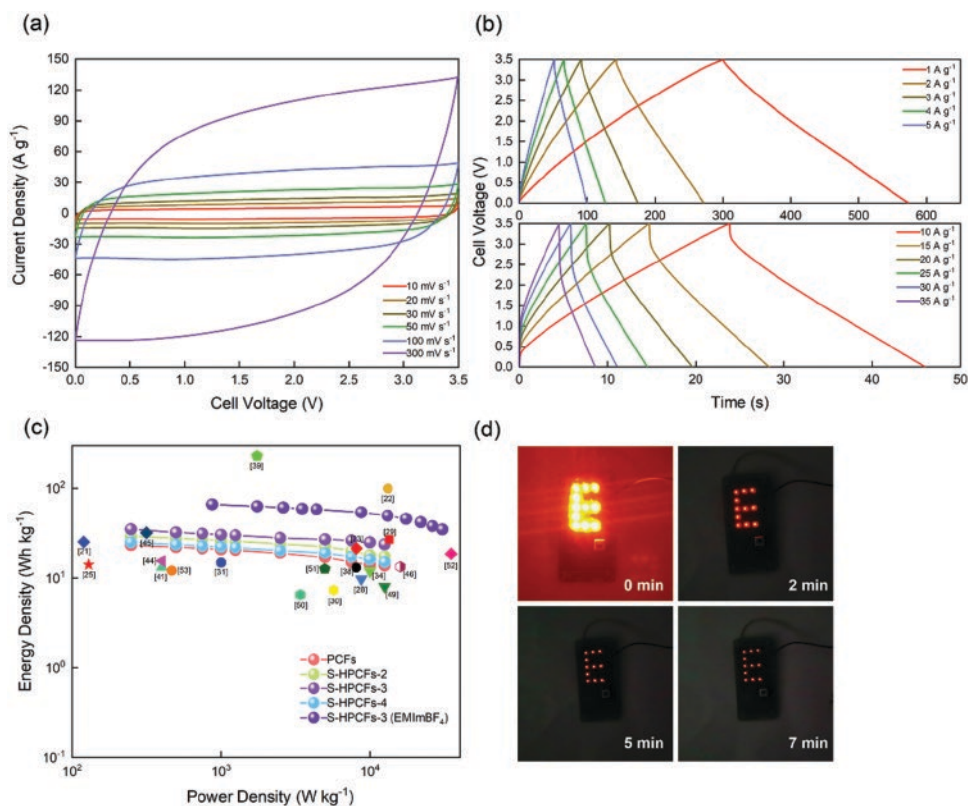
Figure 18.6 (a) CV curves for S-HPCFs-3 in EMImBF$_4$ electrolytes at different scan rates, (b) corresponding GCD curves at various current densities, (c) Ragone curves for both KOH and EMImBF4 electrolytes, and (d) digital photograph of LED lamps. *Reproduced with permission* [37]. *Copyright 2021, Elsevier.*

compared its capacitance to that of undoped activated carbon and porous banana peel carbon. The capacitance in the three-electrode system was 146.1 Fg^{-1}, while the scan rate was 5 mVs^{-1} (Figure 18.7). They discovered that the specific capacitance value of activated carbon was 162.5 Fg^{-1}, with an energy density of 90.7 Wh kg^{-1} and a power density of 1.3 kW kg^{-1} in 6 M KOH at a current density of 0.5 Ag^{-1} due to S doping.

To build a solid-state supercapacitor, another research group used H$_2$SO$_4$/PVA gel as an electrolyte and S-doped laser-generated graphene as an electrode material. The results showed both enhanced areal capacitance (22 mF cm^{-2}) and areal energy density of 1.53 mWh cm^{-1} at an area power density of 25.4 mW cm^{-2} for the produced electrode material has exceptional electrochemical performances (at 15% laser power), namely. After 9000 cycles, the produced S-doped carbon material likewise displayed outstanding capacitance retention of 89.8%. [42] Self-doped S on carbon matrix is superior due to the omission of additional chemicals and is also documented in the literature for supercapacitor devices. At a pyrolysis temperature of 400 °C, the 3 Dl hierarchical porous sulfur-doped carbon aerogel from carrageenan-Fe aerogel displayed high capacitance in both aqueous and organic electrolytes with values of 335 and 217 Fg^{-1} (1 Ag^{-1}). [48] Deng et al. [44] made
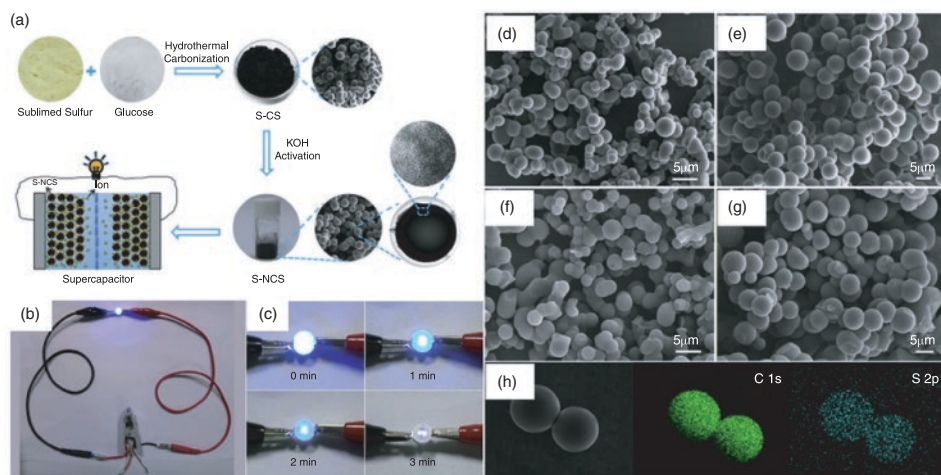
Figure 18.7 (a) Schematic illustration of the preparation of S-NCS, (b) shows two supercapacitors in series after charging can light up LED indicators; (c) different stage of blue LED, (d–g) SEM images of (d) CS-20, (e) S-CS-4, (f) NCS and (g) S-NCS-4. (h) SEM elemental-mapping of S-CS-4 to build a solid-state supercapacitor. *Reproduced with permission* [33]. *Copyright 2017, Elsevier.*

S-doped carbon from lignin biomass and measured specific capacitance in H_2SO_4 and KOH electrolytes. The electrode material had an outstanding specific capacitance of 297 Fg^{-1} in 2 M H_2SO_4 and 213 Fg^{-1} in 6 M KOH (0.5 Ag^{-1}). They also made two solid-state supercapacitor devices with PVA-H_2SO_4 and PVA-KOH gels as solid electrolytes and separators and discovered that both electrolytes had an outstanding capacitance of 140 Fg^{-1} at 0.5 Ag^{-1}.

18.5 Conclusions

Supercapacitors possess different properties, including high energy density typically at high power density, fast charging and discharging rate, long cycle life, and high specific capacitance, and are used as promising and dominating energy storage devices in commercial applications. Biomass-based carbon is widely used as electrode materials in supercapacitors due to its cheapness, unique structure, availability, and environmental friendliness. The limitation of using pure carbon arises due to lacking energy density and specific capacitance. Heteroatom doping is a possible methodology to minimize these drawbacks. Heteroatoms on carbon surface enhance the prepared electrode material's specific capacitance and energy density via fast redox reaction known as pseudocapacitive behavior. Due to its easily polarizable nature, wider bandgap, and unpaired electron of S, S-doped biomass-based carbon gains a tremendous application in the supercapacitor field. However, in the literature, the typical synthesis processes are activation and the carbonization of precursor material. A few have reported synthesizing S-doped carbon without an extra activation process. Hence, one-step synthesis without an extra activation procedure to get high-density S-doped carbon or composite materials would be helpful in the sense of commercial scale for the compact design of high-power energy sources. In addition, using S as an external dopant is not environmentally friendly as an additional chemical is

used in this process. Although in some literature, a single precursor is used as carbon and S source, more and more focus should be given to this protocol. The study discussed in this chapter demonstrates the production of S-doped carbon with high interest and their use in supercapacitors. Although significant progress has been achieved in recent years, more work is needed to create scalable, cost-effective, and long-term synthetic approaches for S-doped carbon. Furthermore, we feel that the information presented here about S-doped carbon will be useful for every energy storage and conversion sector, including supercapacitor technology, battery, metal-ion capacitors, fuel cells, sensors, catalysis, and a variety of other applications.

Acknowledgments

References

1 A. González, E. Goikolea, J. A. Barrena, R. Mysyk, *Renew. Sustain. Energy Rev.* **2016**, *58*, 1189–1206.

2 G. Wang, L. Zhang, J. Zhang, *Chem. Soc. Rev.* **2012**, *41*, 797–828.

3 C. Zhong, Y. Deng, W. Hu, J. Qiao, L. Zhang, J. Zhang, *Chem. Soc. Rev.* **2015**, *44*, 7484–7539.

4 K. Mensah-Darkwa, C. Zequine, P. K. Kahol, R. K. Gupta, *Sustain* **2019**, *11* (2), 414.

5 Q. Ke, J. Wang, *J. Mater.* **2016**, *2*, 37–54.

6 Z. Bi, Q. Kong, Y. Cao, G. Sun, F. Su, X. Wei, X. Li, A. Ahmad, L. Xie, C. M. Chen, *J. Mater. Chem. A* **2019**, *7*, 16028–16045.

7 R. Vinodh, C. V. V. M. Gopi, V. G. R. Kummara, R. Atchudan, T. Ahamad, S. Sambasivam, M. Yi, I. M. Obaidat, H. J. Kim, *J. Energy Storage* **2020**, *32*, 101831.

8 M. A. Aziz, S. S. Shah, S. M. A. Nayem, M. N. Shaikh, A. S. Hakeem, I. A. Bakare, *J. Energy Storage* **2022**, *50*, 104278.

9 S. Najib, E. Erdem, *Nanoscale Adv.* **2019**, *1*, 2817–2827.

10 M. L. Divya, S. Natarajan, Y. S. Lee, V. Aravindan, *ChemSusChem* **2019**, *12*, 4353–4382.

11 C. Liu, S. Zhao, Y. Lu, Y. Chang, D. Xu, Q. Wang, Z. Dai, J. Bao, M. Han, *Small* **2017**, *13*, 1603494.

12 G. S. Dos Reis, H. P. de Oliveira, S. H. Larsson, M. Thyrel, E. C. Lima, *Nanomaterials* **2021**, *11* (2), 424.

13 L. Miao, Z. Song, D. Zhu, L. Li, L. Gan, M. Liu, *Mater. Adv.* **2020**, *1*, 945–966.

14 W. Zhang, R. R. Cheng, H. H. Bi, Y. H. Lu, L. B. Ma, X. J. He, *Xinxing Tan Cailiao/New Carbon Mater* **2021**, *36*, 69–81.

15 S. M. A. Nayem, S. S. Shah, N. Sultana, M. A. Aziz, A. J. S. Ahammad, *Chem. Rec.* **2021**, *21*, 1039–1072.

16 D. Kang, Q. Liu, J. Gu, Y. Su, W. Zhang, D. Zhang, *ACS Nano* **2015**, *9*, 11225–11233.

17 J. Deng, M. Li, Y. Wang, *Green Chem.* **2016**, *18*, 4824–4854.

18 Z. Zhu, Z. Xu, *Renew. Sustain. Energy Rev.* **2020**, *134*, 110308.

19 S. M. A. Nayem, N. Sultana, T. Islam, M. M. Hasan, A. Awal, S. C. Roy, M. A. Aziz, A. J. S. Ahammad, *Electrochemical Sci. Adv.* **2021**, *2*, e2100046.

20 X. Tang, D. Liu, Y. J. Wang, L. Cui, A. Ignaszak, Y. Yu, J. Zhang, *Prog. Mater. Sci.* **2021**, *118*, 100770.

21 P. Thomas, C. W. Lai, M. R. B. Johan, J. Anal, *Appl. Pyrolysis* **2019**, *140*, 54–85.

22 Y. Deng, Y. Xie, K. Zou, X. Ji, *J. Mater. Chem. A* **2015**, *4*, 1144–1173.

23 S. Ghosh, S. Barg, S. M. Jeong, K. Ostrikov, *Adv. Energy Mater.* **2020**, *10*, 2001239.

24 B. Cai, C. Shao, L. Qu, Y. Meng, L. Jin, Front. Mater. Sci. **2019**, *13*, 145–153.

25 Z. Liang, H. Xia, H. Liu, L. Zhang, Y. Zhao, J. Zhou, H. Li, W. Xie, *ECS J. Solid State Sci. Technol.* **2020**, *9*, 021005.

26 W. Cai, K. Li, K. Jiang, D. Lv, Y. Q. Liu, D. Wang, X. Wang, C. Lai, *Diam. Relat. Mater.* **2021**, *116*, 108380.

27 Z. Chen, B. Deng, K. Du, X. Mao, H. Zhu, W. Xiao, D. Wang, *Adv. Sustain. Syst.* **2017**, *1*, 1700047.

28 S. S. Shah, S. M. Abu Nayem, N. Sultana, A. J. Saleh Ahammad, M. Abdul Aziz, *ChemSusChem* **2022**, *15*, e202101282.

29 S. Yaglikci, Y. Gokce, E. Yagmur, Z. Aktas, *Environ. Technol. (United Kingdom)* **2020**, *41*, 36–48.

30 J. Li, S. Ma, L. Cheng, Q. Wu, *Mater. Lett.* **2015**, *139*, 429–432.

31 A. Gopalakrishnan, S. Badhulika, *Renew. Energy* **2020**, *161*, 173–183.

32 F. R. Maria Sundar Raj, N. V. Jaya, G. Boopathi, D. Kalpana, A. Pandurangan, *Mater. Chem. Phys* **2020**, *240*, 122151.

33 S. Liu, Y. Cai, X. Zhao, Y. Liang, M. Zheng, H. Hu, H. Dong, S. Jiang, Y. Liu, Y. Xiao, *J. Power Sources* **2017**, *360*, 373–382.

34 A. Elmouwahidi, J. Castelo-Quibén, J. F. Vivo-Vilches, A. F. Pérez-Cadenas, F. J. Maldonado-Hódar, F. Carrasco-Marín, *Chem. Eng. J.* **2018**, *334*, 1835–1841.

35 S. S. Desa, T. Ishii, K. Nueangnoraj, *ACS Omega* **2021**, *6*, 24902–24909.

36 H. Chen, Z. Zhao, P. Qi, G. Wang, L. Shi, F. Yu, *Int. J. Nanomanuf.* **2019**, *15*, 181–195.

37 S. Wang, Z. Hu, Z. Pan, D. Wang, *J. Alloys Compd.* **2021**, *876*, 160203.

38 X. Ma, L. Zhao, Z. Yu, X. Wang, X. Song, G. Ning, J. Gao, *ChemSusChem* **2018**, *11*, 3766–3773.

39 D. Wang, S. Wang, Z. Lu, *Int. J. Energy Res.* **2021**, *45*, 2498–2510.

40 X. Ma, G. Ning, Y. Kan, Y. Ma, C. Qi, B. Chen, Y. Li, X. Lan, J. Gao, *Electrochim. Acta* **2014**, *150*, 108–113.

41 C. Wang, S. H. Zhang, L. Zhang, R. Xi, D. P. Jiang, Z. Y. Chen, H. Huang, L. Y. Ding, G. B. Pan, *J. Power Sources* **2019**, *443*, 227183.

42 X. Sun, X. Liu, F. Li, *Appl. Surf. Sci.* **2021**, *551*, 149438.

43 M. P. Bondarde, P. H. Wadekar, S. Some, *J. Energy Storage* **2020**, *32*, 101783.

44 Q. Deng, S. C. Abbas, Z. Li, J. Lv, X. Ma, S. Cao, Y. Ni, W. Zhao, *J. Colloid Interface Sci.* **2020**, *574*, 33–42.

45 J. Tian, Z. Liu, Z. Li, W. Wang, H. Zhang, *RSC Adv.* **2017**, *7*, 12089–12097.

46 J. Tian, H. Zhang, Z. Liu, G. Qin, Z. Li, *Int. J. Hydrogen Energy* **2018**, *43*, 1596–1605.

47 M. Demir, A. A. Farghaly, M. J. Decuir, M. M. Collinson, R. B. Gupta, *Mater. Chem. Phys.* **2018**, *216*, 508–516.

48 D. Li, G. Chang, L. Zong, P. Xue, Y. Wang, Y. Xia, C. Lai, D. Yang, *Energy Storage Mater.* **2019**, *17*, 22–30.

49 H. Ji, T. Wang, Y. Liu, C. Lu, G. Yang, W. Ding, W. Hou, *Chem. Commun.* **2016**, *52*, 12725–12728.

50 H. Liu, M. Wang, D. D. Zhai, X. Y. Chen, Z. J. Zhang, *Carbon N. Y.* **2019**, *155*, 223–232.

51 X. Yu, S. K. Park, S. H. Yeon, H. S. Park, *J. Power Sources* **2015**, *278*, 484–489.

52 M. Seredych, T. J. Bandosz, *J. Mater. Chem. A* **2013**, *1*, 11717–11727.

19

Biomass-derived Carbon and Metal Oxides Composites for Supercapacitors

Muhammad Ammar[1], Himadri Tanaya Das[2], Awais Ali[1], Sami Ullah[3], Abuzar Khan[4], Abbas Saeed Hakeem[4], Naseem Iqbal[5], Muhammad Humayun[6], Muhammad Zahir Iqbal[7], and Muhammad Usman[4],*

[1] *Department of Chemical Engineering Technology, Government College University, Faisalabad 38000, Pakistan*

[2] *Center for Advanced Materials and Applications, Utkal University, Vanivihar, Bhubneswar, 751004, Odisha, India*

[3] *K. A. CARE Energy Research and Innovation Center, King Fahd University of Petroleum & Minerals, Dhahran, 31261, Saudi Arabia*

[4] *Interdisciplinary Research Center for Hydrogen and Energy Storage (IRC-HES), King Fahd University of Petroleum and Minerals (KFUPM), Dhahran 31261, Saudi Arabia*

[5] *U.S. Pakistan Center for Advanced Studies in Energy (USPCAS–E), National University of Sciences and Technology (NUST), Islamabad, Pakistan*

[6] *Wuhan National Laboratory for Optoelectronics, Huazhong University of Science and Technology, Wuhan, 430074, China*

[7] *Nanotechnology Research Laboratory, Faculty of Engineering Sciences, GIK Institute of Engineering Sciences and Technology, Topi 23640, Khyber Pakhtunkhwa, Pakistan*

* *Corresponding author*

19.1   Introduction

A supercapacitor is a promising electrochemical energy storage device widely used in electronic devices and electric vehicles. The supercapacitor possesses numerous desirable characteristics of energy storage systems, such as, environmental friendliness, fast charging time, and long cycle life [1, 2]. The rapid improvement of electrochemical efficiency of supercapacitors with high rate capability and long cycling stability in this energy storage system has drawn interest from more and more researchers. Recent advances in material science engineering have opened up new opportunities for supercapacitors by designing efficient electrode materials for their practical applications [3–6]. An ion-permeable separator is used to separate the two electrodes of a supercapacitor to facilitate the transport of ions between them. The electrode material used in a supercapacitor is the most important component since it determines the final performance of the produced supercapacitor. As a result, extensive research exploring novel electrode materials is being conducted to increase the supercapacitor performance. Supercapacitors are divided into three categories based on the charge storage mechanisms: 1. The charge is stored electrostatically via adsorption of ions on the electrode surface in electric double-layer capacitors (EDLC) (uses carbon electrodes). 2. Pseudocapacitor (uses metal oxide electrodes), that stores energy electrochemically via rapid surface-controlled redox processes.

3. Hybrid supercapacitor combines capacitive type nature with Faradaic type and the electrostatic capacitance of EDLC. Because of combining the synergistic effects of carbonaceous materials and metal oxides, hybrid supercapacitors with better energy and power densities could be developed. The hybrid supercapacitor can be an asymmetrical supercapacitor, despite the fact that the electrodes utilized are identical to those of an asymmetrical supercapacitor [7].

Carbon materials are widely applied as efficient electrode materials in supercapacitors with unique structures, high surface area, and good mechanical and electric properties compared to metal oxides/sulfides/phosphides [8–11]. The electrochemical properties of carbon based materials have been improved in many ways [12–14]. Unfortunately, carbon materials as electrode materials suffer from high production costs, toxic chemical treatments, and difficulties in synthesis/fabrication processes such as when producing carbon nanotubes (CNTs) and graphene. Given that, biomass-derived carbon materials have gained attention of industries and academia due to the advantages of them being a natural source, hierarchical structure (porous material synthesis), low cost, and sustainability for wide applications. They also undergo similar processing procedures, such as carbonization, activation, and purification [15]. Different chemicals, such as metallic compounds, may be added to the conversion process, endowing biomass-derived carbon materials with even more capacitive capabilities. Natural porous and heteroatomic structures with a high surface area and defective nature of biomass-derived carbon materials can provide abundant electroactive sites for energy storage and supply ion transport pathways by enhancing electrolyte penetration [16].

Further, biomass-derived carbons with transition metal oxides composites can combine their respective advantages. Biomass-derived carbon can offer high surface area for depositing transition metal oxides to provide maximum electroactive areas. An excellent conductivity of transition metal oxides can effectively promote charge transfer and thus enhance redox reaction kinetics, leading to the supercapacitor's high electrochemical performance [17–19]. Further, robust architectures of biomass-derived carbons can buffer the mechanical stress induced by Faradaic reactions from metallic species during a repeated charging/discharging process, significantly elongating the cycling life of supercapacitors. Therefore, biomass-derived carbon and transition metal oxides composites demonstrate enhanced capacitance, rate performance, energy density, power density, and cyclic life. Beyond that, asymmetric supercapacitors using biomass-derived carbon (as negative electrodes) and transition metal oxides or corresponding composites (as positive electrodes) manifest excellent electrochemical properties [20]. The final production of inherited biomass-derived carbons with a high carbon yield and interconnected 3D nanoporous structure depends on the biomass precursors used. High-performance supercapacitor applications need heteroatom-doped activated carbons with hierarchically linked meso/microporous structures.

This chapter focuses on a comprehensive summary of significant research advances in biomass-derived carbon and transition metal oxides composites with discussions and evaluation of their application as electrode materials for supercapacitors. Various biomass-derived carbon and transition metal oxides composites are summarized categorically. Then, their electrochemical performances are discussed.

19.2 Composites of Biomass-derived Carbon and Metal Oxides

19.2.1 Biomass-derived Carbon and Manganese Oxide Composites

Manganese oxides are widely explored for their active electrochemical properties, such as their redox nature (Mn^{3+} and Mn^{4+}) and wide potential window. MnO_2 exhibits pseudocapacitive behavior with a high theoretical specific capacitance of $1370\,F\,g^{-1}$. The facile synthesis of different phases and morphologies of the manganese oxides and their composite has added advantages as electrodes in a supercapacitor. The problems with manganese oxides-based electrodes are low intrinsic conductivity and low-capacity retention, which can be overcome by compositing it with conducting network of carbon. Such a strategy can also improve the mechanical and chemical stability of the electrodes. Among the nanocomposites, the manganese oxide composites with biomass-derived carbon are sustainable, and cost-effective to collect for use in electrodes. Biomass-derived carbon can be provided with a conductive path for the enhanced electrochemical properties of manganese oxides.

Many researchers have tried various ways to investigate the electrochemical performance of the manganese oxides with biomass-derived carbon nanocomposite as an electrode for supercapacitor applications. Rambutan peels-derived carbon was combined with MnO_2 to produce 3D-porous MnO_2@carbon nanosheets [21]. It was used as a positive electrode and the biomass-derived carbon as a negative electrode which delivered a specific capacity of $25.8\,F\,g^{-1}$ with high energy and power density of $9.2\,Wh\,kg^{-1}$ and $1283.7\,W\,kg^{-1}$, respectively. The device showed stability of 82% even after 5000 cycles. Biomass-derived carbon using radish as raw material synthesized and incorporated MnO_2 by a suitable impregnation method. The prepared composite delivered a high gravimetric capacitance of $557\,F\,g^{-1}$, while the fabricated two-electrode device delivered a high gravimetric capacitance of $447\,F\,g^{-1}$ with energy and power density $248.23\,Wh\,kg^{-1}$ and $4786.44\,W\,kg^{-1}$, respectively [22]. MnO_2 with watermelon soft tissue-derived carbon aerogel (MnO_2@CA) composite synthesized as electrode materials for supercapacitors by a simple and facile hydrothermal approach [23], is illustrated in Figure 19.1. After hydrothermal carbonization and a freeze-drying process, porous carbonaceous aerogels were obtained from watermelon. Further functionalization on the carbonaceous aerogels with precursors of MnO_2 was adopted to achieve high-performance electrode materials. Two reaction systems, (1) $KMnO_4 + Na_2S_2O_3 \cdot 5H_2O$ system and (2) $MnSO_4 \cdot H_2O + (NH_4)_2S_2O_8$ system, were employed to obtain the MnO_2@CA composite. Their results showed a reasonable specific capacitance of $123.5\,F\,g^{-1}$, while carbon derived from hemp stem and composite deposited on MnO_2 nanowires showed a high specific capacitance of $340\,F\,g^{-1}$ [23, 24].

Faidherbia albida fruit shell-derived carbon and MnO_2 were utilized to fabricate the electrodes for a solid-state supercapacitor with a wide potential window greater than 1.6V. The supercapacitor achieved energy and power densities of $32\,Wh\,kg^{-1}$ and $400\,W\,kg^{-1}$, respectively [25]. Similarly, MnO_2 nanosheets with bamboo leaf-derived carbon or conodium-derived hollow carbon spheres composites were used as electrodes for supercapacitors [26, 27]. Even rice husk-derived carbon with MnO_2 nanocomposite delivered a specific capacitance of $210.3\,F\,g^{-1}$ with a good capacity retention rate of 80.2% after 5000 cycles. Thus, the synergistic effect of manganese oxides and biomass-derived carbon is a potential candidate for supercapacitor applications [28].
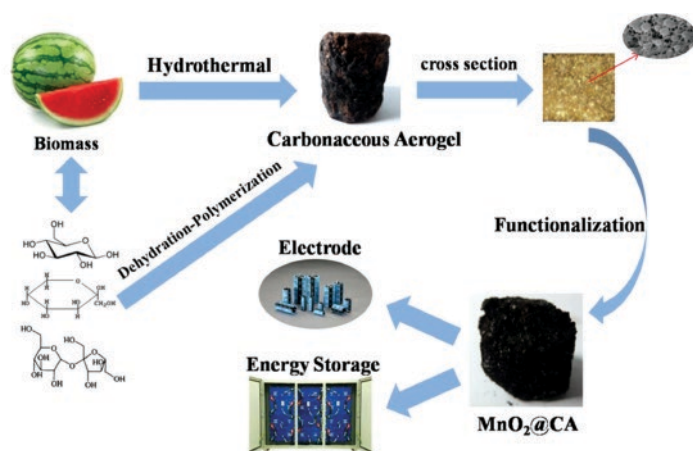
Figure 19.1 Illustration of the strategy and further application for the functional carbonaceous materials that come from watermelon. *Reproduced with permission [23]. Copyright 2014, American Chemical Society.*

19.2.2 Biomass-derived Carbon and Cobalt Oxide Composites

Due to dynamic electrochemical and redox properties, cobalt is highly exploited for energy storage or catalytic applications [29–32]. Apart from the high theoretical capacity ($3560\,Fg^{-1}$), the cobalt oxides electrodes can sustain mechanical and chemical stability in various electrolytes. Usually, the cobalt oxides are incorporated into carbon matrix of different types to generate more surface area, porosity, and high conductivity. Both cobalt oxides and carbon play a vital role in enhancing a supercapacitor's charge storage ability [33, 34]. Many researchers report that the biomass-derived carbon nanocomposite with cobalt oxides can be an efficacious electrode with long-term cycling stability and high capacity.

Co_3O_4@biomass-derived carbon fiber@Co_3O_4 composite was fabricated, which showed excellent electrochemical performance of $892\,Fg^{-1}$ at a current density of $0.5\,A\,g^{-1}$ with high capacitance retention of 88% of initial capacitance after 6000 cycles. The fabricated asymmetric supercapacitor exhibited a high energy density of $33.6\,Wh\,kg^{-1}$ at a power density of $1500\,Wkg^{-1}$ [35]. A 3D-hollow nanocomposite of aloe juice-derived carbon aerogel with Co_3O_4 displayed a high capacity of $1345.2\,Fg^{-1}$ at $1\,Ag^{-1}$. It retained 92.7% of capacity after 10000 cycles, and the asymmetric supercapacitor device delivered a high energy density of $68.17\,Wh\,kg^{-1}$ at a power density of $549\,Wkg^{-1}$ [36]. Interestingly, *Bauhinia vahlii* dry fruits-derived activated carbon composited with Co_3O_4 showed a high specific capacitance of $653\,Fg^{-1}$ at $1\,Ag^{-1}$ and good capacitance retention of 91% even after 8000 cycles [37].

Co_3O_4 was anchored on the surface of agricultural waste-derived carbon; the porous structure enhanced the stability and facilitated the diffusion of electrolyte ions. The material was fabricated for an aqueous and solid-state supercapacitor, and the aqueous supercapacitor displayed a high energy density of $42.5\,Wh\,kg^{-1}$ at a power density of $746\,W\,kg^{-1}$. However, the solid-state supercapacitor showed a high energy density with a good retention rate of 87.1% after 3000 cycles [38]. The functionalized carbon also played a vital role in improving

supercapacitor performance, for example, N-doped porous carbon from waste carbon shell composited with Co_3O_4, which exhibited a high specific surface area of $2430 \, m^2 g^{-1}$ with excellent stability of 95% after 10000 cycles [39]. A porous alkali-treated activated carbon was derived from wheat flour and supported with Co_3O_4 and achieved remarkable specific capacitance of $232.9 \, F g^{-1}$ and excellent capacitance retention capability (80.35%) after 1000 cycles [40].

19.2.3 Biomass-derived Carbon and Copper Oxide Composites

Biomass-derived carbon has been developed to support the copper oxides from structural degradation during electrochemical performance and prevent the agglomeration of copper oxide [41]. The biomass-derived carbon provides a conductive pathway and elongates the cycling stability. Different biomass-derived carbons in composites perform differently as electrodes in supercapacitors according to their morphology, porosity, surface area, and active sites. The interconnected nanostructure provides high diffusion rates for composite electrodes.

Biomass-derived activated carbon incorporated with CuO composite prepared as electrode material for supercapacitors [41]. Peanut shells were used as carbon precursors to prepare the porous carbon using KOH as the activator via a simple two-step process followed by immersion in an aqueous solution of $Cu(CO_2CH_3)_2$ as the Cu precursor and NH_4OH for six hours. The resultant mix solution was dried at $105 \, °C$ to obtain an intermediate product which was then heated at $310 \, °C$ under air for two hours to achieve CuO nanoparticle decorated on porous carbon matrix (CuO-AC) electrode material, as shown in Figure 19.2a. CuO nanoparticles were dispersed homogeneously in the carbon matrix with particle size in the range of 10 to 20 nm and lattice distance was 0.25 and 0.23 nm, corresponding to the (–111) and (111) crystal planes of CuO, respectively, as depicted in Figure 19.2b-d. Also, the homogenous distribution of C, O, and Cu elements was observed on the surface of the carbon matrix, confirming the successful incorporation of CuO in CuO-AC composite, having a high surface area of $2640.55 \, m^2 g^{-1}$. The CuO compositing AC increased the gravimetric capacitance of $530 \, F g^{-1}$ with excellent stability of 92.5% even after 10000 cycles. The device exhibited high energy and power densities of $11.7 \, Wh \, kg^{-1}$ and $628.73 \, W \, kg^{-1}$, respectively.

Bamboo leaf-derived porous carbon was used to fabricate hybrid composite with copper and cuprous oxide as electrode materials for supercapacitors [42]. Moreover, anisotropic carbon stabilized polyaminate copper oxide as the cathode for hybrid supercapacitor was reported as showing high specific capacitance of $694.8 \, F g^{-1}$, and the hybrid device showed high cyclic stability of 91.2% retention after 5000 cycles and high energy and power densities of $13.6 \, Wh \, kg^{-1}$ and $350.3 \, W \, kg^{-1}$ reported, respectively [43]. Cu doped carbon aerogels derived from sodium alginate through a green and facile method with a high surface area of $230.4 \, m^2 g^{-1}$ and showed a specific capacitance of $414.4 \, F g^{-1}$ for supercapacitor application [44].

19.2.4 Biomass-derived Carbon and Nickel Oxide Composites

Nickel materials have been extensively explored in catalysis and energy conversion [45, 46]. This is due to the tuned morphology of nickel oxides by facile synthesis
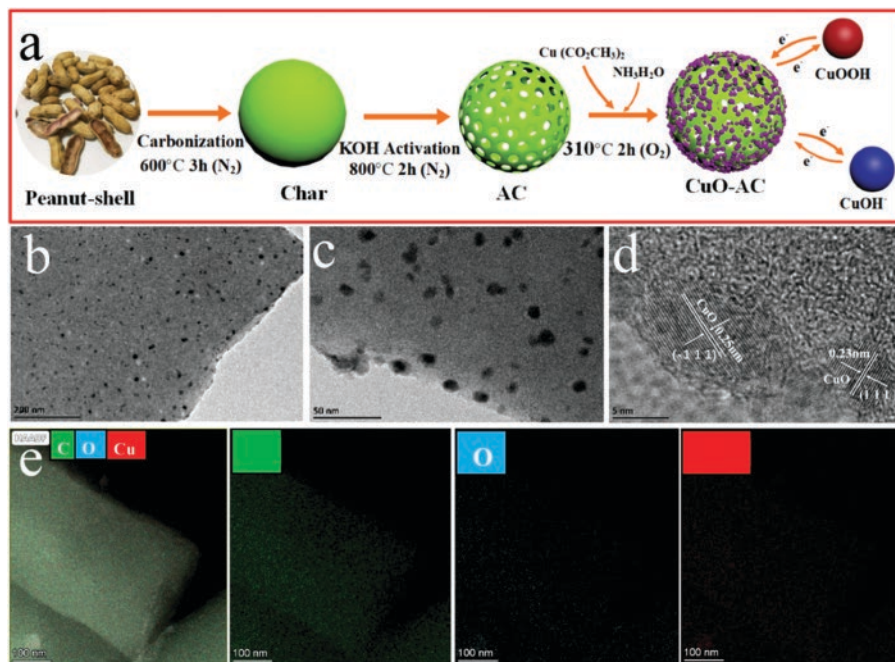
methods. These properties enable them to be efficient electrode materials for supercapacitors. Their swift redox nature facilitates them to achieve remarkable electrochemical performance. But experimentally, the theoretical capacitance has not yet been achieved due to limitations such as loss of capacity, low stability, and conductivity. These drawbacks can be overcome by preparing composite material using nickel oxides and carbon materials, having versatile and favorable structural properties for supercapacitor applications [47]. Among all composites, nickel oxide with biomass-derived carbon composites has been proved relevant for electrochemical devices and widely investigated for supercapacitor applications.

Carbon aerogel by pyrolysis of sodium carboxymethyl cellulose aerogel and composited with NiO possessed a surface area of $175.05 \, \text{m}^2 \, \text{g}^{-1}$ and a specific capacity of $81.67 \, \text{mAh} \, \text{g}^{-1}$ with a retention rate of 94.5% after 5000 cycles [48]. Due to the high surface area, the highly porous carbon electrodes developed from biomass contribute to better electrochemical performances. Lignin-derived mesoporous carbon combined with NiO had a surface area of $852 \, \text{m}^2 \, \text{g}^{-1}$ and delivered a high specific capacitance of $508 \, \text{F} \, \text{g}^{-1}$ [49]. Banana peel waste-derived porous carbon with NiO composite was observed at a high specific capacitance of $811 \, \text{F} \, \text{g}^{-1}$ at a current density of $1 \, \text{A} \, \text{g}^{-1}$, with a high retention rate of 84.55% after 1000 cycles [50]. Carbonized kapok fiber/NiO composite had a microtubular structure designed to obtain high specific capacitance. The fabricated asymmetric device with activated carbon of wide cell voltage (1.6 V) showed energy and power densities of $7.5 \, \text{Wh} \, \text{kg}^{-1}$ and $64.6 \, \text{W} \, \text{kg}^{-1}$, respectively [51].

Lignin-derived mesoporous carbon embedded with NiO composite as electrode material showed a high surface area of $802\,m^2\,g^{-1}$ with a uniform pore size of 3.7 nm. The electrode material exhibited a high specific capacitance of $880.2\,Fg^{-1}$ and a good retention rate of 90.9% after 1000 cycles [52]. NiO nanosheets anchored honeycomb amorphous porous carbon (NiO@PC) composite and successfully enhanced the capacitance up to $500\,Fg^{-1}$ at a high current density of $10\,Ag^{-1}$ [53]. N doped chitosan nanofibers-derived porous carbon nanosheets-Ni composite formed a layered honeycomb structure with a high specific surface area of $1847.4\,m^2\,g^{-1}$ with an N content of 5.16%. The effect of high surface area and nitrogen doping was observed in electrochemical performance, such as a high specific capacitance of $614.6\,Fg^{-1}$, with the energy density of $20.3\,Wh\,kg^{-1}$ at a power density of $240.9\,W\,kg^{-1}$ and stability of 85.6% even after 10000 cycles [54].

19.2.5   Biomass-derived Carbon and Iron Oxide Composites

Iron oxides have received significant attention owing to their abundant natural availability, rich energy storage ability, low cost, and environmental friendliness for their applications in electrochemical energy storage devices. Iron oxides exhibit high theoretical capacity ($926\,mAh\,g^{-1}$), multiple valence states such as Fe^{2+} and $Fe^{3+,}$ and rich redox pairs, which make them promising electrode materials [55, 56]. However, the inherent problems related to iron oxides for supercapacitor applications are their low specific capacitance in aqueous electrolytes due to poor electrical conductivity and poor recycling stability [57]. Numerous attempts have been made to prepare hybrid nanostructured composites by incorporating iron oxides with biomass-derived carbon materials to overcome these issues.

2D-crumpled porous carbon sheet (2D-CCS) has been developed using waste garlic husk to synthesize $Fe_3O_4NAs@2D$-CCS composite [58]. The composite reveals an excellent specific capacitance of $820\,Fg^{-1}$ at $0.5\,Ag^{-1}$, 3–5 times higher than bare Fe_3O_4 NPs, with a remarkable energy density (115.5–65.9 Wh kg^{-1}) and power density (3500–8000 W kg^{-1}) in a pseudocapacitor application. Iron-carbon-based functional material ($Fe_3O_4/Fe_3C@C$) prepared for supercapacitor electrode by iron oxide/carbide, and sustainable bagasse-derived carbon (*Saccharum officinarum*), displayed excellent electrochemical performance due to the synergistic effect of iron oxide/carbide and graphitic layers [59]. $Fe_3O_4/Fe_3C@C$ composite revealed a specific capacitance of $211.6\,Fg^{-1}$ at $0.4\,Ag^{-1}$ in the 2-electrode system and $878\,Fg^{-1}$ at $5\,Ag^{-1}$ in the 3-electrode system with excellent cyclic stability. The energy density of $29.4\,Wh\,kg^{-1}$ and the power density of $807\,W\,kg^{-1}$ were observed. Biochar with an interconnected 3D pore network structure was prepared using activation treatment on *Cladophora glomerata* followed by a slow pyrolysis process. Subsequently, Fe composite biochar was obtained by functionalizing the biochar with H_2SO_4 and HNO_3 for extending the formation of iron oxide via the hydrothermal method. The composite demonstrated remarkable electrochemical performance as a supercapacitor electrode in terms of high specific capacitance, excellent rate capability, and incredible cycle stability [60]. The asymmetric supercapacitor revealed an energy density of $41.5\,Wh\,kg^{-1}$ at a power density of $900\,W\,kg^{-1}$ with stable cycling performance.

Biocarbon (KWB) derived from direct pyrolysis of sugarcane bagasse was used to obtain Fe_3O_4/biocarbon composite (KBFe) via a chemical co-precipitation method [61]. A series of KBFe composite were prepared and denoted as KBFe-1, KBFe-2, KBFe-3, KBFe-4, and

KBFe-5 with the theoretical value of the mass ratio of Fe_3O_4 to KWB being 0.25:1, 0.5:1, 0.75:1, 1:1, 1.5:1, respectively. The surface area and chemical composition of KBFe composite profoundly affected their electrochemical performance. CV curves of KBFe composite revealed the redox peaks indicating the existence of pseudocapacitive function of Fe_3O_4 and the redox reaction of Fe ions (Figure 19.3a). Additionally, the pseudocapacitance reaction of Fe_3O_4 in the KOH electrolyte was accompanied by intercalation of OH^- balance the extra charge with the Fe_3O_4 layers. GCD curves of KBFe were nearly symmetrical to their corresponding discharge curves, indicating that the capacitance was caused by the blend of EDLC and pseudocapacitance (Figure 19.3b). Furthermore, a much larger current response and longer discharge time of KBFe-4 was observed than that of other composites, demonstrating that the KBFe-4 possessed excellent capacitive performance. The specific capacitance of KBFe-4 reached $342\,F\,g^{-1}$ at $1\,A\,g^{-1}$. EIS curves suggested that KBFe-4 revealed the shortest $45°$ diagonal line at the medium frequency region and the most significant slope of a straight line at the low-frequency region, indicating that KBFe-4 had the lowest diffusion resistance than others (c). The specific capacitance of KBFe composite decreased with the increase in the current density, as shown in Figure 19.3d. The specific capacitance of KBFe-4 could reach $171\,F\,g^{-1}$ at the current density of $10\,A\,g^{-1}$ which
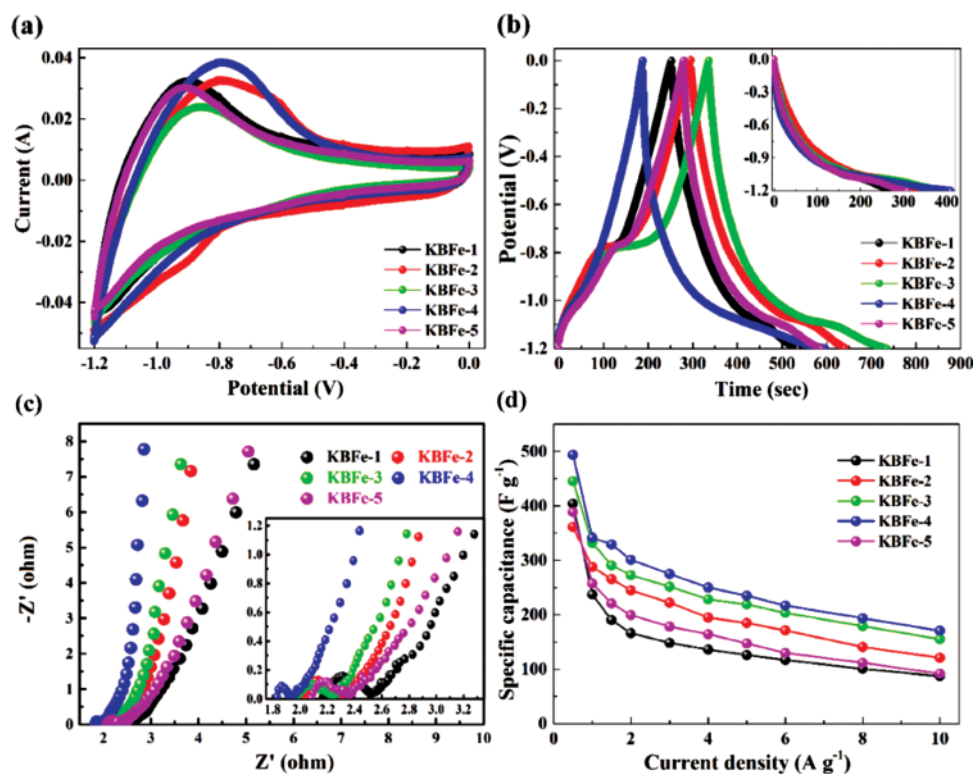
Figure 19.3 (a) CV curves (scan rate of $0.01\,V\,s^{-1}$), (b) GCD curves (current density of $1\,A\,g^{-1}$), (c) EIS curves, and (d) specific capacitance versus current density of KBFe composite. *Reproduced with permission [61]. Copyright 2017, Elsevier.*

suggested that the KBFe-4 has the most excellent fast charge/discharge performance among all the KBFe composite.

3D kenaf stem-derived macroporous carbon (KSPC) was used as support for Fe_3O_4 doped porous carbon nanorods (Fe_3O_4-DCN) to prepare KSPC/Fe_3O_4-DCN nanocomposite via pyrolyzing MIL-88A (iron-based MOFs) and KSPC. The KSPC/Fe_3O_4-DCN nanocomposite possessed a 3D interconnected configuration with combined advantages of Fe_3O_4-DCN having enriched electroactive sites and KSPC owning hierarchical pores, high surface area, and good conductivity [62]. The nanocomposites were employed as supercapacitors and delivered a remarkable specific capacitance of 285.4 F g^{-1} at 1 A g^{-1} with 77.2% capacitance retention after 5000 cycles. Watermelon-derived sponge-like 3D carbonaceous gels (CGs) are used to fabricate Fe_3O_4/CGs composite by incorporating Fe_3O_4 nanoparticles into the networks of CGs, followed by calcination to transform them into magnetite carbon aerogels (MCAs). The porous structure of MCAs facilitated the stable transport of both electrons and electrolyte ions to the electrode surface during the electrochemical process. The MCAs displayed an excellent specific capacitance of 333.1 F g^{-1} at 1 A g^{-1} and remarkable cycling stability with 96% specific capacitance maintenance after 1000 cycles [63]. Persimmon fruit-derived carbon possessed a very porous structure and high surface area for growing yolk-shell structure Fe_3O_4 nanoparticles under hydrothermal conditions, carbonization, and in the microwave-assisted step. The resultant composite with a surface area of 251.36 m^2 g^{-1} offered sufficient active sites for chemical transformation during oxidation and reduction. It achieved remarkable areal capacitance and specific capacitance [64].

19.2.6 Biomass-derived Carbon and Ruthenium Oxide Composites

Ruthenium oxide (RuO_2) is a suitable electrode material for electrochemical energy storage devices because of its high chemical and thermal stability, abundance, and rapid charge/discharge behavior. Due to its fast Faraday redox reaction, good electrical conductivity, high rate capability, large potential window, and high theoretical capacitance (2000 F g^{-1}), ruthenium oxide has been regarded as a promising supercapacitor electrode material [65]. However, its toxic nature, high cost, poor cycling stability, severe agglomeration, and low porosity are tough challenges and limit its electrode applications [66]. Attempts have been made to synthesize composite electrode materials to reduce ruthenium's cost and combine the advantages of ruthenium oxide and the high porosity and cycling stability of biomass-derived carbon materials.

Moringa oleifera fruit shell-derived porous activated carbon (MOC) was used to obtain Ru/MOC composite by dispersing Ru nanoparticles on MOC under continuous ultrasonication, followed by pyrolysis for supercapacitor applications. The Ru/MOC composite revealed desirable textural features and remarkable electrochemical and capacitive properties [67]. A high specific capacitance (291 F g^{-1} at 1 A g^{-1}) with outstanding cycling stability (>90% of capacitance retention after 2000 cycles at 4 A g^{-1}) was achieved. The assembled symmetric supercapacitor provided an energy density of 6.3 Wh kg^{-1} at a power density of 250 W kg^{-1}. Charcoal-derived activated carbon (CAC) was obtained by CO_2 activation to fabricate 3D hetero-RuO_2/CAC composite by the hydrothermal method as a supercapacitor electrode. High conductivity of RuO_2/CAC composite is attributed to

abundant active sites for charge storage and efficient electron transfer that resulted in improved supercapacitor performance [68]. The composite hybrid electrodes displayed a high specific capacitance of $510\,F\,g^{-1}$ at $1\,A\,g^{-1}$ along with 87.05% capacitance retention at $1\,A\,g^{-1}$ for 3000 cycles. Kapok fiber-derived carbon aerogel (CA) was obtained by $NaClO_2$ pretreatment of kapok fiber and carbonization of kapok fiber aerogel. Then, the CA was used to prepare 3D microtubular CA/RuO_2 composite electrode material, which possessed an integrated tubular structure and moderate pore size distribution [69]. The composite showed a remarkable specific capacitance ($433\,F\,g^{-1}$ at $1\,A\,g^{-1}$) with good cycle stability (91.5% capacitance retention after 2000 cycles) in a three-electrode system. The CA/RuO_2 composite as electrode in an asymmetric device displayed an energy density of $8.92\,Wh\,kg^{-1}$ at a power density of $558.12\,W\,kg^{-1}$.

Biomass-derived carbon was used to achieve RuO_2-biomass carbon (RuO_2-BC) composite by combining octyl ammonium salicylate ionic liquid with Ru^{3+} ions, followed by coconut meat and microwave thermal treatment in sequence. Homogenous dispersion of RuO_2 nanoparticles on BC provided an excellent synergetic effect between RuO_2 nanoparticles and BC, and RuO_2-BC composite displayed higher specific capacitance ($907.7\,F\,g^{-1}$) than that of RuO_2 ($548.7\,F\,g^{-1}$) and BC ($150.6\,F\,g^{-1}$) electrodes [70]. The mechanical flexibility and electrochemical durability of the RuO_2-BC supercapacitor were investigated by designing typical hand movements. Figure 19.4 shows that the glove with a supercapacitor can complete various operation conversions. The capacitance retention rate was close to 100% when the glove remained flat for five cycles because the supercapacitor had no folding
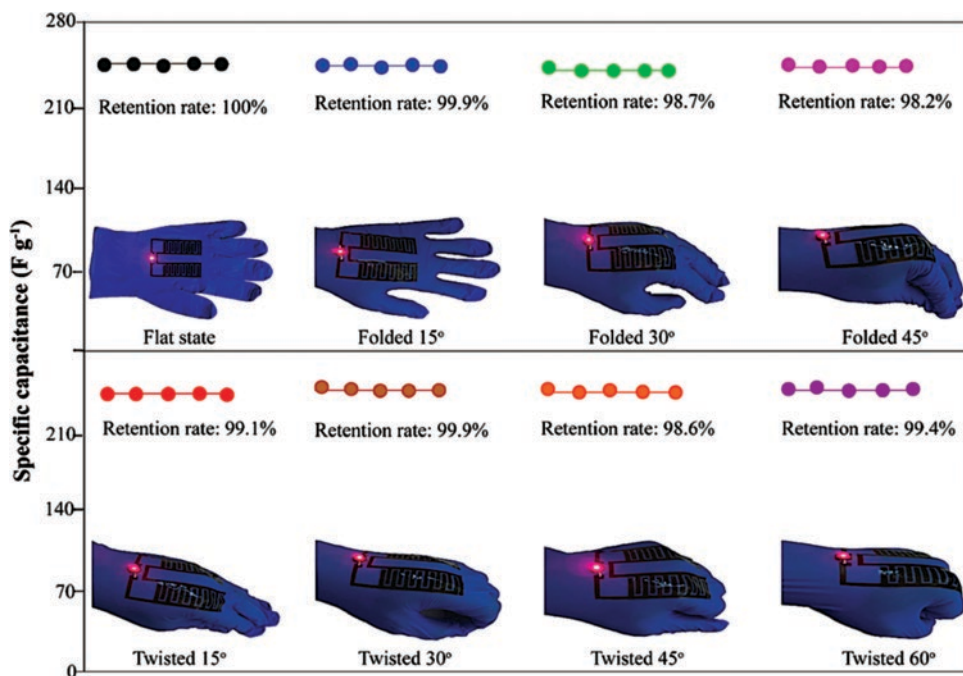
Figure 19.4 Digital photos of the supercapacitor and its specific capacitances at the current density of $20\,A\,g^{-1}$ for 5-cycle. *Reproduced with permission [70]. Copyright 2022, Elsevier.*

or twisting. The capacitance remained almost unchanged for folding angles of 15° and twisting angles of 15°. The capacitance decreased with an increase in folding angle from 30° to 45°. Like holding, a relatively big twisting angle bought a rather significant change in capacitance. However, the capacitance remained at 98.2% when the folding angle was 45°. These findings confirmed that the supercapacitor exhibited excellent flexibility and stability that is attributed to the unique structure of RuO_2-BC. The fabricated symmetric supercapacitor exhibited excellent electrochemical performance and energy density of $378.7\,Wh\,kg^{-1}$ at a power density of $5199.2\,W\,kg^{-1}$.

Corncob-derived activated carbon with high surface area ($3.145\,m^2\,g^{-1}$) and high percentage of micropores (87%) was prepared by thermal treatment and impregnated with RuO_2 to get activated carbon-RuO_2 composite for electrode material in a supercapacitor. The physicochemical properties of activated carbon-RuO_2 composite confirmed the homogenous and high distribution of crystalline RuO_2 particles on the surface of activated carbon, which enhanced their electrochemical properties. The resultant composite showed the specific capacitance of $360\,F\,g^{-1}$ and electric conductivity of $408\,S\,m^{-1}$ [71].

19.2.7 Biomass-derived Carbon and Molybdenum Oxide Composites

Molybdenum oxide (MoO_3) has attracted significant interest as an active electrode for electrochemical energy storage devices due to its low resistivity, metallic conductivity, cost-effectiveness, and environmental benignity. Molybdenum oxide is a promising electrode material for supercapacitors, as it possesses several oxidation states (+2 to +6), high theoretical specific capacity ($1111\,mAh\,g^{-1}$), excellent redox reaction capability, and good electrochemical activity [72]. However, its practical applications are hampered by poor cycling stability due to the lack of efficient electronic/ionic transport pathways [73]. Thus, incorporating molybdenum oxide into porous, sustainable, and low-cost carbon, i.e., biomass-derived carbon, may provide more electroactive sites that effectively enhance the electrochemical properties.

The oxygen-rich and meso/macroporous network of loofa sponge-derived activated carbon was employed to encapsulate MoO_3 nanoflowers by hydrothermal treatment to synthesize a highly capacitive and cost-effective AC-MoO_3 composite. The MoO_3 structure with flower-like morphology provided a high electrochemical assessable surface area for abundant charge storage and reduced the volume stress generated during cycling and distance for electron transport [74]. The composite revealed good electrochemical performance with a specific capacitance of $413\,F\,g^{-1}$ and an excellent rate capability of 76.93%. Moreover, the asymmetric supercapacitor delivered a remarkable energy density ($52.87\,Wh\,kg^{-1}$) at a power density of $3800\,W\,kg^{-1}$.

Goat hair-derived activated carbon used as a cathode and MoO_2@rGO as anode materials were synthesized and applied as a hybrid supercapacitor. Uniform distribution of the nanostructure of MoO_2 on the surface of rGO enhanced the electrical conductivity during cycling in the anode, and porous activated carbon with a high surface area of $2042\,m^2\,g^{-1}$ provided a pathway for the adsorption and desorption of ions, which improved the electrochemical performance of the cathode [73]. Both electrodes revealed excellent electrochemical performance as well as good cycling stability. The hybrid supercapacitor fabricated by these electrodes displayed an energy density of $79\,Wh\,kg^{-1}$ and a power density of $95\,W\,kg^{-1}$. Peanut

shell-derived porous activated carbon (AC) was used to embed the nanostructures of MoO_2 and Mo_2C for fabrication of ($AC/MoO_2/Mo_2C$) composite by a facile in-situ pyrolysis route. The resultant composite was used as the electrode for the symmetric supercapacitor. It displayed an excellent electrochemical performance attributed to the synergistic effect of metal oxide and metal carbide species with the interconnected porous carbon providing favorable properties [75]. The composite manifested an outstanding specific capacitance ($115\,F\,g^{-1}$) with impressive rate capability (58% at $20\,A\,g^{-1}$) and remarkable cycling performance (99.8% Coulombic efficiency after 25,000 cycles). Moreover, an energy density of $51.8\,Wh\,kg^{-1}$ with a power density of $900\,W\,kg^{-1}$ was noted for the symmetric supercapacitor.

19.2.8 Biomass-derived Carbon and Mixed Oxide Composites

Mixed metal oxides have been widely studied as electrode materials for electrochemical storage devices due to their excellent electrical conductivity, low electronegativity, small bandgap with highly active sites, environmental friendliness, and low cost. Mixed metal oxides reveal remarkable electrochemical performance compared to their single metal oxide for supercapacitor applications because of low diffusion resistance, effective electron transport, easy electrolyte penetration, low cost, and high theoretical capacitance [76]. However, the significant drawbacks that limit their supercapacitor applications are the intrinsic rapid capacitance degradation, poor cyclic stability, and low rate capability of mixed oxides as electrode material. Incorporating mixed metal oxides in biomass-derived porous carbon material is a practical approach to solving these problems.

Poplar catkins-derived porous carbon (PC) micro sheets with a thickness of 150–200 nm were modified with polydopamine (PD) and further deposited with ultrathin nickel cobaltite nanosheets ($NiCo_2O_4$ NSs) to form a $NiCo_2O_4$ shell-carbon core sandwich composite ($NiCo_2O_4$ NSs@PD-PC). A pair of redox peaks were observed in all CV curve of the samples, which indicated the typical Faradaic behavior associated with the reversible redox reactions in $NiCo_2O_4$ (Figure 19.5a). The unchanged shape of CV curves of $NiCo_2O_4$ NSs@PD-PC at different scan rates demonstrated excellent electrochemical reversibility and high-rate performance, which was associated with the low resistance of the electrodes (Figure 19.5b). GCD curves of all samples displayed two visible potential plateaus arising from Faradaic redox reactions and lower internal resistance of $NiCo_2O_4$ NSs@PD-PC attributed to the tight coupling effect of PDA and quickly charge transportation (Figure 19.5c). Also, the $NiCo_2O_4$ NSs@PD-PC revealed excellent specific capacity ($256.2\,mAh\,g^{-1}$ at $1\,A\,g^{-1}$), a smaller value of equivalent series resistance (ESR), and good cycling stability (91.36% capacity retention after 5000 cycles) [77]. The $NiCo_2O_4$ NSs@PD-PC//PD-PC hybrid supercapacitor revealed outstanding performance with an energy density of $39.1\,Wh\,kg^{-1}$ at the power density of $799.9\,W\,kg^{-1}$ with 95.5% capacitance retention after 5000 cycles.

3D gelatin-derived carbon-nickel foam (GCNF) was used to grow nanoflower-like $NiCo_2O_4$ by a facile hydrothermal treatment to synthesize binder-free $NiCo_2O_4$/GCNF composite for a high-performance supercapacitor. The resulting composite provided rapid transfer of ions and electrons by enhancing the electroactive surface area due to the nanoflower-like morphology of $NiCo_2O_4$ and improved the skeleton's electrical conductivity owing to the homogenous coating of porous carbon on the surface of the nickel foam [78]. The $NiCo_2O_4$/GCNF composite displayed a specific capacitance of $1416\,F\,g^{-1}$ at $1\,A\,g^{-1}$ and remarkable
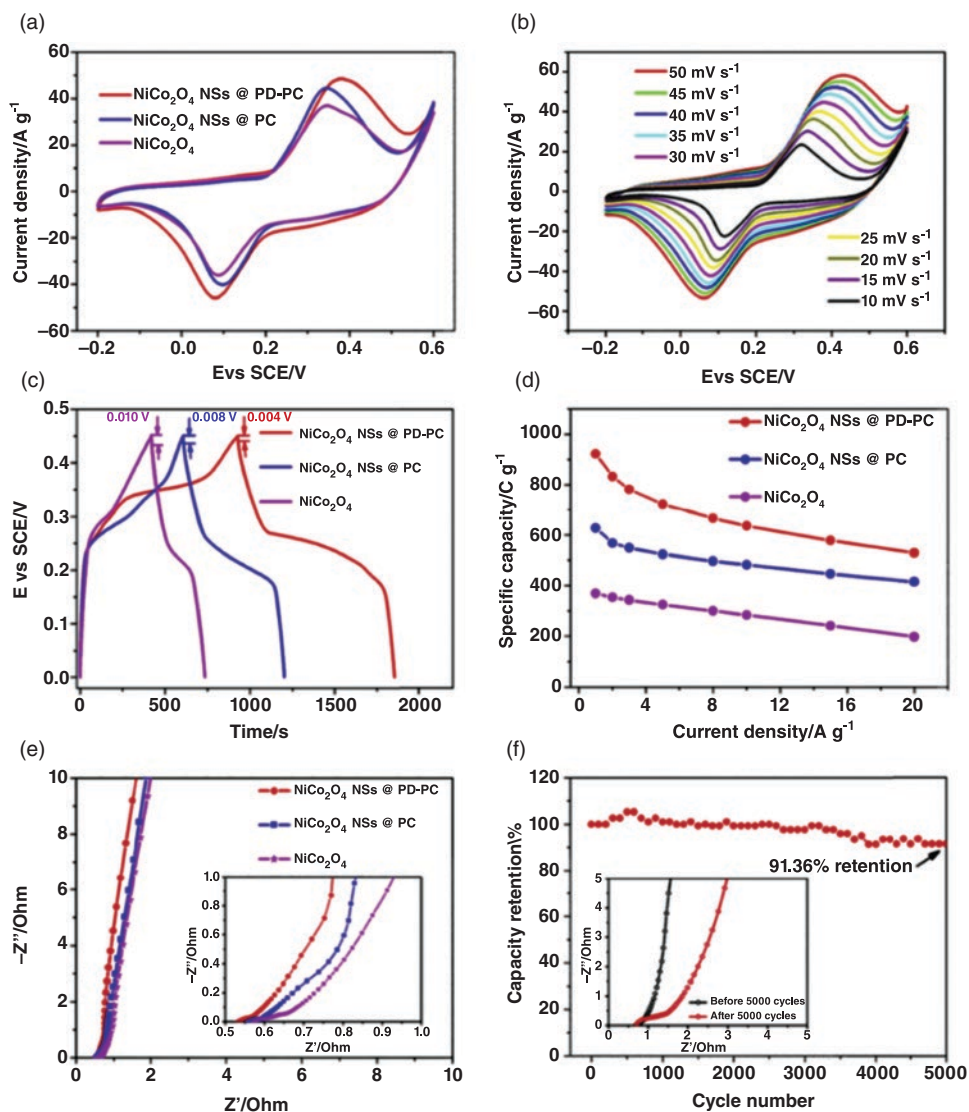
Figure 19.5 CV curves of $NiCo_2O_4$, $NiCo_2O_4$ NSs@PC, and $NiCo_2O_4$ NSs@PD-PC at 30 mV s^{-1}. (b) CV curves of $NiCo_2O_4$ NSs@PD-PC at different scan rates within the potential range of -0.2 to 0.6 V. (c) GCD curves of three electrodes at 1 A g^{-1}. (d) The specific capacity as a function of current density for three electrodes. (e) EIS spectra of three electrodes, inset is the magnified image. (f) Cyclic stability analysis of $NiCo_2O_4$ NSs@PD-PC (up to 5000 cycles) at 10 A g^{-1}, the inset shows the EIS spectra of the electrode materials before and after 5000 cycles. *Reproduced with permission [77]. Copyright 2019, Elsevier.*

cycling performance. The $NiCo_2O_4$/GCNF//activated carbon asymmetric supercapacitor delivered an energy density of 48.6 Wh kg^{-1} at a power density of 749.3 W kg^{-1} with 88.5% capacitance retention after 10000 cycles.

Jackfruit peel-derived activated carbon obtained by chemical activation and 3D microstructure $NiCo_2O_4@Co_3O_4$ composite synthesized via a facile two-step hydrothermal

process was employed to fabricate high energy asymmetric supercapacitor [79]. The outstanding electrochemical performance of the asymmetric supercapacitor was attributed to the building blocks of the porous electrodes. The asymmetric supercapacitor delivered a specific capacitance of $119\,F\,g^{-1}$ and an energy density of $42.5\,Wh\,kg^{-1}$ at a power density of $80\,W\,kg^{-1}$ with excellent cyclability (97% of capacitance retention after 7000 cycles).

Ricinus communis seed-derived honeycomb porous N-doped activated carbon and $NiCo_2O_4@ZnCo_2O_4$ nanocomposite material were employed as electrode materials for supercapacitor applications [80]. Urchin-like $NiCo_2O_4$ displayed superior specific capacity of $150.83\,mAh\,g^{-1}$ at $1\,A\,g^{-1}$ among the other different morphologies of $NiCo_2O_4$ (spherical, rod, and granular). The $NiCo_2O_4$ hybridized with $ZnCo_2O_4$ nanosheets to achieve $NiCo_2O_4@ZnCo_2O_4$ nanocomposite and revealed a significant increase in specific capacitance ($1029\,F\,g^{-1}$ at $1\,A\,g^{-1}$). Moreover, the $NiCo_2O_4@ZnCo_2O_4$//N-doped activated carbon hybrid supercapacitor displayed a specific capacity of $62.78\,mAh\,g^{-1}$ with a maximum energy density of $101.6\,Wh\,kg^{-1}$ at $15500\,W\,kg^{-1}$ and 78.5% capacitance retention after 12000 cycles.

Using loofah biomass as carbon and dicyandiamide as nitrogen sources synthesized 3D N doped porous graphene materials (3D-NPG). Subsequently, $NiMn_2O_4$ nanoparticles were homogeneously dispersed on the 3D-NPG surface using a facile hydrothermal method to form $NiMn_2O_4$/3D-NPG nanocomposite. The $NiMn_2O_4$/3D-NPG nanocomposite revealed unique architecture with a conductive network that facilitated easy interaction between electrolyte ions and $NiMn_2O_4$ nanoparticles and provided a beneficial path for electron transport in the electrochemical reaction [81]. The $NiMn_2O_4$/3D-NPG electrode demonstrated a remarkable specific capacitance ($1308.2\,F\,g^{-1}$ at $1\,A\,g^{-1}$) with outstanding rate capability (77.9% at $15\,A\,g^{-1}$) and good cyclic stability (91.6% capacitance retention after 10000 cycles). The assembled $NiMn_2O_4$/3D-NPG//3D-NPG asymmetric supercapacitor displayed an energy density of $45.25\,Wh\,kg^{-1}$ at $11380\,W\,kg^{-1}$ with impressive cyclic stability.

19.3 Conclusion

This chapter summarizes recently reported literature on the utilization of biomass-derived carbon and transition metal oxides composites as electrode materials for high-performance supercapacitor applications, and focused on the recent development of biomass-derived carbon and transition metal oxides composites as electrode materials for supercapacitors. Biomass-derived carbons possess different sizes, morphologies, pore distributions, interconnected structures, and crystallinities that improve supercapacitors' energy density without affecting their power density and cyclic stability. However, the development of biomass-derived carbon materials is confronted with several challenges such as the different growing environments, harvest time, and nutrition resources of plants at various locations that may cause a huge variety in the size, structure, morphology, and surface properties of biomass-derived carbon. Therefore, considerable research attention is going in to exploring methods to control the biomass-derived carbon properties. The combination of biomass-derived carbons and transition metal oxides facilitates fast redox reaction kinetics and effective charge transfer resulting in high capacitance, rate capability, and cycling

stability of supercapacitors. To obtain desirable physicochemical properties of composites with controllable structures and morphologies, synthesis methods can be reasonably combined so that the intrinsically diverse textures and structures of composite materials can easily be derived.

Acknowledgment

References

1 Y. Li, W. Ou-Yang, X. Xu, M. Wang, S. Hou, T. Lu, Y. Yao, L. Pan, *Electrochim. Acta* **2018**, *271*, 591–598.

2 H. T. Das, S. Dutta, N. Das, P. Das, A. Mondal, M. Imran, *J. Energy Storage* **2022**, *50*, 104643.

3 M. Yaseen, M. A. K. Khattak, M. Humayun, M. Usman, S. S. Shah, S. Bibi, B. S. U. Hasnain, S. M. Ahmad, A. Khan, N. Shah, A. A. Tahir, H. Ullah, *Energies* **2021**, *14*, 7779.

4 S. A. Khan, S. Ali, K. Saeed, M. Usman, I. Khan, *J. Mater. Chem. A* **2019**, *7*, 10159–10173.

5 I. Khan, N. Baig, S. Ali, M. Usman, S. A. Khan, K. Saeed, *Energy Storage Mater.* **2021**, *35*, 443–469.

6 H. T. Das, K. Mahendraprabhu, T. Maiyalagan, P. Elumalai, *Sci. Rep.* **2017**, *7*, 15342.

7 Y. Zhang, S. Yu, G. Lou, Y. Shen, H. Chen, Z. Shen, S. Zhao, J. Zhang, S. Chai, Q. Zou, *J. Mater. Sci.* **2017**, *52*, 11201–11228.

8 R. N. A. R. Seman, M. A. Azam, M. A. Mohamed, *Adv. Nat. Sci.: Nanosci. Nanotechnol.* **2016**, *7*, 045016.

9 Y. Zhu, S. Murali, M. D. Stoller, K. Ganesh, W. Cai, P. J. Ferreira, A. Pirkle, R. M. Wallace, K. A. Cychosz, M. Thommes, *Science* **2011**, *332*, 1537–1541.

10 M. Humayun, H. Ullah, M. Usman, A. Habibi-Yangjeh, A. A. Tahir, C. Wang, W. Luo, *J. Energy Chem.* **2022**, *66*, 314–338.

11 H. T. Das, S. Dutta, T. E. Balaji, N. Das, P. Das, N. Dheer, R. Kanojia, P. Ahuja, S. K. Ujjain, *Chemosensors* **2022**, *10*, 223.

12 M. Usman, M. Humayun, S. S. Shah, H. Ullah, A. A. Tahir, A. Khan, H. Ullah, *Energies* **2021**, *14*, 2281.

13 M. A. Marwat, M. Humayun, M. W. Afridi, H. Zhang, M. R. Abdul Karim, M. Ashtar, M. Usman, S. Waqar, H. Ullah, C. Wang, W. Luo, *ACS Appl. Energy Mater.* **2021**, *4*, 12007–12031.

14 S. S. Shah, H. T. Das, H. R. Barai, M. A. Aziz, *Polymers* **2022**, *14*, 270.

15 S. O. Adio, S. A. Ganiyu, M. Usman, I. Abdulazeez, K. Alhooshani, *Chem. Eng. J.* **2020**, *382*, 122964.

16 Y.-P. Gao, Z.-B. Zhai, K.-J. Huang, -Y.-Y. Zhang, *New J. Chem.* **2017**, *41*, 11456–11470.

17 A. Ali, M. Ammar, M. Ali, Z. Yahya, M. Y. Javaid, S. Ul Hassan, T. Ahmed, *RSC Adv.* **2019**, *9*, 27432–27438.

18 A. Ali, M. Ammar, Z. Yahya, M. Waqas, M. A. Jamal, E. H. M. Salhabi, *New J. Chem.* **2019**, *43*, 10583–10589.

19 M. Ashraf, S. S. Shah, I. Khan, M. A. Aziz, N. Ullah, M. Khan, S. F. Adil, Z. Liaqat, M. Usman, W. Tremel, *Chem. Eur. J.* **2021**, *27*, 6973–6984.

20 C. Chen, Y. Zhang, Y. Li, J. Dai, J. Song, Y. Yao, Y. Gong, I. Kierzewski, J. Xie, L. Hu, *Energy Environ. Sci.* **2017**, *10*, 538–545.

21 M. Li, J. Yu, X. Wang, Z. Yang, *Appl. Surf. Sci.* **2020**, *530*, 147230.

22 H. Zhou, Y. Zhan, F. Guo, S. Du, B. Tian, Y. Dong, L. Qian, *Electrochim. Acta* **2021**, *390*, 138817.

23 Y. Ren, Q. Xu, J. Zhang, H. Yang, B. Wang, D. Yang, J. Hu, Z. Liu, *ACS Appl. Mater. Interfaces* **2014**, *6*, 9689–9697.

24 M. Yang, D. S. Kim, S. B. Hong, J.-W. Sim, J. Kim, -S.-S. Kim, B. G. Choi, *Langmuir* **2017**, *33*, 5140–5147.

25 A. A. Mohammed, C. Chen, Z. Zhu, *J. Power Sources* **2019**, *417*, 1–13.

26 J. Yu, M. Li, X. Wang, Z. Yang, *ACS Omega* **2020**, *5*, 16299–16306.

27 C. Mao, S. Liu, L. Pang, Q. Sun, Y. Liu, M. Xu, Z. Lu, *RSC Adv.* **2016**, *6*, 5184–5191.

28 C. Yuan, H. Lin, H. Lu, E. Xing, Y. Zhang, B. Xie, *Appl. Energy* **2016**, *178*, 260–268.

29 M. Usman, M. Humayun, M. D. Garba, L. Ullah, Z. Zeb, A. Helal, M. H. Suliman, B. Y. Alfaifi, N. Iqbal, M. Abdinejad, A. A. Tahir, H. Ullah, *Nanomaterials* **2021**, *11*, 2029.

30 M. D. Garba, M. Usman, S. Khan, F. Shehzad, A. Galadima, M. F. Ehsan, A. S. Ghanem, M. Humayun, *J. Environ. Chem. Eng.* **2021**, *9*, 104756.

31 L. Yaqoob, T. Noor, N. Iqbal, H. Nasir, M. Sohail, N. Zaman, M. Usman, *Renew. Energy* **2020**, *156*, 1040–1054.

32 R. Razzaq, C. Li, M. Usman, K. Suzuki, S. Zhang, *Chem. Eng. J.* **2015**, *262*, 1090–1098.

33 T. E. Balaji, H. Tanaya Das, T. Maiyalagan, *ChemElectroChem* **2021**, *8*, 1723–1746.

34 A. Ali, M. Ammar, I. Hameed, M. Ali, M. Tayyab, R. Mujahid, I. Ali, M. Zia-ul-haq, M. Ashraf, *J. Electrochem. Soc.* **2020**, *167*, 100509.

35 Z. Shi, L. Xing, Y. Liu, Y. Gao, J. Liu, *Carbon* **2018**, *129*, 819–825.

36 Q. Yin, L. He, J. Lian, J. Sun, S. Xiao, J. Luo, D. Sun, A. Xie, B. Lin, *Carbon* **2019**, *155*, 147–154.

37 B. Sriram, A. Sathiyan, S.-F. Wang, E. Elanthamilan, X. B. Joseph, J. N. Baby, J. P. Merlin, J. C. Ezhilarasi, *J. Solid State Chem.* **2021**, *295*, 121931.

38 Y. Ji, Y. Deng, F. Chen, Z. Wang, Y. Lin, Z. Guan, *Carbon* **2020**, *156*, 359–369.

39 H. S. Kim, M. S. Kang, W. C. Yoo, *Bull. Korean Chem. Soc.* **2018**, *39*, 327–334.

40 Z. Cui, X. Gao, J. Wang, J. Yu, H. Dong, Q. Zhang, L. Yu, L. Dong, *ECS J. Solid. State. Sci. Technol.* **2018**, *7*, M161.

41 Y. Zhan, J. Bai, F. Guo, H. Zhou, R. Shu, Y. Yu, L. Qian, *J. Alloys Compd.* **2021**, *885*, 161014.

42 Q. Wang, Y. Zhang, J. Xiao, H. Jiang, T. Hu, C. Meng, *J. Alloys Compd.* **2019**, *782*, 1103–1113.

43 C. Wan, W. Tian, J. Zhou, Y. Qing, Q. Huang, X. Li, S. Wei, L. Zhang, X. Liu, Y. Wu, *Materials & Design* **2021**, *198*, 109309.

44 Z. Zhai, B. Ren, Y. Xu, S. Wang, L. Zhang, Z. Liu, *Org. Electron.* **2019**, *70*, 246–251.

45 I. U. Din, M. Usman, S. Khan, A. Helal, M. A. Alotaibi, A. I. Alharthi, G. Centi, *J. CO2 Util.* **2021**, *43*, 101361.

46 R. Razzaq, H. Zhu, L. Jiang, U. Muhammad, C. Li, S. Zhang, *Ind. Eng. Chem. Res.* **2013**, *52*, 2247–2256.

47 A. Ali, M. Ammar, A. Mukhtar, T. Ahmed, M. Ali, M. Waqas, M. N. Amin, A. Rasheed, *J. Electroanal. Chem.* **2020**, *857*, 113710.

48 M. Yu, Y. Han, J. Li, L. Wang, *Chem. Eng. J* **2017**, *324*, 287–295.

49 Z. Zhou, F. Chen, T. Kuang, L. Chang, J. Yang, P. Fan, Z. Zhao, M. Zhong, *Electrochim. Acta* **2018**, *274*, 288–297.

50 S. A. Al Kiey, M. S. Hasanin, *Environ. Sci. Pollut. Res.* **2021**, *28*, 1–13.

51 W. Xu, B. Mu, A. Wang, *Electrochim. Acta* **2016**, *194*, 84–94.

52 F. Chen, W. Zhou, H. Yao, P. Fan, J. Yang, Z. Fei, M. Zhong, *Green Chem.* **2013**, *15*, 3057–3063.

53 S. Zhang, Y. Pang, Y. Wang, B. Dong, S. Lu, M. Li, S. Ding, *J. Alloys Compd.* **2018**, *735*, 1722–1729.

54 K. Chen, J. Liu, H. Bian, J. Wei, W. Wang, Z. Shao, *Nanotechnology* **2020**, *31*, 335713.

55 Y. Li, L. Kang, G. Bai, P. Li, J. Deng, X. Liu, Y. Yang, F. Gao, W. Liang, *Electrochim. Acta* **2014**, *134*, 67–75.

56 Z. Wang, C. Ma, H. Wang, Z. Liu, Z. Hao, *J. Alloys Compd.* **2013**, *552*, 486–491.

57 W. Shi, J. Zhu, D. H. Sim, Y. Y. Tay, Z. Lu, X. Zhang, Y. Sharma, M. Srinivasan, H. Zhang, H. H. Hng, *J. Mater. Chem.* **2011**, *21*, 3422–3427.

58 S. Venkateswarlu, H. Mahajan, A. Panda, J. Lee, S. Govindaraju, K. Yun, M. Yoon, *Chem. Eng. J.* **2021**, *420*, 127584.

59 S. R. Manippady, A. Singh, C. S. Rout, A. K. Samal, M. Saxena, *ChemElectroChem* **2020**, *7*, 1928–1934.

60 S. Pourhosseini, O. Norouzi, P. Salimi, H. R. Naderi, *ACS Sustain. Chem. Eng.* **2018**, *6*, 4746–4758.

61 J. Chen, J. Qiu, B. Wang, H. Feng, K. Ito, E. Sakai, *J. Electroanal. Chem.* **2017**, *804*, 232–239.

62 L. Wang, J. Yu, X. Dong, X. Li, Y. Xie, S. Chen, P. Li, H. Hou, Y. Song, *ACS Sustain. Chem. Eng.* **2016**, *4*, 1531–1537.

63 X.-L. Wu, T. Wen, H.-L. Guo, S. Yang, X. Wang, A.-W. Xu, *ACS Nano* **2013**, *7*, 3589–3597.

64 Y. Li, M. Xu, H. Yin, W. Shi, G. I. Waterhouse, H. Li, S. Ai, *J. Alloys Compd.* **2019**, *810*, 151887.

65 C. Zhong, Y. Deng, W. Hu, J. Qiao, L. Zhang, J. Zhang, *Chem. Soc. Rev.* **2015**, *44*, 7484–7539.

66 L. Qie, W. Chen, H. Xu, X. Xiong, Y. Jiang, F. Zou, X. Hu, Y. Xin, Z. Zhang, Y. Huang, *Energy Environ. Sci.* **2013**, *6*, 2497–2504.

67 B.-S. Lou, P. Veerakumar, S.-M. Chen, V. Veeramani, R. Madhu, S.-B. Liu, *Sci. Rep.* **2016**, *6*, 1–11.

68 Y. Zhang, S.-J. Park, *Carbon* **2017**, *122*, 287–297.

69 J. Sun, E. Lei, C. Ma, Z. Wu, Z. Xu, Y. Liu, W. Li, S. Liu, *Electrochim. Acta* **2019**, *300*, 225–234.

70 Z. Cao, R. Li, P. Xu, N. Li, H. Zhu, Z. Li, *J. Colloid Interface Sci.* **2022**, *606*, 424–433.

71 V. Hoffmann, C. Rodriguez Correa, S. Sachs, A. Del Pilar Sandoval-rojas, M. Qiao, A. B. Brown, M. Zimmermann, J. P. Rodriguez Estupiñan, M. T. Cortes, J. M. C. Moreno Pirajan, *Electronic Materials* **2021**, *2*, 324–343.

72 J.-L. Huang, L.-Q. Fan, Y. Gu, C.-L. Geng, H. Luo, Y.-F. Huang, J.-M. Lin, J.-H. Wu, *J. Alloys Compd.* **2019**, *788*, 1119–1126.

73 K. Ramakrishnan, C. Nithya, R. Karvembu, *ACS Appl. Energy Mater.* **2018**, *1*, 841–850.

74 A. Joshi, V. Sahu, G. Singh, R. K. Sharma, *Sustain. Energy Fuels* **2019**, *3*, 1248–1257.

75 N. F. Sylla, S. Sarr, N. M. Ndiaye, B. K. Mutuma, A. Seck, B. D. Ngom, M. Chaker, N. Manyala, *Nanomaterials* **2021**, *11*, 1056.

76 A. Ali, I. Hameed, M. Ammar, R. Mujahid, S. Mirza, *J. Energy Storage* **2021**, *37*, 102472.

77 J. Nan, Y. Shi, Z. Xiang, S. Wang, J. Yang, B. Zhang, *Electrochim. Acta* **2019**, *301*, 107–116.

78 G. Yang, S.-J. Park, *J. Alloys Compd.* **2020**, *835*, 155270.

79 P. Sennu, V. Aravindan, Y.-S. Lee, *J. Power Sources* **2016**, *306*, 248–257.

80 A. J. C. Mary, C. Sathish, P. S. M. Kumar, A. Vinu, A. C. Bose, *Electrochim. Acta* **2020**, *342*, 136062.

81 M. Zhang, Z. Song, H. Liu, T. Ma, *Appl. Surf. Sci.* **2020**, *507*, 145065.

20

Composites of Biomass-derived Materials and Conducting Polymers

Wael Mahfoz[1], Abubakar Dahiru Shuaibu[2], Syed Shaheen Shah[3,4], Md. Abdul Aziz[3,5,*], and Abdul-Rahman Al-Betar[1,3,*]

[1] *Chemistry Department, King Fahd University of Petroleum and Minerals, Dhahran, 31261, Saudi Arabia*

[2] *Material Science and Engineering Department, King Fahd University of Petroleum and Minerals, Dhahran, 31261, Saudi Arabia*

[3] *Interdisciplinary Research Center for Hydrogen and Energy Storage (IRC-HES), King Fahd University of Petroleum & Minerals, KFUPM Box 5040, Dhahran, 31261, Saudi Arabia*

[4] *Physics Department, King Fahd University of Petroleum & Minerals, KFUPM Box 5047, Dhahran, 31261, Saudi Arabia*

[5] *K. A. CARE Energy Research & Innovation Center, King Fahd University of Petroleum & Minerals, Dhahran, 31261, Saudi Arabia*

* Corresponding authors

20.1   Introduction

Energy storage devices have become an essential topic in energy research due to their critical role in sustainable alternative energy usage and storage [1, 2]. A supercapacitor (SC) is considered one of the essential energy storage tools because of its unique properties [3]. SCs generally consist of two electrodes separated by a separator saturated with an electrolyte [4]. Every electrode consists of a current collector covered with an electrode material [2, 4]. There are three types of SC: electrochemical double-layer SC (EDLC), pseudocapacitor, and hybrid [5–7]. The difference between these types is the SC energy storage mechanism. In the case of EDLC, the energy storage mechanism is a double-layer mechanism where the electrode material adsorbs the ions from the electrolyte electrostatically in the charging phase and releases these ions in the discharging phase [8]. In pseudocapacitors, the electrode material contains an active redox material that stores and releases the energy due to its redox reactions [9]. Finally, the hybrid SC used the both previous mechanisms for its charging and discharging phases [10]. As a result, the SC electrode material plays a critical role in the mechanism and performance of SCs [6]. Generally, carbon materials are used to fabricate EDLCs [6, 8], while transition metals oxides, hydroxides, and conductive polymers (CPs) are used to manufacture pseudocapacitors [9].

CPs are organic polymers that can conduct electricity and have unique advantages, including high conductivity, flexibility, low cost, and simplicity of synthesis [11]. Due to these properties, CPs have been used in different electrochemical applications, including sensors [12], corrosion protection [13], water splitting [14], hydrogen generating [15], batteries [16], and SCs [17]. Due to their active redox behavior [18], CPs represent an ideal material for fabrication of SCs, especially pseudocapacitors [18, 19]. For SC fabrication,

using the combination of carbon and CPs has many advantages, including enhancing the active surface of electrode material, improving the SC performance, capacitance, and stability, and decreasing the fabrication cost [19]. Biomass-derived carbon (BDC) is one of the carbon types used successfully and commonly in SC fabrication [20]. Combining biomass carbon with CPs offers many advantages and ways to improve BDC's performance, including increasing the active surface area and wettability, enriching the supercapacitor with pseudocapacitance behavior, and improving the total performance toward capacitance, energy density, and power density [21–23].

BDC syntheses and applications are considered promising fields of science [24–27].BDC studies were triggered by the nanotechnology revolution and inspired by the important discovery of graphene [28–33]. Scientists started searching for new sources of active carbon materials with the nanomaterial's effects and structure. Remarkably, biomass materials have become a rich source for synthesizing different types of active carbon in different sizes and shapes [34, 35]. As a result of the BDC novelty, the BDC-CP-based SC studies are still relatively modest in number. Most BDC-CP-based SC works used the typical PCs of polyaniline (PANI) and polypyrrole (PPy). PANI is considered the most studied CP for its advantages and applications [11, 36]. In addition, PPy is a typical CP used frequently in different research fields [37]. It was predictable that the initial biomass-CP-based SC studies focused on these two precious CPs.

Due to its importance in the biomass-supercapacitor, the combination of BDC and CPs will be discussed in detail. This chapter will cover the basic scientific facts behind the CPs in general and PANI and PPy in particular. Furthermore, the chapter will investigate most of the biomass-CP-based SC studies in detail and predict the future direction of biomass-CP-based SC research.

20.2 BDC-PANI-based SCs

PANI is an organic polymer synthesized from aniline monomer and prepared chemically and electrochemically. PANI is considered one of the oldest conductive polymers, as it was discovered in the nineteenth century by Ferdinand Runge Carl Fritzsche, John Lightfoot, and Henry Letheby [38]. Furthermore, PANI was used in the dye fabric industry at the beginning of the twentieth century. PANI has gotten much attention since 1980, when it was used in different research areas and became the most studied and reported conductive polymer [11]. The polymer characteristics include good temperature resistance, high stability, and electrical conductivity. One of the great advantages of PANI is its ability to form stable and effective composites with a variety of compounds. The BDC-PANI is one of these composites that has been used successfully in the field of SCs . To investigate the synthesis and properties of the composite of BDC-PANI, we have evaluated PANI synthesis and formula from published papers and report synthesis methods of BDC-PANI and the ways to use it as a SC device.

20.2.1 PANI Synthesis Mechanism and Structure

PANI is prepared by oxidative polymerization in an acidic medium. To some extent, the polymerization mechanism is similar in both chemical and electrochemical ways.
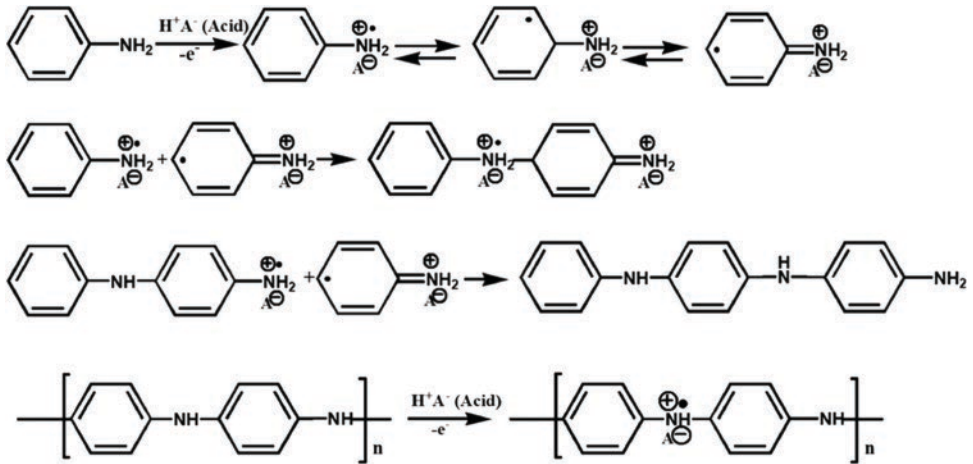
Figure 20.1 PANI electrochemical synthesis mechanism. *Redraw from Ref* [39].

The aniline is initiated by an oxidant initiator in the chemical method and by the applied potential in the electrochemical method (Figure 20.1) [21, 39–42].

The initiation process forms the radical cation of anilinium cation, forming the dimer. Then the oxidation of the dimer and bonding to another anilinium cation leads to the propagation of PANI. The final synthesized PANI structure contains two types of rings which are quinoid and benzenoid ringsas shown below (redraw from Ref [39].).

Quinoid rings **Benzenoid rings**
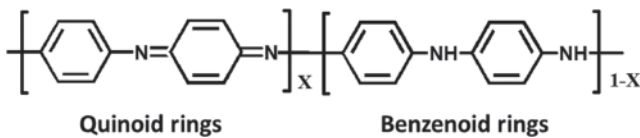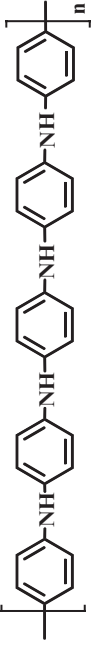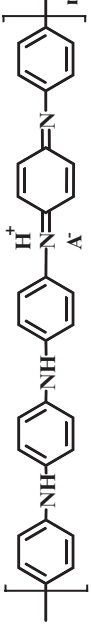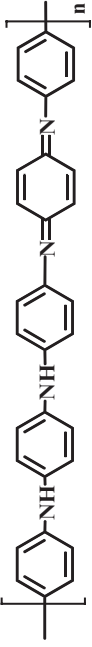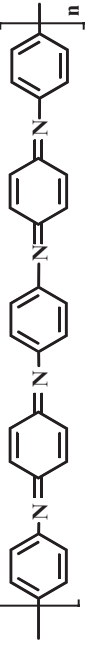
The N atom of PANI is fully oxidized in the benzenoid ring, while it is in a fully reduced state in the quinoid ring. Consequently, the value of X in the above formula, which determines the ratio of the quinoid and benzenoid rings, also determines the type of PANI. We can identify four PANI types: leucoemeraldine, emeraldine base, emeraldine salt, and pernigraniline (Table 20.1) [43–45]. The doped PANI of emeraldine salt is the conductive form of PANI which is formed through biomass carbon-PANI composite synthesis. In general, the PANI emeraldine form is partially oxidized and reduced into the other oxidation states throughout the SC's charging and discharging steps. Consequently, the PANI-based SC is characterized as a pseudocapacitor. Similarly, the BDC-PANI composite-based SC has pseudocapacitance behavior due to PANI and double-layer capacitance behavior due to the BDC.

20.2.2 Synthesis of BDC-PANI Composite

The BDC-PANI composite synthesis depends on the method used to add the PANI to the surface of the BDC. We can identify three primary methods used to synthesize the biomass carbon-PANI composite: (i) in-situ PANI chemical deposition, (ii) ex-situ PANI chemical deposition, and (iii) in-situ PANI electrochemical deposition.

Table 20.1 Forms of PANI. Redraw from ref [45].

PANI form	Status	X Value	Color	Conductivity	Formula
Leucoemeraldine	Completely reduced	0	Colorless	Insulator	
Emeraldine base	Partially oxidized	0.5	Blue	Insulator	
Emeraldine salt	Partially oxidized	0.5	Green	Conductor	
Pernigraniline	Completely oxidized	1	Purple	Insulator	

20.2.2.1 In-situ PANI Chemical Deposition

In-situ chemical deposition of PANI has become the most common method to synthesize the BDC-PANI composite. This method is based on the deposition of PANI on BDC during the formation of PANI. This, in turn, gives the opportunity to form a threaded structure, leading to a stable chemical composite. In general, the monomer of aniline and the initiator are prepared separately in an acidic solution. Then, the BDC is added to one of the solutions. The polymerization of PANI starts by mixing the monomer and the initiator. The PANI is formed throughout and on the surface of the biomass carbon structure. Then the composite is cleaned and prepared for use as an electrode material. In a study by Lyu et al. they modified yeast-derived N-doped microsphere carbon with PANI through an in-situ chemical polymerization to synthesize a BDC-PANI composite [46]. PANI's chemical polymerization occurs directly on the surface of the BDC (Figure 20.2). 20 mg of yeast-derived N-doped microsphere carbon (YC) was mixed with 10 ml of 1 M HCl and 5 ml of ethanol to avoid freezing, which could happen through the low temperature of the PANI polymerization. The aniline was added to the yeast carbon solution and mixed well for two hours at -10 °C. Ammonium persulfate (APS) in a solution of 1 M HCl was used as an initiator at -10 °C and added to the yeast carbon and monomer solution. The polymerization reaction was kept for 24 hours leading to the synthesis of a dark green product. The product was rinsed with ethanol and deionized and kept for freeze drying.

The final dry resultant of yeast carbon (YC)/PANI composite was used to fabricate a symmetrical PANI/YC/aluminum foil/carbon/-based SC. YC/PANI composite was dispersed in deionized water, then dispersed on a glass carbon electrode (GCE) to check the performance of the material in the three-electrode system. The three-electrode system used Ag/AgCl as a reference electrode, a bare Pt wire as a counter electrode, and GCE/yeast carbon/PANI as a working electrode. The experiment was run in a solution of 1 M H_2SO_4 within a potential window of 0–0.8 V. The specific capacitance was 500 Fg^{-1} at a current density of 1 Ag^{-1}. To fabricate a symmetrical two-electrode system, YC/PANI with a ratio of 80 wt.% was mixed with 10 wt% acetylene black and 10 wt.% polyvinylidene fluoride using an organic solution. The resulting slurry was coated on a pellet of titanium foil and dried in an oven with a final
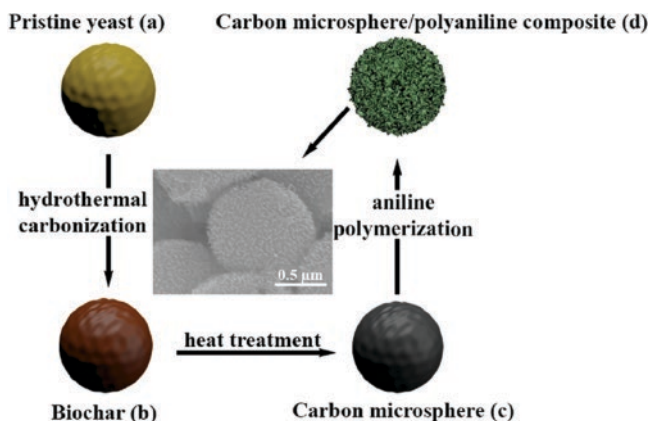
Figure 20.2 Synthesis of YC microsphere-polyaniline composite. *Reproduced with permission* [46]. *Copyright 2018, Elsevier.*

loaded material of 1.5 mg/cm^2. Two symmetrical pellets were put in a 1 M H$_2$SO$_4$ solution overnight for a complete soaking. Then the final SC was fabricated using two symmetrical pieces with a filter paper separator saturated with the electrolyte. The SC was tested within a potential window of 0–1.1 V. The specific capacitance of the fabricated SC was 100 F g^{-1} at a current density of 1 A g^{-1}. The SC achieved an energy density of 16.9 Wh kg^{-1} at a power density of 550 W kg^{-1}. Whereas the stability test shows around 95.4% of the initial capacitance after 5000 cycles.

20.2.2.2 Ex-situ Chemical Polymerization:
In the ex-situ method of chemical deposition of PANI, PANI is prepared chemically by mixing the monomer of aniline and the initiator in an acidic medium. Then, the formed PANI is mixed with the BDC. The product is prepared for use as an electrode material. Ajay et al. used this method to synthesize orange peel-derived activated carbon (OPAC) and PANI nanocomposite for SC fabrication [47]. To prepare the electrode material, OPAC was mixed with prepared PANI of 50 wt.% and mixed well by using mortar and pestle for 30 min. The OPAC-PANI (85%) was mixed with polyvinylidene difluoride (PVDF) (5%) and Ketjan black (10 W%). The mixture was dissolved in N-methyl-2-pyrrolidone (NMP) solvent to prepare a slurry which was coated on a 1 cm x 1 cm Toray carbon paper. The performance of the OPAC-PANI electrode was investigated in a three-electrode system using 1 M KOH (aq.) electrolyte. In a potential window from -1.5 to 0.5 V. The C_{sp} of the OPAC-PANI electrode was 427 F g^{-1} at a scan rate of 2.5 mV s^{-1} with an energy density of 13.44 Wh kg^{-1} at a power density of 19.33 W kg^{-1}. Furthermore, the stability test of the OPAC-PANI electrode was around 70% of the initial capacitance after 5000 cycles. Whereas the OPAC electrode's C_{sp} was only 144 F g^{-1} at scan rate of 2.5 mV s^{-1} with an energy density of 5.27 Wh kg^{-1} at a power density of 17.59 W kg^{-1}.

20.2.2.3 In-situ Electrochemical Polymerization
In contrast to the previous two methods, here PANI is prepared electrochemically on an electrode surface prepared from the synthesized BDC in an acidic medium. Du et al. electro-deposited PANI on BDC from *Enteromorpha prolifera* [48]. *Enteromorpha prolifera* carbon (EPC) was ground with vinylidene fluoride (PVDF) and immobilized on a Pt sheet. The EPC electrode was modified with PANI by in-situ electro-polymerization using a three electrode system. The three electrodes were immersed in 0.3 M aniline solution prepared in 1 M HCl. The PANI was deposited by using the potential of 0.75 V for a specific time. The resulted EPC/PANI was cleaned using deionized water and dried at 60 °C. The EPC/PANI electrode was tested in three-electrode system using 1 M H$_2$SO$_4$ as an electrolyte. The specific EPC/PANI electrode capacitance was 622 F g^{-1} at the current density of 1 A g^{-1}. while the specific capacitance of EPC electrode was only 180 F g^{-1}. Whereas the stability test of the EPC/PANI electrode shows around 87% of the initial capacitance after 2000 cycles.

20.2.3 Factors Influencing Biomass Carbon-PANI Composite Synthesis

20.2.3.1 Effect of Monomer Concentration
Zhang et al. synthesized a porous carbon spheres (PCS) composite derived from γ-cyclodextrin and in-situ chemically-prepared PANI [49]. Their work also studied the

effect of the monomer concentration on the morphological and electrochemical performance of the final fabricated electrode. PCS were prepared as a dispersed solution in a mixture of 1 M HCl and ethanol and mixed with mono-aniline. A solution of ammonium persulfate (APS) in 1 M HCl was added as an initiator. The ratio of APS: monomer used was 1: 1 M. The resultant was dispersed in deionized water to prepare $1\,mg\,ml^{-1}$ solution, and 10 microL was dispersed on a glassy carbon electrode (GCE). The GCE modified with APS-PANI was used as a working electrode, and its capacitance performance was evaluated by GCD techniques using a three-electrode system in 1 M H_2SO_4 electrolyte and applying a potential window from -0.2 to 0.8.

The work tested the effect of the concentration of aniline monomer on the electrochemical performance of the PCS-PANI. Different solutions of aniline concentration, including 5, 10, 20, 30, and 40 mM, were tested. The morphological study of scanning electron microscopy (SEM) illustrates that the surface and pores are covered with PANI when a low concentration of aniline is used, like the concentrations of 5, 10, and 20 mM. On the other hand, using the high concentrations of aniline of 30 and 40 mM shows an expanding growth of PANI on the pores and the surface. Thus, the study recommended the concentration of 20 mM based on the mapping image result, which shows an orderly distribution of C and N atoms on the surface. The electrochemical performance supported the morphological study. The specific capacitance of PCS-PANI electrodes prepared with aniline concentrations of 5, 10, 20, 30, and 40 mM was calculated depending on the GCD measurement. The specific capacitance increases with the increase in the concentration of aniline to reach the highest value of $339.2\,F\,g^{-1}$ at an aniline concentration of 20 mM. Then, the specific capacitance decreases gradually for 30 and 40 mM concentrations, respectively. The specific capacitance of the PCS-PANI electrode was $339.2\,F\,g^{-1}$ at the current density of $1\,A\,g^{-1}$. Where the specific capacitance of PCS electrode was $110\,F\,g^{-1}$, and the specific capacitance of PANI electrode without any biomass adding was $187.1\,F\,g^{-1}$ at the same current density. The energy density of the PCS-PANI electrode was $24.4\,Wh\,kg^{-1}$ at a power density of $7.9\,KW\,kg^{-1}$. Whereas the stability test shows around 98% of the initial capacitance after 3000 cycles.

20.2.3.2 Effect of Biomass Carbon Composition on the PANI Deposition

Shah et al. provided a study on an indium tin oxide electrode (ITO) modified with carbon nanosheets (CNS) derived from *Pithophora polymorpha* and supported with electrodeposited PANI. This study provided a good example of the effect of biomass carbon composition on the PANI deposition and consequently on the fabricated SC performance [21]. In the study, PANI was electrodeposited from a solution of 0.5M aniline in 1M H_2SO_4 using an electrode of ITO modified with CNS derived from *Pithophora polymorpha*. The amperometry technique was used for the PANI electrodeposition at ITO modified with CNS derived from *Pithophora polymorpha* at a potential of 0.75V for 120s. The work used four types of SC that were fabricated from four different electrodes. The four types of electrodes are ITO modified with electrodeposited PANI (PANI/ITO), ITO modified with *Pithophora polymorpha*-derived carbon (C/ITO), C/ITO modified with electrodeposited PANI (PANI/C/ITO), and ITO modified with another type of biomass activated carbon from jute sticks and supported with PANI electrodeposition (PANI/JC/ITO). The same PANI electrodeposition parameters were used in the electrodes modified

with PANI. C/ITO and PANI/ITO-based SCs were tested in order to compare the final performance of the final SCs performancewhereas, PANI/JC/ITO-based SC was used as a comparative material to investigate the effect of biomass carbon type on the PANI electrodeposition. At a current density of $1 \, mA \, cm^2$, the specific capacitance of the C/ITO, PANI/ITO, PANI/C/ITO, and PANI/JC/ITO-based SCs were 37, 77, 176, and $7 \, mF \, cm^2$, respectively. The specific capacitance values show that the capacitance of C/ITO-based SC is improved dramatically by PANI electrodeposition from 37 to $176 \, mF \, cm^2$. Furthermore, the specific capacitance values showed that the capacitance of PANI/ITO-based SC is enhanced from 77 to $176 \, mF \, cm^2$ by using the biomass carbon of *Pithophora polymorpha* as a substrate for PANI electrodeposition. This indicates that the biomass carbon of *Pithophora polymorpha* provides a bigger surface and better structure for PANI electrodeposition. It was clear from the capacitance results that carbon nanosheets (CNS) derived from *Pithophora polymorpha* created a suitable environment for PANI electrodeposition, in contrast to jute stick-derived activated carbon. The main reason for the difference between the two carbon effects on PANI electrodeposition is the difference in their structures. Thus, the characterization study of the CNS derived from *Pithophora polymorpha* illustrated heteroatoms (Mg, Si, P, S, Cl, Ca, Fe, and N)-enriched hierarchical porous carbon.

20.2.4 Properties and Characterization of BDC-PANI SC

As with other BDC-based SC works, the BDC-PANI composite-based SC studies required typical morphological and structural characterization and the electrochemical performance investigation, for example, scanning electron microscope (SEM), x-ray photoelectron spectroscopy (XPS), cyclic voltammetry (CV), galvanostatic charge/discharge (GCD), and stability test for good correlation. In the following section we will examine a set of studies done on BDC-PANI composite based SCs focusing on the method of preparation and fabrication of SC and the specific capacitance performance.

Sahu et al. [22] synthesized PANI-modified mustard oil-derived carbon aerogel (CA) for SC application. The electrode material was prepared based on in-situ chemical polymerization. Initially, mustard oil-derived carbon aerogel was added to a solution of mono-aniline in H_2SO_4. Then, the ammonium persulfate solution, an initiator, was added to the mixture through stirring. The resultant was dispersed onto polished graphite sheets in a solution of isopropyl alcohol to obtain the SC electrode of CA-PANI. An H_2SO_4-PVA gel membrane was used as a separator. The study used the CA-PANI to fabricate an asymmetrical SC of CA/CA-PANI. Where CA was used as a cathode, and CA-PANI was used as an anode. SEM images show the biomass carbon morphological surface before and after deposition with PANI (Figure 20.3). Figure 20.3a-**c** show the biomass carbon surface of CA in different magnitudes. After the deposition process, CA surface was covered with PANI (Figure 20.3d-f). The specific capacitance of CA/CA-PANI-based SC was $64.5 \, F \, g^{-1}$ at the current density of $2.8 \, A \, g^{-1}$. The SC's energy density was $24.4 \, Wh \, kg^{-1}$ at a power density of $7.9 \, KW \, kg^{-1}$. Whereas the stability test shows around 98% of the initial capacitance after 3000 cycles.

XPS is commonly employed as a powerful tool to investigate the chemical composition and presence of functional groups and valency of the elements present in materials,
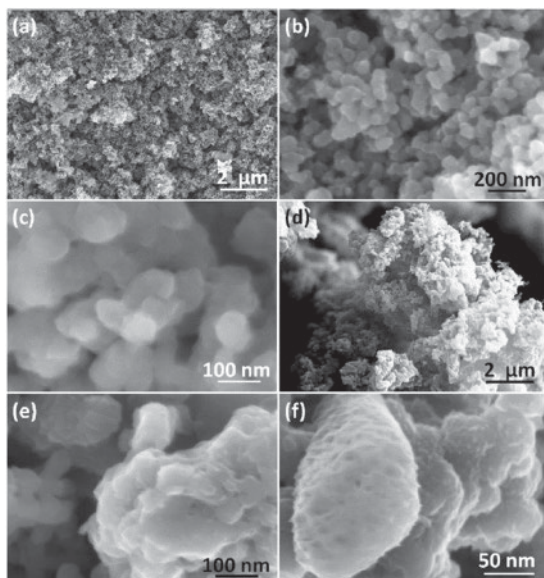
Figure 20.3 SEM images of (a-c) CA and (d-f) CA-PANI. *Reproduced with permission* [22]. *Copyright 2017, Elsevier.*

including BDC-PANI. The study of *Pithophora polymorpha*-PANI-based SC by Shah et al. [21] provided an excellent example of chemical characterization based on XPS (Figure 20.4). The XPS data illustrate the different components of PANI/CNS/ITO electrode material, including C and N, due to the PANI and other elements from the biomass carbon and the substrate material (Figure 20.4a). While (Figure 20.4b-**d**) displays the high-resolution spectra of the C1s, O1s, and N1s.

CV and GCD measurements mainly evaluate the electrochemical performance of the SC, including BDC-PANI-based SC. This includes determining the mechanism of SC's charging and discharging phases and investigating its pseudocapacitance behavior. According to the study of *Enteromorpha prolifera* carbon (EPC)-PANI-based SC by Du et al. [48] the CV measurement illustrates clearly the change in the mechanism of the SC after modification with PANI (Figure 20.5). According to Figure 20.5, the cyclic voltammogram of EPC illustrates a typical double-layer supercapacitor mechanism. On the other hand, the CV of EPC-PANI shows a clear pseudocapacitance behavior due to the two redox peaks corresponding to PANI. Likewise, the GCD of EPC shows a clear shape of an isosceles triangle, indicating the carbon double-layer supercapacitor mechanism (Figure 20.6). In contrast, the GCD of EPC-PANI shows a shape of significant pseudocapacitance behavior.

In the stability test of SC, the biomass carbon-PANI composite shows significant stability throughout the charging/discharging cycles. For example, the aforementioned YC-PANI-based SC offers capacitance retention of 95.4% from the initial capacitance after 5000 cycles (Figure 20.7) [46]. The stability test of YC-PANI illustrates a similar level of stability of YC. The stability test shows low stability for PANI in the same condition.
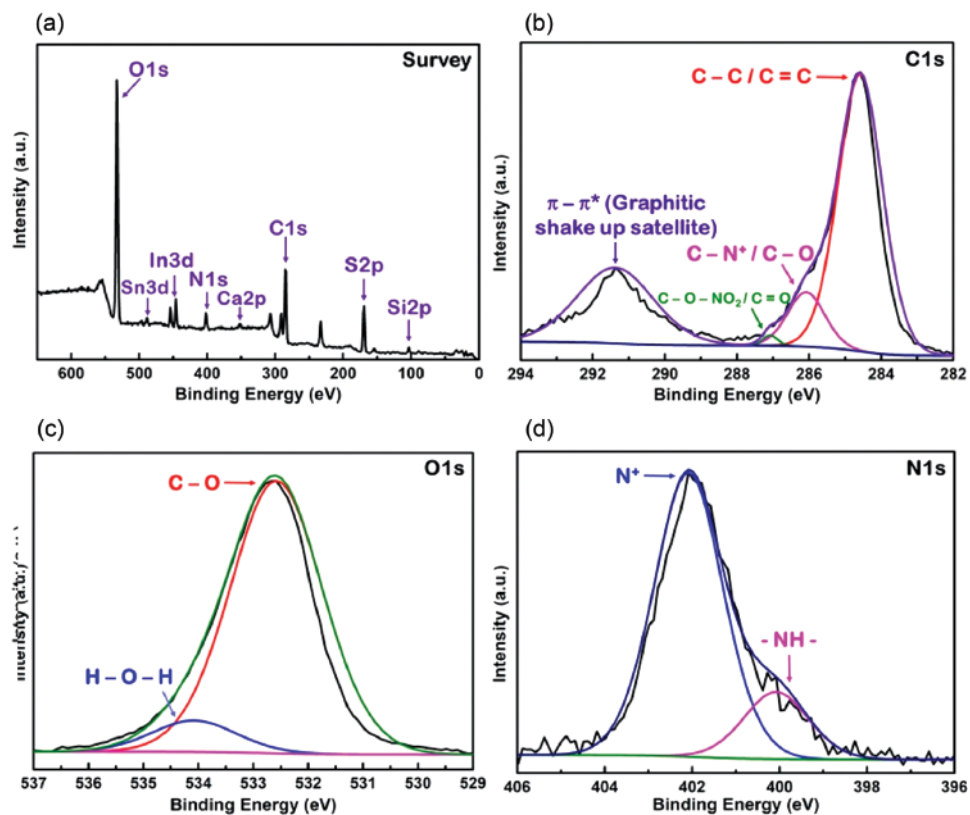
Figure 20.4 XPS of PANI/CNS/ITO (a) and the corresponding spectra of (b) C1s, (c) O1s, and (d) N1s. *Reproduced with permission* [21]. *Copyright 2020, Elsevier.*
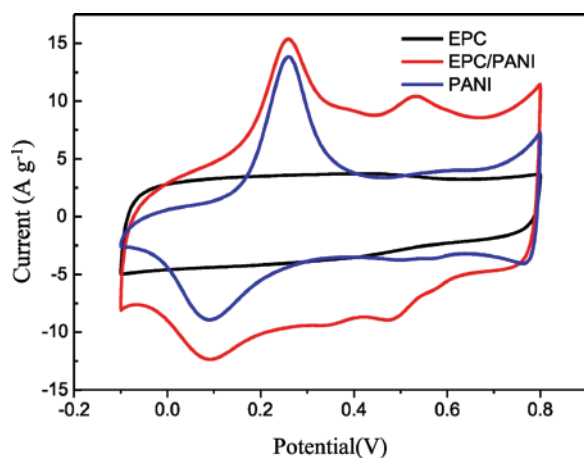
Figure 20.5 CVs of EPC, EPC-PANI, and PANI. *Reproduced with permission* [48]. *Copyright 2017, Elsevier.*
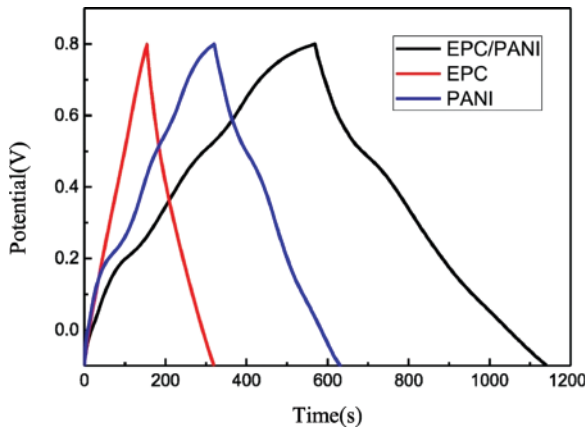
Figure 20.6 GCDs of EPC, EPC-PANI, and PANI. *Reproduced with permission* [48]. *Copyright 2017, Elsevier.*
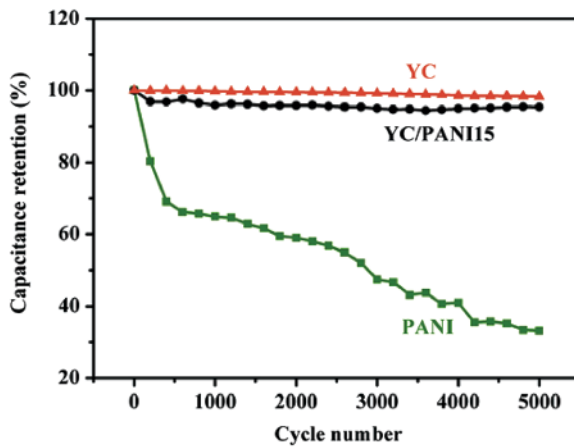
Figure 20.7 Capacitance retention of specific capacitance of the YC/PANI composite. *Reproduced with permission* [46]. *Copyright 2018, Elsevier.*

20.2.5 Fabrication of BDC-PANI-based SCs

Gao et al. synthesized a composite of chitin-derived hierarchically porous carbon microspheres (HCMs) derived from chitin supported with PANI [50]. Firstly, nanofibrous chitin/chitosan microspheres (CCMs) were prepared by dissolving the chitin/chitosan mixture in a solution of ($LiOH/KOH/urea/H_2O$). Then the biomass was stirred in a solution that contained isooctane and Span 85. The biomass was boiled to obtain the CCMs. An acetic acid solution was used to remove the chitosan fiber from the CCMs, and the resultant was marked as CCM-A. The resultant CCM-A was pyrolyzed at 800 °C in the Ar atmosphere to obtain the carbon microsphere (HCM). The PANI was synthesized on the HCM surface by in-situ chemical polymerization of aniline using an APS initiator in $HClO_4$ solution

The HCM-PANI was mixed with acetylene black and tetrafluoroethylene polymer to fabricate the HCM-PANI film electrode. The HCM-PANI film electrodes were used to fabricate a symmetrical SC using 1 M H_2SO_4 as an electrolyte. The SC was tested in a potential window of 0 to 1 V using the two-electrode system. The energy density of the HCM -PANI SC was 8.9 Wh kg^{-1} at a power density of 1644 W kg^{-1}. Whereas the stability test was used CV measurement at a scan rate of 50 mVs^{-1} showing around 90.6% of the initial capacitance after 10000 cycles.

Hu et al. synthesized a biomass carbon derived from chitosan (CS) and modified it with PANI by in-situ chemical polymerization of aniline [51]. After the product was dried, the percentage weight of PANI was calculated by measuring the weight of the sample before and after polymerization. Three samples of CS-PANI were prepared with a different ratio of PANI of 16%, 33%, and 64% of the total mass. The further electrochemical performance showed that the CS-PANI with 33% of PANI gave the best performance and was selected as the optimum value for preparation. The CS-PANI with 33% of PANI was applied to titanium meshes to fabricate a symmetrical SC, with filter paper saturated with 1 M H_2SO_4 as a separator. For a two-electrode system measurement, the specific capacitance of CS-PANI-based SC was 285 Fg^{-1} at the current density of 0.5 Ag^{-1}. The SC energy density was 22.2 Wh kg^{-1} at a power density of 713 W kg^{-1}. Whereas the stability test shows around 80% of the initial capacitance after 5000 cycles.

Yu et al. prepared nitrogen-doped porous carbon derived from wood (NKWC) and then modified the resultant carbon with PANI by in-situ chemical method. The NKWC-PANI was mixed with acetylene black as an electrical conductor and polytertfluorene-ethylene as a binder. Deionized water was added to the mixture to form a paste. The paste was transferred to stainless steel mesh which was used as a current collector. The dried electrode of NKWC-PANI was used as a working electrode, and its electrochemical performance was tested using the three-electrode system in a solution of 1 M H_2SO_4 in a potential window from -0.1 to 0.9 V. A Pt electrode and an Ag/AgCl electrode were used as counter electrode and reference electrode, respectively. The specific capacitance of the NKWC-PANI electrode was 347 Fg^{-1} at the current density of 2 Ag^{-1}. The SC energy density was 44.4 Wh kg^{-1} at a power density of 922 W kg^{-1}.

Tan et al. [52] synthesized a biomass-PANI composite based on porous carbon derived from the dulse plant (DDPC). The DDPC was modified with PANI using aniline as a monomer, and APS as an initiator in an aqueous solution with H_2SO_4 as solvent. Initially, they dissolved DDPC in 1 M H_2SO_4 solution and successively added mono-aniline and the APS to the reaction mass. The resultant of DDPC-PANI was mixed with a graphite material, acetylene black, and polytetrafluoroethylene to form a paste. The resulting paste was used as an electrode material for the stainless steel strip. The DDPC-PANI electrode electrochemical performance was evaluated by using a three-electrode system. The specific capacitance of the DDPC-PANI electrode was 458 Fg^{-1} at the current density of 0.5 Ag^{-1}. In comparison, the specific capacitance of the electrode was higher than the specific capacitance of the DDPC electrode of 218 Fg^{-1}, and the specific capacitance of the PANI electrode of 318 Fg^{-1} at the same current density. Whereas the stability test shows around 66% of the initial capacitance after 5000 cycles. To calculate the energy density and power density, the SC device was fabricated using a DDPC-PANI electrode as an anode and an active carbon electrode as a cathode. It showed an energy density of 9.02 Wh kg^{-1} at a power density of 4.42 KW kg^{-1}.

Wang et al. [53] synthesized the composite of biomass-carbon/PANI from chestnut shell-based activated carbon (CAC) and used it for asymmetrical SC. Then the mono-aniline solution was added to the mixture. To fabricate the SC electrode, initially, the CAC-PANI was mixed with polyvinylidene fluoride (PVDF) N-methyl-2-pyrrolidone to obtain a slurry. Then, the slurry CAC-PANI and polyvinylidene fluoride (PVDF) N-methyl-2-pyrrolidone binder was coated on to a net of stainless-steel and dried. The SC was fabricated using the CAC-PANI electrode as an anode, a tungsten trioxide nanowires electrode as a cathode, a polypropylene film as a separator, and 1 M H_2SO_4 as an electrolyte. The SC electro-performance was tested in a potential window of 0 to 1.5 V, and the obtained specific capacitance of the SC was 274.3 $F\,g^{-1}$ at the current density of 1 $A\,g^{-1}$. The energy density of The SC was 15.4 $Wh\,kg^{-1}$ at a power density of 252 $W\,kg^{-1}$. We tabulated the performances of the developed various BDC-PANI-Based SC performances in Table 20.2 for proper comparison.

20.3 BDC-PPy-based SCs

PPy is identified as a conductive organic polymer synthesized from pyrrole monomer. Like PANI, PPy can be synthesized chemically and electrochemically. Furthermore, PPy has been extensively studied. Due to its properties and stability, PPy is suitable for many electrochemical applications, including SCs.

20.3.1 PPy Synthesis Mechanism and Structure

Pyrrole can be polymerized in a natural aqueous solution and in many organic solvents. The general mechanism of polymerization of pyrrole is like the PANI mechanism polymerization, where the polymerization procedure starts with forming the radical cation of the pyrrole monomer (Figure 20.8) [39]. The initiation process can occur via an oxidative chemical initiator in the case of chemical polymerization or by the applied potential in the case of electrochemical polymerization. The initiation step is followed by forming a dimer from coupling two radical cations. Then, the formed dimer is oxidized to form a radical cation which binds to another cation. This leads to growing the chain of the polymer and forming PPy.

PPy consists of heteroatoms and π-conjugated carbon chains, which is inadequate to achieve high conductivity. However, PPy can gain a high conductivity by the doping process [55].The equation below shows the doping and doping reaction of PPy, redraw from ref [56].
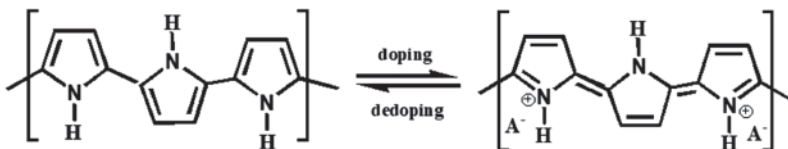
20.3.2 Fabrication of BDC-PPy SCs

Yu et al. synthesized PPy-anchored cattail biomass-derived carbon aerogels starting from raw cattail fibers for supercapacitor application [57]. The entire preparation method of

Table 20.2 Performance of biomass carbon-PANI based supercapacitor devices.

Biomass-derived carbon	Current collector	Electrolyte	Current density ($A\,g^{-1}$)	Potential window (V)	Areal capacitance ($F\,g^{-1}$)	Energy density ($Wh\,kg^{-1}$)	Power density ($W\,kg^{-1}$)	Stability (%@Cycle)	Ref.
Yeast carbon	Titanium foil	1 M H_2SO_4	1	0 to 1.1	100	16.9	550	95.4@5000	[46]
Mustard oil-derived carbon aerogel	Graphite sheets	H_2SO_4-PVA	2.8	0 to 2	64.5	24.4	7900	98@5000	[22]
Orange peel derived carbon	Carbon paper	1 M KOH	$2.5\,mV\,s^{-1}$	-1.5 to 0.5	427	13.44	19.33	70@5000	[47]
Enteromorpha prolifera carbon	Pt sheet	1 M H_2SO_4	1	-0.1 to 0.8	622	-	-	87@2000	[48]
Porous carbon spheres derived from cyclodextrin	GCE	1 M H_2SO_4	1	-0.2 to 0.8	339.2	24.4	7.9	98@3000	[49]
Chitin-derived hierarchically porous carbon microspheres	Same material prepared as a film	1 M H_2SO_4	0.2	0 to 1	76	8.9	1644	90.6@10000	[50]
Carbon derived from chitosan	Titanium mesh	1 M H_2SO_4	0.5	0 to 1.5	285	22.2	713	80@5000	[51]
Nitrogen-doped porous carbon derived from poplar wood sawdust	Stainless steel mesh	1 M H_2SO_4	2	-0.1 to 0.9	347	44.4	922	67@2500	[54]
Dulse-derived porous carbon	Stainless steel strip	1 M H_2SO_4	0.5	-0.2 to 0.7	458	9.02	4420	66@5000	[52]
Chestnut shell-based activated carbon	Stainless steel net	1 M H_2SO_4	0.5	0 to 1.5	274.3	15.4	252	83@1500	[53]
CNS-*Pithophora polymorpha*	ITO	0.1 M HCl	1	0 – 1	176 mF cm^2	24.5 μWh cm^2	500 μW cm^2	>95@1000	[21]
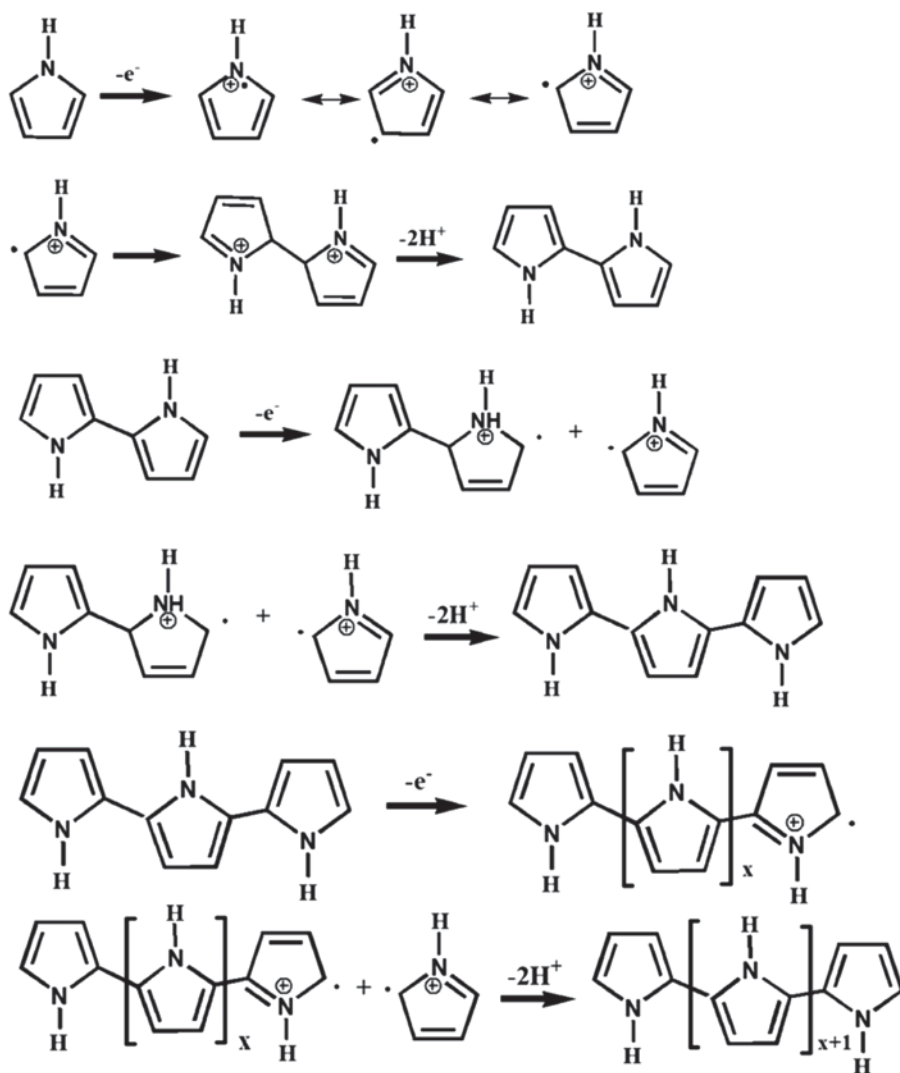
Figure 20.8 Mechanism of PPy synthesis. *Redraw from Ref* [39].

PPy-anchored cattail biomass-derived carbon is schematically described in (Figure 20.9). The PPy-carbon product was cut into 1×1 cm^2 pieces and used as a working electrode in the three-electrode system using 1 M H$_2$SO$_4$ as an electrolyte. The CFCA/PPy electrode capacitance was 419 mF cm^2 at a current density of 1 mA cm^2. The CFCA/PPy electrode shows good stability with capacitance retention of 86.4% after 3000 cycles.

Zhuo et al. [58] synthesized a cellulose carbon aerogel supported with PPy and used the composite successfully in a SC application. To prepare the cellulose carbon, cellulose powder was dissolved in a solution of urea/NaOH/H$_2$O (Figure 20.10). To obtain the cellulose gel, the cellulose solution was temperature-treated for 72 hours at 50 °C. The resulting gel was freeze-dried to create the aerogel. To modify the product cellulose
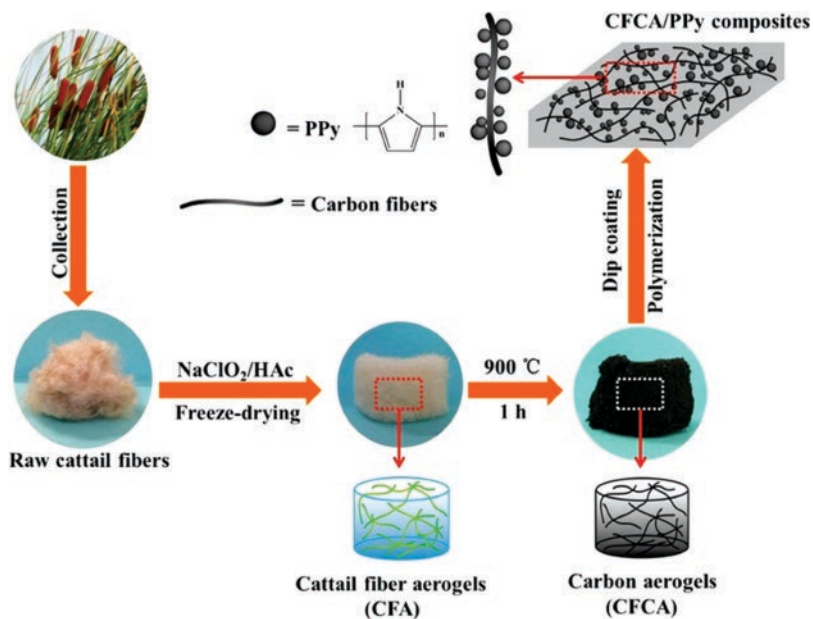
Figure 20.9 PPy-anchored cattail biomass-derived carbon synthesis. *Reproduced with permission* [57]. *Copyright 2018, Elsevier.*
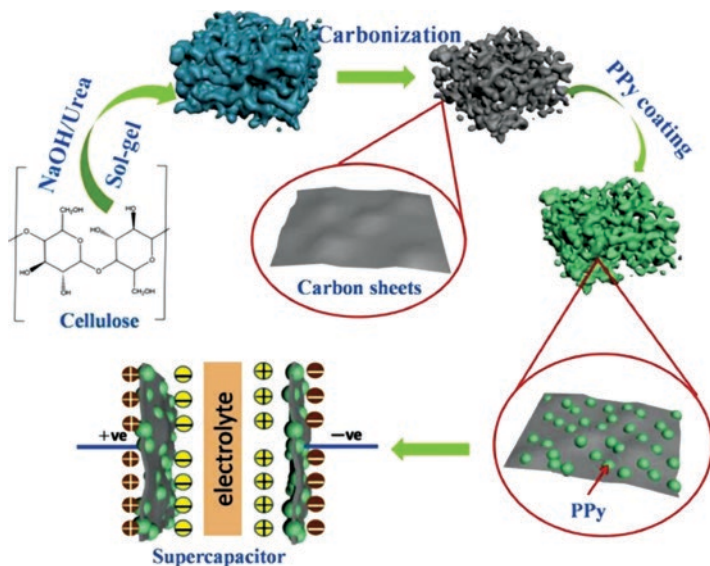
Figure 20.10 Porous cellulose carbon aerogel/PPy composite synthesis. *Reproduced with permission* [58]. *Copyright 2019, Elsevier.*

carbon aerogel with PPy, it was drenched into a pyrrole solution in 0.5 M HCl. Then, an oxidant solution of $FeCl_3 \cdot 6H_2O$ in 0.5 M HCl was added gradually throughout for 30 min. The resultant cellulose carbon aerogel/PPy was cut into slices to prepare a working electrode and clamped between two titanium strip meshes. The cellulose carbon aerogel/PPy performance was tested in the three-system electrode in a potential window from 0.1 to 0.8 V in 1.0 M H_2SO_4. A Pt wire and Ag/AgCl electrodes were used as counter and reference electrodes, respectively. The specific capacitance of the fabricated supercapacitor was 387.6 $F\,g^{-1}$ at a current density of 0.5 $A\,g^{-1}$ with a capacitance retention of 92.6% after 10000 cycles.

dos Reis et al. fabricated a symmetrical SC based on the spruce bark-activated carbon/polypyrrole using in-situ chemical polymerization [59]. The spruce bark was mixed with KOH, with H_2O added, to obtain a homogeneous paste. The paste was dried and pyrolyzed at 900 °C in an inert atmosphere. The resulting carbon was dispersed into a solution of ethyl alcohol and sonicated. Then, prepared internal eggshell membranes was added to the solution and mixed well. The resulting internal eggshell membrane modified with biomass carbon was dried, cleaned, and used as an electrode. The final carbon/internal eggshell membrane electrode was drenched into a solution of $FeCl_3$ which was added later to the monomer solution of pyrrole to form the carbon/PPy composite. To fabricate the SC, two symmetrical electrodes were prepared as a sandwich with a separator of PVA-H_3PO_{4m} membrane. The areal capacitance was 172.5 $mF\,cm^2$ calculated by CV at scan rate of 10 $mV\,s^{-1}$, the calculated energy density was 4.73 $Wh\,kg^{-1}$ at a power density of 320.8 $W\,kg^{-1}$, and the capacitance retention was 60% after 1000 cycles.

Liu et al. [60] used N-doped carbon derived from mesophase pitch and PPy for SC fabrication. Initially, mono-pyrrole was dissolved in a mixture of H_2SO_4 and ethanol and mixed in a silica MCM-48 template to move the PPy oligomer into the template pores. Then, N-methyl pyrrolidone (NMP) was added to dissolve the oligomers and mixed with mesophase pitch (MP). The mixture was pre-oxidized to obtain the PPy and followed with carbonization to obtain the silica template with N-doped carbon. The silica template was removed using HF and the product was cleaned. The resultant was used to fabricate the SC electrodes by mixing with acetylene black and polytetrafluoroethylene in ethanol. The material was dispersed on a stainless-steel strip and dried. The final SC was fabricated by applying two symmetrical electrodes as a sandwich with a filter paper separator saturated in 6 M KOH. The potential window of -1 to 0 V was used to test the SC performance. In two system-electrode systems, the specific capacitance was 110.6 $F\,g^{-1}$ at a current density of 0.2 $A\,g^{-1}$. Energy density was 15.30 $Wh\,kg^{-1}$ at a power density of 399.9 $W\,kg^{-1}$. The capacitance retention was 89.8% after 5000 cycles. We tabulated the performances of the developed various BDC-PANI-based SC performances in Table 20.3 for proper comparison.

20.4 Conclusions

This chapter summarizes in detail the composites derived from BDC and CPs as electrode materials for supercapacitors. BDC-CPs-based supercapacitors as energy storage devices have the advantage of combining the properties of both BDC and CPs. Also, due to its pseudocapacitance properties, the CP supports the electrode material with a high

Table 20.3 Performance of BDC-PPy based supercapacitors.

Biomass-derived carbon	Current collector	Electrolyte	Current density (A g^{-1})	Potential window	Areal capacitance (F g^{-1})	Energy density (Wh kg^{-1})	Power density (W kg^{-1})	Stability (%@Cycle)	Ref.
Cellulose carbon aerogel	The same material	1 M H$_2$SO$_4$	0.5	-0.1 – 0.8	387.6	-	-	92.6@10000	[58]
Mesophase pitch	Stainless-steel	6 M KOH	0.2	-1 – 0	110.6	15.30	399.9	89.8@5000	[60]
CFCA/PPy	The same material -	1 M H$_2$SO$_4$	1	0 – 0.8	419	-	-	86.4@3000	[57]
Spruce bark activated carbon	internal eggshell membrane	PVA-H$_3$PO$_4$	-	0 – 0.8	172.5	4.73	320.8	60@1000	[59]

supercapacitance performance. The main drawback associated with CPs is their mechanical degradation. Various methods have been discussed in detail, including coupling them with BDC to complement their mechanical properties. Due to the importance of the CPs for SCs, it is predictable that more types of CPs will be used to modify the biomass carbon SC and enhance its performance.

Acknowledgments

References

1 Y. Huang, M. Zhu, Y. Huang, Z. Pei, H. Li, Z. Wang, Q. Xue, C. Zhi, *Adv. Mater.* **2016**, *28*, 8344–8364.

2 W.-J. Song, S. Lee, G. Song, H. B. Son, D.-Y. Han, I. Jeong, Y. Bang, S. Park, *Energy Storage Mater.* **2020**, *30*, 260–286.

3 J. Libich, J. Máca, J. Vondrák, O. Čech, M. Sedlaříková, *J. Energy Storage* **2018**, *17*, 224–227.

4 J. Yan, Q. Wang, T. Wei, Z. Fan, *Adv. Energy Mater.* **2014**, *4*, 1300816.

5 S. S. Shah, S. M. A. Nayem, N. Sultana, A. J. S. Ahammad, M. A. Aziz, *ChemSusChem* **2022**, *15*, e202101282.

6 M. Yaseen, M. A. K. Khattak, M. Humayun, M. Usman, S. S. Shah, S. Bibi, B. S. U. Hasnain, S. M. Ahmad, A. Khan, N. Shah, A. A. Tahir, H. Ullah, *Energies* **2021**, *14*, 7779.

7 S. S. Shah, M. A. Aziz, E. Cevik, M. Ali, S. T. Gunday, A. Bozkurt, Z. H. Yamani, *J. Energy Storage* **2022**, *56*, 105944.

8 Y. Wang, L. Zhang, H. Hou, W. Xu, G. Duan, S. He, K. Liu, S. Jiang, *J. Mater. Sci.* **2021**, *56*, 173–200.

9 S. Fleischmann, J. B. Mitchell, R. Wang, C. Zhan, D.-E. Jiang, V. Presser, V. Augustyn, *Chem. Rev.* **2020**, *120*, 6738–6782.

10 S. S. Shah, M. A. Aziz, Z. H. Yamani, *Chem. Rec.* **2022**, *22*, e202200018.

11 M. Beygisangchin, S. Abdul Rashid, S. Shafie, A. R. Sadrolhosseini, H. N. Lim, *Polymers (Basel)* **2021**, *13*.

12 T. Sen, S. Mishra, N. G. Shimpi, *RSC Adv.* **2016**, *6*, 42196–42222.

13 P. P. Deshpande, N. G. Jadhav, V. J. Gelling, D. Sazou, *J Coat. Technol. Res.* **2014**, *11*, 473–494.

14 W. Mahfoz, M. A. Aziz, S. S. Shah, A.-R. Al-Betar, *Chem. Asian J.* **2020**, *15*, 4358–4367.

15 H. M. El-Bery, M. R. Salah, S. M. Ahmed, S. A. Soliman, *RSC Adv.* **2021**, *11*, 13229–13244.

16 P. Sengodu, A. D. Deshmukh, *RSC Adv.* **2015**, *5*, 42109–42130.

17 Q. Meng, K. Cai, Y. Chen, L. Chen, *Nano Energy* **2017**, *36*, 268–285.

18 A. M. Bryan, L. M. Santino, Y. Lu, S. Acharya, J. M. D'Arcy, *Chem. Mater.* **2016**, *28*, 5989–5998.

19 X. Cai, K. Sun, Y. Qiu, X. Jiao, *Crystals* **2021**, *11*, 947.

20 S. Saini, P. Chand, A. Joshi, *J. Energy Storage* **2021**, *39*, 102646.

21 S. S. Shah, M. A. Alfasane, I. A. Bakare, M. A. Aziz, Z. H. Yamani, *J. Energy Storage* **2020**, *30*, 101562.

22 V. Sahu, R. B. Marichi, G. Singh, R. K. Sharma, *Electrochim. Acta* **2017**, *240*, 146–154.

23 S. S. Shah, M. A. Aziz, W. Mahfoz, A.-R. Al-Betar, Conducting Polymers Based Nanocomposites for Supercapacitors in *Nanostructured Materials for Supercapacitors*, (Eds. S. Thomas, A. B. Gueye, R. K. Gupta), Springer, Cham, **2022**, Chapter 22, 485–511, vol. *1*.

24 S. S. Shah, M. A. Aziz, *Bangladesh J. Plant Taxon.* **2020**, *27*, 467–478.

25 S. S. Shah, M. N. Shaikh, M. Y. Khan, M. A. Alfasane, M. M. Rahman, M. A. Aziz, *Chem. Rec.* **2021**, *21*, 1631–1665.

26 N. C. Deb Nath, S. S. Shah, M. A. A. Qasem, M. H. Zahir, M. A. Aziz, *ChemistrySelect* **2019**, *4*, 9079–9083.

27 M. A. Aziz, S. S. Shah, S. M. A. Nayem, M. N. Shaikh, A. S. Hakeem, I. A. Bakare, *J. Energy Storage* **2022**, *50*, 104278.

28 A. K. Geim, *Phys. Scr.* **2012**, *T146*, 014003.

29 M. Ashraf, S. S. Shah, I. Khan, M. A. Aziz, N. Ullah, M. Khan, S. F. Adil, Z. Liaqat, M. Usman, W. Tremel, M. N. Tahir, *Chem. Eur. J.* **2021**, *27*, 6973–6984.

30 S. M. Abu Nayem, S. S. Shah, N. Sultana, M. A. Aziz, A. J. Saleh Ahammad, *Chem. Rec.* **2021**, *21*, 1039–1072.

31 S. Islam, S. S. Shah, S. Naher, M. A. Ehsan, M. A. Aziz, A. J. S. Ahammad, *Chem. Asian J.* **2021**, *16*, 3516–3543.

32 S. S. Shah, H. Yang, M. Ashraf, M. A. A. Qasem, A. S. Hakeem, M. A. Aziz, *Chem. Asian J.* **2022**, *17*, e202200567.

33 M. Usman, M. Humayun, S. S. Shah, H. Ullah, A. A. Tahir, A. Khan, H. Ullah, *Energies* **2021**, *14*, 2281.

34 N. Anzar, R. Hasan, M. Tyagi, N. Yadav, J. Narang, *Sensors Int.* **2020**, *1*, 100003.

35 K. Itami, T. Maekawa, *Nano Lett.* **2020**, *20*, 4718–4720.

36 Z. A. Boeva, V. G. Sergeyev, *Polym. Sci. Ser. C* **2014**, *56*, 144–153.

37 J. Stejskal, M. Trchová, *Chem. Pap.* **2018**, *72*, 1563–1595.

38 S. Rasmussen, *Substantia* **2017**, *1*, 99–109.

39 M. M. Gvozdenović, B. Jugović, J. Stevanović, B. N. Grgur, *Hem. Ind.* **2014**, *68*, 673–684.

40 S. S. Shah, H. T. Das, H. R. Barai, M. A. Aziz, *Polymers* **2022**, *14*, 270.

41 S. S. Shah, M. A. Aziz, A.-R. Al-Betar, W. Mahfoz, *Arab. J. Chem.* **2022**, *15*, 104058.

42 M. M. Hasan, T. Islam, A. Imran, B. Alqahtani, S. S. Shah, W. Mahfoz, M. R. Karim, H. F. Alharbi, M. A. Aziz, A. J. S. Ahammad, *Electrochim. Acta* **2021**, *374*, 137968.

43 G. Inzelt, M. Pineri, J. Schultze, M. Vorotyntsev, *Electrochim. Acta* **2000**, *45*, 2403–2421.

44 A. Pron, P. Rannou, *Prog. Polym. Sci.* **2002**, *27*, 135–190.

45 N. Gospodinova, L. Terlemezyan, *Prog. Polym. Sci.* **1998**, *23*, 1443–1484.

46 L. Lyu, H. Chai, K.-D. Seong, C. Lee, J. Kang, W. Zhang, Y. Piao, *Electrochim. Acta* **2018**, *291*, 256–266.

47 K. Ajay, M. Dinesh, G. Byatarayappa, M. Radhika, N. Kathyayini, H. Vijeth, *Inorg. Chem. Commun.* **2021**, *127*, 108523.

48 W. Du, X. Wang, X. Ju, K. Xu, M. Gao, X. Zhang, *J. Electroanal. Chem.* **2017**, *802*, 15–21.

49 W. Zhang, T. Xia, X. Huo, X. Li, S. Park, L. Lin, G. Diao, Y. Piao, *J. Electroanal. Chem.* **2022**, *920*, 116615.

50 L. Gao, L. Xiong, D. Xu, J. Cai, L. Huang, J. Zhou, L. Zhang, *ACS Appl. Mater. Interfaces* **2018**, *10*, 28918–28927.

51 Y. Hu, X. Tong, H. Zhuo, L. Zhong, X. Peng, *ACS Sustain. Chem. Eng.* **2017**, *5*, 8663–8674.

52 Y. Tan, Y. Liu, Y. Zhang, C. Xu, L. Kong, L. Kang, F. Ran, *J. Appl. Polym. Sci.* **2018**, *135*, 45776.

53 H. Wang, G. Ma, Y. Tong, Z. Yang, *Ionics* **2018**, *24*, 3123–3131.

54 S. Yu, D. Liu, S. Zhao, B. Bao, C. Jin, W. Huang, H. Chen, Z. Shen, *RSC Adv.* **2015**, *5*, 30943–30949.

55 S. Carquigny, O. Segut, B. Lakard, F. Lallemand, P. Fievet, *Synth. Met.* **2008**, *158*, 453–461.

56 P. Camurlu, *RSC Adv.* **2014**, *4*, 55832–55845.

57 M. Yu, Y. Han, Y. Li, J. Li, L. Wang, *Carbohydr. Polym.* **2018**, *199*, 555–562.

58 H. Zhuo, Y. Hu, Z. Chen, L. Zhong, *Carbohydr. Polym.* **2019**, *215*, 322–329.

59 G. S. Dos Reis, R. M. A. P. Lima, S. H. Larsson, C. M. Subramaniyam, M. Thyrel, H. P. de Oliveira, *J. Environ. Chem. Eng.* **2021**, *9*, 106155.

60 M. Liu, W. Li, S. Ruan, Y. Fei, *Energy Fuel* **2020**, *34*, 5044–5051.

21

Composite of Biomass-derived Material and Conductive Material Excluding Conducting Polymer Material

Nasrin Sultana[1], Ahmar Ali[2], S. M. Abu Nayem[1], Syed Shaheen Shah[2,3], Md. Hasan Zahir[4], A. J. Saleh Ahammad[1,*], and Md. Abdul Aziz[3,5,*]

[1] *Department of Chemistry, Jagannath University, Dhaka, 1100, Bangladesh*

[2] *Physics Department, King Fahd University of Petroleum & Minerals, KFUPM Box 5047, Dhahran 31261, Saudi Arabia*

[3] *Interdisciplinary Research Center for Hydrogen and Energy Storage (IRC-HES), King Fahd University of Petroleum & Minerals, Dhahran 31261, Saudi Arabia*

[4] *Interdisciplinary Research Center for Renewable Energy and Power Systems (IRC-REPS), Research Institute, King Fahd University of Petroleum & Minerals, Dhahran, 31261, Saudi Arabia*

[5] *K.A. CARE Energy Research and Innovation Center, King Fahd University of Petroleum & Minerals, Dhahran, 31261, Saudi Arabia*

* *Corresponding author*

21.1   Introduction

An electrode is a discrete and fundamental part of a supercapacitor. The supercapacitor's charge storage mechanism and performance largely depend on the electrode material. Thus, the improvement of electrode material and its morphology has become an interest of many researchers. Generally, traditional carbon materials (graphene, carbon nanotubes, templated carbon) with porous structures and high surface area are the conventional choice for electrode material (primarily for EDLC), as the porous structure can store a large amount of charge [1, 2]. Synthesis of these carbon materials is costly and requires nonrenewable raw materials [1]. Thereby large-scale production and their application as electrode materials are limited. In this regard, synthesizing carbon material with a comparable capacitive performance from a cost-effective, readily available and renewable nature source is desirable for electrode material. Biomass (plants, animal residues, and waste) is a renewable and abundantly available green source of carbon content [3, 4]. BDCs reduce costs and provide porous structured carbon with a tunable opportunity to enhance the supercapacitor performance. Biomass material usually contains a large amount of hemicellulose, cellulose and lignin [4–6]. These biomass components can be converted into desirable activated carbon materials following the appropriate procedure. However, biomass precursors often contain heteroatoms like N, O, P, and S, and appropriate treatment of these biomass precursors results in self-doped activated carbon with improved conductivity and enhanced electrochemical performance [7–9]. Compared with EDLC (which has high power density), pseudocapacitors show high energy density and specific capacitance [10, 11]. In this regard, a composite of BDCs with conductive materials, i.e., metal/metal

nanoparticle, transition metal sulfide, can introduce the Faradaic charge storage mechanism (pseudocapacitance) in EDLC to enhance the energy density and specific capacitance. Also, composite of BDCs with CNTs and rGO helps to enhance conductivity and thereby, high charge storage property is derived [12–15].

21.2 Importance of BDCs Composite with Conductive Materials as an Electrode for Supercapacitors

BDCs as the electrode usually show poor energy density and conductivity [16]. Inappropriate pore size distribution during the carbonization of biomass precursors results in a poor effective surface area for electrolyte ions adsorption and reduces the specific capacitance [17]. Theoretical study shows that there is a proportional relationship between specific capacitance and energy density $\left[E = \frac{1}{2} CV^2 \right]$ [18]. Therefore, an increase in the capacitance property of the BDC electrode will increase the energy density. Developing surface morphology by introducing an appropriate porous structure will provide high specific surface area (SSA) and large charge storage capacity [9, 19–21]. But still, there are some limiting points which reduce the electrochemical performance of BDC electrodes. The conductivity and wettability of electrode materials have an immense effect on the voltametric performance, especially when an aqueous electrolyte is used [22] because intrinsic resistance of poor conducting electrode material makes poor contact with electrolyte ions. Therefore, the low conductivity of electrode material reduces the charge storage capacity and plays a significant role in reducing electrochemical performance. Working on the surface chemistry of BDCs can resolve the issue. Modifying surface chemistry significantly affects conductivity, wettability, and capacitance performance [23, 24]. However, activation and heteroatom doping show great potential to enhance the capacitive performance of BDCs [18, 25]. Composite formation with conductive materials is another way to enhance the electrochemical performance of BDCs. It can reduce the intrinsic resistance of BDCs and thereby shows high charge storage performance. Moreover, the synergistic effect of composite material improves electrode performance by enlarging the specific capacitance value with a reasonable retention rate at long cycles [26, 27].

21.3 Composite of BDCs with Conductive Materials

21.3.1 Composites with Metal Nanoparticles

Metal nanoparticles in the composite material serve as a bridge to fasten the electron transfer and exhibit high capacitance [28]. High conductivity and surface energy of metal nanoparticles leads to high charge storage capacity for the BDCs. Earlier metal particles or/and nanoparticles have been used to prepare BDC composite electrodes, which showed high capacitance performance. The incorporation of Au in BDCs significantly enhanced electrode performance [13, 29, 30]. Ma et al. [30] showed that a composite of porous carbon derived from phoenix tree leaves (PPTLC) and Au nanoparticles exhibited high specific capacitance $440\,\text{F}\,\text{g}^{-1}$. BET analysis also confirmed impregnation of PPTLC with Au

enlarged the specific surface area with uniform sizes of micro- and mesopores. Avila-Brande et al. [29] showed the addition of Au nanoparticles increased the voltammetric capacitance of activated carbon from bamboo waste. Ag particles are also used to advance the BDCs electrodes for high-performance supercapacitors. The gravimetric capacitance value of activated carbon derived from ash was increased by 31% due to the presence of Ag in the activated carbon composite material (Ag-BC). Use of BDCs in this study reduced the production cost by about 92% [31]. Here, the capacitive performance of the activated carbon was accelerated by the irreversible reaction between Ag^+ ions in the electrode and the electrolyte $Li[N(SO_2CF_3)_2]$, as shown below.

$$Ag^+ + Li\left[N\left(SO_2CF_3\right)_2\right] \rightarrow Ag\left[N\left(SO_2CF_3\right)_2\right]\downarrow + Li^+$$
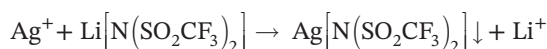
In another study, a hybrid electrode consisting of mainly Ag particles and carbonized wood carbon (CWC derived from poplar catkin) exhibited much better capacitive performance (in KOH electrolyte) than the singly CWC derived from both poplar catkin and poplar fibre [32]. Ru nanoparticle was also incorporated into the BDC to prepare a hybrid electrode for the supercapacitor [33].

As shown in Figure 21.1a, a large shape cyclic voltammetry (CV) curve is observed for the $Ru_{1.0}$-MOC-900 electrode where MOC stands for activated carbons obtained from *Moringa oleifera* fruit shells annealed at 900 °C and the subscript denotes the amount of Ru added in the composite. CV curve also exhibits excellent pseudocapacitance behaviour with EDLC. Figure 21.1d shows the galvanostatic charge-discharge (GCD) curve at different current densities for the $Ru_{1.0}$-MOC-900 electrode. This study also revealed that only the optimized amount of metal in the composite could accelerate the electrode performance. Lei et al. [34] showed when collagen-derived carbon (containing self-heteroatom N) was doped using Mn metal, the conductivity and specific capacitance increased to a high value introducing a Faradaic charge storage mechanism. Co and Cu also show similar behaviour to enhance the electrochemical performance of BDC electrodes [35].

21.3.2 Composite with Transition Metal Sulfides

As well as transition metal oxides, transition metal sulfides are very effective electro-active materials for pseudocapacitors [13, 15, 36–39]. Recently electro-active NiS, CuS, CoS, and MnS have been explored to fabricate electrode material for the high-performance supercapacitor due to their reversible redox process and relatively high theoretical pseudocapacitance value [27, 40]. Peng et al. [41] useds nitrogen-doped pomelo mesocarps-based carbon nanosheet, (N-PMCN) as a positive electrode and $NiSe@MoSe_2$ nanosheet arrays as a negative electrode, a novel asymmetric supercapacitor (ASC) was fabricated that had a high energy density. Figure 21.2 shows due to the special nanosheet array structure of $NiSe@MoSe_2$ and the interconnected sheet-like porous morphology with high nitrogen content (9 wt.%) of N-PMCN. $NiSe@MoSe_2$ demonstrated a maximum specific capacity of 128.20 mAh g^{-1} and a high specific capacitance of 223.0 F g^{-1} at a current density of 1.0 A g^{-1}. The newly constructed $NiSe@MoSe_2$/N-PMCN asymmetric SC device also demonstrated exceptional cycling stability, retaining 91.4% of its capacitance after
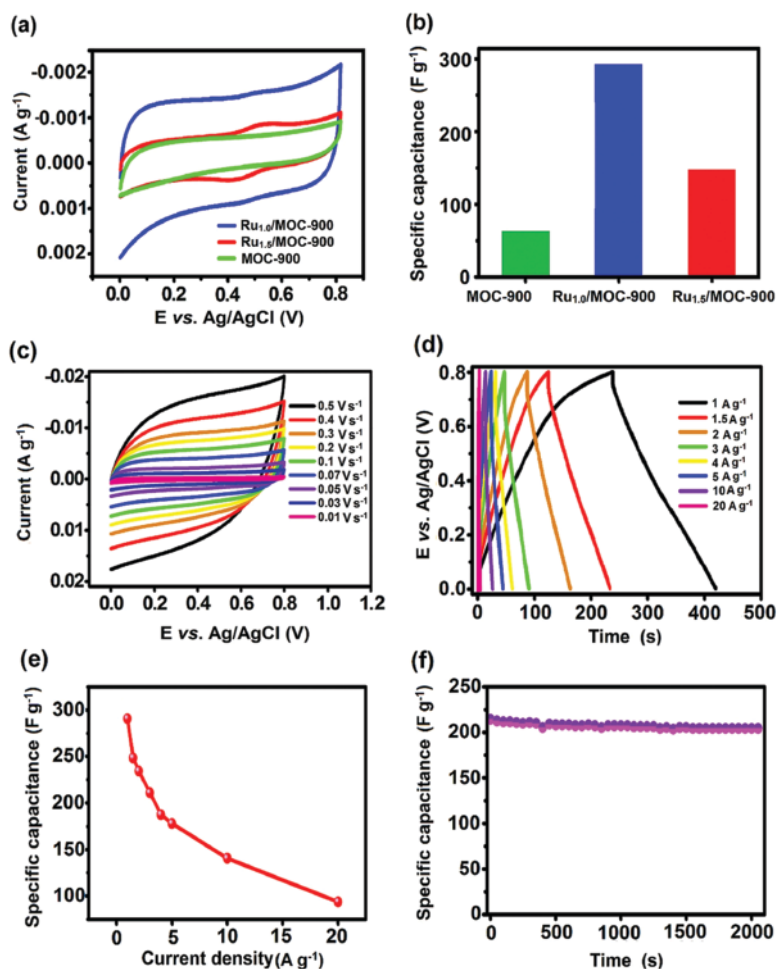
Figure 21.1 The electrochemical capabilities of several MOC-based electrodes. (a) CV graphs were captured at a scanning rate of $10\,mV\,s^{-1}$ in an electrolyte of $1.0\,M\,H_2SO_4$ aqueous. (b) Corresponding capacitances measured for the different electrodes. (c) CV graphs recorded between 10 and $500\,mV$ per second. (d) GCD graphs at different current densities, i.e. $(1-20A\,g^{-1})$. (e) change in specific capacitance with the current density. (f) Test of the cyclic stability at the constant current density of $4.0A\,g^{-1}$. Reproduced with permission [33]. *Reproduced under the terms of the CC BY 4.0 license. Copyright 2016, Lou et al.*

the 5000 cycles in an aqueous electrolyte and having a high energy density of $32.60\,Wh\,kg^{-1}$ at a power density of $415.0\,W\,kg^{-1}$. Its maximum operating voltage is $1.65\,V$. Wang el at [42]. studied the significant effect of ternary metallic sulfide, $NiCo_2S_4$, to enrich the capacitive performance of the activated carbon prepared from gasified rice husk.

21.3.3 Composite with CNTs

Rational incorporation of CNTs (sp^2) into porous structure carbon is desirable to have conductive 3D nanostructures material with full compact merit of all material. CNTs are highly known for their high conductivity, surface area, high chemical stability, and low
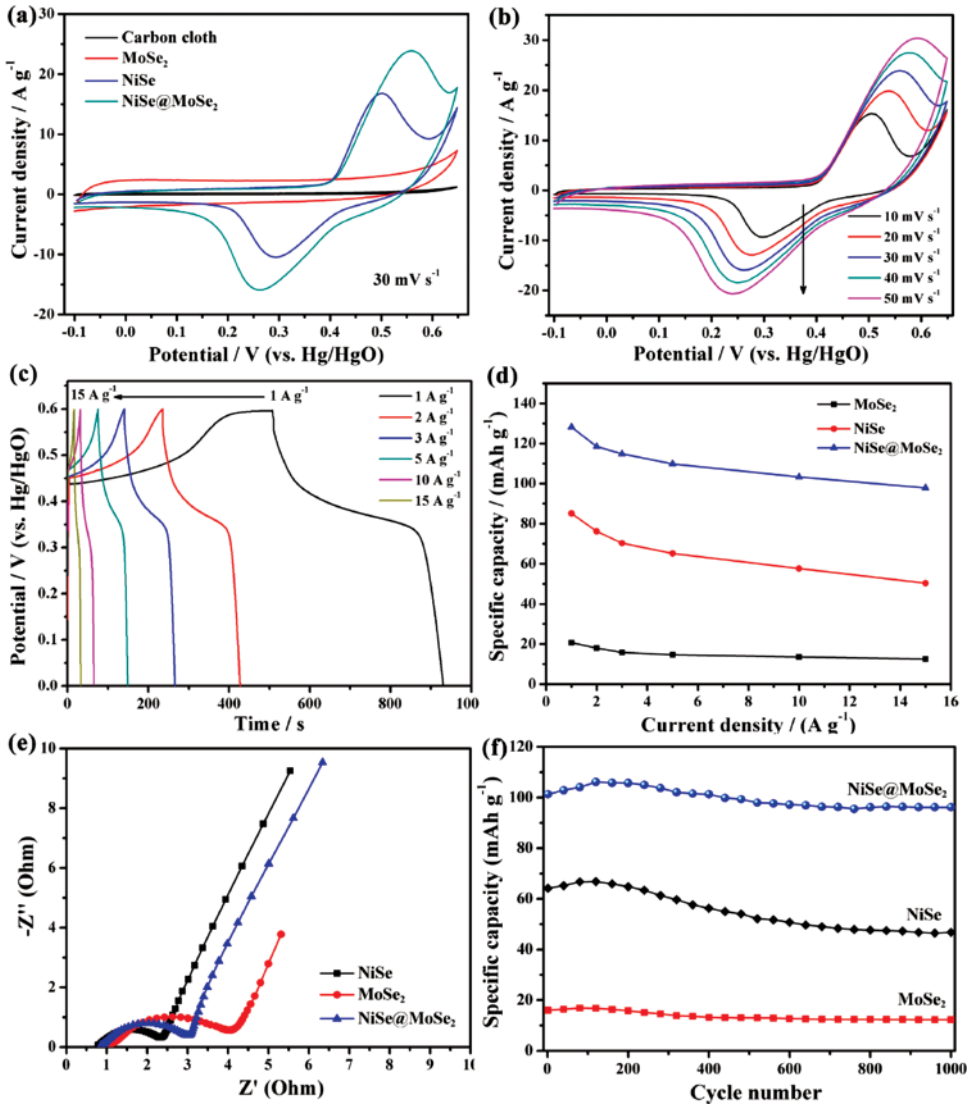
Figure 21.2 (a) $MoSe_2$, NiSe, and NiSe@$MoSe_2$ CV curves in 2.0 M KOH electrolyte (b) NiSe@$MoSe_2$ CV curves at various scanning rates. (c) NiSe@$MoSe2$ at various current densities, GCD curves. (d) Different electrodes' specific capacities at various current densities. (e) Nyquist graphs of $MoSe_2$, NiSe, and NiSe@$MoSe_2$ electrodes. (f) $MoSe_2$, NiSe, and NiSe@$MoSe_2$ electrode cycling stability at $5.0A\,g^{-1}$. *Reproduced with permission [41]. Copyright 2017, American Chemical Society.*

mass density, making them promising materials for energy storage devices [12, 14, 43–45]. Therefore, a composite of CNTs and porous BDCs becomes a potential research interest as it reduces costs and provides a high-performance supercapacitor. An increase in the CNTs amount in the composite material increased the capacitance value of the hybrid supercapacitor. Farma et al. synthesized graphene monoliths from a mixture of CNTs, KOH, and carbon grains obtained from oil palm empty fruit fibres [46]. After activation of the mixture of CNTs and carbon grains at 800 °C in CO_2 gas for one hour, the activated carbon
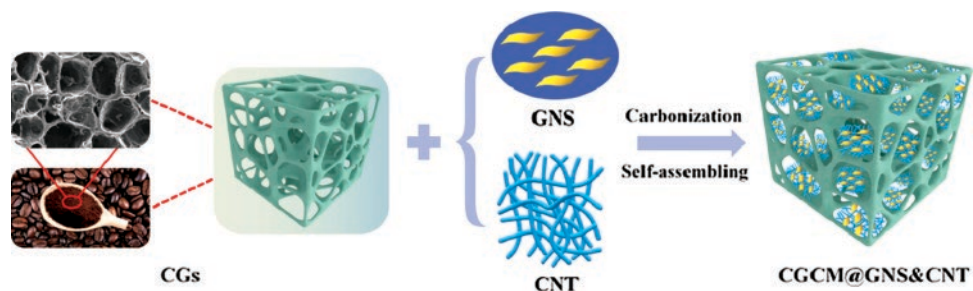
Figure 21.3 Schematic representation for synthesis of CGCM@GNS&CNTs. *Reproduced with permission* [47]. *Copyright 2021, Elsevier.*

monoliths (ACMs) were successfully used to prepare a high-performance supercapacitor. CNTs were also used to change the chemical property of glucose-derived carbon, and the hybrid electrode resulted in a large CV curve in supercapacitor performance [24]. He et al. [47] prepared a three-dimensional (3D) hierarchical porous structure carbon composite (CGCM@GNS&CNTs) incorporating 2D graphene nanosheet (GNS) and 1D CNT into grounded coffee-derived carbon (CGCM) as shown in Figure 21.3. The composite material was used to prepare a symmetric supercapacitor where volumetric capacitance and areal capacitance for composite electrode are evaluated to be $90\,F\,cm^{-3}$ and $441\,mF\,cm^{-2}$, which are much larger than CGCM ($78\,F\,cm^{-3}$ and $290\,mF\,cm^{-2}$) at a current density of $1.0\,mA\,cm^{-2}$. Here, CNT and GNS additives reduce the internal resistance, facilitate ions transfer inside the composite material and enhance the electrochemical performance. Zhou et al. [48] showed charge storage performance of heteroatom N doped BDCs increases with CNT addition and the composite contained a cross-linked three-dimensional porous conductive framework which tremendously facilitates adsorption or desorption of electrolyte ions during the period of charging and discharging process.

21.3.4 Composite with rGO

To achieve a high energy density, the wettability of the BDCs electrode plays an important role. Surface wettability facilitates the adoption of electrolyte ions through the electrode's porous structure, resulting in high charge storage capacity. In addition to BDCs composite, rGO as an additive can increase the hydrophilicity of BDCs due to oxygen having functional groups of rGO [49]. Moreover, rGO also enhances the effective particular surface area of the activated carbon. Generally, rGO has a large theoretical specific surface area (SSA), but an aggregation of rGO sheets drastically reduces the practically obtained SSA and the conductivity [50]. Wang et al. [51] showed in their study that a composite of rGO and biomass-derived activated carbon exhibited a larger surface than individual rGO and activated carbon electrodes. This is because the attachment of activated carbon on the surface of the rGO nanosheet prevents aggregation, providing large SSA and ensuring high conductivity. Guardia et al. also synthesized a BDC composite with rGO that enabled a much higher rate capability and lowered internal resistance of the BDC [52]. Cui et al. [50] reported a composite electrode of biomass-derived porous carbon with rGO.

The porous carbon was hydrothermally prepared from corn cob lignin which was activated in air, and the effect of temperature treatment on the porous carbon performance was studied. Composite of the related porous carbon and rGO showed the lower value of charge transfer resistance even lower than rGO and increased conductivity. Such enhanced conductivity indicates the faster ions/charge transfer efficiency between electrode and electrolyte.

21.4 Preparation of BDCs Composite

Composite formation provides the opportunity to combine the electrochemical performance and advantageous structure of each component. It also combines the disadvantageous physical and chemical properties but selection of materials, optimization and appropriate method to prepare the composite lead to the formation of high-performance electrode material. There are a variety of methods to prepare BDCs and the synthesis of BDC composites can be categorized into two different classes:(i) direct methods and (ii) indirect methods.

21.4.1 Direct Methods

In this method, composites are prepared in a single step. Biomass precursors and additives are treated together. Either pyrolysis or hydrothermal treatment is carried out to form composites of BDCs and conductive materials. In addition to carbonization, heteroatom doping, and activation of the carbonized composite are also used to prepare high-performance electrode material. Rey-Raap at el. studied the effect of multiwall carbon nanotubes (MWCNTs) on the charge storage performance of BDCs [24]. They synthesized the composite by hydrothermal treatment of glucose at 200 °C for 16 hours in the presence of MWCNTs. The amount of CNT in the composite was optimized to have high supercapacitor performance. The hydrothermally treated composite was further processed through both physical and chemical activation. The physical activation was performed under the flow of CO_2 at a temperature of 900 °C for nine hours. The chemical activation was carried out at 700 °C in a nitrogen flow of $50\,cm^3\,min^{-1}$ using KOH as activating agent.

21.4.2 Indirect Methods

The indirect method to synthesize BDC composites consists of two steps. The first step is the carbonization of biomass precursors and the second step is the formation of the composite. Hoang reported a composite made of BDC dot and reduced graphene oxide and prepared in a two-step process [53]. In the first step, cauliflower leaves were washed with Mili-Q water and the carbon dot (CD) prepared by hydrothermal treatment in an autoclave for eight hours at 220 °C. In the second step, a composite of CD and rGO was also synthesized by hydrothermal treatment in an autoclave for 10 hours at 200 °C. The composite (RGO/CD) material with a 2:1 mass ratio revealed a high specific capacitance of $278\,F\,g^{-1}$ at the current density of $0.20\,A\,g^{-1}$.

21.5   Charge Storage Mechanism of BDCs Composite Materials

The charge storage mechanism of a supercapacitor involves either physical adsorption or accumulation of electrolyte ions across the electrode surface, or a fast interface redox reaction. Hence, supercapacitors can be placed into two different categories based on the charge storage mechanism [54, 55]. One is EDLC, where capacitance arises due to the electrostatic accumulation of electrolyte ions (non-Faradaic process), and it strongly relies on the accessible surface area provided by the electrode [52, 53]. Carbon materials are generally used as electrode material for EDLC [56]. Another category of supercapacitors is a pseudocapacitor or redox capacitor, which allows fast and reversible redox reactions between the electrolyte and electro-active species to store charges [57]. In a pseudocapacitor, electrode material contains redox active material such as metal oxide/sulfide and shows high specific capacitance and energy density [58]. However, it also has lower power density and poor stability compared to EDLC [59]. Therefore, it is clear that the elemental composition of the electrode varies the charge storage mechanism and controls the electrochemical performance of the electrode. A composite of EDLC and pseudocapacitive materials can combine the charge storage mechanisms and result in a hybrid electrode that enhances charge storage performance through the Faradaic and non-Faradaic processes. Hence, high electrochemical performance is observed with composite material-based electrodes. Composite of BDC with graphene, rGO and CNTs, follows the same double-layer charge storage mechanism. Still, these additives are essential to improving the surface area and conductivity of the electrode [47]. In addition, biomass-based carbon contains heteroatoms such as N, O, and P, which result in self-doped BDC [35]. These heteroatoms, especially O and N, can incorporate Faradaic pseudocapacitance and increase the wettability and conductivity of BDCs [60, 61].

21.6   Application of BDCs Composite with Conductive Materials as Electrodes for Supercapacitors

A composite material as an electrode effectively improves the electrochemical performance of supercapacitor by introducing more charge storage sites and increasing conductivity. Fabrication of composite material with BDCs and conductive materials reduces the cost and enhances the electrochemical property and shows elevated energy density and power density. In addition, there is plenty of available biomass, which can be classified as plant biomass [62, 63], animal biomass [64, 65], fruit-based [66, 67], and microorganism-based biomass [68, 69]. Fan et al. [70] synthesized a composite electrode made of an N-doped carbon framework (NCCF) derived from cotton and chemically produced rGO. The nitrogen adsorption-desorption isotherm of NCCF-rGO composite revealed a hierarchical porous structure containing mesopores, micropores and macropores, which resulted in a large specific surface area of $398.9 \, m^2 g^{-1}$. Therefore, for NCCF-rGO, a high CV curve was observed in quasi-rectangular form with slight distortion at the edge (Figure 21.4a), which is attributed to the pseudocapacitance behaviour of O-containing functional groups in rGO. The galvanostatic charge-discharge (GCD) curve (Figure 21.4b) for NCCF-rGO showed almost equal charging and discharging time at a current density of $1.0 \, A g^{-1}$,
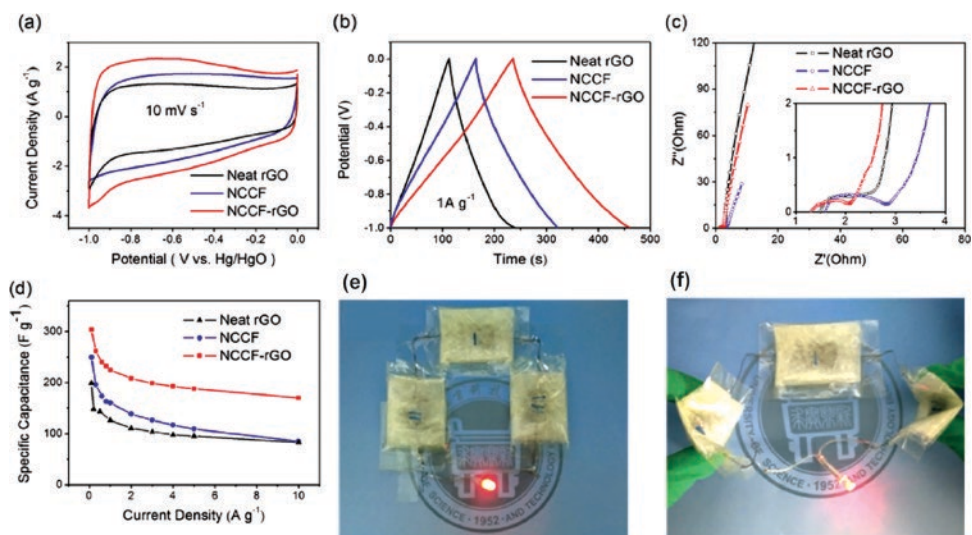
Figure 21.4 The electrochemical performance of the NCCF-rGO all-solid-state supercapacitors was investigated in a PVA/KOH gel electrolyte. (a) CV graph at the scan rate of $10\,mV\,s^{-1}$. (b) GCD graph of the sample at the current density, $1\,A\,g^{-1}$. (c) The inset displayed Nyquist plots and a close-up of the extensive frequency regime. (d) sample specific capacitance at the different current densities. (e, f) Three flexible supercapacitors connected in series to illuminate a red LED light are shown in the images. *Reproduced with permission* [70]. *Copyright 2017, Elsevier.*

representing double-layer capacitance with no potential drop. Figure 21.4d shows a comparative study of the three electrodes where improved energy storage ability up to 305, 225 and $170\,F\,g^{-1}$ at the current densities of 0.10, 1 and $10\,A\,g^{-1}$, respectively, was found for the composite electrode. The NCCF-rGO composite was then used to fabricate a flexible symmetrical supercapacitor, and that supercapacitor showed a high energy density of $20\,Wh\,kg^{-1}$ at a power density of $4000\,W\,kg^{-1}$. Figure 21.4e,f shows the practical applicability of the flexible supercapacitor to light a red LED light.

Wu et al. [16] also used a graphene network (rGO) to prepare highly conductive and high-performance BDC composite electrodes for supercapacitors. Biomass-based activated carbon (ACs) was extracted from straw through ball milling at $500\,rev\,min^{-1}$ for 1 h, and KOH was used to activate the straw-derived carbon. Finally, the composite was prepared by microwave-assisted hydrothermal treatment of ACs and GO. By this process, a highly densified carbon electrode was prepared with a hierarchical porous structure. In the three-electrode system, a high volumetric capacitance, $775\,F\,cm^3$ at $0.5\,A\,g^{-1}$, remained at 74.68% at the current density of $5.0\,A\,g^{-1}$. Such enhanced electrochemical performance of the composite electrode is attributed to the assembly of double-layer capacitance and pseudocapacitance. Here, N-containing groups in the biomass precursors introduced pseudocapacitance in the composite material. In the two-electrode system, the high-density electrode showed gravimetric and voltammetric energy densities of $7.9\,Wh\,kg^{-1}$ and $9.7\,Wh\,L^{-1}$. Hsiao et al. [71] reported composite ($rGO/Oyster/Fe_2O_3$) electrode material prepared with rGO, oyster shell powder (OSPs), and Fe_2O_3 by hydrothermal method. Here OSPs help prevents the restacking of graphene sheets and ensures fast ion transfer and

high surface area for charge storage. The incorporation of Fe_2O_3 over the rGO supports the reversible redox process of the pseudocapacitor material. The composite electrode showed excellent specific capacitance of $473.9\,F\,g^{-1}$ at $5.0\,mV\,s^{-1}$. An asymmetric assembly of the composite electrode with $AC-MnO_2$ resulted in a large operating voltage of 2.2 V. In the two-electrode system, Na_2SO_3 electrolyte was used for the composite anode electrode and Na_2SO_4 electrolyte for the $AC-MnO_2$ electrode. The asymmetric supercapacitor achieved a power density of $2200\,W\,kg^{-1}$ and an energy density of $31.2\,Wh\,kg^{-1}$. Wang et al. constructed a biomass-derived 3D N-doped hierarchical porous carbon (N-HPC) from sodium alginate biomass, and a composite ($Ni_3S_2@Co_9S_8$/N-HPC) was formed by adding nickel sulfide (Ni_3S_2) and nanocrystal attached cobalt sulfide (Co_9S_8) in the hierarchical porous carbon [72]. Here, transition metal sulfide species serve high theoretical specific capacitance and N-doped carbon framework insured excellent electrical conductivity with fast ion transport. Therefore, the synergistic effect of $Ni_3S_2@Co_9S_8$/N-HPC composite resulted in a high specific capacitance of $1970.50\,F\,g^{-1}$ at $0.50\,A\,g^{-1}$ and good cycling stability with 89.5% capacitance retention after 5000 cycles at $10.0\,A\,g^{-1}$. Asymmetric assemble of $Ni_3S_2@Co_9S_8$/N-HPC and HPC ($Ni_3S_2@Co_9S_8$/N-HPC//HPC) in 6 M KOH revealed an impressive energy density of $77.1\,Wh\,kg^{-1}$ at $263.3\,W\,kg^{-1}$ and the energy density stayed as high as $36.1\,Wh\,kg^{-1}$ even at a power density of $25.9\,kW\,kg^{-1}$. Nowadays, semiconducting materials such assilicon carbide (SiC) and titanium nitride, also have been used with porous carbon material to prepare highly conductive composite due to their electrical conductivity and mechanical stability [73, 74]. SiC has the highest potential due to its low band gap, high electron mobility, and favourable chemical stability [75, 76]. In addition, biomass precursors serve as both silicon and carbon resource and led to the successful formation of high-performance BDCs-SiC composite electrodes [76]. Tang et al. [76] reported a high-performance electrode material for charge storage made of a composite of hierarchical porous carbon and SiC (HPC/SiC), where waste villi of bamboo shoot shells (VBSS) were used as green carbon and silicon resources. The high conductivity of SiC and porous carbon structure in HPC/SiC resulted in a specific capacitance of $234.2\,F\,g^{-1}$ at the current density of $1\,A\,g^{-1}$. The composite showed excellent cycling stability with 90.8% retention after 10,000 cycles. Symmetric assemble with HPC/SiC also showed a high specific capacitance of $224\,F\,g^{-1}$ and a good energy density of $25.20\,Wh\,kg^{-1}$ at a power density of $181.1\,W\,kg^{-1}$. A comparative study of charge storage and the performance of different BDC composites electrode is shown in Table 21.1.

21.7 Conclusions

The flexibility to tailor the surface chemistry of biomass-derived activated carbon offers new scope to form composite electrodes using conductive materials. Moreover, a composite of BDCs with conductive material shows high electrochemical performance and provides large SSA and high specific capacitance. In the composite, carbon material serves as the backbone to support the additive material. The synergistic effect within the composite material increases the charge/discharge rate. It exhibits good retention values even after a long cycle life, which makes the composite of BDCs an excellent choice for supercapacitors. However, the synthesis of composite material faces some challenges. BDAC's porous

Table 21.1 Comparative study of different BDC composite electrodes for supercapacitors.

Biomass	Additive	Electrolyte	Surface area (m² g⁻¹)	Specific Capacitance (F g⁻¹)	Stability (Retention @Cycle)	Energy density (Wh kg⁻¹)	Power density (W kg⁻¹)	Ref.
Bacterial cellulose	NiS	2 M KOH	-	1606	87.1@10000	21.5	700	[27]
Ash tree	Ag	2 M LiN((SO$_2$CF$_3$)$_2$)	335	494	98.6@2000	12.8	366	[31]
Poplar catkin	Ag	1 M KOH	745	250	95@5000	...	...	[32]
Camellia oleifera shells	RuNPs	1 M H$_2$SO$_4$	2522	291	90@2000	...	...	[33]
Collagen waste	Mn	1 M KOH	420.27	272.62	81.4@6000	...	...	[34]
Rice husk	NiCo$_2$S$_4$	2 M KOH	653	1680	86@5000	41.6	150	[42]
Wood scraps	CNT	1 M Na$_2$SO$_4$	537.9	215.3	96.2@10000	39.8	940	[43]
Oil palm fruit	CNT	1 M H$_2$SO$_4$	485	85	...	2.1	161	[46]
Pig nails	CNT	6 M KOH	2542.24	293.1	97.0@10000	27.46	874.98	[48]
Coffee grounds	rGO	5 M KOH EMIMTFSI	2620	512 440	87@10000	187.3	438	[49]
Waste water purifier	rGO	1 M H$_2$SO$_4$ 1 M Na$_2$SO$_4$	963	116.8 541	97.85@8000	11.90	469.24	[51]
Straw	rGO	1 M H$_2$SO$_4$	533	628	97.05@10000	7.9	50	[16]
Oyster shell	rGO/Fe$_2$O$_3$NPs	1 M Na$_2$SO$_3$	92.0	473.9	79.4@10000	31.2	2200	[71]
Alginate beads	Ni$_3$S$_2$/Co$_9$S$_8$	6 M KOH	360.1	1970.5	89.5@5000	77.1	263.3	[72]
Bamboo shell	SiC	1 M Na$_2$SO$_4$	1357.9	234.2	90.8@10000	25.20	181.1	[76]

structure helps to store electrolyte ions using different dimensional pore sizes. Appropriate pore size distribution enlarges the ion's availability resulting in good charge-discharge capability and high retention capability. The incorporation of additives can clog the pore structure of the AC and reduce the charge storage space and ion diffusion tunnelling. In this case, optimizing the additive amount to modify the surface physiochemical property can be a practical step. In addition to the optimization of additive, activation parameters, i.e., activation temperature, activation time and optimization of activating agent amount, can also be analyzed to get the best result from composite.

Acknowledgements

References

1 H. Chen, D. Liu, Z. Shen, B. Bao, S. Zhao, L. Wu, *Electrochim. Acta* **2015**, *180*, 241–251.
2 Z. Tan, J. Yang, Y. Liang, M. Zheng, H. Hu, H. Dong, Y. Liu, Y. Xiao, *J. Colloid Interface Sci.* **2021**, *585*, 778–786.
3 J. Wang, X. Zhang, Z. Li, Y. Ma, L. Ma, *J. Power Sources* **2020**, *451*, 227794.
4 A. Aziz, S. S. Shah, A. Kashem, *Chem. Rec.* **2020**, *20*, 1074–1098.
5 V. Pasangulapati, K. D. Ramachandriya, A. Kumar, M. R. Wilkins, C. L. Jones, R. L. Huhnke, *Bioresour. Technol.* **2012**, *114*, 663–669.
6 S. S. Shah, M. N. Shaikh, M. Y. Khan, M. A. Alfasane, M. M. Rahman, M. A. Aziz, *Chem. Rec.* **2021**, *21*, 1631–1665.
7 X. Kang, H. Zhu, C. Wang, K. Sun, J. Yin, *J. Colloid Interface Sci.* **2018**, *509*, 369–383.
8 L. Jiang, L. Sheng, Z. Fan, *Sci. China Mater.* **2018**, *61*, 133–158.
9 S. S. Shah, M. A. Aziz, E. Cevik, M. Ali, S. T. Gunday, A. Bozkurt, Z. H. Yamani, *J. Energy Storage* **2022**, *56*, 105944.
10 Q. Jiang, N. Kurra, M. Alhabeb, Y. Gogotsi, H. N. Alshareef, *Adv. Energy Mater.* **2018**, *8*, 1703043.
11 W. Jiang, D. Yu, Q. Zhang, K. Goh, L. Wei, Y. Yong, R. Jiang, J. Wei, Y. Chen, *Adv. Funct. Mater.* **2015**, *25*, 1063–1073.
12 S. M. Abu Nayem, S. S. Shah, N. Sultana, M. A. Aziz, A. J. Saleh Ahammad, *Chem. Rec.* **2021**, *21*, 1039–1072.
13 M. Usman, M. Humayun, S. S. Shah, H. Ullah, A. A. Tahir, A. Khan, H. Ullah, *Energies* **2021**, *14*, 2281.
14 S. Islam, S. S. Shah, S. Naher, M. A. Ehsan, M. A. Aziz, A. J. S. Ahammad, *Chem. Asian J.* **2021**, *16*, 3516–3543.
15 M. Ashraf, S. S. Shah, I. Khan, M. A. Aziz, N. Ullah, M. Khan, S. F. Adil, Z. Liaqat, M. Usman, W. Tremel, M. N. Tahir, *Chem. Eur. J.* **2021**, *27*, 6973–6984.

16 Q. Wu, M. Gao, C. Jiang, X. Gu, Z. Wang, L. Huang, S. Yu, *J. Power Sources* **2021**, *497*, 229878.

17 X. Luo, S. Chen, T. Hu, Y. Chen, F. Li, *SusMat* **2021**, *1*, 211–240.

18 S. S. Shah, S. M. A. Nayem, N. Sultana, A. J. S. Ahammad, M. A. Aziz, *ChemSusChem* **2022**, *15*, e202101282.

19 S. S. Shah, M. A. Aziz, *Bangladesh J. Plant Taxon.* **2020**, *27*, 467–478.

20 S. S. Shah, M. A. Aziz, W. Mahfoz, A.-R. Al-Betar, Conducting Polymers Based Nanocomposites for Supercapacitors in *Nanostructured Materials for Supercapacitors*, (Eds. S. Thomas, A. B. Gueye, R. K. Gupta), Springer, Cham, **2022**, Chapter 22, pp. 485–511, Vol. *1*.

21 S. S. Shah, E. Cevik, M. A. Aziz, T. F. Qahtan, A. Bozkurt, Z. H. Yamani, *Synth. Met.* **2021**, *277*, 116765.

22 E. Raymundo-Piñero, K. Kierzek, J. Machnikowski, F. Béguin, *Carbon* **2006**, *44*, 2498–2507.

23 Z. Bi, Q. Kong, Y. Cao, G. Sun, F. Su, X. Wei, X. Li, A. Ahmad, L. Xie, C.-M. Chen, *J. Mater. Chem. A* **2019**, *7*, 16028–16045.

24 N. Rey-Raap, M. Enterría, J. I. Martins, M. F. R. Pereira, J. L. Figueiredo, *ACS Appl. Mater. Interfaces* **2019**, *11*, 6066–6077.

25 S. S. Shah, M. A. Aziz, A. K. Mohamedkhair, M. A. A. Qasem, A. S. Hakeem, M. K. Nazal, Z. H. Yamani, *J. Mater. Sci. - Mater. Electron.* **2019**, *30*, 16087–16098.

26 R. Wang, X. Li, Z. Nie, Y. Zhao, H. Wang, *J. Energy Storage* **2021**, *38*, 102479.

27 L. Zuo, W. Fan, Y. Zhang, Y. Huang, W. Gao, T. Liu, *Nanoscale* **2017**, *9*, 4445–4455.

28 M. Vanitha, P. Keerthi, P. Cao, N. Balasubramanian, *J. Alloys Compd.* **2015**, *644*, 534–544.

29 D. Ávila-Brande, D. Arenas-Esteban, L. C. Otero-Díaz, A. Guerrero-Martínez, G. Tardajos, J. Carretero-González, *RSC Adv.* **2015**, *5*, 86282–86290.

30 H. Ma, Z. Chen, X. Gao, W. Liu, H. Zhu, *Sci. Rep.* **2019**, *9*, 17065.

31 L. Kouchachvili, E. Entchev, *Mater. Today Energy* **2017**, *6*, 136–145.

32 Z. Zhang, J. Yang, Y. Han, X. He, J. Zhang, J. Huang, D. Chen, S. Xu, W. Xie, *Appl. Phys. A* **2020**, *126*, 199.

33 B.-S. Lou, P. Veerakumar, S.-M. Chen, V. Veeramani, R. Madhu, S.-B. Liu, *Sci. Rep.* **2016**, *6*, 19949.

34 J. Lei, J. Zhou, J. Li, J. Wen, L. Su, T. Duan, W. Zhu, *Electrochim. Acta* **2018**, *285*, 292–300.

35 M. Zhang, X. Jin, L. Wang, M. Sun, Y. Tang, Y. Chen, Y. Sun, X. Yang, P. Wan, *Appl. Surf. Sci.* **2017**, *411*, 251–260.

36 J. Saravanan, M. Pannipara, A. G. Al-Sehemi, S. Talebi, V. Periasamy, S. S. Shah, M. A. Aziz, G. Gnana Kumar, *J. Mater. Sci. - Mater. Electron.* **2021**, *32*, 24775–24789.

37 S. S. Shah, M. A. Aziz, A.-R. Al-Betar, W. Mahfoz, *Arab. J. Chem.* **2022**, *15*, 104058.

38 M. Yaseen, M. A. K. Khattak, M. Humayun, M. Usman, S. S. Shah, S. Bibi, B. S. U. Hasnain, S. M. Ahmad, A. Khan, N. Shah, A. A. Tahir, H. Ullah, *Energies* **2021**, *14*, 7779.

39 A. Helal, S. S. Shah, M. Usman, M. Y. Khan, M. A. Aziz, M. Mizanur Rahman, *Chem. Rec.* **2022**, *22*, e202200055.

40 H. Yang, Y. Tang, X. Sun, Q. Liu, X. Huang, L. Wang, Z. Fu, Q. Zhang, S. W. Or, *J. Mater. Sci. - Mater. Electron.* **2017**, *28*, 14874–14883.

41 H. Peng, J. Zhou, K. Sun, G. Ma, Z. Zhang, E. Feng, Z. Lei, *ACS Sustain. Chem. Eng.* **2017**, *5*, 5951–5963.

42 H. Wang, D. Wu, J. Zhou, *J. Alloys Compd.* **2019**, *811*, 152073.

43 C. Wu, S. Zhang, W. Wu, Z. Xi, C. Zhou, X. Wang, Y. Deng, Y. Bai, G. Liu, X. Zhang, X. Li, Y. Luo, D. Chen, *Carbon* **2019**, *150*, 311–318.

44 S. M. Abu Nayem, S. S. Shah, N. Sultana, M. A. Aziz, A. J. Saleh Ahammad, *Chem. Rec.* **2021**, *21*, 1038-1038.

45 S. M. A. Nayem, S. S. Shah, N. Sultana, M. A. Aziz, A. J. S. Ahammad, *Chem. Rec.* **2021**, *21*, 1073–1097.

46 A. M. Deraman, I. A. Talib, R. Farma, R. Omar, M. M. Ishak, E. Taer, B. N. M. Dolah, N. H. Basri, N. S. M. Nor, *AIP Conf. Proc.* **2015**, *1656*, 030007.

47 W. He, P.-G. Ren, Z. Dai, X. Hou, F. Ren, Y.-L. Jin, *Appl. Surf. Sci.* **2021**, *558*, 149899.

48 Y. Zhou, Z. Song, Q. Hu, Q. Zheng, N. Jiang, F. Xie, W. Jie, C. Xu, D. Lin, *Superlattices Microstruct.* **2019**, *130*, 50–60.

49 J.-H. Choi, C. Lee, S. Cho, G. D. Moon, B.-S. Kim, H. Chang, H. D. Jang, *Carbon* **2018**, *132*, 16–24.

50 L. Cui, Y. Yang, C. Cheng, L. Xu, Y. Li, M. Jia, X. Dun, X. Jin, *J. Wood Chem. Technol.* **2019**, *39*, 343–359.

51 J. Wang, Q. Li, C. Peng, N. Shu, L. Niu, Y. Zhu, *J. Power Sources* **2020**, *450*, 227611.

52 L. Guardia, L. Suárez, N. Querejeta, V. Vretenár, P. Kotrusz, V. Skákalová, T. A. Centeno, *Electrochim. Acta* **2019**, *298*, 910–917.

53 V. C. Hoang, L. H. Nguyen, V. G. Gomes, *J. Electroanal. Chem.* **2019**, *832*, 87–96.

54 H. Zhou, Y. Zhan, F. Guo, S. Du, B. Tian, Y. Dong, L. Qian, *Electrochim. Acta* **2021**, *390*, 138817.

55 Y. Wang, L. Zhang, H. Hou, W. Xu, G. Duan, S. He, K. Liu, S. Jiang, *J. Mater. Sci.* **2021**, *56*, 173–200.

56 S. Saini, P. Chand, A. Joshi, *J. Energy Storage* **2021**, *39*, 102646.

57 L. L. Zhang, X. Zhao, *Chem. Soc. Rev.* **2009**, *38*, 2520–2531.

58 B. Liu, D. Kong, J. Zhang, Y. Wang, T. Chen, C. Cheng, H. Y. Yang, *J. Mater. Chem. A* **2016**, *4*, 3287–3296.

59 C. Z. Yuan, B. Gao, L. F. Shen, S. D. Yang, L. Hao, X. J. Lu, F. Zhang, L. J. Zhang, X. G. Zhang, *Nanoscale* **2011**, *3*, 529–545.

60 C. Shi, L. Hu, K. Guo, H. Li, T. Zhai, *Adv. Sustain. Syst.* **2017**, *1*, 1600011.

61 M. A. Aziz, S. S. Shah, S. M. A. Nayem, M. N. Shaikh, A. S. Hakeem, I. A. Bakare, *J. Energy Storage* **2022**, *50*, 104278.

62 J. Li, Y. Gao, K. Han, J. Qi, M. Li, Z. Teng, *Sci. Rep.* **2019**, *9*, 17270.

63 M. A. Aziz, S. S. Shah, S. Reza, A. S. Hakeem, W. Mahfoz, *Chem. Asian J.* **2022**, e202200869, https://doi.org/10.1002/asia.202200869.

64 J. Niu, M. Liu, F. Xu, Z. Zhang, M. Dou, F. Wang, *Carbon* **2018**, *140*, 664–672.

65 J. Wang, C. D. Buchman, J. Seetharaman, D. J. Miller, A. D. Huber, J. Wu, S. C. Chai, E. Garcia-Maldonado, W. C. Wright, J. Chenge, T. Chen, *J. Am. Chem. Soc.* **2021**, *143*, 18467–18480.

66 N. C. Deb Nath, S. S. Shah, M. A. A. Qasem, M. H. Zahir, M. A. Aziz, *ChemistrySelect* **2019**, *4*, 9079–9083.

67 C. K. Roy, S. S. Shah, A. H. Reaz, S. Sultana, A.-N. Chowdhury, S. H. Firoz, M. H. Zahir, M. A. A. Qasem, M. A. Aziz, *Chem. Asian J.* **2021**, *16*, 296–308.

68 H. Zhu, J. Yin, X. Wang, H. Wang, X. Yang, *Adv. Funct. Mater.* **2013**, *23*, 1305–1312.

69 S. S. Shah, M. A. Alfasane, I. A. Bakare, M. A. Aziz, Z. H. Yamani, *J. Energy Storage* **2020**, *30*, 101562.

70 Y.-M. Fan, W.-L. Song, X. Li, L.-Z. Fan, *Carbon* **2017**, *111*, 658–666.

71 C. Hsiao, C. Lee, N. Tai, *Electrochim. Acta* **2021**, *391*, 138868.

72 S. Wang, Z. Xiao, S. Zhai, H. Wang, W. Cai, L. Qin, J. Huang, D. Zhao, Z. Li, Q. An, *J. Mater. Chem. A* **2019**, *7*, 17345–17356.

73 D. Tang, R. Yi, W. Zhang, Z. Qiao, Y. Liu, Q. Huo, D. Wang, *Mater. Lett.* **2017**, *198*, 140–143.

74 T. Wang, K. Li, S. An, C. Song, X. Guo, *Appl. Surf. Sci.* **2019**, *470*, 241–249.

75 C. Shao, F. Zhang, H. Sun, B. Li, Y. Li, Y. Yang, *Mater. Lett.* **2017**, *205*, 245–248.

76 Q. Tang, X. Chen, D. Zhou, C. Liu, *Colloids Surf. A Physicochem. Eng. Asp.* **2021**, *620*, 126567.

Part 4

Binding Materials, Electrolytes, Separators, and Packaging Materials from Biomass for Supercapacitors

22

Biomass-based Electrolytes for Supercapacitor Applications

S. M. Abu Nayem[1], Santa Islam[1], Syed Shaheen Shah[2,3], Nasrin Sultana[1], M. Nasiruzzaman Shaikh[4], Md. Abdul Aziz[2,4,], and A. J. Saleh Ahammad[1,*]*

[1] Department of Chemistry, Jagannath University, Dhaka, 1100 Bangladesh
[2] Interdisciplinary Research Center for Hydrogen and Energy Storage (IRC-HES), King Fahd University of Petroleum & Minerals, Dhahran, 31261, Saudi Arabia
[3] Physics Department, King Fahd University of Petroleum & Minerals, KFUPM Box 5047, Dhahran, 31261, Saudi Arabia
[4] Interdisciplinary Research Center for Hydrogen and Energy Storage (IRC-HES), King Fahd University of Petroleum & Minerals, Dhahran, 31261, Saudi Arabia
* Corresponding authors

22.1 Introduction

In light of the increasing depletion of fossil fuels and the massive pollution caused by use of fossil fuels, electrochemical energy storage (EES) devices have received significant interest. Supercapacitors (SCs) are excellent alternatives among EES devices for resolving future energy crises and reducing environmental pollutants. SCs have impressive characteristics, such as longer cycle life (>500,000 cycles), higher power density (>10 kW kg^{-1}) with fast discharging/charging rate (in seconds), and high energy efficiency (near to 100%) compared with conventional EES devices such as batteries and fuel cells [1–4]. Though the overall operating performance of any EES devices depends mostly on both power and energy density, as well as other factors, SCs inherently possess lower energy density, which limits the ultimate applicability where high power and energy density are required. As a result, SCs are being extensively investigated to improve energy density so that these can compensate for the shortcomings of fuel cells and batteries. It has been found that power density (P) and energy density (E) both show proportional relation to the cell voltage (V) built up across the electrode, which is shown in Equations (22.1) and (22.2) [2, 3].

$$E = \frac{CV^2}{2} \tag{22.1}$$

$$P = \frac{E}{t} \tag{22.2}$$

Therefore, increasing the working cell voltage can be a useful and practical approach to enhance energy and power density. The types of electrolytes, followed by the stability, influence cell voltage drastically (when the electrodes are stable within the potential

region). For instance, the potential operational window of an aqueous electrolyte is 1.0–1.3 V, while ionic liquid and organic electrolytes-based SCs have potential windows of 3.5–3.4 V and 2.5–2.7 V, respectively [4]. Even liquid electrolytes are quite prominent in SCs applications; these are caustic, poisonous, and responsible for potential leakage. Using organic polymer electrolytes to replace liquid electrolytes can reduce the possibility of leaking in SCs. However, the polymer matrix containing liquid electrolytes can improve ionic conductivity during charge transfer followed by storage at the interface. Synthetic organic polymer preparation typically necessitates a large amount of resource consumption and raises environmental concerns because they are not biodegradable. As a result, creating polymer electrolytes derived from sustainable biomass sources has sparked intense scientific interest. Electrolytes produced from biomass, such as starch, cellulose, chitosan, soybean protein, and others, are gaining popularity because of their low cost, renewability, excellent mechanical characteristics, and environmental friendliness [3–5].

22.2 Biomass-based Electrolytes

Electrolytes are not only involved in the charge storage mechanism but also help to get high cell voltage. Thus, the electrolyte plays an essential role in improving power and energy density. An ideal electrolyte needs to have some specific characteristics, including enhanced ionic conductivity, wide electrochemical potential window, chemical inertness to cell components, high chemical/thermal stability, safe, non-toxic, and be economically affordable [1]. Though it is challenging to meet all the prerequisites at once, tremendous work has been done to achieve an electrolyte with electrochemical stability in a wide potential window and temperature range, and that is non-toxic, cost-effective, and environmentally friendly [6–8]. Meanwhile, biopolymer electrolyte (BPE) derived from biomass sources has become a popular choice to study and use as the electrolyte in EES devices due to its unique properties, such as it being compatible with various solvents, biodegradable, inexpensive, abundant, and with a good film-forming ability [7, 8]. In addition, polymer electrolytes possess a solid physique but are amorphous in nature; they have ionic conductivity comparable to liquid electrolytes [9]. BPEs obtained from the conversion or extraction of biomass, generally take the form of gel polymer electrolytes (GPE) and solid-state polymer electrolytes (SPE) [3]. By dissolving inorganic salts in a polar polymer chain, SPE can be obtained, providing necessary anions and cations that make the polymers ionically conductive [10]. Ionic migration experiences translational motion into a free space formed by the continual redistribution of free spaces in the polymeric material, which is the process of SPE [11]. For the high capacitance performance of EES devices, GPEs are more attractive since they can trap significant liquid electrolytes and hence possesses higher ionic conductivity [12]. GPE generally contains polymeric frameworks, supporting electrolytic salts and organic solvents [13]. In traditional GPE, polymeric frameworks are used as a host matrix, providing i) a solid matrix that is flexible enough for easy design, ii) accepts the added salt in the matrix, iii) the volume changes during the charging/discharging of devices, and iv) dissociates the salt and facilitates the ion transport and accommodation [9]. Biopolymeric host matrix for GPE prepared from natural polymers such as chitosan, dextrin, cellulose, and starch are suitable over synthetic polymers for environmental reasons and have been widely studied but have yet to get desired results as electrolytes for

commercial use [10, 14–16]. Hydrogel polymers containing a high amount of water and cross-link renewable polymers become a potential replacement for organic solvents (which are prone to catch fire) for next-generation SCs [13]. In synthesizing hydrogel electrolytes, cross-linking agents are often used to carry out cross-linking bonds in the polymer chain and increase the mechanical properties [17]. In case of bio-hydrogel electrolytes, poly (ethylene glycol) diacrylate, formaldehyde, and glutaraldehyde are some common cross-linking agents. In such hydrogel electrolytes ionic conductivity follows the ionic transportation mechanism through the porous channel produced by a hydrogen bonded cross-linking network [11]. Owing to the unique structure, large potential window and thermal stability of ionic liquid (IL), ionogel is getting tremendous interest from the scientific community. Biopolymer (from biomass) based ionogel and hydrogel electrolytes have shown good response in the preparation of high performance solid-state SCs [4, 18, 19]. Both GPE and SPE provide good fixability to design high performance SCs.

22.3 Factors Affecting the Ionic Conductivity of the Biopolymer Electrolyte

22.3.1 Polymer Blending

For electrolyte preparation, the use of two or more polymers as hosts is better than using a single polymer, as it can enhance thermal stability, mechanical strength, and availability of ion hopping sites. Because of this, polymer hybrids or blends are extremely promising and considered as revolutionary research, as they widen the chain flexibility and mobility, therefore leading to an increase in the conduction qualities because of the blend's ability to give more coordinating positions. These blended polymers are mainly copolymers made of two polymers linked together by comparatively weak interactions like van der Waals forces and H-bonding. Polymers are made up of two parts: crystalline and amorphous phases. It is generally understood that the amorphous area is primarily responsible for ionic conduction, and polymer blending aids in producing highly amorphous regions within the blended polymers. This enhanced amorphous phase is responsible for the movement of the local chain segment, which leads to the movement of ions and thus the conductivity of ions can be improved [20, 21]. In addition, the mechanical and other physical/chemical characteristics of a single polymer are insufficient to provide this wide variety of applications in supercapacitor devices; the primary disadvantages of single polymer-based SPEs include low ionic conductivity at ambient temperatures and poor electrode-electrolyte interaction as compared to liquid electrolytes. As a result, one polymer mixed with other polymers, can function as a host electrolyte, to overcome the flaws in the individual polymers [22].

22.3.2 Addition of Dopant

The conductivity of pristine polymer is low, and the problem of low conductivity in a polymer can be solved by salt incorporation. Because of the presence of polar groups in the polymer structure, a polymer can act as a host in an electrolyte system. Thus, dissolving

ionic ions can improve the BPE characteristics. The conduction process of the electrolyte can be modified due to the formation of a dative bond between the ions of the dissolved salts with the functional groups of the polymers. In a nutshell, salt ions form dative bonds with the lone pair electrons of functional groups in polymeric chains, increasing salt dissociation and ionic conductivity. Salt selection is critical in polymer-salt electrolytes. Strong inorganic acid-based electrolyte suffers chemical degradation, hence need to solve this problem. Li salts are considered the best salts because they have the highest electrochemical characteristics, but their high cost, scarcity, and flammability have motivated scientists to seek alternatives [23–25].

22.3.3 Addition of Plasticizer

Using plasticizers in the BPE manufacturing method enhances the amorphous area of the BPE. Plasticization also improves the dissolving characteristics of dopant salts by assisting the the degree of dissociation of dopant salts and offering a greater number of conducting pathways in which mobile ions can move, resulting in increased electrolyte ionic conductivity. The choice of plasticizer is based on a high dielectric constant; in the literature, glycerol is the most commly-used plasticizer [26].

22.3.4 Addition of Filler

Incorporating a nanofiller into the BPE can be a viable approach to improve ionic conductivity. Additionally, the mechanical strength and thermal stability of SPEs can be dramatically increased by the addition of nanofillers, resulting in enhanced ionic conductivity. The nanofiller with high dielectric constant, strong Lewis acid characteristics and high surface area is the best choice for enhancing the ionic conductivity [27].

22.3.5 Addition of Ionic Liquids

Ionic liquids (IL) may decrease transitory coordinative links among polymer molecules in the crystalline area, causing polymer chains to become more flexible and polymer complexes to become more amorphous. Adding a significant amount of IL to the BPE system provides more free ions and enhances the polymer's segmental mobility in proportion to the enhancement of conductivity. In addition, IL possesses different properties, including high ionic conductivity, non-volatile and non-flammable, non-toxic, negligible vapour pressure, wide decomposition temperature range, and wide electrochemical potential window (up to 6V), which makes IL a potential candidate for enhancing the ionic conductivity of BPE [28, 29].

22.3.6 Addition of Metal Complexes

Another significant criterion for improving BPEs ionic conductivity is adding metal complexes. Due to the interactions of metal complexes with polymer functional groups, which break hydrogen bonding among polymer chains, metal complexes enhance the amorphous phase of polymers and provide more accessible paths for ion conduction. Moreover, the

inclusion of metal complexes also enhances other conduction parameters such as dynamism which is mainly known as mobility (μ), charge transfer density (n), and diffusion coefficient (D) of both cations and anions. In addition, reducing the energy bandgap can be accomplished by incorporating metal complexes, which brings tremendous benefits in supercapacitor applications [20, 30–32].

22.4 Biomass-based Electrolytes for Supercapacitor

22.4.1 Solid-state Polymer Electrolytes

Typically, solid-state polymer electrolytes (SPE) can be obtained by dissolving metal salts in a polymeric matrix and dissociating them into metal cations and counter anions. Because these polymers are ionically conductive, they have received a lot of interest because they can be used in various electrochemical devices. Different types of SPE, such as cellulose-, chitosan- and starch-based SPEs, are presented in the following sections.

22.4.1.1 Cellulose-based SPE

The most common biopolymer found in nature is cellulose, which is insoluble in water. To dissolve cellulose into water, it must first be modified. For example, adding methyl chloride to cellulose (methylation) turns it into methylcellulose (MC). MC has various properties, including excellent film-forming characteristics, thermal and mechanical strength, electrical properties, and biocompatibility. MC contains β-(1,4)-glycosidic bonds attached to methyl substituents in linear chains with different functional groups of C–O–C, O–CH$_3$, and O–H, which provides a lone pair of electrons for ionic conduction. Another fascinating characteristic of MC is its amphiphile nature, which arises from the hydrophobic polysaccharide and hydrophilic carboxylic functional group [16, 33–35]. In the literature, different polymeric hybrid hosts based on MC have been fabricated with other polar functional groups containing polymers such as chitosan (CS) [32, 33, 35, 36], poly(vinyl alcohol) (PVA) [16, 37], dextran (DX) [38], and potato starch (PS) [39]. Most polymer blends have been synthesized by following the solution casting method (SCM). The charge transfer ability of the polymer blend electrolyte can be increased by adding salts or inorganic acid. The addition of salts as a dopant into the polymeric matrix is superior compared to the addition of inorganic acids because of chemical degradation and incompatibility in the practical application of the latter. According to the literature, among different salts, ammonium salts (e.g., NH$_4$I, NH$_4$SCN) are used mostly as a dopant in biopolymer matrix over sodium and lithium salts because of environmental pollution due to lithium salts, comparable fast dissociation of ions of ammonium salts, and presence of NH$_4^+$ and H$^+$ ions which enhance the ionic conductivity (linear sweep voltammetry (LSV) for highest conductivity shown in Figure 22.1) and thermal stability [36]. Furthermore, plasticizer incorporation (high dielectric constant polar solvents) enhances the dissociation of dopant, thermal properties of the electrolyte, amorphousness, and ionic conductivity, hence the electrolyte performance in SC applications. For example, infusing ammonium nitrate (NH$_4$NO$_3$) as dopant and glycerol as plasticizer from potato starch (PS)-MC mixed SPE, Hamsan et al. [39] manufactured a solution cast SPE. The potential window for the electrolyte was found as 1.88 V through the evaluation of LSV.
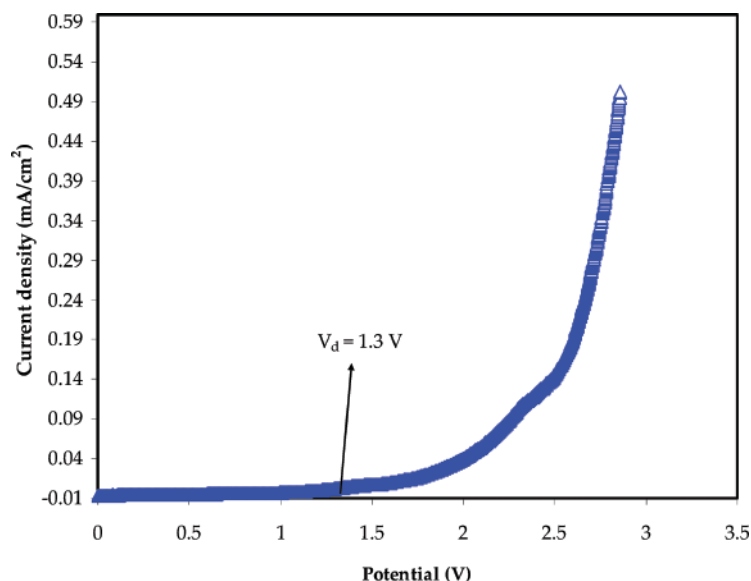
Figure 22.1 LSV graph of the highest conducting electrolyte at 0.02 V/s. *Reproduced with permission* [36]. *Reproduced under the terms of the CC-BY-4.0 license. Copyright 2021, Aziz et al.*

22.4.1.2 Chitosan-based Electrolyte

One of the most abundant polymers on earth next to cellulose is chitosan (CS), one of chitin's derivatives. It can be obtained by dissolving N-deacetylated chitin in dilute acidic solutions. It has a β-(1→4) 2-amino-2-deoxy-D-glucose-(D-glucosamine) structure in its polymeric chain and it has shown excellent mechanical strength, and chemical and thermal stability up to 200 °C. Another noteworthy feature of CS is its capacity to be moulded into various shapes, from hydrogels to porous scaffolds to films. Because it has different lone pairs containing functional groups, including OH, C–O–C, and NH_2 in its polymeric chain, ion transportation from one electrode to another becomes feasible. However, the conductivity of CS is low; the problem of low conductivity in CS is solved by salt incorporation and plasticizer addition. Because of the presence of such polar groups in the CS structure, CS can act as a polymer host in an electrolyte system, dissolving ionic ions and exhibiting polymer electrolyte characteristics [40, 41]. In the literature, CS-based BPE is reported where $LiCOOCH_3$ [23], NH_4NO_3 [40], and magnesium acetate ($Mg(CH_3COO)_2$) [42] have been exploited as effective ion sources, while glycerol is used as plasticizer material. Hamsan et al. [43] employed SCM to make a CS-based biopolymer, using CS as the polymer host, $MgCl_2$ as an ion source, and glycerol as the plasticizer. At room temperature, a solution of 1g of CS in 40 mL 1% CH_3COOH solution was obtained after three hours. Thereafter, 0.66 gram of $MgCl_2$ was added into the solution via magnetic stirring for a couple of hours to get a clear solution of polymer salt complexes. Finally, after adding different weight percentages of glycerol, a plasticized polymer was obtained. The highest DC ionic conductivity of the CS:$MgCl_2$ electrolyte system was found to be 1.03×10^{-3} S cm^{-1} when 40 wt.% glycerol was added. The addition of metal complexes also enhances the conductivity of BPE. Aziz et al. [30] dispersed Ni metal complex into plasticized CS-$Mg(CH_3COO)_2$-based BPE. Prior to the addition of metal complex, they dispersed 1 g

of CS in 50 mL of 1 wt.% CH_3COOH solution then added 40 wt.% of $Mg(CH_3COO)_2$ salt and magnetically stirred to get homogeneous dispersion followed by addition of 42 wt.% of glycerol for plasticization. From ultraviolet-visible (UV-vis) spectroscopy and x-ray diffraction spectroscopy (XRD) (Figure 22.2), the incorporation of Ni-metal complexes was confirmed. Enhanced cycles (1000) were observed in case of CS-glycerol-$Mg(CH_3COO)_2$-Ni, while only 400 cycles during charging and discharging for CS-glycerol-$Mg(CH_3COO)_2$ was found in the EDLC application. Hadi et al. [20] prepared CS-based polymer electrolyte by introducing Zn(II)-complex into the mixture of CS and ammonium iodide (NH_4I), followed by adding glycerol as a plasticizer.

When the polymer electrolyte was 30 wt.% glycerol with CS:NH_4I:Zn(II)-complex, a smooth and uniform surface morphology without any phase separation was revealed by field emission scanning electron microscopy (FESEM), lowering bulk resistance and assisting conducting ions to transfer easily, resulting in ion conductivity. The electrochemical stability was 1.37 V for the prepared (30 wt.% glycerol with CS:NH_4I:Zn(II)-complex) electrolyte system. In another study, a dilute solution of zinc metal complex (10 mL) was added into 40 wt.% glycerol plasticized sample of CS:NH_4F electrolyte and
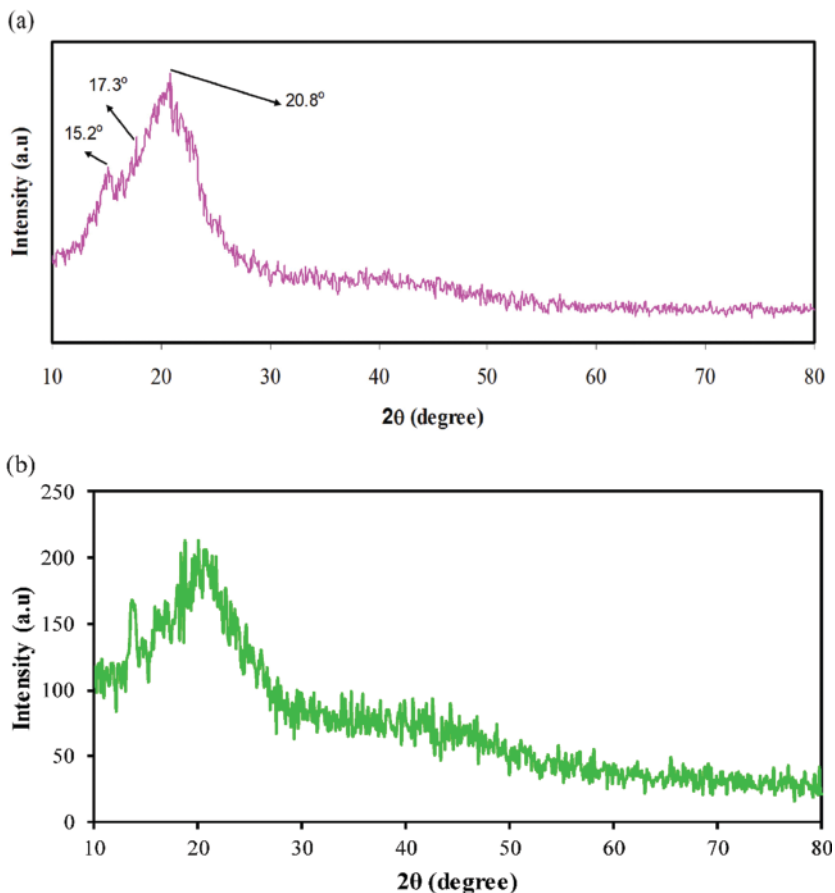
Figure 22.2 XRD patterns of (a) pure CS and (b) CS:$Mg(CH_3COO)_2$:Gly:Ni CS systems. *Reproduced with permission* [30]. *Reproduced under the terms of the CC-BY-4.0 license. Copyright 2021, Aziz et al.*

exhibited excellent ionic conductivity, which was found as 1.71×10^{-3} S cm^{-1}, while without using zinc metal complex (40 wt.% glycerol with CS:NH$_4$F), about 9.52×10^{-4} S cm^{-1} results [31]. The excellent charge storage behaviour was confirmed by cyclic voltammetry shown in Figure 22.3. The blending polymer host is superior to a single
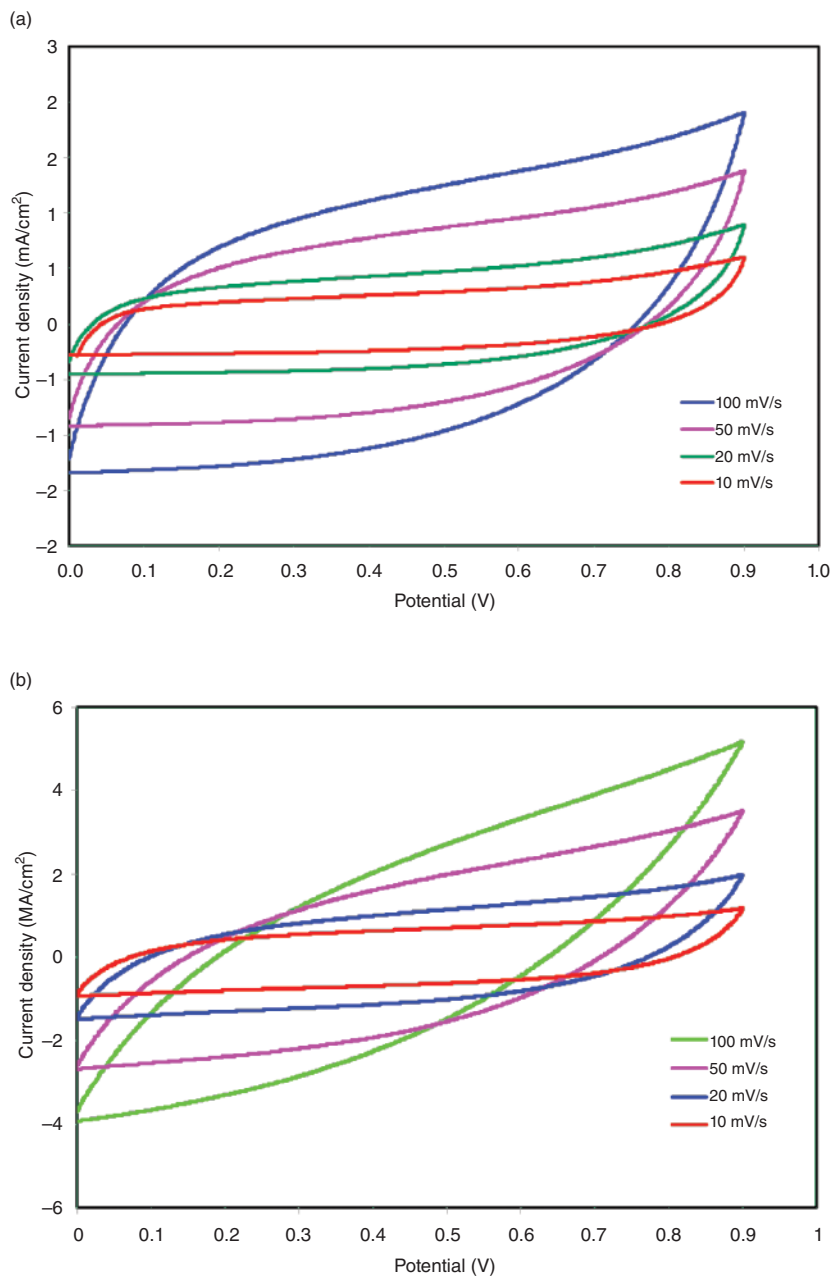
Figure 22.3 CV curves of the engineered EDLC using (a) CSNHG$_4$ and (b) CSNHG$_5$ electrolyte at different scan rates. *Reproduced with permission* [31]. *Reproduced under the terms of the CC-BY-4.0 license. Copyright 2020, Asnawi et al.*

polymeric host. To utilize these opportunities, CS was blended with other polymers such as PVA [10, 24], poly(ethylene oxide) (PEO) [21, 44], and DX [26], to prepare the polymeric host to different salts.

Aziz et al. [44] blended an optimum amount of 70 wt.% CS with 30 wt.% PEO and added different amounts of $LiClO_4$ to obtain $CS:PEO:LiClO_4$ electrolytes via SCM. In brief, 70% CS and 30% PEO were dissolved separately in 50 mL of 1% acetic acid for 120 minutes at room temperature. Then the two solutions were mixed and magnetically stirred to get a homogeneous blended polymer solution. Finally, $CS:PEO:LiClO_4$ was obtained by introducing $LiClO_4$ into a blended polymer solution. When $LiClO_4$ was 40 wt.%, the synthesized polymer exhibited a maximum DC conductivity of 7.34×10^{-4} S cm^{-1}. The specific capacitance of the prepared electrolyte in EDLC application was 6.88 F g^{-1}.

22.4.1.3   Starch-based Electrolytes

Starch is another green polysaccharide polymer consisting of amylase (linear structure) and amylopectin (branched structure) and which has a variety of properties, including low cost, abundance, superior steel adhesion features, high solubility, good film-forming ability along with enhanced recrystallization stability of the amorphous phase, and it is renewable raw material with good biocompatibility. The linear portion comprises -(1,4)-linked D-glucopyranosyl chains, while the branching portion comprises a junction made up of -(1,6)-linked polysaccharide chains. Amylose's linear shape enables salt contact more than amylopectin's branching structure, which adds a steric barrier to starch-salt interaction. However, amylopectin (double helices) reduces the polymer chain mobility due to this steric barrier. Since starch with high amylose content is highly amorphous, it is preferable to use it as a polymer host in electrolytes [45, 46]. Chauhan et al. [45] selected corn starch crosslinked with glutaraldehyde (GA) as polymeric host and $NaClO_4$ salt for starch-salt interaction to make flexible electrolyte membranes. A suitable amount of corn starch and $NaClO_4$ (starch/salt ratio varied from 1:0.1 to 1:1) were dispersed in methanol separately and then mixed together. Then 2 ml of GA was added, and finally, the entire solution was agitated at 40 °C for three hours to create a homogenous solution, which was then allowed to dry at room temperature. From Nyquist plots, it was observed that the highest conductivity was found at a 1:0.9 starch/salt ratio. A similar method was performed to prepare arrowroot starch-based electrolyte and it was compared with a corn starch-based electrolyte system [46]. It has been found that the association of salt with corn starch is high compared to arrowroot starch, thus the excess electric field is required to dissociate at the electrode. A higher electrochemical stability window was observed and confirmed by using LSV for corn starch-based electrolytes. Corn and arrowroot starch-based approaches had ambient conductivities of 1.00×10^{-2} S cm^{-1} and 5.60×10^{-3} S cm^{-1}, respectively. Graphene oxide (GO) was employed by Azli and his groups [28] for the chemical modification of the starch to improve the film-forming characteristic of the starch by combining both potato starch (PS) and GO. They also employed lithium trifluoromethanesulfonate ($LiCF_3SO_3$) in this SPE research since it contains big and bulky anions that may be delocalized to promote salt dissociation and solubility.

However, since $LiCF_3SO_3$ has a poor ionic conductivity at ambient temperature, they incorporated IL (1-butyl-3-methylimidazolium chloride ([Bmim][Cl])) into a PS/GO/$LiCF_3SO_3$ electrolytic system. Differential scanning calorimetry (DSC) analysis revealed that the addition of 30 wt.% [Bmim][Cl] into the PS/GO/$LiCF_3SO_3$ electrolytic system

Figure 22.4 Transparent and free-standing starch-chitosan-based film. *Reproduced with permission* [49]. *Copyright 2015, Elsevier.*

caused a decrease in glass transition temperature (T_g) values from 36.5 to 17.5 °C resulting higher ionic conductivity. The addition of IL (1-butyl-3- methylimidazolium hexafluorophosphate ($BmImPF_6$)) to corn starch and lithium hexafluorophosphate ($LiPF_6$) (polymer-salt system) via solution casting technique extended the electrochemical potential window of polymer electrolytes more than that of ionic liquid–free polymer electrolyte [29]. An alternative conduction pathway for ions in the polymer matrix via hydroxyl groups on the surface of nanofillers was generated due to the addition of 4 wt.% TiO_2 nanofiller to the starch-LiOAc (lithium acetate) complex. This was confirmed by Fourier transform infrared (FTIR) spectra [27]. As well as these examples, other starch-based blended polymers have been used as hosts, such as ST-CS, potato starch (PS)-MC, ST-poly(styrene sulphonic acid) (PSSA), PS-CS. Lithium perchlorate ($LiClO_4$), NH_4Cl, NH_4NO_3, NH_4F have been used as dopants, with glycerol as a plasticizer, to fabricate SPE via solution casting methods for supercapacitor applications [39, 47–49]. One example of electrolyte film is shown in Figure 22.4 [49].

22.4.2 Gel Polymer Electrolyte (GPE)

GPE is a unique substance that combines the flexibility and stability of a solid with the ease of liquid dispersion of a liquid. Because of possessing both liquid-like ionic conductivity and solid-like structural and mechanical features, GPEs are considered promising candidates for SC applications.

22.4.2.1 Cellulose-based Polymer Gel Electrolyte

Most cellulose-based GPEs use cellulose to confine the liquid electrolyte within the cellulose structure, resulting in significantly more ionic conductivity than SPEs. The linked cellulose chains provide the mechanical stability for supercapacitors to operate in bending mode without sacrificing electrochemical performance. However, there have challenges to

having a full-cellulose matrix with both solid ionic conductivity and mechanical integrity. Different cellulose-based gel polymer electrolytes have been developed to address this issue, with the help of different liquid solvent and salts [50]. An example is where cellulose was dissolved in a precooled NaOH/urea solution (freeze-thawing method), and hydrogels were produced using a low temperature crosslinking method in the presence of the cross-linking agent epichlorohydrin (EPI) [13]. SEM images confirmed the porous architecture of the prepared hydrogel (cellulose/NaOH hydrogels), which was responsible for the ion migration in the constructed symmetric supercapacitor system that used N-doped graphene (NG) hydrogels as electrodes. This constructed symmetric capacitor demonstrated an enhanced specific capacitance of $98.8\,F\,g^{-1}$ at $1\,A\,g^{-1}$, superb cyclic stability with a maximum energy density of $13.5\,Wh\,kg^{-1}$ while the power density was $496.4\,W\,kg^{-1}$ at the optimized condition of electrolytes. To widen the electrochemical potential window and extend the cycle life of the supercapacitor, a gel polymer electrolyte was proposed based on the trapping of highly concentrated $ZnCl_2$ into cellulose matrix with Ca^{2+} ions worked as a crosslinking agent for enhancing the strength of hydrogel [12]. The constructed supercapacitor exhibited an energy density of $192\,Wh\,kg^{-1}$ while the power density was $499\,W\,kg^{-1}$ and $58\,Wh\,kg^{-1}$ at an extremely high-power density of $16976\,W\,kg^{-1}$ with high retention of capacitance (94.7%) after 5000 cycles. In addition, the cellulose-based hydrogel was prepared by dissolving microcrystalline cellulose via stirring at $50\,°C$ for 30 min in IL/DMSO (IL = N,N′-dimethyl-N-ethylpiperazinium acetate ([DMEPpz][Ac]) and DMSO = dimethyl sulfoxide) mixed solvent followed by immersing that cellulose solution into deionized water and then immersing in $2\,M$ lithium acetate (LiAc) aqueous solution to obtain swell electrolyte [51]. Pérez-Madrigal et al. [50] investigated the influence of several parameters such as the degree of cross-linking, post-washing treatment, cellulose concentration, supporting electrolyte concentration to the gel polymer hydrogel, and the cellulose amount. Where NaCl was used as a supporting electrolyte, citric acid solutions were used as a crosslinking agent with poly(3,4-ethylene dioxythiophene) (PEDOT) electrodes. The post-washing treatment involved re-absorption of supporting electrolytic salt with or without lyophilization, 10 or 20 wt.% of carboxymethyl cellulose sodium salt (NaCMC) was employed as a polymer matrix. The overall schematic diagram is shown in Figure 22.5.

Among numerous gel electrolytes, ionogels have three-dimensional (3D) polymer or inorganic networks containing ionic liquids (ILs). The ILs serve as both carrier ions and solvents to provide excellent ionic conductivity, a broad electrochemical window, strong chemical and thermal stability, as well as non-flammability. On the other hand, the solid networks serve as a structured matrix to give mechanical strength. Ionogels are inherently more stable than other gels using volatile solvents because ILs are nonvolatile and have a low vapour pressure [52]. To optimize the effect of ionogels, a large amount of IL is needed to add into a 3D polymer matrix, which adversely affects the mechanical properties and makes electrolytes brittle.

To overcome this limitation, Rana and his group [52] used facile solution chemistry to design dual networking of renewable, highly conducting, and very durable cellulose-based ionogels. To create dual networked ionogels, they chose 1-butyl-3-methylimidazolium bis(trifluoromethylsulfonyl)imide ([BMIM][TFSI]) IL and 1,3-dimethylimidazolium methyl phosphite ([DMIM][(MeO)(H)PO$_3$]) mixture to dissolve pristine cellulose, and then 2-hydroxyethyl methacrylate (HEMA) monomer was polymerized
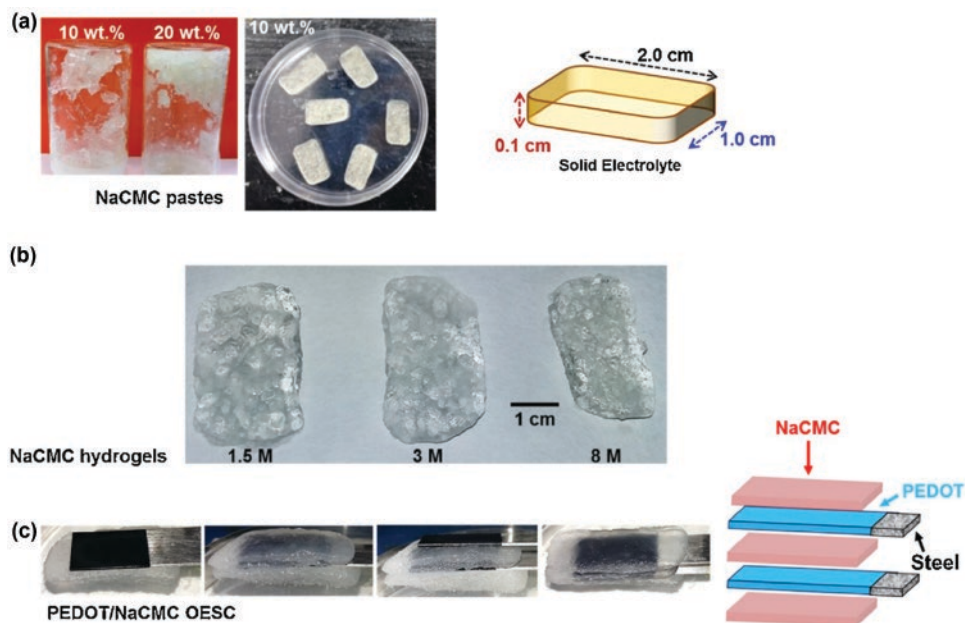
Figure 22.5 (a) Pieces obtained after moulding the NaCMC pastes (10 or 20% wt. cellulose) with a hydraulic press. The dimensions of the pieces are displayed on the right. (b) NaCMC hydrogels cross-linked using citric acid solutions at different concentrations (1.5, 3 or 8 M). (c) Photographs displaying the assembly of the different elements of the PEDOT/NaCMC ESCs. A scheme of the supercapacitor is displayed on the right. *Reproduced with permission* [50]. *Copyright 2018, Elsevier.*

in the presence of the first cellulose network. The cellulose-based ionogel electrolyte (excellent ionic conductivity and electrochemical stability, see Figure 22.6) between two activated carbon electrodes delivers high specific capacitance and rate capability of $174 \, F \, g^{-1}$ and 88% at 120 °C at a cell voltage of 2.5 V. In addition regenerated cellulose nanoparticle (RCN) were used as a regulator to prepare cellulose based ionogels [53], manganese dioxide (MnO_2) and reduced graphene oxide (RGO) nanosheet-piled hydrogel films and novel bacterial cellulose (BC)-filled polyacrylic acid sodium salt-Na_2SO_4 (BC/PAAS-Na_2SO_4) neutral gel electrolyte [54] and Ag and polyaniline (PANI) nanoparticles coated on cellulose nanofibrils (CNF) aerogel [55], have been reported for supercapacitor applications.

22.4.2.2 CS and Starch-based Gel Electrolyte

To create safe devices e.g. thin-film or stacked cells, energy storage systems need to meet the flexibility or durability of any solid-state electrolytes. Yamagata et al. [56] prepared CS-based gel polymer electrolyte by mixing 2 wt.% aqueous solutions of CS with a crosslinking agent 10 wt.% sodium hydroxide aqueous solution followed by washing with distilled water. Thereafter immersing in a significant excess of ethanol for 24 h, then again rinsed with ethanol and subsequent immersion in 1-ethyl-3-methylimidazolium tetrafluoroborate (EMImBF₄). During 5000 cycles, supercapacitor devices showed Coulombic efficiency at more than 99.9% while using activated carbon and the synthesized electrolyte
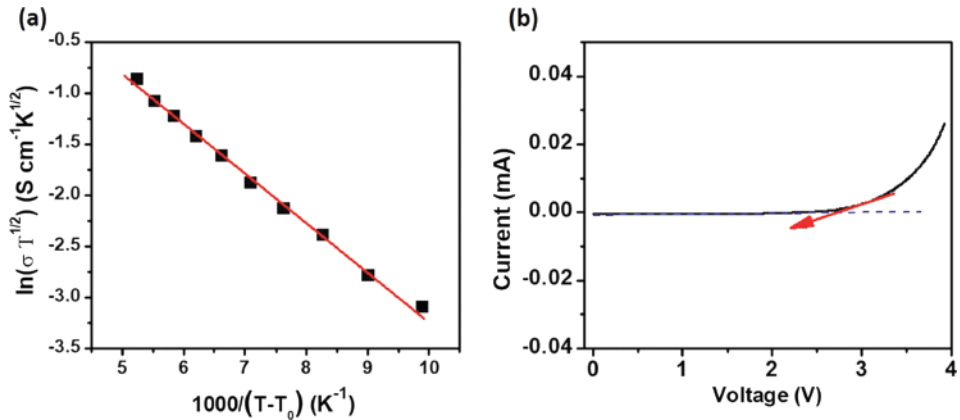
Figure 22.6 (a) VTF plot of log (ionic conductivity) vs. inverse temperature, (b) LSV curve of CpHEMA/C-p-cellulose ionogels at 30 °C. *Reproduced with permission* [52]. *Copyright 2020, Elsevier.*
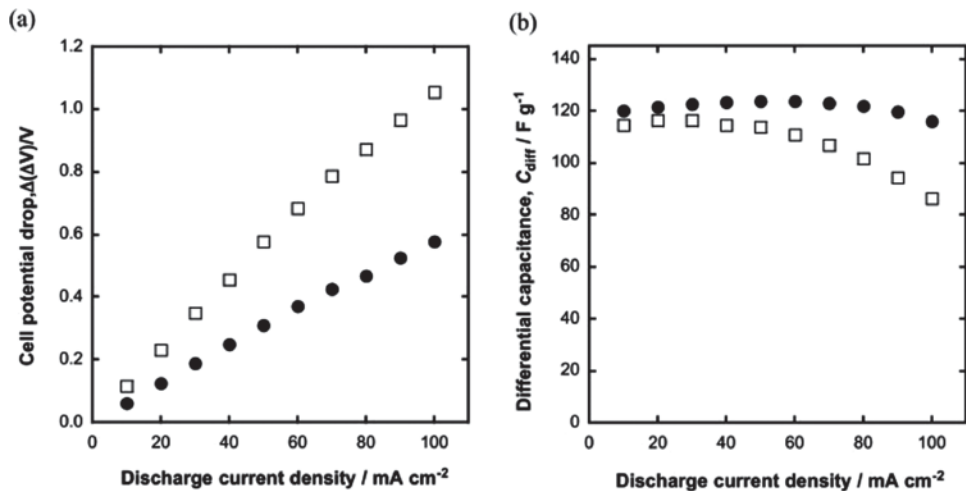
Figure 22.7 (a) Cell potential drop and (b) differential capacitance estimated using the charge-discharge profile of the model cell with Chi/EMImBF$_4$ (●) and liquid EMImBF$_4$ (□). Current density: 10–100 mA cm^{-2}; cell potential: 0–2.5 V. *Reproduced with permission* [56]. *Copyright 2012, Elsevier.*

(Figure 22.7). They also observed the influence of CS above the activated carbon as electrode material in supercapacitor performance with the gel polymer. It was observed that the cell voltage drops (ΔV_{drop}) were reduced by 0.09 V while using Chi + ACFC electrodes (ΔV_{drop} for Chi + ACFC was 0.15 V, and that for ACFC was 0.24 V) [57]. Furthermore, carboxylated chitosan-graft-polyacrylamide-lithium sulfate (CYCTS-g-PAM-Li$_2$SO$_4$) as a modified supramolecular carboxylated chitosan hydrogel electrolyte was prepared by using a free radical polymerization of acrylamide monomers in carboxylated chitosan (CYCTS) solution with N,Ń-methylene bisacrylamide (MBA).

Special advantages of CYCTS-g-PAM-Li$_2$SO$_4$ (2.25 MPa) were found: higher ionic conductivity (1.74×10^{-2} S cm^{-1}), greater electrolyte absorbability (280%), and increased

mechanical qualities [58]. The starch-based electrolyte was prepared using thermoplastic starch (TPS) (from the mixture of corn starch and citric acid) powder, mixing with distilled water, followed by corn starch via the ultrasonication method. It was discovered that 10% citric acid containing hydrogel is most suitable gel polymer electrolyte for printed batteries or supercapacitors and it reached a specific capacitance of roughly $35\,F\,g^{-1}$ or $279\,mF\,cm^{-2}$ without extra electrolyte [59].

22.4.2.3 Lignin-based Polymer Gel Electrolyte

Lignin is an aromatic heteropolymer with many carbonyls, phenolic, or phenolate groups. Lignin-based hydrogel electrolytes can be synthesized by chemical crosslinking between poly(ethylene glycol) diglycidyl ether (PEGDGE, $M_n = 500$) and lignin [60]. The phenolic groups of lignin function as nucleophiles, while PEGDGE acts as a source of epoxy groups, resulting in lignin-based dry gels via ring-opening polymerization. These cross-linked lignin hydrogel electrolytes are mechanically robust (523% swelling ratio) and have high ionic conductivity ($10.35\,mS\,cm^{-1}$) owing to having high mechanical/dimensional stability and a large amount of water uptake resulting from the unique cross-linking chemistry. A simple acid soaking technique was used to transform chemically crosslinked lignin hydrogel into high-mechanical hybrid double crosslinked (physical and chemical crosslinking) lignin hydrogel (DC lignin hydrogel) through the development of lignin hydrophobic aggregation interaction [61]. Moreover, protonation of unreacted phenol and carboxyl groups within the lignin structure is produced by acid soaking of the chemically crosslinked lignin hydrogel, resulting in the development of hydrophobic interactions among lignin chains. These synthesized DC lignin hydrogels have a higher ionic conductivity, mechanical strength, and cyclic loading-unloading compression performance than chemically crosslinked lignin hydrogel.

22.4.2.4 Soybean Protein Isolate

Soybean protein isolate (SPI) is used as a matrix material for supercapacitor electrolyte preparation due to its environmentally friendly nature [62]. However, SPI's lower mechanical strength, unsatisfactory processability, and poor water stability limit its use in supercapacitors. To overcome these drawbacks, a crosslinking agent, ethylene glycol diglycidyl ether (EGDE), is used to prepare a series of crosslinked membranes (SPI/EGDE) with SPI via SCM [62]. Even though the water resistance of the synthetic SPI/EGDE membrane has been improved, the ionic conductivity of SPI/EGDE is lower than pure SPI, resulting in poor electrochemical performance of SC. These issues can be addressed by adding a very hydrophilic polymer into the crosslinked structure. For example, due to its outstanding hydrophilicity and film-forming ability, hydroxyethyl cellulose is mixed with SPI and saturated with 1M Li_2SO_4 to create GPEs which used in SP. The synthesized GPE exhibits enhanced ionic conductivity and capacitive performance with water-resistant characteristics [63]. The capacitive performance of SPI-based GPE can also be enhanced by introducing redox mediators into the electrolyte [64]. Using SPI as the polymer matrix, potassium iodide (KI) as the redox mediator, and Li_2SO_4 as the neutral electrolyte, Z. Xun et al. [64] created an SPI-based redox GPE. When SPI-Li_2SO_4-100wt.% KI is employed as the electrolyte material, the specific capacitance is $224.19\,F\,g^{-1}$, which is 156% greater than SPI-Li_2SO_4.

22.5   Conclusion

BPE materials have piqued researchers' attention in SCs applications. BPEs reduce the cost and environmental risk and provide a wide operating potential window, flexibility, and high mechanical property supporting the creration of portable and wireless high-performance SCs. In recent years, for preparing BPE cellulose, CS, DX, starch, and SPI have been used in SCs providing great stability, strong ionic conductivity, a broad potential window, and mechanical robustness. In SCs, biomass-based hydrogel electrolytes have been extensively explored with promising results. Compared with hydrogels, biomass-based ionogels are highly stable because the distribution of ILs in 3D polymer networks is nonvolatile with minimal vapour pressure. Although significant progress has been seen in BPEs, some challenges still limit their use in commercial applications. BPEs generally have low ionic conductivity and viscosity thus, a small value of specific capacitance is observed. Hence improvement of the ionic conductivity of BPEs is needed. The development of ionic conductivity of BPE via blending with other polymers, incorporation of dopant salts, the addition of plasticizer, the addition of metal complexes, and the addition of nanofiller and ionic liquid are reported in the literature and summarized here briefly. Utilization of this process requires optimizing the mechanical strength and ionic conductivity of prepared BPE. These novel components are designed to increase SCs performance by performing one or more useful functions. These methods provide reference direction for improving BPEs for use in SC applications in the future. Research focus will continue toward biomass-based quasi-solid-state electrolytes, such as GPE, to meet the needs of new flexible and wearable SC energy storage devices.

Acknowledgements

References

1 L. Xia, L. Yu, D. Hu, G. Z. Chen, *Mater. Chem. Front.* **2017**, *1*, 584–618.

2 L. Zhang, X. S. Zhao, *Chem. Soc. Rev.* **2009**, *38*, 2520–2531.

3 H. Parsimehr, A. Ehsani, *Chem. Rec.* **2020**, *20*, 1163–1180.

4 C. Zhong, Y. Deng, W. Hu, J. Qiao, L. Zhang, J. Zhang, *Chem. Soc. Rev.* **2015**, *44*, 7484–7539.

5 S. Lin, F. Wang, Z. Shao, *J. Mater. Sci.* **2021**, *56*, 1943–1979.

6 S. B. Aziz, M. H. Hamsan, R. M. Abdullah, M. F. Z. Kadir, *Molecules* **2019**, *24*(13), 2503.

7 M. H. Hamsan, S. B. Aziz, M. F. Shukur, M. F. Z. Kadir, *Ionics* **2019**, *25*, 559–572.

8 I. Stepniak, M. Galinski, K. Nowacki, M. Wysokowski, P. Jakubowska, V. V. Bazhenov, T. Leisegang, H. Ehrlich, T. Jesionowski, *RSC Adv.* **2016**, *6*, 4007–4013.

9 N. Srivastava, *Supercapacitor Technology* **2019**, *61*, 121–140.

10 S. B. Aziz, J. M. Hadi, E. M. Elham, R. T. Abdulwahid, S. R. Saeed, A. S. Marf, W. O. Karim, M. F. Z. Kadir, *Polymers* **2020**, *12*(9), 1938.

11 F. G. Torres, G. E. De-La-Torre, K. N. Gonzales, O. P. Troncoso, *ACS Appl. Energy Mater.* **2020**, *3*, 11500–11515.

12 L. Yang, L. Song, Y. Feng, M. Cao, P. Zhang, X. F. Zhang, J. Yao, *J. Mater. Chem. A* **2020**, *8*, 12314–12318.

13 H. Wang, J. Wu, J. Qiu, K. Zhang, J. Shao, L. Yan, *Sustain. Energy Fuels* **2019**, *3*, 3109–3115.

14 S. B. Aziz, M. H. Hamsan, W. O. Karim, M. F. Z. Kadir, M. A. Brza, O. G. Abdullah, *Biomolecules* **2019**, *9*(7), 267.

15 A. S. A. Khiar, A. K. Arof, *World Acad. Sci. Eng. Technol. 59 2011*, **2011**, *5*, 23–27.

16 S. B. Aziz, M. M. Nofal, M. F. Z. Kadir, E. M. A. Dannoun, M. A. Brza, J. M. Hadi, R. M. Abdulla, *Materials* **2021**, *14*(8), 1994.

17 H. Yang, Y. Liu, L. Kong, L. Kang, F. Ran, *J. Power Sources* **2019**, *426*, 47–54.

18 L. Cao, M. Yang, D. Wu, F. Lyu, Z. Sun, X. Zhong, H. Pan, H. Liu, Z. Lu, *Chem. Commun.* **2017**, *53*, 1615–1618.

19 D. Zhao, C. Chen, Q. Zhang, W. Chen, S. Liu, Q. Wang, Y. Liu, J. Li, H. Yu, *Adv. Energy Mater.* **2017**, *7*, 1700739.

20 J. M. Hadi, S. B. Aziz, S. R. Saeed, M. A. Brza, R. T. Abdulwahid, M. H. Hamsan, R. M. Abdullah, M. F. Z. Kadir, S. K. Muzakir, *Membranes* **2020**, *10*(11), 363.

21 S. B. Aziz, R. T. Abdulwahid, M. H. Hamsan, M. A. Brza, R. M. Abdullah, M. F. Kadir, S. K. Muzakir, *Molecules* **2019**, *24*(19), 3508.

22 Y. N. Sudhakar, M. Selvakumar, *Electrochim. Acta* **2012**, *78*, 398–405.

23 A. S. F. M. Asnawi, S. B. Aziz, M. M. Nofal, M. H. Hamsan, M. A. Brza, Y. M. Yusof, R. T. Abdilwahid, S. K. Muzakir, M. F. Z. Kadir, *Polymers* **2020**, *12*(6), 1433.

24 M. Brza, S. B. Aziz, S. R. Saeed, M. H. Hamsan, S. R. Majid, R. T. Abdulwahid, M. F. Z. Kadir, R. M. Abdullah, *Membranes* **2020**, *10*(12), 381.

25 M. H. Hamsan, S. B. Aziz, M. A. S. Azha, A. A. Azli, M. F. Shukur, Y. M. Yusof, S. K. Muzakir, N. S. A. Manan, M. F. Z. Kadir, *Mater. Chem. Phys.* **2020**, *241*, 122290.

26 S. B. Aziz, M. A. Brza, I. Brevik, M. H. Hafiz, A. S. F. M. Asnawi, Y. M. Yusof, R. T. Abdulwahid, M. F. Z. Kadir, *Polymers* **2020**, *12*(9), 2103.

27 A. C. W. Ong, N. A. Shamsuri, S. N. A. Zaine, D. Panuh, M. F. Shukur, *Ionics* **2021**, *27*, 853–865.

28 A. A. Azli, N. S. A. Manan, S. B. Aziz, M. F. Z. Kadir, *Ionics* **2020**, *26*, 5773–5804.

29 C. W. Liew, S. Ramesh, *Carbohydr. Polym.* **2015**, *124*, 222–228.

30 S. B. Aziz, E. M. A. Dannoun, M. H. Hamsan, R. T. Abdulwahid, K. Mishra, M. M. Nofal, M. F. Z. Kadir, *Membranes* **2021**, *11*(4), 289.

31 A. S. F. M. Asnawi, S. B. Aziz, M. M. Nofal, Y. M. Yusof, I. Brevik, M. H. Hamsan, M. A. Brza, R. T. Abdulwahid, M. F. Z. Kadir, *Membranes* **2020**, *10*(6), 132.

32 E. M. A. Dannoun, S. B. Aziz, M. A. Brza, M. M. Nofal, A. S. F. M. Asnawi, Y. M. Yusof, S. Al-Zangana, M. H. Hamsan, M. F. Z. Kadir, H. J. Woo, *Polymers* **2020**, *12*(11), 2531.

33 S. B. Aziz, M. H. Hamsan, M. M. Nofal, S. San, R. T. Abdulwahid, S. R. Saeed, M. A. Brza, M. F. Z. Kadir, S. J. Mohammed, S. Al-Zangana, *Polymers* **2020**, *12*(7), 1526.

34 S. B. Aziz, I. Brevik, M. H. Hamsan, M. A. Brza, M. M. Nofal, A. M. Abdullah, S. Rostam, S. Al-Zangana, S. K. Muzakir, M. F. Z. Kadir, *Polymers* **2020**, *12*(10), 2257.

35 S. B. Aziz, A. S. F. M. Asnawi, M. F. Z. Kadir, S. M. Alshehri, T. Ahamad, Y. M. Yusof, J. M. Hadi, *Polymers* **2021**, *13*(8), 1183.

36 S. B. Aziz, E. M. A. Dannoun, M. H. Hamsan, H. O. Ghareeb, M. M. Nofal, W. O. Karim, A. S. F. M. Asnawi, J. M. Hadi, M. F. Z. A. Kadir, *Polymers* **2021**, *13*(6), 930.

37 S. B. Aziz, I. Brevik, M. A. Brza, A. S. F. M. Asnawi, E. M. A. Dannoun, Y. M. Yusof, R. T. Abdulwahid, M. H. Hamsan, M. M. Nofal, M. F. Z. Kadir, *Materials* **2020**, *13*(21), 5030.

38 S. B. Aziz, M. A. Brza, K. Mishra, M. H. Hamsan, W. O. Karim, R. M. Abdullah, M. F. Z. Kadir, R. T. Abdulwahid, *J. Mater. Res. Technol.* **2020**, *9*, 1137–1150.

39 M. H. Hamsan, M. F. Shukur, M. F. Z. Kadir, *Ionics* **2017**, *23*, 3429–3453.

40 S. B. Aziz, M. A. Brza, I. Brevik, M. H. Hamsan, R. T. Abdulwahid, S. R. Majid, M. F. Z. Kadir, S. A. Hussen, R. M. Abdullah, *Polymers* **2020**, *12*(11), 2718.

41 M. H. Hamsan, M. M. Nofal, S. B. Aziz, M. A. Brza, E. M. A. Dannoun, A. R. Murad, M. F. Z. Kadir, S. K. Muzakir, *Polymers* **2021**, *13*(8), 1233.

42 M. H. Hamsan, S. B. Aziz, M. F. Z. Kadir, M. A. Brza, W. O. Karim, *Polym. Test.* **2020**, *90*, 106714.

43 M. H. Hamsan, S. B. Aziz, M. M. Nofal, M. A. Brza, R. T. Abdulwahid, J. M. Hadi, W. O. Karim, M. F. Z. Kadir, *J. Mater. Res. Technol.* **2020**, *9*, 10635–10646.

44 S. B. Aziz, M. H. Hamsan, M. A. Brza, M. F. Z. Kadir, R. T. Abdulwahid, H. O. Ghareeb, H. J. Woo, *Results Phys.* **2019**, *15*, 102584.

45 J. K. Chauhan, M. Kumar, M. Yadav, T. Tiwari, N. Srivastava, *Ionics* **2017**, *23*, 2943–2949.

46 J. K. Chauhan, D. Yadav, M. Yadav, M. Kumar, T. Tiwari, N. Srivastava, *SN Appl. Sci* **2020**, *2*, 899.

47 S. B. Aziz, M. H. Hamsan, W. O. Karim, A. S. Marif, R. T. Abdulwahid, M. F. Z. Kadir, M. A. Brza, *Ionics* **2020**, *26*, 4635–4649.

48 Y. N. Sudhakar, M. Selvakumar, *J. Appl. Electrochem.* **2013**, *43*, 21–29.

49 M. F. Shukur, M. F. Z. Kadir, *Electrochim. Acta* **2015**, *158*, 152–165.

50 M. M. Pérez-Madrigal, M. G. Edo, M. G. Saborío, F. Estrany, C. Alemán, *Carbohydr. Polym.* **2018**, *200*, 456–467.

51 D. Kasprzak, I. Stępniak, M. Galiński, *J. Solid State Electrochem.* **2018**, *22*, 3035–3047.

52 H. H. Rana, J. H. Park, G. S. Gund, H. S. Park, *Energy Storage Mater.* **2020**, *25*, 70–75.

53 M. Zhu, L. Yu, S. He, H. Hong, J. Liu, L. Gan, M. Long, *ACS Appl. Energy Mater.* **2019**, *2*, 5992–6001.

54 H. Fei, N. Saha, N. Kazantseva, R. Moucka, Q. Cheng, P. Saha, *Materials* **2017**, *10*(11), 1251.

55 X. Zhang, Z. Lin, B. Chen, W. Zhang, S. Sharma, W. Gu, Y. Deng, *J. Power Sources* **2014**, *246*, 283–289.

56 M. Yamagata, K. Soeda, S. Ikebe, S. Yamazaki, M. Ishikawa, *Electrochim. Acta* **2013**, *100*, 275–280.

57 K. Soeda, M. Yamagata, S. Yamazaki, M. Ishikawa, *Electrochemistry* **2013**, *81*, 867–872.

58 H. Yang, X. Ji, Y. Tan, Y. Liu, F. Ran, *J. Power Sources* **2019**, *441*, 227174.

59 A. Willfahrt, E. Steiner, J. Hötzel, X. Crispin, Appl., *Phys. A Mater. Sci. Process.* **2019**, *125*, 474.

60 J. H. Park, H. H. Rana, J. Y. Lee, H. S. Park, *J. Mater. Chem. A* **2019**, *7*, 16962–16968.

61 T. Liu, X. Ren, J. Zhang, J. Liu, R. Ou, C. Guo, X. Yu, Q. Wang, Z. Liu, *J. Power Sources* **2020**, *449*, 227532.

62 P. Huo, S. Ni, P. Hou, Z. Xun, Y. Liu, J. Gu, *Polymers* **2019**, *11*(5), 863.

63 Z. Xun, S. Ni, Z. Gao, Y. Zhang, J. Gu, P. Huo, *Polymers* **2019**, *11*(11), 1895.

64 Z. Xun, Y. Liu, J. Gu, L. Liu, P. Huo, *J. Electrochem. Soc.* **2019**, *166*, A2300–A2312.

23

Biomass-based Separators for Supercapacitor Applications

S. M. Abu Nayem[1], Santa Islam[1], Syed Shaheen Shah[2,3], Abdul Awal[1], Nasrin Sultana[1], A. J. Saleh Ahammad[1,*], and Md. Abdul Aziz[2,4,*]

[1] *Department of Chemistry, Jagannath University, Dhaka 1100, Bangladesh*
[2] *Interdisciplinary Research Center for Hydrogen and Energy Storage (IRC-HES), King Fahd University of Petroleum & Minerals, Dhahran 31261, Saudi Arabia*
[3] *Physics Department, King Fahd University of Petroleum & Minerals, KFUPM Box 5047, Dhahran 31261, Saudi Arabia*
[4] *K. A. CARE Energy Research and Innovation Center, King Fahd University of Petroleum & Minerals, Dhahran, 31261, Saudi Arabia*
* *Corresponding authors*

23.1 Introduction

With advancements in science and technology, portable and wearable electronic systems have seen tremendous growth in a variety of applications, including a variety of sensors, electronic skin, and other flexible electronic devices (e.g., notebook computers, smart glasses, mobile phones, automatic doors, smart watches, intelligent bracelets, window locks, hybrid electric vehicles, and so on). As a result, the creation of portable and wearable energy storage technologies has become a global goal [1–7]. Among different established energy storage systems, supercapacitors are a promising and environmentally friendly energy conversion/storage solution due to their high electric capacitance value, high charge and discharge efficiency, high power density, and high capacitive retention over thousands of cycles [8–13]. During the charge storage process, supercapacitors typically obey two main mechanisms: electrical double-layer capacitance and pseudocapacitance [14, 15]. Between the electrode and electrolyte interface, a double layer is formed where charge storage is caused by a non-Faradaic process that is related to its capacitance value in an electrical double-layer capacitor (EDLC). On the other hand, pseudocapacitance is caused by the fast-Faradaic reaction that occurs when electrons are transferred from the electrode to the electrolyte ions [5, 16]. The performance of supercapacitors is determined by their structural components, which include two electrodes, an electrolyte (or mixture of different electrolytes such as aqueous and organic or aqueous and ionic liquid electrolyte), a separator, and current collectors. Two electrodes are separated in supercapacitors by a porous membrane that is submerged in an electrolytic solution (Figure 23.1) [8, 17]. In an effort to increase electrochemical performance, much emphasis has been placed on electrode materials and
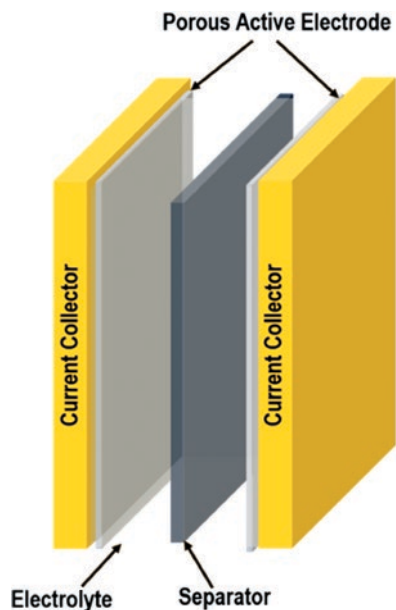
Figure 23.1 Principle structure of supercapacitor with essential elements.

architectures rather than electrolytes and separators [18]. The transportation of the ions of the electrolyte is also a vital issue in determining capacitor performance.

It is widely recognized that the separator is one of the crucial parts affecting the device's overall performance [19]. When the cathode and anode are in direct contact, the separator functions as a physical barrier, preventing a short circuit and allowing the liquid electrolyte ions to move quickly [20]. The separator should be dielectric in nature as well as chemically and electrochemically stable in the electrolytic solution [21]. During the charging and discharging process, the separator must be thin and porous enough to facilitate the flow of ions in the electrolyte. Using a separator that can be stretched without ripping can considerably improve the safety of flexible supercapacitors [6]. The separator must be chemically inert to the other components, notably the electrolyte. It should have low internal resistance and avoid introducing any additional unwanted elements into the workspace, such as humidity, gases, and especially air, which are likely to be present in its pores [19, 22]. Traditional energy storage systems have used separators made of commercial polyolefin-based membranes. The hydrophobic nature of these commercial polyolefins decreases the electron transfer rate while applying a high charge/discharge current, which may cause dimensional instability due to internal short circuits. In addition, the Nafion membrane has also been used commercially as a supercapacitor separator in the current market. However, the high cost and limited raw material limit its application in supercapacitor separators [23, 24].

There are different properties of separators, such as porosity, pore size, chemical stability, thermal conductivity, thickness, hydrophilicity, ionic conductivity, cheapness and flexibility which influence supercapacitor performance [10, 19, 23, 25, 26]. As a result, research into separator material selection for electrochemical capacitors is crucial in order to achieve the best values for these properties.

In recent years biomass has been extensively researched in different fields of application, such as supercapacitors, electrochemical sensors, dye-sensitized solar cells, and environmental remediations [27–31]. Due to their fantastic mechanical qualities, biocompatibility, biodegradability, and low cost, with incredibly strong, extensible, and robust features, renewable-source (especially cellulose) derived separators have sparked a lot of research interest in the electrochemical energy storage application world [32]. To solve the energy crisis, exploring renewable sources to prepare separator materials has become more urgent and significant. In this chapter, we summarize the development of the production of separators from sustainable biomass sources and their uses in supercapacitors.

23.2   Preparation of Biomass-based Separators

Via a thorough overview of the literature, many preparation processes for biomass-based separators have been discovered, such as phase-inversion [18, 33–36], simple freeze-thawing technique [37], TEMPO oxidation method [24], freeze-drying process [38], electrospinning process [39], and activation process [40].

The phase-inversion process generally involves a transformation of one phase to another, creating some unique properties such as lower crystallinity, higher thermal stability, flexibility, higher tensile strength, porous structure, and foldable nature [18, 33, 34]. The typical manufacturing of hydrogel film as a separator includes a dispersion of crystalline cellulose in an organic solvent, gelation, and subsequent replacement of the organic solvent with water. During the replacement process, the cellulose chains reorganized, resulting in an enlarged white regenerated cellulose hydrogel. After solidification and drying, a freestanding membrane is created [18, 36]. Hu et al. [36] prepared an ecofriendly cellulose film for the supercapacitor separator. The sandwich method was employed to assemble the supercapacitor device (SCD) (electrode/separator/electrode) (Figure 23.2). For instance, to prepare regenerated porous cellulose supercapacitor separator film by simply dissolving cellulose into the lithium chloride (LiCl) or dimethylacetamide (DMAc) solvent Teng et al. [34] used a simple phase inversion process. Initially, they prepared activated cellulose from the mixture of microcrystalline cellulose and DMAc by heating at 120 °C, stirring for three hours, then filtration and subsequent drying at 60 °C. Finally, the cellulose film was obtained by dissolving activated cellulose into LiCl/DMAc solvent followed by heating at 120 °C, stirring for three hours, cooling for 24 hours and subsequently washing with distilled water and freeze-drying. No chemical
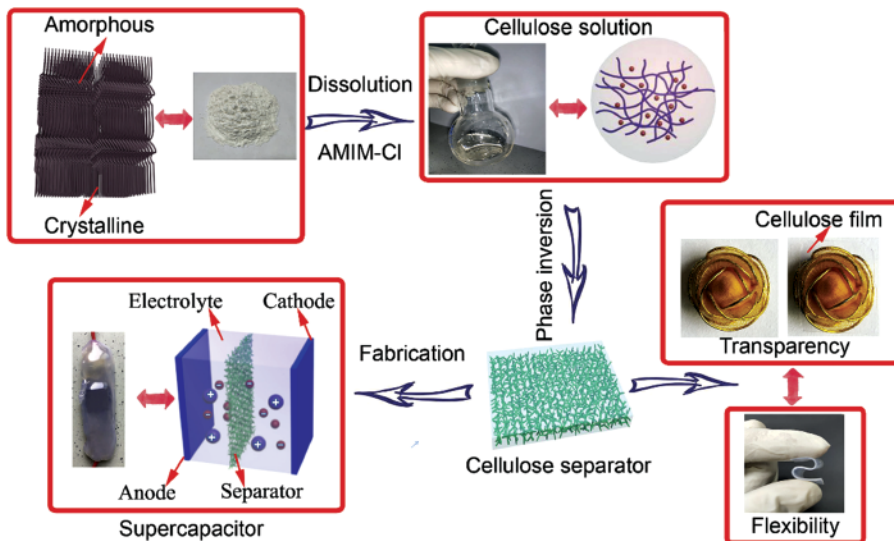
Figure 23.2   The preparation of porous cellulose film and the assembly of SCDs. Reproduced with permission [36]. *Copyright 2020, Elsevier.*

reaction occurred during the phase inversion process to prepare cellulose film from microcrystalline cellulose, which was confirmed by the FTIR spectral analysis of microcrystalline cellulose and regenerated cellulose film. They found that regenerated cellulose film with a cellulose concentration of ~8% exhibited higher thermal stability, lower crystallinity, and high tensile stress, which was obtained from fourier transform infrared spectroscopy (FTIR), x-ray diffraction (XRD), thermogravimetric analysis (TGA), derivative thermogravimetry (DTG), and tensile tester analysis.

Another study used a self-enhancing approach to create a composite hydrogel film by inverting the phases of microcrystalline cellulose and bacterial cellulose. In this study, a NaOH-urea solution was used to disperse microcrystalline cellulose. Then, bacterial cellulose was added to the solution mentioned above; after the H_2SO_4 treatment, a composite hydrogel film was produced. The SEM image exhibited the nanoporous structure of the prepared hydrogel surface while the meso- and macroporous structure of the cross-sectional view of the prepared hydrogel was observed, which indicated a more hydrophilic nature of the prepared hydrogel film [35]. Lignin sulfonate/SWCNT/holey reduced graphene oxide (Lig/SWCNT/HrGO) film showed a high tensile strength of 121.8 MPa. Different amounts of bacterial cellulose (BC) were added to microcrystalline cellulose (MCC) to prepare self-enhancing cellulose hydrogels. Mechanical performance without breaking structure under different deformations assures the flexibility of the fabricated system (Figure 23.3) [35]. The addition of polyvinyl alcohol (PVA) solution into the three freeze-thawing cycles and stirred homogeneous solution of microcrystalline cellulose, urea and NaOH, also produced cellulose/PVA composite gel after freezing for 12 hours and followed by removal of residual NaOH and urea using deionized water. The prepared composite gel exhibited excellent toughness with easily elongated behaviour without fracture [37].

In another report, Lima and coworkers [39] designed a flexible and stretchable supercapacitor by coating the inner electrode with electrospun cellulose acetate fibres as a separator and the outer electrode coiled around the separator. To prepare the separator, they used cellulose acetate solution in acetone and dimethylacetamide (DMAc) solvent with a 2:1 (wt.) proportion. Then using a1 mL syringe, they deposited an electrospun cellulose acetate membrane onto the inner electrode surface. Torvinen et al. [41] have prepared pigment-CNF separator-substrates with ~7% dispersions for the printed graphene and carbon nanotube supercapacitors systems, where the composite typically contained 80% pigment and 20% cellulose nanofibrils (CNF). The prepared composite separator exhibited flexibility, thermal stability, and sufficient strength properties.

It was also reported that the separator membrane of the supercapacitor was obtained via the simple addition of polyvinyl alcohol and chitosan. Briefly, the membrane was obtained by mixing and stirring the chitosan solution (in 1% acetic acid solvent), polyvinyl alcohol solution (in water solvent and heated at 120 °C), and subsequent solidification for two days. The prepared solid membrane was soaked with1 M H_2SO_4 and used as the separator [42]. Hashim and coworkers [23] prepared a separator for supercapacitor applications from the resultant mixture of hybrid polymer electrolyte PVA (70%) and phosphoric acid (H_3PO_4) (30%) submerged in a solution of polymethyl (methacrylate) and lauroyl chitosan (PLC). Furthermore, for supercapacitor purposes, Raja et al. [19] introduced a separator created from a blended mixture of chitosan and
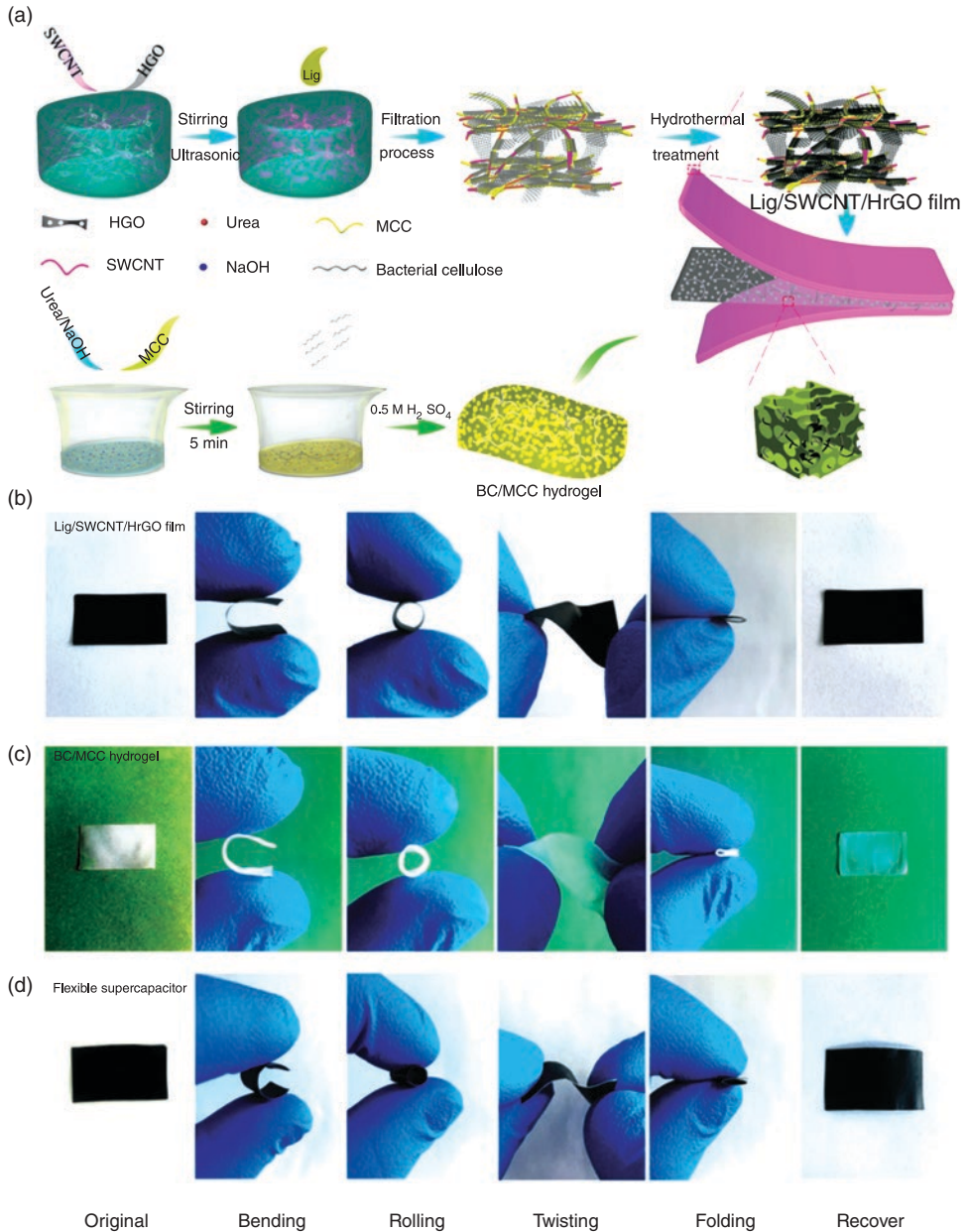
Figure 23.3 (a) Schematic illustrations of the preparation of Lig/SWCNT/HrGO film and self-enhancing BC/MCC hydrogel for wearable supercapacitor. (b) The Lig/SWCNT/HrGO film, (c) BC/MCC self-enhancing hydrogel and (d) flexible supercapacitor under bending, rolling, twisting and double folding situations. *Reproduced with permission* [35]. *Copyright 2020, American Chemical Society.*

chitosan/poly(ethylene glycol)-ran-poly (propylene glycol) [Ch/poly(EG-ran-PG)] in a 1:1 weight ratio. SEM imaging confirmed the exceptional properties of this fabricated membrane, including excellent thermal stability and enhanced tensile strength with a layered structure containing pores of 2–7 μm in diameter.

In recent years, eggshells becoming an important biowaste and are composed of a hierarchical macroporous 3D network and calcified shell with layered assembly. Typically, organic eggshell membranes (ESM) contain collagen types I, V, and X, as well as glycosaminoglycans, sialoprotein, and several other chemical functional groups, such as amino, carboxyl, and hydroxyl groups, which have become of interest for biomass-based supercapacitors. Natural eggshell membranes are made up of three distinct layers, the outer shell membrane, an inner shell membrane, and the final one is the limiting membrane. This limiting membrane surrounds the egg white and the outer shell membrane, which can be easily isolated from eggshells and possesses a high decomposition temperature of >220 °C and strong mechanical strength, making it a promising contender to replace traditional filter-based separators in supercapacitor applications [43–48]. For example, Yu et al. [47] prepared eggshell membrane as a separator from biowaste egg shells. Initially, they washed the eggshells with deionized water (DI) and manually removed the particular limiting and inner shell membranes. Then the remaining eggshell was treated with 1 M HCl acid resulting in a $CaCO_3$ free organic membrane. They characterized the prepared sample using different analytical techniques. SEM imaging confirmed the presence of a macroporous structure with a pore diameter of 1–3 μm. The TGA and tensile stress-strain curve (Figure 23.4) confirmed that the prepared membrane was thermally stable and possessed such mechanical strength as a potential separator that is required for high performing supercapacitor applications.

In addition, low water absorption and minimum degree of swelling of manufactured ESM supported its applicability as a supercapacitor separator. In another report, Das et al. [43] also used the procedure mentioned above with a slight difference to prepare ESM. They initially washed and cleaned the eggshells with cold water to remove white albumin attached to the raw eggshell membrane and yolk. They then used a 10% (v/v.) HCl acid treatment on the washed eggshell and converted it into an organic eggshell membrane by etching away the $CaCO_3$. Then the ESM was rinsed with acetone and 2-propanol then dried and used as a separator. In another study, a binary combination of maleic anhydride (MA) and polyethylene glycol-lignin (PEG-L) in a glove box under a nitrogen atmosphere with varying charge ratios was cast in a mold cavity containing poly(tetrafluoroethylene) (PTFE) film, followed by coating with another sheet of (PTFE) film. In this case a hydraulic hot-press machine was used to melt the mixture in the (PTFE) film mold, while polycondensation occurred at 200 °C for four hours under a pressure of 5 MPa. After cooling, the resultant bipolyester film was scraped from the (PTFE) mold and collected. It was then cleaned with acetone and utilized as separator material after removing the solvent by dry filter paper, whilst complete drying was done by keeping it over P_2O_5 in a vacuum oven at 50 °C under reduced pressure overnight. The resultant film showed a maximum tensile strength of 45.6 MPa and a maximum tensile modulus of 2.4 GPa, respectively, at a charged molar ratio of 6.6/3.4 [48]. A terpolyester film was prepared using a mixture of NaCl, polyethylene glycol (PEG) (500,000), and MA and PEG-L under nitrogen pressure in a glove box. The terpolyester film was obtained by maintaining the above conditions; the use of NaCl was

responsible for the porous structure of terpolyester film. This terpolyester film possessed excessive elongation (94%) of all the films examined and was flexible enough to fold like a paper without breakage. Both the bipolyseter and tripolyester film were used as a separator, where tripolyester film showed enhanced capacitance values [49]. The hot-pressed condition was also used in other research to prepare a quaternary-based flexible separator film. To prepare 2,2,6,6–tetramethylpiperidine–1–oxyl (TEMPO) oxidized cellulose nanofiber (TOCN) lignin-based polyester film (LPF) (TOCN-LPF), a quaternary mixture of polyethylene glycol-lignin (PEG-L), polyethylene glycol with a molar mass of 500 kDa (PEG500k), maleic anhydride (MA), and TOCN was blended and hot pressed under 5 MPa at 200 °C for four hours. Finally, after hot pressing under the specified conditions, a NaCl combination with TOCN-LPF generated a porous TOCN-LPF film. The prepared film

(a)

(b)
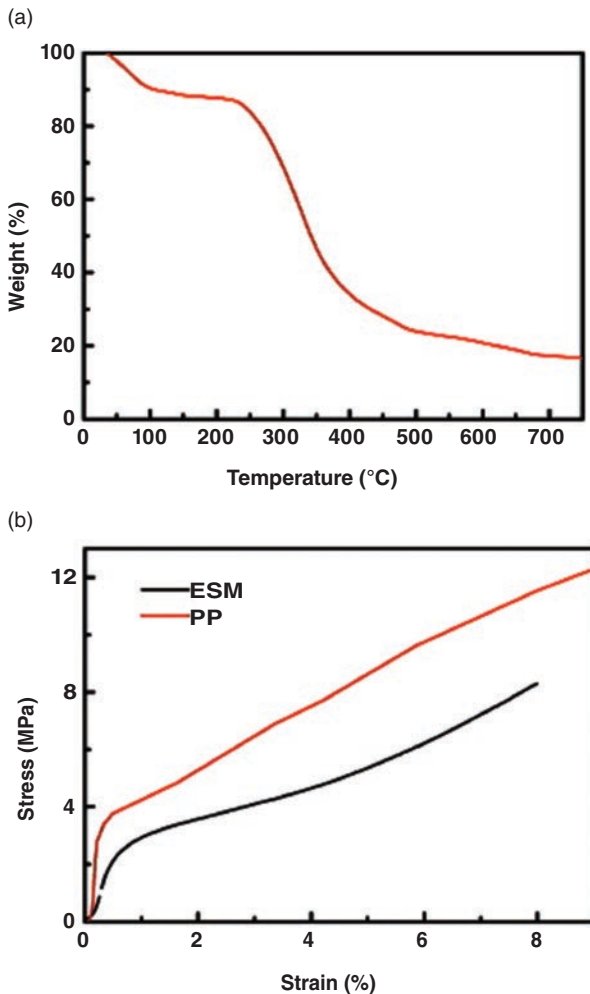
Figure 23.4 (A) TGA curve of the ESM and (B) tensile stress-strain curves of the ESM and PP. *Reproduced with permission* [47]. *Copyright 2012, Elsevier.*

exhibited excellent tensile strength, higher thermal stability, higher viscoelastic moduli, and the highest strain energy density for 1%-TOCN-LPF [50]. Similarly, various separator films were also prepared using sources of raw biomass such as soybean leaf [38], orange peel [51], kelp [52], rice straw [24], wood pulp [53], silk fiber [32], and fish swim bladder [54]. Sun et al. [51] used orange peel to assemble a supercapacitor. Orange peel inherently contains a natural porous channel structure with a porosity of 74.6%, which is undoubtedly high enough to allow the electrolytic ions to pass easily. This porous structure added an extra benefit to the separator (Figure 23.5) [51].

Islam et al. [24] used rice straw as a biomass source to prepare cellulose nanofibrils (CNF) membranes. The step-by-step synthesis method of this process involved initially preparing bleached pulp from dried rice straw by alkali treatment, washing and acid treatment. Then CNF was obtained by TEMPO oxidation of dried, bleached pulp (microcellulose). Finally, the CNF membrane was obtained by casting the CNF solution into a mold of 12 cm × 12 cm, followed by drying in the oven at 45 °C for 12 hours and maintaining a continuous air flow. Different CNF membrane thicknesses were obtained by varying the concentration of poured CNF solution. FTIR and XRD analysis indicated the formation of the CNF membrane from the TEMPO oxidation method. The higher thermal stability of prepared CNF was obtained from TG and DTG analysis.

The TEM picture clearly reveals a well-distributed CNF with a consistent dimension of roughly 10 nm in width. This indicates that to generate a more uniform CNF, TEMPO-mediated oxidation is a suitable approach for defibrillating and separating the
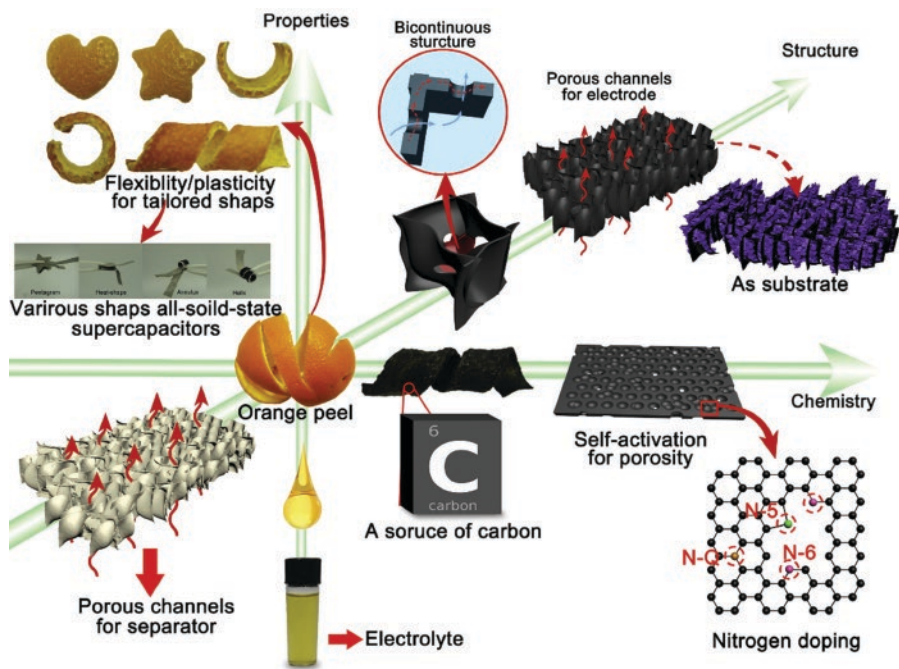
Figure 23.5 Schematic illustration of utilization of orange peel for fabricating supercapacitors. *Reproduced with permission* [51]. *Copyright 2018, Elsevier.*

micro-sized cellulose. In another report, Tan and his colleagues [32] created silk nanofibrils (SNFs) directly by liquid-exfoliating genuine silk strands. They first degummed silk threads from Mori cocoons by boiling them in a 0.5 wt.% Na_2CO_3 solution for 30 minutes. The protein denaturant deep eutectic solvent (PD-DES)-exfoliated silk nanofibers were then made by combining PD-DES with degummed *Bombyx mori* silk fibres. The high-yield SNFs were prepared by sonicating the silk/water combination. The sonication was conducted for four hours at 40 kHz frequency in a KQ- 400DE ultrasonic bath (400 W) and to keep the bath temperature at room temperature during sonication, a water-cooling coil and an ice bath were adjusted and followed by centrifugation. Finally, dispersed SNFs were vacuum filtered using nylon filtration membranes having a pore size of 0.2 μm and diameter of 5.0 cm to yield SNF membranes for the supercapacitor separator. SNF membranes were made up of tightly packed nanofibrils. Again the fibrous and linked porous structure with pores ranging from 100 to 200 nanometers was confirmed by SEM image. Furthermore, nano-fibrillated cellulose (NFC) and cellulose nanocrystal (CNC) are employed in the supercapacitor as a solution-processed separator layer [55].

23.3 Application of Biomass-based Separator in Supercapacitors

As a part of supercapacitor devices, separator film is used to prevent short circuits and pass ions from one side to another. A literature survey found that separator film prepared from biomass exhibited excellent super capacitive performance. It also found that cellulose film and its derivative from biomass are primarily prepared and used as separators. In these circumstances, Xu et al. [36] proposed porous cellulose separators for supercapacitor application, which also has special properties like transparency and is renewable. This was prepared via the phase-inversion method with 1-Allyl-3-methylimidazolium chloride as a solvent. The supercapacitor constructed with the prepared separator film exhibited excellent capacitive behaviour. They optimize cellulose concentration during separator preparation via super capacitive performance. It was observed that the cellulose concentration of 7 wt.% exhibited higher charge-discharge efficiency of 98.58% at 3 A g^{-1}, lower equivalent series resistance of 0.5 Ω and areal capacitance of 1.15 F cm^{-2} at 5 mV s^{-1}. In another research, Lv and coworkers [56] prepared a flexible integral separator for a supercapacitor device based on bacterial cellulose (BC). Conductive polyaniline (PANI) was deposited on BC by peeling off one side of multi-layered PANI/BC and filtering KOH-activated pyrolysis PANI/BC (KPBC). The digital structure is shown in Figure 23.6. The bacterial cellulose was employed as the integrated electrode-separator matrix to decrease the inner resistance (2.48 solution resistance), and increase cycling capabilities (remaining 100% through 2500 charge/discharge cycles), which can be attributed to having a linked network structure. Figure 23.6e-h shows the entire device's construction and flexibility.

The areal-specific capacitance (C_{sa}), volumetric capacitance and mass-specific capacitance were found as 43 mF cm^{-2}, 28.3 F cm^{-3}, (C_{sp}) and 54.4 F, respectively at the current density of 0.1 A g^{-1}. The tensile strength of the film supercapacitor was also proven to be good. Furthermore, lighter, and thinner supercapacitors are readily available, and
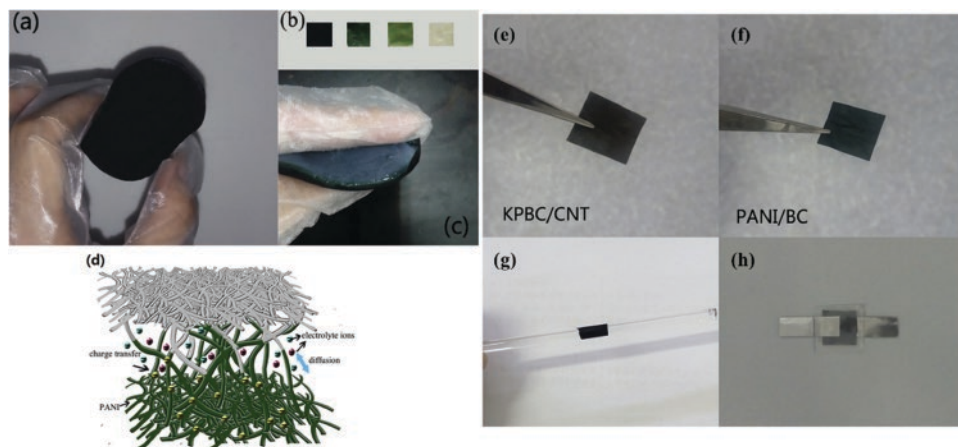
Figure 23.6 Digital pictures of (a) dried PANI/BC//BC film, (b) different peeled layers from one side of PANI/BC film, (c) wet PANI/BC//BC film. (d) Schematic of ions diffusion in the PANI/BC//BC film. (e) one side of KPBC/CNT, (f) the other side of PANI/BC, (g) the flexible PANI/BC//KPBC/CNT film, (h) the all-solid-state flexible supercapacitor made by PANI/BC/KPBC/CNT film. *Reproduced with permission* [56]. *Copyright 2017, Elsevier.*

supercapacitor production is straightforward, low-cost, and convenient. Moreover, to fabricate an asymmetric supercapacitor the eggshell membrane (ESM) was also used as a separator material. The AC-300//n-ESM//MnO$_2$/AC-KOH asymmetric supercapacitor was cycled reversibly in a voltage region of 0–1.5 V in 1.0 M Na$_2$SO$_4$ electrolyte, which showed an energy density of 14 Wh kg^{-1} and an exceptional power density of 150 W kg^{-1}. In 1.0 M Na$_2$SO$_4$, the supercapacitor also exhibited a high specific capacitance of 478.5 F g^{-1}, and the natural ESM-based bio separator has an excellent ion conductivity and cycle life [45]. In another study, a supercapacitor was built employing ESM as a separator, carbon nanotubes (CNT) ink coated ESM as electrodes, and KOH as an electrolyte. At a phase angle of -45°, the developed ESM-based capacitor displayed a frequency response as rapid as 4500 Hz. The high-frequency capacitor maintained an approximately rectangular form in the cyclic voltammogram even at the scan rate of 1 kV s^{-1} and had outstanding cycling stability of 98.6% after 200,000 cycles [43]. Wang and his colleagues [51] utilized biomass resources in supercapacitor applications to maximize environmental and economic benefits. Their study used orange peel (mesocarp) as a separator, while orange peel juice with PVA as an electrolyte and orange peel-derived monolithic porous carbon as electrode material. The constructed supercapacitor from easily available orange peel resources showed a high areal capacitance of 3987 mF cm^{-2}. In another study, Islam and coworkers [24] prepared a cellulose nanofibril separator from rice straw biowaste and constructed supercapacitor devices. By optimizing the thickness of the prepared cellulose nanofibrils separator during characterization, they found that a thickness value of 30 μm had a higher percentage of porosity with a uniform pore distribution and the highest percentage of mesopore and higher electrolyte uptake ability. The separator film of 30 μm thickness exhibited the highest capacitance value of 150.7 F g^{-1} with a high energy density of 30.2 Wh kg^{-1} and power density of 240.0 W kg^{-1} at a current density of 0.1 A g^{-1} in a 1 M Na$_2$SO$_4$ electrolyte solution.

Furthermore, the biomass-derived separator-based supercapacitor cell showed excellent capacitance retention and coulombic efficiency (100%) over 5000 cycles.

23.4   Conclusions

Supercapacitors play an essential role in energy storage/conversion application because of their simple principle, pulse power supply, enhanced cyclic stability, and high dynamic of charge propagation. Electrode materials, electrolytes, and separators are essential parts of supercapacitor design. Separators properties such as porous structure, electrolyte uptake, chemical and electrical stability, thickness, flexibility, ionic conductivity, and thermal stability, play a crucial role in supercapacitor performance. A separator film from biomass sources is gaining tremendous attention for supercapacitor devices and can be a potential candidate for commercialization. This chapter provides a glimpse of the preparation of separator membranes from biomass and their application in supercapacitor devices. However, for future research on preparing separator membranes from biomass, we should focus more and more on the properties mentioned above. The thickness of the separator film should be based on its porous architecture (more porosity with a small pore diameter) as lower porosity and bigger pore size have a negative impact on the supercapacitor performance. We also should keep in mind that the separator film should be chemically and electrochemically inert, especially to the electrolyte during the supercapacitor separator film design from biomass.

Flexibility is an essential parameter for portable and wearable electronic devices; hence this should also be kept in mind during separator film and corresponding supercapacitor device fabrication. Also, facile electrolyte movement and comparable ionic conductivity are crucial properties of an ideal separator film. Hence, the separator film prepared from the biomass should possess a higher electrolyte uptake property and highly ionic conductivity. Most of the research focuses on cellulose-based separator membranes, and the future direction of protein, starch, chitosan, and lignin-derived separator can be focused extensively. The other biomass sources, such as trees, plants, fungi, algae, and other biowaste containing abundant cellulose, protein, and starch, should be included in bringing future research into preparing separator films. There is also a lot of potential for future research into the extraction process of biomass-based chemical components such as cellulose, lignin, and chitosan, which are converted into separator film. Finally, an environmentally benign, cost-effective ideal separator film with excellent capacitive behaviour is a prerequisite for future research on biomass-based separator film and its application as supercapacitor devices.

Acknowledgements

References

1 M. Zhou, H. Zhang, Y. Qiao, C. M. Li, Z. Lu, *Cellulose* **2018**, *25*, 3459–3469.

2 Y. Bai, W. Zhao, S. Bi, S. Liu, W. Huang, Q. Zhao, *J. Energy Storage* **2021**, *42*, 103058.

3 S. Ahankari, D. Lasrado, R. Subramaniam, *Mater. Adv.* **2022**, *3*, 1472–1496.

4 Q. Huang, Y. Yang, R. Chen, X. Wang, *EcoMat* **2021**, *3*, e12076.

5 G. Ma, M. Dong, K. Sun, E. Feng, H. Peng, Z. Lei, *J. Mater. Chem. A* **2015**, *3*, 4035–4041.

6 C. Y. Bon, L. Mohammed, S. Kim, M. Manasi, P. Isheunesu, K. S. Lee, J. M. Ko, *J. Ind. Eng. Chem.* **2018**, *68*, 173–179.

7 M. A. Aziz, S. S. Shah, S. M. A. Nayem, M. N. Shaikh, A. S. Hakeem, I. A. Bakare, *J. Energy Storage* **2022**, *50*, 104278.

8 M. Sharma, A. Gaur, *J. Energy Storage* **2021**, *38*, 102500.

9 Y. Z. Zhang, Y. Wang, T. Cheng, W. Y. Lai, H. Pang, W. Huang, *Chem. Soc. Rev.* **2015**, *44*, 5181–5199.

10 X. Liu, C. Men, X. Zhang, Q. Li, *Small* **2016**, *12*, 4973–4979.

11 S. Islam, M. M. Mia, S. S. Shah, S. Naher, M. N. Sheikh, M. A. Aziz, A. J. S. Ahammad. *Chem. Rec.* **2022**, *22*, e202200013.

12 S. S. Shah, H. T. Das, H. R. Barai, M. A. Aziz, *Polymers (Basel)* **2022**, *14(2)*, 270.

13 C. K. Roy, S. S. Shah, A. H. Reaz, S. Sultana, A. N. Chowdhury, S. H. Firoz, M. H. Zahir, M. A. Ahmed Qasem, M. A. Aziz, *Chem. – An Asian J.* **2021**, *16*, 296–308.

14 R. Arthi, V. Jaikumar, P. Muralidharan, *Energy Sources, Part A Recover. Util. Environ. Eff* **2019**, *latest article*, doi:10.1080/15567036.2019.1649746.

15 T. Islam, M. M. Hasan, S. S. Shah, M. R. Karim, F. S. Al-Mubaddel, M. H. Zahir, M. A. Dar, M. D. Hossain, M. A. Aziz, A. J. S. Ahammad, *J. Energy Storage* **2020**, *32*, 101908.

16 S. S. Shah, S. M. A. Nayem, N. Sultana, A. J. S. Ahammad, M. A. Aziz, *ChemSusChem* **2022**, *15*, e202101282.

17 J. P. Meng, Y. Gong, Q. Lin, M. M. Zhang, P. Zhang, H. F. Shi, J. H. Lin, *Dalt. Trans.* **2015**, *44*, 5407–5416.

18 D. Zhao, C. Chen, Q. Zhang, W. Chen, S. Liu, Q. Wang, Y. Liu, J. Li, H. Yu, *Adv. Energy Mater.* **2017**, *7*, 1700739.

19 M. Raja, B. Sadhasivam, R. Janraj Naik, R. Dhamodharan, K. Ramanujam, *Sustain. Energy Fuels* **2019**, *3*, 760–773.

20 T. He, R. Jia, X. Lang, X. Wu, Y. Wang, *J. Electrochem. Soc.* **2017**, *164*, E379–E384.

21 Y. M. Shulga, S. A. Baskakov, V. A. Smirnov, N. Y. Shulga, K. G. Belay, G. L. Gutsev, *J. Power Sources* **2014**, *245*, 33–36.

22 B. Szubzda, A. Szmaja, M. Ozimek, S. Mazurkiewicz, *Appl. Phys. A Mater. Sci. Process.* **2014**, *117*, 1801–1809.

23 M. A. Hashim, L. Sa'adu, M. Bin Baharuddin, K. A. Dasuki, *J. Mater. Sci. Res.* **2013**, *3*, 25–29.

24 M. A. Islam, H. L. Ong, A. R. Villagracia, K. A. Khairul, A. B. Ganganboina, R. A. Doong, *Ind. Crops Prod.* **2021**, *170*, 113694.

25 P. Tammela, H. Olsson, M. Strømme, L. Nyholm, *J. Power Sources* **2014**, *272*, 468–475.

26 L. S. Godse, V. N. Karkaria, M. J. Bhalerao, P. B. Karandikar, N. R. Kulkarni, *Energy Storage* **2021**, *3*, e204.

27 S. M. A. Nayem, N. Sultana, T. Islam, M. M. Hasan, A. Awal, S. C. Roy, M. A. Aziz, A. J. S. Ahammad, **2021**, *2*, e2100046.

28 S. M. A. Nayem, N. Sultana, M. A. Haque, B. Miah, M. M. Hasan, T. Islam, M. M. Hasan, A. Awal, J. Uddin, M. A. Aziz, A. J. S. Ahammad, *Molecules* **2020**, *25(20)*, 4773.

29 S. S. Shah, M. N. Shaikh, M. Y. Khan, M. A. Alfasane, M. M. Rahman, M. A. Aziz, *Chem. Rec.* **2021**, *21*, 1631–1665.

30 S. S. Shah, M. A. Aziz, *Bangladesh J. Plant Taxon.* **2020**, *27*, 467–478.

31 S. M. A. Nayem, S. S. Shah, N. Sultana, M. A. Aziz, A. J. S. Ahammad, *Chem. Rec.* **2021**, *21*, 1039–1072.

32 X. Tan, W. Zhao, T. Mu, *Green Chem.* **2018**, *20*, 3625–3633.

33 S. Yong, N. Hiller, K. Yang, S. Beeby, *Proceedings* **2019**, *32(1)*, 15.

34 G. Teng, S. Lin, D. Xu, Y. Heng, D. Hu, *J. Mater. Sci. Mater. Electron.* **2020**, *31*, 7916–7926.

35 Z. Peng, W. Zhong, *ACS Sustain. Chem. Eng.* **2020**, *8*, 7879–7891.

36 D. Xu, G. Teng, Y. Heng, Z. Chen, D. Hu, *Mater. Chem. Phys.* **2020**, *249*, 122979.

37 Y. Ji, N. Liang, J. Xu, D. Zuo, D. Chen, H. Zhang, *Cellulose* **2019**, *26*, 1055–1065.

38 Q. Yao, H. Wang, C. Wang, C. Jin, Q. Sun, *ACS Sustain. Chem. Eng.* **2018**, *6*, 4695–4704.

39 N. Lima, A. C. Baptista, B. M. M. Faustino, S. Taborda, A. Marques, I. Ferreira, *Sci. Rep.* **2020**, *10*, 7703.

40 L. Jin, K. Wei, Y. Xia, B. Liu, K. Zhang, H. Gao, X. Chu, M. Ye, L. He, P. Lin, *Mater. Today Energy* **2019**, *14*, 100348.

41 K. Torvinen, S. Lehtimäki, J. T. Keränen, J. Sievänen, J. Vartiainen, E. Hellén, D. Lupo, S. Tuukkanen, *Electron. Mater. Lett.* **2015**, *11*, 1040–1047.

42 A. Maddu, R. A. Nugroho, E. Rustami, S. Arjo, M. Hidayat, *J. Phys. Conf. Ser.* **2019**, *1171*, 012043.

43 S. Das, M. Manuraj, R. B. Rakhi, A. Ajayaghosh, *J. Energy Storage* **2022**, *45*, 103799.

44 D. Dahlan, N. Sartika, E. L. Astuti, N. E. Taer, *Mater. Sci. Forum* **2015**, *827*, 151–155.

45 P. Yang, J. Xie, C. Zhong, *ACS Appl. Energy Mater.* **2018**, *1*, 616–622.

46 N. S. M. Nor, M. Deraman, R. Omar, E. Taer, A. R. Farma, N. H. Basri, B. N. M. Dolah, *AIP Conf. Proc.* **2014**, *1586*, 68–73.

47 H. Yu, Q. Tang, J. Wu, Y. Lin, L. Fan, M. Huang, J. Lin, Y. Li, F. Yu, *J. Power Sources* **2012**, *206*, 463–468.

48 E. Taer, M. A. Sugianto, S. R. Taslim, I. D. Dahlan, M. Deraman, *Adv. Mater. Res.* **2014**, *896*, 66–69.

49 K. Koda, S. Taira, A. Kubota, T. Isozaki, X. You, Y. Uraki, K. Sugimura, Y. Nishio, *J. Wood Chem. Technol.* **2019**, *39*, 198–213.

50 S. Taira, M. Kurihara, K. Koda, K. Sugimura, Y. Nishio, Y. Uraki, *Cellulose* **2019**, *26*, 569–580.

51 C. Wang, Y. Xiong, H. Wang, Q. Sun, *J. Colloid Interface Sci.* **2018**, *528*, 349–359.

52 J. Zeng, L. Wei, X. Guo, *J. Mater. Chem. A* **2017**, *5*, 25282–25292.

53 J. Han, H. Wang, Y. Yue, C. Mei, J. Chen, C. Huang, Q. Wu, X. Xu, *Carbon* **2019**, *149*, 1–18.

54 A. Maitra, S. K. Karan, S. Paria, A. K. Das, R. Bera, L. Halder, S. K. Si, A. Bera, B. B. Khatua, *Nano Energy* **2017**, *40*, 633–645.

55 S. Tuukkanen, S. Lehtimäki, F. Jahangir, A. P. Eskelinen, D. Lupo, S. Franssila, *ESTC 2014-5th Electron. Syst. Technol. Conf.* **2014**, doi: 10.1109/ESTC.2014.6962740.

56 X. Lv, G. Li, D. Li, F. Huang, W. Liu, Q. Wei, *J. Phys. Chem. Solids* **2017**, *110*, 202–210.

24

Binding Agents and Packaging Materials of Supercapacitors from Biomass

Md. Mehedi Hasan and Md. Rajibul Akanda*

Department of Chemistry, Jagannath University, Dhaka, Bangladesh
* Corresponding author

24.1   Introduction

Supercapacitors (SCs) are capacitors with increased capacity and substantially higher capacitance than conventional capacitors. Its lower voltage limits essentially bridge the chasm between rechargeable and electrolytic capacitors. Compared to electrolytic capacitors, SC's energy storage capacity per unit volume or mass is typically 10 to 100 times more. Additionally, SCs have a significantly faster charge transfer rate than conventional batteries and can withstand more charge-discharge cycles than rechargeable batteries [1].

Various applications, such as uninterruptible power supply, electric vehicles, home and communal energy storage, demanded the commercial development of ecofriendly, biomass-derived, and cost-effective electrical energy storage devices [2–8]. Equivalent series resistance (ESR) is a predominant factor that commonly determines the potentiality of those devices [9, 10], and reduction of ESR of SCs means the output capability of the devices reaches its theoretical limits. Finding the mechanism for lowering ESR of SCs and developing activity is one of the recent focuses of research in this area [10]. The preparation of electrodes with minimum internal electrical resistance is a crucial way to decrease ESR. Careful selection of additives, conductive materials, and carbon sources for the electrode's active materials (AM) can effectively resolve this issue. These substances are needed for pliable electrodes, effective binding materials, and packaging materials.

The performance of SCs is correlated with other key variables, such as the highest specific power, as well as a comparison with other batteries. It has been found that common SCs have a high specific power maximum of about $2\text{--}3 \text{ kW} \text{kg}^{-1}$, whilst batteries have a maximum of about $400 \text{ W} \text{kg}^{-1}$. But a drawback of SC is its lower limit of specific power (about $4\text{--}5 \text{ Wh kg}^{-1}$) compared to batteries (about $35\text{--}40 \text{ Wh} \text{kg}^{-1}$) [11]. Importantly, SCs life cycle (more than ~100000 cycles) is much higher than batteries (~1000 cycles). Moreover, the charging and discharging of SCs can be completed quickly. Therefore, both SCs and batteries are used in electrical power systems.

The overall efficiency and safety of the SCs depend on the components of binding materials. The feature of binding materials can control and the production capability and efficiency using various methods of energy storage devices. The properties of binders, such as porosity, pore size and shape, and zeta potentials, should be evaluated carefully to improve the lifetime of energy storage devices. Nowadays, the safety issue of energy storage devices and supercapacitors has drawn great attention worldwide. In order to improve the safety performance of energy storage devices/supercapacitors, many safety devices and actions have been developed, such as pressure release vents, thermal fuses, positive temperature coefficient (PTC) shutdown separators, and non-flammable electrolytes, etc [12]. Even though these components have greatly improved the safety performance of Li-ion batteries, 100% prevention of thermal runaway of energy storage devices/supercapacitors has still not yet been realized. Especially after end-of-life (EOL), the spent energy storage devices/supercapacitors are in a mixture of different conditions. Their safety devices are frequently defective and cannot prevent fire incidents. Depending on precautions and packaging, these devices can go into thermal runaway during transportation and storage. The further progression of the incident is heavily dependent on the surrounding conditions, especially the thermal insulation materials, which need to be investigated scientifically. Thus finding suitable packaging material that can prevent the thermal runway is significant.

This chapter demonstrates how improvements in the quality and assembly of the binding materials and packaging materials can allow commercial SCs to achieve higher specific power. To do so, this chapter discusses the binding materials and packaging material's role, types, functions, and futures and, importantly, focuses on preparing binding materials and packaging materials from natural sources or biomass to develop SCs.

24.2 Binding Materials/Binders

24.2.1 Principle of Binders

Binding materials sustain a strong link between the electrode and the active material particles within the electrode of energy storage devices. These binding materials are usually inert and play an essential part in developing the energy storage device. The selection of binding materials is correlated with the AM of electrodes. Binders have long been made by mixing with the powdered active electrode material, which performs two roles. First, maintaining the electrode material's structural integrity and second, improving adhesion properties between the active electrode material and current collector. This means that the binder should hold all particulate matter in close proximity without degrading the porosity and without reducing the ionic conductivity on the working electrode surface [13]. The electrode binder percentage usually differs between $5 \sim 20$ wt.%. But in a few cases, a stable electrode requires a higher binder concentration [14, 15]. Traditional binders such as poly(vinylidene fluoride) (PVDF) and polytetrafluoroethylene (PTFE) are usually electrical insulators, therefore using a large amount would undoubtedly lower the electrical conductivity of the electrode, ultimately improving ESR and decreasing the SC performance. Types of novel binders and production methodologies have been researched with the aim of reducing the internal electrical resistance of

SCs. Typical binders are metal nanoparticles, sulfur for nano-carbon (like nanotubes or nanofiber) electrodes [16], a mixture of ionic liquids (acts as a unique plasticizer), and polymer like poly(vinylidene fluoride-hexafluoropropylene) (PVDF-HFP) [17], natural cellulose [18], and conductive polymers and their derivatives [19]. A few of those conducting polymers, such as traditional PVDF and PTFE, can dissolve only in toxic and environmentally dangerous organic solvents. In addition to environmental concerns, it is beneficial for the methods used to result in electrodes that consider water-soluble materials as binders as they allow for easy dispersion [20] and wetting when the electrolyte is an aqueous solution [21]. Researchers have looked into a wide range of binding materials, including polyvinyl alcohol [21], acryl S020 [22], and carboxymethyl cellulose [23], that are used in industrial processes for the fabrication of carbon electrodes, but they are susceptible to bacterial growth [22]. However, sodium carboxymethyl cellulose, lithium carboxymethyl cellulose, and xanthan gum are electrically nonconductive cellulose-based salts. Additionally, the usage of poly (3,4-ethylene dioxythiophene), a costly binder that is electrically conductive, was examined [24]. Also, polyacrylic acid, nafion, polyvinyl pyrrolidone, and conductive polymers like polyaniline and polypyrrole have also been employed as the binder for SC fabrication [25–28]. Literature suggests that the performance of the SCs is considerably affected by the binding material and type of binder used [29, 30]. Summarizing the research articles mentioned above and patent applications, it can be said that high-performance electrodes for SCs that are capable of stable operation, low ESR, and high capacitance are still needed. Also, it is necessary to find cost-effective electrode fabrication techniques as well. Biomass-based binding materials can be a suitable choice for research or investigation because they can improve the performance of SCs and make them environment-friendly.

24.2.2 Importance of Binding Agents in SCs

A literature review has already established that, in contrast to the significant improvement of other components for the SCs, the proper selection of binders and binding agents is crucial in improving the cycle efficiency and electrode mechanical properties [31–33]. To prevent active materials from detaching during electrode operation, binders bind conductive agents and AMs together and cohere with electrode material substrates. The function of the binder should offer sufficient strength during electrode creation and suitable pore diameters. However, cohesive or binding chemicals invariably cover some pores or surface regions of active materials. Therefore, the electrochemical performances of SCs will be directly influenced by the characteristics of binders and their content in the electrodes [34]. Thus, to make SCs ecofriendly and cost-effective, selecting an appropriate binding agent from biomasses is crucial.

24.2.3 Biomass-derived Binding Agents for SCs

An important aspect of selecting a suitable binder is how to hold all particle debris in close vicinity without reducing not only ionic conductivity but also the porosity of the electrode [35]. Here, a brief description of the biomass-derived binding agents recently used is discussed below. From the literature, it was found that biomass-derived binders used are natural polysaccharides (arabic gum (AG) and xanthan gum (XG)) [36], cellulose fiber (kraft

pulp) [37], nanocellulose [38], starch [39], chitosan [40], and PS/GG (potato starch/guar gum) mixture [41]. Other biomass-derived polysaccharides with similar properties should be investigated as binding materials to improve SCs further.

24.2.3.1 Natural Polysaccharides (AG and XG)

Water-soluble biopolymers made from natural polysaccharides are more affordable and environmentally benign than other organic binders. By improving the transportation of electrolyte ions, polysaccharide-based binders can boost the capacity of the electrode. [24] AG and XG are natural biopolymers that consist of polysaccharides. The molecular formula shown in Figure 24.1 indicates the presence of negatively charged hydroxyl and carboxylate groups on these biopolymers. These functionalities are essential components for the binders to produce significant flexibility, better adhesive properties, and significant electrode-electrolyte contact within the electrodes [42].

Figure 24.2a–2d shows the SEM images of hybrid mixture, MoO_3/CNT, and electrodes under different states. The TEM of the MoO_3/CNT hybrid (Figure 24.2a inset) clearly demonstrates the small MoO_3 nanoparticles affixed to the CNTs' exterior surface and inside the tube. MoO_3/CNT/Ni combined with XG and AG binders represents the Mo/C/Ni, Mo/C/NiAG, and Mo/C/Ni/XG, respectively. According to the Mo/C/Ni morphology (Figure 24.2b), the Ni foam's pores on the outside and inside have both been sonochemically coated with a thin layer of MoO_3/CNT hybrid. Natural binders were used to coat the Ni foam with a more MoO_3/CNT hybrid, as seen in Figures 2c and 2d.

The electrochemical behavior of Mo/C/Ni/XG and Mo/C/Ni/AG is shown in Figure 24.3. The CV curve of the Mo/C/Ni electrode is shown in the figure alongside two other electrodes (Mo/C/Ni/AG and Mo/C/Ni/XG) made use of natural polysaccharides as binders within 0.15 to 0.45 V potential range and 5 mV s^{-1} scan rate. It can be seen that the peak areas of the natural polysaccharides modified electrodes (Mo/C/Ni/AG and Mo/C/Ni/XG) are higher than the unmodified electrode (Mo/C/Ni). That means that the addition of natural polysaccharides improves supercapacitive performance in the electrodes. The unmodified electrode has a lower specific capacitance than the modified electrodes. Due
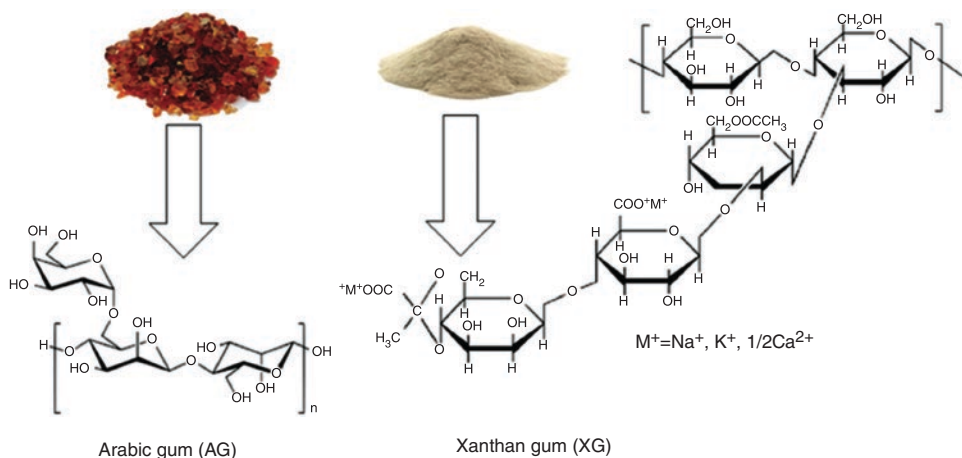
Figure 24.1   The forms and molecular formulas of AG and XG.
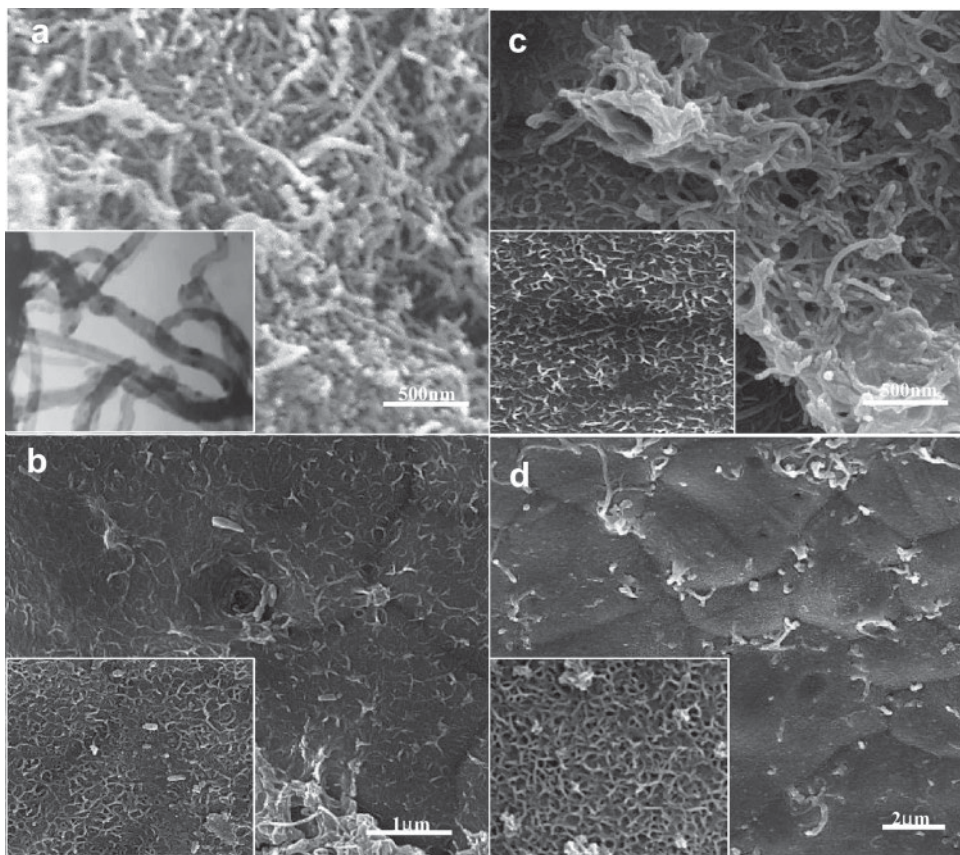
Figure 24.2 SEM images of a) hybrid mixture MoO₃/CNT, b) bare electrode, c) AG, and d) XG electrodes. *Reproduced with permission* [36]. *Copyright 2020, Springer.*
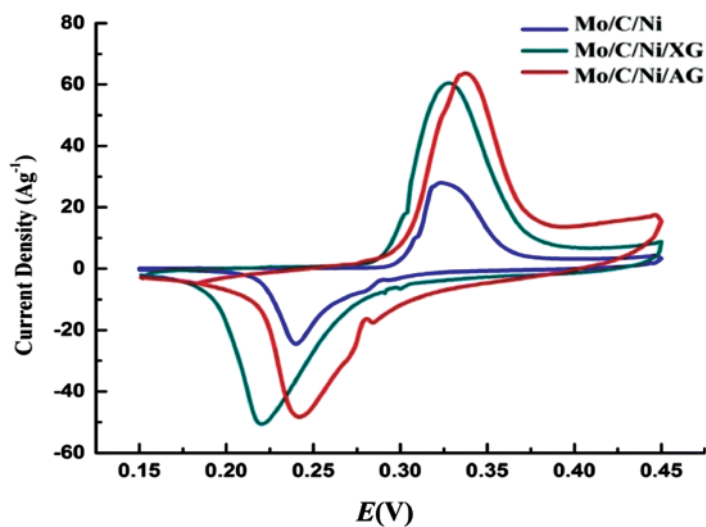
Figure 24.3 Cyclic voltammograms of the three electrodes: unmodified (Mo/C/Ni), and modified (Mo/C/Ni/XG and Mo/C/Ni/AG), respectively, at 5 mV s⁻¹ scan rate. *Reproduced with permission* [36]. Copyright 2020, Springer.

to the strong ionic conductivity of the charged biopolymers the electrode-electrolyte contact is improved, and capacity is increased.

24.2.3.2 Cellulose Fiber (Kraft Pulp)

Cellulose and its derivatives are widely employed in several applications as binding agents and dispersion agents. An environmentally beneficial substitute for oil-based polymer binding agents is cellulose-based binders. The electrical resistance of electrodes made of refined fibers or kraft pulp was the smallest. Surprisingly, the specific capacitances of all electrical double-layer capacitors (EDLCs) were comparable, with the cellulose nanofiber EDLC having a specific capacitance value a little lower [37]. Figure 24.4 shows the molecular structure of kraft pulp. Figure 24.5 shows the current vs. potential curves from the CV observations of the EDLC. The observations of CV

Kraft pulp · Molecular formula
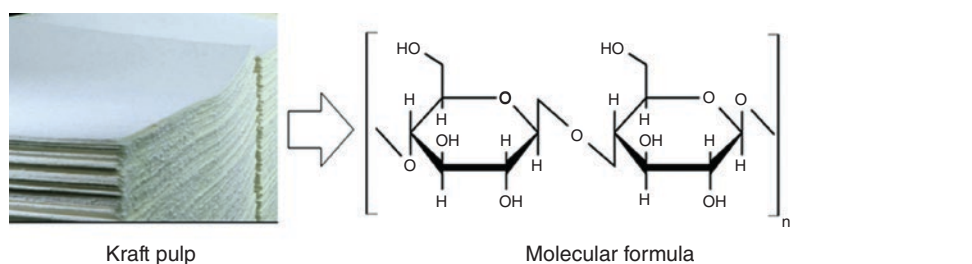
Figure 24.4 The form and molecular formula of kraft pulp, used as cellulose binders.
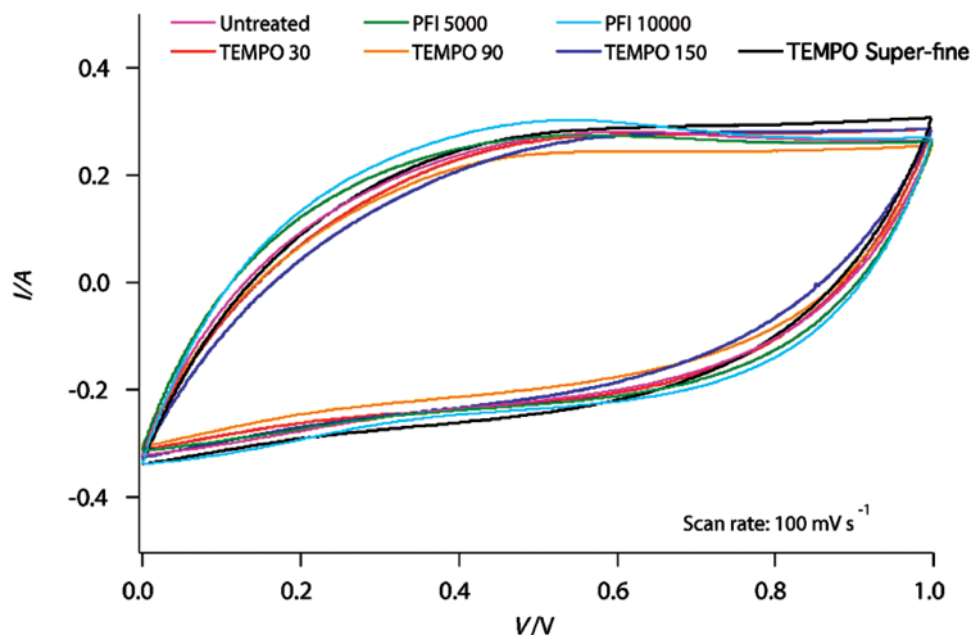
Figure 24.5 CV of electric double-layer capacitors at 100 mVs^{-1} with electrodes made of cellulose from kraft pulp. *Reproduced with permission* [37]. *Reproduced in accordance with the CC BY-NC-ND 4.0 license. Copyright 2018, Andres et al., published by Elsevier.*

behavior confirmed the occurrence along with charging and discharging. The used CNFs from the highest quality of cellulose were predicted to work best as a binder and dispersant. However, given that CNFs show the maximum electrical resistance owing to the production of CNF films on the electrode surface, our findings demonstrate that CNFs are not the optimum material to utilize for electrodes. Thus, these dispersions must be refined and dehydrated directly after their preparation. In conclusion, the use of microfibrillated cellulose (MFC), (2,2,6,6-Tetramethylpiperidin-1-oxyl) TEMP oxidized fiber, including TEMP super fine as an electrode binding material for EDLCs is preferred since it is cost-effective and has significant dispersion stability as well as the best electrical properties [37].

24.2.3.3 Starch

Starch is considered the second most prevalent natural biomaterial: it is ecofriendly (because it is renewable and biodegradable), affordable, and generally accessible [43–45]. As a result, starch has been employed as a binder and an adhesive in various sectors for many years [46]. The molecular formula and functionalities of starch is shown in Figure 24.6 below.

The electrodes with starch binders were repeatedly charged and discharged within 0.0 to 0.25V at a current of 25 Ag^{-1} to determine their long-term stability. As shown in Figure 24.7, the magnitude of capacitance (solid green curve) after 50,000 cycles (capacitance retention of 95% in comparison with the initial value) and coulombic efficiency of 98% indicates that starch may be used as a conductive glue and electrode binder in EDLCs with extended life spans [39].

24.2.3.4 Chitosan

Chitosan is a naturally derived polymer from chitin that is strongly N-deacetylated. Chitosan is a linear polysaccharide that is generated from the exoskeleton of crustaceans, and from fungus, and insect carapace chitin deacetylation. It mainly consists of uniformly distributed -(1–4)-linked D-glucosamine and N-acetyl-D-glucosamine units [47, 48]. The functionalities of the chitosan structure are shown in Figure 24.8. A chitosan binder exhibited higher thermal stability up to 200 °C. Due to its simplicity of manufacture, low cost, high surface area, and flexibility, chitosan is a good choice as a binder material [49]. Because of chitosan's superior matrix ion adsorption, non-toxicity, and high retention capacity, using it as an electrode binder offers certain benefits to batteries, including solid electrochemical performance [50].

Starch   Molecular formula
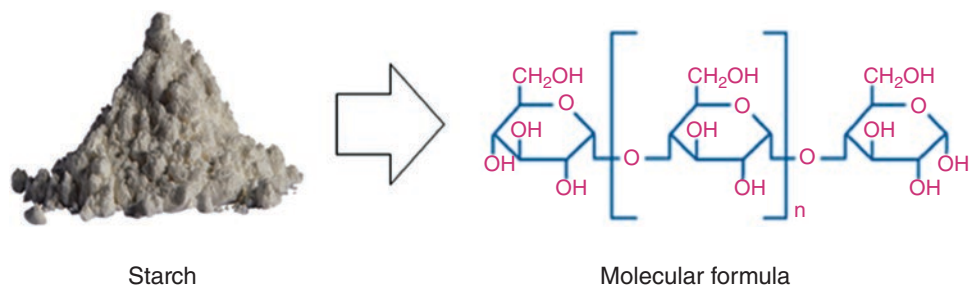
Figure 24.6   The form and molecular formula of starch as binders.
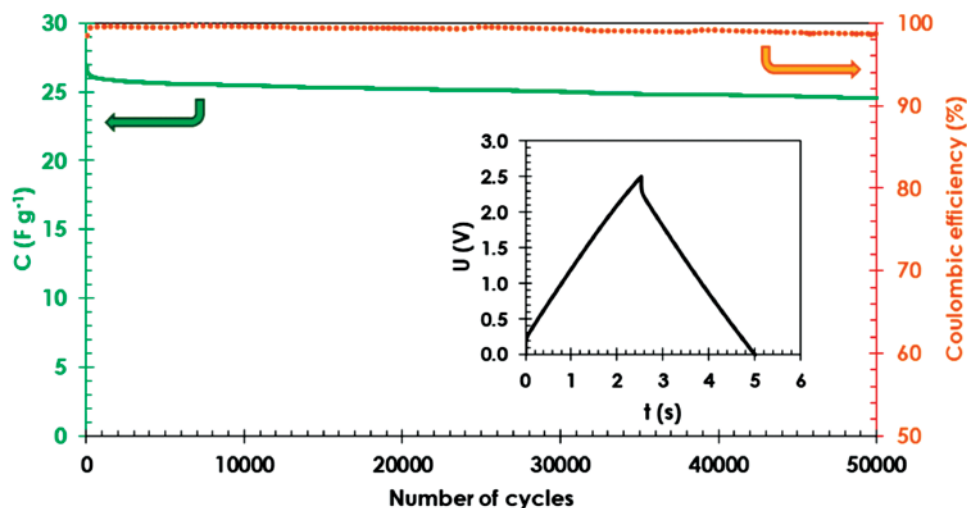
Figure 24.7 Starch-based EDLC cells cyclability within $0.0 \sim 2.5$ V range with a current density of 25 A g^{-1} and 1 mol L^{-1} TEABF$_4$ in an electrolyte of ACN. The solid and dotted lines, are used to illustrate capacitance levels and coulombic efficiency, respectively. The electrode material is made up of 80 weight % activated carbon (YP 80F), 10 weight % carbon black (Super C65), and 10 weight % starch. *Reproduced with permission* [39]. *Reproduced in accordance with the CC-BY-4.0 license. Copyright 2019, P. Jeowski et al., published by MDPI.*
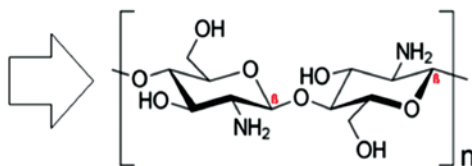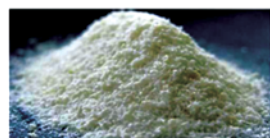
White chitosan   Molecular formula

Figure 24.8 The form and molecular formula of chitosan as binders.

The capacitive value of the graphene-chitosan-based electrodes was investigated at scan speeds from 5 to 100 mV s^{-1}, by observing CVs (Figure 24.9) [40]. All of the graphene electrodes with various weight % of chitosan binder also at a higher scan rate (100 mV s^{-1}) demonstrated their quasi-rectangular CV behavior, a manner typical of carbon-based materials [34]. The CV curve incorporated regions increase with scan rates.

The CV and galvanostatic charge/discharge (GCD) curves were run under various bending situations (0°, 90°, 180°, and restored state) to show the graphene electrode's flexibility and stability with a 10 wt% chitosan binder (Figure 24.10) [40]. The schematic illustrations show how graphene adheres to nickel foam at the bending point. It demonstrates the bond's tensile strength and shows no peeling behavior when being bent (Figures 24.10b and 10c). Figure 10d proved a strong connectivity between graphene and Ni foam by the chitosan binder, due to similar binder morphology at various bending states from the initial condition in terms of cracking or peeling effects. Previous studies have suggested that
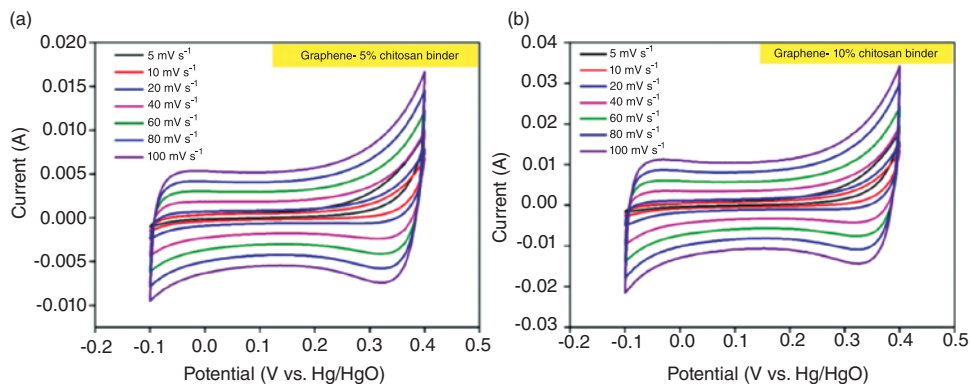
Figure 24.9 CV curves of the graphene-chitosan electrode at various scan rates (a) with 5 wt% and (b) with 10 wt.% chitosan binder proportions. *Reproduced with permission* [40]. *Reproduced under terms of the CC BY-NC-ND 4.0 license. Copyright 2021, Salleh et al., published by Elsevier.*

the hydrophilic (-COOH and -OH) functional groups can be hydronated to polycationic material in acid conditions, producing the connection between graphene sheets through strong bonding [51]. This procedure involved making a slurry of graphene and chitosan in acetic acid. As a result, significant bonding and dispersion were observed between graphene and chitosan, making chitosan a fantastic binder for the graphene electrode. The bending process barely changes the physical characteristics of the samples. The samples' structure can be completely reversed back to its original form. The electrochemical performance is unaffected by the modest differences in the CV curves of 10% electrodes in various bending states (Figure 24.10e). All of the conditions resulted in the same shape of the curves; however, the current varied slightly. The bending operation does not significantly affect the efficiency of the GCD, indicating that the manufactured material has outstanding bending performance and may be a great choice for a wearable device (Figure 24.10f).

24.2.3.5 Potato Starch/ Guar Gum (PS/GG) Mixture

Guar gum (GG) is a natural polysaccharide from guar beans. GG varies from starches through its backbone composed of (1–4)-bonded D-mannopyranose units that carry short side chains as shown in Figure 24.11. Single (1–6)-bonded -D-galactopyranose units make up these side chains (Figure 24.11). GG is utilized in various applications, from food additives to hydraulic fracturing. It is recognized to significantly enhance the viscosity of low concentration solutions in which the solvent is water [52]. The main components of potato starch (PS) granules are the polysaccharides amylose and amylopectin, which are packed closely together. The main linear component is amylose, which makes up 20–30%; nevertheless, some of it is slightly branched.

The most promising mixing ratio for PS/GG is 3:1, denoted as PS75/GG25. The electrochemical properties of the PS75/GG25-based electrodes were investigated and found to be satisfactory when used as the electrode [41]. The top curve in Figure 24.12 depicts the electrochemical signal for a completely empty Al current collector. In this illustrative test, the cyclic voltammograms display an oxidation peak (irreversible) caused by the dissolution of aluminum and subsequent loss with multiple cycling due to passivation events.
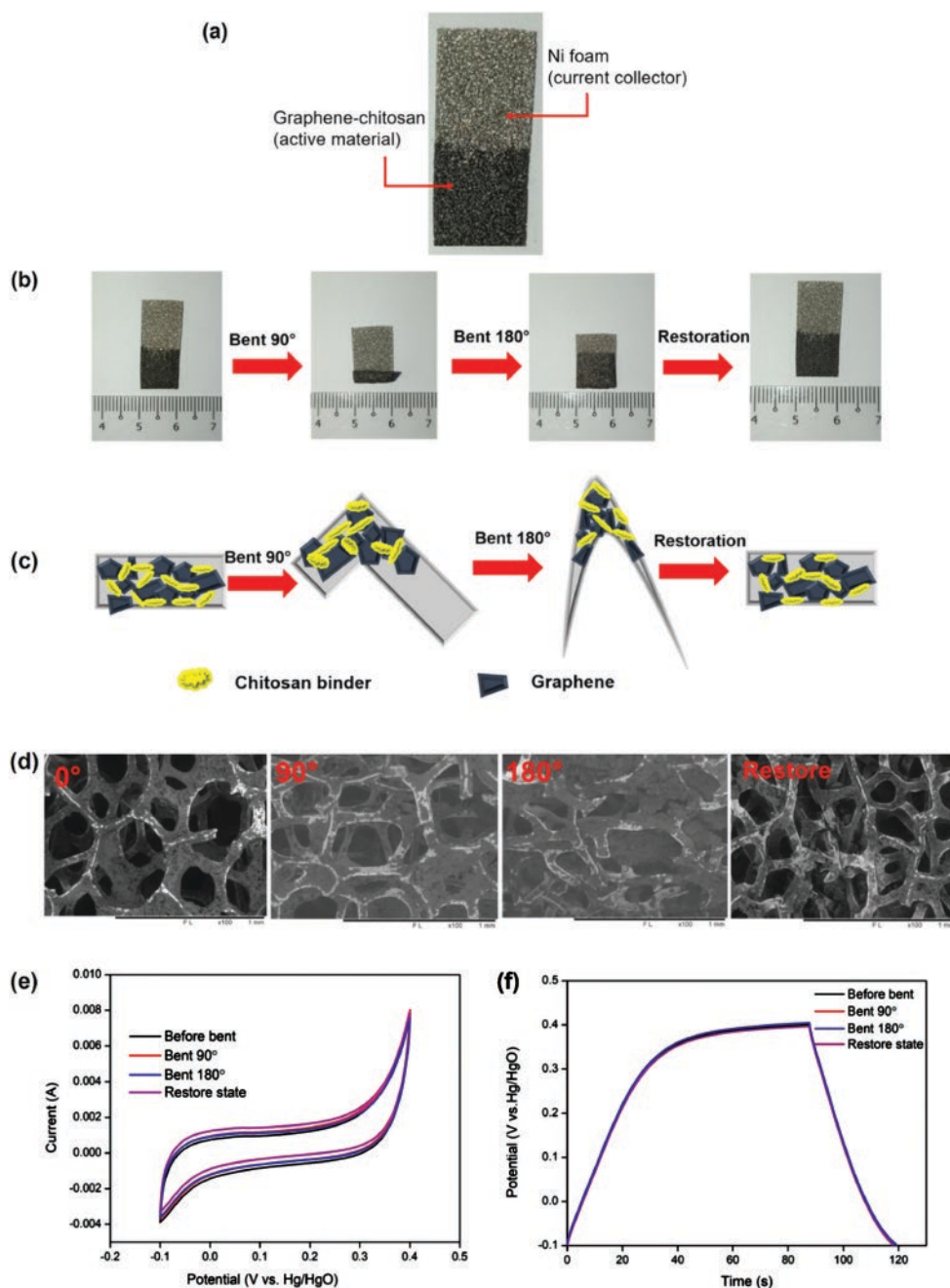
Figure 24.10 An electrode made of (a) graphene and chitosan (10%), (b) the electrode being bent at various angles, (c) a schematic diagram, (d) an SEM image of the electrode, (e) CVs, and (f) GCDs of graphene and chitosan (10%) at various bending states. *Reproduced with permission* [40]. *Reproduced under terms of the CC BY-NC-ND 4.0 license. Copyright 2021, Salleh et al., published by Elsevier.*
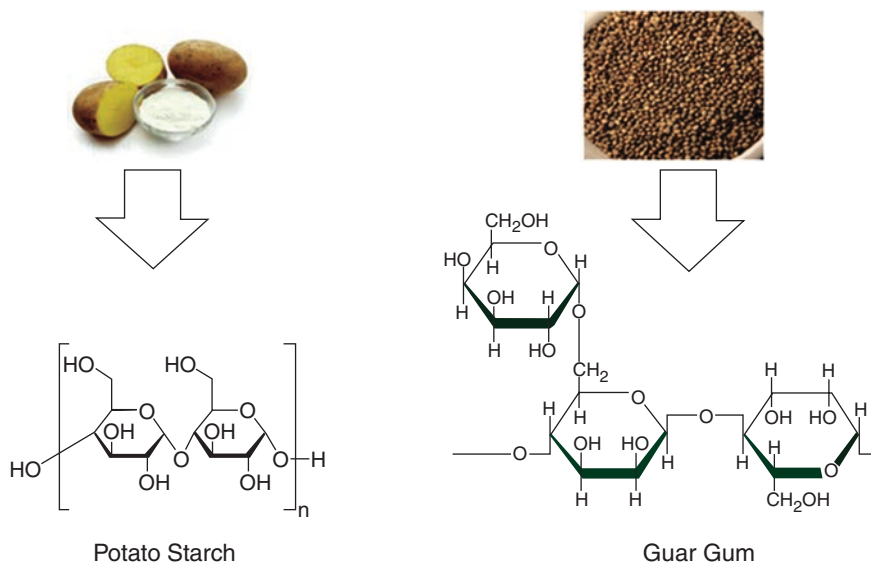
Figure 24.11   The forms and molecular formulas of GG and PS used as binders.

Binder-coated Al electrodes also exhibit the same oxidation peak in the voltammograms, where the onset is founded at potentials much earlier. Reduced current was recorded during multiple cycles, signifying passivation, occuring with binder-coated Al electrodes. At last, the binder was found to be unreactive towards any of the employed electrolytes [41].

Electrochemical impedance spectroscopy (EIS) studies on PS75/GG25-based AC electrodes were carried out to examine the effects of the binder. A number of electrochemical cells were examined using CMC and PS75/GG25 electrodes with active material loadings of $3.5 \, mg \, cm^{-2}$ (standard loading) and $7.0 \, mg cm^{-2}$ (high loading). The EIS of the prepared electrodes is shown in Figure 24.13. Even though the standard loading system's overall impedance differs from the high loading system, the impedance spectra of the electrodes (Figure 24.13A, 24.13B) may be characterized by the same circuit (see Figure 13C). Interestingly, high-loading-type cells exhibit two distinct semicircles in the same frequency range (see Figure 13D). This suggests that the electrode layer/current collector interface could still be improved, as the EIS results show a minor electrode resistance disadvantage for PS75/GG25 against CMC.

The voltage hold trial is shown in Figure 24.14A. The PS75/GG25 electrodes clearly allow for capacitance retention performance that is on par with CMC. It is correct for the high-loading electrodes that exhibit a somewhat elevated equivalent series resistance. Thus, this type of high-loaded electrode can significantly enhance the active material/current collector ratio without affecting performance. The same kind of coin cells were used to test the cycling performance of the electrodes, but they were subjected to quick, constant current charge/discharge cycles instead. As shown in Figure 24.14B, the findings demonstrate that the rate performance of electrodes based on PS75/GG25 is largely equal to those based on CMC. At very high currents, the capacitance of all cells is only slightly impacted. The cycle data as a whole clearly confirms that PS75/GG25 is the same as CMC, instead permitting a two-fold increase in mass loading.
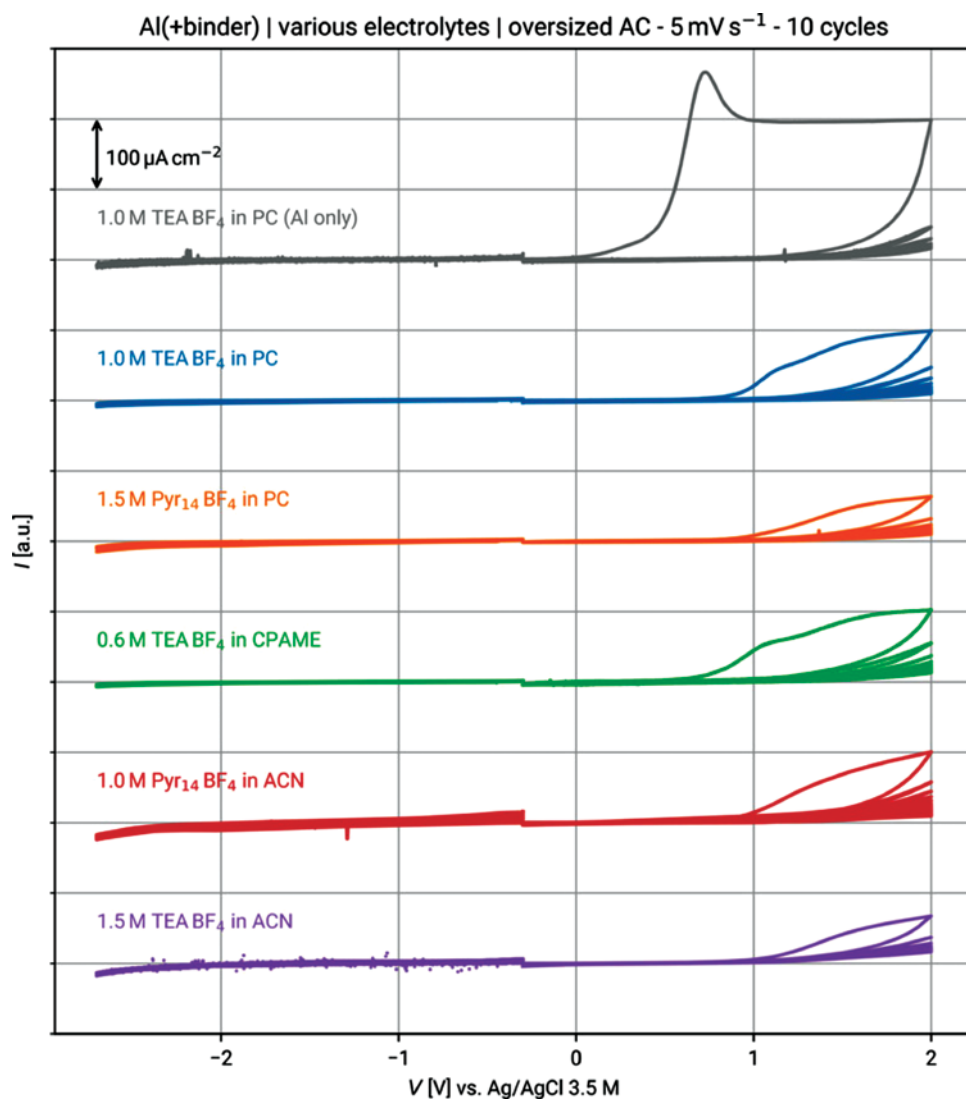
Figure 24.12 CV recorded for the binder in various electrolytes. Voltammograms, recorded at 5 mV s^{-1}, of pristine and binder-coated Al electrodes in various electrolytes. *Reproduced with permission* [41] *Reproduced under the term CC BY 4.0 license. Copyright 2020, Ruschhaupt et al., published by Wiley.*

In conclusion, it was discovered that the best coating rheology could be produced from the 3:1 ratio of PS and GG, allowing for flexible high-mass loading electrodes with high solid contents. The bending tests for the survival of PS75/GG25 were up to 7 mg cm^{-2}, double that of carboxymethyl cellulose (CMC). SEM microscopy showed less crack formation during drying and good dispersion of the conductive additives and the active substance. It was demonstrated that PS and GG are stable at the average drying air temperatures, allowing for quick drying. PS75/GG25 electrodes' rate capabilities were quite comparable to those of CMC-based electrodes. Thus, PS/GG-based binders are a possible replacement for CMC. So it can be said that functional biomass-derived materials can be studied in detail to check their suitability as binding agents of SCs.
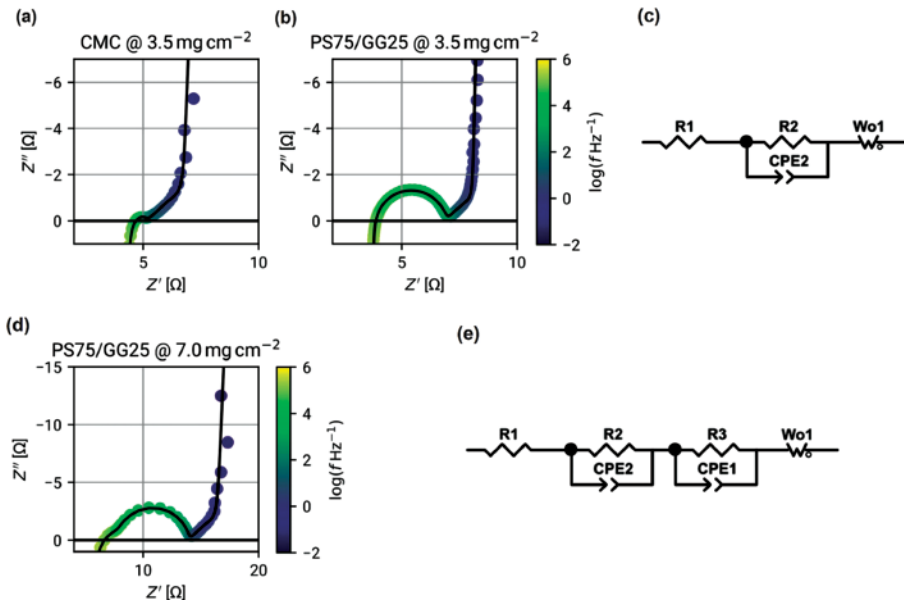
Figure 24.13 EIS spectra of cells using CMC and PS75/GG25-based electrodes in 1 m TEA BF$_4$ in PC, UDC=0 V, UAC=5 mV. (A) The CMC-based electrodes' spectrum with uniform loading. (B) The PS75/GG25-based electrodes' spectrum with uniform loading. Modeling a circuit to fit the spectra in (A) and (B) where the semicircles are connected to the RQ element's model of interfacial resistance processes (R2, CPE2). They have been linked to the contact resistance between the current collector and the carbon atoms. Higher R2 values can be seen in PS75/GG25. (D) Highly loaded PS75/GG25-based electrodes' spectra. (E) A model of an equivalent circuit that fits the spectrum in (D). *Reproduced with permission* [41] *Reproduced under the term CC BY 4.0 license. Copyright 2020, Ruschhaupt et al., published by Wiley.*

24.3 Packaging Materials

24.3.1 Principle and Importance of Packaging Materials in SCs

When building flexible SC devices, the packaging strategy and materials are also crucial considerations because the encapsulation gives the devices mechanical support and shields them from the surroundings. Commercial SCs are produced by compacting the electrodes, separator, and electrolytes before wrapping them in flexible plastic, like polyethylene terephthalate [53], which is a favoured material for conventional packaging. However, there are still a lot of issues that need to be resolved, such as pressure control during compression, ecofriendly packing materials, cost of packaging, and electrolyte leakage (particularly for liquid and gel-state electrolytes) [54]. The pictorial representation of SCs encapsulated by packaging material shown by Wang et al. in 2016 helps to realize the position and function of packaging materials in the SCs [55]. In the next section, we focused on packaging materials from biomass to solve most of the above-mentioned problems.

24.3.2 Biomass-derived Packaging Materials for SCs

Encapsulation of SC devices by biomass-derived materials protects the devices from the outside environment. It can easily decompose and mix with biological systems and soil
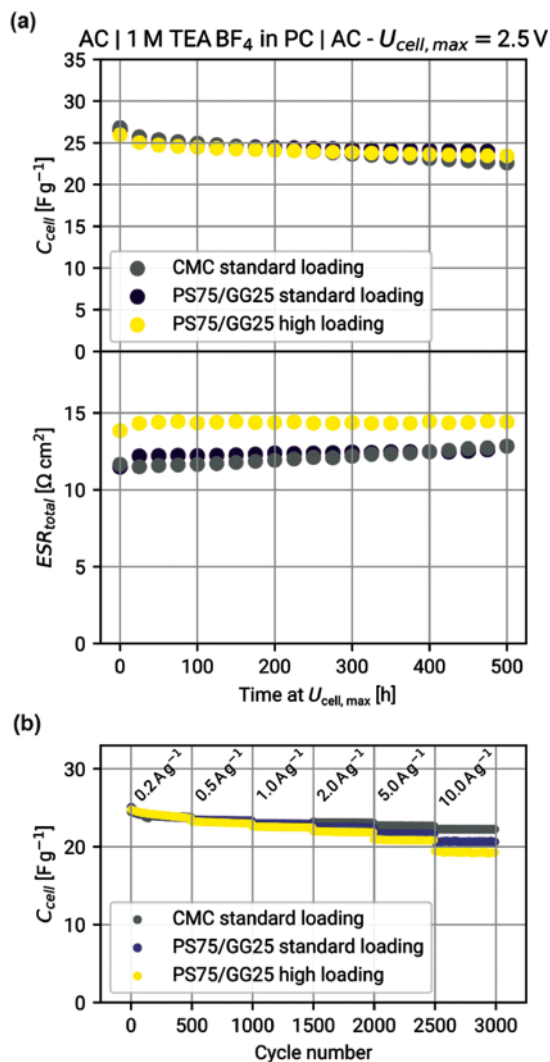
Figure 24.14 Performance of symmetric cells during cycling. (A) As voltage-hold trials progress, capacitance retention and ESR show increasing behavior. At regular mass loading (3.5 mg cm^{-2}), PS75/GG25 electrodes displayed the same capacitance as CMC electrodes, and high mass loaded (7.0 mg cm^{-2}) electrodes exhibited slightly enhanced ESR but the same capacitance. (B) Electrodes rate performance loaded with various binders. *Reproduced with permission* [41]. *Reproduced under the term CC BY 4.0 license. Copyright 2020, Ruschhaupt et al., published by Wiley.*

within a short time after disposing of the SCs. Thus, it is essential to find biomass-derived packaging materials and sources that can be used in the near future. The literature indicates that gelatin from biomass has been mainly used as packaging materials. The gelatin-based film exhibits excellent mechanical and barrier qualities, low production costs, biodegradability, and environmental friendliness [56]. A brief description is given below. Understanding this description could help us find other likely packaging materials.

24.3.2.1 Gelatin

Collagens from animals' bones and skin undergo hydrolysis to produce a gelatin. The extraction processes, animal types, age, and collagen types all significantly impact the physicochemical properties of the gelatin that is generated [57]. Two categories of gelatin can be distinguished based on the pretreatment of the gelatin during the extraction process. Acid-treated pretreatment yields type A gelatin, which has an isoionic point of 6 to 9, and alkali-treated pretreatment yields type B gelatin, which has an isoionic point of 5. Gel tensile and viscosity properties of extracted gelatin are indicators of gelatin quality. The gel strength, commonly referred to as the "bloom" value, indicates how rigid and robust the gelatin is. It is also a reflection of the gelatin's molecular weight, which is typically between 30 and 300 bloom. A higher bloom value indicates greater gelatin strength. The typical collagen sources from which gelatin can be derived are porcine [58], bovine [59], fish [60], poultry [61], and insects [62]. Gelatin sheets were employed as the packing materials in many food processes and medical capsulations [55]. The gelatin was digested (in situ) at room temperature of 25 °C when sheets of it were submerged in a simulated stomach fluid and moved in a horizontal direction [55]. A cross-sectional area of 160 μm x 1090 μm is observed in a gelatin sheet which expands due to the gastric fluid diffusion into the gelatin's polymeric network, shrinks due to the gelatin's digestion, and finally becomes identical to simulated gastric fluid after 2.5 hours. This gelatin sheet is considered to have been dissolved since it has no mechanical strength to function as a package. Due to the limitation in the horizontal plane, the maximum strain is only 17% during this phase (swelling and shrinking) in the horizontal direction. In comparison, in the thickness direction, ε thickness is found to be 261%. This quasi-1D digestion process can be explained by a theoretical study considering the chemical reaction, mass diffusion, mechanical deformation, etc. Moreover, the above study showed good agreement between the experimental result and simulation results for the time evolutions of the strains (ε horizontal and ε thickness). Numerous earlier experiments conducted by various teams have demonstrated that crosslinking treatment extends the shelf life of gelatin in humid, acidic, and hot settings [63–65].

A new sustainable wood fiber-based packaging material called Paptic Tringa has been introduced by the recently finished sustainable innovations business Paptic. The manufacturer claims that it can be classified as new material as it does not contain paper, nonwoven, or plastic components. Paptic tringa is expecting to convince the consumers, brand owners, and merchants that it is the "best choice for sustainable and reusable packaging solutions". Paptic claims that Paptic Tringa has a distinctive appearance and feel and supports all common printing and converting procedures. The usage of single-use plastic packaging is ultimately reduced throughout the value chain thanks to the sustainable packaging material's sturdy, resilient, and flexible characteristics.

Natural fibers like cotton and jute fiber can be considered as packaging materials. But one of the problems of cotton fiber is that its production is not environmentally friendly, consumes a huge amount of water, and emits greenhouse gases. Again, jute fiber is commonly rougher, uncomfortable, and has much lowering tensile strength than cotton fiber. Importantly natural fibers may show minimal conductivity. So additional research needs to be done to make it fully non-conducting, cost-effective, and improve its tensile strength. Besides this, non-conducting biomass-derived materials can be studied further to find other packaging materials.

24.4 Conclusions

This chapter clearly establishes the importance and suitability of biomass-derived binding agents and packaging materials for developing environment-friendly SCs. The biodegradability, porosity, and cost-effectiveness make biomass-derived functional materials promising binding agents, and the additional non-conducting properties of biomass materials good as packaging materials for SCs. Materials like natural polysaccharides, cellulose fiber, nanocellulose, starch, chitosan, and potato starch/ guar gum mixture have been successfully utilized as binders. Biomass-derived gelatin having non-conducting properties is used successfully as a packaging material. Still, lots of biomaterials are available in nature, having the required properties to allow them to be used as binding materials. A lot more research is needed to evaluate their suitability in SCs. Many insulating biomass-derived materials can be studied further to find more packaging materials. Jute fiber, cotton fiber, mucilage, wool, linen, pectin, and natural rubber can be studied in the future to check their suitability as binding and packaging materials. The future is highly promising for further improvements in the SC sector.

Acknowledgments

References

1 F. Häggström, J. Delsing, *Energy Harvest. Syst.* **2018**, *5*(3–4), 43–51.

2 S. Lu, K. A. Corzine, M. Ferdowsi, *IEEE Trans. Veh. Technol.* **2007**, *56*(4), 1516–1523.

3 M. Mastragostino, F. Soavi, *J. Power Sources* **2007**, *174*(1), 89–93.

4 J. D. Yanq, K. Y. Ho, K. S. Wook, L. S. Hyun, *J. Power Sources* **2003**, *114*(2), 366–373.

5 M. B. Camara, H. Gualous, F. Gustin, A. Berthon, *Proc CESIIEEE 5th International Conference on Power Electronics and Motion Control* **2006**, I–5.

6 R. A. Dougal, S. Y. Liu, R. E. White, *IEEE Trans Compon Packaging* **2002**, *25*(3), 120–131.

7 T. Kiniyo, T. Senjyu, T. Urasaki, H. Fujita, *IEEE Trans. Energy Convers.* **2006**, *21*(3), 221–227.

8 P. Srithoffi, M. Aten, R. Parashar, *Proc. 3rd lET International Conference on Power Electronics. Machines and Drives* **2006**, 354–360.

9 R. Kötz, M. Carlen, *Electrochim. Acta* **2000**, *45*, 2483–2498.

10 S. S. Shah, M. A. Aziz, E. Cevik, M. Ali, S. T. Gunday, A. Bozkurt, Z. H. Yamani, *J. Energy Storage* **2022**, *56*, 105944.

11 S. S. Shah, S. M. A. Nayem, N. Sultana, A. J. S. Ahammad, M. A. Aziz, *ChemSusChem* **2022**, *15*, e202101282.

12 P. G. Balakrishnan, R. Ramesh, T. Prem Kumar, *J. Power Sources* **2006**, *155*, 401–414.

13 S. S. Shah, E. Cevik, M. A. Aziz, T. F. Qahtan, A. Bozkurt, Z. H. Yamani, *Synth. Met.* **2021**, *277*, 116765.

14 P. Mitchell, X. Xi, L. Zhong, B. Zou, *US Patent 7851238*, **2010**.

15 L. T. Lam, N. P. Haigh, C. G. Phyland, D. A. J. Rand, *US Patent 8232006*, **2012**.

16 Y. N. Kim, *US Patent 8278010*, **2012**.

17 W. Lu, *US Patent 8277691*, **2012**.

18 S. S. Jeong, N. Böckenfeld, A. Balducci, M. Winter, S. Passerini, *J. Power Sources* **2012**, *199*, 331–335.

19 A. Zhamu, B. Z. Jang, *US Patent 7875219*, **2011**.

20 V. V. Dementiev, R. C. West, R. J. Hamers, K. Tse, *US Patent 7466539*, **2008**.

21 B. Park, J. Choi, *Electrochim. Acta* **2010**, *55*, 2888–2893.

22 E. Pohjalainen, S. Räsänen, M. Jokinen, K. Yliniemi, D. A. WorsleY, J. Kuusivaara, J. Juurikivi, R. Ekqvist, T. Kallio, M. Karppinen, *J Power Sources* **2013**, *226*, 134–139.

23 J. Drofenik, M. Gaberscek, R. Dominko, F. W. Poulsen, M. Mogensen, S. Pejovnik, J. Jamnik, *Electrochim. Acta* **2013**, *48*, 883–889.

24 F. M. Courtel, S. Niketic, D. Duguay, Y. Abu-Lebdeh, I. J. Davidson, *J. Power Sources* **2011**, *196*, 2128–2134.

25 K. T. Lee, C. B. Tsai, W. H. Ho, N. L. Wu, *Electrochem. Commun.* **2010**, *12*, 886–889.

26 M. Kang, J. E. Lee, H. W. Shim, M. S. Jeong, W. B. Imb, H. Yoon, *RSC Adv.* **2014**, *4*, 27939–27945.

27 A. Varzi, A. Balducci, S. Passerini, *J. Electrochem. Soc.* **2014**, *161*, A368–A375.

28 M. Aslan, D. Weingarth, N. Jäckel, J. S. Atchison, I. Grobelsek, V. Presser, *J. Power Source* **2014**, *266*, 374–383.

29 K.-C. Tsay, L. Zhang, J. Zhang, *Electrochim. Acta* **2012**, *60*, 428–436.

30 Q. Abbas, D. Pajak, E. Frąckowiak, E. F. Béguin, *Electrochim. Acta* **2014**, *140*, 132–138.

31 S. Najib, E. Erdem, *Nanoscale Adv.* **2019**, *1*(8), 2817–2827.

32 S. S. Shah, M. N. Shaikh, M. Y. Khan, M. A. Alfasane, M. M. Rahman, M. A. Aziz, *Chem. Rec.* **2021**, *21*, 1631–1665.

33 B. Song, F. Wu, Y. Zhu, Z. Hou, K.-S. Moon, C.-P. Wong, *Electrochim. Acta* **2018**, *267*, 213–221.

34 Z. Zhu, T. Shuihua, Y. Jiawei, Q. Xiaolong, D. Yuxiao, Q. Renjie, G. M. Haarberg, *Int. J. Electrochem. Sci.* **2016**, *11*, 8270–8279.

35 L. Kouchachvili, N. Mafei, E. Entchev, *J. Solid State Electrochem.* **2014**, *18*, 2539.

36 S. Bayatpour, M. Afsharpour, Z. Dini, H. M. Naderi, *J. Mater. Sci. - Mater. Electron.* **2020**, *31*, 6150–6615.

37 B. Andres, C. Dahlström, N. Blomquist, M. Norgren, H. Olin, *Mater. Des.* **2017**, *141*, 342–349.

38 J. Jose, V. Thomas, V. Vinod, R. Abraham, S. Abraham, *J. Sci. - Adv. Mater. Dev.* **2019**, *4*, 333–340.

39 P. Jeżowski, P. L. Kowalczewski, *Polymers* **2019**, *11*(10), 1648.

40 N. A. Salleh, S. Kheawhom, A. A. Mohamad, *Results Phys.* **2021**, *25*, 104244.

41 P. Ruschhaupt, A. Varzi, S. Passerin, *Chem. Sus. Chem.* **2020**, *13*, 763–770.

42 M. Murase, N. Yabuuchi, Z. J. Han, J. Y. Son, Y. T. Cui, H. Oji, S. Komaba, *Chem. Sus. Chem.* **2012**, *5*, 2307.

43 R. A. Gross, B. Kalra, *Science* **2002**, *297*, 803–807.

44 D. R. Lu, C. M. Xiao, S. J. Xu, *Express Polym. Lett.* **2009**, *3*, 366–375.

45 A. Makowska, A. Szwengiel, P. Kubiak, J. Tomaszewska-Gras, *Starch* **2014**, *66*, 895–902.

46 H. M. Kennedy, in *ACS Publication Series*, **1989**, *385*, Ch. 23.

47 L. Chai, Q. Qu, L. Zhang, M. Shen, L. I. Zhang, H. Zheng, *Electrochim. Acta* **2013**, *105*, 378–383.

48 S. S. Alias, S. M. Chee, A. A. Mohamad, *Arabian J. Chem.* **2017**, *10*, S3687–98.

49 L. Ng, A. Mohamad, *J. Membr. Sci.* **2008**, *325*, 653–657.

50 X. He, P. Song, X. Shen, Y. Sun, Z. Ji, H. Zhou, B. Li, *Cellulose* **2019**, *26*(17), 9349–9359.

51 N. A. Choudhury, P. W. C. Northrop, A. C. Crothers, A. Jain, V. R. Subramanian, *J. Appl. Electrochem* **2012**, *42*, 935–943.

52 R. J. Chudzikowski, *J. Soc. Cosmet. Chem.* **1971**, *22*, 43–60.

53 I. Nam, S. Park, G. P. Kim, J. Park, J. Yi, *Chem. Sci.* **2013**, *4*, 1663–1667.

54 V. K. Thakur, G. Q. Ding, J. Ma, P. S. Lee, X. H. Lu, *Adv. Mater.* **2012**, *24*, 4071–4096.

55 X. Wang, W. Xu, P. Chatterjee, C. Lv, J. Popovich, Z. S. L. Dai, M. Y. S. Kalani, S. E. Haydel, H. Jiang, *Adv. Mater. Technol.* **2016**, *1*, 1600059.

56 N. S. Said, N. K. Howell, N. M. Sarbon, *Food Rev. Int.* **2021** *37*.

57 M. C. Gómez-Guillén, B. Giménez, M. E. López-Caballero, M. P. Montero, *Food Hydrocolloids* **2011**, *25*, 1813–1827.

58 T. N. Azira, I. Amin, Y. B. C. Man, *Int. Food Res. J.* **2012**, *19*(3), 1175–1180.

59 R. N. Hafidz, C. M. Yaakob, I. Amin, A. Noorfaizan, *Int. Food Res. J.* **2011**, *18*, 813–817.

60 N. Rosli, N. M. Sarbon, *Int. Food Res. J.* **2015**, *22*(2), 699–706.

61 N. M. Sarbon, F. Badii, N. K. Howell, *Food Hydrocolloids* **2013**, *30*(1), 143–151.

62 A. A. Mariod, H. Fadul, *Food Sci. Technol. Int.* **2014**, *21*(5), 380–391.

63 M. M. Welz, C. M. Ofner, *J. Pharm. Sci.* **1992**, *81*, 85.

64 G. A. Digenis, T. B. Gold, V. P. Shah, *J. Pharm. Sci.* **1994**, *83*, 915.

65 C. M. Ofner, Y. E. Zhang, V. C. Jobeck, B. J. Bowman, *J. Pharm. Sci.* **2001**, *90*, 79.

Part 5

Biomass-Based Supercapacitors: Future Outlooks and Challenges

25

Biomass-based Supercapacitors: Lab to Industry

Syed Shaheen Shah[1,2,3], Md. Abdul Aziz[1,4,], Muhammad Usman[1], Abbas Saeed Hakeem[1], Shahid Ali[1], and Atif Saeed Alzahrani[1,5]*

[1] *Interdisciplinary Research Center for Hydrogen and Energy Storage (IRC-HES), King Fahd University of Petroleum & Minerals, KFUPM Box 5040, Dhahran 31261, Saudi Arabia*

[2] *Physics Department, King Fahd University of Petroleum & Minerals, KFUPM Box 5047, Dhahran 31261, Saudi Arabia*

[3] *JSPS International Research Fellow, Department of Material Chemistry, Graduate School of Engineering, Kyoto University, Kyotodaigaku Katsura, Nishikyo-ku, Kyoto 615–8520, Japan*

[4] *K. A. CARE Energy Research and Innovation Center, King Fahd University of Petroleum & Minerals, Dhahran, 31261 Saudi Arabia*

[5] *Materials Science and Engineering Department, King Fahd University of Petroleum & Minerals, Dhahran, 31261 Saudi Arabia*

* Corresponding author

25.1 Introduction

Due to the smart electronics industry's ongoing development, there is a tremendous need for high-performance supercapacitors that are long-lasting, affordable, and lightweight for portable and smart electronic devices. Researchers have recently become more interested in designing and creating novel energy storage materials and supercapacitors as a result of the rapid growth in improvements in the creation of portable electronic systems. A potential energy source that could provide a long-term answer to the world's energy needs is solar energy. The low cost, high efficiency, and specialized design of solar cell technology have led to its commercialization. Solar cell-based solar energy harvesting has been extensively researched. However, the intermittent nature and variation in solar radiation is the main obstacle to the continuous real-time applications of solar cells because of their fluctuating and unstable output power supply to the load. Integrating solar cells with supercapacitors can reduce the power output fluctuation, providing a constant and uninterrupted power supply to the load. In this regard, a few scientists have evaluated and demonstrated a combination of solar cells and supercapacitors as self-powering and energy-storage devices [1–3]. There has been much reporting on the electrochemical performance of electric double-layer capacitors over the past few decades [4–9].

The supercapacitor market is anticipated to reach US$8.3 billion in 2025 with a nearly 30% compound annual growth rate (CAGR). When international renewable energy applications first entered the market in 2010, there were noticeable changes in the different categories of supercapacitors, as shown in Figure 25.1(a). This growth rate is attributed to the increasing demand for these supercapacitors in automotive applications, such as regenerative braking and start-stop systems for reducing fuel consumption. In the upcoming
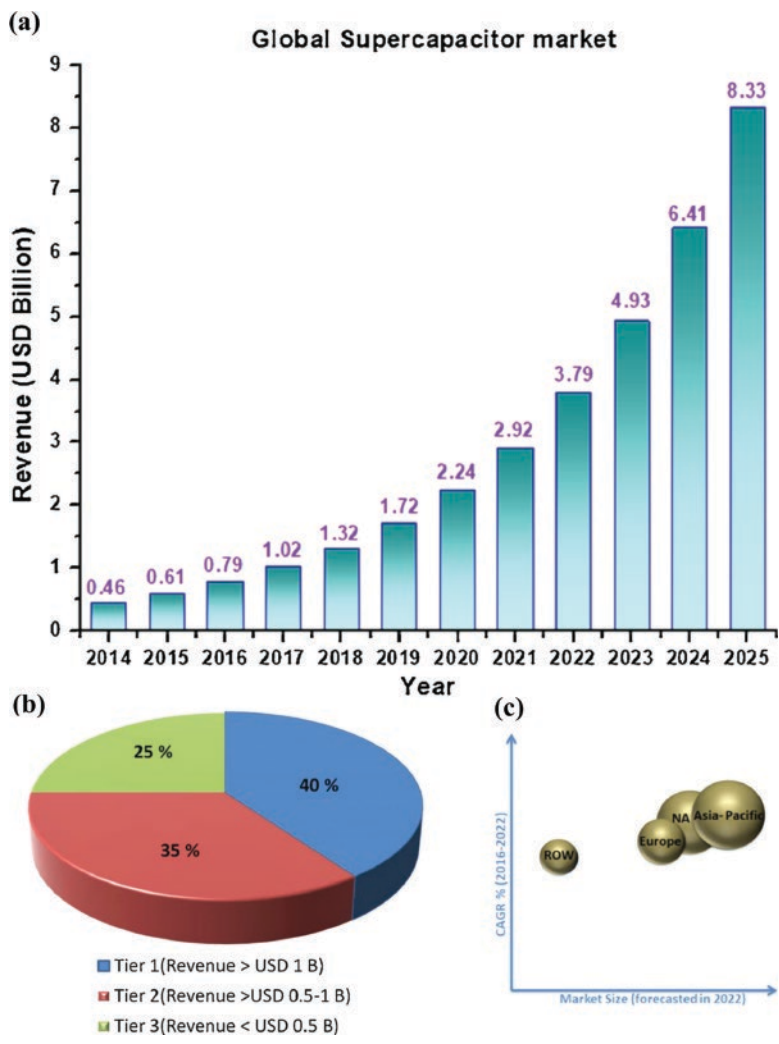
Figure 25.1 (a) Global supercapacitor market, (b) consumption of supercapacitors based on the types of companies, and (c) consumption of supercapacitors by region. *Reproduced with permission [10]. Copyright 2020, Elsevier.*

years, hybrid supercapacitors are expected to experience exponential expansion [10]. Additionally, Figure 25.1(b) shows the distribution of supercapacitor consumption based on the type of industry categorized by revenue, which is often grouped into three categories. Information about the region's base consumption is shown in Figure 25.1(c). The Asia Pacific (APAC) areas show the most significant contribution. The development of startups in this area stimulates market expansion. The industrial sectors in North America and Europe grew after APAC. Energy storage systems are widely used in Australia, Singapore, South Korea, and Japan in renewable energy projects. Government agencies in several Asian nations have also hybridized their transport networks, contributing to APAC holding

the lion's share of the supercapacitor market. The principal cost of the material is found to be the main barrier to market expansion. Recently, some supercapacitors have incorporated graphene, a highly conductive substance that is more expensive than activated carbon. Despite the reasons impeding the market development for supercapacitors, much research is being conducted to reduce overall costs and increase the market's adoption of supercapacitors [10].

Biomass is a naturally renewable and sustainable carbon precursor that could be easily converted to highly efficient carbon for supercapacitors. Although a lot of work has been done on developing biomass carbonaceous-based materials for supercapacitors, most of this carbon has only been tested in coin cells in the lab. Cylindrical or pouch cell devices have shown little commercial utility [11]. There are three primary packaging types – cylindrical cells, pouch cells, and coin cells – that are frequently used in manufacturing large supercapacitors. Electrode sheets and separators are rolled into cylindrical or prismatic hard case cells and spiral wound before being placed within the matching metallic cylinder or prism. Following electrolyte filling and final sealing, the current collector tabs are next soldered to the rolled sheets. These two designs are advantageous because they enclose the large-surface-area electrodes in a small casing, which reduces internal cell resistance, and because the metallic casing ensures the cell is moisture-free with a straightforward closure. The industry and the scientific community have recently focused a lot of attention on the prismatic pouch cell design as a potential alternative for supercapacitors. This design involves stacking electrodes, sheets, and separators one on top of the other inside a polymer bag. The primary benefit of a pouch cell is its incredibly adaptable construction, which enables the stacking of any number of electrodes into the required configuration, provided that each soldered current collector tab is correctly connected to the corresponding terminals in the cell. These parts are combined within a polymer bag to allow volume expansion. Thus, a high degree of cell capacity customization can be achieved without too many issues. The pouch cell design also has the lowest volume at the module level and the highest packaging efficiency of all the packaging designs, with a space utilization rate of up to 95%. These characteristics lead to thinner devices with lower electrochemical series resistance and higher energy and power densities than cylindrical cells in terms of volumetric and gravimetric calculations [12].

A supercapacitor's size, type, and intended purpose must all be considered while packaging it. Mobile electronics, such as phones, cameras, and other devices, use thin prismatic supercapacitors. PC-board and other items are stored in coin-type cans. The end plates of a supercapacitor must make good contact with its electrodes during packaging to lower electrochemical series resistance. To prevent oxidation processes that could lead to gas evolution, the packaging must be able to protect the electrochemical system from oxygen and water vapor. The employed container must be capable of withstanding the pressure caused by the electrochemical breakdown. The container may occasionally have a weak spot built in for safety when there is a risk, such as an overcharge. The cell will be able to open softly as a result. Preferably, the container's weight should be one-tenth that of the supercapacitor cell [13]. This chapter discusses the market trends for biomass-based supercapacitors, the essential qualities of biomass that can be utilized in supercapacitors, the technology readiness level (TRL), as well as information on the characteristics of supercapacitor devices and applications made by a variety of researchers.

25.2 Pre-requisites and Need for Biomass-based Supercapacitors for Industrialization

Biomass-based supercapacitors are expected to be part of the ongoing growth of energy storage devices for large scale in the near future. To play a part in such a rapidly growing industry, biomass-based supercapacitors should have long-term stability, high energy density, low cost, high power density, low toxicity, worldwide availability of materials, compatibility with the electrical device, easy modulation, be safe, and have excellent sustainability. By having such outstanding characteristics, biomass-based supercapacitors can attract the market and will be used in various industrial applications. In order to enhance the electrochemical capabilities of energy generation and storage systems, carbon-based materials are now essential [4–6, 14–16]. As a result, the problem of source depletion for synthesizing these materials must be addressed, and researchers must devise imaginative and practical solutions. Recent research indicates that biomass provides a real solution to address this problem, with a range of benefits. Reliable modifications are required, particularly for supercapacitors, and biomass-derived carbon-based materials are critical. Following significant research, it was discovered that a long-lasting, low-cost precursor is required for biomass to produce extremely porous carbon molecules. At this point, it should be emphasized that these technologies contribute to waste recycling in accordance with the win-win principle and do not only give a means of producing high-value supplies. According to the studies, biomass materials improve the electrochemical adhesion of the ions, increasing the electrode's specific capacitance and improving the supercapacitor's cycling performance and stability [7–9, 15–26]. The selection of biomass, the synthesis technique, the pretreatment, and the kind of supercapacitor are all critical aspects in manufacturing biomass-based goods. Precursor material and pretreatment are essential factors because the precursor content and pretreatment technique heavily influence pore size and dispersion. Because heteroatom doping to biomass-derived materials provides exceptionally high conductivity, composite materials are favored in many supercapacitor applications. Because a biomass-derived synthesis is a green synthesis technique, rather than using excessively risky chemical pretreatments [27, 28], the researchers should choose an acceptable precursor biomass material that has these qualities. Overall, biomass is a very beneficial resource for building the next generation of low-cost, environmentally friendly supercapacitor electrode materials.

25.3 Feasibility of Biomass-based Supercapacitors for Industry

Aside from a material aspect, several factors relating to electrode processing conditions and a cell assembly, such as electrode thickness/density, cell pressure, and pre-conditioning process, can significantly alter the performance of a supercapacitor cell as indicated by capacitance and internal resistance. A supercapacitor can be made in a few steps, which involve preparing a homogeneous mixture of components, creating an electrode layer on a current collector sheet, assembling the cells, and packing. To assess an electrode material in a full cell configuration in a laboratory setting, a pair of tiny electrodes with an area of a few cm^2 or mF capacity are often packed in a coin cell or its derivatives, such as a Swagelok

cell. However, a demonstration of a large-capacity cell is required to assess the cell's performance from a practical standpoint and as a first step toward commercialization. A high-capacity cell must be packaged in a pouch or cylindrical cell. Unfortunately, the published research offers little information, and the guidelines for producing a cell in such a container are proprietary in the industrial domain. Recently, it has been reported that efforts have been made to scale up the size of supercapacitors to coin cells to an even larger format, notably a pouch cell, highlighting challenges with electrode preparation. The pouch cell packing appears to be the preferred format in literature due to its ease of use, low cost of processing, industrial compatibility, and minimal footprint design [29].

25.3.1 Coin Cell-based Supercapacitors

Coin cell-based supercapacitors are the easiest to fabricate using biomass-based materials. Karaman et al. [30] described a straightforward and affordable method for creating 3D graphene line hierarchical porous carbon structures from agricultural waste materials with a finely controlled pore structure, a high specific surface area, and improved electrochemical activity (using orange peels). In order to provide comprehensive inspiration for the engineering and design of high-energy, low-cost aqueous supercapacitors based on carbon networks made from biomass, this work integrates state-of-the-art advancement. Graphene-like porous carbon made from agricultural waste was used to make a coin cell-type symmetrical supercapacitor that was tested using both 12 M $NaNO_3$ (water-in-salt) and 1 M Na_2SO_4 (salt-in-water) electrolytes. The supercapacitor cell used in the water-in-salt electrolyte had a wide operating voltage range of 2.3 V. The measured power and energy density values were comparable to those of commercially available, high-performance double-layer electrical capacitors. Developing high-rate electrochemical energy storage systems based on carbonaceous materials obtained from biomass will be made possible with the help of such fundamental discoveries. Kumar et al. [31] fabricated symmetrical coin cell supercapacitors using carbon derived from American poplar fruits. They tested in two different electrolytes, KOH (6 M aqueous electrolyte, up to 1.4 V) and 1 M Et_4NBF_4/AN (organic electrolyte, up to 2.5 V). The schematic representation for the fabrication of a coin cell-based supercapacitor (symmetric) is illustrated in Figure 25.2(a). The symmetrical coin cell supercapacitor under 6 M KOH offered a noteworthy 58.71 Fg^{-1} specific capacitance at 1 Ag^{-1} current density, 7.99 $Whkg^{-1}$ energy density at 372 Wkg^{-1} power density and additionally exceptional cyclic durability with conserved 80.2% of initial specific capacitance after 10000 GCD cycles. Meanwhile, the coin cell-based symmetrical supercapacitor under 1 M Et_4NBF_4/AN electrolyte exhibited an increased specific capacitance of 31.68 F g^{-1} at a current density of 1 Ag^{-1}, high energy density (13.75 $Whkg^{-1}$), and excellent cyclic durability with conserved 60.5% of initial specific capacitance after 10000 GCD cycles. The corresponding cyclic voltammograms, GCD curves, and cyclic stability of the fabricated coin cell-based supercapacitor in 1 M Et_4NBF_4/AN and 6 M KOH electrolyte are given in Figure 25.2(b-e). The reported coin cell-based symmetric supercapacitor paper thus advises using waste American poplar fruit as a sustainable carbon source for the creation of hierarchical porous carbon for applications in energy storage devices. Similarly, in three different aqueous electrolytes, Misnon et al. [32] reported on how physically and chemically activated carbon made from oil palm kernel shells stored charges electrochemically. Activated carbon electrodes produced from oil palm kernel shells and separated by fiberglass separator and electrolyte were used to develop the coin cell (CR2032)
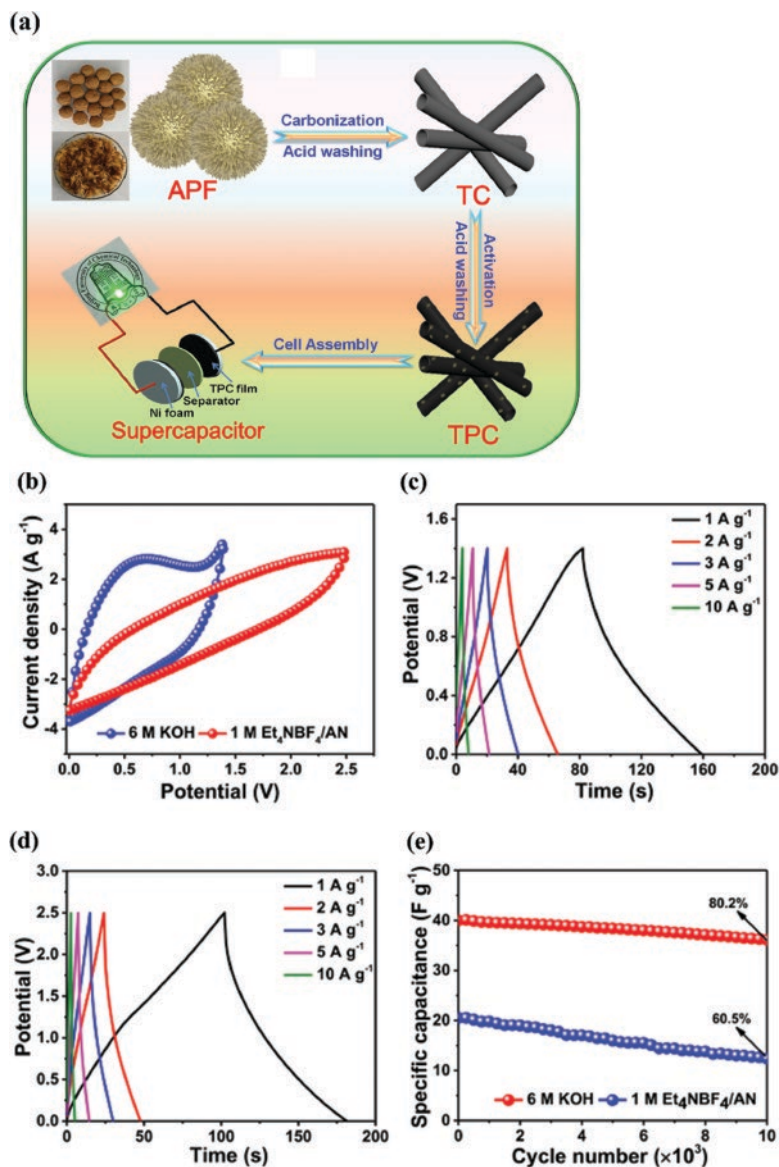
Figure 25.2 (a) Schematic representation for fabricating coin cell supercapacitor using carbon derived from American poplar fruits. (b) Cyclic voltammograms at 50 mV/sec in different electrolytes. GCD profiles in (c) 6 M KOH and (d) 1 M Et_4NBF_4/AN electrolytes at different current densities. (e) Cyclic performance of the symmetric supercapacitor. *Reproduced with permission* [31]. *Copyright 2020, Elsevier.*

based supercapacitors. The respective achievable operating potentials of these devices ranged from 1.0 V to 2.0 V for 1 M Na_2SO_4, 6 M KOH, and 1 M H_2SO_4. The Na_2SO_4 electrolyte produced maximum specific energy of 7.4 Wh kg^{-1} with a specific power of 300 W kg^{-1}. The supercapacitor stability for 3500 cycles revealed capacitance retention in all the manufactured devices in the 78 to 114% range.

A simple method to fabricate a new hierarchical porous carbon using readily available, inexpensive jujube fruits as a viable carbon source for making innovative supercapacitors was proposed by Yang et al. [33]. The naturally derived porous carbon from jujube fruits was produced by combining carbonization and activation with NaOH processes. In order to create well-organized micropores with a significant specific surface area of 1134.9 m^2g^{-1}, NaOH was used as an activating agent with excellent productivity and low cost. Additionally, a symmetrical coin-type supercapacitor based on the produced carbon technology offered high specific energy of 23.7 $Whkg^{-1}$ at a specific power of 629 Wkg^{-1} and exceptional long-term durability with a loss 6% of specific capacitance after 10000 GCD cycles in an organic electrolyte of 1 M Et_4NBF_4/AN. In terms of large specific capacitance, excellent rate ability, extraordinarily long cyclic life, and excellent energy density, the obtained coil cell-based supercapacitor demonstrated exceptional electrochemical performance in a larger operating potential window of (2.5 V). The research shows that cheap and sustainable carbon sources can be obtained from readily available jujube fruits to create high-performance supercapacitors. A coin-type symmetric supercapacitor was built using a porous polypropylene separator, two prepared electrodes, and the same mass of biomass waste from carbon derived from *Camellia oleifera* [34]. Due to its high specific capacitance of 275 Fg^{-1}, high energy density of 9.55 $Whkg^{-1}$ (at a power density of 478 Wkg^{-1}), and excellent cyclic stability with 99% capacitance retention after 10000 GCD cycles, the obtained coin cell-based symmetric supercapacitor was a promising energy storage device for electrochemical energy storage. Gong et al. [35] created a one-step procedure to transform bamboo char into three-dimensional porous graphitic biomass carbon, and we looked into how well it performed electrochemically as an electrode material for supercapacitors. The manufactured coin cell type-symmetric supercapacitor generated a 20.6 $Whkg^{-1}$ energy density at a 12 $kWkg^{-1}$ power density. This method demonstrated significant promise for the future low-cost, ecofriendly, and industrial-grade manufacture of carbon compounds from renewable biomass for advanced energy storage applications.

The supercapacitor cyclic stability increases and becomes environmentally friendly when a PVA/KOH gel electrolyte is used [36]. In practical applications, the built coin-type assembled symmetric prototype redox-enhanced supercapacitor in the gel electrolyte (PVA/KOH/ARS) demonstrated significant capacitance, cyclic stability for 2000 cycles, and synergistic power-energy output properties. Utilizing alizarin and carbon derived from lignosulfonate in charge storage devices is a step toward making energy storage and conversion technologies green and sustainable. In the past ten years, there has been a surge in interest in creating more environmentally friendly, simple, and affordable ways to use resources that are abundant and renewable in nature. This relieves worries about tainted water supplies and stores renewable energy. Because of their availability, simplicity of processing, customizable surface qualities, and relative affordability, carbon compounds generated from biomass has attracted much attention. Aruchamy et al. [37] showed how *Parthenium hysterophorous*, a common and hazardous weed, has the potential to be transformed into porosity-enriched ultrahigh surface area activated carbon, which has a surface area of 4014 m^2/g and a sizable amount of porous volume. The supercapacitor device constructed utilizing the carbon material as manufactured has a considerable 270 Fg^{-1} specific capacitance and outstanding capacitance retention of 98.5% even after 30000 GCD cycles. The synthesis of *Parthenium hysterophorous*-derived carbon and the corresponding coin cell type supercapacitor fabrication and their electrochemical performances are shown in Figure 25.3(a). The mesopore-dominated activated carbon electrode design has significantly improved the electrolyte breakdown voltage and energy
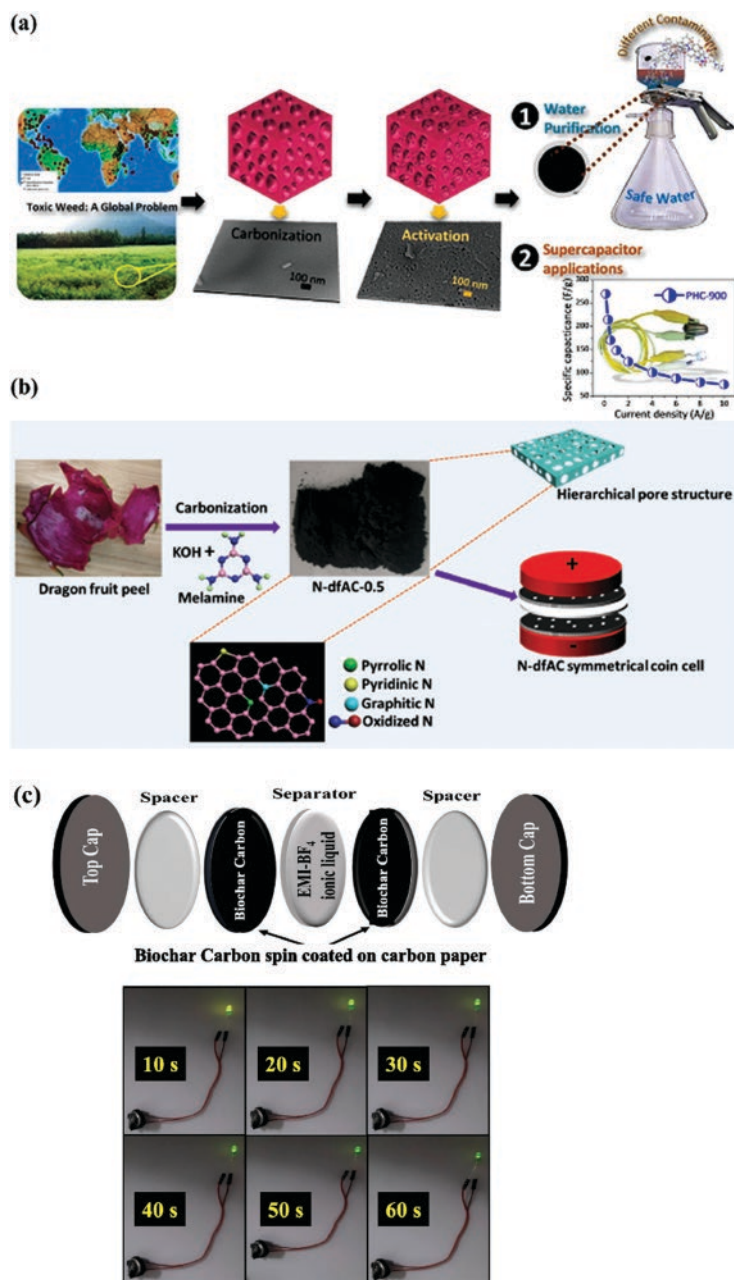
Figure 25.3 (a) Synthetic scheme for producing *Parthenium hysterophorous*-derived activated carbon and coin cell type supercapacitor fabrication. *Reproduced with permission* [37]. *Copyright 2022, Elsevier.* (b) Fabrication of coin cell-based symmetric supercapacitor from dragon fruit peel-derived nitrogen-doped carbon. *Reproduced with permission* [38]. *Reproduced under the terms of the CC BY-NC-ND 4.0 license. Copyright 2021, American Chemical Society, Gandla et al.* (c) Schematic illustration of biochar-based coin cell-based supercapacitor assembly and the corresponding performance with glowing LEDs. *Reproduced with permission [39]. Reproduced under the terms of the CC BY-NC-ND 4.0 license. Copyright 2022, Elsevier, Husain et al.*

density of supercapacitors. Under the synergistic action of KOH as the activating agent and melamine as the dopant, N-doped mesoporous-dominated hierarchical activated carbon was produced using the dragon fruit peel, a plentiful biomass precursor (Figure 25.3(b)) [38]. The electrode with the ideal N-doping content had the highest specific capacitance ($427 \, \mathrm{F \, g^{-1}}$) and the best cyclic stability in aqueous 6 M KOH electrolytes (123% up to 50000 GCD cycles). The authors created a 4.0 V symmetric coin cell supercapacitor with tremendous energy and power densities of $112 \, \mathrm{Wh \, kg^{-1}}$ and $3214 \, \mathrm{W \, kg^{-1}}$, respectively, in organic electrolytes. After 5000 GCD cycles at the working voltage of 3.5 V, the cell has a much longer cycle life than commercial YP-50 AC (capacitance retention of 60%). The capacity of mesopores to allow a diffuse ion layer with a longer Debye length and the carbon's polar N-doped species, which enhance capacitance and ion transport, both contribute to the higher voltage window. By carefully adjusting their pore architectures, the findings offer a novel method for developing biomass materials that are sustainable and friendly to the environment into high-capacity and high-working voltage coin-based supercapacitors. With the coin cell assembly, supercapacitor assembly is simple and repeatable, as shown in Figure 25.3(c).

Similarly, various coin cell-based supercapacitors have been reported which use various biomass-derived carbon materials such as bagasse-derived carbon [40], *Ganoderma lucidum* residues-based porous carbon [41], pear-derived graphene aerogels [42], bean dregs derived carbon [43], peeled ginger derived heteroatom-doped microporous carbon nanosheets with few-layer graphene [44], lotus root derived highly porous carbon [45], N-doped algae-derived porous carbons [46], waste tea derived activated carbon [47], bamboo-based hierarchical porous carbon [48], bamboo shavings derived petal-like N-O-codoped hierarchical porous carbon [49], and garden biomass waste derived mesoporous biochar [39]. The electrochemical performances of various coin cell-based supercapacitors are tabulated in Table 25.1.

25.3.2 Pouch Cell-based Supercapacitors

Pouch cell-based supercapacitors in high demand in the market due to high energy densities, larger potential windows, and compatibility with various industrial applications. Inal et al. [47] used a chemical approach to manufacture inexpensive activated carbon from biomass. When utilized as the electrode material in the supercapacitor, this activated carbon underwent a second heat treatment right away, which greatly enhanced the electrochemical performance. Moreover, the pouch cell supercapacitor version of the coin supercapacitor device, which was made from activated carbon, was scaled up successfully without sacrificing performance. The heat-treated AC sample was used to make the supercapacitor devices, which performed well electrochemically when both aqueous and organic electrolytes were present. Kongthong et al. [50] reported composite of MnO_2 nanofibers and pineapple leaf-derived porous N-doped activated carbon (PALF-NAC) as electrode materials for high-performance pouch cells and coin cell supercapacitors. Figure 25.4 displays a schematic for producing coin cells and pouch cells-based supercapacitors.

The performance and scaling potential of the prototype pouch cell supercapacitor were evaluated. With respective energies and powers of $26.8 \, \mathrm{Wh \, kg^{-1}}$ and $120.5 \, \mathrm{W \, kg^{-1}}$, the supercapacitor demonstrated a significant capacitance of $120 \, \mathrm{F \, g^{-1}}$ at a current density of $10 \, \mathrm{mA \, cm^2}$. With 87% capacitance retention after 1000 cycles, such a pouch device also demonstrated excellent stability. Veerasubramani et al. [51] reported a pouch cell with a flexible type hybrid supercapacitor based on laboratory waste tissue paper-derived honeycomblike

Preparation of PALF-AC
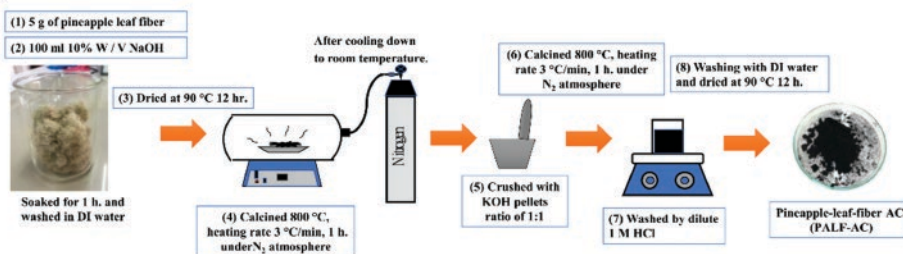
Preparation of PALF-NAC
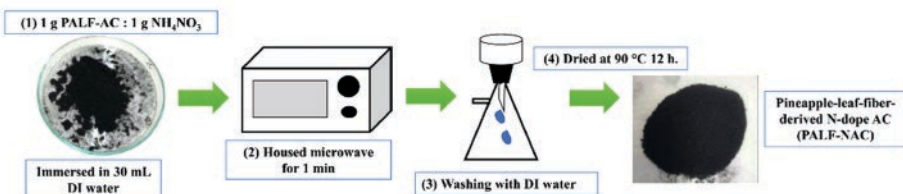
Preparation of α-MnO₂ nanofiber
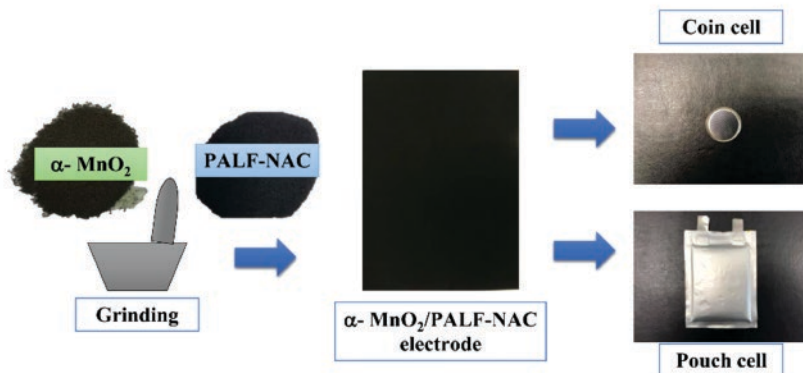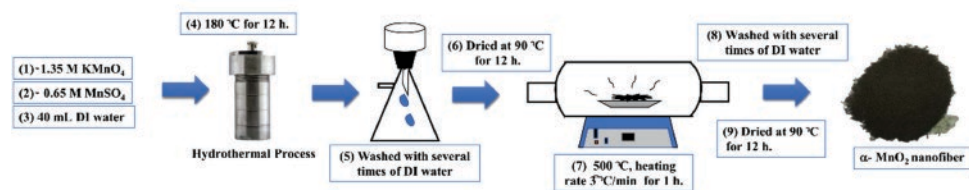
Figure 25.4 Supercapacitors based on coin cells and pouch cells are depicted schematically. *Reproduced with permission* [50]. *Reproduced under the terms of the CC BY-NC-ND 4.0 license. Copyright 2022, Elsevier, Kongthong et al.*

porous carbon (LTHAC). The highly flexible, pouch-style hybrid supercapacitor in the liquid electrolyte was built using the cobalt hydroxide-cobalt molybdate ($Co(OH)_2/CoMoO_4$) core-shell structure (prepared by electrochemical deposition) sandwiched with the prepared porous carbon. The $Co(OH)_2/CoMoO_4$ positive electrode and porous LTHAC negative electrode used in the construction of the pouch-type hybrid supercapacitor displayed

an extended working voltage of 1.5 V in 2 M KOH electrolyte and had the capacity to store up to 167.5 Wh cm^2 of energy. Interestingly, the produced pouch-type supercapacitor displayed outstanding flexibility under various bending conditions and incredible cyclic stability with >98% capacitance retention even after extended cycles. The device's functionality was also shown by coupling it with a solar cell to run different kinds of LEDs and seven-segment displays for applications that require self-powered devices.

Potphode et al. [52] outlined a promising technique for converting biowaste into porous carbon to create a functional electrode for developing long-lasting pouch cell-type supercapacitors. To create partially graphitic carbon nanosheets linked to the porous carbon, *Borassus flabellifer* fruit skin (BFFS) was carbonized in an inert atmosphere and then activated with KOH. Surface chemistry and porosity were modified by altering the carbonization and activation temperatures to gain significant control of the investigated physiochemical parameters. The resulting BFFS-derived porous carbon exhibits excellent energy storage potential due to its distinct shape and specific surface area of 1750 m^2/g^{-1}. A significant volume portion of the BFFS has micro- and mesoporosity due to the distinctive mineral composition, which produced a highly porous architecture. The specific capacitance of pouch cell symmetric supercapacitors made with 1 M H$_2$SO$_4$ and EmimBF$_4$ (ionic liquid) as electrolytes attained 202 and 208 F g^{-1}, respectively. The supercapacitor's performance based on carbon electrodes made from biomass was reasonably stable, and the cycling stability of up to 94% at a 2 A g^{-1} current density confirms the potential of activated carbon produced from BFFS for the development of supercapacitors made from biowaste electrodes. Ojha et al. [53] prepared holey graphitic carbon nano-flakes from puffed rice (HGCNF) and used them as electrode materials for symmetric pouch cell supercapacitor fabrication. Figure 25.5(A) illustrates the fabrication of electrodes from the HGCNF, and the corresponding pouch cell assembly is shown in Figure 25.5(B). The fabricated pouch cell showed promise for converting the cell design to a commercial level when three series-connected cells were charged to 3 V, as shown in Figure 25.5(C).

A straightforward, one-step pyrolysis process was used to prepare a ternary doped carbon material (with B, N, and P) from hemp fiber biomass [54]. The resultant carbon exhibited excellent qualities, including mixed morphologies with square, diamond-like, and cylindrical-shaped morphologies that demonstrate heteroatom doping into the carbon networks, which facilitated quick ion transfer, great diffusion rates, and competent electrode/electrolyte interfaces, and improved supercapacitive properties. The study thus provided a promising strategy for increasing the electrochemical energy storage potential by heteroatom doping. By combining the synergistic effects of the heteroatoms B, N, and P, the carbon electrode was able to produce a maximum half-cell specific capacitance of 520 F g^{-1} at 1 A g^{-1}. These heteroatoms increase electrical conductivity, facilitate electrolyte ion migration to the active electrode material, and increase fast charge transfer reactions. The most significant full-cell specific capacitance for the symmetric pouch-cell supercapacitor was 262.56 F g^{-1} at a current density of 1 A g^{-1}. The constructed symmetric pouch-cell supercapacitor provided a maximum energy density of 118 Wh kg^{-1} and a maximum power density of 5759 W kg^{-1} with an enlarged potential window of 1.8 V and 99.7% capacitance retention over 10000 GCD cycles. The outstanding outcome thus points to the potential of this biomass-based carbon with a pouch cell assembly, an environmentally friendly and inexpensive method of synthesizing biomass-based material as an alternative electrode material for energy storage and conversion. For a range of electrochemical energy storage applications, it is crucial to
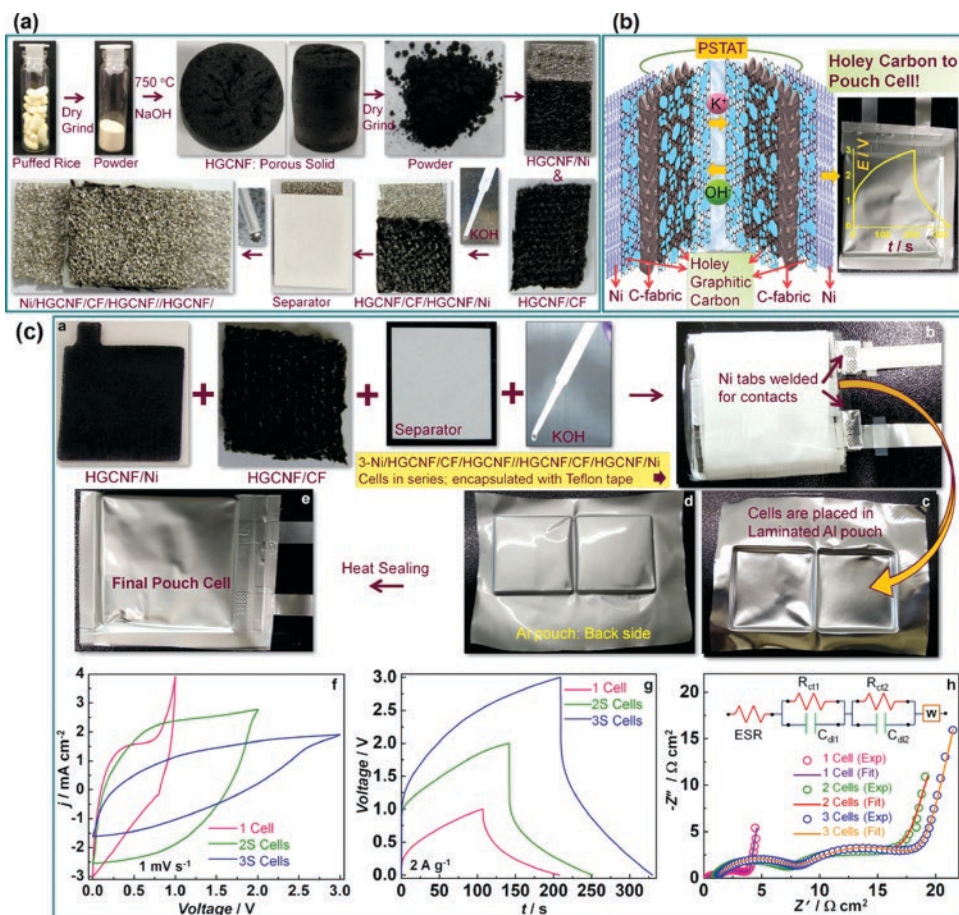
Figure 25.5 (A) Step-wise fabrication of symmetric supercapacitor using the puffed rice-derived holey graphitic carbon nano-flakes. (B) A schematic for pouch cell supercapacitor demonstration, and (C) the corresponding pouch cell supercapacitor with their electrochemical performances. *Reproduced with permission* [53]. *Copyright 2021, Elsevier.*

building electrodes with high mass loading while preserving outstanding electrochemical characteristics. A hierarchically porous activated carbon electrode was reported by Hung et al. [55] with a more significant mass loading ($8.5\ mg\,cm^{-2}$). The propylene carbonate-based electrolyte in the pouch-type symmetric device demonstrated high-rate capability and good cyclic. On the other hand, a pouch-type symmetric supercapacitor delivered a capacitance of 32.4 F and capacitance retention of 96% after 30000 GCD cycles. The intriguing characteristics of the pouch cell supercapacitor and the advantageous features of the produced electrode are credited with the corresponding electrochemical performances.

A combination of low-cost electrochemically exfoliated graphene and activated carbon derived from the waste of the tea industry was used to create scalable, highly stable supercapacitor electrodes [56]. The stability of the hybrid electrodes was noticeably improved at high current densities. Using an aqueous electrolyte, the first electrochemical performances of activated carbon and graphene were investigated using button-sized cells. The hybrid materials were created by combining activated carbon and graphene at various mass

percentage ratios, and under the same testing conditions they were evaluated as supercapacitor electrodes. Compared to the original activated carbon, the capacitance stability of the electrodes at high currents was enhanced by roughly 45%. This hybrid electrode accomplished the maximum gravimetric capacitance ($110\,\mathrm{F\,g^{-1}}$). The hybrid electrode was tested utilizing an organic electrolyte after being built up to a pouch cell-based supercapacitor device. The organic electrolyte was chosen for scaling up because of its greater voltage range. The pouch cell performed just as well in the organic electrolyte as the coin cell, with a gravimetric capacitance of $85\,\mathrm{F\,g^{-1}}$.

25.3.3 Cylindrical Cell-based Supercapacitors

Cylindrical supercapacitors are the best energy storage options for use in electric vehicle applications due to their safety, high power, and capacitance. In this regard, materials containing activated carbon must be developed and used economically in supercapacitors. Researchers have paid a lot of attention to the production of carbon-based materials for use in supercapacitors. However, laboratory testing on the coin-cell scale is the extent of research on and using such materials. Recently, a small number of researchers reported cylindrical supercapacitors made of biomass that might be useful for commercial applications. Nanaji et al. [11] fabricated activated carbon nanosheets from petroleum coke with a specific surface area of $2394\,\mathrm{m^2\,g^{-1}}$. They also showed that these activated carbon sheets can be used in commercial applications by developing a cylindrical supercapacitor with a high potential of 2.7 V and excellent capacitance of 1200 F. The step-wise fabrication of the cylindrical supercapacitor is shown in Figure 25.6. The cylindrical supercapacitor displayed a high capacitance of 1202 F, 1.22 Wh of stored energy, and a gravimetric energy density of $20.2\,\mathrm{Wh\,kg^{-1}}$. The electrochemical performances of the fabricated cylindrical supercapacitor are shown in Figure 25.6A-F. The built-in supercapacitor showed a lot of promise in terms of electrochemical properties that could be used in commercial applications. It was roughly compared to a supercapacitor that is currently on the market and was about the same size as the native cylindrical device. The investigation also showed that cheap petroleum coke with high carbon content was employed to fabricate petroleum coke carbon-based supercapacitors, which can be used as a substitute for commercial carbon-based supercapacitors.

Using a self-templating technique along with NaOH activation, waste straw cellulose was converted into a three-dimensional hollow tubular porous carbon [57]. Due to its substantial specific surface area, high mesoporosity ratio, and low resistance, the prepared carbon demonstrated exceptional electrochemical performance for use in supercapacitors. The carbon electrode displayed a high specific capacitance of $312.57\,\mathrm{F\,g^{-1}}$ and superior cyclic stability with capacitance retention of 93% after 20000 GCD cycles in 6 M KOH at a current density of $0.5\,\mathrm{A\,g^{-1}}$. A cylindrical supercapacitor that produced energy densities of $8.67\,\mathrm{Wh\,kg^{-1}}$ at a power density of $3.50\,\mathrm{kW\,kg^{-1}}$ in 6 M KOH and $28.56\,\mathrm{Wh\,kg^{-1}}$ at a power density of $14.09\,\mathrm{kW\,kg^{-1}}$ in $1\,\mathrm{M\,Et_4NBF_4/PC}$ electrolyte showed that the prepared carbon could be used in this way. This study provided an efficient method for using biomass waste and a quick, ecofriendly method for producing hierarchical porous carbon for electrochemical energy storage devices. Nanaji et al. [58] used jute sticks as a carbon precursor to synthesize nanoporous carbon with a structure resembling graphene and examined the electrochemical characteristics of cylindrical supercapacitors. The activation temperature controlled the ratio of amorphous carbon to the graphene-like network that makes up the produced nanoporous carbon. As the activation temperature
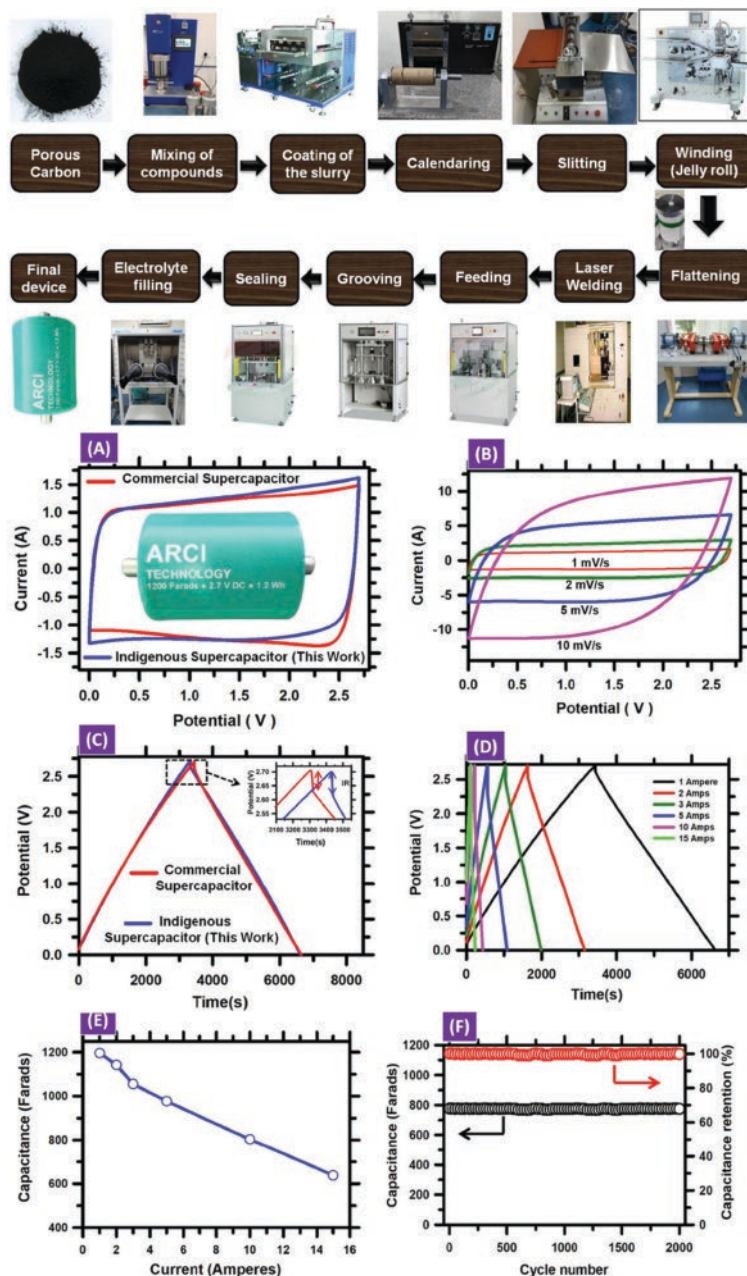
Figure 25.6 Photographs showing the step-by-step fabrication of a cylindrical supercapacitor with the prepared porous carbon from petroleum coke. (A) Comparative CV curves at a scan rate of 1 mV s^{-1} for commercial and lab-fabricated cylindrical supercapacitors, (B) CV curves at different scan rates for the lab-fabricated cylindrical supercapacitor, (C) comparative GCD profiles at a current of 1 A for commercial and lab fabricated cylindrical supercapacitors, (D) GCD profiles at various currents for the lab fabricated cylindrical supercapacitor, (E) capacitances at different currents, and (F) cyclic stability of the lab fabricated cylindrical supercapacitor. *Reproduced with permission [11]. Copyright 2022, Elsevier.*

was increased, the amorphous carbon changed into a stable graphene-like network with a high specific surface area of 2396 m^2 g^{-1}, a graphene-like sheet-like shape, and a highly organized graphitic sp2 carbon. The nanoporous carbon was examined in both aqueous and organic electrolytes for supercapacitor applications, and the material exhibited outstanding electrochemical performance in both situations. It showed good rate capability and high specific capacitance of 282 Fg^{-1} while retaining over 70% of capacitance at high current rates. Benchmark analyses showed that the nanoporous carbon was superior to commercially available supercapacitive carbon. The constructed symmetric supercapacitor displayed an impressive energy density of 20.6 Wh kg^{-1} at a high power density of 33600 Wkg^{-1}. A cylindrical supercapacitor with a 20 F capacitance and a 2.7 V voltage was developed and tested for use in practical applications using a nanoporous carbon electrode. The electrode material's high specific surface area and ideal pore size distribution, along with the ordered graphene network's robust electrical conductivity, are what give the electrode its exceptional electrochemical performance. These results demonstrated how straightforward, reasonably priced, and environmentally friendly materials could be created for use in commercial energy storage applications. The electrochemical performances of various commercially viable supercapacitors are tabulated in Table 25.1.

25.4 Industrial Applications of Biomass-based Supercapacitors

Supercapacitors are electrical energy storage systems that can store a lot of energy and discharge it quickly. Although they cannot currently match the energy content of Li-ion batteries in the industrial market, their capacity is growing yearly. They are already employed as accessory components to store braking energy and supply the necessary boost during rapid accelerations, thereby improving the industry's (especially electric vehicles) economy. In order to prepare for their potential use in industry, should the current trends in electrical storage continue, this discussion will briefly elaborate on the state-of-the-art materials, technology, and applications while introducing the industrial aspects of biomass-based supercapacitors. The comparison of Li-ion batteries and supercapacitors to be used in electric vehicles is shown in Figure 25.7.

Batteries were once considered the primary method of electrical energy storage for off-grid applications. Batteries will still be utilized for this purpose, but supercapacitors, a more contemporary form of electric energy storage device, are expected to replace or significantly augment traditional battery storage. Power handling and environmental sustainability are the two most crucial areas where supercapacitors are needed. The transition away from fossil fuel-burning internal combustion engines has produced a gap between the high power needs of these engines and the power that battery technology can deliver. The battery is the most expensive component overall, especially in modern electric vehicles, where the size is often determined by the highest power handling demand rather than the minimum range that the vehicle must be able to go between charges. Furthermore, repetitive high-power charging and discharging shortens the lifespan of batteries, reducing them from a few thousand to just a few hundred cycles. On the other hand, supercapacitors excel at high-power handling. Importantly, they may do so without hurting the device or reducing its longevity, which is normally rated at least 500000 cycles for goods now on the market. They can typically handle power loads up to 100 times larger than those of Li-ion batteries [59].

Table 25.1 Electrochemical performances of various commercially viable supercapacitors, reported in the literature.

Electrodes	Supercapacitor Type	Specific Capacitance ($F\,g^{-1}$) @ Current Density ($A\,g^{-1}$)	Electrolyte	Energy Density ($Wh\,kg^{-1}$)	Power Density ($W\,kg^{-1}$)	Capacitance Retention (%) @ Cycle No.	Ref.
Orange peel-derived carbon	Coin Cell	70 @ 0.5	12 M $NaNO_3$	38	9.15×10^3	86.2 @ 10000	[30]
American poplar fruit-derived carbon	Coin Cell	31.68 @ 1.0	1 M Et_4NBF_4/AN	13.75	624	60.5 @ 10000	[31]
Oil palm kernel shell-derived activate carbon	Coin Cell	75 @ 0.6	1 M Na_2SO_4	7.4	300	114 @ 3500	[32]
Jujube fruits derived porous carbon	Coin Cell	54.7 @ 1.0	1 M Et_4NBF_4/AN	23.7	629	94 @ 10000	[33]
Camellia oleifera-derived carbon	Coin Cell	275 @ 0.5	2 M H_2SO_4	9.55	478	99 @ 10000	[34]
Bamboo char-derived porous graphitic carbon	Coin Cell	48.1 @ 0.2	EMIM TFSI	20.6	12×10^3	84 @ 5000	[35]
Lignosulfonate-derived hierarchical porous graphitic carbon	Coin Cell	68.04 @ 0.5	PVA/KOH/ARS	9.45	100.06	99.7 @ 2000	[36]
Dragon fruit peel-derived N-doped carbon	Coin Cell	53 @ 2 mA/cm^2	1 M $TEABF_4$/AN	112	664	109 @ 5000	[38]
Garden biomass waste derived mesoporous biochar	Coin Cell	228 @ 1.0	1 M H_2SO_4	7.91	...	88 @ 5000	[39]
Bagasse derived carbon	Coin Cell	228 @ 0.5	6 M KOH	25.6	226	100 @ 10000	[40]
Ganoderma lucidum residues based porous carbon	Coin Cell	252 @ 0.5	6 M KOH	6.1	5000	99.9 @ 10000	[41]
Pear-derived graphene aerogels	Coin Cell	133.53 @ 2.0	EMIM-TFSI	56.80	620.26	83 @ 10000	[42]
Peeled ginger-derived heteroatom-doped few-layer graphene-like microporous carbon nanosheets	Coin Cell	70 @ 0.1	1 M H_2SO_4	9.67	200	93.3 @ 3500	[44]
Lotus root-derived highly porous carbon	Coin Cell	273 @ 0.34	6 M KOH	9.0	80.8	94 @ 2000	[45]

Material	Cell Type	Specific Capacitance (@ current)	Electrolyte	Energy Density	Power Density	Cyclic Stability (% @ cycles)	Ref.
N-doped algae-derived porous carbons	Coin Cell	190 @ 0.2	6 M KOH	...	...	98 @ 8000	[46]
Waste tea-derived activated carbon	Coin Cell	140 @ 0.1	1 M Et_4NBF_4/ACN	...	...	98 @ 10000	[47]
Bamboo shavings derived hierarchical porous carbon	Coin Cell	160 @ 0.5	6 M KOH	15.3	290	94.2 @ 10000	[49]
Waste tea-derived activated carbon	Pouch Cell	100 @ 0.1	1 M Et_4NBF_4/ACN	...	...	92.5 @ 10000	[47]
$PALF\text{-}NAC@MnO_2$	Pouch Cell	120 @ 10 mA/cm^2	1 M H_2SO_4	26.8	120.5	87 @ 1000	[50]
$LTHAC@CoMoO_4/Co(OH)_2$	Pouch Cell	107 @ 2 mA/cm^2	2 M KOH	33.5	3750	98.64 @ 2500	[51]
BFFS-derived porous carbon	Pouch Cell	208 @ 0.5	$EmimBF_4$	...	...	94 @ 10000	[52]
HGCNF	Pouch Cell	232 @ 0.5	6 M KOH	68	2.5×10^3	96 @ 10000	[53]
B, N, and P-doped carbon material from hemp fiber biomass	Pouch Cell	262.56 @ 1.0	6 M KOH	118	5759	99.7 @ 10000	[54]
Hierarchically porous activated carbon	Pouch Cell	77.8 @ 1 mA/cm^2	$TEABF_4$/PC	17.5	661.7	96 @ 30000	[55]
Tea industry waste-derived activated carbon and graphene	Pouch Cell	58 @ 1.0	1 M Et_4NBF_4/AC	...	...	90 @ 10000	[56]
Petroleum coke-derived carbon	Cylindrical Cell	1200 F @ 1 mA	1 M Et_4NBF_4/AC	20.2	32.8×10^3	91 @ 2000	[11]
Straw cellulose waste-derived carbon	Cylindrical Cell	141.64 @ 0.5	1 M Et_4NBF_4/PC	28.56	14.09×10^3	92.93 @ 20000	[57]
Jute stick-derived graphene-like porous carbon	Cylindrical Cell	131 @ 0.5	6 M KOH	20.6	33600	85 @ 10000	[58]
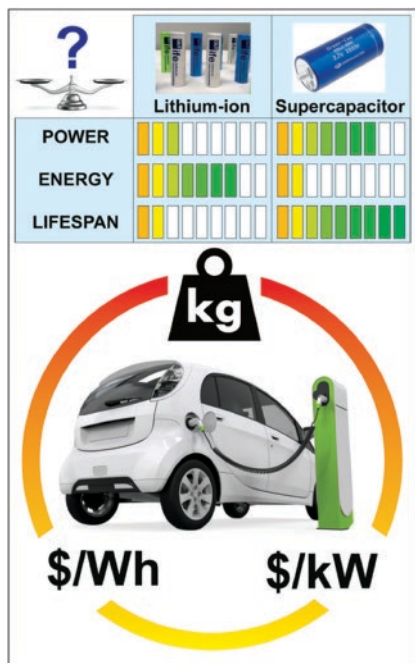
Figure 25.7 Supercapacitors: A potential new power source for electric vehicles. *Reproduced with permission* [59]. *Copyright 2019, Elsevier.*

The drawback of modern supercapacitors is their energy density, or their inability to provide continuous power for long periods of time [9]. In order to boost supercapacitor energy density, a lot of research is being done [9, 18, 24, 60]. Supercapacitors can only support other automotive power sources, such as batteries and fuel cells, which are unable to meet the power requirements of regenerative braking and quick acceleration due to their poor energy density. Despite this difference, a direct comparison of the standard electrical storage metric of $/kWh is erroneous because the size of battery packs is controlled by power rather than energy. Supercapacitors can cost up to USD$10,000/kWh, whereas Li-ion batteries now cost as little as USD$250/kWh [59]. It is clear that there is an optimization issue given the metric of $/kW, where Li-ion batteries are at least ten times cheaper than supercapacitors. Technical factors that increase the complexity of the problem include supercapacitors' increased electrical efficiency, longer longevity, and batteries' extended lifecycle when their loading is maximized. Technical and societal issues will strongly impact the field, including range expectations, autonomous vehicle policy, and infrastructure development. The finest electric vehicle- powering solutions, which would entail predictions that consider at least all of the previously described factors, are still far from being produced.

Biomass-based materials can be used to lower the overall cost of supercapacitors and offer high efficiency to compete at the industrial and commercial level. Using electricity to power cars is the transportation sector's response to the greenhouse gas emissions caused by fossil fuels. Biomass-based supercapacitors have thus started to enter the mid-sized vehicle market. The automotive industry has adopted widespread commercialization of biobased products, albeit in an infant stage. Therefore, it is customary to assess the numerous disadvantages of using biobased materials and select the best path for further research and development in this field. This article discusses various biobased product applications in supercapacitors and ongoing research in this field to replace petroleum and crude oil-based sources with biobased sources. Electrodes play a critical role in the overall performance and other crucial components of supercapacitors. The typical electrode materials used in supercapacitors are conducting polymers, transition metal oxides, and carbon-based materials such as activated carbon, carbon nanotubes, and graphene. Surface area and pore size distribution are crucial factors to consider when selecting an electrode material. They are in charge of the ion absorption capacity of the electrodes, which directly affects the amount of energy that can be stored in them. Heteroatoms like oxygen and nitrogen function as electron acceptors and donors in the form of functional groups, and they support reversible redox processes. Biomass-based

materials make suitable electrodes for supercapacitors due to their adaptable surface and morphological characteristics and the presence of various oxygenated functional groups.

The environmentally friendly conversion of biomass waste into a high-performance, cost-effective electrical energy storage devices has attracted a lot of scientific and technological interest [4, 28, 60, 61]. The main challenges for supercapacitor developers are the high manufacturing costs and low energy densities of supercapacitors. In order to overcome these difficulties, Vijayakumar et al. [62] reported the fabrication of excellent durable supercapacitor electrodes derived from industrial waste cotton used as a sustainable and affordable carbon resource, as described in Figure 25.8(a, b). The improved electrodes had a greater energy density, charged more quickly, and held up better over time. The resulting supercapacitor electrode displayed good volumetric capacitance of $87\,F\,cm^3$ at a current density of $1\,A\,g^{-1}$ due to the simultaneous attainment of high active mass loading ($9\,mg\,cm^2$) and a maximum voltage
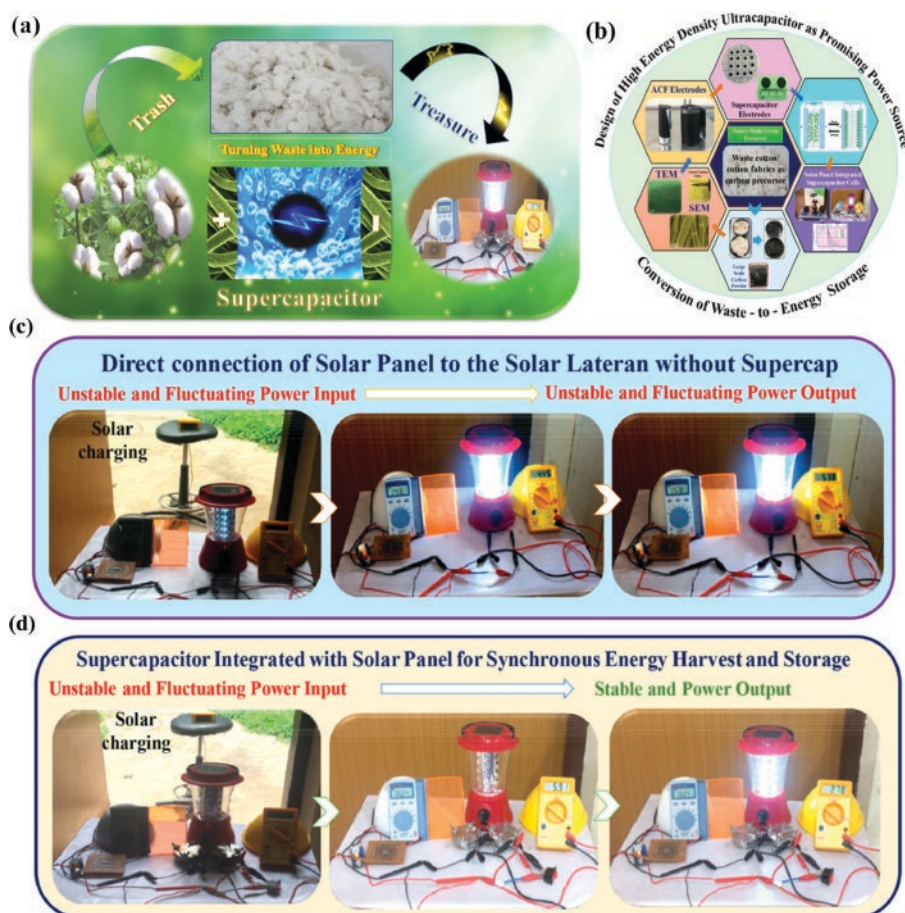
Figure 25.8 (a) Schematic representation of turning biomass into an energy application via supercapacitor. (b) Conceptualization of a large-scale and sustainable process for producing activated carbon from waste cotton for a supercapacitor with a high energy density. The practicality of supercapacitor cells incorporated into solar panels; (c) direct solar panel connection powers LED lighting and (d) energy storage and energy harvesting hybrid LED lights powered by a solar supercapacitor. *Reproduced with permission [62]. Copyright 2019, American Chemical Society.*

window of 3.2 V. A greater volumetric energy density of 30.94 Wh/L was produced. The supercapacitor electrodes also showed exceptional durability up to 15000 GCD cycles, even at higher voltages of 3.2 V. One explanation for this is that electrolyte ion transport can be accelerated even at high current loads by an interconnected porous network of activated carbon fibers with a large electrolyte ion accessible surface area ($1893 \ m^2 \ g^{-1}$). Strong capacitance retention at a high current with a high voltage, which is very interesting, clearly demonstrated the presence of the ideal carbon electrode pore size, which can match with the electrolyte ion size for a rapid capacitive response. The solar-powered supercapacitor, which also functions as a self-powering energy harvest and storage device, was integrated to power the commercial solar lantern, as shown in Figure 25.8(c, d). The individual solar panel and supercapacitor cell performances were tested independently before they looked into the integrated system. The solar panel that was directly attached to a solar lantern (40 LED lights) without a supercapacitor was investigated to determine how well the solar panel performed on its own. Figure 25.8(c) makes it abundantly evident that the electricity coming from the solar panel is unpredictable and variable and that a solar lantern's load is simultaneously linked to the fluctuating power input. However, a solar-powered device that had two supercapacitor cells connected in series was put to the test. The solar panel, which had an open circuit potential of 0–6 V and a 3 W power output, worked as an energy harvester to charge the supercapacitor when exposed to solar light. The supercapacitor cells were connected to the solar panel for charging. A solar lantern was utilized as a load to link the supercapacitor terminals. As shown in Figure 25.8(d), it was found that in this integrated system, the solar panel functions as the energy source that charges the supercapacitor cells, which can then provide steady power to the LED lights in the solar lantern without any power fluctuations. The supercapacitor's extremely quick charge-discharge characteristic made it particularly advantageous for various commercial applications. The findings demonstrated that a solar panel and supercapacitor device combination is a desirable and efficient ultrafast next-generation device that simultaneously converts and stores energy. This study provides an easy-to-use synthetic technique for making cost-effective, high-performance supercapacitor electrodes for real-time supercapacitor applications.

25.5 Technology Readiness Level for Commercialization

Technology readiness level (TRL) is a measure to judge the difference between development and deployment. There are various levels of technology readiness from 1 to 9. The lower TRL represents the early stage, while the high TRL shows the maturity of the technology. The definition for various TRLs is given in Table 25.2.

Due to the high demand for efficient and high-power energy storage, supercapacitors have gained significant attention in research and development. This increase in research has led to the development of supercapacitors that have been applied in several areas, especially in transportation and renewable energy. Currently, the application of supercapacitors in buses and trains promises its TRL 9 [65–68]. Biomass-based supercapacitors have been prepared on a large scale at the industrial level; however, their applications at the industrial level are at the developing stage, and efforts are needed to enhance the TRL of biomass-based supercapacitors. However, researchers could identify the TRL of the developed supercapacitor as per the criterion given in Table 25.2.

Table 25.2 TRL definition.

TRL	Definition
TRL 1	Basic principles observed and reported
TRL 2	Conceptualization of the technology
TRL 3	Experimental and analytical proof of concept
TRL 4	Technology validation in the laboratory
TRL 5	Technology validation in a relevant environment
TRL 6	Technology demonstrated as a prototype in the relevant environment
TRL 7	Prototype a pre-commercial scale
TRL 8	First of a kind of commercial system
TRL 9	Full commercialization application

Modified from published reports [63, 64].

25.6 Conclusions

In light of considerable research and problems connected to biomass-based supercapacitors, this chapter focuses on numerous essential vital components that define the performance and use of biomass-based supercapacitors in the contemporary energy sector worldwide. The research that is currently available in the literature can be used to avoid some of the challenges in biomass-based supercapacitors, which create hurdles in their industrialization. The current situation of the global market, as well as the demand for supercapacitor use and the number of manufacturing businesses working in the global energy sector, have all been provided with relevant data. The number of countries in which energy is produced has also been presented. The most recent research on each method discusses the classification of biomass-based supercapacitors and the unique parameters of each approach and helps differentiate it from the others. These parameters assist in distinguishing each technique from the others. We have elaborated on the electrode materials and the composites. To make headway in the field of biomass-based supercapacitor research, fresh strategies that boost the performance of supercapacitors are necessary. Greater capacitances, strong cycling stability, and adequate rate capability must all be guaranteed by these techniques. We extensively discussed how the carbon materials, conventional electrolytes, newly adopted electrolytes, and their ionic conductivity all work together to enhance the electrochemical behavior of biomass-based supercapacitors. Even though some encouraging discoveries have been made in the biomass-based supercapacitor field, producing supercapacitors capable of meeting the demand for energy at the industrial level is still challenging. One must possess in-depth knowledge of the mechanisms underlying energy storage at the electrode and electrolyte interfaces, optimize the electrode design to create hierarchical agglomerated porous structures, and achieve favorable interactions at the electrode and electrolyte interfaces to improve the performance of supercapacitors. Then, and only then, will it be possible to boost the performance of supercapacitors . Due to the rising demand for supercapacitors in various applications, the market is likely to increase rapidly. These supercapacitors vary in size, capacitance, energy, power, and voltage and are sometimes built for specialized uses. Murata Technology, Eaton, Maxwell, Nippon Chemi-Con, and

Nesscap dominate the supercapacitor market. These significant organizations invested much in supercapacitor research and development to meet demand and stay ahead of competitors. Biomass is essential for supercapacitors' cost-effectiveness, high-quality carbon electrodes, non-toxic electrolytes, and packaging materials. Commercial applications utilize biomass-based supercapacitors scaled from experimental to industrial. This chapter discussed biomass-based supercapacitors' market trends, biomass's essential qualities, and researchers' supercapacitor devices and components. According to the authors of several studies, the only way to meet the energy demand is to rely on ongoing research to enhance the production of high-performance biomass-based supercapacitors. It is possible to speculate that the performance of supercapacitors will soon be improved and that their costs will also be optimized at some point in the not-too-distant future. Engineers and researchers will benefit from this chapter's information by adopting the best technique and type of biomass-based supercapacitor for industrial applications.

Acknowledgments

References

1 X. Xiao, T. Li, P. Yang, Y. Gao, H. Jin, W. Ni, W. Zhan, X. Zhang, Y. Cao, J. Zhong, L. Gong, W.-C. Yen, W. Mai, J. Chen, K. Huo, Y.-L. Chueh, Z. L. Wang, J. Zhou, *ACS Nano* **2012**, *6*, 9200–9206.

2 T. Chen, L. Qiu, Z. Yang, Z. Cai, J. Ren, H. Li, H. Lin, X. Sun, H. Peng, *Angew. Chem. Int. Ed.* **2012**, *51*, 11977–11980.

3 J. Bae, Y. J. Park, M. Lee, S. N. Cha, Y. J. Choi, C. S. Lee, J. M. Kim, Z. L. Wang, *Adv. Mater.* **2011**, *23*, 3446–3449.

4 S. S. Shah, E. Cevik, M. A. Aziz, T. F. Qahtan, A. Bozkurt, Z. H. Yamani, *Synth. Met.* **2021**, *277*, 116765.

5 A. Aziz, S. S. Shah, A. Kashem, *Chem. Rec.* **2020**, *20*, 1074–1098.

6 S. S. Shah, M. N. Shaikh, M. Y. Khan, M. A. Alfasane, M. M. Rahman, M. A. Aziz, *Chem. Rec.* **2021**, *21*, 1631–1665.

7 A. K. Mohamedkhair, M. A. Aziz, S. S. Shah, M. N. Shaikh, A. K. Jamil, M. A. A. Qasem, I. A. Buliyaminu, Z. H. Yamani, *Arab. J. Chem.* **2020**, *13*, 6161–6173.

8 M. M. Hasan, T. Islam, S. S. Shah, A. Awal, M. A. Aziz, A. J. S. Ahammad, *Chem. Rec.* **2022**, *22*, e202200041.

9 S. S. Shah, M. A. Aziz, Z. H. Yamani, *Chem. Rec.* **2022**, *22*, e202200018.

10 K. V. G. Raghavendra, R. Vinoth, K. Zeb, C. V. V. Muralee Gopi, S. Sambasivam, M. R. Kummara, I. M. Obaidat, H. J. Kim, *J. Energy Storage* **2020**, *31*, 101652.

11 K. Nanaji, A. Nirogi, P. Srinivas, S. Anandan, R. Vijay, R. N. Bathe, M. Pramanik, K. Narayan, B. Ravi, T. N. Rao, *J. Energy Storage* **2022**, *55*, 105650.

12 D. Bhattacharjya, D. Carriazo, J. Ajuria, A. Villaverde, *J. Power Sources* **2019**, *439*, 227106.

13 U. S. Sani, I. H. Shanono, *Akgec Int.l J. Technol.* **2016**, *6*, 1–7.

14 S. S. Shah, M. A. Aziz, *Bangladesh J. Plant Taxon.* **2020**, *27*, 467–478.

15 N. C. Deb Nath, S. S. Shah, M. A. A. Qasem, M. H. Zahir, M. A. Aziz, *ChemistrySelect* **2019**, *4*, 9079–9083.

16 C. K. Roy, S. S. Shah, A. H. Reaz, S. Sultana, A.-N. Chowdhury, S. H. Firoz, M. H. Zahir, M. A. A. Qasem, M. A. Aziz, *Chem. Asian J.* **2021**, *16*, 296–308.

17 M. Ashraf, S. S. Shah, I. Khan, M. A. Aziz, N. Ullah, M. Khan, S. F. Adil, Z. Liaqat, M. Usman, W. Tremel, M. N. Tahir, *Chem. Eur. J.* **2021**, *27*, 6973–6984.

18 M. A. Aziz, S. S. Shah, S. M. A. Nayem, M. N. Shaikh, A. S. Hakeem, I. A. Bakare, *J. Energy Storage* **2022**, *50*, 104278.

19 S. I. Basha, S. S. Shah, S. Ahmad, M. Maslehuddin, M. M. Al-Zahrani, M. A. Aziz, *Chem. Rec.* **2022**, *22*, e202200134, https://doi.org/10.1002/tcr.202200134.

20 S. Islam, M. M. Mia, S. S. Shah, S. Naher, M. N. Shaikh, M. A. Aziz, A. J. S. Ahammad, *Chem. Rec.* **2022**, *22*, e202200013.

21 T. Islam, M. M. Hasan, S. S. Shah, M. R. Karim, F. S. Al-Mubaddel, M. H. Zahir, M. A. Dar, M. D. Hossain, M. A. Aziz, A. J. S. Ahammad, *J. Energy Storage* **2020**, *32*, 101908.

22 M. Rauf, S. S. Shah, S. K. Shah, S. N. A. Shah, T. U. Haq, J. Shah, A. Ullah, T. Ahmad, Y. Khan, M. A. Aziz, K. Hayat, *J. Saudi Chem. Soc.* **2022**, *26*, 101514.

23 S. S. Shah, M. A. Alfasane, I. A. Bakare, M. A. Aziz, Z. H. Yamani, *J. Energy Storage* **2020**, *30*, 101562.

24 S. S. Shah, M. A. Aziz, A.-R. Al-Betar, W. Mahfoz, *Arab. J. Chem.* **2022**, *15*, 104058.

25 S. S. Shah, M. A. Aziz, E. Cevik, M. Ali, S. T. Gunday, A. Bozkurt, Z. H. Yamani, *J. Energy Storage* **2022**, *56*, 105944.

26 S. S. Shah, M. A. Aziz, W. Mahfoz, A.-R. Al-Betar, Conducting Polymers Based Nanocomposites for Supercapacitors in *Nanostructured Materials for Supercapacitors*, (Eds. S. Thomas, A. B. Gueye, R. K. Gupta), Springer, Cham, **2022**, Chapter 22, pp. 485–511, vol. *1*.

27 M. Usman, M. Y. Khan, T. Anjum, A. L. Khan, B. Hoque, A. Helal, A. S. Hakeem, B. A. Al-Maythalony, *Membranes* **2022**, *12*, 1055.

28 S. S. Shah, M. A. A. Qasem, R. Berni, C. Del Casino, G. Cai, S. Contal, I. Ahmad, K. S. Siddiqui, E. Gatti, S. Predieri, J.-F. Hausman, S. Cambier, G. Guerriero, M. A. Aziz, *Sci. Rep.* **2021**, *11*, 6945.

29 G. A. Safitri, K. Nueangnoraj, P. Sreearunothai, J. Manyam, *Curr. Appl. Sci. Technol.* **2020**, *20*, 124–135.

30 C. Karaman, O. Karaman, N. Atar, M. L. Yola, *Phys. Chem. Chem. Phys.* **2021**, *23*, 12807–12821.

31 T. R. Kumar, R. A. Senthil, Z. Pan, J. Pan, Y. Sun, *J. Energy Storage* **2020**, *32*, 101903.

32 I. I. Misnon, N. K. M. Zain, R. Jose, *Waste Biomass Valorization* **2019**, *10*, 1731–1740.

33 V. Yang, R. Arumugam Senthil, J. Pan, T. Rajesh Kumar, Y. Sun, X. Liu, *J. Colloid Interface Sci.* **2020**, *579*, 347–356.

34 X. Bo, K. Xiang, Y. Zhang, Y. Shen, S. Chen, Y. Wang, M. Xie, X. Guo, *J. Energy Chem.* **2019**, *39*, 1–7.

35 Y. Gong, D. Li, C. Luo, Q. Fu, C. Pan, *Green Chem.* **2017**, *19*, 4132–4140.

36 T. Wang, S. Hu, D. Wu, W. Zhao, W. Yu, M. Wang, J. Xu, J. Zhang, *J. Mater. Chem. A* **2021**, *9*, 11839–11852.

37 K. Aruchamy, K. Dharmalingam, C. W. Lee, D. Mondal, N. Sanna Kotrappanavar, *Chem. Eng. J.* **2022**, *427*, 131477.

38 D. Gandla, X. Wu, F. Zhang, C. Wu, D. Q. Tan, *ACS Omega* **2021**, *6*, 7615–7625.

39 Z. Husain, A. R. Shakeelur Raheman, K. B. Ansari, A. B. Pandit, M. S. Khan, M. A. Qyyum, S. S. Lam, *Mater. Sci. Eenrgy Technol.* **2022**, *5*, 99–109.

40 Z. Tan, J. Yang, Y. Liang, M. Zheng, H. Hu, H. Dong, Y. Liu, Y. Xiao, *J. Colloid Interface Sci.* **2021**, *585*, 778–786.

41 M. Xu, A. Wang, Y. Xiang, J. Niu, *J. Clean. Prod.* **2021**, *315*, 128110.

42 Y. Myung, S. Jung, T. T. Tung, K. M. Tripathi, T. Kim, *ACS Sustain. Chem. Eng.* **2019**, *7*, 3772–3782.

43 C. Ruan, K. Ai, L. Lu, *RSC Adv.* **2014**, *4*, 30887–30895.

44 A. Gopalakrishnan, C. Y. Kong, S. Badhulika, *New J. Chem.* **2019**, *43*, 1186–1194.

45 R. Rajendiran, M. Nallal, K. H. Park, O. L. Li, H.-J. Kim, K. Prabakar, *Electrochim. Acta* **2019**, *317*, 1–9.

46 J. Wang, P. Zhang, L. Liu, Y. Zhang, J. Yang, Z. Zeng, S. Deng, *Chem. Eng. J.* **2018**, *348*, 57–66.

47 I. I. Gurten Inal, Z. Aktas, *Appl. Surf. Sci.* **2020**, *514*, 145895.

48 G. Qiu, Z. Miao, Y. Guo, J. Xu, W. Jia, Y. Zhang, F. Guo, J. Wu, *Colloids Surf. A Physicochem. Eng. Asp.* **2022**, *650*, 129575.

49 G. Qiu, Y. Guo, Y. Zhang, X. Zhao, J. Xu, S. Guo, F. Guo, J. Wu, *Ind. Eng. Chem. Res.* **2022**, *61*, 16034–16049. 10.1021/acs.iecr.2c02815.

50 T. Kongthong, C. Poochai, C. Sriprachuabwong, A. Tuantranont, S. Nanan, N. Meethong, P. Pakawatpanurut, T. Amornsakchai, J. Sodtipinta, *J. Sci-Adv. Mater. Dev.* **2022**, *7*, 100434.

51 G. K. Veerasubramani, A. Chandrasekhar, Sudhakaran, M. S. P., Y. S. Mok, S. J. Kim, *J. Mater. Chem. A* **2017**, *5*, 11100–11113.

52 D. Potphode, S. Saha, C. S. Sharma, *J. Electrochem. Soc.* **2020**, *167*, 140508.

53 M. Ojha, X. Liu, B. Wu, M. Deepa, *Fuel* **2021**, *285*, 119246.

54 S. S. Gunasekaran, S. Badhulika, *Int. J. Hydrog. Energy* **2021**, *46*, 35149–35160.

55 T.-F. Hung, T.-H. Hsieh, F.-S. Tseng, L.-Y. Wang, -C.-C. Yang, -C.-C. Yang, *Nanomaterials* **2021**, *11*, 785.

56 İ. I. Gürten, *Turk. J. Chem.* **2021**, *45*, 927–941.

57 Z. Chen, X. Wang, B. Xue, Q. Wei, L. Hu, Z. Wang, X. Yang, J. Qiu, *ChemSusChem* **2019**, *12*, 1390–1400.

58 K. Nanaji, V. Upadhyayula, T. N. Rao, S. Anandan, *ACS Sustain. Chem. Eng.* **2019**, *7*, 2516–2529.

59 M. Horn, J. MacLeod, M. Liu, J. Webb, N. Motta, *Econ. Anal. Policy* **2019**, *61*, 93–103.

60 S. S. Shah, H. T. Das, H. R. Barai, M. A. Aziz, *Polymers* **2022**, *14*, 270.

61 A. J. S. Ahammad, N. Odhikari, S. S. Shah, M. M. Hasan, T. Islam, P. R. Pal, M. A. Ahmed Qasem, M. A. Aziz, *Nanoscale Adv.* **2019**, *1*, 613–626.

62 M. Vijayakumar, A. Bharathi Sankar, D. Sri Rohita, T. N. Rao, M. Karthik, *ACS Sustain. Chem. Eng.* **2019**, *7*, 17175–17185.

63 T. Altunok, T. Cakmak, *Adv. Eng. Softw.* **2010**, *41*, 769–778.

64 J. Straub, *Aerosp. Sci.Technol.* **2015**, *46*, 312–320.

65 F. Odeim, J. Roes, A. Heinzel, *IEEE Trans. Veh. Technol.* **2016**, *65*, 5783–5788.

66 D. Lemian, F. Bode, *Energies* **2022**, *15*, 5683.

67 H. Y. Tong, *Sustain. Cities Soc.* **2019**, *48*, 101588.

68 P. V. Radu, A. Szelag, M. Steczek, *Energies* **2019**, *12*, 1291.

26

Future Directions and Challenges in Biomass-Based Supercapacitors

Syed Shaheen Shah[1,2], Md. Abdul Aziz[1,3,], Muhammad Ali[1], Muhammad Usman[1], Sikandar Khan[4], Farrukh Shehzad[5], Syed Niaz Ali Shah[6], and Sami Ullah[3]*

[1] *Interdisciplinary Research Center for Hydrogen and Energy Storage (IRC-HES), King Fahd University of Petroleum & Minerals, KFUPM Box 5040, Dhahran 31261, Saudi Arabia*

[2] *Physics Department, King Fahd University of Petroleum & Minerals, KFUPM Box 5047, Dhahran 31261, Saudi Arabia*

[3] *K. A. CARE Energy Research and Innovation Center, King Fahd University of Petroleum & Minerals, Dhahran, 31261, Saudi Arabia*

[4] *Department of Mechanical Engineering, King Fahd University of Petroleum and Minerals, Dhahran 31261, Saudi Arabia*

[5] *Department of Chemical Engineering, King Fahd University of Petroleum & Minerals, Dhahran31261, Saudi Arabia*

[6] *Center for Integrative Petroleum Research, King Fahd University of Petroleum and Minerals, Dhahran 31262, Saudi Arabia*

* Corresponding author

26.1 Introduction

Future energy production and collection from renewable sources must be efficient and environmentally friendly, both in storage, and in use. The latter will utilize environmentally friendly fuel cells, batteries, and supercapacitors, whereas the former will rely on sources like solar, wind, or biomass refineries. Biomass is a resource that is particularly important for the principles of green engineering because it provides the opportunity to create thermochemical energy while also generating a waste product useful for creating components with excellent performance for electrochemical energy storage systems [1, 2].

According to their method of storing, pseudocapacitors, hybrid supercapacitors, and electrochemical double-layer capacitors (EDLCs) are different types of supercapacitors [3, 4]. While pseudocapacitors store charges through redox reactions, EDLCs do so via reversible ions adsorption at the electrode–electrolyte interface. The former uses mostly conductive polymers and metal oxides, and the latter uses carbonaceous electrode materials such as carbon nanofibers, activated carbon, carbon nanotubes, and graphene [5, 6]. Compared to EDLC electrodes, pseudocapacitive materials generally have a larger specific capacitance. However, carbon-based materials often offer a better rate and cyclic stability. Biomass-derived porous materials have been the main products evaluated in the search to

find more sophisticated electrode materials for supercapacitors [3, 4, 7]. To obtain outstanding performance, reasonable electrode material designs that consider the particular surface area, porous shape, and degree of graphitization are important. Because of their substantial specific surface area, hierarchically porous frameworks, and high structural stability, carbon produced by biomass has received considerable attention in the field of materials used for energy storage [4, 8–10]. Supercapacitors can attain high specific capacitance, high charge/discharge rates, and a long lifespan. Researchers have effectively created nanostructured carbon materials from various biomasses in all three dimensions for supercapacitor electrodes. Popular carbon materials with exceptional structure and competitive chemical performance include graphene and carbon nanotubes. Despite their effective application, energy storage materials still have a lot of issues. For instance, environmental degradation and sustainability challenge the chemical vapor deposition technique applied to create graphene from fossil fuels. Active carbon made from petroleum coke and graphite is nonrenewable and contaminative [11, 12]. Furthermore, under extremely difficult circumstances, nanostructured carbons are frequently produced from them.

Renewable biomass, like that from plants or animals, can be seen as an advantageous for the environment, as they release less pollution into the atmosphere. Among the energy storage materials, biomass with naturally occurring hierarchical structures as a precursor might be a viable option. Given that biomass is made from regenerative plants or animals, it is more affordable than other types of nanostructured materials. Additionally, there is a lot of research being done right now on how to make electrodes out of biomass, which is a very renewable resource. Biomass is the most easily accessible carbon precursor from plants, animals, or marine life. On the other hand, figures indicate that animal husbandry or living waste might cause critical environmental problems. As a result, it is believed that employing biomass in the production of activated carbon for supercapacitor electrodes is an effective way to address the issues of disposing of agricultural or daily-living biomass. Active electrode materials from biomass can naturally acquire specific porosity and layered topologies. Recently, there has been a lot of interest in developing activated electrode materials for electrochemical energy storage using biomass. Numerous active electrode materials from biomass have been created using hydrothermal carbonization, chemical activation, or physical activation [1, 13–17].

Evaluation of the performance of the different active materials when used as electrodes in supercapacitor applications and their straightforward comparison is a fairly challenging procedure because the absolute value of specific capacitance is most frequently used to describe a supercapacitor's performance, depending on several factors. Comparing data from similar systems, such as an electrode or device capacitance, which pertains to 3- or 2-electrode cells, should give one confidence. The electrode capacitance can be calculated from the capacitance of a 2-electrode symmetric device, although the calculated value is typically different from that obtained from a 3-electrode system [3]. Because it substantially impacts capacitance performance, the kind of electrolyte used, such as aqueous, organic, ionic liquid, gel, or even redox and hybrid electrolytes, should also be carefully investigated. Last but not least, when comparing capacitance values obtained using different techniques, such as cyclic voltammetry (CV), galvanostatic charge-discharge (GCD), or electrochemical impedance spectroscopy (EIS) measurements, it is imperative to verify that the data were collected under comparable settings for the supercapacitor charge state and, obviously, at same rates of applied voltages [14].

Batteries, the most common form of electrical energy storage, provide enough power for a variety of functions and requirements in daily life. Batteries transmit power slowly, as

seen in a Ragone plot in Figure 26.1 while storing a huge amount of energy in a comparatively small mass and volume. Therefore, they are only useful in systems that need much power and speedy storage. However, owing to their higher power density, superior durability, and rapid GCD cycles, electrochemical capacitors, often referred to as supercapacitors, have drawn considerable interest as an alternative to or in addition to batteries in energy storage systems. Creating novel processes to convert lignin into sustainable chemicals and useful materials is a vital step toward the high-value use of lignocellulosic biomass. Carbon materials made from lignin have a lot of potential

Figure 26.1 Ragone plot for capacitors, supercapacitors, and batteries.

for use in chemical and energy engineering, catalysis, and environmental cleanup. This study gives the state-of-the-art sciences and technologies for the controllable synthesis of lignin-derived carbon materials. Additionally, the controlling approaches for crystalline engineering, pore structure, and morphology are comprehensively described and critically examined. Future developments in the study of materials made of lignin include cost-effective, accurate carbonization tuning, and green chemical engineering. Future research directions have been suggested to develop lignin-derived carbon materials for practical uses [18, 19].

The production of porous materials requires natural biomass with interconnected channels and various microstructures, which affect the specific surface area of carbonized materials. Therefore, critically evaluating the choice of probable precursors from various biomass sources was deemed important. The purpose of this chapter is to showcase recent developments in synthesizing carbon compounds from various biomass precursors. The classic nanostructured electrode materials still have issues, for example, their low production rate, high cost, difficulties in heteroatoms doping, and ecologically toxic by-products. The detailed discussion of the impact of pore structure, surface characteristics, and graphitic degree on electrochemical performance may aid in the rational development of future biomass-derived carbon materials for supercapacitors. We also provide the data science and experimentation methods used to draw high-level links between structural features and electrochemical characteristics, revealing the most important influences on supercapacitor capacitance and power density [7, 9, 20–22]. The advancement of biomass-based supercapacitors has also been highlighted, along with its existing difficulties and future prospects.

By considering the various important aspects such as reducing the temperature to get excellent carbon for supercapacitors, unifying the methods for membrane preparation from biomass, providing enough concentration in developing high-performance electrolytes from biomass, developing the simple method for packaging materials, scaling up in an easy way with low cost, recycling the generated gas during pyrolysis as fuel, focusing on techno-economic analysis, preparing compatible supercapacitors with various instruments e.g. heart monitor (the current challenge is to meet up the optimum potential and capacitance), overcome safety concerns (e.g. minimizing the heat generation), and minimizing IR drop would bring up the biomass-based supercapacitors to a commercial level. Therefore, this systematic study will serve as a resource for other researchers interested in developing
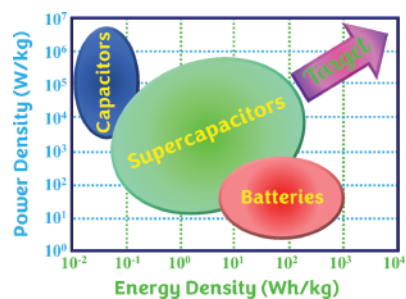
biomass-based supercapacitors as an alternative to conventional supercapacitors and batteries made of biomass materials.

26.2 Biomass-based Supercapacitors and Future Directions

Materials science, nanotechnology, and process engineering advancements progressively make it possible for biomass to be used in cutting-edge energy storage technologies. Notably, materials generated from biomass that vary from renewable organic biomolecules or biopolymers to inorganic multi-dimensional carbonaceous materials can support "green energy storage" systems by acting as sustainable components [15]. This section provides a thorough analysis of the production and possible use of biomass and biomass-derived components for high-performance supercapacitors. Understanding the associated biomass processing is given particular attention. Biomass utilization as electrode supports, active materials, binder materials, separators, and solid-state electrolytes in supercapacitors are methodically offered and discussed. The results showed that biomass has enormous capabilities for creating high-performance "green energy storage" systems that, in varying degrees, use environmentally friendly and sustainably produced supercapacitor components. In order to speed the industrialization of biomass, special attention should be paid to improving the processing technologies to optimize biomass use with high efficiency and low cost. Due to their natural abundance, exceptional capabilities, and distinctive architectures, biomass-based materials have become one of the most promising and sustainable components for various electrochemical energy storage and conversion systems. Biomass-based materials have been widely used as separators, electrolytes, binders, and substrate supports for various electrochemical applications because of their appealing electrochemical properties, which include stability throughout a large working voltage and high stability in various solvents [23].

Zea mays (corn) wastes were used in electrochemical energy storage devices by Hamidreza et al. [24]. The separator, electrolyte, binder, and electrodes – the four essential components of supercapacitors – can all be made from leftover corn. The plentiful and inexpensive biomasses considerably enhance the electrochemical characteristics of electrochemical energy storage devices, such as electrochemical durability and high specific capacitance, while reducing the environmental pollution. Moreover, due to the plentiful availability of raw ingredients, adequate electrochemical effectiveness, high-conductivity, and low-cost, carbonaceous materials generated from nanocellulose have also drawn considerable interest in ecofriendly energy storage [23, 25]. Due to the low-cost and environmental friendliness of biomass-derived materials and their derivatives and the simple fabrication processes, biomass-based electrochemical techniques are considered capable candidates for future "green" and renewable energy systems. Using biomass-derived materials, particularly carbonaceous materials, in a supercapacitor may help the electronic industries grow economically.

26.2.1 Utilization of Biomass-derived Carbonaceous Materials as Supercapacitor Electrodes

A variety of electrochemical applications require carbonaceous materials because of their variable capacity for charge storage and electron transmission. Carbon nanotubes,

graphene, carbon nanofibers, graphite, and activated carbon are a few examples of the many allotropic forms of carbon that are extensively employed as fundamental electrode materials in contemporary electrochemistry. For electrochemical energy storage applications, electrochemical sensors, electrochemical water oxidation, and other electrochemical processes, carbonaceous materials, for instance, are utilized as electrode materials. When used in electrochemical detection, bare electrodes usually have poor repeatability, weak electrocatalytic properties, a surface fouling effect, and the inability to discriminate between different identities. Thus, adding nanocarbon can considerably enhance the electrochemical performance of bare electrodes, including their sensing efficiency [26–28]. Activated carbon electrodes have a wide range of beneficial properties, but there are also a number of fascinating and important fundamental properties that need to be studied, such as transport phenomena, molecular sieving activity, the relationship between electrochemical performance and surface chemistry, and many more. Mao et al. [29] reported several nanocarbons for electrochemical applications, such as sensing, electrocatalysis, and energy storage. The performance of electrochemical sensors will be enhanced, and supercapacitor devices will be able to deliver more power thanks to the usage of nano-architecture carbon in electrode design [30]. Additionally, this indicates a significant future potential for nanocarbon in electrochemistry. The production of carbon-based active materials has been widespread, so it is vital to provide clever and useful tools to aid in and optimize material selection for the intended applications. Because of their exceptional electrical conductivity, porous topology, large specific surface area, and special stability, electrodes made from biomass-derived activated carbon are effective for supercapacitors. In addition to their pertinent physicochemical characteristics, carbonaceous materials from biomass may be created for very little money and come in various shapes with adaptive porosity, conductivity, and surface functioning.

Energy storage systems made from biomass are gaining popularity. Waste biomass can be carbonized and used as conductive additives and electrodes for sodium-ion, lithium-ion, metal-sulfur, and metal-oxygen batteries. Furthermore, with very little chemical modification, numerous biomolecules with redox-active groups can be employed as electrodes [31]. A special class of nanostructures for improving electrochemical applications is provided by biomass-derived carbon materials with outstanding electrochemical performance, particularly for sustainable electrochemical energy conversion and storage applications. Tao et al. [13] prepared carbon nanofibers made from walnut shells (waste biomass) by dissolving the biomass, electrospinning, and carbonizing the fibrils. They investigated the effects of high-temperature carbonization and thoroughly characterized the structural characteristics, morphology, and specific surface area of walnut shell-derived carbon nanofibers. Their electrochemical efficiency as Li-ion battery (LIB) electrode materials was also investigated. The results showed that the prepared carbon nanofibers anode exhibited high specific capacities of up to ~272 mAh g^{-1} at a current density of 30 mA g^{-1}, excellent rate capacities, and good cycling performance after 200 GCD cycles. The walnut shells derived carbon nanofibers electrodes, their FESEM images, and the corresponding electrochemical performances are shown in Figure 26.2. This report showed the enormous potential for transforming cheap biomass into high-value carbon for use in energy storage technologies such as supercapacitors.

Due to their distinctive and perfect structures and exceptional electrical, thermal, and mechanical properties, graphene and carbon nanotubes have received the greatest
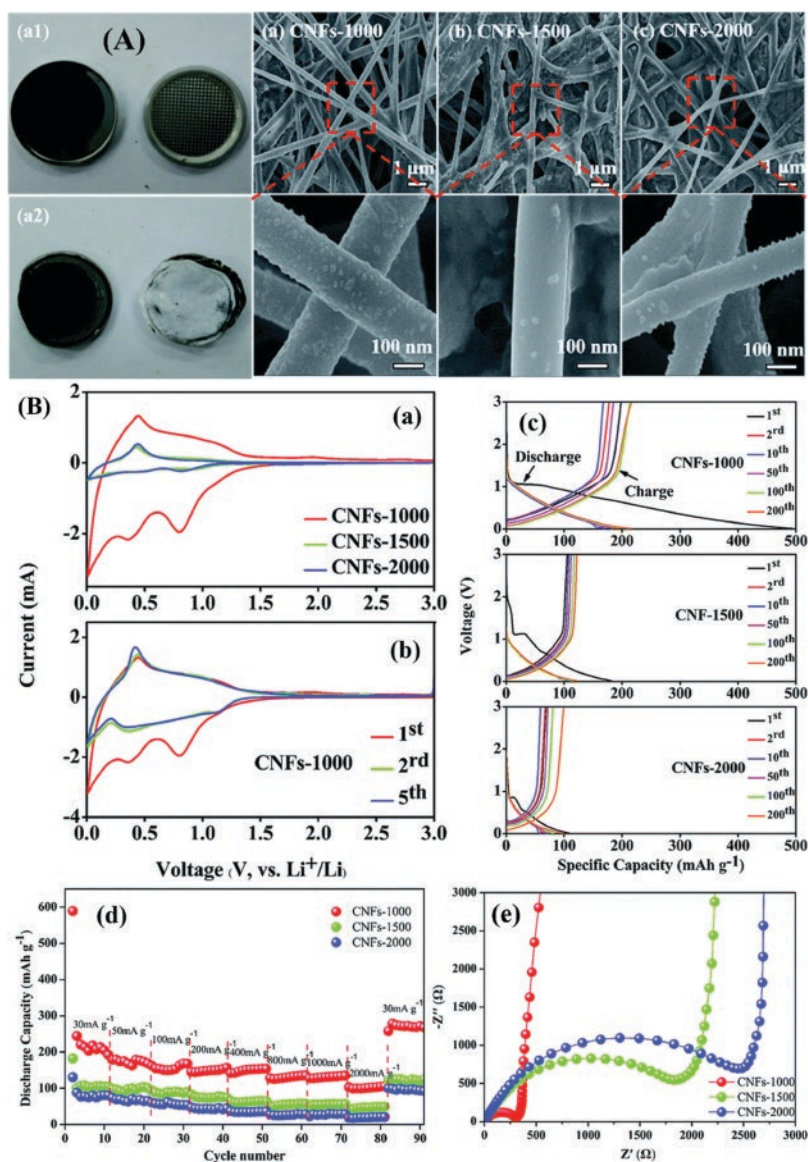
Figure 26.2 (A) Photographs of the carbon nanofibers electrode (a1) before and (a2) after stability and (a–c) FESEM micrographs of the carbon nanofibers electrodes after 200 GCD cycles. (B) Various electrochemical analyses of the LIBs. Cyclic voltammograms of the carbon nanofibers (a) 1st cycle at a 0.5 mV sec^{-1} scan rate of and (b) at first five cycles, (c) GCD curves of the carbon nanofibers at a 100 mA g^{-1} current density, (d) discharge capacities of the carbon nanofibers at different current rates, and (e) Nyquist plots of the carbon nanofibers. *Reproduced with permission* [13]. *Reproduced under the terms of the CC BY 3.0 license. Copyrights 2018, Tao et al.*

attention as the most valuable carbon nanomaterials. Creating sustainable, affordable, and environmentally benign carbon sources is fueled by previously unheard-of uses and market demand for graphene and carbon nanotubes. Materials made from biomass are cheap, renewable, and carbon-rich. Recent research reports the developments in producing

high-quality graphene and carbon nanotubes from various dissimilar biomass sources and their uses in electrochemistry, photocatalysis, and water purification [32]. The graphene and carbon nanotubes from biomass show new pathways for creative, high-performance supercapacitors. Recently Shah et al. [33] reported the production of electrochemically active and extremely stable jute sticks derived 3D interconnected graphene frameworks (3D-JGF) via an easy and effective green synthesis method. 3D amorphous activated carbon was initially produced from jute sticks at 850 °C in a nitrogen environment. After being heat treated at 2700 °C in an argon environment, the resulting 3D amorphous activated carbon converted to 3D-JGF, as shown in Figure 26.3(a). The produced 3D-JGF exhibited graphene-like nanosheet-type morphology (Figure 26.3(b–e)), demonstrated a very dynamic nature for the electrooxidation of sulfide, and exhibited an extremely stable nature in heat and chemical conditions. This research could be seen as making a significant contribution to developing an efficient and affordable method for producing 3D-JGF from biomass that could be utilized in high-performance supercapacitors.

Due to its cost, natural availability, high heteroatom concentration, and environmental friendliness, using carbon materials obtained from biomass is an effective solution to address various problems. Biomass-derived carbons differ from conventional nanostructured electrode materials because they already possess hierarchical structures. The development of porous carbon frameworks for supercapacitors has made considerable steps in terms of gravimetric performance in the last several years employing biomass wastes or residues. The majority of these evaluations, however, did not consider their volumetric performance. Notably, studies have demonstrated that using volumetric capacity rather than gravimetric performance to assess the GCD capacity of supercapacitors is more trustworthy and accurate. Recent studies have mainly focused on supercapacitor electrodes made from biomass with exceptional volumetric performance. Specifically, well-defined porous structure and morphology offer superior mass transport and many active sites; naturally, abundant heteroatoms offer superior charge transfer kinetics and improve surface
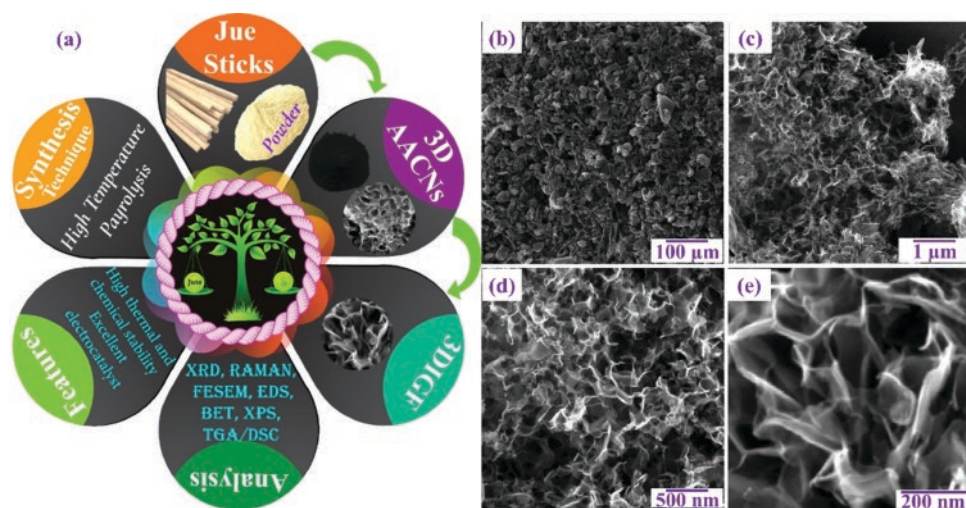
Figure 26.3 (a) Synthesis and features of jute sticks derived 3D-JGF and (b–e) FESEM micrographs at various magnifications. *Reproduced with permission* [33]. *Copyright 2022, Wiley.*

wettability, and trace metal doping results in increased pseudocapacitance due to the quick Faradaic reaction of metal redox couples. The fixed dimensions and structures of biomass species are cited as the fundamental disadvantage of biomass-derived carbon compounds, as they provide fewer design and modification options than traditional carbon materials. Low packing density and particular capacitance result in generally poor volumetric performance [34].

Energy demand is increasing due to a growing world population and rising living standards. The rapid growth of portable devices, technological developments, and hybrid electric vehicles have contributed to the urgent and expanding need for high-power, clean, sustainable energy sources. Currently, most of the energy we use is provided by fossil fuels. Global warming and the discharge of hazardous compounds are two environmental problems caused by using fossil fuels as an energy source. Developing high-power and high-energy density alternative energy storage and conversion technologies is crucial for resolving this problem. As a result, significant effort is being made to create sustainable and renewable energy sources.

26.2.2 Utilization of Biomass-derived Materials as Solid Electrolytes for Supercapacitors

The engineering of solid-state ionic conductors having efficient mechanical, optical, and electrical properties specifically created for practical use is one of the most recent advancements in electrochemistry. Additionally, there is a noticeable interest in low-cost, environmentally-friendly materials that support sustainability and recycling [35–37]. Solid-state electrolytes were created from regenerated biomass that addresses these issues and satisfied the requirements for electrochemical applications [36–38]. Solid electrolytes are interesting possibilities for advanced electrochemical applications because of their flexibility, viscoelasticity, and ionic conductivity. Solid electrolytes are employed in electrochemical devices, such as supercapacitors, fuel cells, and electrochromic devices, in addition to LIBs [39]. Solid polymer electrolytes have several benefits over liquid electrolytes, involving the absence of electrolyte leakage, the absence of internal shorting, and the creation of fireproof reaction products at the surface of electrodes. They can be used as an ion-conducting electrolyte by chemically modifying biomass-based cellulose to conduct ions at ambient temperature. This is possible because cellulose's unique linear chain molecular structure consists of continuous glucose units with several surface hydroxyl groups [40, 41].

Similarly, developing solid electrolytes for electrochemical applications depends on lignin and hemicellulose. Green natural lignocellulose was used to create a high-performance gel polymer electrolyte for LIBs [42]. Natural lignin was employed as a matrix to make gel polymer electrolytes to investigate an ecologically friendly and green gel polymer electrolyte. Lignin, liquid electrolytes, and water can be used to make the fabrication process quick and simple [43]. A biodegradable composite polymer membrane was created by creating polyvinylpyrrolidone (PVP) on a lignin matrix. Next, the necessary gel polymer electrolyte was created by absorbing the liquid electrolyte [44]. LIBs and supercapacitors now use liquid electrolytes; however, solid polymer electrolytes have the advantages of being flexible, non-flammable, and non-leaking. Biomass-based nanocellulose was used by Hengfei et al. [45] to develop solid electrolytes., as demonstrated in Figure 26.4. The
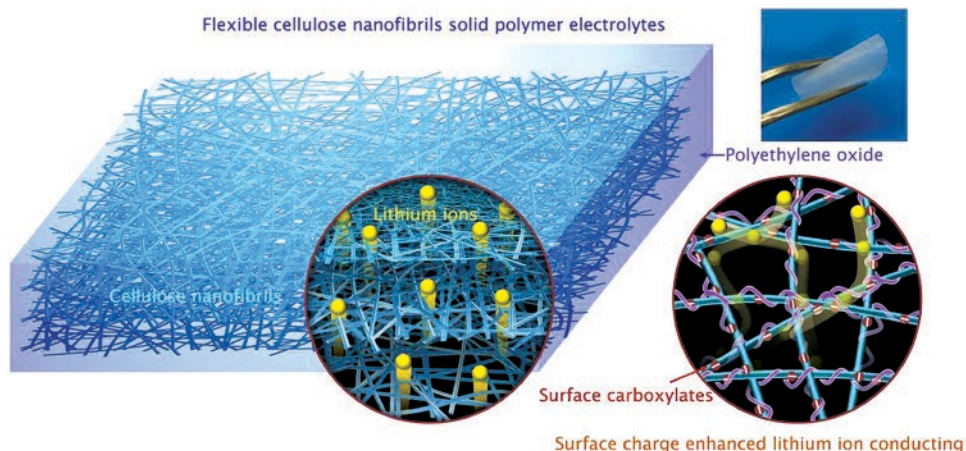
Figure 26.4 Biomass-derived solid electrolyte for LIBs. *Reproduced with permission* [45]. *Copyright 2020, Elsevier.*

increased surface charge density of the nanocellulose-based solid electrolytes causes an improvement in ionic conductivity. With its great electrochemical stability at high temperatures, the newly created solid electrolyte is promising to replace liquid electrolytes in supercapacitors. Various biomasses can be used as effective and environmentally friendly sources in creating solid electrolytes by considering the uses of nanocellulose, hemicellulose, cellulose, and lignin.

26.2.3 Utilization of Biomass-derived Materials as Electrodes for Supercapacitors with other Conducting Materials

Biomass-based materials hold great potential for developing electrochemical energy storage technologies [46]. The rapid expansion of modern society has made the problem of meeting the ever-increasing need for energy a significant one, and this problem will only worsen in the years to come. There has been a significant amount of focus placed on the research and development of energy storage systems that are affordable, sustainable, and kind to the environment. Batteries and supercapacitors have shown enormous promise as prospective power sources for portable gadgets, hybrid electric vehicles, and large-scale energy storage systems [46, 47]. In addition to improving performance and safety, the most difficult concerns for energy storage system development are lowering overall costs, realizing environmentally friendly processes, utilizing abundant and environmentally friendly raw materials, and creating systems that are as simple as possible.

In addition to a wide range of potential possibilities, materials generated from biomass have garnered increasing interest as desirable components of a wide variety of electrochemical energy storage systems [48–50]. Carbonized nanocellulose fibers, which have many surface functions, can combine with activated carbon to form a strongly linked composite. This composite is then utilized to improve the performance of electrodes, which are utilized in supercapacitors [51, 52]. Even today, topics such as energy storage from renewable sources while protecting the environment are very important. Converting energy,

storing it, and providing enough of it are the three most significant obstacles humanity must overcome in this century to properly protect the environment. With its unique structure and extraordinary qualities, nanocellulose has emerged as a viable and sustainable nanomaterial in this context. These properties include great stability in most solvents, natural abundance, high specific modulus, and low toxicity. Nanocellulose is a good contender for the construction of green renewable energy storage devices due to its low cost, easy availability, and simple synthesis procedures. Because of its low cost and ecofriendly nature, it is easily accessible [53].

Electrodes are essential components in producing high-performance supercapacitors, a process that requires outstanding electrochemical performance and adaptability [12, 20, 54, 55]. Both nanocellulose and graphene are excellent choices for electrode materials in supercapacitors. Due to its high chemical reactivity, excellent mechanical flexibility, and biodegrading capacity, nanocellulose is frequently used as a substrate material for electrical devices. Xing et al. [56] examined the layout, composition, and construction of the nanocellulose and graphene composites used for supercapacitors. Figure 26.5 provides a diagrammatic illustration of supercapacitors based on nanocellulose and graphene.

Lithium-ion batteries have established themselves as the primary power source for portable electronic gadgets due to their high output voltage, significant lifespan, and high energy density [46]. Three primary parts make up a LIB: the electrodes, the electrolytes, and the separators. The materials that make up the electrodes are the most important factor to consider when analyzing the performance of batteries. Nanocellulose has the potential to be used with other conductive materials to accelerate the development of more effective electrodes for LIBs.

Due to the inherent characteristics and structures of nanocellulose, one of its many potential applications that has garnered increasing attention is for energy storage. The tremendous application opportunities of nanocellulose-based materials in energy storage
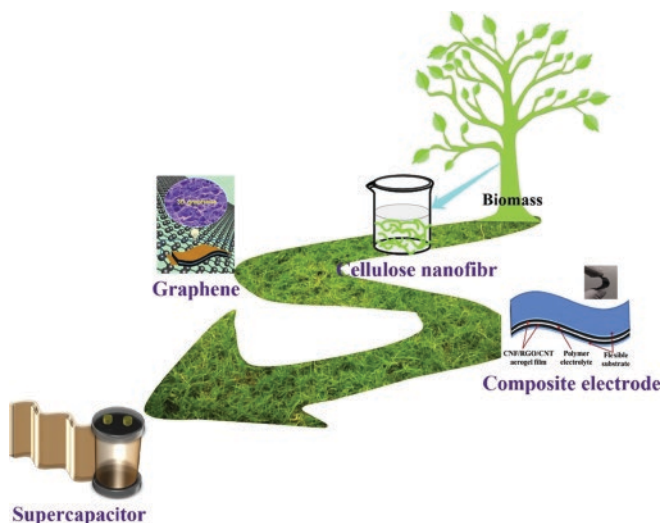
Figure 26.5 A schematic design of supercapacitors based on biomass-based nanocellulose and graphene. *Reproduced with permission* [56]. *Copyright 2019, Elsevier.*

applications will become clear once fundamental knowledge has been attained. This investigation showed that nanocellulose possesses both an application potential and an amazing value as a support nanomaterial for energy storage. Biomass-derived nanocellulose may soon become substantial and powerful multifunctional nanomaterials thanks to the development of more improved procedures for preparation, processing, and characterizations. These nanomaterials have a enormous potential for applications involving electrochemical energy storage, especially in supercapacitors.

Since there is a requirement for producing carbon materials of outstanding quality for usage in various applications, biomass consisting of lignocellulose can also be turned into carbon materials through pyrolysis. The thermal degradation of biomass cellulosic materials into carbonaceous materials under an inert atmosphere is referred to as biomass pyrolysis. This decomposition often takes place at temperatures more than 400 °C. The characteristics of processed carbon materials are extremely dependent on the types of biomass used and the techniques used to prepare them [25]. The primary processes involved in preparing novel carbon materials include pyrolysis, activation, and the pre-treatment of raw materials [20, 25]. Because the compositions and characteristics of the various biomass resources are so highly diverse, the characterization of the biomass feedstock is particularly crucial in determining whether or not it is suitable for conversion into carbon compounds. Various agricultural byproducts, include date palm leaves [57], *Syzygium cumini* leaves [58], *Albizia procera* leaves [59–61], banana leaves [54], tal palm leaves [26], nettle fiber clone [9], *Pithophora polymorpha* filaments [55], and jute sticks/fibers [7, 19, 25, 28, 33, 62–64], sources that have been used in the production of carbon products at a minimal cost. However, a great deal of research has been done to transform jute into innovative carbonaceous materials, comprising nanocarbon, for useful applicationssuch as energy storage, sensors, and waste-water treatment, due to its environmental friendliness, high carbon content, biodegradable nature, and low ash content [7, 25, 26, 28, 54, 55, 58, 59, 61].

Jute-derived carbon has been the subject of extensive research over the past few years, including the production of nanocarbon via direct pyrolysis to adjust the properties of carbon materials, such as surface functionality, pore characteristics, morphology, and surface area, to increase its suitability for real-world applications [7, 19, 25, 28, 33, 62–65]. Similar to this, activation – the process by which biomass is transformed into activated carbon – is crucial for creating high-quality carbon products. Physical activation and chemical activation are additional categories for the activation process. Our research group has reported the full specifics of the activation procedure [25]. A few of the preparations of the nanocarbon that is generated from biomass are also briefly explained [19, 25].

At a temperature of 800 °C, Aziz et al. [66] generated jute-derived activated carbon nanosheets by activating the carbon with sodium bicarbonate. Figure 26.6 presents a simplified diagrammatic representation of the jute-derived activated carbon nanosheets preparation procedure. In addition to this, they utilized a straightforward acid treatment to accomplish carboxylic acid functionalization of the jute-derived activated carbon nanosheets. The carboxylated jute-derived activated carbon nanosheets demonstrated a significantly greater surface area in comparison to other types of nanocarbon, such as carboxylated CNTs [66]. When it came to the removal of the heavy metal Pb^{2+} from water, the carboxylated jute-derived activated carbon nanosheets demonstrated outstanding effectiveness. For the synthesis of porous jute-derived carbon with a graphene-like structure,
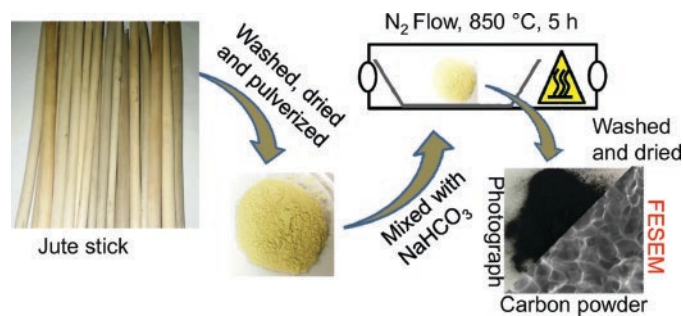
Figure 26.6 Schematic representation for jute-derived activated carbon nanosheets preparation. *Reproduced with permission* [66]. *Copyright 2019, Springer-Verlag GmbH Germany, part of Springer Nature.*

Nanaji et al. [67] utilized a straightforward activation technique as well. In another investigation, the same group found that jute sticks could be the source of jute-derived carbon with graphitic porous nanosheet-type morphology [68]. The produced jute-derived carbon was utilized in two distinct applications: one as electrode material for an ultrafast supercapacitor [67] and the other as an electrode material for a LIB [68]. Recently, Shaheen et al. [7] created extremely effective porous hierarchical jute-derived activated carbon nanosheets by pyrolyzing jute sticks using a straightforward pyrolysis method. The electrochemical energy storage performance of two different types of activated carbon, one commercially available and the other produced by jute-derived activated carbon nanosheets, were examined and compared. These activated carbons were utilized as electrode materials. Activated carbons were utilized in conjunction with a bioelectrolyte based on glycerol to create electrochemical double-layer supercapacitor devices. The jute-derived activated carbon nanosheets-based supercapacitor generated a maximum specific capacitance of 150 $F g^{-1}$ at a 10 mV sec^{-1} scan rate. This specific capacitance is significantly higher than the specific capacitance of commercially available activated carbon-based supercapacitors, which is only 29 $F g^{-1}$ at 10 mVsec^{-1}. The supercapacitor based on jute-derived activated carbon nanosheets demonstrated a specific energy density of 20 Wh kg^{-1} at a specific power density of 500 W kg^{-1} with outstanding performance even after being subjected to 10000 GCD cycles. The scientists conducted a study in which they evaluated the performance of commercially available activated carbon to that of the jute-derived activated carbon nanosheets not including conductive additives for use in supercapacitor applications. They found that the treated jute-derived activated carbon nanosheets showed potential as a candidate for use in energy storage materials.

Raziyeh et al. [69] have developed various biomass-derived nanoporous activated carbons with varying pyrolysis temperatures and activation agent (KOH) to carbon ratios. The prepared activated carbon had a morphology that was primarily nanofibers, and it demonstrated a large surface area (up to 2580 $m^2 g^{-1}$). The activated carbon was utilized as a nano-adsorbent to assess its applicability concerning the adsorption of H_2S and CO_2. Figure 26.7 displays the FESEM micrographs of the biomass-derived activated carbon obtained under various experimental settings. To create activated carbon from jute sticks, Asadullah et al. [70] used a combination of physical and chemical activation techniques. To produce activated carbon, several activating agents were necessary for the physical and chemical
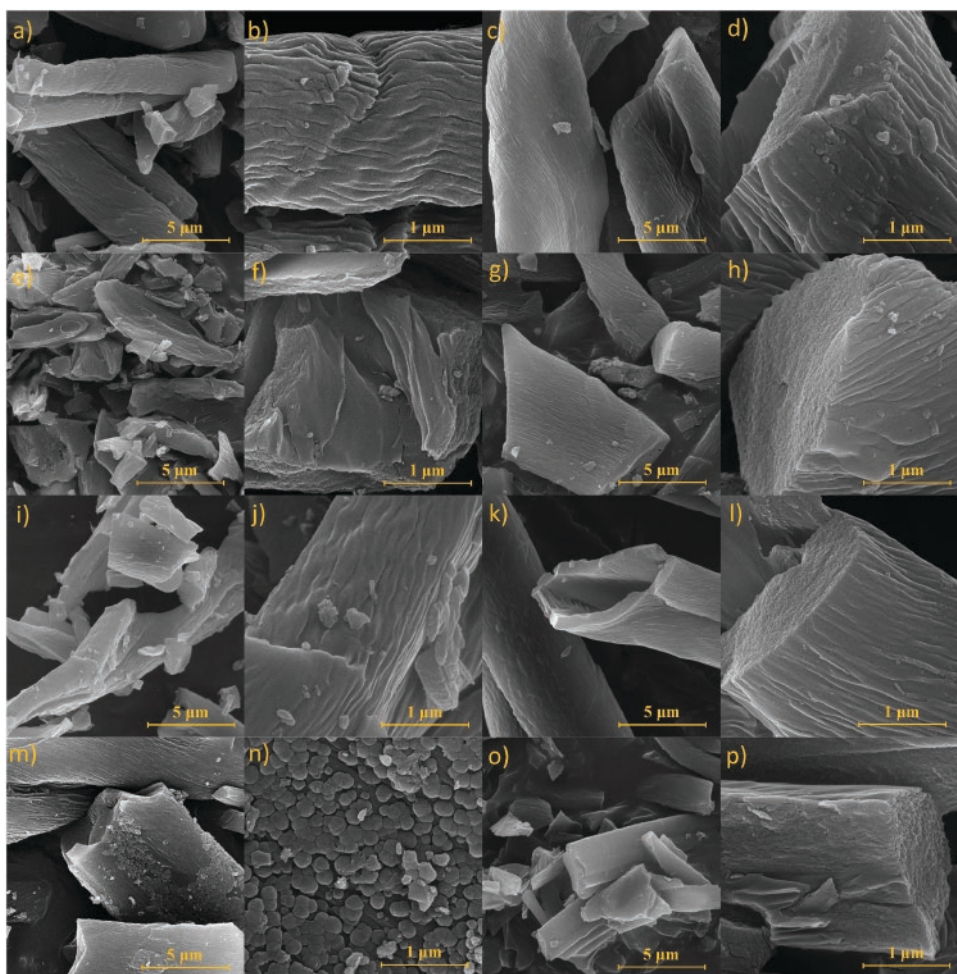
Figure 26.7 FESEM images of the jute-derived activated carbon synthesized at different experimental conditions. *Reproduced with permission* [69]. *Copyright 2021, Elsevier.*

activations of jute (fibers and sticks). These activating agents included $NaHCO_3$ [7, 66], $CuCl_2$ [16], KOH [17, 67, 68, 71, 72], H_3PO_4 [73–78], CO_2 [77, 79], steam [70, 79–81], and $ZnCl_2$ [28, 70, 79, 81]. Because its pores or actual particle sizes are in the nano ranges, biomass-derived carbon materials, in their entirety, can generally be considered to be a form of nanocarbon. Biomass-derived carbon has been utilized in the fields of water treatment [70, 75, 79, 82], electrochemical sensors [28, 66], and energy storage [7, 67, 68, 83].

Recently, it has been revealed that natural jute fiber can be used in ecofriendly energy systems, including supercapacitors and sensors [84]. In order to demonstrate an appealing environmental solution in numerous industrial applications, they created supercapacitor-powered fabricated sensors utilizing biocompatible and sustainable jute fibers. Food packaging is an essential component of the food industry and aids in maintaining food and drink storage hygienically to maintain food safety. Toxins harmful to human health can be released from many packing materials, including plastic, polyethylene, and other

materials. Nanocellulose paper will be a great resource for packaging in the food safety industry. Given the rigorous standards for food safety and environmental awareness, cellulose nanofibers are an excellent choice for biodegradable food packaging. Agricultural food packaging has made use of them [85]. Nanocellulose has been utilized in the food sector as hydrophobic coatings, packaging films, and reinforcing agents for hydrophobic polymers in nanocomposites [86]. One of the remarkable developments of nanotechnology is the development of nanocellulose-based bio-composites, which can be used in packaging applications to replace traditional petroleum-based plastics that are not biodegradable. A study showed that nanocellulose-based bio-composites could be a viable alternative to conventional packaging materials with improved characteristics. Jute fibers could be treated in an industrial setting in a natural, clever, and inexpensive way to encourage the reinforcement's attachment to the matrix in jute fiber-reinforced composite parts. Plant genetic material could be preserved using hydrophobic polymers by cryopreservation. Additionally, nanocellulose was employed to create thermoelectric paper and an ultrafiltration membrane [87–89].

Despite being abundant in nature, using lignin and cellulose nanofibers for energy storage is still a work in progress. This could be caused, among other things, by the carbon production of heat-treated lignin and cellulose nanofibers. After carbonization, the carbon production of cellulose and lignin is decreased to 40% and 10–30%, respectively. Another significant obstacle is the poor electrochemical performance of electrospun lignin/cellulose nanofibers in supercapacitors. Compared to PAN and other carbon compounds made from petroleum, lignin/cellulose nanofiber electrodes perform noticeably poorer. The electrospinning technique can create fine nanofibers if the fiber shape is controlled. However, several factors can impact how nanofibers form. It is still difficult to adjust all of these factors at once and how it affects the resulting nanofiber. This is because improving every parameter at once needs multiple trials runs. Such tests are ineffective and time-consuming. Aqueous electrolyte use restricts the cell voltage of supercapacitors to around 1.0 V to prevent supercapacitor rupture caused by hydrogen gas development on the negative electrode and oxygen gas evolution on the positive electrode at higher potentials. Manufacture of high-performance supercapacitors based on lignin or cellulose precursors usually employ aqueous electrolytes [90].

26.2.4   Application of Computational Methodologies in Biomass-based Supercapacitors

It is challenging to directly measure equilibrium properties and non-equilibrium ion transport at the nanoscale in experiments because they differ significantly from bulk systems. Understanding the mechanisms and properties of various transport processes in the electrolytes, porous electrodes, and at the interface of the electrodes and electrolytes at the nanoscale is essential for enhancing the performance of supercapacitors through computational and theoretical research methods. Numerous computational and theoretical methods, including density functional theory (DFT) [2, 91], molecular dynamics simulation (MD) [92, 93], Grand Canonical Monte Carlo (GCMC) [94, 95], mean-field theory (MFT) [96], and machine learning (ML) [97–99], have been extensively utilized in the study of ionic transport and charging dynamics, electrical double layer capacitance, quantum

capacitance, and pseudocapacitance. Within the scope of DFT, MD, GCMC, MFT, and ML approaches, equilibrium thermodynamic-based simulations can be done to analyze the electrical double layer (EDL) structures and capacitances in various electrode pore geometries and electrolyte components. By minimizing the grand potential, we may derive the density profiles of the solution species, including anions, cations, and solvent molecules, within the pore [100]. The differential capacitance of electric double layers in ionic liquids and its association with the surface charge density, ion size, and concentration has been established using classical DFT [101]. Based on the electronic structure of the electrode material, which can be estimated using electronic DFT, quantum capacitance also significantly influences the supercapacitor's overall capacitance [2]. By computationally integrating the equations of motion for individual atoms, MD simulation tries to predict the EDL structural and specific capacitance of thermodynamic systems. The MD simulation outcomes depend on the force fields employed for electrode/electrolyte interactions. Kiyohara et al. [94, 95] proposed constant voltage GCMC as a viable method for solving thermodynamic equilibrium problems at the electrode–electrolyte interface for a two-electrode system with planar electrodes and the hard-sphere ion model.

Dynamic DFT has enormous potential as an alternative multiscale technique for studying non-equilibrium ion transport in porous electrodes and optimizing materials and processes. The Poisson-Nernst-Planck equations omit ionic steric effects and electrostatic correlations, whereas dynamic DFT provides a thorough and effective method for describing them [102–104]. Using approximations to represent steric effects and electrostatic interactions, a MFT can be utilized to capture the "bell" or "camel" shaped differential capacitance curves that are frequently studied in experiments [96]. Moreover, the published experimental data has been utilized for training ML models to study the capacitance of carbon-based supercapacitors [97–99]. The data-driven method can be used as an alternate method to build useful correlations between the material's properties and their performance without invoking physical details.

26.3 Biomass-based Supercapacitors and Challenges

The usage of biomasses as one of the primary precursors for the electrode materials used in supercapacitors is on the rise. First, it is a readily available and inexpensive resource, which motivates researchers and entrepreneurs. Supercapacitors made from biomass have a power density of 1 to 10 kW kg^{-1}, which is very promising compared to batteries. This is because batteries charge and discharge more slowly than supercapacitors. Carbon-based electrodes made from biomass have a very long shelf life, allowing supercapacitors to use these electrodes to store charges for a very long time. Supercapacitors are also suitable for military applications since they can maintain their capacitance after millions of cycles at temperatures between 40 and 70 °C because of their minimal heat losses. Researchers have produced and used activated carbon obtained from biomass for various purposes over the years, depending on their structural and chemical compositions. However, the most recent research makes a lot of noise regarding producing activated carbon using biomass because of its simple synthesis technique, high specific surface area, powerful conductivity, and hierarchical pore size distribution. The pre-carbonization procedure and the activation

step are two essential processes in the current trends to manufacture activated carbon from biomass. Although little progress has been made in this area, pre-carbonization is an important step in creating very porous carbon. To produce sheets of highly conductive and nanoporous activated carbon, it has been shown that the acid treatment approach employed in pressurized Teflon bombs is more effective than low-temperature heating. These results highlight the pre-carbonization process's significance in influencing the final activated carbon's high conductivity, heteroatom doping, and porosity. Additionally, for biomass-derived carbon to work effectively with EDLC, an ideal balance of pore size, specific surface area, and high conductivity is needed. Thus, after pre-carbonization, the porosity and specific surface area of activated carbon can be modified using contemporary synthesis methods such as chemical, physical, chemical, or microwave-assisted activation methods. Chemical activation techniques are more expensive and complicated than physical processes, which produce high-quality products but call for handling and employing dangerous substances. Despite being superior in terms of saving time, money, special circumstances, and high-temperature equipment, microwave activation and synthesis techniques in industrial settings are still in their infancy. However, due to their superior scalable method, simple synthesis, and improved carbonization and activation procedures, ongoing efforts are required to manufacture highly porous and activated carbon from biomass [105]. In addition to the many benefits of biomass-based supercapacitors, there are several significant challenges, as indicated in Figure 26.8. It is challenging to fully embrace lignin or cellulose nanofiber electrode materials despite the vast array of benefits they offer in energy storage due to a number of serious drawbacks. The various barriers to the widespread use of lignin/cellulose-based electrode materials are discussed in this section.

One of the most crucial elements is the biocompatibility of biomasses, which may be evaluated primarily through ecotoxicity, life cycle evaluation, and leaching behavior studies. Studies on ecotoxicity are mostly used to determine whether a biomass product poses a threat to the environment. A chemical-specific technique and a toxicity-based approach are commonly used for an ecotoxicity test. However, a combination of both methods using biomass source materials and their aqueous/gaseous extracts is the most effective method for carrying out ecotoxicity testing. If at least one pollutant concentration surpasses the predefined threshold values or if at least one biological test is successful, the biomass materials are considered economically viable in this test. The chemical activation of biomass materials is a common process that increases specific surface area while also leaving behind various toxic chemicals that are difficult to remove. Additionally, it is often still uncertain how mobile leftover pollutants are. Also, the preparation of carbon from biomass require high temperatures, which is a challenging process. The industrialization standard and the environment are major obstacles to the widespread use of biomass-based supercapacitors. For different applications, specialized standards should be established; these specifications relate to the current collector's electrolyte, porosity, and biomass slurry coating. The other challenge is scaling up research for laboratory-level materials with approved procedures that may be used on a bigger

Figure 26.8 Various challenges in biomass-based supercapacitors.

scale. The primary issue in processing biomass-based supercapacitors on a big scale is the reduced activated carbon yield. This problem can be resolved by correctly combining the precursor with the carbonization and activation processes in one tank. The graphitic structure can also be created by incorporating catalysts and organic chemicals in the precursors to include more carbon. Due to their EDLC phenomenon, carbon-based supercapacitors made from biomass have a significantly lower energy density. To get around this, the energy density of the biomass precursors can be increased by doping them with heteroatom dopant atoms before or after carbonization. Nevertheless, the potential operating window can be increased by using organic, ionic liquid, redox, and polymer gel electrolytes. The specific capacitance and potential window are concurrently increased when both requirements are met, considerably increasing the energy density. Engineering has little control over the processes that lead to the carbonization and graphitization of biomass precursors. This results in the random distribution of micro-, meso-, and macropores over the carbonized biomass, which reduces the effectiveness of ion and charge transfer. To regulate the graphitized carbon's pore size distribution and orientation, various engineering techniques can be applied to precursors created from biowaste. To achieve this, alternative activators or activation processes, such as hydrothermal and air activation, could be utilized in place of the currently employed activation agents, resulting in biomass-derived carbon with higher nitrogen levels and self-supporting qualities. Additionally, nothing is known about the precise addition of surface chemistry and pore size distribution on the electrochemical performance of biomass-based supercapacitors. As a result, scientists are always examining how specific porosity variables affect the performance of electrochemical systems. Quantifying sustainability in using risky chemicals, difficult processing techniques, harmful gas emissions, etc., is a big problem for materials made from biomass. Therefore, reducing these negative impacts is preferable as is choosing extremely sustainable processing methods. Researchers recently suggested creating hybrid supercapacitors, which combine batteries-based and biomass-based supercapacitors, to increase performance. This method results in quick acceleration, reliable starting in cold weather, extended battery life, and braking energy recovery. Numerous uses are advanced, especially in hybrid electric vehicles. In addition to these uses, supercapacitors are also currently used to start internal combustion engines instead of conventional lead acid batteries, for high-speed localized energy delivery, to start electric motors in industrial installations, and for voltage stabilization along electric railway lines, which eliminates the need for extra supply wires by storing and delivering energy to trains when they accelerate.

Biomasses as precursors play a crucial role in developing a greener and more sustainable carbon synthesis techniques for creating activated carbon for energy storage applications due to their widespread availability and quantity. It is still uncertain how to choose the best biomass resources and tie these features to electrochemical performances to generate suitable micro and nanostructures (in terms of pore shapes and sizes) by activating carbon preparation processes. The high surface area of EDLC candidates can be combined with the pseudocapacitive action of a second component in the resulting structures by nitrogen doping. It is necessary to examine and optimize several aspects of this approach, including which N-dopant to employ and in what proportion. Such data are missing from current investigations. It is challenging to maintain doping concentration and ratio during pyrolysis and activation. An additional understanding of the electrochemical pathways is required to examine the impacts of heteroatom doping on biomass-based activated carbon in terms

of rate capability, chemical stability, cycling performance, and capacitive retention. The notion that all green devices with the required energy and power density to compete with conventional batteries and capacitors may be manufactured affordably and easily is supported by a single-step effort to produce N-doped carbon derivatives. Building viable carbon electrodes for supercapacitors will require more work to scale up the production of activated carbon electrodes made from biomass. To advance the industry must provide ecofriendly, high-performance materials and long-range hybrid vehicles. Building environmentally acceptable batteries that use biomass wastes as carbon sources rather than potentially harmful materials is essential [106].

Since the morphologies of biomass are often irregular, it can be difficult to precisely control pore properties like shape and structure, which affect rate performance and power density. Additionally, it is unknown how pore size, surface area, and surface chemistry affect the electrochemical performance of supercapacitors made from biomass for energy storage. Researchers still struggle with understanding the ion diffusion process in the hierarchical pore structure. It is possible to use biomass to make flexible electrodes. A new field of study will result from this. With continuous research on this topic, there may be excellent opportunities to achieve practical usage of biochar materials in renewable energy conversion and storage [98]. While lignin and cellulose nanofiber electrode materials provide many benefits for energy storage, several significant drawbacks make it challenging to employ these materials effectively. The various barriers to the widespread use of lignin and cellulose-based electrode materials will be described in this section.

A composite filament made of lignin and cellulose nanofibres (CNFs) was recently created by Geng et al. [107] using a microfluidic spinning process and in situ interfacial complexation procedures. The carbonization and stabilization of the hierarchical assembly of well-ordered lignin/CNFs crosslinked with biomass chitosan led to the creation of biomass-based CFs with fine graphitic microcrystals. The CF tensile strength may reach 1648 MPa when the lignin content was 75 weight percent, exceeding most values noted in the literature. From plant protein-lignin precursors, Yang et al. [108] created self-standing nitrogen-doped CF networks. In preparing them it was difficult to keep the fiber structure throughout the carbonization process. The results demonstrated that electrospun fibers with protein-to-lignin ratios ranging from 50:50 to 20:80 might retain their fibrous structure after carbonization. This discovery has the potential to increase the value of plant proteins and lignin as waste products from agricultural processing. However, cellulose's poor carbon yields severely restrict its use as a precursor for carbon fibers. Biomass products from agriculture and forestry have a lot of potential as starting points for the production of sustainable activated carbons used in supercapacitor applications. Although significant efforts have been made to design supercapacitors up to this point, there are still a number of difficulties that need to be resolved in order to further enhance the electrochemical performance of materials in supercapacitor applications.

26.4 Conclusions

In conclusion, it is sustainable and affordable to use abundant biomass to create biomass-based materials with outstanding electrochemical characteristics for supercapacitors. The chemical makeup, pore structure, and experimental settings all significantly impact the electrochemical performance. To produce a high-quality biomass-based product, good

design must be used in selecting the source material and the suitable pyrolysis or activation procedure. Given the variety of biomass resources, a thorough investigation of the electro-capacitive characteristics of biomass species and organs has been conducted for this chapter. Analysis of the precursor in terms of plant, microbial, and animal remnants is a useful practice, and distinct potential qualities should be summarized to maximize biomass-based active carbon's electrochemical properties. The preparation of 0D–3D interconnected porous frameworks, heteroatom doping, and the degree of graphitization, which can increase the energy and power densities, are examples of how they differ from structure and compositional design. The successful conversion of biomass to nanostructured carbon creates a new method for utilizing naturally occurring frameworks. Several significant obstacles and opportunities are highlighted in developing biomass-based carbon in super-capacitors, even though advanced research on the material has demonstrated comparably high electrochemical performance, high-rate capability, and cycling ability. A broad guideline for the development of next-generation energy storage devices may be found in this chapter. It is a potential area for developing renewable and biomass-derived materials. Thus, the research should focus on free-standing supercapacitors, excellent electrochemical performance, and favorable mechanical qualities. Highly conductive and flexible carbon electrode materials are produced using the two main techniques for producing free-standing carbon materials: simple one-step carbonization and activation preparation processes and the deposition or embedding of carbon nanotubes onto stretchable or flexible substrates. These supercapacitors have dramatically increased energy density without compromising their power capacity. Additionally, biomass-based binder-free supercapacitors will advance this promising area of electrical energy storage and work to find ways to use it practically in the near future. This progress report presents a comprehensive summary of recent advances in the rational design and fabrication of innovative supercapacitor materials produced from biomass. Additionally, it methodically explores the key elements – from fundamental chemistry to operational assembly – that significantly impact the volumetric performance of materials obtained from biomass. By considering the various important aspects such as reducing the temperature to get excellent carbon for supercapacitors, unifying the methods for membrane preparation from biomass, providing enough concentration in developing high-performance electrolytes from biomass, developing the simple method for packaging materials, scaling up in an easy way with low cost, recycling the generated gas during pyrolysis as fuel, focusing on techno-economic analysis, preparing compatible supercapacitors with various instruments, overcome safety concerns, and minimizing IR drop would brought up the biomass-based supercapacitors to a commercial level. Therefore, this systematic study will serve as a resource for other researchers interested in developing biomass-based supercapacitors as an alternative to conventional supercapacitors and batteries made of biomass materials. We hope our timely study will provide future supercapacitor device designers with a beneficial overarching framework.

Acknowledgments

References

1 J. L. Goldfarb, G. Dou, M. Salari, M. W. Grinstaff, *ACS Sustain. Chem. Eng.* **2017**, *5*, 3046–3054.

2 S. S. Shah, M. A. Aziz, E. Cevik, M. Ali, S. T. Gunday, A. Bozkurt, Z. H. Yamani, *J. Energy Storage* **2022**, *56*, 105944.

3 S. S. Shah, S. M. A. Nayem, N. Sultana, A. J. S. Ahammad, M. A. Aziz, *ChemSusChem* **2022**, *15*, e202101282.

4 S. S. Shah, M. A. Aziz, Z. H. Yamani, *Chem. Rec.* **2022**, *22*, e202200018.

5 C. Zhong, Y. Deng, W. Hu, J. Qiao, L. Zhang, J. Zhang, *Chem. Soc. Rev.* **2015**, *44*, 7484–7539.

6 G. Wang, L. Zhang, J. Zhang, *Chem. Soc. Rev.* **2012**, *41*, 797–828.

7 S. S. Shah, E. Cevik, M. A. Aziz, T. F. Qahtan, A. Bozkurt, Z. H. Yamani, *Synth. Met.* **2021**, *277*, 116765.

8 M. A. Aziz, S. S. Shah, S. M. A. Nayem, M. N. Shaikh, A. S. Hakeem, I. A. Bakare, *J. Energy Storage* **2022**, *50*, 104278.

9 S. S. Shah, M. A. A. Qasem, R. Berni, C. D. Casino, G. Cai, S. Contal, I. Ahmad, K. S. Siddiqui, E. Gatti, S. Predieri, J.-F. Hausman, S. Cambier, G. Guerriero, M. A. Aziz, *Sci. Rep.* **2021**, *11*, 6945.

10 M. M. Hasan, T. Islam, S. S. Shah, A. Awal, M. A. Aziz, A. J. S. Ahammad, *Chem. Rec.* **2022**, *22*, e202200041.

11 C. Lu, S. Xu, C. Liu, *J. Anal. Appl. Pyrolysis* **2010**, *87*, 282–287.

12 M. Ashraf, S. S. Shah, I. Khan, M. A. Aziz, N. Ullah, M. Khan, S. F. Adil, Z. Liaqat, M. Usman, W. Tremel, M. N. Tahir, *Chem. Eur. J.* **2021**, *27*, 6973–6984.

13 L. Tao, Y. Huang, X. Yang, Y. Zheng, C. Liu, M. Di, Z. Zheng, *RSC Adv.* **2018**, *8*, 7102–7109.

14 M. Athanasiou, S. N. Yannopoulos, T. Ioannides, *Chem. Eng. J.* **2022**, *446*, 137191.

15 C. Jin, J. Nai, O. Sheng, H. Yuan, W. Zhang, X. Tao, X. W. Lou, *Energy Environ. Sci.* **2021**, *14*, 1326–1379.

16 Y. Dou, X. Liu, K. Yu, X. Wang, W. Liu, J. Liang, C. Liang, *Diamond Relat. Mater.* **2019**, *98*, 107514.

17 K. Ojha, B. Kumar, A. K. Ganguli, *J. Chem. Sci.* **2017**, *129*, 397–404.

18 M. Yaseen, M. A. K. Khattak, M. Humayun, M. Usman, S. S. Shah, S. Bibi, B. S. U. Hasnain, S. M. Ahmad, A. Khan, N. Shah, A. A. Tahir, H. Ullah, *Energies* **2021**, *14*, 7779.

19 S. S. Shah, M. N. Shaikh, M. Y. Khan, M. A. Alfasane, M. M. Rahman, M. A. Aziz, *Chem. Rec.* **2021**, *21*, 1631–1665.

20 T. Islam, M. M. Hasan, S. S. Shah, M. R. Karim, F. S. Al-Mubaddel, M. H. Zahir, M. A. Dar, M. D. Hossain, M. A. Aziz, A. J. S. Ahammad, *J. Energy Storage* **2020**, *32*, 101908.

21 S. S. Shah, M. A. Aziz, W. Mahfoz, A.-R. Al-Betar, Conducting Polymers Based Nanocomposites for Supercapacitors in *Nanostructured Materials for Supercapacitors*, (Eds: S. Thomas, A. B. Gueye, R. K. Gupta), Springer, Cham, **2022**, Chapter 22, pp. 485–511, Vol. *1*.

22 S. S. Shah, H. T. Das, H. R. Barai, M. A. Aziz, *Polymers* **2022**, *14*, 270.

23 C. Chen, L. Hu, *Acc. Chem. Res.* **2018**, *51*, 3154–3165.

24 H. Parsimehr, A. Ehsani, *Chem. Rec.* **2020**, *20*, 1163–1180.

25 A. Aziz, S. S. Shah, A. Kashem, *Chem. Rec.* **2020**, *20*, 107, 1074–1098.

26 A. J. S. Ahammad, N. Odhikari, S. S. Shah, M. M. Hasan, T. Islam, P. R. Pal, M. A. Ahmed Qasem, M. A. Aziz, *Nanoscale Adv.* **2019**, *1*, 613–626.

27 S. S. Shah, M. A. Aziz, M. Oyama, A.-R. F. Al-Betar, *Chem. Rec.* **2021**, *21*, 204–238.

28 A. J. S. Ahammad, P. R. Pal, S. S. Shah, T. Islam, M. M. Hasan, M. A. A. Qasem, N. Odhikari, S. Sarker, D. M. Kim, M. A. Aziz, *J. Electroanal. Chem.* **2019**, *832*, 368–379.

29 X. Mao, G. C. Rutledge, T. A. Hatton, *Nano Today* **2014**, *9*, 405–432.

30 M. A. Aziz, S. S. Shah, M. A. J. Mazumder, M. Oyama, A.-R. Al-Betar, *Chem. Asian J.* **2021**, *16*, 1570–1583.

31 C. Liedel, *ChemSusChem* **2020**, *13*, 2110–2141.

32 Y. Zhou, J. He, R. Chen, X. Li, *Mater. Today Sustain.* **2022**, *18*, 100138.

33 S. S. Shah, H. Yang, M. Ashraf, M. A. A. Qasem, A. S. Hakeem, M. A. Aziz, *Chem. Asian J.* **2022**, *17*, e202200567.

34 H. Jin, J. Li, Y. Yuan, J. Wang, J. Lu, S. Wang, *Adv. Energy Mater.* **2018**, *8*, 1801007.

35 S. M. Abu Nayem, S. S. Shah, N. Sultana, M. A. Aziz, A. J. Saleh Ahammad, *Chem. Rec.* **2021**, *21*, 1039–1072.

36 S. M. A. Nayem, S. S. Shah, N. Sultana, M. A. Aziz, A. J. S. Ahammad, *Chem. Rec.* **2021**, *21*, 1073–1097.

37 S. M. Abu Nayem, S. S. Shah, N. Sultana, M. A. Aziz, A. J. Saleh Ahammad, *Chem. Rec.* **2021**, *21*, 1038-1038.

38 P. Duarte, S. Pereira, I. Cunha, A. Pimentel, M. Dionísio, E. Fortunato, R. Martins, L. Pereira, *Front. Mater.* **2020**, *7*, 269.

39 C. Vilela, A. J. D. Silvestre, F. M. L. Figueiredo, C. S. R. Freire, *J. Mater. Chem. A* **2019**, *7*, 20045–20074.

40 J. Zhang, J. Fu, X. Song, G. Jiang, H. Zarrin, P. Xu, K. Li, A. Yu, Z. Chen, *Adv. Energy Mater.* **2016**, *6*, 1600476.

41 J. Fu, J. Zhang, X. Song, H. Zarrin, X. Tian, J. Qiao, L. Rasen, K. Li, Z. Chen, *Energy Environ. Sci.* **2016**, *9*, 663–670.

42 W. Ren, Y. Huang, X. Xu, B. Liu, S. Li, C. Luo, X. Li, M. Wang, H. Cao, *J. Mater. Sci.* **2020**, *55*, 12249–12263.

43 S.-D. Gong, Y. Huang, H.-J. Cao, Y.-H. Lin, Y. Li, S.-H. Tang, M.-S. Wang, X. Li, *J. Power Sources* **2016**, *307*, 624–633.

44 B. Liu, Y. Huang, H. Cao, A. Song, Y. Lin, M. Wang, X. Li, *J. Solid State Electrochem.* **2018**, *22*, 807–816.

45 H. Qin, K. Fu, Y. Zhang, Y. Ye, M. Song, Y. Kuang, S.-H. Jang, F. Jiang, L. Cui, *Energy Storage Mater.* **2020**, *28*, 293–299.

46 W. Chen, H. Yu, S.-Y. Lee, T. Wei, J. Li, Z. Fan, *Chem. Soc. Rev.* **2018**, *47*, 2837–2872.

47 R. Fang, S. Zhao, Z. Sun, D.-W. Wang, H.-M. Cheng, F. Li, *Adv. Mater.* **2017**, *29*, 1606823.

48 S. Dutta, J. Kim, Y. Ide, J. Ho Kim, M. S. A. Hossain, Y. Bando, Y. Yamauchi, K. C. W. Wu, *Mater. Horiz.* **2017**, *4*, 522–545.

49 M. M. Pérez-Madrigal, M. G. Edo, C. Alemán, *Green Chem.* **2016**, *18*, 5930–5956.

50 L. Nyholm, G. Nyström, A. Mihranyan, M. Strømme, *Adv. Mater.* **2011**, *23*, 3751–3769.

51 Z. Li, J. Liu, K. Jiang, T. Thundat, *Nano Energy* **2016**, *25*, 161–169.

52 S. M. Alshehri, J. Ahmed, A. N. Alhabarah, T. Ahamad, T. Ahmad, *ChemElectroChem* **2017**, *4*, 2952–2958.

53 J. Jose, V. Thomas, V. Vinod, R. Abraham, S. Abraham, *J. Sci-Adv. Mater. Dev.* **2019**, *4*, 333–340.

54 C. K. Roy, S. S. Shah, A. H. Reaz, S. Sultana, A.-N. Chowdhury, S. H. Firoz, M. H. Zahir, M. A. A. Qasem, M. A. Aziz, *Chem. Asian J.* **2021**, *16*, 296–308.

55 S. S. Shah, M. A. Alfasane, I. A. Bakare, M. A. Aziz, Z. H. Yamani, *J. Energy Storage* **2020**, *30*, 101562.

56 J. Xing, P. Tao, Z. Wu, C. Xing, X. Liao, S. Nie, *Carbohydr. Polym.* **2019**, *207*, 447–459.

57 M. A. Aziz, D. Theleritis, M. O. Al-Shehri, M. I. Ahmed, M. Qamaruddin, A. S. Hakeem, A. Helal, M. A. A. Qasem, *ChemistrySelect* **2017**, *2*, 4787–4793.

58 N. C. Deb Nath, S. S. Shah, M. A. A. Qasem, M. H. Zahir, M. A. Aziz, *ChemistrySelect* **2019**, *4*, 9079–9083.

59 S. S. Shah, M. A. Aziz, A. K. Mohamedkhair, M. A. A. Qasem, A. S. Hakeem, M. K. Nazal, Z. H. Yamani, *J. Mater. Sci. - Mater. Electron.* **2019**, *30*, 16087–16098.

60 A. K. Mohamedkhair, M. A. Aziz, S. S. Shah, M. N. Shaikh, A. K. Jamil, M. A. A. Qasem, I. A. Buliyaminu, Z. H. Yamani, *Arab. J. Chem.* **2020**, *13*, 6161–6173.

61 I. A. Buliyaminu, M. A. Aziz, S. S. Shah, A. K. Mohamedkhair, Z. H. Yamani, *Arab. J. Chem.* **2020**, *13*, 4785–4796.

62 S. M. Abu Nayem, S. S. Shah, S. B. Chaity, B. K. Biswas, B. Nahar, M. A. Aziz, M. Z. Hossain, *Arab. J. Chem.* **2022**, *15*, 104265.

63 M. A. Aziz, S. S. Shah, S. Reza, A. S. Hakeem, W. Mahfoz, *Chem. Asian J.* **2022**, *17*, e202200869, https://doi.org/10.1002/asia.202200869.

64 M. R. Hasan, T. Islam, M. M. Hasan, A.-N. Chowdhury, A. J. S. Ahammad, A. H. Reaz, C. K. Roy, S. S. Shah, I. Al, M. A. Aziz, *J. Phys. Chem. Solids* **2022**, *165*, 110659.

65 S. S. Shah, M. A. Aziz, *Bangladesh J. Plant Taxon.* **2020**, *27*, 467–478.

66 M. A. Aziz, I. R. Chowdhury, M. A. J. Mazumder, S. Chowdhury, *Environ. Sci. Pollut. Res.* **2019**, *26*, 22656–22669.

67 K. Nanaji, V. Upadhyayula, T. N. Rao, S. Anandan, *ACS Sustain. Chem. Eng.* **2019**, *7*, 2516–2529.

68 K. Nanaji, T. N. Rao, U. Varadaraju, S. Anandan, *Int. J. Energy Res.* **2020**, *44*, 2289–2297.

69 R. Ahmadi, M. S. Alivand, N. H. M. H. Tehrani, M. Ardjmand, A. Rashidi, M. Rafizadeh, A. Seif, F. Mollakazemi, Z. Noorpoor, J. Rudd, *Chem. Eng. J.* **2021**, *415*, 129076.

70 M. Asadullah, M. Asaduzzaman, M. S. Kabir, M. G. Mostofa, T. Miyazawa, *J. Hazard. Mater.* **2010**, *174*, 437–443.

71 J. H. Khan, F. Marpaung, C. Young, J. Lin, M. T. Islam, S. M. Alsheri, T. Ahamad, N. Alhokbany, K. Ariga, L. K. Shrestha, Y. Yamauchi, K. C.-W. Wu, M. S. A. Hossain, J. Kim, *Microporous Mesoporous Mater.* **2019**, *274*, 251–256.

72 T. Ramesh, N. Rajalakshmi, K. S. Dhathathreyan, *Ren. Energy Env. Sust.* **2017**, *2*, 4.

73 R. K. Ghosh, D. P. Ray, S. Chakraborty, B. Saha, K. Manna, A. Tewari, S. Sarkar, *Int. J. Environ. Anal. Chem.* **2020**, *101*, 2171–2188.

74 M. Asadullah, M. A. Rahman, M. A. Motin, M. B. Sultan, *Adsorp. Sci. Technol.* **2006**, *24*, 761–770.

75 M. I. Jahan, M. A. Motin, M. Moniuzzaman, M. Asadullah, *Indian J. Chem. Technol.* **2008**, *15*, 413–416.

76 Q. X. Liu, T. Ji, L. F. He, Q. Gao, *Appl. Mech. Mater.* **2012**, *184-185*, 1428–1432.

77 N. H. Phan, S. Rio, C. Faur, L. Le Coq, P. Le Cloirec, T. H. Nguyen, *Carbon* **2006**, *44*, 2569–2577.

78 T. B. Devi, D. Mohanta, M. Ahmaruzzaman, *J. Ind. Eng. Chem.* **2019**, *76*, 160–172.

79 C. Nieto-Delgado, D. Partida-Gutierrez, J. R. Rangel-Mendez, *J. Clean. Prod.* **2019**, *213*, 650–658.

80 C. F. Rombaldo, A. C. Lisboa, M. O. Mendez, A. R. Coutinho, *An. Acad. Bras. Ciênc.* **2014**, *86*, 2137–2144.

81 M. Asadullah, M. S. Kabir, M. B. Ahmed, N. A. Razak, N. S. A. Rasid, A. Aezzira, *Korean J. Chem. Eng.* **2013**, *30*, 2228–2234.

82 J. H. Khan, J. Lin, C. Young, B. M. Matsagar, K. C. Wu, P. L. Dhepe, M. T. Islam, M. M. Rahman, L. K. Shrestha, S. M. Alshehri, T. Ahamadg, R. R. Salunkh, N. A. Kumar, D. J. Martin, Y. Yamauchi, M. S. A. Hossain, *Mater. Chem. Phys.* **2018**, *216*, 491–495.

83 C. Zequine, C. Ranaweera, Z. Wang, P. R. Dvornic, P. Kahol, S. Singh, P. Tripathi, O. Srivastava, S. Singh, B. K. Gupta, *Sci. Rep.* **2017**, *7*, 1174.

84 L. Manjakkal, F. F. Franco, A. Pullanchiyodan, M. Gonzálezjiménez, R. Dahiya, *Adv. Sustain. Syst.* **2021**, *5*, 2000286.

85 F. Li, H.-Y. Yu, -Y.-Y. Wang, Y. Zhou, H. Zhang, J.-M. Yao, S. Y. H. Abdalkarim, K. C. Tam, *J. Agric. Food. Chem.* **2019**, *67*, 10954–10967.

86 W. Wang, Z. Yu, F. K. Alsammarraie, F. Kong, M. Lin, A. Mustapha, *Food Hydrocoll.* **2020**, *100*, 105411.

87 S. Xiao, R. Gao, L. Gao, J. Li, *Carbohydr. Polym.* **2016**, *136*, 1027–1034.

88 T. Xu, Q. Jiang, D. Ghim, K. K. Liu, H. Sun, H. G. Derami, Z. Wang, S. Tadepalli, Y. S. Jun, Q. Zhang, S. Srikanth, *Small* **2018**, *14*, 1704006.

89 Q. Jiang, D. Ghim, S. Cao, S. Tadepalli, -K.-K. Liu, H. Kwon, J. Luan, Y. Min, Y.-S. Jun, S. Singamaneni, *Environ. Sci. Technol.* **2019**, *53*, 412–421.

90 A. A. Adam, J. Ojur Dennis, Y. Al-Hadeethi, E. M. Mkawi, B. Abubakar Abdulkadir, F. Usman, Y. Mudassir Hassan, I. A. Wadi, M. Sani, *Polymers* **2020**, *12*, 2884.

91 J. Wu, Z. Li, *Annu. Rev. Phys. Chem.* **2007**, *58*, 85–112.

92 Y. Qiu, Y. Chen, *J. Phys. Chem. C.* **2015**, *119*, 23813–23819.

93 G. Feng, R. Qiao, J. Huang, B. G. Sumpter, V. Meunier, *ACS Nano* **2010**, *4*, 2382–2390.

94 K. Kiyohara, K. Asaka, *J. Chem. Phys.* **2007**, *126*, 214704.

95 K. Kiyohara, K. Asaka, *J. Phys. Chem. C.* **2007**, *111*, 15903–15909.

96 M. Jitvisate, J. R. T. Seddon, *J. Phys. Chem. Lett.* **2018**, *9*, 126–131.

97 M. Zhou, A. Gallegos, K. Liu, S. Dai, J. Wu, *Carbon* **2020**, *157*, 147–152.

98 J. Wang, X. Zhang, Z. Li, Y. Ma, L. Ma, *J. Power Sources* **2020**, *451*, 227794.

99 H. Sui, H. Li, X. Zhu, D. Chen, G. Wu, *Chemosphere* **2016**, *144*, 1950–1959.

100 D.-E. Jiang, J. Wu, *Nanoscale* **2014**, *6*, 5545–5550.

101 K. Ma, C. Lian, C. E. Woodward, B. Qin, *Chem. Phys. Lett.* **2020**, *739*, 137001.

102 M. Z. Bazant, *Acc. Chem. Res.* **2013**, *46*, 1144–1160.

103 I. Sprague, P. Dutta, *Electrochim. Acta* **2011**, *56*, 4518–4525.

104 E. Karimi-Sibaki, A. Kharicha, M. Wu, A. Ludwig, J. Bohacek, *Ionics* **2018**, *24*, 2157–2165.

105 S. Sundriyal, V. Shrivastav, H. D. Pham, S. Mishra, A. Deep, D. P. Dubal, *Resour. Conserv. Recycl.* **2021**, *169*, 105548.

106 G. S. D. Reis, H. P. D. Oliveira, S. H. Larsson, M. Thyrel, E. C. Lima, *Nanomaterials* **2021**, *11*, 424.

107 L. Geng, Y. Cai, L. Lu, Y. Zhang, Y. Li, B. Chen, X.-F. Peng, *ACS Sustain. Chem. Eng.* **2021**, *9*, 2591–2599.

108 J. Yang, Y. Wang, J. Luo, L. Chen, *ACS Omega* **2018**, *3*, 4647–4656.

Index

WILEY END USER LICENSE AGREEMENT

Go to www.wiley.com/go/eula to access Wiley's ebook EULA.